THE STRUCTURAL GEOLOGY OF THE NAUKLUFT NAPPE COMPLEX AND ITS RELATIONSHIP TO THE DAMARA OROGENIC BELT, SOUTH WEST AFRICA/NAMIBIA

CHRISTOPHER JOHN HUBERT HARTNADY

Thesis submitted in fulfilment of the requirements for the degree of Doctor of Philosophy in the Faculty of Science of the University of Cape Town

1978

ABSTRACT

The Naukluft nappe complex has been quoted as a classic example of gravity gliding tectonics (Korn & Martin, 1959). Situated close to the southern margin of the Damara orogenic belt, it provides a key to the persistent controversy over the correlation of the "geosynclinal" Damara Supergroup with the Nama Group on the Kalahari craton. It also contains critical evidence bearing on the timing and large-scale geodynamics of the Late Precambrian-Early Palaeozoic Damara orogeny, particularly the hypothesis that it involved plate tectonic processes of subduction and continental collision in the southern zones.

In the southern part of the Damara orogenic belt, macroscopic structural criteria visible on LANDSAT imagery permit the definition of a distinct *Khomas Ridge province* which can be further subdivided into four major tectonic zones, here labelled KR-I to KR-IV from south to north. The northern boundary of the Khomas Ridge province is a fundamental discontinuity of sub-vertical orientation and since it can be traced (or inferred where disrupted by late intrusions) for at least 350 km along strike it is assumed to cleave deeply through a major part of the lithosphere. The northern zones KR-III and KR-IV comprise the deep and lithologically monotonous Khomas Trough, which is the true "eugeosyncline" of the Damara belt. Zones KR-II and KR-III especially are characterized by strongly-developed, early tectonic foliations. In zone KR-III, the main foliation dips northwestwards at an angle of about 30° and the zone includes the remarkable Matchless Amphibolite. Zone KR-II is characterized by complex poly-phase deformation patterns involving southward-vergent recumbent folds and thrust nappes. Zone KR-I is a marginal part of the Damara belt, which was formerly classified as part of the southern foreland. The imprint of Damaran deformation and low- to very-low-grade metamorphism in this zone is clear, even on the macroscopic scale. Due to poor exposure and its intrinsically diffuse nature, the exact locus of the southern boundary of zone KR-I is difficult to trace. Although the Naukluft nappe complex falls well within and is the highest tectonic element of zone KR-I, it can be regarded as part of the (locally subhorizontal) boundary between zones KR-I and KR-II since it displays transitional structural styles and includes some characteristic KR-II lithological units. The present revision of the stratigraphy of the Naukluft nappe complex aims at drawing a clearer distinction between the basic tectonic units (thrust-sheets or nappes) and eight lithostratigraphic formations.

The oldest stratigraphic units in the nappe complex are the *Noab* and *Büllsport Formations* which represent two slightly different facies, dune-beach and tidal flat, of a dolomite-clastics assemblage, probably deposited along a northward-facing coastline. In contrast, all younger lithostratigraphic units in the Naukluft complex were apparently derived from tectonically active provenances in the north. The *Remhoogte Formation* grades from conglomeratic phyllites in the northwest to fine-grained, slaty metapelites in the southeast and contains local, deformed limestone and carbonate breccia members. In the central part of the Naukluft complex, it is overlain unconformably by the

Blässkranz Formation, which is a thick limestone and dolomite breccia interpreted as a submarine slump deposit ("olistostrome"). It contains some pebbles and boulders which are identifiable as Noab and Büllsport lithologies, as well as rare granitoid basement clasts. The *Tsabisis Formation*, which is distinguished by a thin volcaniclastic member, follows conformably in the local succession. The *Klipbokrivier Formation*, which is the upper unit in an overlying nappe, is correlated with the Remhoogte Formation on Lithological grounds. At the base of the enigmatic S. Pavian nappe, the *Aubschlucht Formation* is a sequence of arkosic sandstone, conglomerate and siltstone with a characteristic hematitic pigment in most parts. Its relative stratigraphic position is uncertain because lithologically it is unique in the Naukluft complex. It most resembles the Kamtsas Formation northeast of the nappe complex, but this correlation is controversial because it implies that the Kamtsas Formation is a syn-orogenic Damaran deposit. The youngest unit, the *Zebra River Formation*, is a sequence of quartzite, shales, limestones and dolomites which is subdivided into five members and tentatively correlated with the underlying, autochthonous Zaris Formation in the Nama Group.

The present analysis of structural geometry has concentrated on presenting an accurate picture of lithostratigraphic boundary and thrust-contact relationships and has initiated the construction of a computerised base of fabric data collected at precisely located field sites.

Five major thrust-sheets are now distinguished in the Naukluft nappe complex. In the northern region, the dolomitic *Kudu nappe*, which has undergone very little internal ductile deformation, overlies the largely pelitic *Northern Pavian nappe* with a major tectonic discontinuity. This contact is subhorizontal over an extensive area and has been gently folded and locally faulted by later structures. In the central and eastern parts of the nappe complex, the main planar tectonic fabric steepens and the two northern nappes have been displaced over the intricately imbricated sequence of (in descending tectonic order) the *Southern Pavian*, *Western Dassie* and *Eastern Dassie nappes*. Within the W. Dassie nappe, there is a conspicuous change in structural style and fabric orientation between the segments comprised of the imbricated Büllsport Formation and the openly folded Zebra River Formation, respectively. The greatly inhomogeneous nature of Naukluft structure is related to large contrasts in rock ductility, particularly of the dolomites with respect to other lithologies, but also reflects a complicated history of syn-orogenic sedimentation.

The Naukluft nappe complex shows five distinct deformational episodes (D_1 to D_5), defined mainly by unconformity relationships between lithostratigraphic elements within individual nappes and subsequent correlation of these events between nappes. The D_1 *episode* was responsible for the production of complex planar fabric development in the northern phyllites of the Remhoogte Formation, and is evidenced by the erosional truncation of Remhoogte lithologies at the base of the Blässkranz Formation. The D_2 *episode* resulted in the displacement of the Noab and Büllsport dolomites over the Blässkranz and Tsabisis depositional basin. Because of the very low ductility of the

massive and sandy dolomites, the Kudu nappe segment of the thrust-sheet was little deformed, but the better layered Büllsport facies was intensely imbricated in the toe region of the nappe. A mixed layer of marble and phyllite, which formed a viscous *decollement* zone between the original Kudu nappe and its substratum, shows complex deformation phenomena, including refolding recumbent folds. The minimum cumulative Kudu nappe displacement during D_1 and D_2 is estimated as 33 km toward azimuth 170°. At this stage a major hiatus in orogenic activity appears to have intervened in the Naukluft region, allowing the accumulation of a molassic Aubschlucht Formation and subsequently the shallow marine transgression of the Zebra River basin across the former nappe front. Renewed orogenesis in the *D_3 episode* involved large-scale re-imbrication of the frontal zone of the older Kudu-N. Pavian nappe complex in an arcuate pattern which is ascribed to a type of indentation tectonics. A minimum 16 km displacement of the Kudu nappe toward azimuth 170° is estimated to have occurred during D_3. A part of the Zebra River Formation was incorporated in the re-imbricated zone as the S. Pavian nappe, but a great area of the Zebra River in the W. Dassie nappe was apparently only locally affected by intense D_3 deformation close to the main D_3 *decollement*. After the deposition of the upper, Onis dolomite and limestones, during the *D_4 episode*, the Zebra River Formation in the W. Dassie nappe was openly folded about northeasterly-trending axes. The displacement of the entire Naukluft nappe complex, as an effectively rigid plate, over the northern part of the Nama basin is regarded as having occurred in a slightly later but distinct *D_5 episode*. A minimum cumulative D_4 and D_5 displacement of 35 km towards azimuth 125° is estimated.

For the early stages of Naukluft nappe evolution, a gravity spreading model is preferred in which the main D_2 viscous *decollement* zone developed at a depth of about 15 km beneath a southward surface slope of at least 3°. The thrust surfact itself was northward-dipping. Deformation structures in the marble zone indicate relatively high shear stresses (20–50 MPa) at strain-rates close to $10^{-11}s^{-1}$. Inferred temperature and confining pressure within the deformation zone are 350–400°C and about 400 MPa, respectively. For the final (D_5) emplacement stage, an evaporitic precursor to the Unconformity Dolomite, constituted a thin layer of very low viscosity and probable associated high pore fluid pressure deforming under a basal shear stress of less than 5 MPa. D_5 overthrusting took place at a much higher level in the crust and may have involved down-slope gravity gliding towards the end of the episode.

Three major features of the Khomas Ridge province suggest that the Damara orogenesis was related to oceanic crustal subduction and continental collision. Firstly, the existence of a thick monotonous prism of metasedimentary schist, which despite its deformation, is physically similar to modern fore-arc basin deposits and is chemically similar to the average andesite, may be used to obtain an estimate of the length of the oceanic slab that was consumed, provided that the almost entirely volcanogenic origin of the deposit is assumed and that subduction-related petrological models of andesite genesis are accepted. Secondly, the unique concentration of belts

of mafic and also ultramafic rock in zones KR-II and KR-III can be interpreted either as deformed and dismembered ophiolitic material or as interstratified mafic volcanics of the type found typically in fore-arc or trench environments in Phanerozoic belts. Thirdly, the southward increase in the intensity of deformation within the Khomas Ridge province, culminating in a slab-like zone of shallow, northward dip and complex polyphase fold and thrust structure, can be interpreted as the product of a simple shear displacement of the Khomas Ridge province over the north-western margin of the Kalahari craton for a distance of the order of 100 km. The evolution of the Naukluft nappe complex is related to the collision of the Kalahari craton with the southern Damara subduction zone, driven by the gravitational sliding into the mantle of a wide, dense oceanic slab.

ACKNOWLEDGEMENTS

The Naukluft project was initiated by the late Professor John de Villiers for whose support and enthusiasm I remain sincerely grateful; his untimely death before the main results of this work had begun to emerge is deeply regretted. I am also grateful to Professor J. G. Ramsay for first suggesting to me that the Naukluft structures were worthy of re-investigation, and to Professor Henno Martin, who guided me on an introductory field trip and who has maintained a constant interest in my progress ever since.

Professor E.S.W. Simpson supported me on my return to the University of Cape Town, and my thanks are due to him and to Professor A.M. Reid for making the facilities of the Department of Geology available to me.

The continued support and very great patience of my supervisor, Assoc. Prof. P. Joubert, has been most appreciated. I have also benefitted from numerous discussions on Damaran geology with my colleagues in the Precambrian Research Unit, particularly Professor A. Kröner (now at the University of Mainz) and Mr. S. T. Malling. The late Dr. Vaclav Vajner helped considerably with the preparation of the tectonic data-base system, which was developed during the course of this project. Others who assisted enormously with that aspect were Dr. A.R. Duncan and Mr. J.P. Willis of the Department of Geochemistry, whose own data system was the model for the one which I have developed.

The finite element study of the deformation of a materially inhomogeneous system was begun at the Imperial College of Science and Technology, London, during the tenure of a British Council scholarship. I am grateful to Dr. A.W.B. Siddans for introducing me to this field of tectonophysical research. Dr. N.C. Gay has continued to encourage me in this direction.

I am pleased to acknowledge the hospitality of the farmers in the Naukluft area, in particular the late Mr. G. Jackson and Mrs. Jackson, of Nauzerus, Mr. and Mrs. O. Voigts of Blässkranz and Mrs. H. Sauber of Büllsport. The support of the Department of Nature Conservation and Tourism in SWA/Namibia in allowing me free access to the Naukluft Mountain Zebra Park is also gratefully acknowledged.

The Geological Survey of South West Africa has always been extremely helpful to me, and I am particularly thankful to Mr. L. Engelbrecht and Dr. P.J. Hugo, who have also acted as co-ordinators for the National Geodynamics Project in the Damara orogenic belt. Other Survey officers who have helped me with their interest and support are Drs. R. McG. Miller, K.E.L. Schalk and G.J.B. Germs.

Financial support for this project was received through the C.S.I.R., as part of the South African National Geodynamics Programme.

For technical help in the preparation of this work, I am grateful to Miss. P. Eloff for transforming my amateurish drawings into fine diagrams and maps and to Mrs. J. Elliott for typing the manuscript. For draft typing, proof reading, copying, collating and generally helping me in ways too numerous to mention, I shall always be grateful to my wife, Pamela.

CONTENTS

		Page
I	INTRODUCTION	1
A	OROGENIC THEORIES, NAPPES, GRAVITY TECTONICS AND THE NAUKLUFT MOUNTAINS	1
B	THE NAUKLUFT NAPPE COMPLEX	5
1	General setting	5
2	Objectives of the present project	7
II	THE DAMARA OROGENIC BELT AND ITS SUBDIVISION IN THE KHOMAS RIDGE REGION	13
A	INTRODUCTION	13
B	GENERAL DATA ON THE OROGENIC BELT	14
1	Definition of the belt and the Geodynamics study area	14
2	Surface shape of the orogenic belt in plan	15
3	Surface shape of the segment in elevation	17
4	Geophysical Data - The deep structure of the segment	19
5	Time relations	23
C	SUBDIVISION OF THE DAMARA OROGENIC BELT	31
1	Previous large-scale zonation	31
2	The Khomas Ridge province	32
3	Boundaries of the Khomas Ridge province	33
4	Description of the tectonic zones	35
5	Concluding remarks	39
III	STRATIGRAPHY IN THE NAUKLUFT NAPPE COMPLEX AND THE SOUTHERN MARGINAL ZONES OF THE DAMARA BELT	41
A	INTRODUCTION	41
1	Stratigraphy in zone KR-I	41
2	Stratigraphy in Zone KR-II	46
3	Lithostratigraphy in the Naukluft Complex	49

			Page
B	DOLOMITIC FORMATIONS OF THE KUDU AND DASSIE NAPPES		54
	1	Noab Formation	54
	2	Büllsport Formation	62
	3	Regional Aspects of the Noab and Büllsport Formations	67
C	BLACK LIMESTONE ("SCHWARZKALK") BEARING FORMATIONS OF THE KUDU AND NORTHERN PAVIAN NAPPES		71
	1	Klipbokrivier Formation	71
	2	Remhoogte Formation	73
	3	Blässkranz Formation	80
	4	Age and correlation of black limestone-bearing formations of the Kudu and Northern Pavian nappes	88
D	TSABISIS FORMATION		90
	1	Introduction	90
	2	Description	91
	3	Relationships to adjacent units	95
	4	Depositional environment	96
	5	Correlation and age of the Tsabisis Formation	98
E	ZEBRA RIVER FORMATION		99
	1	Introduction	99
	2	Description	100
	3	Relationships to adjacent units	104
	4	Depositional environment	104
	5	Correlation and age of the Zebra River Formation	105
F	FORMATIONS OF THE SOUTHERN PAVIAN NAPPE		107
	1	Introduction	107
	2	Description	107
	3	Relationships to adjacent units	109
	4	Depositional environment	109
	5	Correlation and age of the S. Pavian Formations	110

			Page
IV	STRUCTURAL GEOMETRY OF THE NAUKLUFT COMPLEX		113
	A	INTRODUCTION	113
		1 General remarks	113
		2 Methods of structural analysis	113
	B	STRUCTURAL GEOMETRY	116
		1 Shape of the nappe complex and definition of the constituent nappes	116
		2 Structure of the North-west (NW) and Northern (N) areas	120
		3 Structure of the Central (C) area	141
		4 Structure of the South-eastern (SE) and South-central (SC) areas	148
		5 Structure of the Western (W) and South-western (SW) areas	160
V	KINEMATIC AND DYNAMIC ANALYSIS OF NAUKLUFT NAPPE EMPLACEMENT		168
	A	ASPECTS OF NAUKLUFT KINEMATICS	168
		1 Role of unconformities in defining deformation episodes	168
		2 Correlation of deformation episodes	169
		3 Kinematic reconstruction of nappe emplacement	172
		4 Some aspects of brittle and ductile deformation kinematics	181
	B	DYNAMIC INTERPRETATION OF NAUKLUFT NAPPE EMPLACEMENT	188
		1 Evidence of the mechanical state of thrust surfaces during D_2 and D_3	189
		2 Origin and mechanical state of the Unconformity Dolomite	197
		3 Analysis of the relative importance of gravitational and longitudinal compressive forces in Naukluft nappe tectonics	202
VI	GEODYNAMIC INTERPRETATION OF THE DAMARA OROGEN		206
	A	INTRODUCTION	206
		1 The asthenolith hypothesis	206
		2 Some geophysical aspects of modern geodynamic theory	207

			Page
B		A REALISTIC MODEL FOR THE DAMARA OROGENY	213
	1	Major indications for plate tectonics	213
	2	Implications of plate theory to the interpretation of the Khomas schists	216
	3	The Matchless Amphibolite : a possible ophiolite	228
VII		CONCLUSIONS	235
		REFERENCES	242

PLATES

ANNEXURE I : Geological map of the Naukluft nappe complex

ANNEXURE II : Sections through the Naukluft nappe complex

FIGURES

No.		follows page
1	Locality map of central SWA/Namibia	5
2	Physiographic map of central SWA/Namibia	6
3	Generalised map of Damara orogenic belt	14
4	Bouguer gravity anomaly map of central SWA/Namibia	19
5	Correlation diagram of Late Precambrian sequences on the Congo craton	28
6	Tectonic zonation of the Khomas Ridge province	33
7	Interpretation of LANDSAT image E-1058-08210	36
8	Major lithostratigraphic units of zone KR-1	43
9	Pipe-like (? defluidisation) structures in Noab dolomite	58
10	Stratigraphic column for the N. Pavian nappe	73
11	Sketch of crenulation cleavage microstructure in Remhoogte phyllite (Type II)	74
12	Detail sketch of mineral and grain relationships in Type II Remhoogte phyllite	75
13	Sketch of microstructure and chlorite porphyroblastesis in Type I Remhoogte phyllite	76
14	Model for the origin of the Blässkranz carbonate breccias	85
15	Detailed stratigraphic column for Tsabisis volcaniclastic member at locality 30009	90
16	Detailed stratigraphic column for Tsabisis volcaniclastic member at locality 30079	90
17	Sketch of tuffaceous and agglomeratic layer in a Tsabisis hand specimen	93
18	Stratigraphic column for the Zebra River Formation	100
19	Local stratigraphic columns for the S. Pavian nappe	107
20	The five major nappe units of the Naukluft complex	117
21	Location of the seven structural data regions	120
22	Structural map of the Kuibis Formation in the Abbabis area	121
23	Orientation diagrams for SS and S_1 in the Nama Group of the NW area	123

No.		follows page
24	Internal structure of the N. Pavian nappe in a segment along the north-western boundary of the nappe complex	125
25	Orientation diagrams for the giant tectonic inclusion in the north-western part of the N. Pavian nappe	126
26	Cross-sectional sketch illustrating N. Pavian and Kudu nappe structure along the north-western nappe boundary	127
27	- ditto -	127
28	Orientation diagrams for the Remhoogte Formation in the N and NW areas	131
29	Orientation diagrams for post-S_1 deformation of the Remhoogte Formation in the N and NW areas	133
30	Orientation diagrams for Remhoogte linear structures	134
31	Fold trends in the N, NW and C areas of the Naukluft complex	136
32	Orientation diagrams for the Noab Formation in the N and NW areas	139
33	Orientation diagrams for the Klipbokrivier Formation	139
34	Distribution and structure of lithostratigraphic units in the N. Pavian nappe of the C area	141
35	N. Pavian-Kudu nappe relationships in the northern part of Blässkranz	141
36	Orientation diagrams for SS in the N. Pavian formations of the C area	143
37	Orientation diagrams for S_1 and L_1 in the N. Pavian nappe of the C area	143
38	Orientation diagrams for S_1 structure types in the N. Pavian nappe of the C area	144
39	Orientation diagrams for S_1 and L_{1X} in the Remhoogte, Blässkranz and Tsabisis Formations separately	144
40	Structures in the N. Pavian nappe west of Pavianskopf	145
41	Orientation diagrams for the Kudu nappe and its lower contact zone in the C area	146
42	Map of imbricate structure in the E. Dassie nappe	149
43	Orientation diagrams for SS in the Büllsport Formation of the SE area	150

No.		follows page
44	Panoramic section sketch of the nappe pile west of the Tsondab valley on Büllsport	151
45	Structural map of the nappe front around Büllsport	152
46	Cross-sectional sketch showing W. Dassie-E.Dassie nappe contact relationships	152
47	Orientation diagrams for S_1 in the W. Dassie nappe of the SE area	153
48	Orientation diagrams for structures in Büllenkopf and the Polizeischlucht (Büllsport area)	154
49	Orientation diagrams for SS and L_1 FAX in the W. Dassie nappe	155
50	Orientation diagrams for S_1 and L_{1X} in the W. Dassie nappe	155
51	Orientation diagrams for the S. Pavian nappe	157
52	Orientation diagrams for the Kudu nappe in the SC area	157
53	Map of fold trends and major structural domains in the Zebra River Formation	161
54	Contact relationships at the base of the Zebra River Formation on Tsams Ost 2	162
55	Orientation diagrams for the Büllsport and Zebra River Formations of the W and SW areas	164
56	Detail map of lithostratigraphy and structure in a critical region of the Naukluft Mountain Zebra Park	165
57	Sketch map of nine localities critical to kinematic interpretation of Naukluft nappe evolution	169
58	Reconstruction of Naukluft nappe emplacement	173
59	Sketch maps relating to the problem of S. Pavian nappe emplacement during the D_3 deformation episode	175
60	Postulated pre-D_3 configuration of imbricate zone of the W. Dassie and E. Dassie nappes	179
61	Total displacement of the Kudu nappe related to some major features of the south-western Damara belt	180
62	Idealised model of the tectonic imbrication process	182
63	Graph relating shortening to bedding dip resulting from tectonic imbrication	185

No.		follows page
64	Graph of nappe thickness versus length/thickness ratio (after Elliott, 1976a) illustrating relative importance of compressive to gravitational stresses driving thrust sheets	203
65	Model of temperature distribution at depth a peak of Damaran post-tectonic metamorphism (after Haack, 1976)	214
66	Structural cross-section of the Khomas Trough and its possible modern analogue in the Guatemalan continental margin	217
67	Map showing distribution of bodies of mafic and ultramafic rock in zones KR-II and KR-III of the Khomas Ridge province	232

TABLES

No.		follows page
1	Summary of Otavi Group stromatolite palaeontology	28
2	Precambrian stratigraphy of Khomas Ridge zone KR-I (south-western part)	41
3	Tectonic and stratigraphic units of the Naukluft nappe complex	119
4	Fabric statistical parameters for the Nama group structures in the NW area	124
5	Fabric statistical parameters for the Remhoogte Formation structures in the NW and N areas	132
6	Fabric statistical parameters for the Kudu nappe structures in the NW and N areas	132
7	Fabric statistical parameters for the N. Pavian nappe bedding (SS) structures in the C area	142
8	Fabric statistical parameters for the N. Pavian nappe cleavage (S_1) structures in the C area	144
9	Fabric statistical parameters for the E. Dassie (E.D.), W. Dassie (W.D.), S. Pavian (S.P.) and Kudu nappe bedding (SS) structures in the SE and SC areas	150
10	Fabric statistical parameters for the W. Dassie (W.D.) and Kudu nappe cleavage (S_1) structures in the SE and SC areas	156
11	Tectonostratigraphic history of the Naukluft nappe complex	168
12	Composition of the Khomas Schist	218
13	Models of Khomas Trough Evolution	224

CHAPTER I

INTRODUCTION

A. OROGENIC THEORIES, NAPPES, GRAVITY TECTONICS AND THE NAUKLUFT MOUNTAINS

H.B. de Saussure (b. 1740), the "founder of Alpine Geology" is recorded to have said that the study of mountains, better than anything else, would permit us to arrive at a theory of the Earth (Collet, 1935, p.3). The study of the processes and causative forces of *orogeny*, which has been defined as the *profound deformation of rock bodies along restricted zones and within a limited time interval* (Dennis, 1967, p.112) and is usually followed by the uplift of these restricted crustal belts to form mountain chains, remains as vital now to understanding the nature of the solid Earth as de Saussure considered it to be almost two centuries ago. This can be gauged from the intensity of the present-day controversy between so-called fixed crust (or "fixist") and mobile crust (or "mobilist") theories of orogeny.

Fixist theories of orogeny are based on the concept that all observed structural phenomena can be explained by dominantly vertical oscillations of the Earth's crust (Haarman, 1930; Van Bemmelen, 1933; Beloussov, 1962). Mobilist theories of orogeny are based on the concept that large horizontal relative displacements take place between rigid blocks of the Earth's crust and that these horizontal boundary displacements account for observed deformation phenomena in orogenic zones. The argument between the two viewpoints falls, in the first instance, entirely within the domain of *kinematics*, the study of motion and could therefore be settled conclusively by observing the final geometric configuration of geological structures, the initial or earlier geometric configuration of which is either well known or tightly constrained by ancillary geological evidence. Basically, this involves the quantitative estimation of displacements and strain or deformation in orogenically deformed rock bodies (Ramsay, 1969).

In the case of large overthrusts in former sedimentary formations which are datable by palaeontological methods, evidence for sometimes very large lateral movements of extensive bodies of rock is quite clear and unambiguous. In this connection, the recognition in the Alps of the Glarus overthrust by Escher in 1841 and its subsequent explanation by Bertrand (1884), is a classic milestone in tectonic geology. This was the beginning of the *nappe* concept of a large, *sheet-like tectonic unit which has been transported from its original site of emplacement by movement along a predominantly subhorizontal floor* (definition modified from Dennis, 1967, p.111). The obvious kinematic inference to be drawn from this kind of evidence is that large horizontal boundary displacements have indeed occurred within and about orogenic zones.

However, on account of the then unacceptably large horizontal displacements that were implied by the field relationships of some nappes a displacement of about 150 km was claimed by Bailey (1910, p.587) for the Scandinavian overthrust described by Törnbohm (1896) - and of the inability of the rocks in relatively thin nappe structures to withstand the powerful lateral stresses required to overcome frictional-sliding resistance along the basal thrust plane (Smoluchowski, 1909), the nappe concept was not uncritically received. On the first count, an alternative explanation for nappe phenomena which did not involve such radical crustal shortening was sought in the old geological hypothesis of gravity tectonics.

Gravity tectonics is defined (Dennis, 1967, p.85) as the "*process and result of rock deformation primarily under the influence of gravity*". The hypothesis was used early in the history of the nappe concept to explain the Pre-alpine and Helvetic structures as a result of gravitational sliding of sedimentary cover rocks from the uplifted crystalline basement to the south of their present positions. Their hypothesis, as later elaborated, emphasized "flowage" or pervasive plastic deformation of the sliding masses, rather than rigid-body gliding on a single discrete surface. Dennis (1967, p.86) articulates the difference between these two components of the general gravity tectonics hypothesis as follows:

> "Gignoux (1948, p.740) distinguishes clearly between *gliding* and *flow* under the influence of gravity. Thus de Sitter (1956) uses the name "gravity gliding tectonics" and Dennis (*in* Korn & Martin, 1959) uses "gravity tectonics", which implicitly includes both flow and gliding, as displayed in the Naukluft Mountains."

Thus, from the research in the Alpine nappes, a *dynamic* hypothesis was elaborated which assigned the inferred movements of the nappe structures to a specific force, namely the body force of gravity involving the mass of the moving nappe itself. In other words, the simultaneous gliding and flow of a nappe is produced under the action of nappe's own weight. Such a hypothesis obviously involves important assumptions about the mechanical constitution, the "rheological" or flow behaviour, of the rock materials found within the nappes.

Following Alpine research developments of the 1940's, a trend developed in structural geology towards placing increased emphasis on the force of gravity to explain large lateral movements of rock. Temple (1968, p.696), for example, stated:

> "Numerous examples of overthrusting, previously thought to be the result of shortening of the crust, are now convincingly explained as the result of downslope gliding. This has led many geologists to de-emphasize crustal compression as a major force in mountain building. The same reasoning has given credence to theories which account for all observed structural phenomena primarily by vertical uplift. Compression, if present at all, plays only a secondary role."

The emergence of the theory of plate tectonics (Wilson, 1965; McKenzie & Parker, 1967; Le Pichon, 1968; Morgan, 1968) has seen, in some respects, a dramatic reversal of the trend to which Temple refers. In classic regions such as the Alps and Himalayas, crustal compression, developed during the collision of previously separated continental masses, has again come to be emphasized as the major force in the building of those mountain chains and the deformation of the rocks within them (Mitchell & Reading, 1969; Dewey & Bird, 1970; Dewey, Pitman, Ryan & Bonnin, 1973; Le Fort, 1975). Even in the case of the Pre-alpine nappes, the so-called "fatherland" of the gravity tectonics concept, the exclusive role of gravity as the immediate causative force of rock deforma-

tion has been challenged (Lemoine, 1973).

The Naukluft Mountains of South West Africa have figured prominently in the theory of gravity tectonics since Korn & Martin's 1959 description of the nappe phenomena there. This is illustrated by the use of the Naukluft nappes as a classic example of gravity deformation in Holmes (1965, p.1145) and by the above quotation from Dennis (1967). At a time of general re-appraisal of orogenic and tectonic theories, it is therefore quite appropriate that the evidence from the Naukluft structures also be re-examined. However, the nature of this re-examination deserves some special comment.

Previous structural work in the Naukluft region (Cloos, Korn & Martin, 1937; Korn & Martin, 1959) was done prior to the rise of the "geometrical approach to structural geology" (Weiss, 1959, p.62), which is in general characterised by rigorous attention to precise measurement of quantitative orientation and location data in the field, by the application of broadly statistical techniques to the analysis of this data (Turner & Weiss, 1963) and more recently, by the rigorous application of the mathematical theory of strain and deformation to naturally deformed rock bodies (Ramsay, 1967). Furthermore, the description of the Naukluft phenomena preceded, by a short while, the development and elaboration of a quantitative physical theory for the mechanism of large-scale overthrusting and gravity gliding, by Hubbert & Rubey (1959) and others. In respect of both the quantitative geometrical and kinematic description of Naukluft rock structures and the quantitative dynamic analysis of these phenomena, there remained much work to be done.

The recent development of the quantitative kinematic theory of plate tectonics (Le Pichon, Francheteau & Bonnin, 1973) and recent geodynamic research into the driving forces of plate motion (Harper, 1975; Solomon, Sleep & Richardson, 1975; Forsyth & Uyeda, 1975) holds out the prospect, as yet largely unrealised, of explaining orogenic development quantitatively in terms of motions, forces, heat and mass exchanges at convergent plate boundaries. Tentative attempts to use quantitative plate kinematics to this end have been made for certain parts of the system of Mesozoic-Cenozoic orogenic belts by Atwater (1970) and Dewey and others (1973). However, the technical difficulties facing such reconstructions for earlier geological time are formidable

(Dewey, 1975) and moreover, the extension of plate concepts and techniques to Precambrian orogenic belts remains most controversial (Sutton, 1976). In the case of the Damara orogenic belt, to which the Naukluft nappe complex is closely related in time and space, there is at present a clear division between different workers over the issue of the applicability of a plate tectonic analysis. This, too, is part of the general context in which re-examination of the Naukluft Mountains takes place, namely, the framework of the South African contribution to Working Group 9 - "History and Interactions of Tectonic, Metamorphic and Magmatic Processes" - of the International Geodynamics Project (Geodynamics Project in South Africa, 1975).

B. THE NAUKLUFT NAPPE COMPLEX

1. General setting

a. Location and dimensions

The Naukluft nappe complex falls within a rectangular area bounded by latitudes 23° 45'S and 24° 30'S and longitudes 16° 00'E and 16° 30'E (Fig. 1 and Annexure I). The nappe complex itself is elongate in a NE-SW direction having a maximum length of about 70 km and a maximum width of about 30 km. These dimensions and the roughly elliptical plan shape of the complex, indicate that it covers an area not less than 1650 km^2. Though somewhat smaller, they are comparable with the dimensions of the Pre-alpine nappe complex of the Chablais and the Prealpes Romandes (Debelmas & Kerckhove, 1973; Lemoine, 1973), the equivalent dimensions of which are approximately 130 km, 40 km and 4000 km^2. The lowest exposed part of the Naukluft nappe complex is at an elevation of 1240 m above mean sea-level and the highest part of the complex is at an elevation of 1994 m. This indicates that it has a present-day thickness of at least 750 m.

The lateral dimensions of the Naukluft nappe complex shortly after its emplacement are unknown but may well have been very similar to those of the above-mentioned Alpine-analogue, for the Naukluft complex has obviously been subject to considerable post-emplacement uplift and erosion, most of which occurred during Lower Palaeozoic times.

b. Physiography

The Naukluft region straddles the divide between the westward-draining systems of the Tsondab and Tsauchab Rivers, on the one hand and the eastward draining system of the upper Fish River, on the other (Fig.1). Between the trace of the drainage divide and the inner 1200m desert plain, there is a zone of heavily-dissected, mountainous topography with summit plateaux close to 2000 m. This Great Escarpment is a feature which has been inherited from the time of break-up of the West Gondwana continent and in the course of its parallel retreat from the original site of rifting, has left behind a great coastal plain pediment, the present day morphology of which has been shaped mainly by Tertiary transgressions and regressions of the Atlantic Ocean.

It is primarily the present location of the Escarpment and the magnificent mountain- and cliff-side exposures that it provides, that has facilitated the recognition and accurate structural interpretation of the Naukluft nappe complex. At the same time however, a great portion of the complex, both vertical and lateral, was removed irrevocably. It is evident from the metamorphic state (lower greenschist facies) of some Naukluft formations that the present preserved vertical thickness of about 1 km is not a true reflection of its original thickness at least in the north-eastern part of the nappe pile.

In the geomorphology of the Naukluft area, there is evidence that some of the existing valley topography is the exhumed remnant of a sub-Karoo, U-shaped glacial valley topography, since outliers of Permo-Carboniferous tillite have been found at elevations between 1400 and 1600 m. (Korn & Martin, 1959, p.1050). These outliers lie at least 200 m below the very conspicuous summit erosion level in the Naukluft Mountains, which was considered by Korn & Martin (*op.cit.*) to be also of pre-Karoo age. This surface lies mainly between 2000 m and 1800 m elevation, sloping very gently eastwards, away from the escarpment zone. It is at an equivalent elevation to the Khomas Peneplain (Mabbutt, 1955) which is at about 2000 m elevation in the Khomas Highlands and in shoulders fringing the Auas Mountains, farther north-east along the southern margin of the Damara orogenic belt (Fig. 2).

The Tsondab River valley divides the Naukluft nappe complex into two

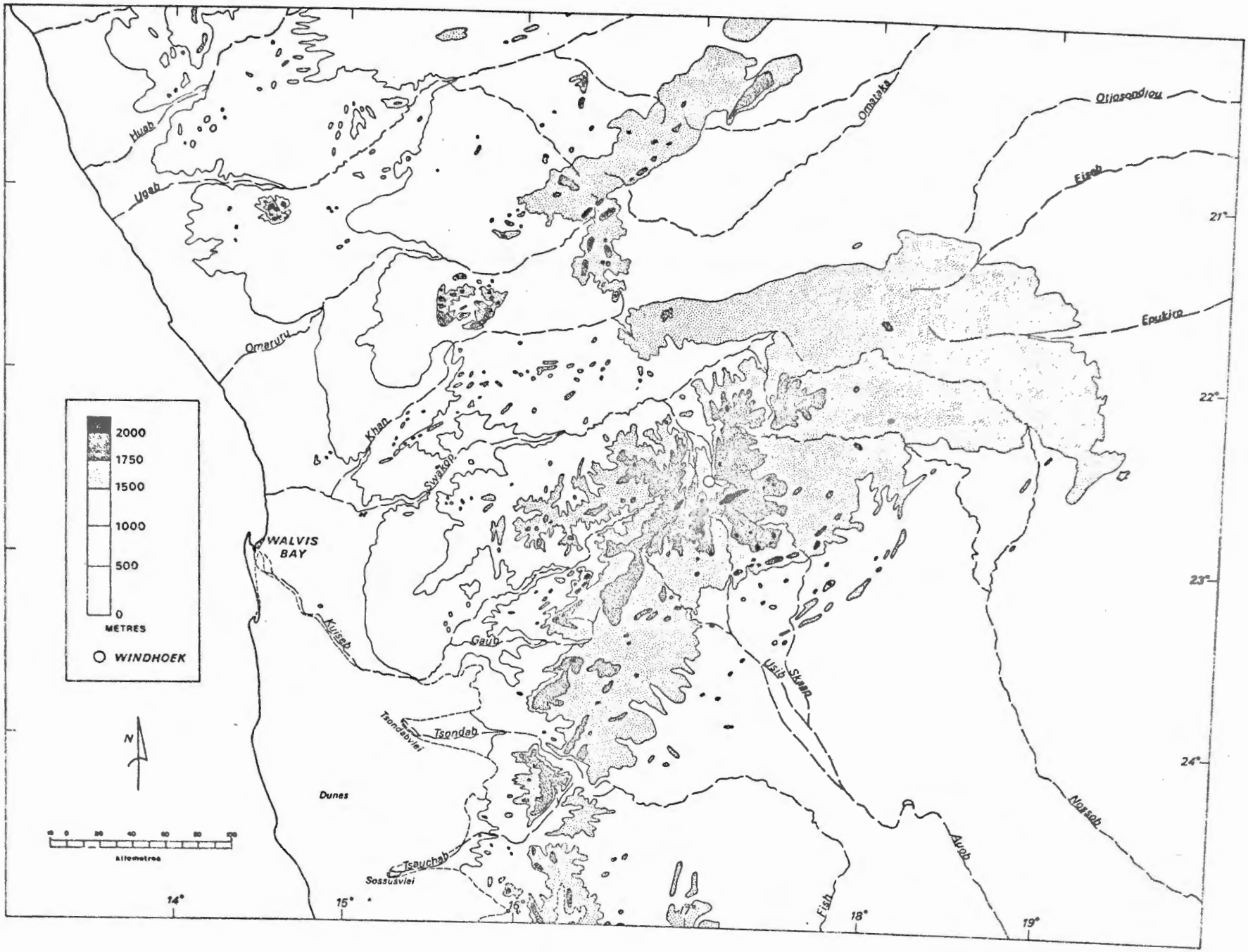
Huab
Ugab
Omaruru
Khan
Swakop
Omatako
Otjosondjou
Eiseb
Epukiro
Kuiseb
Gaub
Usib
Skaap
Tsondab
Tsondabvlei
Dunes
Tsauchab
Sossusvlei
Nossob
Auob
Fish
WALVIS BAY
2000
1750
1500
1000
500
0
METRES
WINDHOEK
N
Kilometres
14°
15°
16°
17°
18°
19°
21°
22°
23°
24°

approximately equal halves, (Annex. I). The south-western part of the complex forms the Naukluft Mountains *sensu stricto*, in the triangular area bounded by the Tsondab and Tsauchab Rivers and the Namib Desert inner plains (Fig. 2). The upper part of the Tsondab River near Büllsport has exhumed a U-shaped valley originally carved by southward flowing Permo-Carboniferous glaciers. A small patch of tillite, west of the Büllenkopf on Büllsport, containing boulders obviously derived from the gneissic massif north-west of the nappe complex is evidence for this and explains the spectacular breaching of the otherwise prominent nappe front by a small, intermittent stream (Plate 1).

c. Communications

The main road between Walvis Bay and Maltahöhe passes through the Naukluft region via the Tsondab River valley (Fig. 1), making the latter the most accessible part of the nappe complex. Büllsport, at the nappe front, is reached from Windhoek via a road through Rehoboth and Klein Aub. Abbabis, north-west of the nappe complex, can be reached directly from Windhoek via a road through Rehoboth and Nauchas, which also passes through the northern part of the nappe complex along parts of the Noab River valley (Annex. IA).

In general, access to the northern and eastern parts of the nappe complex, along these roads and local farm tracks, is fair. Access to the rugged western fringes of the Naukluft Mountains proper, from a secondary road between Abbabis and Maltahöhe, is more difficult. Despite reasonable primary access by farm roads, most parts of the Naukluft nappe complex can only be reached on foot, because of the mountainous and dissected nature of the terrain.

Most of the south-western Naukluft Mountains now fall within the Naukluft Mountain Zebra Park, which by 1976 had been enlarged to include the farms Naukluft, Ubusis, Felseneck and Die Valle (Annex. IA).

2. Objectives of the present project

a. Structural geometry and the mechanics of rock deformation

The project was originally conceived as a comprehensive study, using modern

methods of structural analysis, of the geometry and mechanics of rock deformation in a nappe complex with a known internal stratigraphy (Korn & Martin). It was believed that the nappe pile had been emplaced by gravity-sliding from the basement massif to the north-west, around Nauchas, so that the boundary stress and displacement conditions during deformation as well as confining pressures and temperature, could be well constrained from field evidence.

One particular aspect of rock deformation in the Naukluft nappes which was considered especially important was the well-displayed effect of ductility contrasts between different rock types, which from field observation alone (Korn & Martin, 1959) showed the order of increasing ductility to be limestone-shale-quartzite-dolomite. The contrasting mechanical behaviour of the two kinds of carbonate rock, especially where they occur together as pebbles in certain formations, was clearly worthy of further study with a view to quantifying the ductility or viscosity contrasts in terms of recent theoretical and experimental results (e.g. Gay, 1968a, b). It therefore seemed that, with its good exposures and low metamorphic grade, the Naukluft nappe complex might prove exceptionally instructive about the deformation in inhomogeneous geological materials.

b. The Damara-Nama correlation problem

Apart from its inherent interest for structural geology, it also seemed likely that the Naukluft nappe complex would provide a definite key to the perennial problem of the late-Precambrian stratigraphy of SWA/Namibia; namely, the controversial issue of the relative age and correlation of the widespread, "geosynclinal" Damara Supergroup, in the central and northern parts of the territory and the "platform facies" Nama Group, in the southern part of the territory.

After a period in which the Damara-Nama correlation had been generally out of favour (cf. Martin, 1965), it has recently been restated (cf. Kröner, 1971; Toens, 1975) while, simultaneously, objections to it were cited (Germs, 1972, 1974). It was accordingly felt that the Naukluft nappe complex, which originally occupied an intermediate palaeogeographical position between the Damara geosyncline and the Nama basin, might either show definite indications of a continuous change from shelf to geosynclinal facies, or firm stratigraphic evidence

showing the Damara formations to be older than the Nama Group.

c. The Geodynamics Programme

The Naukluft project was incorporated into the South African National Geodynamics Programme during 1974. The objective of Working Group 9B, concerned with the Damara orogenic belt, was originally formulated as follows (Clifford, Martin & Nicolaysen, 1972) :

> "*Definition of the continuity of the basement and the layered strata across the entire orogenic belt*
> ..... to understand whether:
> (a) the geosyncline was formed on a continuous Precambrian continental type crust and this crust maintained, though greatly altered by anatexis and granite intrusion, a continuous physical character before, during and after the Damara orogeny
>
> *or*
>
> (b) the crust was broken by a major downgoing subduction zone at some critical stage
>
> *or*
>
> (c) the orogenic drama was caused by collision of entirely separate plates."

At the time of the project's incorporation, a preliminary working hypothesis had been established, as a result of initial investigations in the Naukluft Mountains and reconnaissance along the southern margin of the Damara belt, which favoured alternative (c) and pointed to the region of the Matchless Amphibolite as a probable zone of continental suturing (Hartnady, 1973, unpublished document submitted to South African Committee for the International Union of Geological Sciences - SACUGS). Elaborating this model so that its consequences can be fully explored in the field, has been a principal objective of the present work, since it bears strongly on the deformation and emplacement history of the Naukluft nappe complex and on the Damara-Nama correlation problem.

d. Development of computer methods in structural analysis

In the context of an emerging "continuum mechanics approach to structural geology" (e.g. Ramsay & Graham, 1970; Hobbs, 1971; Ramsay, 1976), the use of computer methods in routine statistical processing and display of structural orientation data (e.g. Loudon, 1964; Starkey, 1970; Mahtab *et al.*, 1972), the recent advances in applying finite-element analysis techniques to tectonophysical problems in structural geology and geotectonics (e.g. Dietrich & Onat, 1969; Douglas, 1970; Stephansson & Berner, 1971; Bott & Dean, 1972; Shimazaki, 1974) and contemporary interest in the application of modern data-base principles to the collection, storage and retrieval of geological field data (e.g. Wynne-Edwards *et. al.*, 1970; Bowen & Botbol, 1975; Bouillé, 1976), there is a clearly developing need for an integrated system in which a sufficient range of techniques is brought together to provide the researcher with an effective tool for :

(i) storing, retrieving and processing numerical data;
(ii) marshalling the data or derived parameters as input to computer-based mathematical models of rock deformation problems, and
(iii) creatively experimenting with complex ideas about relationships between structural geometry and finite strain distribution in three dimensions (or four, if time is included)

Each of these three aspects belongs to a distinct level of application. The first is at the level of simple routine; the second, at a more sophisticated modelling level; and the third, at a level, as yet largely unrealised, of "computer-aided thought" or "artificial intelligence" (cf. Perkins & Hammond, 1975).

"The essence of computer-aided thought is the effective interfacing of the conceptual prowess of man with the manipulative capability of the computer" (*op. cit.*, p.174). The impediments to the achievement of this appear to be mostly of human origin. Firstly, the idea has not yet been made generally comprehensible to the researcher in structural geology and there is a consequent lack of motivation to explore its application. Secondly, the acquisition of the necessary expertise, either of the structural geologist in computer science

or the computer scientist in structural geology, requires much time and effort.

The preliminary exploration of this field was one of the objectives of the Naukluft project.

e. Synopsis

There is certain dichotomy between the last-mentioned methodological objective and those concerned with substantive questions about the tectonic history of central SWA/Namibia and this dichotomy is reflected in the structure of the present thesis. It is, however, believed that this dichotomy itself reflects the present intermediate state of science in structural geology, which is experiencing a revolution through the impact of new ideas, theories and methods imported from continuum mechanics and materials science and at a different level, through the impact of the geophysical theory of plate tectonics.

Since it can be argued that the development of the theory of plate tectonics required the digital computer for its realisation (Bullard *et. al.*, 1965) and that the full application of continuum mechanics theory in structural geology is technically impracticable without considerable assistance from digital computer techniques (such as finite-element analysis) because of the otherwise generally intractable nature of realistic boundary-value problems in tectonophysics, it is considered that the digital computer is an essential part of the paradigmatic foundation (Kuhn, 1970) of modern tectonic science. Realising this concept in the form of a practical, working system of generalised, portable computer programmes capable, in principle, of integrating field, theoretical and experimental aspects of tectonics in its operational procedure is a fundamental task which, in the writer's opinion, should be at the core and not the periphery of the science.

Despite the evident dichotomy between the statement and preliminary exploration of this ideal, in the Appendix to this thesis and the degree to which it has actually been realised within the field context of the Naukluft project and the Damara geodynamics programme, it is hoped that the nucleus at least of the future development of such a system has been provided. In the field, the Naukluft Mountains and the southern zones of the Damara belt have, in fact, pre-

sented problems in the tectono-stratigraphic relationship between tectonics and sedimentation and in large-scale fracture mechanics which, strictly speaking, still lie largely outside the scope of these developments.

CHAPTER II

THE DAMARA OROGENIC BELT AND ITS SUBDIVISION IN THE KHOMAS RIDGE REGION

A. INTRODUCTION

One major problem in elaborating geotectonic hypotheses for Precambrian orogenic belts is the difficulty of searching through the bulk of the literature in order to take account of all relevant evidence and also the subjective way in which much of the work on continental tectonics is presented. In order to obviate this, an attempt is made here to use the "Data for Orogenic Studies Questionnaire" (Spencer, 1974) as a model. This attempt, in fact, revealed a quite appalling lack of data for the Damara belt which is not framed within, or does not assume, some form of geotectonic hypothesis, such as the geosynclinal theory. It also revealed that there is a very large degree of imprecision in the definition of major tectonic and stratigraphic units within the belt.

Since the abovementioned questionnaire was designed for a survey of Mesozoic-Cenozoic orogenic belts, in which palaeontological control on the age of formations and the dating of tectonic events is generally quite good, it was also found that some of the questions which presupposed a reasonably precise knowledge of time relationships were practically unanswerable in the context of a Late-Precambrian orogeny. Nevertheless, the attempt to describe both recent and much older orogenic areas in a common, standardised format is believed to be useful and instructive and to point most clearly either to major gaps in our knowledge of Precambrian belts or to major differences between modern and Precambrian orogenic processes.

The structure of the present chapter therefore follows the structure of the "Data for Orogenic Studies Questionnaire" quite closely, in that attention is given first to a general description of the Damara belt and then to the question of its subdivision into major structural zones. The latter are defined in the questionnaire as "conveniently chosen stratigraphic-tectonic units, the

geographical boundaries of which may be shown as lines on a map and which include rocks of all structural levels within the geographical limits of the zone" (Spencer, 1974).

At this point, recent LANDSAT imagery is used in conjunction with geophysical and other evidence discussed in the first section to set boundaries to a major tectonic subdivision of the Damara belt along its southern margin. Partly following Gevers (1934), who first recognised it as a structurally-distinct unit, it is called the *Khomas Ridge province*. This is subdivided in turn, into four distinct structural zones in the abovementioned sense. A detailed tectono-stratigraphic description of each of these zones, as presupposed in Part 3 of the orogenic studies questionnaire, is not yet possible, but many aspects of such a description are treated separately later (cf. Chapter III) when the relationship of Naukluft tectono-stratigraphy to that of the immediately adjacent Khomas Ridge zones is discussed.

B. GENERAL DATA ON THE OROGENIC BELT

1. Definition of the belt and the Geodynamics study area

The northern and southern margins of the Damara orogenic belt, as previously understood and as presently suggested, are illustrated on an accompanying diagram (Fig. 3) which also shows the location of the study strip or "geotraverse" selected as part of the South African National Geodynamics programme.

In SWA/Namibia, the Damara belt is about 450 km wide in the western end of the segment which trends north-east towards Botswana. The average width of the belt may be somewhat less than this however, since there are indications that it tapers significantly eastwards.

It is evident that the Damara belt contains rocks deformed during more than one Precambrian orogeny, since large inliers of highly deformed, pre-Damaran gneissic basement are exposed in the northern, central and southern parts of the belt, where they have been called the Kamanjab, Abbabis and Rehoboth inliers respectively (Martin, 1965). There is however, still some

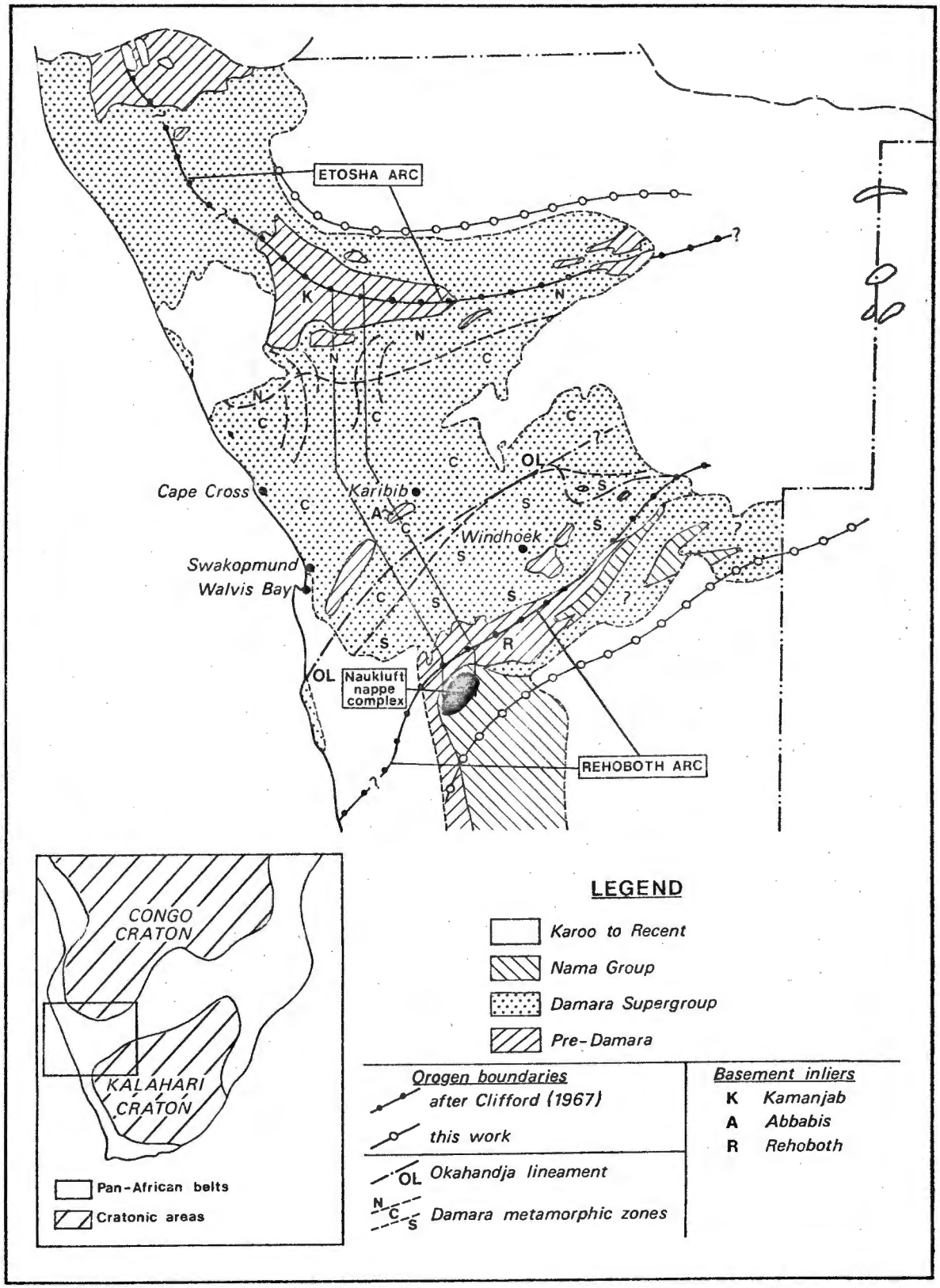

Figure 3. Generalised map of the Damara orogenic belt illustrating its metamorphic zonation (after Clifford, 1967), structural trends, location of the major basement inliers and of the Geodynamics study strip.

uncertainty over the nature of the Damara orogeny itself. The question is whether, in the 450 Myr interval from -900 Myr to -450 Myr, there was only one orogeny and if so, of what precise duration? There is some evidence which suggests that this period may encompass more than one orogeny, as defined by Spencer (1974).

2. Surface shape of the orogenic belt in plan

a. Margins of the belt

The northern margin of the Damara orogenic belt as a whole is somewhat indefinite because of lack of exposure around the southern margin of the Ovamboland Etosha Basin. It is possible to locate it arbitrarily along the line where Damara [1] formations disappear beneath Phanerozoic continental sediments, on the grounds that these Damara rocks are gently folded up to this line, but probably are unfolded north of it. This definition of the northern margin may however, be disputed since it is traditional rather to define the northern margin of the Damara orogenic belt along the southern margin of the Kamanjab inlier where the imprints of strong polyphase deformation and low-grade metamorphism become obvious.

The southern margin of the Damara orogenic belt has been traditionally defined to coincide with the limits of outcrop of the "eugeosynclinal" Swakop Group (cf. Martin, 1965). However, it has recently become evident that a strong overprint of Damaran deformation and metamorphism occurs south of the Swakop Group outcrops in the Rehoboth inlier. Damaran deformation is also obvious in the northern parts of the Nama Group (Germs, 1974) and in pre-Nama rocks formerly grouped in the "Tsumis Formation" (cf. Schalk, 1973). Lack of exposure generally inhibits precise definition of the boundary between deformed

[1] Note that the name Damara has been applied to a major stratigraphic unit, the Damara Supergroup (Kröner, 1974a) as well as to a major geotectonic unit, the Damara orogenic belt.

and undeformed rocks in these younger formations. Close to the escarpment between the Namib desert and the inland plateau, however, a distinct boundary is visible on LANDSAT imagery between folded and faulted Lower Schwarzrand (Nama) beds and unfolded beds of the Upper Schwarzrand Terminal Clastic Member. This intra-Schwarzrand unconformity (Germs, 1972, 1974) can be considered to fall along a gradational southern margin of the Damara orogenic belt.

b. Along-strike continuation of the belt

Strictly speaking, the Damara orogenic belt is not observed to extend beyond the sides of the segment chosen for description here. Westwards, it passes beneath thin superficial deposits of the Namib desert coastal pediplain and then out to sea. Eastwards it is largely concealed by later rocks of the inland Kalahari Basin. If a revised definition of its southern margin is adopted, it is evident that the Damara belt extends a considerable distance of about 1000 km eastwards through Botswana in the form of the Ghanzi Ridge. Furthermore, if the evidence of gravity data (Reeves & Hutchins, 1975; Reeves, 1977), photogeological lineament analysis (Viljoen *et al.*, 1975) and geomagnetic deep sounding (De Beer *et al.*, 1976) is accepted, it extends continuously through to the Lake Kariba region where it links with the Luangwa-Kariba Belt of southern Zambia (Ramsay & Ridgway, 1977). There is however, no clear geophysical or geological evidence of any direct link with the Lufilian Belt of northern Zambia and Zaire. South-westwards of the segment chosen, an offshore connection between the Damara and Gariep orogenic belts is postulated (Kröner, 1974b Kröner & Jackson, 1974).

c. General trend of the belt

The geometrical pattern of the Damara belt is apparently that of two large arcs, a south-westward convex "Etosha arc" in the north and a north-westward convex "Rehoboth arc" in the south (Fig. 3). The internal structure of the northern arc appears to be complex. Although the Etosha arc and the Kamanjab inlier are convex toward the south-west, the foliation and fold trends of the deformed rocks in the metamorphic part of the belt show a smaller scale eastward convex arc on the west of the Summas Mountains and a north-westward

convex arc on the east of the same mountains. . More precise tectonic relationships between the southern, Rehoboth arc and the northern structures have yet to be determined. From inspection of airphoto mosaics however, it seems that structures related to the northern arcs are overprinted by structures related to the larger southern arc in the region of the Omaruru River.

3. Surface shape of the segment in elevation

Along the northern margin of the Damara belt near the Kamanjab inlier, the average elevation is about 1000 m above sea-level, but along the southern margin of the belt, the average elevation is closer to 1500 m (cf. Fig. 2). The highest 5% of the ground within the belt is in excess of about 2250 m and lies close to the southern margin. This feature falls within an area which is usually called the Khomas Hochland (or Khomas Highlands) and was described structurally by Gevers (1934) as the Khomas Ridge.

The earliest recognisable geomorphological surface is the Permo-Carboniferous sub-glacial one recognisable beneath outliers of Karoo tillite in various parts of the belt. Along the Khomas Ridge this surface reaches altitudes of about 2300 m. The prominent Khomas Highlands land surface, at about 2000 m along the Khomas Ridge, is probably of Jurassic-Cretaceous age and may form part of the "Gondwana" land surface before the opening of the South Atlantic in the early Cretaceous (Valanganian, c.-128 Myr; Larson & Ladd, 1973). South of the Khomas Ridge, there appear to be at least two "steps" of Tertiary age at about 1700 m and about 1400 m, forming part of the "African" land surface (Mabbutt, 1955). The coastal plain pediment of the Namib desert, rising from sea-level to altitudes of about 1100 m over a distance of about 140 km, is probably of Miocene-Pliocene age, as is the inland land surface passing beneath the sediments of the Kalahari Group.

It has been suggested (Spreitzer, 1966) that the inclined Namib plain consists of several surfaces related to higher still-stands of sea-level; the breaks between surfaces being placed at 200, 400, 600 and 900 m above present sea-level. Closer to the coast, near Gobabeb, terraces and their deposits along the Kuiseb River, at 6, 20 and 42 m above the river bed reflect Quater-

nary fluctuations in sea-level and climate related to the Pleistocene glaciations (Goudie, 1972). The Kuiseb has a mouth which shows evidence of a buried channel about 25-30 m below present channel level (Vegter, 1953), indicating that there was once a lower base level associated with a lower level of the sea. At Swakopmund on the coast, raised terraces have been reported at 4-6, 12 and 14-16 m above sea-level (Spreitzer, 1966). Indications of differences between late Tertiary and Quaternary land surfaces north and south of the Kuiseb River are noted by Selby (1976), who has suggested that the area south of the Kuiseb is "tectonically different" from the area north of the Kuiseb (*op. cit.*, p.6).

The Kuiseb River course approximately marks the position where the Great Escarpment is deflected from the coast-parallel trend which it maintains for about 500 km from the Orange River. The Escarpment swings inland toward the Okahandja vicinity, becoming more or less parallel to the tectonic trend of the Khomas Ridge. In other words, the Escarpment approximately follows the Rehoboth arc. It has been suggested that the Escarpment dates back to pre-Dwyka times in the Kaokoveld branch of the belt (Martin, 1953). The recent discovery (Faupel, 1974) of a small Dwyka outlier on Komanuab, near the head of the Nausgomab valley, a tributary of the Kuiseb, appears to allow a similar conclusion to be drawn for the Escarpment in the Khomas Ridge region (Martin, 1975). Dwyka glacial valleys north of the Khomas Ridge and west of the present Escarpment appear to have been carved by westward-flowing ice. In contrast, Dwyka glacial valleys within and north-east of the Naukluft Mountains and east of the present Escarpment, appear to have been carved by ice flowing eastward to a Permian marine basin with a coastline now at about 1400 m above sea-level (Martin & Wilcewski, 1970).

It is evident therefore, that the present Escarpment has been deflected in the Kuiseb region so as to follow a pre-existing geomorphological divide which has been in existence for almost 300 Myr. Dwyka glaciers were apparently flowing in opposing directions off a mountain chain which rose at least 1000 m above sea-level in Permian times. This mountain chain is still represented by the peaks which rise above all the younger land surfaces: the Naukluft Mountains (1994 m); Gamsberg (2347 m); Hakos Mountains; Charlottenberg (2144 m); Billstein (2250 m); Oamites Mountain (2144 m); Sternberg; Moltkeblick (2484 m);

Wortel Mountain; Hamis Mountain (2009 m) and Kamtsas Mountain (2010 m) are a few of the prominences in the Khomas Ridge chain. Moltkeblick, in the Auas Mountains, is the highest peak of the chain and is second in altitude only to the Brandberg, in the northern part of the belt. The Brandberg however, is an isolated massif of erosion resistant Karroo plutonic and subvolcanic rocks, while the Auas Mountains and their surroundings constitute the largest region of high topography (>2000 m) in the territory (cf. Fig. 2).

On physiographic and geomorphological grounds, it is clear that the Khomas Ridge is a distinct and important entity within the Damara orogenic belt as a whole. Geophysical evidence, to be discussed briefly in the next section, reinforces this conclusion.

4. Geophysical data - The deep structure of the segment

a. Gravity data

Gravity data from the Damara belt have been provided by Kleywegt (1967). A Bouguer anomaly map with 10 milligal contour intervals is given in Fig. 4 . On this map, some important anomalies have been labelled for the purposes of of the following description.

The most conspicuous feature of the Bouguer anomaly pattern is the large negative anomaly (KR) associated with the Khomas Ridge. The KR anomaly reaches -180 milligal near the eastern end of the Ridge, making it one of the largest known negative Bouguer anomalies in Southern Africa. The anomaly has a trough-like form in the west, the axis of the trough coinciding with the zone of highest topography on the Khomas Ridge. The gravity field in this region is clearly concordant with both the main tectonic and the main topographic trend. In the extreme west, near the Naukluft Mountains, this anomaly curves toward the south-west, mimicking the form of the Rehoboth Arc, at the same place shoalling to about -140 milligals. Farther south-westward it becomes obscured by the continental edge effect.

South of this particular negative anomaly - a positive anomaly (RB) is associated with the Rehoboth basement inlier. This broad domical anomaly

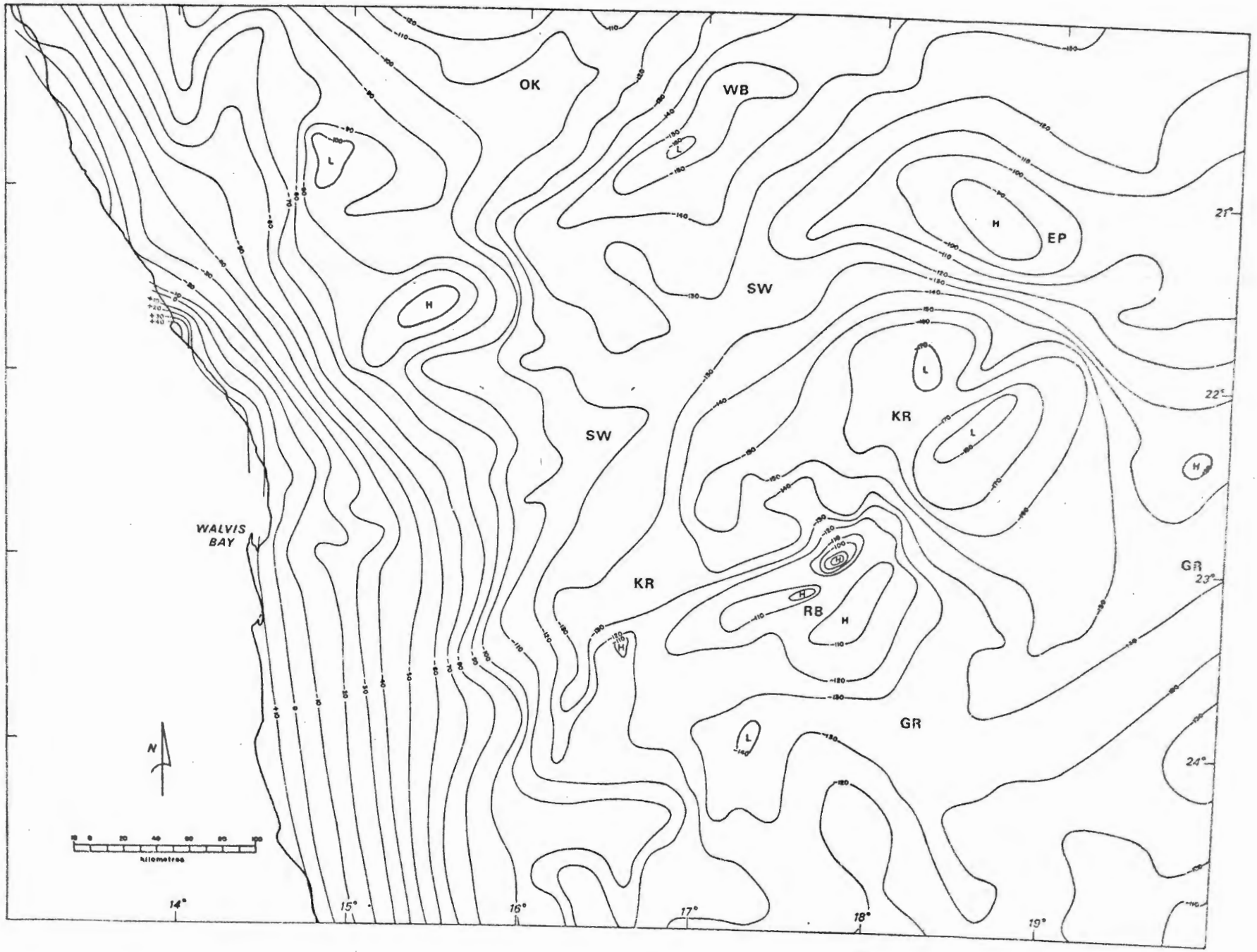
OK
WB
SW
EP
SW
KR
KR
RB
GR
GR
WALVIS BAY
N
Kilometres
14°
15°
16°
17°
18°
19°
21°
22°
23°
24°

contains two smaller, peak-like positive anomalies one of which reaches -80 milligals. These appear to be associated with local near-surface concentrations of dense mafic rock. The pronounced linear gradient between the KR negative and RB positive anomalies appears to coincide with a line of strong faulting and mylonitisation.

South of the RB positive anomaly another trough-like negative anomaly (GR), coinciding with the northern part of the Nama Basin and with the apparent axis of the pre-Nama Tsumis sedimentary trough, is evidently the south-westward extension of the major negative anomaly found along the Ghanzi Ridge in Botswana (Reeves and Hutchins, 1975). Near Witvlei, the KR and GR negative anomalies in fact appear to merge and constitute one reason for considering the tectonic association between the Khomas Ridge and the Ghanzi Ridge to be a close one in space and time.

In the east of the segment, a prominent positive anomaly (EP) of -90 milligals near the Epukiro Omuramba has a west-northwesterly trend quite oblique to the KR anomaly trend. The steep gradient between the KR and EP anomalies appears to reflect a major change in crustal structure, the exact tectonic significance of which is not yet known. One possible hypothesis is that the southern and central tectonic zones of the Damara orogenic belt curve round sharply south-eastwards in a north-eastwards convex arc and terminates in the Epukiro region. There is some evidence for this hypothesis from reconnaissance photogeological mapping (Porada, Schmidt & Wittig, 1972) and ground geological reconnaissance (J.L.Blaine, personal communication) in the regions east of Okahandja.

The EP positive gravity anomaly appears to curve round westwards to follow a subdued positive ridge (SW) which approximately coincides with the Swakop River course. North of the curving region, near Okahandja, there is a local zone of narrow north-south trending gravity anomalies. These are associated with a zone of north-south trending ridges, underlain by Karoo sediments and dolerite intrusions and may reflect a belt of early north-south-trending Damaran structure.

Farther north-eastward, a conspicuous trough-like negative anomaly (WB) coincides with the outcrop area of Karoo sediments (Etjo beds) in the Waterberg

Plateau continuing northward, the next major feature in the segment is an extensive ridge-like positive anomaly (OK) which coincides with the large Okonguarri antiform (Guj, 1974) and extends south-westwards to cross the outcrop area of the pre-Swakop Group rocks recently named the "Tsaun Formation" (Botha *et al.*, 1974).

The multiple reversals of the gravity gradient in a section across the Damara belt, from the GR anomaly in the south to the OK anomaly in the north, can be taken as evidence that the Damara orogenic belt is no simple "geosyncline" (Kleywegt, personal communication). The Bouguer anomaly pattern can be used to divide the Damara orogenic belt into component parts characterised chiefly by paired positive and negative anomalies.

A small negative isostatic anomaly of about -20 milligals coincides with the KR Bouguer anomaly (Kleywegt, 1967). This anomaly has presumably been inherited from the time of the Damaran orogeny and is supported and maintained by the fundamental strength of the lithosphere. The Damara orogenic belt is otherwise in approximate isostatic equilibrium.

b. Electromagnetic data

A major electrical conductivity anomaly, detected by geomagnetic deep sounding (De Beer *et al.*, 1975; De Beer *et. al.*, 1976) coincides approximately with the EP positive anomaly (Fig. 4). This anomaly trends nearly westwards towards the upper parts of the Omaruru River. Near the Botswana border, however, it curves around in a south-westerly convex arc to trend north-eastward along a line coinciding with the northern margin of the Ghanzi Ridge. According to De Beer *et al.* (1976), the conductivity anomaly and the seismic activity of the Okavango region probably reflects the extension of the East African Rift Valley across Southern Africa (cf. Fuller, 1972) following old lines of weakness established in Late Precambrian times. If the conductivity anomaly does indeed reflect Damaran tectonic trends, then its form in the Epukiro region could be considered further evidence against a direct along-strike continuation of the central Damara belt in the Okavango region of Botswana.

Regional magnetic data are available for parts of the central Damara orogenic

belt within the segment described here. All anomalies are apparently concordant with the main tectonic and topographic trends. In the central Damaran region the principal anomaly pattern appears to be associated with inliers of Nosib Group or pre-Nosib basement (Jacob, 1974). Along the lower Swakop River, there is a striking contrast between the magnetic anomaly patterns over the so-called Abbabis Swell (Gevers, 1963) and those over the northern parts of the Khomas Trough (R. McG. Miller, personal communication). The distinct line separating the two patterns coincides with a belt of steeply dipping and highly deformed schist. This belt forms a distinct tectonic lineament which on LANDSAT imagery (cf. Section C below) is observed to extend north-eastwards to Gross Barmen near Okahandja where a belt of right-lateral shearing was postulated by Gevers (1963). Detailed structural mapping (Blaine, 1977) confirms the existence of a major tectonic discontinuity, some 6 km north of Gross Barmen. It would seem that regional magnetic data could be used to track this discontinuity eastward across regions of poor or no exposure.

c. Present-day seismic activity in the segment

The Damara orogenic belt appears to be currently active seismically, but at a very low level. During a recent seismic refraction survey in the segment the occurrence of natural tremors was noted (R.W.Green, personal communication). This activity may be linked with the microseismic activity recently studied in the Okavango Swamp region of Botswana (Scholz *et al.*, 1976). This and the abovementioned electrical conductivity anomaly, is speculatively considered to reflect the extention or concurrent propagation of the East African Rift Valley across Southern Africa. Large-scale control of this process by Late-Precambrian tectonic anisotropy seems probable.

In an early review of seismic activity in South West Africa (Korn and Martin, 1951), an association between tremors felt and the escarpment regions was noted. In some instances, for example, the Changans earthquake swarm of November, 1932, the activity seems to be associated with the north-south-trending faults and master-joint systems of post-Karoo age. Only in one instance, a north-northwest-trending fault near Sesriem south-west of the Naukluft mountains, is there documented evidence of recent displacement along such structures. Here

the present land surface is uplifted on the east by about 5 m along a youthful scarp about 20 km long. Assuming the relationships between fault length L(cm), displacement D(cm) and earthquake magnitude M derived by King and Knopoff (1968),

$$\log LD^2 = 2{,}24M - 4{,}99$$

one may speculate that this event was accompanied by a shock of magnitude M = 6,2.

5. Time relations

a. Basement rocks

Basement rocks - defined as the structural element (or elements) showing evidence of movements and/or metamorphism completed prior to those in the orogeny in question and characterised by a distinct structural pattern differing from that of the orogenic belt in question - occur within the orogenic segment in at least three large inliers. The Kamanjab inlier, near the northern margin, contains rocks that have given isotopic ages ranging between 2000 Myr and 1700 Myr (Burger, Clifford & Miller, 1976). The Abbabis inlier and recently discovered south-western extensions in the central part of the orogenic belt, yield isotopic ages close to 2000 Myr (Burger, Kröner and Jacob, personal communications). The Rehoboth inlier contains rocks with isotopic ages between 1630 Myr and 900 Myr (Burger & Coertze, 1975; Hugo & Schalk, 1974).

In the Rehoboth inlier, however, it is not yet clear to what extent rocks falling within the 1300 to 900 Myr age range are basement, *as defined above*. Allowing for progressive changes, the structural pattern and metamorphic grade of these rocks is not distinctly different from that of adjacent Damara Supergroup rocks. They have evidently been strongly affected by the Damara orogeny, but the evidence for a prior orogenic episode is ambiguous. It is instead possible that the 1300 to 900 Myr age range reflects a period of *anorogenic* igneous activity with concurrent continental sedimentation (but see Watters, 1976). This problem is currently being investigated (Malling, in preparation).

b. Oldest rocks deformed for the first time

In the southern part of the Damara belt, therefore, the oldest rocks apparently deformed for the first time during the Damara orogeny are various volcanic and volcaniclastic formations (Opdam Formation, Nauzerus Formation, Grauwater Formation, Doornpoort Formation; cf. Martin, 1965; Schalk, 1973; Hugo & Schalk, 1974), the isotopic ages of which cluster around 1100 Myr. These may be the northern extensions of the Sinclair Group (Watters, 1974), the lower more mafic parts of which have recently given Rb-Sr isochron ages at around 1300 Myr to 1250 Myr. (Kröner, 1976a; Watters, personal communication). In the northern part of the Damara Belt, the oldest rocks deformed for the first time during the Damara orogeny, are the various local clastic and subordinate volcanic formations of the Nosib Group.

The age of the Nosib Group is the subject of some controversy at the present time. Isotopic ages ranging between 740 Myr and 930 Myr (Burger & Coertze, 1973, 1975) have been obtained on units from the Naauwpoort Formation (Frets, 1969) which is said to be related to the Nosib Group and recent Rb-Sr analysis of Naauwpoort material (Oas syenite) indicates an age close to 800 Myr (Kröner, personal communication). In contrast, an age of 1100 ± 35 Ma has been reported for the Chela Formation of Southern Angola, also said to be related to the Nosib Group (Kröner, 1976a). There is palaeontological evidence which indicates a Middle Riphean (1350 to 950 Myr) age for the lower part of the Otavi Group (Cloud & Semikhatov, 1969; Germs, 1972) which overlies the Nosib Group. Long-range correlation of the Nosib and Otavi Groups with very similar lithological sequences in the Katanga and West Congo basins also suggests ages of about 1100 to 1000 Myr for its basal parts (Cahen, 1970; Lepersonne, 1974; Clemmey, 1977). Finally, there is recent palaeomagnetic data which suggests that the Nosib Group is between 1100 and 1000 Myr in age (McElhinny & McWilliams, 1977).

There are two possibilities which might resolve these apparent contradictions. The first is that the 740 - 800 Myr ages from the Naauwpoort Formation are too young because the samples dated were collected from an area of greenschist facies metamorphism (cf. the 930 Myr age reported by Burger & Coertze, 1975).

The second possibility is that the Naauwpoort Formation is not related to the Nosib Group but is significantly younger, perhaps falling within the lower part of the Tsumeb Subgroup (upper Otavi Group). This is rendered more probable by the observation (Guj, 1974; Miller, 1974) that the volcanics of the Upper Naauwpoort Formation interfinger with, or intersect, the sedimentary breccias (tillites or mixtites) of the Chuos Formation, which elsewhere marks a regional unconformity between the Abenab and Tsumeb Subgroups within the Otavi Group (Hedberg, 1975). Until further attention is given to resolving the problem, serious uncertainty must exist about the age of the Nosib Group in the northern part of the Damara belt. This uncertainty confuses the issue of chronostratigraphic correlation across the belt.

c. Youngest deformed rocks

The youngest deformed rocks along the southern margin of the Damara belt are the shales and sandstones of the lower Schwarzrand Formation (Germs, 1972). The lower Schwarzrand and underlying Kuibis Formations of the Nama Group show a fauna (cf. Germs, 1972, 1974) which has affinities with the Late-Precambrian Ediacara fauna of the Adelaide geosyncline in Australia (Glaessner, 1969), but also with the crybricyathid fauna of the lowermost Cambrian (Tommotian) of Siberia, USSR (Stanley, 1976). Accepting the traditional age of the basal Cambrian at 570 Myr (cf. Harland, 1975), the lower Schwarzrand Formation cannot be greatly older. The youngest deformed rocks along the northern margin of the Damara orogenic belt are the sandstone and shale formations of the Mulden Group (cf. Frets, 1969), of uncertain age not less than about 500 Myr but probably also Late-Precambrian. According to Germs (1974, 1975), the base of the Mulden Group is probably older than the base of the Nama Group.

d. The oldest undeformed rocks

The oldest undeformed rocks within the orogenic belt generally are the Dwyka-age glacials of the Karoo sequence. The age of the Dwyka Group in southern Africa is said to be Sakmarian (Lower Permian or c. 270 Ma; McLachlan & Anderson, 1975). In SWA/Namibia the exhumed glacial landscape beneath the tillite, which now coincides approximately with the present land surface, may be about

300 Myr in age. Within the broadly gradational southern margin of the Damara belt however, an unconformity between slightly folded lower Schwarzrand and unfolded upper Schwarzrand rocks (Terminal Clastic Member; Germs, 1972) has been found. In southern South West Africa, the Terminal Clastic Member is found within a roof pendant of the Bremen igneous complex (Germs, 1972). The Bremen pluton has not itself been isotopically dated, but by association with the nearby Kuboos pluton, age of about 550 Myr is generally accepted. The Terminal Clastic Member is therefore older than 550 Myr. As these upper Schwarzrand rocks lie barely within the margins of the Damara belt, they could be accepted as the oldest undeformed rocks within it.

e. Initiation of mobility

The initiation of mobility - defined as "continued movements of the lithosphere involving either elevation, depression or lateral movement of parts of the crust of the order of 1 km in 10^7 years or faster, assessed by either deposition or erosion of sedimentary piles, or by the development of tight folding, or by thrusting, or by strike-slip faulting or (in some cases) by metamorphism" (Spencer, 1974) - cannot be clearly recognised within the central parts of the Damara belt due to the effects of later deformation, metamorphism and extensive granitic magmatism. Nevertheless, in traversing from the northern margin of the belt southwards, it is possible to regard the vertical and horizontal transition from the dominantly quartzite-carbonate sedimentation of the Otavi and lower Swakop Groups to the thick metamorphosed shale-sandstone succession (Kuiseb Formation) in the upper Swakop Group (Khomas Subgroup) as representing the initiation of Damaran mobility. Further south, this initiation of mobility can be recognised along the northern boundary of the so-called Khomas Trough where the clastic sequence is thickest. This locality is marked by the conspicuous Okahandja Lineament as well as major facies and thickness changes between carbonate and clastic parts of the upper Swakop succession (Jacob, 1974; Blaine, 1977). The flysch-like Khomas clastics south of the Okahandja Lineament have been estimated to be at least 10 km thick (Hälbich, 1970; Porada, 1973). Assuming they were deposited within a time span of 100 Myr giving a minimum rate of deposition of 0,1 mm yr^{-1}, they would fulfil one of the criteria listed in

the above definition of mobility. It has been tentatively concluded (Blaine, 1977) from detailed structural analysis in the Okahandja Lineament zone that early phases of deformation in the central Damara belt are not at all represented in an upper schist formation of the Khomas Trough. This may imply some form of tectono-stratigraphic unconformity between the central and southern zones of the Damara orogenic belt and between the lower and upper parts of the Damara cover sequence. The regional extent and significance of this finding has yet to be tested, but it recalls the question raised early in this chapter about the multiplicity or otherwise of the orogenic episode(s) in the Damara belt. It also raises questions about the possible diachroneity of the initial orogenic mobility in the Damara belt, even if a single episode of prolonged orogeny is assumed. For example, the evidence just cited can be interpreted to mean that the principal phases of the Damara orogeny are significantly younger in the southern zone of the Damara belt.

Dating the initial orogenic mobility is therefore a difficult problem, principally because of the lack of precise information on the age of different parts of the Damara sequence. The present uncertainty over the age of the Nosib and lower Otavi Groups has already been mentioned above. There is also no unequivocal direct evidence relating to the age of the upper Otavi (Tsumeb Subgroup) and Swakop Groups. Early conventional Pb-Pb determinations on lead ores from deposits located within the Tsumeb Subgroup have given ages of 770 and 790 Myr (cf. Burger & Coertze, 1973) but the interpretation of these results is debatable.

In the central zone, near Karibib, early syn-tectonic dioritic bodies associated with the Salem granitic suite (Gevers, 1931b; Smith, 1965) have recently yielded U-Pb zircon ages close to 800 Myr (Burger & Kröner, personal communications). These have been emplaced within the lower part of the Khomas succession (Smith, 1965). It is therefore suggested that the age of initiation of mobility in the central part of the Damara belt is perhaps greater than 800 Myr, if only slightly. Acceptance of this standpoint implies that the major part of the Damara cover sequence, i.e. the Nosib, Otavi and Swakop Groups in the northern and central regions, falls within the age range from about 1100 Myr

to 800 Myr. On the other hand, it is possible to argue that the apparent high age is inherited from a population of early rounded zircons, the presence of which was formerly interpreted to favour an origin of the Salem suite by metasomatic "granitisation" of Khomas schist (Smith, 1965) and that the result places a maximum and not a minimum limit on the age of the Swakop Group.

The fundamental issue affecting estimates of the initiation of mobility in the northern and central zones of the Damara belt is the age range covered by the clastic-carbonate shelf or "miogeosynclinal" Nosib and Otavi-Swakop sequences and the present choice is between sparse and conflicting evidence which suggests 1100-800 Myr, on the one hand and 800-600 Myr, on the other. Three major considerations cause the present writer to favour the earlier age range. These are:

(i) the lithological correlation of the Damara sequence with remarkably similar and very widespread clastic-carbonate assemblages elsewhere on the Congo craton, but especially well-represented in the Katanga and West Congo basins (Cahen, 1970; Lepersonne, 1974);
(ii) the hypothesis that the principal glacial formations of these areas, i.e. the mixtite at the base of the Haut Shiloango group in the West Congo basin, the "Grand conglomerat" at the base of the Lower Kundelungu group in the Katanga basin and the Chuos Formation at the base of the Tsumeb Subgroup in the Damara sequence, are all approximately contemporaneous (cf. Fig. 5);
(iii) the published age determinations of about 1050 Myr for the Middle part of the Roan Group in the Katanga basin and of about 950 Myr for igneous rocks closely associated with the "Grand conglomerat" (Cahen, 1970; Clemmey, 1977); and
(iv) the evidence of stromatolite palaeontology in the Otavi Group (Cloud & Semikhatov, 1969; Hedberg, 1975) which is strongly suggestive of Middle Riphean ages (cf. Table 1)

The chronostratigraphic correlation of the major Late-Precambrian sequences on

TABLE 1

SUMMARY OF OTAVI GROUP STROMATOLITE PALAEONTOLOGY
(after Hedberg, 1975)

Stromatolite	Stratigraphic unit (Subgroup)	Age range (Myr)
Conophyton sp.	Abenab and Tsumeb	>600
Conophyton ressoti	Upper Abenab	650 - 950
Baicalia aff. B. rara	Lower Abenab	810 - 1400
Conophycus cylindricus	Lower Abenab	980 - 1500
Conophycus lituus	Lower Abenab	980 - 1500

Note: Hedberg (1975) estimated an age range of 560 - 800 Myr for the Otavi Group. This may be due to the importance ascribed to the U-Pb ages of c. 740 Myr and c. 770 Myr obtained from zircons in the Naauwpoort Formation (Burger & Coertze, 1973).

the Congo craton is represented in Fig. 5 . Two possible hypotheses for the correlation of the Damara and West Congo-Katanga sequences are proposed, each recognising the chronostratigraphic significance of the glacial formations. The first possibility, in which the Chuos Formation is correlated with the "Grand conglomerat", is the favoured one.

It may be imagined that the initiation of orogenic mobility is more easily recognised and dated along the low-grade to non-metamorphic southern margin of the Damara belt. As this was one of the objectives of the present work in the Naukluft nappe complex and so as not to prejudice the presentation of structural and stratigraphic evidence from the complex, discussion will be reserved for a later chapter.

f. Cessation of mobility

Cessation of orogenic mobility by Middle Cambrian times may be indicated by ages of about 510 Myr obtained for late- to post-tectonic pegmatites in the central part of the belt (Nicolaysen, 1962) and for part of the Donkerhoek granite batholith (Faupel, 1974). K-Ar model ages of metamorphic biotites (Clifford, 1967; Haack & Hoffer, 1976) range from about 520 Myr to 420 Myr (i.e. Middle Cambrian to Lower Silurian), but these certainly represent an interval of slow cooling from peak metamorphic temperatures to the c. 300°C argon diffusion threshold in biotite (Haack, 1976). Since the pattern of K-Ar ages is not significantly different across major tectonic features such as the Okahandja Lineament, it has been concluded that all major post-tectonic relative uplifts within the Damara belt (particularly of the southern zone relative to the central zone) were completed before -485 Myr (Haack & Hoffer, 1976).

Fabric evidence indicates that the growth of metamorphic biotite over most of the southern zone of the Damara belt post-dates all major deformational episodes (Hälbich, 1970; Hoffer, 1975). This may imply that the orogenic mobility had largely ceased before -550 Myr, which is the estimated time of maximum geothermal gradients in the belt (Haack, 1976).

It is probable that the cessation of orogenic mobility is best indicated

within the Nama Group stratigraphy on the foreland Kalahari craton, particularly near the unconformities at the top of the Schwarzrand Group (Germs, 1974). A minimum age of about 550 Myr is indicated for the uppermost Schwarzrand beds from palaeontological and indirect isotopic evidence.

f. Distinct phases of mobility

The recognition of distinct phases of mobility, defined as relatively brief periods of time when mobility was particularly in evidence, poses problems which are far less tractable in Precambrian orogenic belts than in Phanerozoic, particularly Mesozoic-Cenozoic, orogens where such phases may generally be recognised by stratigraphic unconformities separating palaeontologically datable series, or by thick fossiliferous deposits of rapidly accumulated flysch-type clastic sediments. In the Late Precambrian the shortest time-span reliably resolved by isotopic dating techniques is about 25 Myr, compared to about 5 Myr in the case of Mesozoic-Cenozoic orogenic belts (Spencer, 1974). Also the deeper levels of erosion of Precambrian orogenic belts, combined with their long and often complex post-orogenic thermal histories, tend to efface the record of early orogenic events affecting post-basement formations.

Polyphase deformation, recognised by overprinting relationships between tectonic fabrics, have been widely reported from the Damara belt (Roering, 1961; Smith, 1965; De Waal, 1966; Frets, 1969; Guj, 1970; Hälbich, 1970; Nash, 1971; Miller, 1972; Jacob, 1974; Von Groote-Bidlingmaier, 1974; Porada & Wittig, 1976; Botha *et al.*, 1974; Kasch, 1976; Blaine, 1977). Correlation of these deformation phases between widely separated regions has been attempted (cf. Jacob, 1974, p.55-57; Botha *et al.*, 1974), but the validity of large-scale extrapolations remains questionable in view of new evidence that structural histories of different zones may differ considerably across narrow belts of dislocation or high strain, such as the Okahandja Lineament (Blaine, 1977). There is also a fundamental question about the synchroneity of deformation phases over wide areas in view of evidence from young orogenic belts and also from experimental studies that deformation "fronts" may propagate serially through large plastically deforming systems, thereby affecting different parts of the system at different times.

Accordingly there may be no direct correspondence between deformation phases defined by purely tectonic, fabric criteria and phases of orogenic mobility defined by tectono-stratigraphic criteria. The Naukluft nappe complex, in which a relatively high structural level of the Damara belt is still preserved, is perhaps a good example of this, with respect to its relationship to adjacent tectonic zones in the Damara belt.

These considerations point to the need for a systematic subdivision of the Damara belt into tectonic zones with well-defined boundaries and with internal structures and constitutions which are different from adjoining parts of the Earth's crust. The dynamic analysis of rock structure (cf. Turner & Weiss, 1963, p.9) in the Damara belt is otherwise not possible if boundary stress and displacement conditions for major units cannot be specified, at least in principle.

C. SUBDIVISION OF THE DAMARA OROGENIC BELT

1. Previous large-scale zonation

The Damara orogenic belt covers an area in excess of 250 000 km and the main north-east trending segment of it is at least 450 km wide, which is more than double the distance from the northern stable platform of Austria to the southern stable platform of North Italy across the Eastern Alps. Different parts of the belt differ widely in their lithological constitution and their tectonic, metamorphic and magmatic histories. The first problem therefore, is to establish a subdivision of the Damara belt into convenient tectonic zones based on generally accepted and objective structural criteria.

In the previous sections, the threefold subdivision of the inner, obviously metamorphosed part of the belt into northern, central and southern zones (Fig. 3) on the basis mainly of metamorphic and magmatic characteristics (Clifford, 1967), has been implicitly acknowledged. The central zone is characterised by high-grade metamorphism and granite formation, while the northern and southern zones are flanking areas of medium- and low-grade metamorphism.

It is convenient to accept this broad subdivision, while at the same time substituting new definitive characteristics based on structural rather than metamorphic criteria. This may involve slight revision of the boundaries originally drawn between these zones.

2. The Khomas Ridge province

In previous sections of this chapter, it has been indicated that there is field and geophysical evidence for a major discontinuity within the Damara belt, which separates the southern and central zones as previously defined (Clifford, 1967). Further discussion of the central and northern zones of the belt is beyond the immediate scope of the present work. The tectonic evolution of the southern zone however, is directly relevant to the structural analysis of the Naukluft nappe complex. As structural and metamorphic data from this zone accumulate, it is increasingly evident that there are major differences between the tectonic evolution of this region and more northerly parts of the Damara belt. It is also evident that it has its own internal substructure which enables it to be further subdivided into discrete structural zones, as defined in the"Data for Orogenic Studies Questionnaire" (Spencer, 1974).

The name *Khomas Ridge province* is therefore proposed as a convenient designation of this southern division of the Damara belt. It derives from an early tectonic subdivision of central SWA/Namibia by Gevers (1934, p.247-250).

Previous subdivisions of a part of the Khomas Ridge province have been made by Hälbich (1970) and Porada & Wittig (1975). The latter authors distinguish about ten "isotectonic domains" based upon a systematic classification of mesoscopic structural styles from an extensive sample of outcrops in the Khomas Trough. However, the present attempt at tectonic zonation aims rather at defining *macroscopic* structural criteria for the recognition of major zones, such as might be represented on geological maps at scales between 1:250 000 and 1:1 000 000, or seen on LANDSAT images at scales between 1:500 000 and 1:1 000 000. Hälbich's (1970) subdivision of the Khomas Trough into Northern and Southern belts is partly based on such criteria and has accordingly been followed here. The two main criteria employed in distinguishing tectonic zones in the present study are:

(i) a zone should be distinguishable macroscopically from those adjacent to it by virtue of some characteristic structural pattern or large-scale textural feature; and

(ii) the boundaries between zones should be preferably, but not necessarily, marked by surfaces (or narrow belts) of structural and/or stratigraphic discontinuity.

On the basis of these principles, the Khomas Ridge province may be subdivided into four distinct tectonic zones (Fig. 6). These are labelled from south to north by the Roman numerals I - IV. It is tentatively proposed that they be given names as follows:

Zone I	-	Naukluft Mountains/Kharubeam Hills zone
Zone II	-	Hakos Mountains/Auas Mountains zone
Zone III	-	Eros Mountains zone
Zone IV	-	Ovitoto Mountains zone

The idiosyncratic feature of this nomenclature is that each zone is named after some conspicuous physiographic high region in the zone. This feature and the name of the province as a whole ("Khomas", the regional name, is the Nama word for mountains), is to emphasize the fact that these are true *orogenic* zones. Whatever argument there may be about other parts of the Pan-African system of "mobile" belts (cf. Watson, 1976, p.636), there can be absolutely no question that tectonic mobility in the Khomas Ridge province was responsible for building a major mountain range. This is evident still in the present-day physiography, in the exhumed geomorphology and directions of glacier flow during the Dwyka ice age and in the large negative Bouguer anomaly which characterises most of the Khomas Ridge province.

3. Boundaries of the Khomas Ridge Province

a. Northern boundary : the Okahandja Lineament

The northern boundary of the Khomas Ridge province deserves special attention. On LANDSAT images E-1095-08271 and E-1058-08203, it is clearly visible as a gently-curving major lineament separating regions of marked tonal contrast

and very different structural pattern. This lineament, which can also be recognised on aeromagnetic maps (R.McG. Miller, personal communication), is now called the *Okahandja Lineament*. In the field, the Okahandja Lineament is evidently a complex phenomenon, having been established early in the deposition of the Swakop Group, coincident with a zone of pronounced sedimentary facies change affecting the lower part of the Khomas sequence (Jacob, 1974; Blaine, 1977). This is interpreted to mean that it was then a narrow zone of strong vertical movement between the relatively uplifted Abbabis Swell (Gevers, 1963) and the deeply downwarped Khomas Trough. In a later stage of its evolution, the Okahandja Lineament appears to have been a zone of significant strike-slip movement. Local right-lateral shear zones have been described near the lineament (Gevers, 1963; Nieberding, 1976). The main discontinuity, a few kilometres north of Gross Barmen, has been analysed in detail (Blaine, 1977) and marked differences in the tectonic evolution of blocks on either side of the lineament have been demonstrated. Here too fabric evidence points to a late history of right-lateral strike-slip movement.

At its western extremity, the Okahandja Lineament is partly obscured beneath superficial coastal pediplain deposits of the Namib desert north of the Kuiseb River and becomes completely obscured beneath large Recent dunes on passing south of the River near a prominent bend on its lower course. East of Okahandja, in a region of generally rather poor exposure, the lineament appears to be severely deflected into a north-south trend (see portion of Fig. 6 , after Porada, Schmidt & Wittig, 1972). This 40 km north-south trending segment appears to form an eastern terminator to the main part of the Khomas Trough. A short distance north of the eastern extensions of the Matchless Amphibolite, the structure reverts to its original trend. At this point the Okahandja Lineament appears to have linked up with the western extension of the *Epukiro Lineament*, which is here proposed as a designation for a sharp rectilinear zone of contact between Damaran and pre-Damaran formations parallel to the straight, presumably structure-controlled course of the Epukiro Omuramba. No mechanical explanation of the deflection of the Okahandja-Epukiro structure can now be proposed as field structural mapping of these regions has not yet been carried out. It may however, be speculated that the sigmoidal form of

the structure is related to the evidence for right-lateral shearing movements seen elsewhere in the Khomas Ridge province.

The southern boundary of the Khomas Ridge province, which is also the southern boundary of the Damara orogenic belt as a whole, is a more diffuse phenomenom and therefore not easily defined. Over most of the eastern regions of Fig. 6, the tectonic boundary is obscured beneath deposits of the Karoo Supergroup or Recent wind-blown sand sheets from the Kalahari desert. In the northern part of the Nama basin however, a boundary may be drawn close to the exposed unconformity (Germs, 1972, 1974) between the lower part of the Schwarzrand Formation and the upper part (Terminal Clastic Member) of the same. From field observation (Germs, personal communication) and from LANDSAT imagery (cf. Viljoen, Viljoen, Grootenboer & Longshaw, 1975) it is clear that the lower Schwarzrand was gently folded over a zone some 50 km wide south of the Naukluft nappe complex. The western continuation of the southern boundary in the north-northwest-faulted pre-Nama formations of the Great Escarpment region is problematic.

4. Description of the Tectonic Zones

In the following paragraphs, a brief description of the main structural and lithostratigraphic characteristics of Zones I to IV and the three boundaries between them, will be given. This will be concerned mainly with the surface structural appearance of each zone as seen on LANDSAT images, but where appropriate some attention will be paid to the deep structure as indicated by field structural analysis (Hälbich, 1970; Schalk, 1973).

a. Zone I

Formerly, this zone has not been considered as an integral part of the Damara belt, but rather loosely regarded as part of the southern foreland. However, the presence of major fault zones and mylonite belts in crystalline basement and volcanic rocks of the Rehoboth inlier and the evident late-Damaran folding of Nama and pre-Nama cover rocks in this zone (cf. Schalk, 1973; and LANDSAT images E-1058-08212 and E-1147-08160) favour its inclusion in the Khomas

Ridge province. The major open folds in the cover rocks show rectilinear or gently curving north-easterly trends. There is also the appearance of an en-echelon arrangement between adjacent gently plunging anticlines and synclines, with nearby fault zones being slightly oblique to the traces of fold axial planes.

b. Zone Boundary I/II

In its western portion, this boundary has been located along a spectacular, narrow zone of very intense mylonitization of the crystalline rocks of the Rehoboth inlier, the Areb mylonite belt (Hartnady, 1975a). This belt was previously described as a stratigraphic unit consisting of "sheared leptite" (De Waal, 1966). To the north-east, the boundary is drawn coincident with a zone of subvertical faulting and intense mylonitic deformation, approximately marking the southern margin of the Khomas Trough and the southward extent of Swakop Group rocks (Schalk, 1973). This zone of strong faulting has long been recognised as the "Hamib fault-line" (Gevers, 1934). In the north-east it appears to meet the Epukiro Lineament at an acute angle (see Fig. 6).

Although, strictly speaking, the Naukluft nappe complex forms the uppermost tectonic element of Zone I, it can be regarded as part of the Zone boundary I/II, since it displays structural styles intermediate between those characteristics of these zones. These relationships are discussed in more detail in a later chapter.

c. Zone II

This zone undoubtedly forms the tectonic and physiographic axis of the Khomas Ridge province. It contains all the major topographic prominences of the Khomas Ridge, such as Gamsberg (2347 m) and Möltkeblick (2484 m); is situated over the axis of a Bouguer anomaly (< -180 mgal) indicating a present crustal thickness of about 55 km; and contains structures and tectonic fabrics indicative of the most intense deformation seen anywhere in the Damara belt (cf. De Waal, 1966; Hälbich, 1970; Kasch, 1976).

On surface, it is characterised by a complicated structural pattern of widely divergent foliation trends, although the principal trends evident are

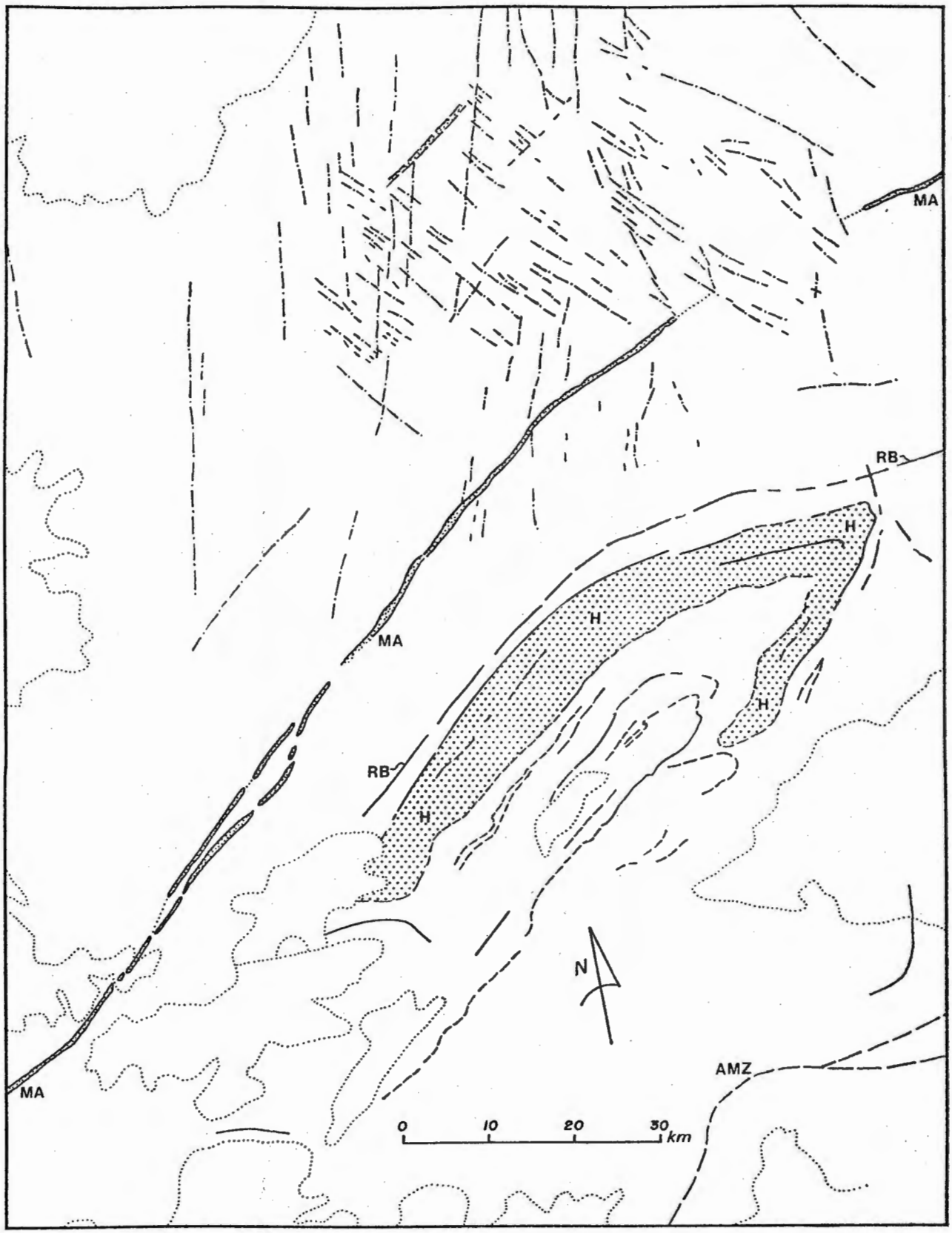
MA
RB
H
H
H
MA
RB
H
N
MA
AMZ
0
10
20
30
km

parallel to the zone boundaries. The complex trend pattern is evidence of polyphase refolding of shallow-dipping early structures, including late "cross-folding", which is transverse or en-echelon to the zone boundaries. Even on LANDSAT images, the complex lithostratigraphic constitution of this zone is clearly evident, with the great tectonic windows of pre-Damaran basement, such as the Rietfontein inlier and the Seeis Dome, showing up as areas of lighter tone and smoother texture. The refolded quartzitic nappe of the Horasib and Hakos mountains (De Waal, 1966) can be clearly seen on LANDSAT image E-1058-08210 (Fig. 7).

On the ground, the general structural character of this zone is one of southward-vergent, large-scale recumbent, early folding and nappe over-thrusting (cf. the Gurumanas nappe of Hälbich, 1970; the Auas Mountains thrusts of Guj, 1969 and sections in Kasch, 1976). On this account, the zone has informally been termed the "Southern Thrust belt" (Miller, personal communication).

d. Zone boundary II/III

In the west this boundary has been located along the so-called "Red Band" (De Kock, 1934; De Waal, 1966), which shows up clearly as a dark, curving lineament on LANDSAT image E-1058-08210. The "Red Band" - a peculiar, granofelsic, locally ferruginous and calcareous, quartzo-felspathic rock - is traceable into the northern quartzite layers of the Auas Mountains and the zone boundary in this region has been drawn so as to coincide with the lithostratigraphic boundary between the Auas felspathic quartzites and the overlying Windhoek biotite schists (Hälbich, 1970). In the east the boundary apparently swings gently so as to become parallel to the Epukiro Lineament before finally merging with the latter.

e. Zone III

Although this zone appears the simplest of all, with respect to both surface structural pattern and structure in a vertical plane, it is probable that this apparent simplicity is highly deceptive.

On LANDSAT image E-1058-08210, this zone is characterised by a finely lineated texture parallel to the zone boundaries. The most conspicuous tonal

feature in this zone is a dark lineament about 2 km wide, which represents the Matchless Amphibolite (Kröner, 1976b). The Matchless Amphibolite, running parallel to the boundaries bisects Zone III. The northern half of the zone is slightly wider than the southern half. The zone tapers from a maximum width of about 45 km in its central segment to about 10 km near its eastern extremity, where in a region of very poor exposure it too appears to merge into the Epukiro Lineament.

On the ground, Zone III is characterised by "parallelschieferung" (Porada & Wittig, 1975), i.e. apparently strict parallelism between the main tectonic foliation and a lithological layering evidently inherited from original sedimentary bedding. The main foliation striking strictly parallel to the zone boundaries, dips at an average angle of about 30° to the north-west. This schistosity is characterised by a strongly developed early lineation which plunges northwestward or north-northwestward, apparently parallel to the axes of rare, tight to isoclinal minor folds of "intrafolial" style. There appears to be some controversy over the genesis of the main foliation. According to Hälbich (1970) it is a second-phase "transposition" schistosity (S_2), but according to Kröner (1976b) it is a first-phase axial-planar foliation (S_1). From a geodynamic point of view, it is most important to resolve this question, because it is fundamental to understanding the tectonophysical evolution of the Eros mountains zone and the Khomas Ridge province as a whole.

f. Zone boundary III/IV

This zone boundary is not easy to trace purely on the basis of LANDSAT imagery. If falls roughly midway in the 90 km wide outcrop area of the monotonous biotite schists of the Khomas Trough. However, there do appear to be subtle macroscopic surface texture differences between the northern and southern belts of Khomas schist. These differences are reflected mainly in the spatial (orientation and spacing) characteristics of several strikingly evident sets of post-tectonic master joints (Fig. 7). A qualitative analysis seems to indicate that there is a large-scale domainal structure in master-joint development which may be related to the tectonic fabric and stress distribution

in the rocks in which the joint system has developed. This idea can best be pursued by attempting to develop a quantitative spatial or textural "signature" on the basis of which an objective geometric classification of joint domains may be possible. The location of Zone boundary III/IV is in part dictated by these considerations.

The most important macroscopic difference between Zones III and IV however, is the presence in the latter of the large, upright early synformal structures, some of which may be traced for distances close to 100 km (Hälbich, 1970). Zone boundary III/IV has been drawn so as to reflect this division.

g. Zone IV

The main macroscopic structural feature of this zone has been mentioned above. Four major synforms in this zone are represented in Fig. 6 , after Hälbich (1970). These are from south to north, the Gorogoneib, Berlin, Gemsboknek and Gross Barmen synclines. They are characterised by the development of a subvertical axial-planar foliation (s_1) which has been described as a "metamorphic banding cleavage" (Hälbich, 1970). This cleavage mimics a fine millimetre-scale, varve-like bedding in the more homogeneous parts of the Khomas schist, but is easily recognisable as a tectonic structure where it crosses original sedimentary layering.

5. Concluding Remarks

The recognition of the Khomas Ridge province as a discrete part of the Damara orogenic belt and its subdivision into four major tectonic zones, each having a distinct structural character which enables it to be distinguished easily from neighbouring domains, has been shown to be possible. For this purpose LANDSAT imagery, controlled by ground observations, has been used. Colour prints of some of the images used in this study have been published (Viljoen *et al.*, 1975; Geodynamics Project in South Africa, 1975) and are therefore already generally available for inspection of some of the features described above and illustrated in Fig. 6 .

The mechanical or geodynamic significance of this subdivision of the Khomas Ridge province into four subparallel structural zones remains an outstanding question, which will be treated in a later chapter. The immediate objective of the present section however, is simply to clarify the large-scale tectonic setting of the Naukluft nappe complex and to provide a terminology which will be useful when structural and stratigraphic relationships between the Naukluft complex and adjacent tectonic units are discussed.

CHAPTER III

STRATIGRAPHY IN THE NAUKLUFT NAPPE COMPLEX AND THE SOUTHERN MARGINAL ZONES OF THE DAMARA BELT

A. INTRODUCTION

Following identification of Khomas Ridge structural zones I and II (hereafter abbreviated as zones KR-I and KR-II) as major tectonic units, it is appropriate to focus briefly on their regional internal stratigraphy before describing the lithostratigraphy of the Naukluft nappe complex.

1. Stratigraphy in zone KR-I

a. General outline

The stratigraphy of the southernmost structural zone is outlined in Table 2. This table represents formations identified in the south-western part of zone KR-I, in the immediate vicinity of the Naukluft nappe complex and does not include formations in the Naukluft complex itself.

In general, the rocks in this zone fall into five major stratigraphic units. At the base, there is a complex assemblage of metamorphic rocks of variable grade, including low- to medium-grade schists and metavolcanics of the *Elim Formation* (De Waal, 1966) and various gneissic and migmatitic rocks which may, in part, be older. These rocks were formerly classed as a lowermost "granitised" part of the Marienhof Formation (Martin, 1965). They are overlain, at a major unconformity, by generally low-grade metavolcanic and metasedimentary rocks of the *Rehoboth Group* (South African Committee for Stratigraphy - SACS, in preparation), which includes various formations previously included in the Dordabis System (Martin, 1965), such as the Opdam Formation and part of the former Skumok Formation. Various high-level intrusive igneous rocks of calc-alkaline affinity, ranging from plutons of tonalite, granodiorite and granite to dyke-swarms of quartz- and rhyolite-porphyry, appear to be associated with the eruptives of the Rehoboth Group. Locally, the history of igneous activity

is complex and the emplacement of individual members of this intrusive suite, is separated by episodes in which swarms of mafic dykes, of at least two generations, have been emplaced. North of the Naukluft complex, the felsic members of the suite have been grouped together as the *Nauchas Granite suite* (after De Waal, 1966). The large Alberta Complex, a metamorphosed layered mafic intrusive (De Waal, 1966), was emplaced earlier than Nauchas suite, but later than a major mafic dyke-swarm. The *Nauzerus Formation* (Hugo & Schalk, 1974), the youngest member of the Rehoboth Group in the Naukluft area, is younger than the Nauchas granites and apparently contemporaneous with late rhyolite-porphyry dykes which transect the high-level plutonic rocks.

A clear distinction between the Rehoboth Group and the basal part of the overlying *Nuwedam Group* (SACS, in preparation) is unfortunately not easily made. The *Grauwater Formation*, as previously defined (Schalk, 1973), formerly included the Nauzerus Formation as a lower member. Its distinctive feature in the Naukluft area, is a conglomerate which contains abundant pebbles and cobbles of Nauzerus-type felsic volcanics and rhyolite-porphyry, but the formation also includes layers of mafic volcanic rock and is locally intruded by diabfasic dykes similar to those which have been emplaced in pre-Nauzerus rocks. Felsic volcanics, like those of the Nauzerus Formation, are also found intercalated in the lower Doornpoort Formation (Schalk, 1973), but the latter is not seen to be intruded by the later mafic dykes (Handley, 1965; Schalk, 1973). The *Klein Aub Formation* is entirely free of volcanic or intrusive igneous rocks.

The Nuwedam Group is overlain unconformably by the Kamtsas Formation, the type-area of which is Kamtsas Mountain in the southern part of zone KR-II, but which is very widespread as the bulk of the former Tsumis Formation in zone KR-I (Martin, 1965). The problems of re-defining the latter unit were discussed by Schalk (1973), after it had been discovered that the name "Tsumis Formation" was a collective term for five different formations. This name has since been abandoned, as the lower units are included in the Nuwedam Group and the Kamtsas and Blaubeker formations stand alone as separate stratigraphic entities. The Blaubeker Formation (De Waal, 1966; Schalk, 1973) is apparently glaciogenic (Kröner & Rankama, 1972).

The *Nama Group* overlies these formations disconformably to paraconformably. In the Naukluft area, the basal part of the Nama Group is represented by the *Kuibis Formation* (Germs, 1972, 1974), but farther north-east in zone KR-1, the *Buschmannsklippe Formation* (Martin, 1965), which may itself be a complex entity (Germs, personal communication), apparently forms the base of the Nama Group.

The regional distribution of these various stratigraphic units and their relationship to some major structural features is illustrated in Fig. 8. South of the Areb mylonite zone (AMZ) and the Hamib Fault (HF), this diagram only represents individual units equivalent to and younger than the Nauzerus Formation. The pre-Nauzerus formations which make up the major part of the Rehoboth inlier have too complex a distribution pattern to be represented at a suitable scale.

In the Nama basin south of the *Schwarzrand Formation* (SR) outcrop, in which folded patterns recognisable on LANDSAT imagery have been traced, the unconformable Terminal Clastic Member (TCM) of the Schwarzrand Formation and seven distinct formations within the Fish River Subgroup (FR_1-FR_7) are also represented.

b. Large-scale tectonostratigraphic relationships

A conspicuous large-scale feature evident in the stratigraphic distribution pattern of zone KR-I is its twofold division into a southern subzone (KR-IA), in which formations older than the Nauzerus Formation are areally insignificant and a northern subzone (KR-IB), in which formations younger than the Nauzerus Formation are areally insignificant. The boundary between these subzones coincides, in the north-eastern part of Fig. 8, with a major fault (cf. Schalk, 1973). Exposures in this region are poor, but the fault appears to post-date the Buschmannsklippe Formation. Near the Naukluft complex, the contact zone between the Nauzerus and Grauwater Formations on the north, and the Doornpoort and Klein Aub Formations on the south, is also poorly exposed but there is evidence in adjacent outcrops for a major dislocation here also. There is a complex pattern of smaller scale faulting, drape-folding and locally intense shearing in the northern block (cf. de Waal, 1966), which clearly pre-dates deposition of the Kuibis Formation. It is clear however, that lesser relative movement along this zone continued into post-Kuibis times, particularly west of the Naukluft complex,

where the apparent south-western extension of the same zone emerges. Here, on Die Valle 226 (Annex.I), the Kuibis Formation has been folded into a tight syncline along a contact between highly sheared Nauzerus felsites and a less-deformed granite body. The latter is apparently overlain unconformably by folded Grauwater conglomerates and quartzites.

The subzone KR-IB has obviously been uplifted greatly relative to the subzone KR-IA in pre-Nama times. The apparent right-lateral displacement of the Nauzerus-Grauwater contact west and north-east of the Naukluft complex is evident farther north-east along the fault in the pattern of stratigraphic contacts between the pre-Doornpoort, Doornpoort, Kamtsas and Blaubeker Formations. In this area, (cf. "window" A in Fig. 8), there are indications that the major displacements along the dislocation occurred before the deposition of the Kamtsas Formation, as the Doornpoort and pre-Doornpoort strata have been strongly deformed into near-vertical orientations and are overlain, at a pronounced unconformity (Schalk, 1973, Plate I), by shallow-dipping Kamtsas beds on which the overlying Blaubeker Formation follows paraconformably in a major syncline. If major displacements had taken place in post-Kamtsas, pre-Buschmannsklippe (Nama) times, such relationships would not be expected. Near the Naukluft complex, the base of the Kamtsas Formation is overlapped by the basal Kuibis quartzite about 4 km south of the fault zone and so the relationship between the fault zone and the Kamtsas Formation cannot be seen directly. The Klein Aub Formation however, displays a well-developed tectonic cleavage dipping steeply northward, which is not as conspicuous in the Kamtsas quartzites which are relatively unstrained. Furthermore, the unconformable truncation of major fold structures in the Klein Aub Formation east of the Naukluft complex (cf. Schalk, 1973, Plates II and III) shows clearly that a significant episode of post-Klein Aub, pre-Kamtsas deformation occurred. It can therefore be inferred that the division of zone KR-I into an uplifted northern zone comprising most of the so-called Rehoboth basement inlier and a depressed southern zone underlain by the Nama sedimentary basin in the south-west and the Tsumis sedimentary basin in the north-east (extending farther into the Ghanzi basin of Botswana), was probably established in immediate pre-Kamtsas times, although this relationship has been obscured by post-Kamtsas and post-Nama reactivation of the structure.

c. Chrono-stratigraphic correlation and interpretation of the Rehoboth Group in subzone KR-IB.

From the age relationships summarised (by "rounding-off to the nearest 25 Myr) in the right-hand column of Table 2 (after Burger & Coertze, 1973, 1975; Hugo & Schalk, 1974 and preliminary new Rb-Sr data of Malling, in preparation), it is most probable that the formations of the Rehoboth Group, including intrusives of the Nauchas suite, are the northern equivalents of the Sinclair Group (Watters, 1974) and that the main episodes of magmatic activity were concentrated in the period from about -1250 Myr to -1100 Myr; some reported ages (cf. Hugo & Schalk, 1974) range as low as about 900-950 Myr but the reliability or significance of ages younger than 1100 Myr is questionable, in view of the sheared condition and low-grade, hydrated metamorphic state of much of the Rehoboth Group outcrop.

A recent interpretation of the Sinclair-Rehoboth magmatic activity (Watters, 1974, 1976) has emphasized the calc-alkaline character of many of the igneous rocks. It has been proposed that subzone KR-IB, in which high-level plutons apparently intrude a carapace of penecontemporaneous extrusives, constitutes the axis of a hypothetical "Rehoboth Magmatic Arc" (cf. Watters, 1976) which formed as a result of south-eastward subduction of oceanic crust at a trench situated about 150-200 km to the north-west, i.e. close to the trace of the Okahandja Lineament as defined in the previous chapter.

In the writer's opinion, this interpretation remains in doubt. In contrast to an interpretation of Rehoboth magmatism as related to a geotectonic environment of plate convergence, the close structural and chronostratigraphic association of the Sinclair-Rehoboth rocks with major mafic dyke swarms extending for many hundreds of kilometres (and locally reaching amazingly high density), as well as layered mafic intrusives like the Alberta Complex, can rather be correlated with a tectonic environment of rifting or plate separation. Work is presently in progress in order to test the petrological consanguinity of members of the Rehoboth Group in the area north of the Naukluft nappe complex, to place constraints on their age range and possible mode and locus of origin, and to elucidate their post-emplacement tectonic and metamorphic history (Malling, in

preparation).

If the plate convergence hypothesis is correct, then the Rehoboth Group magmatic activity, much of the post-Rehoboth, pre-Kamtsas tectonic activity, as well as the early uplift of subzone KR-IB relative to KR-IA, could be associated with a (hypothetical?) c. 1100 Myr-old episode called the "Irumide orogeny" (Clifford *et al.*, 1967; De Villiers & Simpson, 1974). If however, the Rehoboth magmatic activity is found to be of an *anorogenic* kind, then the existence of a pre-Damaran "Irumide orogeny" in central SWA/Namibia may be called seriously into question. There is as yet, no confirmed independent metamorphic or isotopic age evidence for its existence (Malling, personal communication) and for reasons which are dealt with later in this thesis, the pre-Kamtsas deformation described above is not considered to reflect "Irumide" tectonic activity, because the chronostratigraphic correlation of the Kamtsas Formation with the Nosib Group of northern SWA/Namibia is doubted.

2. Stratigraphy in Zone KR-II

Stratigraphic analysis in zone KR-II is severely complicated by inhomogeneous and extremely intense Damaran deformation in basement and cover rocks alike, which is locally inferred to have produced large-scale inversions of the original stratigraphic sequence (De Waal, 1966; Hälbich, 1970; Kasch, 1976). Basement inliers, like those at Rietfontein and Seeis (Fig. 6), owe their exposure within the Damaran cover sequence in part to their incorporation as thrust wedges during early phases of deformation, in part to subsequent refolding of the early nappe structures. There are other, much smaller basement gneiss lamellae within the Damara sequence in the Gamsberg Pass region due north of the Naukluft Mountains, for example and in the Omitara region in the far north-east of Zone KR-II (Kasch, 1976). The extent and local structure of these large-scale tectonic inclusions has yet to be determined.

By far the most spectacular tectonic structure in zone KR-II and one which is critically important to stratigraphic interpretation in this zone, is the giant thrust at the base of the Damara cover sequence. This structure was first identified and described in detail in the Gurumanas area as the local "Gurumanas

nappe" by Hälbich (1970), where the truncation of lithostratigraphic formations and early tectonic structures at the base of the Damara sequence is best exposed. The structure was not, however, extended beyond the Gurumanas area, despite the fact that the lithostratigraphic and structural patterns mapped along the western margin of the Rietfontein inlier clearly indicate the same phenomena (cf. Hälbich, 1970). The structure at this locality can be linked with the evidence for a major thrust contact at the base of the Damara sequence in the Auas Mountains, south of Windhoek (Guj, 1969). Martin (1974) described a *decollement* at the base of an outlier of Damara rocks at Probeer, adjacent to the Areb mylonite zone, about 30 km north-west of the Naukluft complex and Martin & Porada (personal communications) have observed a similar structure at Spaarwater, about 20 km farther west. Recent reconnaissance by Bickle & Coward (1977) in the Corona and Nauas Poort regions has provided further evidence for a major tectonic dislocation and the suggestion that the total horizontal displacement on it may be about 100 km, if it is correlated directly with the *decollement* at the base of the Naukluft nappe complex.

Recognition of the basal Damara thrust has been slow, as the above brief history indicates. For this reason, its influence on stratigraphic interpretation along the southern margin of the Damara belt has, as yet, been minimal. Most workers appear to accept that there has been no major stratigraphic inversion at the level of the thrust, or indeed within the tectonic assemblage above it. In view of the well-exposed structural relationships within the Naukluft nappe complex, this opinion is incomprehensible to the writer. Although somewhat beyond the scope of the present field investigation, brief reconnaissance of the Duruchaus-Damara contact near Gurumanas and of the Kamtsas-Damara contacts near Oamites Mine and Wortel Poort, has indicated that the Damara formations everywhere have a far more complex internal structure than the Duruchaus or Kamtsas Formations (cf. Bickle & Coward, 1977). In the Gurumanas area, it is evident that a major part of the deformation of the Damara sequence was completed prior to its southward thrusting over the simply deformed Duruchaus assemblage. At Wortel Poort ("window" B in Fig. 8), it is apparent that early folding of the Damara schists possibly preceded deposition of the Kamtsas Formation in Wortel Mountain (cf. Hälbich, 1970, Plate IV). It is therefore a considered opinion that the present model of stratigraphy in zone KR-II rests

on a fundamental misapplication of the principle of superposition in a tectonically-imbricated terrain in which the order of structural stacking does not reflect the original depositional sequence.

This opinion is supported by a piece of circumstantial stratigraphic evidence which has hitherto gone unremarked and unexplained. Mafic dykes, intrusions and related extrusives are very abundant in the pre-Duruchaus formations of the Rehoboth inlier. They are entirely absent from all major outcrops of Duruchaus and Kamtsas lithotypes (Schalk, 1973; Hälbich, 1970). The overlying Damara sequence of zones KR-II and KR-III, however, is once again riddled with mafic to ultramafic intrusive and extrusive bodies, of which the Matchless Amphibolite is merely the largest and most conspicuous example. The present stratigraphic interpretation obliges us to accept that there were two major periods of mafic magmatic activity, the second of which left absolutely no trace in rocks older than those in which it is now reflected. The writer is unwilling to accept that this is a reasonable hypothesis.

As an alternative, it is tentatively proposed that the mafic magmatic activity in the allochthonous Damara tectonic assemblage of zone KR-II may have been chronostratigraphically equivalent to a pre-Duruchaus episode of mafic dyke intrusion in the autochthonous crystalline basement. From the present knowledge of quantitative age relationships in the Rehoboth inlier, this hypothesis has the presently awkward consequence for Damara Supergroup stratigraphy that it requires the major part of the sequence in the southern part of the Khomas Trough to be approximately 1100 Myr old and that, far from being a facies equivalent of the Nama Group, the Damara sequence may be chronostratigraphically correlatable with part of the Sinclair Group on the Kalahari craton.

It has been necessary to discuss these problems of zone KR-II and the possibilities that they raise for radically new interpretations of stratigraphy, in order to adequately sketch the background to the present structural and stratigraphic investigation in the Naukluft nappe complex. It has already been noted that the Naukluft complex can be considered as part of the boundary structure between zones KR-I and KR-II and in many respects it forms a microcosm of zone KR-II structure and the larger problem of tectonostratigraphic correlation across major thrust surfaces in Precambrian rocks.

3. Lithostratigraphy in the Naukluft Complex

a. General remarks

Prior to the start of the present investigation, there existed no comprehensive, published account of lithology and stratigraphic relationships in the Naukluft nappe complex, apart from the few paragraphs devoted to these aspects by Korn & Martin (1959). A more detailed account of the Nama Group stratigraphy had, however, recently been given by Germs (1972), but the lithostratigraphy of the Naukluft area remained effectively undescribed. Since it had been noted that there was a close link between sedimentation and tectonic deformation in the Naukluft area (Korn & Martin, 1959), analysis of structural geometry in the nappe complex had necessarily to be combined with close stratigraphic subdivision of the major nappe units, with the aim of isolating lithological markers suitable for the purposes of structural mapping. In the course of this work, it became evident that identification of important thrust-planes was sometimes possible only by prior recognition of repetition in some highly characteristic part of a stratigraphic sequence. It became evident also that a complex history of deformation was recorded by erosional unconformities within the stratigraphic sequences of individual nappes. In the Naukluft complex, structural and stratigraphic analyses are therefore closely complementary.

The generally unfossiliferous character of the Late-Precambrian Naukluft rocks presents a major obstacle to a full knowledge of chronostratigraphic and hence structural relationships in the complex. It is, however, possible that future work on the stromatolites and occasional oncolitic, catagraphic and other structures of evident biological origin in Naukluft limestones and dolomites, which were encountered in the course of this work and are briefly reported below, may allow a consistent biostratigraphy to be erected. If so, many of the outstanding problems of correlation across major tectonic boundaries in the nappe complex may be resolved.

The proper analysis of depositional environments and facies changes is another aspect of Naukluft stratigraphy which, falling within the scope of sedimentology, is only briefly touched on here. It is nevertheless apparent

that it has important implications for structural development of the Naukluft nappes, inasmuch as (1) tectonics and sedimentation were effectively synchronous during the deposition of the younger units and (2) the lithological facies pattern of the older, pre-tectonic units are distinctly different from those of the younger syn-tectonic units and may contain important clues to their correlation with formations outside the nappe complex.

b. Problems of tectonostratigraphic nomenclature

Originally, seven distinct stratigraphic formations or "series" were recognised in the Naukluft complex. These were regarded as part of the "Naukluft facies" of the "Nama System" (Korn & Martin, 1959). In sequence, these seven series were arranged as follows:

(7) Klipbok Series
(6) Kudu Series
(5) Dassie Series
(4) Pavian Series, northern facies
(3) Pavian Series, southern facies
(2) Zebra Series
(1) "Unconformity Dolomite"

All seven units were considered to overlie the foreland Schwarzrand Series above an erosional unconformity marked by a thin yellow-weathering dolomite and to be correlated with the Fish River Series of the Nama System much farther south.

With the adoption of a new code of stratigraphic nomenclature in Southern Africa (cf. South African Commission for Stratigraphy - SACS, 1971), the above-mentioned names are automatically invalidated, since the fundamental lithostratigraphic unit is the *formation* which should ideally be named after a locality from which a stratotype has been formally described; the Naukluft "series" have been named after animals. As a matter of temporary expediency, the original names have recently been used with the term "series" replaced by "formation", in interim reporting (cf. Hartnady, 1974, 1975, 1976; Münch, 1975). With increasingly detailed lithostratigraphic subdivision of the original units and a new appreciation of the structural relationships and correlation, it has become necessary to abolish the old system entirely and to build a new nomen-

clature in the approved style.

The original nomenclature may, however, still be partly preserved in the informal naming of individual tectonic units, i.e. thrust sheets or nappes. Formerly, no clear distinction between tectonic and stratigraphic units was drawn, since it was considered that the nappes are "merely sheared-off sediment packs which remain, more or less, in their true stratigraphic sequence" (Korn & Martin, 1959, p.1062). This concept is shown in the present study to be incorrect. In the Naukluft nappe complex, older rock units have indeed been thrust over younger ones for great distances. It is therefore necessary to distinguish clearly between individual tectonic units, or nappes and the lithostratigraphic formations within them. Since nappe and lithostratigraphic nomenclature largely coincide in the original work (Korn & Martin, 1959), it is both possible and convenient to use most of the original stratigraphic names in order to refer to structural entities.

The Naukluft nappe complex has a complex imbricate structure which has developed serially in the course of an extended and apparently episodic deformation history. In general, the structurally higher northern nappes were emplaced earlier over the structurally lower southern nappes as the deformation front migrated relatively south or south-eastwards. The apparent structural sequence of the five major nappes, from south to north, is therefore as follows:

(5) Kudu nappe
(4) Northern Pavian nappe
(3) Southern Pavian nappe
(2) Eastern Daasie nappe
(1) Western Dassie nappe

These five major tectonic units together constitute the Naukluft nappe complex which, in the eastern regions of the mapped area, overlies a still lower allochthonous unit, namely

(0) Rietoog nappe

(Münch, 1975). The stratigraphy of the latter is not considered here.

It is important to note that the Kudu nappe, as presently mapped, is not

precisely the same as the Kudu Series, as originally mapped. The Kudu nappe includes both the former Kudu Series and the Klipbok Series, for which possible new formational names are proposed below. The Northern Pavian nappe includes all the former "Pavian Series, northern facies", but is now recognised as a tectonic entity with a complex internal lithostratigraphic constitution. At least three mappable lithostratigraphic formations and one erosional unconformity, exist within the Northern Pavian nappe. A special importance attaches to the uppermost formation, the Tsabisis Formation, of the Northern Pavian nappe, since it represents an episode of felsic volcanism in the history of Naukluft sedimentation and deformation, which had previously escaped notice. The Southern Pavian nappe is largely equivalent to the former "Pavian Series, southern facies" except for a small region at its north-eastern extremity, near Pavianskopf (X = + 233 000 m, Y = + 68 500 m) which has been re-interpreted as part of the Kudu nappe (cf. Chapter IV). The Dassie nappe is likewise largely the same as the former Dassie Series except for an area immediately below the Pavian nappes, which was formerly mapped as Kudu Series. Structural relationships between the Dassie and Zebra formations are complex, in that the Dassie nappe is locally thrust over the Zebra units, but the major plane of contact between Dassie and Zebra rocks is a relatively little-deformed erosional unconformity overlain by the latter.

c. Stratigraphic models of the Naukluft sequence

The last observation necessitates a major revision of former models of stratigraphy in the Naukluft complex (cf. Korn & Martin, 1959, Fig. 8). As indicated in the tabulation of original stratigraphic units, earlier in this section, the Zebra Series was formerly considered to be the oldest formation. This idea has subsequently been criticised from different standpoints by Martin (1974), Hartnady (1974) and Münch (1975). In the original stratigraphic model, a correlation of formations within the Naukluft nappes, was based on conspicuous "colouration differences" (Korn & Martin, 1959) which imply significant differences in sedimentary facies and depositional environment. The assumed lower group of formations included the Zebra Series and the two facies of the Pavian Series which are dominated by green- and blue-coloured sediments, notably green chloritic

shales and blue-black bituminous limestones, which may indicate a deeper or colder water depositional environment with reducing chemical conditions. The assumed upper group of formations included the Dassie Series and the Kudu Series, which are conspicuous for red- and purple-coloured sediments, evidently indicating a shallower or warmer water depositional environment with strongly oxidizing chemical conditions. The Klipbok Series remained the odd-formation-out in this model.

In the course of the present investigation, a revised version of this conceptual model was tentatively suggested which included the Klipbok Series (Hartnady, 1974). The revised model envisaged first the deposition of the Kudu and Dassie formations in a tectonically stable shallow-water environment, followed by the onset of tectonic instability, deepening of the sedimentary basin and subsequent accumulation of the Zebra, Pavian and Klipbok formations. The main episode of thrusting internal to the Naukluft nappe complex was considered to have taken place only after deposition of the latter units. This provisional model of stratigraphic relationships is now known to be flawed in several respects. The essential point nevertheless remains that the oxidized "red" formations are older and pre-tectonic and the "blue-green" formations are younger and syn-tectonic.

The major flaws in this later stratigraphic model are (i) the attempt to relate supposed facies changes in the younger group of formations to changes between north-facing continental shelf and slope environments (*op. cit.*, p.85) and (ii) the attempt to correlate the entire Naukluft stratigraphic sequence directly with the lower Nama Group (*op. cit.*, p. 87-88). These features of the model should be disregarded, but they do serve to illustrate the need for more information on sedimentological aspects of Naukluft stratigraphy.

For the purposes of lithostratigraphic description, the essential features of this stratigraphic model are assumed and the formations of the Naukluft complex are divided into the following major categories:

(i) Dolomitic formations of the Kudu and Dassie nappes;

(ii) Blue-black limestone-bearing pelitic formations of the Kudu and Pavian nappes;

(iii) The Tsabisis Formation of the Northern Pavian nappe;

(iv) Formations of the Zebra nappe;

(v) The Formations of the Southern Pavian nappe.

These categories cover all the formations of the Naukluft complex, with the exception of an extremely small wedge of highly deformed pinkish dolomite, calcareous quartzite and red shale which occurs at the base of the Northern Pavian nappe on Nauzerus West 229 (near X = 205 000 m, Y = 70 000 m). This occurrence, which does not warrant further description, appears to be a detached and overridden fragment of the Dassie nappe. It is of greater tectonic than lithostratigraphic importance.

The formations of category (i) are certainly the oldest in the Naukluft Complex and the formations of category (iv) are certainly the youngest in the Naukluft Complex. Within categories (ii) and (iii), however, some uncertainty remains about relative ages of individual formations in different nappes. In category (v), a conglomeratic member, consisting mainly of purplish-brown arkosic grits, in the lower part of the Southern Pavian nappe is an anomaly as regards sedimentary facies which makes it difficult to relate to other units of the complex. The volcaniclastic Tsabisis Formation, in the Upper Northern Pavian nappe, is also an anomaly in that it represents an oxidizing shallow-water depositional environment. Both of these anomalous sedimentary units indicate that the disjunction of pre-tectonic and syn-tectonic sedimentary facies, postulated in the abovementioned stratigraphic model, may not be a completely sharp one.

B. DOLOMITIC FORMATIONS OF THE KUDU AND DASSIE NAPPES

1. Noab Formation

a. Introduction

The Noab Formation corresponds to the "Kudu Series" of Korn & Martin (1959). Consisting mainly of massive dolomites with quartzitic intercalations, it underlies all the high ground in the northern part of the Naukluft nappe complex and

is therefore a most conspicuous stratigraphic unit.

The derivation of the proposed new name is the farm Noab 10, where most of the characteristic lithologies of this formation are represented. The unit, however, has a wide distribution in the northern and central parts of the nappe complex, extending south-westwards to Arbeid Adelt and southwards to the northern parts of Naukluft and Büllsport. As noted below, however, there is a systematic change of facies in a southerly direction which represents a complete transition into the most prominent dolomitic unit of the southern Naukluft area, namely the Büllsport Formation (formerly the "Dassie Series"). This facies variation is most important for palaeogeographic reconstruction. It does, however, complicate the problem of choosing a representative stratotype for the Noab Formation and also raises the question of whether the Noab and Büllsport Formations should continue to be distinguished by different names.

Another complicating factor in the formal stratotype description of the Noab Formation is that of defining its lower boundary. The problem is that the structural base of the Noab Formation is also the sole of a giant thrust nappe, the Kudu nappe,and it is most obvious at several localities that this tectonic contact truncates sedimentary bedding and the internal stratigraphy of the Kudu nappe. This phenomenon was formerly described incorrectly as a truncation of "downward-facing" tectonic slices and folds. The lower parts of the Noab sequence appear to be situated in the north-western parts of the Kudu nappe and the base of the Kudu nappe may cut southwards across progressively younger parts of the sequence. South of Remhoogte, however, this apparently simple pattern is complicated by secondary southward-vergent imbrication of the Kudu nappe.

The selection of the Noab area as most suitable for stratotype description is, in part, because of its central situation between the stratigraphically lower north-western and stratigraphically higher south-eastern parts of the formation.

b. Description

(i) Sequence

In their stratigraphic section of the "Kudu Series", Korn & Martin (1959, Fig. 8) distinguished eight members of the formation and estimated a total thickness of about 325 m. Their sequence with approximate thicknesses is as follows:

(top)	dolomite	(75 m)
	quartzite	(5 m)
	dolomite	(110 m)
	sandy dolomites and dolomitic sandstones	(35 m)
	yellow and white platy dolomite	(5 m)
	brown and purple shale	(10 m)
	laminated limestone	(55 m)
(base)	purple shale	(25 m)

Unfortunately, the precise location from which this sequence was obtained was not recorded and it could not be confirmed in the present field study.

The lower three units of the "Kudu Series" do not form part of the Noab Formation. Insofar as they are part of the Kudu nappe in its southern and south-eastern frontal zone, they represent a tectonite zone, i.e., rocks of relatively low viscosity which constituted the shear zone between the Kudu nappe and its substratum and were largely derived by tectonic ablation of the substratum. In the case of the "purple shale" (actually a hematitic slate or phyllite), it is clear that it originally formed and today still forms, part of a younger sequence below the Kudu nappe, called the Tsabisis Formation. The "laminated limestone" is actually a highly deformed marble zone, containing boudinaged and folded layers of green and purple phyllite.

In the Noab area, a broad subdivision of the Noab Formation into two principal parts is possible. A lower sequence consists mainly of flaggy to thin-bedded dolomites with abundant intercalations of sandy dolomite and dolomitic sandstone. The latter have a characteristic appearance due to well-sorted and well-rounded quartz grains with an average diameter of about 0,5 - 1 mm. Thin beds of shale and pinkish, thin-bedded limestone are also common intercalations in the lower sequence, as are intraformational dolomite breccias containing

angular to sub-rounded clasts of fine-grained and sandy dolomite in a dolomitic (occasionally partly silicified) cement. These rock types often appear together in relatively thin cyclothemic units as follows:

(top) sandy dolomites
thin-bedded pink limestone
grey-purple shale
(base) dolomite breccia

The probable environmental significance of these features will be discussed after petrographic description of some of the rock types.

The upper part of the Noab Formation consists of an apparently monotonous sequence of thick-bedded to massive, fine-grained dolomites. Over wide areas south-east of Noab these upper dolomites are so fine-grained and massive that it is difficult to discern the bedding orientation within them. Thin cherty bands are apparent in places. These have been observed to replace oolitic layers in the upper Noab dolomites north of the Tsondab valley (e.g., localities 30044 and 30071).

(ii) Lithology

The so-called "*sandy dolomites*", while not the most abundant, are at least the most distinctive rock type in the northern Noab Formation. There is a complete gradation from apparently fine-grained dolomites with very sparsely scattered, well-rounded grains of quartz and dolomitic sandstone, in which quartz grains are tightly packed with only an interstitial cement of dolomite (and usually some ferruginous material). Average grain size in individual specimens varies from 0,5 mm (CH37) to about 1,5 - 2,0 mm (CH43, CH46).

On close inspection, the "matrix" of dolomite, in which the quartz grains appear to be suspended, can be seen to consist of partly recrystallised, well-rounded dolomite grains of approximately the same size range. Microscopically, it is particularly evident that prior to diagenesis the unconsolidated rock consisted of varying proportions of clastic carbonate and siliceous grains. The clastic carbonate grains comprise various types, many having a finer, more complex internal structure which is truncated at the grain boundaries. Fine-grained, dark, carbonaceous varieties are particularly conspicuous in thin

section (CH40).

Interbedded with the northern sandy dolomites and other varieties in the northern Noab Formation are coarse dolomitic breccias of apparently intraformational habit. Some consist of sub- to well-rounded clasts, ranging in diameter from about 2 mm to 2 cm, of a variety of dolomite types, including fine carbonaceous types and coarser oolitic species (CH29B). A minor proportion of siliciclastic material is also present in these dolomite conglomerates. Other breccia types consist essentially of angular, flat clasts of the immediately surrounding dolomite type, suspended in a fine-grained dolomitic matrix, which may also contain abundant fine angular quartz grains (CH39).

South of the Tsondab River valley, on the farm Blässkranz, the Noab Formation undergoes a perceptible change of facies. Brownish-weathering, fine-grained calcareous quartzites, varying in thickness from a few millimetres to several centimetres or decimetres, are conspicuously interbedded with fine-grained, pinkish-coloured dolomite (Plate 2). Both the quartzites and the dolomite show abundant evidence of shallow-water structures such as ripple-marking and current-bedding and the dolomite may contain chert-replacement lenses and nodules (Plate 3). The sandy dolomite is not present in this facies. Where the Noab dolomites are massive and do not contain calcareous quartzite layers, there is locally evidence for the presence of vague columnar stromatolitic structures (e.g., CH154 from locality 50129).

In some of the massive, but finely layered pink dolomite beds, an unusual columnar structure is found which in plan resembles a circular burrow having a diameter of approximately 1,5 cm (CH155). It is generally composite in structure, having an irregularly shaped core of quartz surrounded by a shell of sparry calcite or dolomite. In section, these "burrows" may be up to 10 cm long. They appear to start and end at bedding-planes marked by thin lenses or films of material similar to that which fills them and to cut sharply across the fine layering between such planes (Fig. 9). In some cases they are not columnar in shape but are more like nodules. It is probable that these structures are not of biological origin but are infilled cavities ("bird's-eyes") resulting from inorganic processes, perhaps related to the original presence of

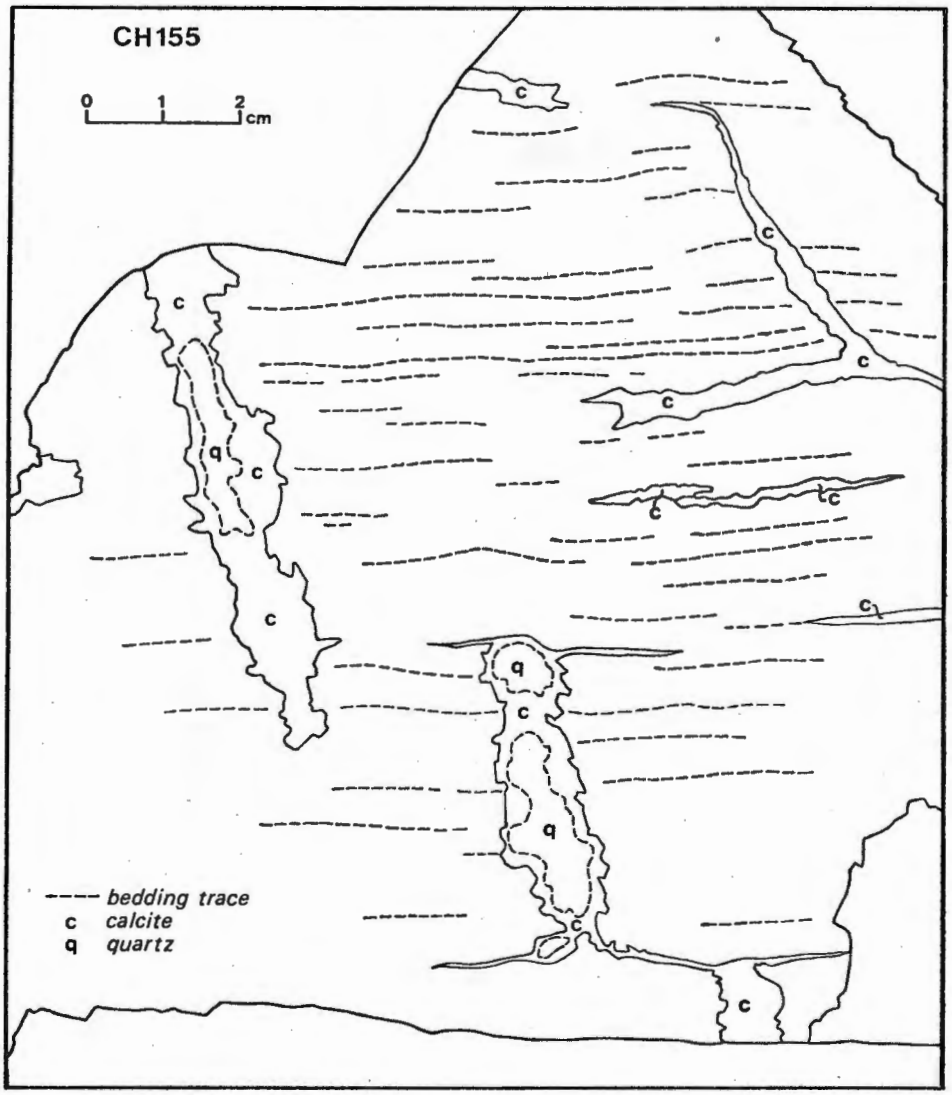

Figure 9. Sketch of pipe-like features in Noab Formation dolomite, interpreted as channels of defluidisation during algal bioherm growth (after Cloud *et.al.*, 1974).

evaporite minerals within the proto-dolomite sequence.[1]

Dolomite breccias are also present in the southern Noab sequence, generally in very close association with flaser-bedded calcareous quartzite layers. Typically, these are "flat-pebble" breccias containing disrupted thin crusts of dolomite (sometimes observed in brecciated, fold-like forms) suspended in a matrix of finer dolomite flakes and calcareous quartzite (CH131). In one case, at least, the breccia grades upward over about 10 cm into calcareous quartzite which has a ripple-marked upper surface. Deposition by tidal currents in shallow tidal channels seems the most probable explanation for these phenomena.

This southern facies of the Noab Formation clearly represents a transition to the lithologies of the Büllsport Formation.

c. Relationships to adjacent units

The Noab Formation is in contact with the following units of the Naukluft nappe complex; arranged in order of geographical appearance from north to south:

Remhoogte Formation
Klipbokrivier Formation
Blässkranz Formation
Tsabisis Formation
Büllsport Formation

The Remhoogte Formation, the Blässkranz Formation and the Tsabisis Formation are components of the Northern Pavian nappe. The Noab Formation overlies these units discordantly on a major thrust contact. The Klipbokrivier Formation is a component of the Kudu nappe: it rests unconformably upon the Noab Formation. On the evidence of lithology, the Büllsport Formation is a southern facies of the Noab Formation but the latter now overlies it on a tectonic contact which effectively defines the base of the Northern Pavian nappe.

d. Depositional environment

Dolomites are known to form at the present time in close association with evaporites under hypersaline conditions. The hypersaline interstitial fluids, responsible for dolomitisation, may be brine-enriched due to evaporation from

[1] *Note:* Identical structures are described in Cloud *et.al.*, (1974).

a shallow, partly isolated body of sea-water with reflux seepage back to the open sea, or to evaporation from a supratidal surface (sabkha) in arid regions, i.e. "evaporative pumping".

It is generally accepted that hypersaline basins must have been partially isolated from the open sea by some sort of sill or bar, in order to account for the brine enrichment. Otherwise dense brine would tend to escape oceanwards by means of a bottom current. An organic reef, or a sand bar, is an effective physical barrier against such a counter-flow. In the Noab basin, it is probable that the main "sandy dolomite" facies of the Noab Formation represents a bar of calcareous beach sand which isolated a large, shallow tidal embayment in which the south-easterly parts of the Noab Formation were deposited.

The northern sandy dolomites are well-sorted and consisted originally of well-rounded quartz and carbonate grains of approximately the same size, i.e., generally between 0,5 mm and 2,0 mm diameter. Some of the carbonate grains show a concentric zonation, indicating oolite formation, probably around a silicate nucleus, but others (cf. CH40) show a complex internal structure of fine-grained carbonate, siliceous material and iron oxides which indicates their origin by erosion and re-working of older calcareous beds. It is probable that the good sorting and coarse grain-size is due to a combination of wave- and wind-winnowing of finer material. The coarse dolomite conglomerates showing rounded fragments of irregular shapes and sizes and which occasionally also show iron-oxide pebble-coatings and interstitial quartz cement (cf. CH29B), can be interpreted as surface lag deposits formed on subaerial wind-stripped terraces, such as might be formed landward of beach-front dunes. Dessication cracks in very fine-grained dolomites in the Noab Formation (cf. Plate 4 from station 10064) testify to subaerial exposure also of dolomitic muds being deposited in low-energy, protected environments, probably landward of the barrier-island beach-zone.

On superficial inspection, much of the Noab Formation sandy dolomite appears to have resulted from aeolian transport of siliciclastic detritus (quartz and some felspar) into fine dolomitic silts or muds, thereby forming an apparent "wackestone" in which silicate grains are suspended in a carbonate matrix.

However, microscopic study generally shows the "matrix" to be comprised of partly recrystallized dolomite grains similar in size and shape to the more conspicuous quartz sand. The concept of strong offshore winds along a desert coast blowing relatively coarse continent-derived detritus into *quiet* depositional environments is therefore not generally tenable. But the concept of aeolian transport of mixed siliciclastic and carbonate sand into a beach- and surf-zone cannot be discounted. It is therefore suggested that the Noab Formation dolomitic quartz-sand and sandy dolomite deposits are a Late-Precambrian analogue of the present-day Umm Said quartz-sand dunes of Qatar which are rapidly migrating into the sea on a leeward coast in the Persian Gulf (Shinn, 1973). No definite large-dune foreset slopes have yet been observed in the Noab Formation to confirm this hypothesis, but this could be ascribed to re-working in the beach-zone.

Aeolian dune-beach complexes are also found on windward coasts of the Persian Gulf, as at Abu Dhabi for example (Purser & Evans, 1973). These result from large-scale oolitic sand production in the tidal deltas, much of which is driven by wave action onto the coastal barrier and piled up by the wind into dunes reaching altitudes of about 10 m (Evans *et al.*, 1973). The relative abundances of siliciclastic grains in the Noab Formation, however, do not suggest a similar kind of tidal delta source unless large quantities of medium-coarse quartz sand were being contributed to the tidal deltas, by longshore drift from a nearby fluviatile delta.

Lateral wedging of some sandy dolomite units in the Noab Formation (e.g. near station 20040) could perhaps be related to original dune-beach forms. At 20040, the wedging sandy dolomite is overlain by a dolomite-pebble breccia, interpreted as a surface lag deposit, which in turn is overlain by pinkish cherty dolomitic limestone with red shale intercalations, interpreted as fine continent-derived sediment marking a phase of regression. The following thick sandy dolomite sequence evidently represents a further transgressive phase.

Tectonic imbrication is naturally a complicating factor in interpreting the original sedimentary structure of the Noab Formation. The frequently-observed angular discordance between bedding in the Kudu nappe and tectonic

foliation in marble/phyllite zone at the base of the nappe, described in a subsequent chapter, bears a superficial resemblance to a large-scale dune foreset structure. It is possible that this was partly inherited from an original sedimentary structure at the interface between horizontally bedded lagoonal marly shales and transgressive, dune-bedded dolomitic sandstone.

2. Büllsport Formation

a. Introduction .

The Büllsport Formation corresponds to the "Dassie Series" of Korn & Martin (1959). It consists of interbedded flaggy dolomites, fine-grained calcareous quartzites and minor amounts of purple shale in the western and southern parts of the outcrop area. In the south-east and east, however, there is a considerable thickness of purple pelitic rock at the base of the Dassie nappe. This continues to be included within the Dassie nappe as part of the Büllsport Formation, although a case can be made for its correlation with the upper part of the Tsabisis Formation.

The derivation of the proposed name is the farm Büllsport from which the characteristic lithological sequence has been defined (Korn & Martin, 1959, Fig. 8 ; Martin, 1974). It is noteworthy that this sequence has been defined within a tectonic slice or imbrication which itself is part of a larger thrust zone separating the western part of the Dassie nappe from its eastern section. In practice, this intense deformation of the Büllsport Formation, together with original change of sedimentary facies, means that it is extremely difficult to trace members of the formation, even the characteristic middle unit, for long distances laterally.

The same difficulties that are experienced in applying formal lithostratigraphic classification procedures to the Noab Formation are present to a far greater degree in the Büllsport Formation, because of the greater intensity of brittle and ductile tectonic deformation.

b. Description

(i) Sequence

The former "Dassie Series" was subdivided into seven members, having a total thickness of about 265 m (Korn & Martin, 1959, Fig. 8). The sequence, with approximate thicknesses, is as follows:

(top)	white dolomite	(45 m)
	chert-banded dolomite	(75 m)
	thin-bedded quartzites alternating with purple shales	(40 m)
	red limestone	(20 m)
	brown dolomite with sand streaks	(40 m)
	laminated limestone	(15 m)
(base)	purple shale	(30 m)

The same reservations that apply to the basal part of the former "Kudu Series" also hold with respect to the purple shale and "laminated limestone" (foliated marble or marble-phyllite zone) in this representation of Büllsport Formation lithostratigraphy. Good exposures of the contact on Spitskop Suidwes, between the lower purple phyllite zone of the Dassie nappe and the overlying, imbricated Büllsport dolomite formations show discordances and tectonic truncation features at the base of the dolomites indicative of significant relative movement. The contact is, in many respects, similar to that between the upper purple slates of the Tsabisis Formation and the overlying Kudu nappe in the Tsondab River valley.

In this instance, however, it cannot definitely be shown that the pelitic formation is transitional downwards into a volcaniclastic sequence which is the defining characteristic of the Tsabisis Formation. Furthermore, on Spitskop Suidwes, fine-grained calcareous quartzites and pinkish dolomites typical of the bulk of the Büllsport Formation are observed to be interbedded with purple siltstones and slates for a considerable distance beneath the above-mentioned contact zone. Small traces of syngenetic copper mineralisation (malachite staining) which have been observed elsewhere within the Büllsport and Noab Formations are also present here. For these reasons, this unit is maintained within the Büllsport Formation although, strictly speaking, it is a distinct mappable unit which could (and probably should) be separated as a sedimentary facies into which the Büllsport Formation probably graded in a southerly direction.

In general, the Büllsport Formation seems easily divisible into three

principal parts; a lower carbonate unit, a middle clastic unit of very characteristic appearance and an upper carbonate-quartzite sequence. The lower division comprises the brown dolomite and "red limestone" units of Korn and Martin (1959). The upper division comprises their "chert-banded" and white dolomite units.

(ii) Lithology

The interbedded dolomite and calcareous quartzite facies described above for the Noab Formation is also typical of most parts of the Büllsport Formation. In the lower part of the Büllsport Formation the dolomites are generally a deeper pink or reddish colour and the calcareous quartzite layers usually have thin interbeds or "drapes" of purple shale.

Near locality 40002, within the lower Büllsport sequence, thin layers of carbonate-cemented arkosic sandstone have been observed. Microscopically, this can be seen to contain poorly sorted, angular grains of quartz, quartzite, felspar and a few lithic fragments, ranging in size from less than 0,5 mm to just over 2 mm (CH101). The felspar is predominantly a pinkish K-felspar but a few clasts of albite-twinned plagioclase are also present.

The middle part of the Büllsport Formation consists entirely of a thin-bedded quartzite-purple shale facies. Ripple-marking and small-scale cross-bedding are conspicuous features of the quartzite layers. Plate 5 illustrates the character of bedding in this part of the sequence, together with a typical ripple-marked block and another with crack-structures formed by the dessication of the thin shale drapes between some quartzite beds.

The upper part of the Büllsport Formation generally consists of pale dolomites interbedded with fine-grained white sandstones of a more orthoquartzitic composition. However, festoon cross-bedded layers of buff calcareous quartzite, weathering with a characteristic brown limonitic crust, are common also in the upper dolomite sequence. Layering in the dolomite beds is frequently indicative of small, domical stromatolitic structures (Plate 6). Dolomitised oolites with concentric zoning have been observed in thin section (e.g. CH133) along with fragments of other dolomite types in fine

breccia beds.

Lenses and nodules of reddish-brown jasperoid and black chert have been observed within some dolomite beds in the upper Büllsport sequence. Near locality 40036, for example, lenses of black and purplish-red chert replace oolitic layers in a bed of grey dolomite.

On lithological grounds, there is difficulty in drawing a clear distinction between the upper Büllsport sequence and a unit identified later in this chapter as the Neuras Member of the Zebra River Formation. Both are characterised by interbedded pale dolomite and quartzitic sandstone. In the Spitskop Suidwes area and also along the southern boundary of the Büllsport Formation between Naukluft and Die Valle, it locally appears as if the upper Büllsport sequence grades upwards with increasing interbeds of quartzitic sandstone into the lower part of a conformably-overlying Zebra River Formation. On the regional scale, however, there is an obvious unconformity between the Büllsport and Zebra River Formations (cf. also Korn & Martin, 1959).

In upper Büllsport (?Neuras) white dolomites on Naukluft, variously sized up to 5 cm nodules of quartz with framboidal or mammilary surfaces have been observed, scattered within certain dolomite beds. These bear a superficial resemblance to some nodular forms of the "burrow" (?birds-eye) structure, described above, from the Noab Formation. The possibility that these are quartz-replaced anhydrite nodules (Tucker, 1976) may be suggested, but further work is needed to confirm this.

c. Relationships to adjacent units

Along its northern boundary, the Büllsport Formation is in tectonic contact with the Remhoogte Formation in the Northern Pavian nappe, the Noab Formation in the Kudu nappe and various formations within the enigmatic Southern Pavian nappe. Within the Naukluft complex, it is in contact with the Zebra River Formation to the south. This contact is well exposed over a distance of about 15 km between Die Valle and Naukluft. It was previously recorded that the "Dassie Series" here appears to intrude the Zebra Series tectonically and to "underthrust it" (Korn & Martin, 1959, p.1057). Mapping

during the present project has shown this idea to be incorrect. There is no evidence for "underthrusting" at the contact which dips gently south-westward. Instead it is clear that the contact is a normal sedimentary one at which the Zebra River Formation overlies the Büllsport Formation unconformably. The same contact is visible within a tectonic slice in the frontal part of the nappe on Spitskop Suidwes (cf. also Korn & Martin, 1959, Fig. 13). It has recently been claimed (Münch, 1975) that the latter contact actually represents the incorporation of part of the Nama Group from the underlying Rietoog nappe into the Naukluft complex but, in the present writer's opinion, the earlier interpretation (Korn & Martin, 1959) is to be preferred.

It has also been claimed (Hartnady, 1974) that the contact between the Büllsport and Zebra River Formations re-appears in the extreme south of the Naukluft complex above the cliffs of the Johann-Albrecht-felsen, implying correlation of the cliff dolomites with the uppermost Büllsport Formation. This tentative interpretation is now retracted, since it has been discovered that a paraconformable dolomite-quartzite member of variable thickness exists at the base of the Zebra River Formation also along the latter's main contact with the imbricated Büllsport Formation.

In the south-eastern front of the Naukluft nappe complex, the Büllsport Formation overlies the highly-deformed Kuibis Formation in the Rietoog nappe at a thrust contact defined by the peculiar Unconformity Dolomite.

d. Depositional environment

The most probable depositional environment for the Büllsport Formation, like that of the southern Noab Formation, is a tidal flat into which carbonate material (oolites, formed in a beach-zone) was transported landward during high tides and mixed with terrigenous siliciclastic material (calcareous quartzites). Cross-bedding, flaser-bedding and ripple-mark structures are evidence of tidal current action and the dolomite breccias may be tidal channel fills. Dessication cracks phenomena also point to intertidal zone sedimentation. Stromatolitic dolomites probably formed in the algal flats (or upper intertidal zone), while the dolomites with nodular and "bird's-eye" structures (anhydrite-replacement?) reflect processes in the supratidal zone or *sabkha*.

The greater abundance of siliciclastic material, which becomes dominant in the middle Büllsport sequence and the presence of a ferruginous, purple shale-siltstone facies in the extreme south-east, may be interpreted as evidence of a transition from a marginal marine to a non-marine environment.

3. Regional aspects of the Noab and Büllsport Formations

a. Interpretative model of the sedimentary basin

The foregoing description of the principal dolomitic units of the Naukluft nappe complex is by no means complete and much sedimentological work could be done in order to improve upon concepts of their depositional environment and history. This has probably been neglected because of the impression previously created of intensive plastic folding of these units on all scales. The impression is not justified since, over large areas, original sedimentary structures and sequences are extremely well preserved and the formations have experienced very little pervasive plastic deformation away from the immediate vicinity of listric thrust-faults and the basal nappe gliding surfaces. This is due to the very low ductility of dolomitic rocks (cf. Heard, 1976). In the Naukluft nappe complex, the thicker parts of the dolomite sequence have moved as effectively rigid plates.

A full investigation of Noab and Büllsport sedimentology is outside the scope of the present study but is relevant to it in one chief respect. In the previous model of relationships between tectonics and sedimentation, the Noab and Büllsport Formations were considered to have been deposited in a southward-sloping northern margin of the subsiding Nama basin (Korn & Martin, 1959). If this were indeed so then it should be reflected in the pattern of facies variation between the Noab and Büllsport type-areas. It is apparent, however, that lithology and sedimentary structures lend very little, if any, support to the previous model. The siliciclastic component in both formations clearly becomes more important southwards, probably indicating a provenance of terrigenous detritus in that direction. Shallow-water to inter-tidal zone sedimentary structures also become more important southwards, particularly in

the Büllsport Formation. Thirdly, the majority of palaeocurrent indicators that the writer has observed point to transport of sedimentary material from south-east to north-west.

In the hope of encouraging further investigation of these aspects, it is suggested here that the Noab and Büllsport Formations were deposited under arid conditions along a north-westward-facing shoreline, fronted seawards by a barrier of dune-beaches similar to those found along the Trucial Coast of the Persian Gulf. The sandy dolomites of the Noab Formation were formed here. Shoreward, this coast was marked by a complex of intertidal flats and lagoons in which the Büllsport Formation was deposited. This complex probably graded southward into a largely non-marine zone in which deep-red, fine-grained terrigenous sediments accumulated along with evaporites (including dolomite) and some syngenetic copper deposits, the former representing occasional incursions of salt-water. This facies zone is now represented by the purple siltstone and slate unit in the south-eastern part of the Büllsport Formation. One may imagine that still farther southward this facies zone merged with a coastal-plain environment of braided streams or alluvial fans.

Since the Naukluft complex has been emplaced from the north-west, it is conceivable that these last-mentioned non-marine facies zones are still preserved in the southern foreland of the Damara belt beneath the Kuibis Formation and can be linked with their equivalent in the nappe. Before a brief consideration of the possible correlatives, it is perhaps significant to remark that a transgressive zone of transition from a sabkha facies, in which extensive dolomitisation has occurred, to a semi-continental evaporite-shale facies provides practically ideal material and boundary conditions for the development of large-scale thrust-nappe tectonics. The reason for this is the extreme contrast in ductility between very strong dolomites, on the one hand and very weak evaporites and shales, on the other (cf. Heard, 1976). Any subsequent body or surface forces applied to such a sabkha dolomite complex and acting in a shoreward direction, will cause it to detach and move easily as a rigid body over its low-viscosity substratum (Kehle, 1970). This appears to have occurred in the Naukluft Mountains and may also explain the common association of the rock dolomite with large-scale overthrust complexes in the Pre-alpes, eastern

Crete and Papua-New Guinea.

b. Correlation and age of the Noab and Büllsport Formations

The Büllsport Formation has recently been correlated with an identical rock sequence in the Probeer synform, immediately north-west of the Areb mylonite zone and about 25 km north-west of the margin of the Naukluft complex (Martin, 1974). The Probeer sequence was formerly described as part of the "Verloren Stage" in the "Hakos Series" of the "Damara System" (De Waal, 1966, following the old stratigraphic nomenclature). The *Hakos Formation* is now subdivided differently in its type area into the Chaibis and Chausib Members (Porada & Wittig, 1976), the latter being a distinctive turbidite sequence apparently grading laterally into the Chaibis felspathic quartzites. The status of other parts of the former Verloren Stage, at Probeer and in an extensive region south-west of the Hakos Mountains around Spaarwater, is still uncertain. It is, however, clear that there is very little in common between a relatively deep-water turbidite sequence like the Chausib Member and a shallow-water to tidal-flat association like the Probeer, Noab and Büllsport Formations. Furthermore, tectonic reconstruction of the sedimentary basin of the Chausib sequence indicates that it was derived from the north (Porada & Wittig, 1976), whereas the facies variation and sedimentary structure of the Noab-Büllsport association suggests a southerly provenance. For these reasons, a correlation between the Noab-Büllsport Formation and the Hakos Formation is simply untenable. The correlation of the Büllsport and Probeer Formations still holds but the relationship of the latter to the Swakop Group along the southern margin of the Khomas Trough is evidently in need of re-examination.

The Probeer sequence was originally described as part of the "Duruchaus Series" (De Kock, 1934), now the Duruchaus Formation. The reasons for this obviously relate to the close lithological resemblance between the western parts of the Duruchaus Formation, beneath the Gurumanas nappe (Hälbich, 1970) and the Probeer Formation. The writer has inspected the western Duruchaus outcrops near the road between Windhoek and Nauchas and is impressed by the similarity of the rock association there to parts of the southern Noab Formation and northern Büllsport Formation. The distinctive pink-red dolomite interbedded with

fine-grained, ripple-marked calcareous quartzite (and locally thinly draped by purplish shale with dessication cracks) is highly characteristic. Correlation of the Noab-Büllsport group with the Duruchaus Formation is therefore strongly suggested.

Finally, there is a probable link between the purple siltstone and shale division in the south-eastern part of the Büllsport Formation with the Kagas Member of the Klein Aub Formation. The Kagas Member consists essentially of hematitic calcareous shales with interbedded calcareous quartzites (Handley, 1965; Schalk, 1973). Some thin limestone bands are also present and Klein Aub mine exploits a stratiform copper deposit within the Kagas Member. Prospecting trenches have been excavated in a malachite-stained calcareous quartzite bed within the purple shale-siltstones of the Büllsport Formation on Spitskop Suidwes and this obviously suggests a correlation between the Büllsport and Klein Aub Formations.

In conclusion, it is considered that the lithofacies of the Noab and Büllsport Formations is so highly distinctive that their correlation with similar formations surrounding the Naukluft complex at no great distance is a relatively simple matter. These units are the Probeer, Duruchaus and Klein Aub Formations. Apart from the sedimentological characteristics that these formations have in common, they contain a widespread syngenetic Fe-Cu-Ag mineralization, which is economically important at Klein Aub, Oamites and the Witvlei prospect (Toens, 1975). While a correlation of the Duruchaus and Klein Aub Formations has been suggested before on these grounds, it would appear that the actual facies transition between the two units is now preserved only in the Büllsport Formation of the Naukluft nappe complex.

The age of these formations is not directly known since they contain no easily datable materials. An age of 1132 Myr has been obtained for the Doornpoort Formation (Burger & Coertze, 1973) and this places a maximum limit on the age of the overlying Klein Aub Formation. Accepting the abovementioned correlations the Noab and Büllsport Formations may be as much as 1000 Myr in age.

C. BLACK LIMESTONE - ("SCHWARZKALK") BEARING FORMATIONS OF THE KUDU AND NORTHERN PAVIAN NAPPES

1. Klipbokrivier Formation

a. Introduction

The Klipbokrivier Formation corresponds to the "Klipbok Series" of Korn & Martin (1959). It is restricted to the northern part of the Kudu nappe and takes its name from the small stream south-west of the farmstead on Noab.

It is preserved to a maximum thickness of about 150 m in several isolated synclinal structures where, being less resistant to erosion than the surrounding Noab dolomites, it underlies areas of low relief and generally poor exposure.

b. Description

(i) Sequence and lithologies

The sequence as preserved comprises two main parts. The lower part consists of dominant greenish sandy shales grading locally into fine-grained subgreywacke. These rocks have generally been transformed into cleaved slaty rocks, but strain is heterogeneous and outcrops can be located (e.g.20047) where they are practically undeformed and fine details of sedimentary bedding are preserved. This part of the sequence is most deformed where it has been wedged into imbrication zones in the Noab dolomite, or where large slabs of the latter have been thrust over the Klipbokrivier Formation, as at the Grenzberg (near X = +212 500 m, Y = +72 500 m).

The upper part of the preserved Klipbokrivier sequence generally forms a resistant capping to low ridges. The rock is a breccia consisting of very angular fragments of black limestone and subordinate grey dolomite set in a fine-grained matrix of orange-brown weathering grey limestone. The latter makes up a variable proportion of the rock, but is mostly a cement to densely-packed limestone and dolomite clasts of irregular shape and size. The grey dolomite fragments in the rock are generally larger than the black limestone clasts, some being several metres in diameter. The average breccia fragment

has a long-axis length of about 5 - 10 cm. Plate 7 illustrates typical features of this rock.

(ii) Deformation

The Klipbokrivier carbonate breccias have been deformed in the same episode which produced the slaty cleavage in the underlying pelites. The black limestone fragments show moderate to large, ductile strains. Larger dolomite blocks and boulders have remained undeformed, testifying to the very large ductility contrast between dolomite and limestone, while smaller dolomite fragments - generally those which were initially elongate - have undergone brittle fracture and extension with calcite filling the voids thus created (Plate 8). A "streaky" white calcite veining is a conspicuous feature of the limestone component of the rock and is unusual in being orientated subparallel to the principal extension direction (X) on cleavage surfaces. It evidently reflects an early phase of brittle fracture and vein formation in the limestone which preceded the principal phase of ductile deformation.

c. Relationships to adjacent units

The Klipbokrivier Formation overlies the Noab Formation unconformably. This is shown by large-scale structural relationships in the Noab River valley between localities 20040 and 20041 and the valley farther to the south-east, where undeformed Klipbokrivier shales are in direct (though poorly exposed) contact with part of the Noab Formation below a conspicuous marker sequence of grey dolomite breccia-pink limestone-sandy dolomite in the latter. It is shown also by the presence of the characteristic Noab sandy dolomite as large clasts within the Klipbokrivier breccia.

South-east of the abovementioned localities the Klipbokrivier Formation overlies a higher part of the Noab sequence paraconformably (locality 20047). This suggests an episode of pre-Klipbokrivier faulting in the Noab Formation.

In a few localities, outcrops of the Klipbokrivier Formation are in very close proximity to those of the Remhoogte Formation, the intervening Noab Formation having been thinned or eliminated by post-Klipbokrivier faults. Superficially, there may appear to be no great difference between Remhoogte and Klipbokrivier pelites where the latter are strongly cleaved. This can

result in local misidentification in the field. Microscopically, however, distinct differences in fabric development and metamorphism are observed between nearby Remhoogte phyllites and Klipbokrivier slates.

d. Depositional environment

Because of the limited areal extent and rather poor exposures, reconstruction of depositional environment is difficult. There can, however, be little doubt that the Klipbokrivier Formation was deposited in a shallow-marine environment under conditions of tectonic instability. Deeper water quiet conditions probably prevailed during the deposition of the lower shales and subgreywackes and (in an adjacent shallower region) of bituminous limestones. Abrupt uplifts and emergence in the limestone facies area then resulted in the large-scale submarine slumping of the breccia formation over the marine shale facies. The incorporation of fragments of Noab dolomite in the slump breccia indicates that movement along major faults in the dolomite formations was responsible for this slumping episode.

2. Remhoogte Formation

a. Introduction

The Remhoogte Formation corresponds to the lower part of the "Pavian Series, northern facies" of Korn & Martin (1959). It forms the major part of the Northern Pavian nappe, as defined in the present work. In the north-western part of the nappe, the Remhoogte Formation alone is found but towards the south-east two distinct upper units appear within the nappe.

In strict terms, it may be preferable to refer to the Remhoogte Formation as the "Remhoogte epimetamorphic suite" since it consists of several different rock types, including "conglomerates", breccias, phyllites, quartzites and marbles, which are all highly deformed and metamorphosed in the lower greenschist facies. The structure is too complex and the exposure too limited to permit the determination of any definite original stratigraphic sequence. In fact, it is doubtful if this could be done, since the rocks appear to have been

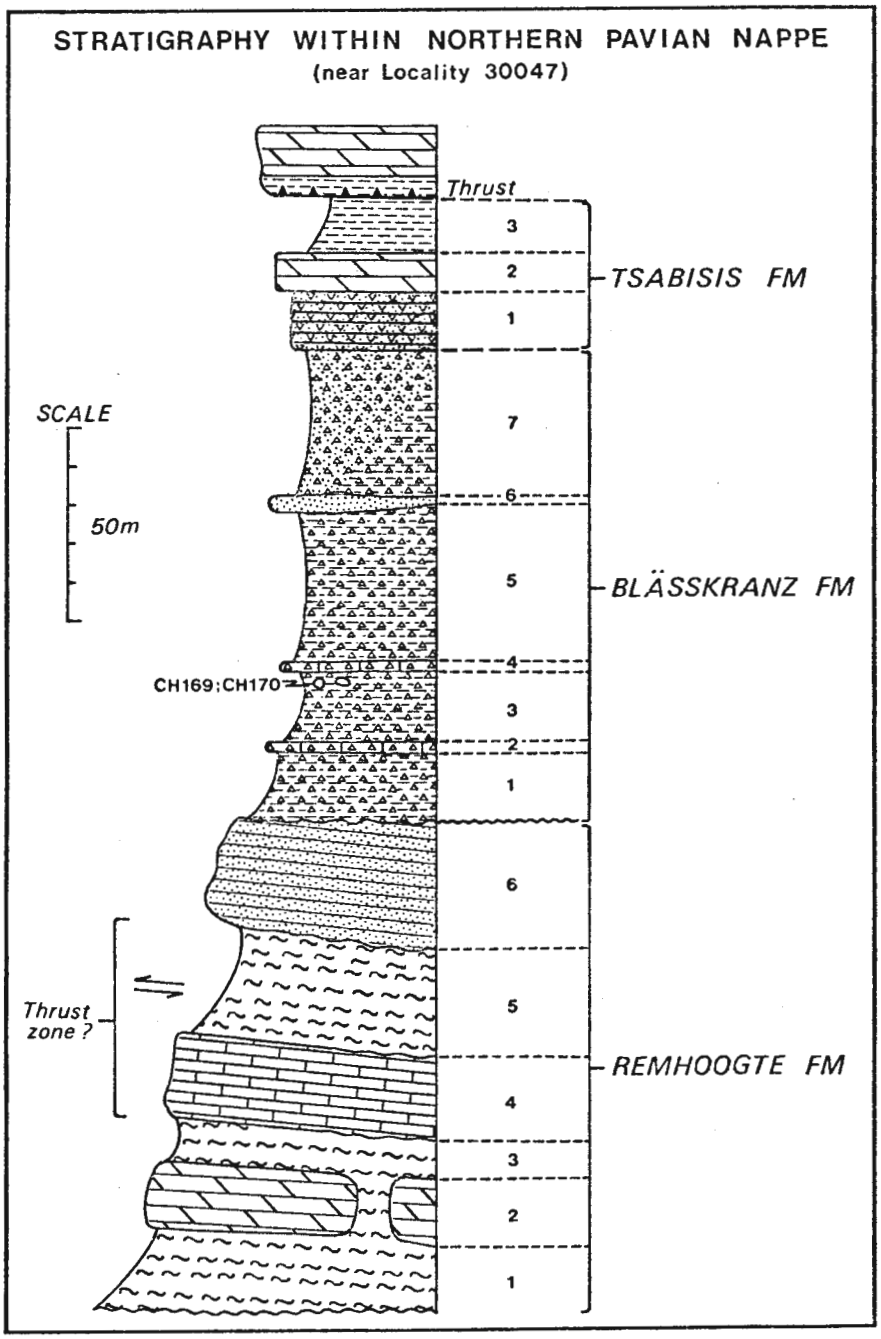

Figure 10. Stratigraphic column for the Northern Pavian nappe on the farm Blässkranz.

assembled from a number of different original sedimentary sources by tectonic processes. This is best seen along the north-western margin of the Naukluft nappe complex, where the phenomenon of the tectonic incorporation or "accretion" of large exotic units, up to 5 km in lateral dimensions and several tens of metres in thickness is clearly demonstrable (cf. Chapter IV, Section 2). The northern Remhoogte Formation can therefore be described as a "melange". The southern exposures of the formation in the Tsondab River valley nevertheless show a sequence of rock types which may reflect an original stratigraphy (Fig. 10).

b. Description

(i) "Conglomerates" and breccias

In the northern Naukluft complex, the bulk of the former "Pavian Series" was said to consist largely of "boulder shales" gradational from "brown arenaceous shales" farther south (Korn & Martin, 1959). Rocks approximating to this description are found along the north-western margin of the complex between Abbabis and Nauzerus West; they are, in fact, pebbly phyllites and schists which have been very highly deformed and significantly metamorphosed near the boundary of the lower greenschist facies.

In this region many of the clastic inclusions, ranging in size from pebbles to small boulders, are of gneissic basement rocks resembling deformed Piksteel granodioritic gneiss (CH10C). In thin section, cataclastic deformation phenomena in remnant felspar augen are abundant (e.g. cracked and "bent" twin lamellae) and quartz augen show impressive plastic deformation lamellae and mortar structure. Original biotite in the rock has been completely chloritised, along with the development of fine white mica from original K-felspar, but very fine flakes of a new, brown, strongly pleochroic mica are present within shear zones and it is suspected that this mineral may be stilpnomelane.

The matrix of these conglomeratic phyllites shows abundant quartz veins in a highly deformed, folded and boudinaged condition. In places (e.g. locality 10055) the "conglomerate" is dominated by large ellipsoidal and angular inclusions of vein quartz and it is possible that many of these have

been formed by brecciation and/or boudinage of quartz veins. In other words, the conglomerates may not have been formed by sedimentary processes but as a tectonic breccia or *melange*.

(ii) Phyllites

In the northern Remhoogte Formation, two types of phyllite may be distinguished. The first type is the greenish-brown highly crenulated phyllite (or more accurately, semi-schist) which is found in generally close association with the conglomerates or breccias. The second type is found farther south in fine-grained meta-pelites which have not been crenulated to any significant degree.

Microscopically, the difference between these two types of phyllite is great. In the first type, the principal foliation is itself an early crenulation cleavage (s_2) which deforms a still earlier schistosity (s_1) defined by a sub-parallel compositional layering and chlorite-white mica fabric, crosscut by thin, folded quartz veins. The latter have been further deformed and boudinaged during the formation of s_2 which microscopically appears as a fine lenticular microlithon structure, varying from 50 to 150 μm in normal thickness, comprised of alternating layers of orientated, fine-grained late chlorite-white mica and folded, coarser grained, early chlorite-white mica (Fig. 11). The principal crenulation foliation, s_2, has been crenulated itself on a scale ranging from microns to a few centimetres, in a later phase of deformation forming s_3 and folding early lineation structures (e.g. locality 10061 and Plate 34).

Qualitative X-ray diffraction analysis of northern Remhoogte phyllites (CH38, CH48) reveals that they consist essentially of quartz, white mica (probably phengite), chlorite and albite, generally in that order of decreasing abundance. The sharp nature of the 10 Å mica peak indicates a crystallinity index, H_b, of less than 125 (after Weber, 1972a), estimated roughly using the quartz of the specimen (CH38) as an internal standard. The boundary between the greenschist facies (low grade) and pumpellyite-prehnite-quartz facies (hyper-low grade) is taken at H_b = 100 (Weber, 1972b).

This may indicate that the grade of metamorphism in the northern

Remhoogte phyllites falls just short of the greenschist facies. There are, however, two features of the phyllites which may indicate that the grade of metamorphism is just above the boundary between low and very-low grades. In the highly crenulated phyllite type (CH38), the growth of a brown, pleochroic micaceous mineral with a parallel extinction pattern typical of biotite is observed. This mineral is present in trace amounts in the rock but is locally quite abundant along some s_2 cleavage planes (Fig.12). Its small grain size (<50 μm), however, inhibits accurate optical identification. It is possibly not biotite, but stilpnomelane.

The slight brownish colour of the northern phyllites is due to the presence of similar brown pleochroic mineral in very fine-grained white mica aggregates (e.g. CH10A), but in these cases it is possible that the mineral is oxidised chlorite. In the same rock, many cleavage surfaces are also stained with an extremely fine layer of limonitic iron oxide. The presence of biotite has therefore yet to be positively demonstrated.

The second feature of the Remhoogte phyllites which indicates that they may fall just within the greenschist facies is the presence of macroscopically visible chlorite porphyroblasts in the second type of phyllite mentioned above. In this type of phyllite, the main cleavage planes (s_1) are not significantly deformed by later crenulations and the average grain-size of the rock is less than in the more northerly, first phyllite type. Under a hand-lens magnification or even with the naked eye, small orientated dark spots can be observed on a fresh cleavage surface. Their orientation defines the conspicuous "grain" or stretching lineation in the rock, which is generally at high angles to the obvious lineation defined by the bedding-cleavage intersection. Microscopically, these spots are observed to consist of a pale-green, pleochroic chlorite with anomalous lavender-blue birefringence colours (Mg-chlorite?). Their habit is unusual in that the basal cleavage is orientated almost at a right-angle to the basal cleavage of the much finer grained chlorite and mica in the matrix of the phyllite. This s_1-defining chlorite-mica fabric also bows around the larger chlorite porphyroblasts, forming clear microscopic pressure shadow structures at the fringes of some. In most specimens (e.g. CH48, CH20, CH21), the chlorite "porphyroblasts" are composite structures and seem to have

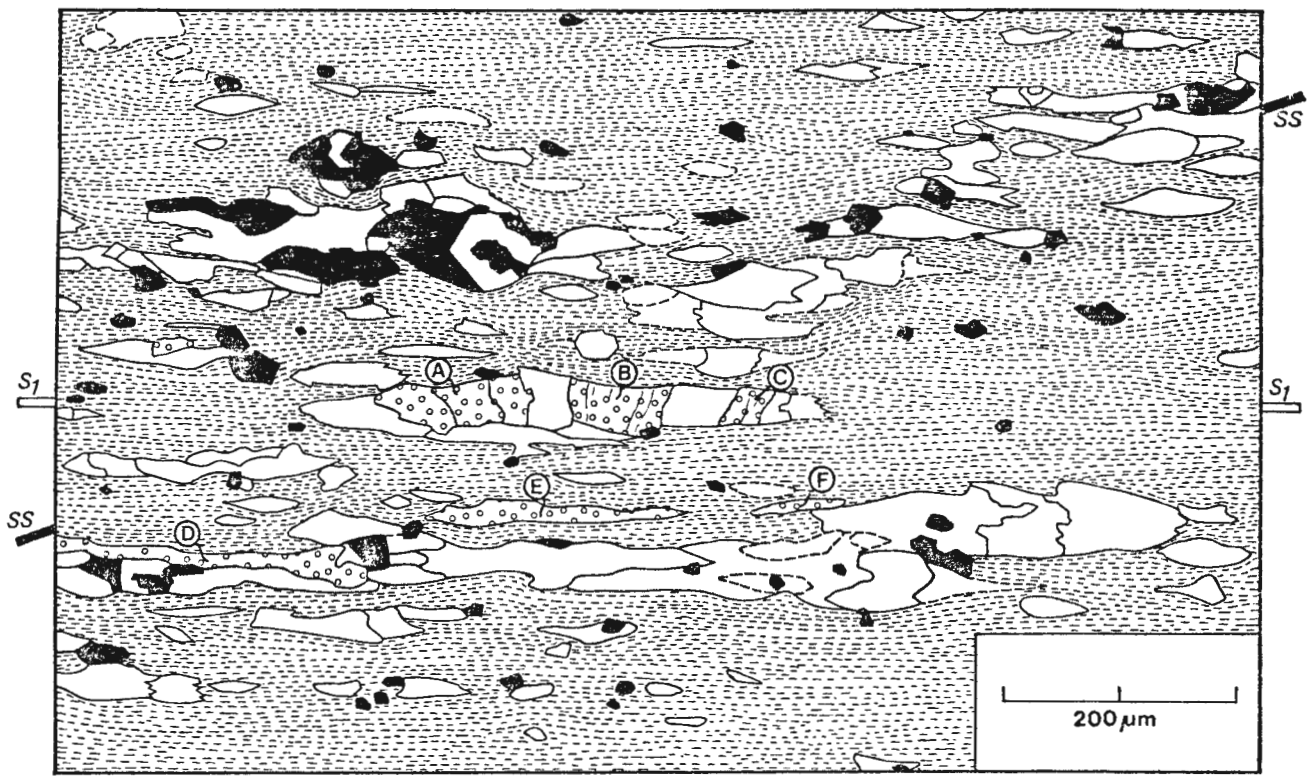

Figure 13. Microstructure of Type I phyllite foliation in the Remhoogte Formation (specimen CH48 from locality on Remhoogte Pass road near X = +218 500 m, Y = +73 000 m), showing main cleavage s_1 defined by fine chlorite and phengite, trace of original bedding (ss), flattening and micro-boundinage of quartz grains with some pressure shadow effects, and chlorite porphyroblastesis, in spaces between quartz fragments (sites A-C) or as large flakes in s_1 (sites D-F).

formed by growth of chlorite in the void space between microboudinaged fragments of pre-existing quartz (and felspar?) clastic grains (cf. Fig. 13). These features generally indicate extensions of at least 100% in a direction parallel to the phyllitic cleavage. In many other instances, no such mechanism can be invoked to explain the chlorite growth since the porphyroblasts are not composite and consist of chlorite alone. Even in these cases, however, the basal crystallographic cleavage in the chlorite porphyroblasts is more or less orthogonal to the rock cleavage in the surrounding matrix and pressure-solution and pressure-shadow phenomena are still present at the porphyroblast margins, indicating that their growth was synkinematic. In the largest example observed (CH21A), the ellipsoidal porphyroblast measures 1200 x 400 µm in section, exhibits large pressure shadows at the boundary segments along its major axis and shows a thin selvedge of matrix darkened by insoluble residue at the boundary segments facing the compressional direction.

According to Weber (1972b), the thickness of chlorite porphyroblasts in metapelitic chlorite-mica aggregates can be related almost linearly to illite crystallinity and hence to metamorphic grade; at the boundary between low and very-low grades it should be approximately 50 µm. The fact that the Remhoogte phyllites contain chlorite porphyroblasts with dimensions greatly in excess of that figure, indicates that they were metamorphosed in the greenschist facies.

In specimen CH48, a single porphyroblast of a mica with conspicuous pleochroism (from light yellow to brown-black) and an extinction and birefringence resembling that of biotite, was noted. It is assumed to be stilpnomelane.

The phyllites and metapelitic subgreywackes of the Tsondab River area have not been studied in detail. It is, however, apparent that their grade of metamorphism is not quite as high, as the growth of lustrous white mica on cleavage planes is not as obvious and no chlorite porphyroblastesis could be seen with the naked eye. It is therefore probable that the facies boundary between the greenschist and pumpellyite-prehnite-quartz facies can be mapped within the Naukluft complex and that it is situated south of the Remhoogte Pass area (on the Nauchas-Abbabis road) and north of the Tsondab River valley.

(iii) Quartzites

In the mountain slopes on the northern side of the Tsondab River, the highest lighological unit in the Remhoogte Formation is a zone of deformed and laminated micaceous quartzites (Fig. 10). It is overlapped in places by the unconformably overlying Blässkranz Formation. Near locality 30028, it contains large, overturned to partly recumbent fold structures which have a south-eastward vergence and overlies an intensely deformed phyllite zone (up to 30 m thick) containing characteristic composite veins of quartz and pinkish calcite. The latter may in future prove useful for oxygen-isotope geothermometry in the Naukluft complex.

(iv) Carbonate rocks

Immediately underlying the abovementioned phyllite zone is a conspicuous 2 - 5 m zone of blueish-grey marble which is extensively veined by white "streaky" calcite. This marble, originally a black, bituminous limestone is highly deformed and probably marks a major zone of relative movement between the overlying quartzite and phyllite units in the Remhoogte Formation and those which underlie it.

The local stratigraphic sequence near locality 30032, on Blässkranz, in this zone of carbonate rocks, is as follows:

Blueish-grey marble	(2-5 m)
green phyllitic slates	(10 m)
grey dolomite	(1 m)
green phyllitic slates	(1 m)
black limestone (oolitic) with limestone-dolomite breccia	(5 m)
greenish arenaceous phyllites (meta-subgreywackes)	(?)

Thicknesses are approximate because of deformation of the sequence but the rocks are in normal stratigraphic order on the evidence of graded bedding in the lowermost unit.

The grey dolomite unit is more conspicuous farther eastward toward Tsabisis but may be locally absent. On a large scale, it seems to occur in dumpy lenticular bodies, which may reflect boudinage of an originally uniform dolomite layer during ductile flow of the surrounding rocks.

The black oolitic limestone unit, which is dominantly a carbonate breccia formation, is similar to the rock types of the overlying Blässkranz Formation except that it is much thinner and the breccia clast size is finer. The clast types consist of limestone, oolitic limestone with partly dolomitised oolites and dolomite (some of which may be oolitic). A particularly interesting feature of this breccia, in which it differs from the Blässkranz breccias, is that the carbonate matrix of the breccia contains *individual* partly-dolomitised oolites (CH161). This shows that the breccia was formed by a mixture of consolidated and unconsolidated sedimentary material originally derived from a zone of agitated, hypersaline, shallow water. This mixture of materials was then transported abruptly into a deep-water (?) environment in which graded subgreywackes were accumulating.

In the north-western part of the Remhoogte Formation, other large bodies of blueish-grey marble, including breccia formations, thin boudinaged dolomite zones and zones of highly deformed marly phyllite, are found. The thin former shale layers within the marly phyllites display peculiar "chocolate-tablet" boudinage structure, with fibrous calcite filling the resultant veins (Plate 9). A dolomite bed about 0,6 m thick, between a zone of marly phyllite and overlying blue marble, is also spectacularly boudinaged (Plate 10) showing that in these northern carbonate units there has been a large amount of bedding-parallel extensional strain.

Since these north-western carbonate units within the Remhoogte Formation are bounded entirely by tectonic contacts and are therefore, in a sense, "exotic", it is impossible to establish their precise relationship to their immediate surroundings and to the carbonate zones near the Tsondab River.

c. Relationships to adjacent units

Along the north-western and northern margins of the Naukluft complex, the Remhoogte Formation overlies the Kuibis Formation above a major tectonic discontinuity marked by the Unconformity Dolomite (Korn & Martin, 1959); the latter is usually about 1 m thick beneath the Remhoogte Formation. In the north-west it is overlain in turn by the Noab Formation at an older and equally major tectonic discontinuity, which is marked in places by the development of a zone

of mixed marble and phyllite.

Towards the south-east, however, there is an important contact within the Northern Pavian nappe at which the Remhoogte Formation is unconformably overlain by the Blässkranz Formation. Farther south-east, the Remhoogte Formation overlies the Büllsport and locally a tectonic slice of the Noab Formation. This contact, which extends from the Blässkranz-Büllsport boundary north-eastward through the Tsabisis area is yet another major tectonic discontinuity within the Naukluft complex.

d. Depositional environment

Because of the complex internal structure of the Remhoogte Formation and the uncertainties about stratigraphic relationships between its more metamorphosed north-western parts and the slightly less metamorphosed south-eastern section in which a local stratigraphic sequence can be recognised, there is little which can presently be said on this subject.

Attention, however, is drawn to remarks made above, in connection with the carbonate rocks of the south-eastern sequence, about the incongruous juxtaposition of contrasting deep- and shallow-water sedimentary facies. In this respect, the Remhoogte Formation, together with the overlying Blässkranz Formation, represents an interesting example of large-scale sedimentary *melange* formation, complicated by the later incorporation of the sedimentary *melange* complex into a large-scale tectonic *melange*.

3. Blässkranz Formation

a. Introduction

The Blässkranz Formation corresponds to a part of the former "Pavian Series, northern facies" (Korn & Martin, 1959) formerly described as "brown boulder shales" and erroneously correlated with the siliciclastic conglomerates in the Remhoogte Formation. The Blässkranz Formation, however, consists exclusively of limestone-and-dolomite breccias with interbedded black limestone layers. It is extensively distributed in the south-eastern part of the Northern Pavian nappe, originally covering an area of at least 15 x 40 km (600 km^2). The name

derives from the exposures of the formation around a prominent Tertiary tufa cliff called the "Blässkranz", after which the farm is named (cf. Korn & Martin, 1959, Plate 2). The area at which the base and top of the formation are best exposed is found on the mountain slope in the north-eastern corner of Blässkranz (Fig. 10). It is relatively undeformed here and the section above locality 30047 could therefore serve as a stratotype.

b. Description

(i) Lithology

The characteristic rock type of the Blässkranz Formation is a remarkable breccia consisting of an extremely wide size-range of angular, very poorly sorted "chips", pebbles, cobbles, boulders and blocks of black limestone and grey dolomite embedded in a fine matrix ranging in composition from limestone (locally dolomitized) through marl to shale. One large block of black limestone, with a length close to 10 m, has been observed with a marginal structure indicating that it was spalling smaller fragments of limestone into the surrounding breccia during the latter's formation (locality 30022, Plates 11 & 12). This is regarded as an indication of an origin by rapid down-slope slumping of a thin, lithified limestone layer.

(ii) Composition of inclusions

The majority of the inclusions in the breccia are of fine-grained dark blue-grey or black bituminous limestone. Some inclusions consist of an oolitic variety of this rock, or show distinct thin oolitic layers. The oolites occasionally show compositional zoning with cores and/or thin margins of dolomite.

Fine-grained grey dolomite constitutes a lesser proportion of the breccia inclusions. Occasional inclusions of an oolitic variety of dolomite are observed, particularly in the vicinity of the Tsubgaus Valley, north of the Blässkranz farmstead. It is difficult to determine whether these clasts are related to similar oolitic dolomites in the upper part of the Noab Formation, or whether they are related to the partly dolomitised, oolitic black limestone clasts found elsewhere in the Blässkranz Formation. The presence of rare brown and black oolitic chert inclusions in the Tsubgaus region, along with red-brown jasper fragments, is considered to be indicative of the Noab and Büllsport Forma-

tions, as similar silica replacement features are quite widespread in the latter.

A few inclusions of typical northern Noab sandy dolomites have been observed within the breccias (e.g. locality 30020 on Tsabisis Oos), but these are relatively rare. A very minor proportion (probably less than 1%) of the inclusions consist of highly sheared and (hydrothermally?) altered igneous rocks (CH157, CH159, CH169, CH170) representative of the crystalline basement of the Rehoboth inlier or its satellites within orogenic zone KR-II.

At one single point, below locality 30079, it was observed that a boulder of finer grained carbonate breccia had been incorporated within the main breccia. It is therefore evident that breccia formation within the Northern Pavian nappe occurred in at least two episodes. The older breccia inclusion was probably derived from an equivalent of the Remhoogte breccia unit which underlies the Blässkranz Formation. Alternatively, since the Blässkranz Formation is a composite of several (at least four) breccia units, it is possible that a lower unit was partly "cannibalised" to provide the breccia-within-breccia inclusion.

(iii) Composition of matrix

The matrix of breccia varies in composition from a fine shaly limestone or dolomite, through a marly shale or phyllite to a fine arenaceous shale. In the upper parts of the sequence (unit 7 in Fig. 10) the latter may grade locally into a fine-grained bedded sandstone containing angular dolomite and limestone clasts. In general, the matrix in the upper western parts of the Blässkranz breccia tends to be arenaceous; the matrix in the lower western parts of the breccia sequence tends to be phyllitic; and in the thin south-eastern sequence it tends to be entirely calcareous. This is probably an important clue to the direction of sedimentary transport in the breccias.

(iv) Bedding structure

On a large scale, the breccias have a distinctly bedded structure (cf. Fig. 10) reflecting in part large-scale and local compositional changes in the matrix and proportion or size of clasts (Plate 13). This appears to show that, in whatever manner the breccia components were transported into the depositional basin, they were probably subjected to some later sedimentary reworking.

The stratigraphic section (Fig. 10) shows seven distinct members. Units 1, 3 and 5 are composed of massive carbonate breccias with a shaly matrix. Each of these is capped by a thinner unit, showing a small-scale bedded structure. The lower units 2 and 4 are composed of finer grained bedded breccias with a calcareous matrix, while the upper unit 6 consists of a fine-grained calcareous quartzite grading downwards into shaly carbonate breccia. Unit 7 is a carbonate breccia with a more arenaceous matrix grading downward and eastwards into a shaly type; it too has a smaller scale bedded structure in its upper parts where interbedded thin calcareous quartzites and carbonate breccia reflect a transition (over a few metres at most) into the lower member of the overlying Tsabisis Formation. The calcareous quartzite interbeds range in thickness here from about 1 cm to 1 m (e.g. localities 30038-39).

Small-scale sedimentary bedding structures within the Blässkranz Formation are also most conspicuous at the very base of the formation at locality 30011 on the farm Tsabisis Oos. The Blässkranz Formation is here observed in practically undeformed condition (Plate 14), grading downward into a fine-grained basal layer in which sporadic lenses of coarser breccia are distributed (Plate 15). This remarkable large-scale reverse grading is undoubtedly significant for the mechanics of breccia formation at this point. Plate 15 illustrates a detail of the bedding structure at this locality in which a thin bed of fine, reverse-graded dolomite breccia is overlain by a very fine-grained limestone with a larger "dropstone"-like inclusion of dolomite.

(v) Thickness

The maximum thickness attained by the Blässkranz breccias is approximately 120 m in the north Blässkranz area (cf. Fig. 10). On the southern side of the Tsondab valley, tectonic deformation inhibits accurate thickness measurements. The formation, however, clearly thins towards the east since it is only 10 m in total (undeformed) thickness at locality 30012 on Tsabisis Oos.

c. Relationships to adjacent units

The Blässkranz Formation overlies the Remhoogte Formation with a distinct

unconformity (cf. Fig. 35), which can be observed at several localities on the northern side of the Tsondab River valley (e.g. below 30009 and 30079 and around 30028). The contact between the Blässkranz and Remhoogte Formations, though generally not well exposed in detail, appears abrupt. It is remarkable that there are no obvious inclusions of Remhoogte silicic rock types, such as the phyllites and quartzites, within the Blässkranz Formation, despite the appearance of oolitic limestone, dolomite and carbonate breccia inclusions which were probably derived from this unit.

The Blässkranz Formation is itself overlain conformably by the Tsabisis Formation at a thin transitional zone at which units of the two formations are interbedded. Over a wide area, however, the Blässkranz Formation is overlain directly by the massive dolomites of the Noab Formation at a major tectonic discontinuity which, from north-west to south-east, truncates the Remhoogte-Blässkranz and Blässkranz-Tsabisis contacts in turn.

d. Depositional environment

The Blässkranz Formation has been compared to a tillite (Korn & Martin, 1959; Kröner, 1974d) and to Alpine wildflysch (Korn & Martin, 1959). The term "wildflysch" is perhaps not appropriate to describe these rocks as, in modern usage, it refers to a chaotic sheared clastic deposit with an assemblage of rocks from only one tectonic environment. The Blässkranz Formation, however, contains blocks from more than one tectonic environment, including rock types from an older dolomite nappe by which it was subsequently overridden and also including scattered blocks of deformed crystalline or gneissic basement. It could therefore be described as a sedimentary *melange*, in the current sense of a mappable body of mixed assemblages in a sheared shaly matrix. The related descriptive term "olistostrome", referring to a sedimentary *melange* deposit with an unsheared matrix is also locally applicable to these rocks (cf. Plate 14).

The controversy over the Blässkranz Formation concerns the issue of the exclusive role of submarine slumping or debris-flow mechanisms in its formation or, alternatively, the role of other agencies such as glacial ice in the transport of the breccia components into the depositional basin. "Dropstone"

phenomena like that illustrated in Plate 15 are cited as evidence in favour of glacial transport mechanisms and it has been suggested that the spalling features illustrated in Plates 11 and 12 can be explained by ice action (G.M. Young, personal communication). Alternative non-glacial explanations are, however, at hand for both features. Interblock collisions during the final phase of momentum loss in a high-speed submarine slide can explain the apparent spalling from large blocks as part of the general process of disruption of a formerly coherent limestone-dolomite body. The "dropstone" illustrated does not actually pierce or deflect fine layering in the dolomitic limestone, which appears to have banked up around it. Together with the underlying reverse-graded fine breccia, it can be explained by a process of bottom-current winnowing of slumped material, or being approximately equidimensional it may simply have rolled into position down the distal slope of a newly arrived slump mass.

It is more difficult to explain the apparently random distribution of rare blocks of basement gneiss in the Blässkranz Formation. Any proposed mechanism of breccia formation must also provide the mechanism by which these rare inclusions became detached and incorporated. Transport of exotic material by glaciers or ice-bergs into a basin in which concurrent limestone and dolomite formation was taking place can be suggested but the palaeoclimatic objections to this hypothesis are obvious. An alternative hypothesis of tectonic (i.e. cataclastic) disruption of the basement along major fault zones and the local incorporation of near-surface fault-breccia into submarine slides which have themselves been triggered by earthquakes, slope oversteepening and sudden "de-buttressing" due to faulting, is suggested here.

The proposed mechanism for Blässkranz breccia formation is illustrated in Fig. 14. Deposition of limestone in a shallow-marine environment (oolites and dolomitisation) over a major fault-zone is envisaged. Motion on this fault is assumed to occur in "stick-slip" cycles. In the intervals in which the fault is "stuck", sedimentary deposition proceeds normally. Sudden slip on the thrust fault effectively "de-buttresses" the newly-deposited material on the hanging-wall side of the fault-trace and, aided by probable slope oversteepening which occurred slowly during the build-up of elastic strain

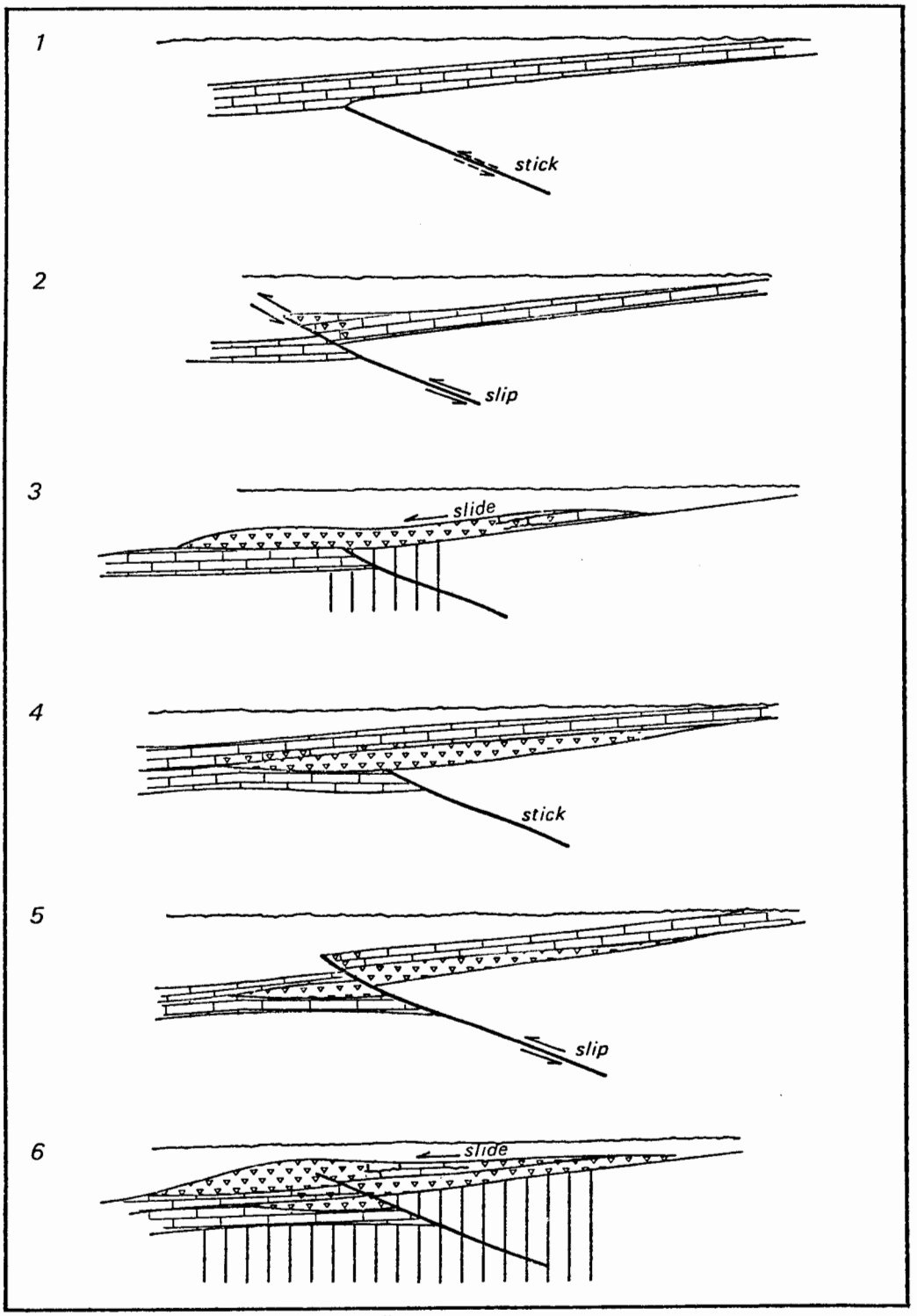

Figure 14. Two cycles of the three-stage, stick-slip-slide mechanism of Blässkranz breccia formation.

about the fault zone and also by transient earthquake stresses, this material slides down-slope over the footwall.

The "stick-slip-slide" cycle may be repeated several times to cause the accumulation of several distinct olistostromes, locally separated by bedded limestones or by bedded breccia forming the re-worked upper portion of a previous debris flow. The latter features, which are common in parts of the Blässkranz Formation, are probable indications that the Blässkranz debris-flows (in contrast to the Remhoogte breccia) did not move great distances down-slope into deep-water environments.

Depending on the amount of slip on the fault, relative to the thickness of carbonate sediments which have accumulated above it, it is possible that parts of the brecciated and sheared basement were exposed at surface and were accordingly incorporated in the subsequent debris flow. This is entirely consistent with the internally sheared and cataclastically-deformed condition of these basement blocks which also show mineralogical evidence (e.g. extensive replacement sericitisation of felspar and quartz-calcite veining) of intense hydrothermal alteration, all of which apparently pre-dates their incorporation into the Blässkranz Formation.

There are places beneath the Kudu nappe where the dolomitic Blässkranz Formation seems to grade upwards into brecciated dolomite of the Noab Formation. At these localities (e.g. above 30029) the impression is created that the Blässkranz breccias formed as a kind of tectonic melange or "friction carpet" beneath the advancing Kudu nappe. Elsewhere, however, the intervening presence of the Tsabisis Formation renders this hypothesis untenable but, because the contact zone between the two formations is not well-exposed and locally sheared (e.g. below locality 30079), it is essential to be certain that this contact is itself not a thrust. The presence of a dolomite-purple shale facies in the Tsabisis Formation, part of which was formerly included in the "Kudu Series" (Korn & Martin, 1959), enhances the latter possibility, but field investigation of the contact zone between Tsubgaus and Tsabisis completely eliminates it. At locality 30043 especially, there can be no doubt that there is simply a conformable sedimentary transition between the two formations.

Despite the elimination of the tectonic melange hypothesis for most of the Blässkranz breccia, it is probable that it is locally in contact with true tectonic megabreccia developed near the base of the Kudu nappe. In this respect, a possible Mesozoic analogue of the Blässkranz breccias is probably represented by the gradations from sedimentary dolomite breccia with water-laid features into tectonic megabreccia and so-called "chaos material", described from the Silurian Hills of San Bernadino County, California (Kupfer, 1960). Longwell's (1951) hypothesis for a similar rock-type may be quoted in this connection:

> "...differences between a breccia of this type and the chaos may in some circumstances be gradational. A thrust block above a fault with moderate to low inclination presumably would supply fragments of exceptional size, would aid gravity in propelling the debris down-slope,and conceivably might progressively override the debris, to form a chaos sheet of large dimensions" (*op.cit.*, p.354).

Another possible analogue, in this case Palaeozoic, is represented by the Cow Head limestone conglomerates of Newfoundland (Kindle & Whittington, 1958). This example is especially instructive since, by palaeontological dating of the larger blocks, it has been shown that the conglomerates, in a thin 300 m sequence, originated during the long time-span (about 75 Myr) from the Middle Cambrian to Middle Ordovician. The Cow Head Group is also explained by the serial submarine sliding of strata "of a limited horizon only" (*op.cit.*, p.340) from submarine thrust faults of minor surface displacement.

In connection with these Phanerozoic analogues, it is relevant to note that they have both formed in the tectonic environment of a major subduction zone, in close association with the emplacement of ophiolite or ophiolitic melange nappes. A further parallel with this tectonic environment can be drawn in a comparison between the Blässkranz olistostromes and the carbonate-breccia olistostromes at the base of the Vourinos ophiolite nappe in Greece (Naylor & Harle, 1976); this comparison is remarkable in also including the rock types which occur in the base of the overlying Tsabisis Formation.

4. Age and correlation of black limestone-bearing formations of the Kudu and Northern Pavian nappes

a. Correlation between nappes

The Klipbokrivier, Remhoogte and Blässkranz Formations all contain characteristic dark, bituminous limestone beds and carbonate breccia units. Furthermore, associated green chloritic shales and phyllites are common to the Klipbokrivier and Remhoogte Formations. The "striking" resemblance of the Klipbokrivier breccia limestones to those in the Pavian nappe was noted by Korn & Martin (1959, p.1060). With the evidence for a major inversion of original stratigraphy about the Kudu and Northern Pavian nappe contact, it could be assumed that there is a direct correlation between the limestone-pelitic facies in these nappes. The younger age of the "Klipbok Series" with respect to the "Pavian Series" was formerly regarded as proved by the presence of characteristic sandy dolomite inclusions from the Noab Formation in the former and their absence from the latter (Korn & Martin, 1959).

This observation no longer applies to the relationship between the Klipbokrivier Formation and the Blässkranz Formation, since sandy dolomite and other oolitic chert inclusions characteristic of the Noab Formation have been observed in both units. It probably still applies to the relationship between the Klipbokrivier breccia and the minor breccia units within the Remhoogte Formation, but does not necessarily mean that the Remhoogte Formation is older than the Noab Formation while the Klipbokrivier and Blässkranz Formations are both younger; it may simply indicate that the Kudu nappe had not become fully emergent at the time that parts of the Remhoogte Formation were being deposited. The presence of boulders of gneissic basement in the "boulder shales" of the northern Remhoogte Formation, on the other hand, suggests that the Noab Formation either never existed in, or had already been completely eliminated by erosion from, the provenance of those rocks.

The sequence of events which can be inferred from observations of lithology and stratigraphy in the Kudu nappe and the lower parts of the Northern Pavian nappe is therefore as follows:

(i) Deposition of the Noab and Büllsport Formations, probably somewhere to the north of the present Nauchus highlands;

(ii) Reversal of the northward palaeoslope, uplift along the southern margin of the Damara belt and exposure of basement cordilleras resulting in rapid deposition of shales, subgreywackes and coarse conglomerates in a shallow (?) marine basin where local accumulations of dark, bituminous, occasionally oolitic, limestones and dolomites were forming in sub-environments that were protected (by orogenic topography ?) from influx of clastic material;

(iii) Uplift and emergence of the dolomite Kudu and Dassie nappes (probably as a single unit) resulting in early deformation and erosion of the part of the Remhoogte Formation and faulting within the dolomite nappe;

(iv) Subsidence of the Kudu nappe and the deformed Remhoogte Formation leading to deposition of further chloritic shales and subgreywackes and allochthonous limestone breccia unconformably on the Noab Formation (Klipbokrivier basin) and deposition of limestone and dolomite breccias unconformably upon the Remhoogte Formation on a steeper southward slope subject to episodes of submarine slumping (Blässkranz basin); probably related to further nappe movements, tectonic oversteepening of basin slopes and triggering of slumps by associated earthquake activity.

In this model of the stratigraphic evolution of the Kudu nappe and part of the Northern Pavian nappe, the Blässkranz and Klipbokrivier Formations are correlated but the Remhoogte Formation (or at least those parts of it that immediately underlie the Blässkranz Formation) is considered to be slightly older. The general tectonic and sedimentary environment of both groups of rocks was, however, practically identical and the age difference implied by the unconformable relationships can be interpreted as evidence of the southward migration of a foredeep basin in the front of an advancing complex of crystalline basement and (later) dolomite nappes. In this respect, the Klipbokrivier and Blässkranz basins are simply "successors" to the Remhoogte basin.

b. Other correlations

Minor occurrences of black limestone breccia are found elsewhere within the Naukluft complex, in the Southern Pavian nappe and in part of the Zebra River Formation. A similar rock type is also reported from the Kuibis Formation in the Rietoog nappe (Korn & Martin, 1959, p.1054). In general, it is true that

the black limestone-green shale facies is typical of the Kuibis Formation in the Nama Group. On purely lithological grounds, it therefore seems natural to correlate all formations of this facies with the Kuibis Formation, regardless of the local unconformities which might separate them. These unconformities can be considered as basin margin phenomena, reflecting the southward migration of the orogenic front bounding the foredeep basin, but this simple concept faces severe difficulties in connection with the uppermost unit of the Northern Pavian nappe, the Tsabisis Formation and the lowermost unit of the Southern Pavian nappe, the Aubschlucht Formation.

c. Age

Evidence discussed in the following section indicates an age close to 650 Myr for the Blässkranz Formation.

D. TSABISIS FORMATION

1. Introduction

The Tsabisis Formation includes the uppermost part of the former "Pavian Series, northern facies" but also incorporates the lowermost part of the former "Kudu Series", on grounds that are explained below. The formation is characterised by the presence of a thin unit of volcaniclastic rocks at its base, which had previously escaped notice.

Like the Blässkranz Formation, the Tsabisis Formation is confined to the south-eastern parts of the Northern Pavian nappe. It is most extensively represented on the farms Tsabisis and Tsabisis Oos, from which its name is derived, but the sections in which the lower part of the formation is best exposed occur on the steep mountain slopes in the north-east corner of Blässkranz (localities 30009 and 30079). These mountain sections (Figs. 15 and 16) may be regarded as the stratotype for the lower boundary and most characteristic parts of the Tsabisis Formation.

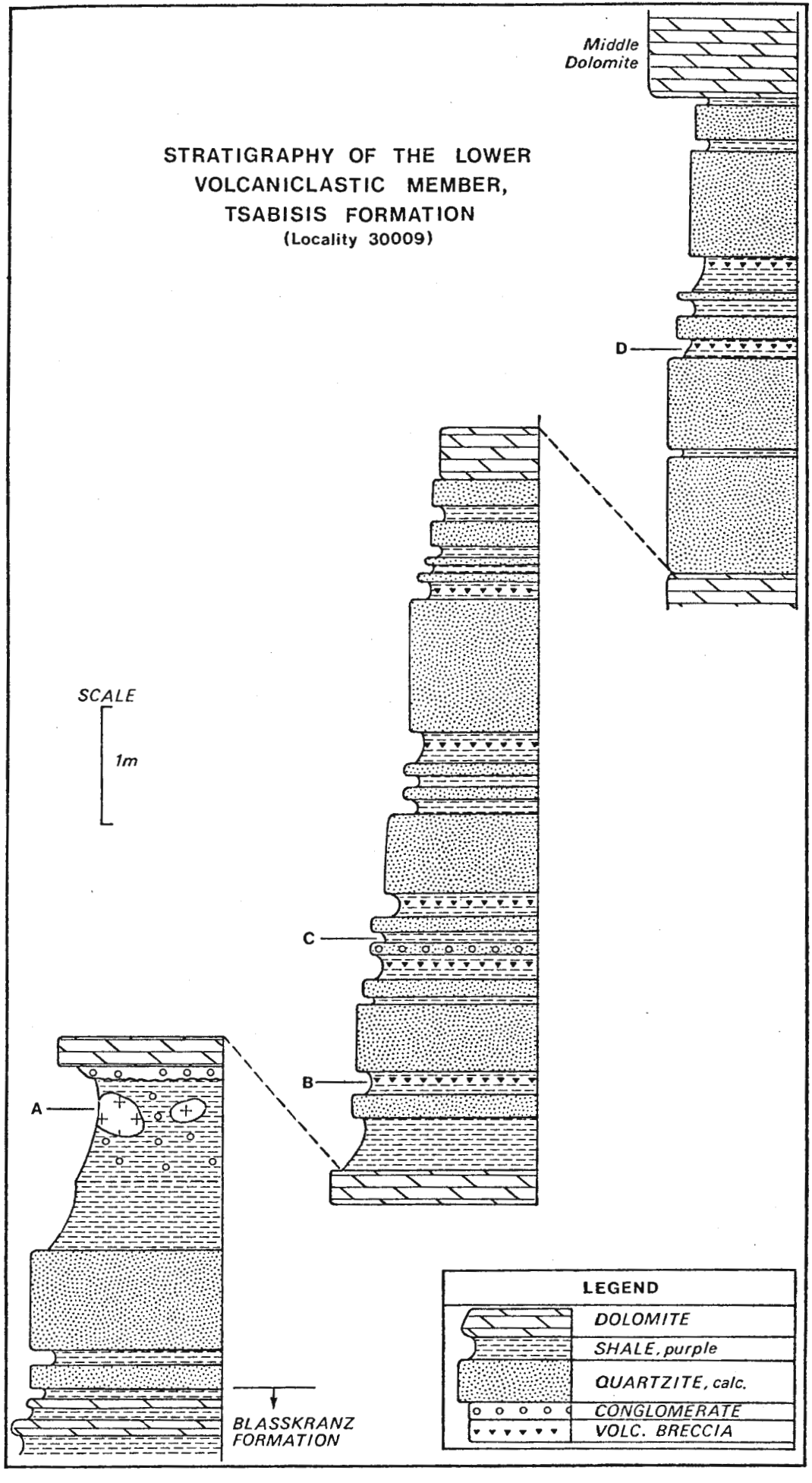
STRATIGRAPHY OF THE LOWER VOLCANICLASTIC MEMBER, TSABISIS FORMATION
(Locality 30009)
Middle Dolomite
D
C
B
A
SCALE
1m
BLASSKRANZ FORMATION
LEGEND
DOLOMITE
SHALE, purple
QUARTZITE, calc.
CONGLOMERATE
VOLC. BRECCIA

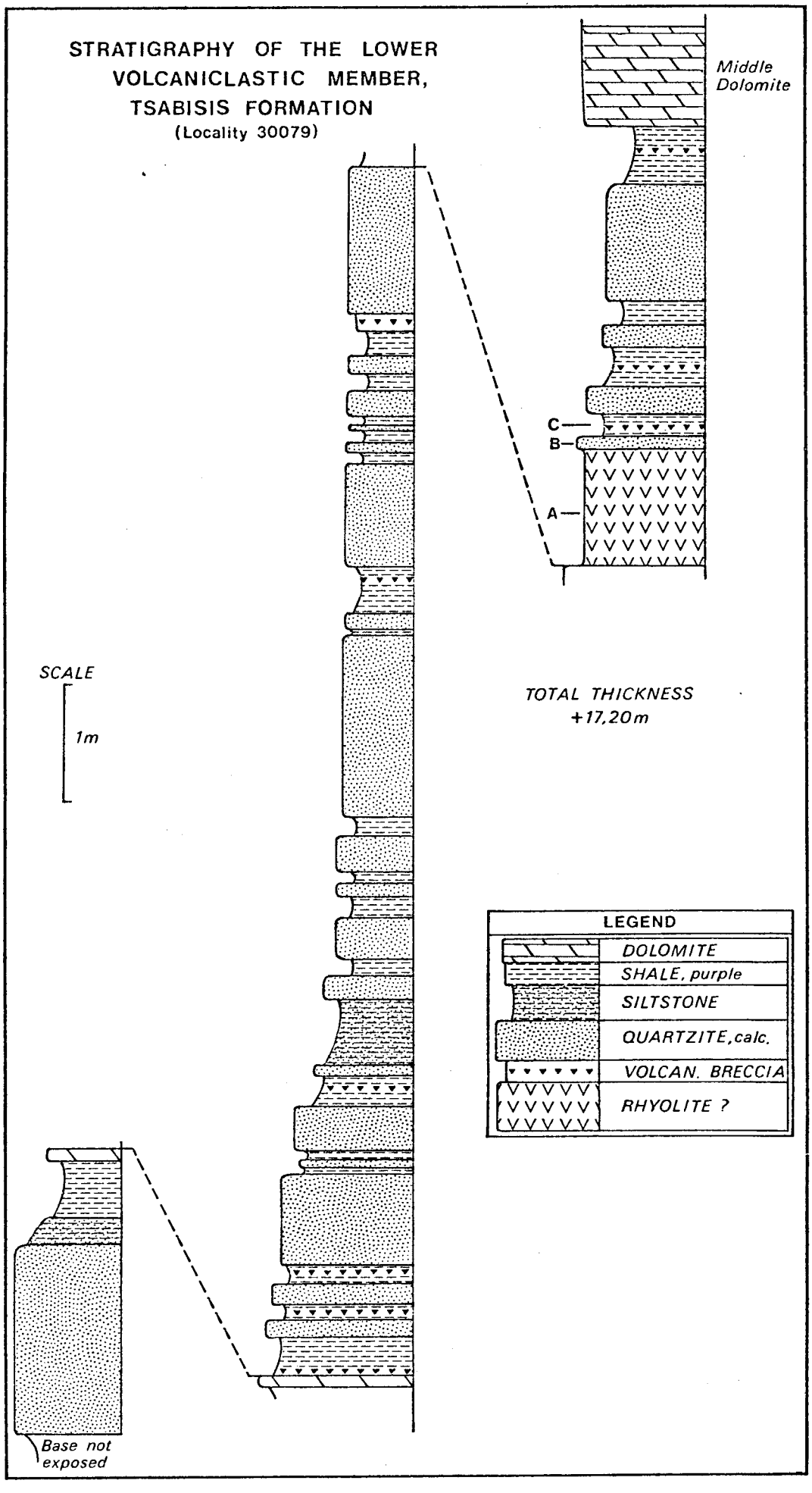
STRATIGRAPHY OF THE LOWER VOLCANICLASTIC MEMBER, TSABISIS FORMATION
(Locality 30079)
Middle Dolomite
C
B
A
SCALE
1m
TOTAL THICKNESS
+17,20m
LEGEND
DOLOMITE
SHALE, purple
SILTSTONE
QUARTZITE, calc.
VOLCAN. BRECCIA
RHYOLITE ?
Base not exposed

2. Description

a. Stratigraphic sequence

The Tsabisis Formation consists of three distinct members: a lower volcaniclastic unit, a middle dolomite member and an upper sequence of purplish, hematitic shales (slates) with thin dolomite interbeds (Fig. 35). The middle and upper parts of the sequence are not further described but the thin lower unit has been stratigraphically analysed in great detail at two well-exposed sections in the stratotype area (Figs. 15 and 16).

These show that the dominant rock-type in the unit is a fine-grained calcareous sandstone or coarse siltstone, very similar to that which is interbedded with the uppermost parts of the Blässkranz Formation. Interbedded with these generally quartzitic layers, are purplish shales and siltstones which constitute the next most abundant rock type. They grade into tuffaceous volcaniclastic breccias, ranging in scale from millimetre-thin microbreccia layers (Plate 16) to "boulder beds" up to a metre or more in thickness and containing some clasts several decimetres in diameter (Plate 17).

Within the principal stratotype section at locality 30009 (Fig. 15) two thin but conspicuous brown dolomite beds divide the sequence into three parts. The upper dolomite is not present in the section at 30079 (Fig. 16), which is less than 500 metres distant and its place in the sequence appears to be taken by a layer of (autoclastically?) brecciated felsitic or microgranitic material (Plate 18). Much farther eastward, however, at locality 30024 on Tsabisis Oos two identical brown dolomite layers appear within the lower Tsabisis Formation, indicating that these episodes of chemical sedimentation are indeed traceable over a wide area and that the threefold subdivision of the volcaniclastic member of the Tsabisis Formation, implicit in the stratigraphic section, is generally valid.

The "boulder shale" lying immediately below the first dolomite in the section at locality 30009 (Plate 17) is also not present farther north-eastward; it is, however, remarkable that a thin, characteristic double layer of green microbreccia within purple shale (Plate 16 and upper right of Plate 18)occurs

at the same level in both sections, i.e. at level marked D in Fig. 15 and C in Fig. 16. The fact that a single layer of volcanic material less than 5 cm in thickness was deposited uniformly over a distance of at least 500 m seems to point conclusively to a pyroclastic origin and a complete lack of later sedimentary re-working.

b. Lithology

(i) Calcareous sandstone and siltstone

Macroscopically these rocks are very fine-grained and finely layered within individual beds which tend to be quite massive (cf. Plate 16, upper right). Microscopically they are seen to consist of angular, frequently lath-shaped clasts of quartz with ubiquitous felspar (mainly K-felspar but probably also some plagioclase). Average grain size may vary from less than 0,05 mm (CH82) to about 0,2 - 0,5 mm (CH86). The coarser grained variety is more felspathic (up to 15% K-felspar) and the matrix is more siliceous (illite/phengite and chlorite in CH86, as opposed to pure carbonate in CH82). The grains are partly suspended in the matrix, giving the rock a wacke-like texture. Conspicuous trace components are zircon grains (CH86) and scattered pelletal aggregates of glauconite (CH82, CH86). Scattered grains of hematite, partly limonitised, are also characteristic.

The discovery of glauconite in these rocks is significant for both the original sedimentary and later metamorphic environmental conditions. In the prehnite-pumpellyite quartz facies of very-low grade metamorphism, glauconite reacts with quartz and chlorite to form stilpnomelane and K-felspar (Frey, 1973). It would therefore seem that there is a distinct difference in metamorphic grade between the Remhoogte phyllites and the Tsabisis siltstones and slaty shales.

Near the base of the Tsabisis Formation, poorly sorted, coarser grained (up to 5 - 10 mm) felspathic sandstone may contain isolated inclusions of limestone or dolomite derived from the underlying Blässkranz Formation (CH84).

(ii) Purple siltstone and shale

There is a complete gradation from the former rock types to coarse siltstones with a deep purplish hue, by increase in the proportion of matrix

containing finely disseminated grains of hematite. There is generally a fine compositional layering in these rocks on the scale of 1 - 5 mm with some indication of size-grading (CH80).

Microscopically the larger clasts are seen to consist of almost equal amounts of quartz and usually highly altered K-felspar, all are extremely angular and poorly sorted, many having tabular or elongate wedge shapes (CH80, CH87). Because altered ("sericitised") K-felspar clasts are randomly interspersed with unaltered K-felspar grains, the conclusion seems inescapable that the alteration occurred prior to their incorporation as clastic fragments in the sediment. The fact that the grain-size of the white mica in the altered clasts is significantly larger than that of the fine white mica in the matrix (CH87), suggests that the cause of the alteration was not simply weathering but intense hydrothermal activity ("propylitization").

These remarks apply also to the minor proportion of altered volcanic fragments that occur in the siltstones. Many of these have unusual shapes which make it virtually certain that they were pyroclastically derived and incorporated in the siltstone with a minimum of sedimentary re-working (CH87). Along with K-felspar such as microcline and microperthite, a very small proportion of the clasts observed in thin section are of deep-seated metamorphic and igneous rock types including exotic fragments of biotite granite or gneiss and some mylonitic quartz schist. From this it is inferred that the centre of explosive volcanism, active during deposition of the Tsabisis Formation, was not separated from crystalline basement by a great thickness of sedimentary rocks.

The existence of centimetre-scale exotic basement fragments embedded in purple shale is illustrated in Plate 19 (from layer marked C in Fig.15). Low in the stratotype sequence (layer marked A in Fig. 15), the purple shales grade into remarkable "boulder shales", containing inclusions of exotic rock types, mainly sheared granitoids, up to 0,5 m in diameter (Plate 17). The precise mechanism by which these blocks were transported and deposited in volcaniclastic shales remains an intriguing question; if they too are pyroclastic ejecta, their size presumably implies that the Tsabisis depositional basin and the volcanic source were in relatively close proximity and that the source had

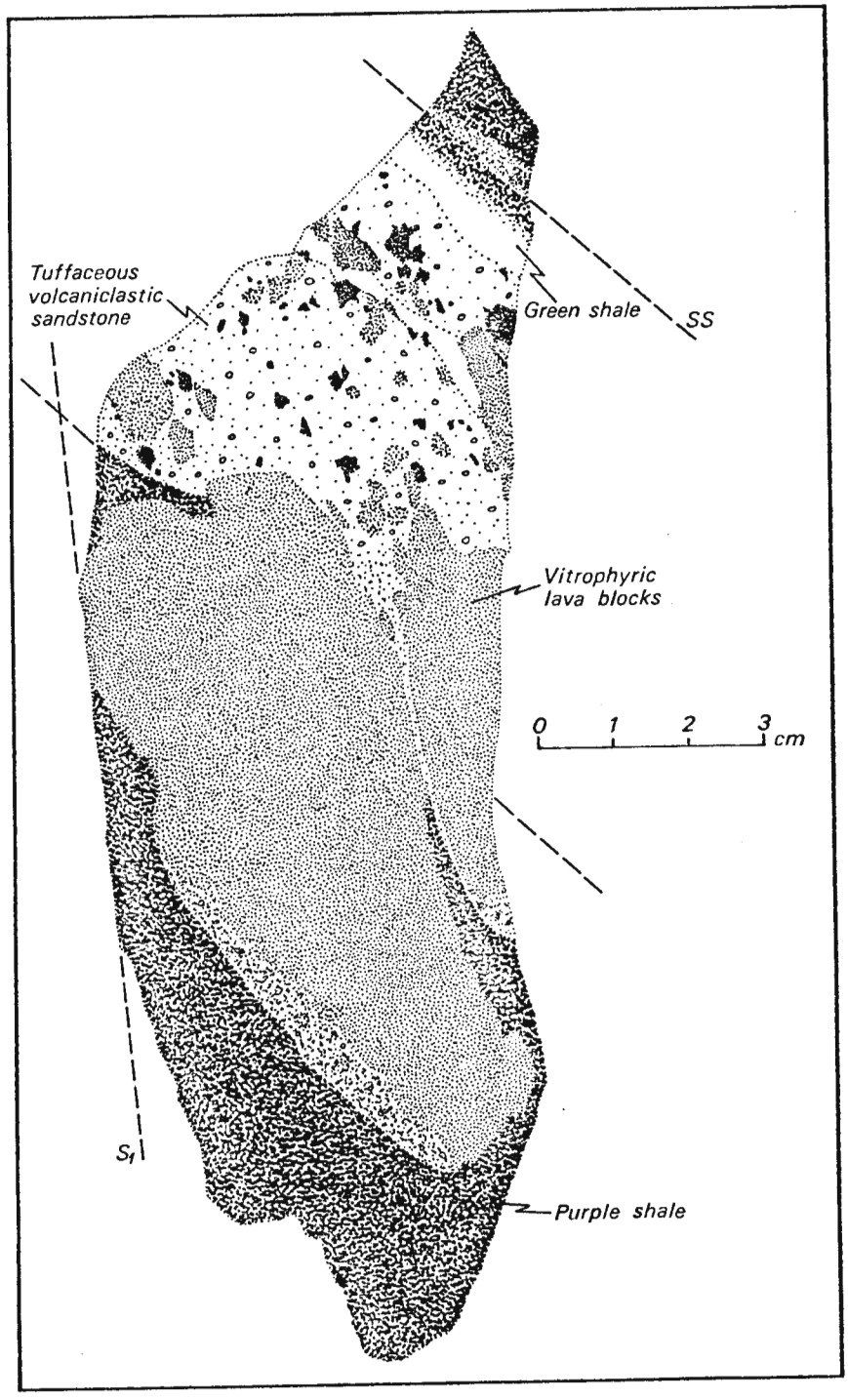

Figure 17. Sketch of a hand specimen of a tuffaceous volcaniclastic sandstone layer in purple slaty shale of the Tsabisis Formation, collected near locality 30002 on farm Blässkranz. Larger blocks of a vitrophyric volcanic rock measuring up to 10 x 3 cm in section are conspicuous at the base of the sandstone layer.

enormous explosive power. The majority of the exotic inclusions in the boulder shales are of porphyritic (CH92) and vesicular (CH91) felsic volcanic rocks.

(iii) Volcaniclastic sandstone and breccias

The purple siltstone, locally grading from the calcareous sandstone beds, in turn grade locally into volcaniclastic sandstones and microbreccias. The shard-like shape of many crystal clasts in these rocks, particularly of quartz, is striking (CH95), elongate isoceles-triangular and rhombic forms, many with concave boundaries, being common in thin section. In contrast, some coarser types of volcaniclastic sandstone are conspicuous for the presence of sub-rounded to well-rounded clasts of quartz and K-felspar, mostly with thin hematite coating (CH83). A significant proportion of the lithic fragments (all volcanic) are also highly ferruginised, their original (glassy?) matrix having been almost totally replaced by opaque hematite. Most have microporphyritic textures with fine laths of felspar (0,1 mm in length) randomly orientated in a semi-opaque devitrified matrix, but some have trachytic textures (CH89).

The interstitial matrix consists mainly of extremely fine-grained white mica and quartz with subordinate chlorite. Some epidote has formed, apparently from small clasts of plagioclase in the matrix, consistent with very-low grade metamorphism during the moderate deformation and cleavage of the rock.

The rocks described in the sections as volcaniclastic breccia are apparently a kind of lapilli tuff (Plate 20). These layers are generally 5 - 10 cm thick and enclosed within purple volcaniclastic shale beds. Most of the lapilli are irregularly shaped brownish fragments of fine-grained volcanic rock with characteristic felty, hyalopilitic, pilotaxitic or even trachytic textures; many show marginal alteration to a light yellowish-green colour and some are completely discoloured in this way (CH88). With this type of volcanic material, there also occurs a darker, more coarsely porphyritic type which occurs as angular blocks up to 5 cm in length (cf. Plate 20, upper left part of central breccia layer). This rock (e.g. in CH88) also has a felty matrix in which fine felspar microlites (now completely sericitised) are distributed in a semi-opaque matrix; this matrix encloses 2 - 3 mm K-felspar phenocrysts several of which show perthitic intergrowth textures.

(iv) Felsite/microgranite (?)

Intercalated within the upper part of the volcaniclastic sequence at locality 30079, is an 80 cm-thick layer of brecciated felsitic material (layer marked A in Fig. 16) resting above a thick calcareous quartzite bed and overlain with a clear sedimentary contact by a thinner quartzite layer; it cannot therefore be intrusive (Plate 18). In thin section (CH119) it is seen to consist of quartz and partly sericitised K-felspar with an average grain size of about 2 mm. The remarkable feature of the rock is the cataclastic (?) deformation, which is evident in fractured felspar grains with quartz-calcite veining and the associated plastic deformation of the quartz grains, reflected by undulose extinction and deformation lamellae passing locally into a subgrain mosaic structure. This deformation clearly predates deposition of the overlying sandstone layer since the latter incorporates a rounded boulder of the deformed felsite (Plate 18) and is itself only slightly deformed. There are no obvious effects of this deformation on the underlying layer either.

The emplacement of this rock unit remains imperfectly understood.

(v) Dolomite

No further remarks on these intercalations are necessary, except that they may mark diastems in the volcaniclastic sequence during which slight erosion, followed by the formation of an evaporitic (later dolomitised) crust took place under playa-like conditions.

3. Relationships to adjacent units

As mentioned several times previously, the Tsabisis Formation overlies the Blässkranz Formation with a conformable and partly transitional contact. The lower boundary can be defined as the calcareous quartzite immediately overlying the last carbonate breccia layer. The upper boundary of the Tsabisis Formation is tectonic; it is overlain by the Noab Formation in the Kudu nappe. The two formations are, however, separated by a zone of approximately 10 m thick, consisting of highly deformed pinkish marble with purple phyllite intercalations. This tectonic zone is not seen where the Kudu nappe overlies units of the Remhoogte and Blässkranz Formations directly, but is widespread at the base of the nappe

south-east of the Tsabisis Formation exposures. From this observation it is assumed that the marble-phyllite zone may, in part at least, be a sheared mass of the upper Tsabisis Formation, which became entrained at the toe of the nappe.

The Tsabisis Formation also locally overlies a slice of the Kudu nappe in the gorge of the Tsondab River between Büllsport and Blässkranz, immediately west of Pavianskopf. This is one of the means of recognising that a later thrusting episode has deformed the Kudu nappe in this region.

4. Depositional environment

The lower part of the Tsabisis Formation evidently represents a gradual shallowing of the tectonically unstable marine basin which existed during deposition of the Blässkranz Formation. In the calcareous sandstone and siltstone units, cross-bedding (some of the festoon type) is locally conspicuous and of course, the sedimentary material with its volcanic component is terrigenous. The presence of glauconite in these rocks is an indicator of a marine environment and also of very slow sedimentation.

The volcaniclastic component in the lower Tsabisis Formation is clearly derived from a highly explosive source with a dacitic to rhyolitic composition. The origin of perhaps the majority of the particles in the volcaniclastic breccias and also the purple shaly siltstones seems obviously pyroclastic on account of their angular, tabular or shard-like shape. The coarse terrigenous epiclastic material found in some layers along with the pyroclastic particles is also exotic, since it is difficult to reconcile the presence of coarse, rounded fragments of iron oxide-coated quartz and microcline with slow sedimentation in a shallow marine basin; it is therefore assumed that this material was entrained along with the pyroclastic material near the volcanic source.

These particles, together with the larger exotic boulders of gneissic basement rock, seem to indicate firmly that the volcanic source was situated on land above sea-level. Although the outcrops of the Tsabisis Formation are too restricted to provide firm evidence as to the source direction relative to

the present situation of the Northern Pavian nappe, there is some indication from the greater abundance of coarse "boulder shale" volcaniclastics in the Tsabisis Oos area that it lay to the north or north-east; this is consistent with the evidence for the direction of the earlier source of the Blässkranz debris-flows.

The change of environment represented by the middle Tsabisis "white dolomite" member probably reflects the extinction of volcanic activity and disappearance of the small land-mass which it formed, thus accounting for the complete absence of a siliceous terrigenous component in this member. The similarity of this unit and the overlying purple shale member to parts of the Büllsport Formation is considered to support the possibility that the latter had now become partly emergent above a thrust-plane at the base of the Dassie nappe and was contributing material to the shallow basin over which it was advancing.

In this model, this last event is considered to be the culmination of the tectonic activity and gradual shallowing of the Blässkranz-Tsabisis sedimentary basin. With the passage of the Dassie nappe (at that stage forming the leading edge of the Kudu nappe; cf. Chapter IV) over the Tsabisis Formation, the sedimentary history of the Northern Pavian nappe was finally brought to a close.

The association of olistostromic breccia formation with succeeding calc-alkaline volcanic activity in a sedimentary basin which was later overridden by a major nappe structure is highly significant. A comparable association of olistostromes and calc-alkaline volcaniclastic rocks, also lying above a tidal-flat dolomite facies and subsequently overridden by a large thrust nappe, is described from the Ayios Nicolaos complex in Northern Greece (Naylor & Harle, 1976). In this case, however, the overlying nappe is the Vourinos ophiolite, interpreted as a fragment of oceanic crust. Reconstructing the tectonic evolution of the Naukluft complex (Chapter IV), it is evident that the Northern Pavian nappe was originally situated within the KR-II tectonic zone, in an area now partly occupied by highly deformed formations containing mafic rocks which can be interpreted as an ophiolitic *melange* complex. The olistostrome-volcaniclastic association of the Blässkranz and Tsabisis Formations is considered to support the interpretation of the KR-II zone as a subduction complex.

5. Correlation and age of the Tsabisis Formation

The lithological association represented by the Tsabisis Formation, is as yet, unique in the southern zones of the Damara belt. It has not been recognised in zone KR-I and is unlikely to have gone undiscovered elsewhere in this zone which is not highly deformed and is metamorphosed only to low grade. In zone KR-II, however, volcanic rocks equivalent to the Tsabisis Formation may be present but may have escaped recognition because of the much more intense Damaran deformation and metamorphism in this zone. A possibility is the so-called "Red Band" (De Kock, 1934; De Waal, 1966) for which an origin as an acid volcanic unit has been suggested (R. McG. Miller, personal communication).

Elsewhere in SWA/Namibia, the nearest lithological sequence comparable with the Tsabisis Formation and Blässkranz Formation is found near the Rosh Pinah mine about 420 km to the south of the Naukluft complex, near the Orange River. In units formerly described as the Kapok Formation and Numees Formation and now placed in the lower Hilda Formation of the Gariep Group (Kröner, 1974b), a sequence of acid volcanics and pyroclastics overlying a "quartzite-diamictite-carbonate" sequence has been identified (Hoffmann, 1972). The latter appears to correspond with the Blässkranz olistostromes. The lower Hilda rocks have been intensely deformed in partly recumbent structures with an eastward vergence, apparently during an episode in which a large nappe, including an apparent ophiolite complex (the Grootderm Formation; Kröner, 1974b) and widespread glaucophane-schist occurrences (Kaiser, 1926), overrode them from the west. An age of approximately 720 Myr is presently accepted for the Hilda Formation.

Reconnaissance attempts have been made to date the Tsabisis volcanic materials (Hartnady, 1975a; Kröner, 1976) and a four-point whole rock Rb-Sr errorchron of 633 ±55 Myr has been provisionally reported (Reid & Kröner, in Kröner, 1976a). The significance of this age estimate is still uncertain, since it is clear from petrographic observation that the volcanic material was extensively altered hydrothermally (propylitised) prior to its incorporation in the volcaniclastic sediments, where it probably underwent further diagenetic change. Fragments of older gneissic rock were mixed with the juvenile volcanic material in the sediment and moreover the whole system subsequently underwent very

low-grade metamorphism in a system in which fluids probably played a prominent role, as evidenced by quartz-calcite veins associated with the formation of rock cleavage. The usefulness of a whole-rock isochron approach to dating the Tsabisis Formation is severely circumscribed by these factors.

Nevertheless, in the absence of any firm contradictory evidence, an age of approximately 650 Myr can be accepted for the Tsabisis Formation. This also represents a likely maximum age for the Nama Group and it can be argued on the basis of structural evidence and lithostratigraphic comparison that the rocks of the Northern Pavian nappe are all definitely older than the Kuibis Formation. If the comparison of the Northern Pavian nappe formations with the Hilda Formation is valid, the age of the Tsabisis Formation may be closer to, or even greater than, 700 Myr.

E. ZEBRA RIVER FORMATION

1. Introduction

The Zebra River Formation is the renamed former "Zebra Series" (Korn & Martin, 1959), the new name deriving from the Zebra River on farm Lemoenputs (cf. *op.cit.*, Pl. 1 and Annex. I of this work). It is characterised by interbedded grey dolomites and sandy shales or siltstones, with minor proportions of calcareous quartzite, conglomerate and black bituminous limestone.

The Zebra River Formation is extensively developed over the south-western part of the Naukluft complex, but a small detached tectonic outlier occurs in the nappe front east of Büllsport and it is probable that a major part of the S. Pavian nappe may correlate with certain members (Annex. I). Five easily recognisable members of the Zebra River Formation have been identified and mapped throughout a major part of its outcrop area. This lithostratigraphic mapping emphasizes the great difference between the structural style of this formation and other units within the Naukluft complex.

2. Description

a. Stratigraphic sequence

The five members of the Zebra River Formation are comprised of three dominantly carbonate (i.e. dolomite) units and two dominantly clastic units. A stratigraphic section of the formation is given below (Fig. 18) which shows that a further subdivision of each of these "members" is possible. In fact, it appears as if each of the members of the Zebra River Formation should have formational status at the present scale of mapping and that the Zebra River sequence should be raised in rank to Subgroup or Group status. Pending more detailed attention to the sedimentology and palaeontology of the Zebra River units, with particular reference to their probable correlation with a part of the Nama Group outside the Naukluft nappe complex, the present lithostratigraphic nomenclature therefore remains provisional.

A remarkable feature of the Zebra River sequence is the abruptness of contacts between the dolomite facies and the clastic facies. This lack of transitional contact relationships suggests that several important hiatuses in sedimentation exist within the generally conformable sequence (G.J.B. Germs, personal communication). In fact, conformable contact relationships, which are widespread in the western and southern part of the Zebra River outcrop, give way eastwards to at least one major intra-sequence unconformity.

The provisional stratotype from which the stratigraphic section (Fig. 18) has been compiled in near locality 70010 on Ubusis at the south-western front of the Naukluft complex, in the cliffs of the Johann-Albrecht-Felsen (cf. Korn & Martin, 1959). These exposures and the stratigraphy and structure displayed therein are illustrated photographically in Plates 21-24. The carbonate members of the sequence form steep cliffs, whereas the two intervening clastic members form slopes of more subdued relief and gentler angle (cf. Plate 24 in which the entire Zebra River Formation is illustrated). Each of these members has been named after a farm on which it is thickest or otherwise best represented, but more detailed stratotype sections from these localities have not yet been prepared. Because of the scarcity of named

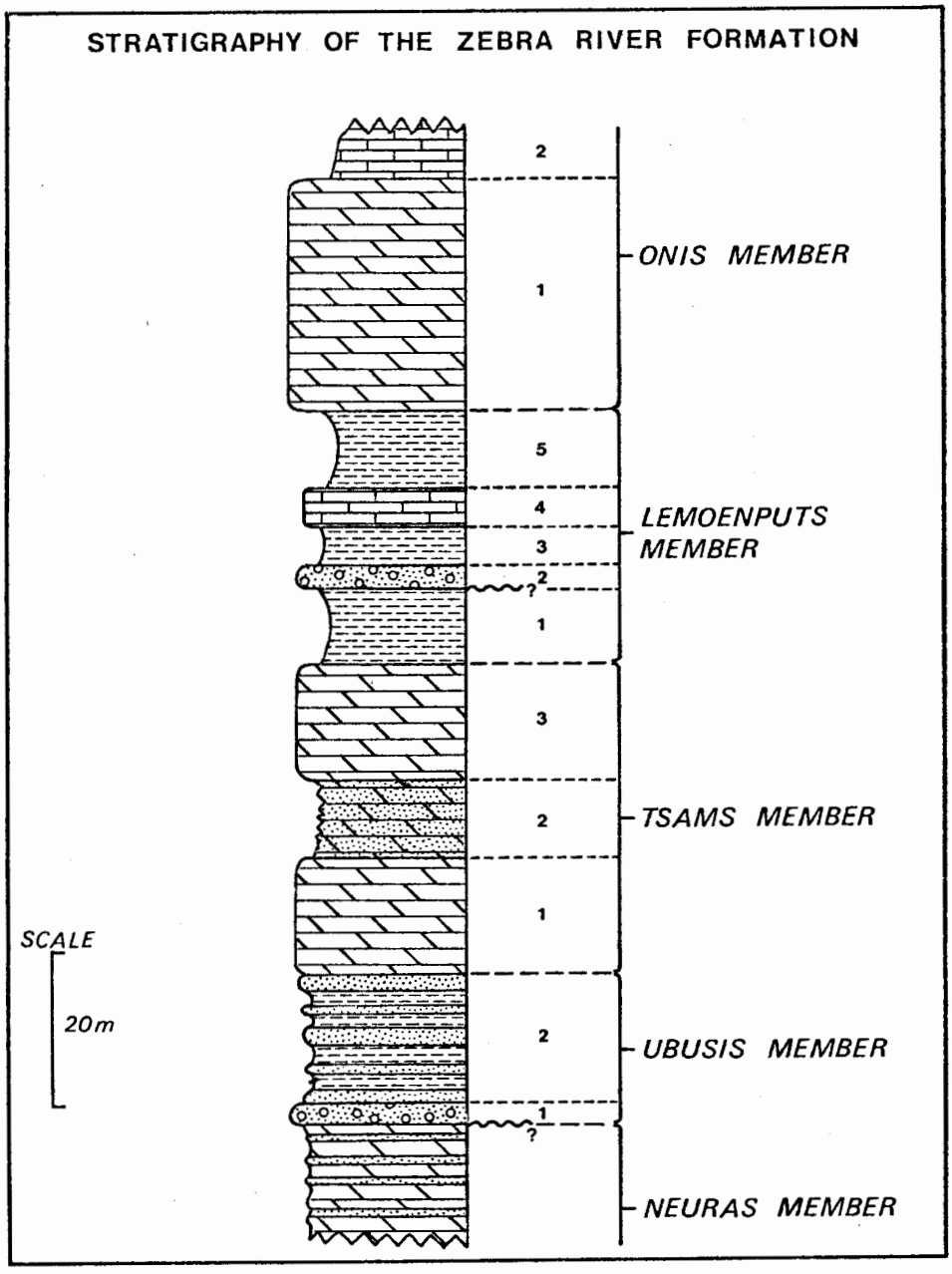

Figure 18. Stratigraphic column for the Zebra River Formation, showing its subdivision into three dominantly carbonate and two dominantly clastic members, and the further subdivision of these members into "beds" of uniform lithological composition.

localities in this terrain, two of the members are named after farms on which they are either only marginally represented (i.e., the Neuras Member) or which are simply overlooked by adjacent cliff-side exposures (i.e., the Onis Member which is not actually present on farm Onis but is best exposed in the cliffs adjacent to its north-western boundary; cf. Plate 24).

b. Lithology

(i) Neuras Member

The basal dolomite unit consists of about 50 m of whitish dolomite regularly interbedded with thin dark layers of quartzitic sandstone, some dolomite beds being themselves sandy in places. It has its maximum development in the extreme south of the Naukluft complex (e.g. Plate 21) where it forms a zone of vertical cliffs immediately above the Unconformity Dolomite. Going eastwards along the nappe front, this zone thins noticeably until it disappears near the Naukluft stream (cf. Annex. I).

In the north of the Zebra River outcrop, the Neuras Member dolomites unconformably overlie similar dolomites of the imbricated upper Büllsport Formation (Fig. 54), and have a locally complex internal structure (described below in Chapter IV). The lithological similarity between Neuras and Büllsport dolomites and the eastward thinning and eventual disappearance of the unit along this northern contact also, formerly led the writer to misclassify the Neuras Member dolomites as "uppermost Dassie Formation" (Hartnady, 1974, p.85).

(ii) Ubusis Member

The type section for this member is in the upper part of the Johann-Albrecht-Felsen where it forms a conspicuous dark unit between the lighter-coloured, more resistant dolomites of the Neuras and Tsams Members (Plate 21). In the northern outcrop area on Tsams Ost, there is an obvious angular unconformity at the base of the Ubusis clastics (Fig. 54). The contact with the Neuras Member becomes progressively conformable eastwards,

but with the eventual overstepping of the latter the unconformity between the Ubusis Member and the Büllsport Formation is very pronounced. In the south the Neuras-Ubusis contact appears quite conformable.

The characteristic basal unit of the Ubusis Member ("Bed" 1 in the section of Fig. 18) is a coarse-grained feldspathic gritstone which is locally conglomeratic in the north-east where the Ubusis Member and the Büllsport Formation are in direct contact. The felspar is a pinkish microcline (CH62) so it is evident that a granitic terrain was exposed relatively nearby during the lower Ubusis deposition. The overlying clastics ("Bed" 2, Fig. 18) are interbedded dark siltstones and white, fine-grained quartzites.

(iii) Tsams Member

The contact between the Ubusis and Tsams Members appears everywhere conformable but is generally most abrupt, although a few thin, dark dolomitic intercalations are present in Ubusis siltstones in the north-western outcrop area. Along the southern nappe front it seems likely that a hiatus in sedimentation and possibly an erosional disconformity is represented by the contact (cf. base of lower Tsams dolomite in centre of Plate 22).

The Tsams Member everywhere has a characteristic three-layer or "sandwich" structure (Fig. 18) in which two thick, homogeneous dolomite layers ("Beds" 1 and 3, Fig. 18) are separated by a zone of thinly bedded, reddish-weathering calcareous quartzites ("Bed" 2). The lower dolomite is typically dark grey in colour and rich in discontinuous cherty layers, whereas the upper dolomite is much lighter-coloured and more regularly bedded with evidence of domal stromatolitic layering near the top.

(iv) Lemoenputs Member

This upper clastic unit appears to follow conformably on the upper Tsams dolomite, though the contact evidently represents a sudden change in sedimentary environment.

The dominant rock type of the Lemoenputs Member is a greenish-grey

siltstone or fine-grained subgreywacke ("Beds" 1, 3 and 5, Fig. 18), containing angular clasts of quartz and some feldspar suspended in a very fine, now recrystallised phyllosilicate matrix. A characteristic feature of this rock (CH64) appears to be the relative abundance of coarser clastic "flakes" of white mica, as evidence of a provenance of (?low-grade) metamorphic rocks.

The central part of the Lemoenputs Member is dominated by two more resistant layers of different lithology (cf. Plate 23.) The lower layer ("Bed" 2 in Fig. 18) is a remarkable conglomerate containing well-rounded clasts of vein quartz, ranging in diameter from about 2 mm to 2 cm, mixed with flat angular clasts of dark, fine-grained dolomite and a few, generally subangular fragments of quartzo-felspathic material. The matrix is a fine carbonate-phyllosilicate mixture (CH116). The upper layer is a black, bituminous limestone ("Bed" 4, Fig. 18). Parts of this unit appear to contain fragments of the Nama shelly fossil *Cloudina*, but thin section examination has so far yielded no positive identification (G.J.B. Germs, personal communication).

The Lemoenputs Member, and its unmistakable double marker beds 2 and 4, can be mapped throughout the outcrop area of the Zebra River Formation (cf. Annex. I). In the north-west, the black limestone unit shows some effects of partial dolomitisation.

(v) Onis Member

This mainly dolomitic unit appears to conformably overlie the Lemoenputs Member over most of the western outcrop area, but in the east a conspicuous unconformity is visible at several localities where the Onis and Tsams Members come into contact.

The lower part of the Onis Member is a light grey dolomite ("Bed" 1, Fig. 18), which may locally exceed 50 m in thickness (Plate 24). This passes gradually in places into an overlying sequence of oolitic black limestone ("Bed" 2). In the extreme east of the Zebra River outcrop, however, it appears that the Onis limestone may overlap the Onis dolomite

and transgresses onto lower parts of the Zebra River sequence.

3. Relationships to adjacent units

The Zebra River Formation overlies the Kuibis Formation at a major tectonic discontinuity, the Naukluft sole thrust, marked by the Unconformity Dolomite. Along its north-eastern boundary within the Naukluft complex, however, it rests on the Büllsport Formation above a significant erosional unconformity. Towards the south-east, this contact is truncated by a major thrust surface within the nappe complex and the Büllsport Formation is locally emplaced over parts of the Zebra River sequence.

4. Depositional environment

The sudden alternations of carbonate and clastic members in the sequence and the evidence of progressive unconformities separating the major litho-stratigraphic components, testify to a tectonically unstable depositional basin which was alternately starved of, or flooded with clastic detritus.

Deposition of the Neuras Member was probably closely related to the emergence of the imbricated Büllsport Formation in the Dassie nappe, with the Neuras dolomites being eroded and redeposited Büllsport dolomite and some of the interbedded thin quartzites representing material brought in from a more distant basement provenance. Sudden influx of coarser grained more quartzo-felspathic detritus to form the basal Ubusis grits and conglomerate probably reflects the greater uplift and emergence of the latter source, resulting in the eventual burial of the outstanding Büllsport topography beneath the Ubusis Member.

Equally suddenly the emergent basement massif appears to have been depressed below sea-level so that the major supply of clastic detritus to the Zebra River basin effectively ceased in Tsams Member times. Some bituminous limestones may have then accumulated in a restricted euxinic environment, to

be succeeded in a shallowing basin by calcareous quartzites and (stromatolitic) limestone formed in an intertidal zone and subsequently to be completely dolomitised by supratidal processes.

In the following Lemoenputs depositional episode, basement uplift of a metamorphic provenance is evident in the rapid influx of fine-grained poorly-sorted clastic detritus. This was interrupted twice : firstly, when local uplift of the basin took place and a system of braided streams spread briefly across the sedimentary surface carrying characteristically fluviatile conglomeratic detritus; secondly, when the supply of clastic detritus suddenly ceased (perhaps due to the intervening uplift of a dolomite nappe), and oolitic limestone was deposited near sea-level in a restricted basin.

Finally, as far as the presently preserved Zebra River section is concerned, conditions of exclusively carbonate deposition in a shallow marine environment were established in a deepening basin, reflected by the upward transition from dolomite to black limestone. Tectonic conditions remained unstable as reflected by local unconformities at the base of, and even within the Onis succession.

In general it appears that the Zebra River Formation is a syn-tectonic deposit formed in a shallow marine basin on the foreland of a rising orogenic belt. The sedimentary character of different parts of the sequence appears to have been controlled by the nature of the nearest emergent cordilleras. When quartzo-felspathic basement of igneous or metamorphic rocks was emergent, the major clastic members of the sequence were laid down in the fore-deep trough, but for most of the time the rising basement provenance appears to have been cut off by an intervening chain of carbonate ridges or islands (probably built up by Noab dolomite of the Kudu nappe) which dammed up the inflow of clastic material and allowed dolomites and limestone to accumulate.

5. Correlation and age of the Zebra River Formation

The Zebra River Formation gives the very strong impression of being a

basin-edge facies of the Kuibis Formation in the Nama Group (G.J.B. Germs, personal communication). When traced northward from the Zaris Mountains toward Felseneck at the southern base of the Naukluft nappe complex, the Kuibis Formation is seen to contain grey dolomite members closely similar in appearance to the Tsams and Onis dolomites of the Zebra River Formation; these have formed in the upper parts of the lower two black limestone members of the Kuibis Formation.

The existence of three sedimentary cycles in the Zaris Mountains section of the Schwarzkalk Limestone Member of the Kuibis Formation was illustrated by Korn & Martin (1959, Pl.2, Fig. 2; see also Plate 25 of this work), each cycle beginning with fine clastic sedimentation, followed by non-stromatolitic limestone and ending with stromatolitic limestone or dolomite (Germs, 1972, p.9). Germs (*op.cit.*, p.11) has drawn attention to the role, during this period, of a tectonic island near the present Naukluft Mountains in shedding detrital material into the Kuibis basin. It seems most probable that the alternating clastic-carbonate succession of the Zebra River Formation can be linked with the above-mentioned Kuibis cyclicity, once the detailed Kuibis stratigraphy of the Felseneck section becomes known. The latter task was beyond the scope of the present investigation which was largely limited to the Naukluft nappe complex. At present, it is tentatively hypothesised that the basal grit of the Ubusis Member may correlate with the Basal Clastic Member of the Kuibis Formation (Germs, 1972), and that the carbonate units of the Tsams, the middle Lemoenputs and the Onis Members correspond to the upper carbonate divisions of the three Kuibis cycles.

The age of the Zebra River Formation is discussed below in connection with the S. Pavian nappe sequence.

F. FORMATIONS OF THE SOUTHERN PAVIAN NAPPE

1. Introduction

In the original description of Naukluft stratigraphy (Korn & Martin, 1959), a "Southern facies of the Pavian Series" was differentiated, whereas in the present work it is recognised that, as there is a Northern Pavian nappe which has tectonic boundaries discordant to its internal stratigraphy, there is also a Southern Pavian nappe (cf. Chapter IV) and these nappes cannot be compared as one lithostratigraphic facies to another.

The Southern Pavian nappe is a thrust-bounded body about 15 km long and 1,5 km wide, with a maximum exposed thickness of about 400 m. It contains lithologies apparently belonging to two quite distinct sedimentary facies, which in their present position outcrop in the near-frontal region of the Naukluft complex west of the Tsondab valley on Büllsport and Naukluft (Annex. I).

2. Description

a. Stratigraphic sequence

Three local stratigraphic sections through the Southern Pavian nappe have been compiled at the same scale in Fig. 19; the sections from localities 50118 and 50018 are at the southern and middle parts of the Tsondab valley outcrop on Büllsport, and the section from locality 50019 is at the southern front of the S. Pavian nappe about 5 km south-west of the Tsondab valley. All were chosen for being relatively undeformed internally and therefore preserving original sequence and thickness relationships between different lithologies.

It is apparent in all three sections that the S. Pavian sequence is immediately divisible into two parts, which are probably separated by a disconformity or unconformity, although no angular discordance was seen. The upper formation, which is further subdivided into four members (labelled 1-4 in Fig. 19), shows relatively minor facies change between local sections, and for reasons outlined below is correlated with the lower part of the Zebra

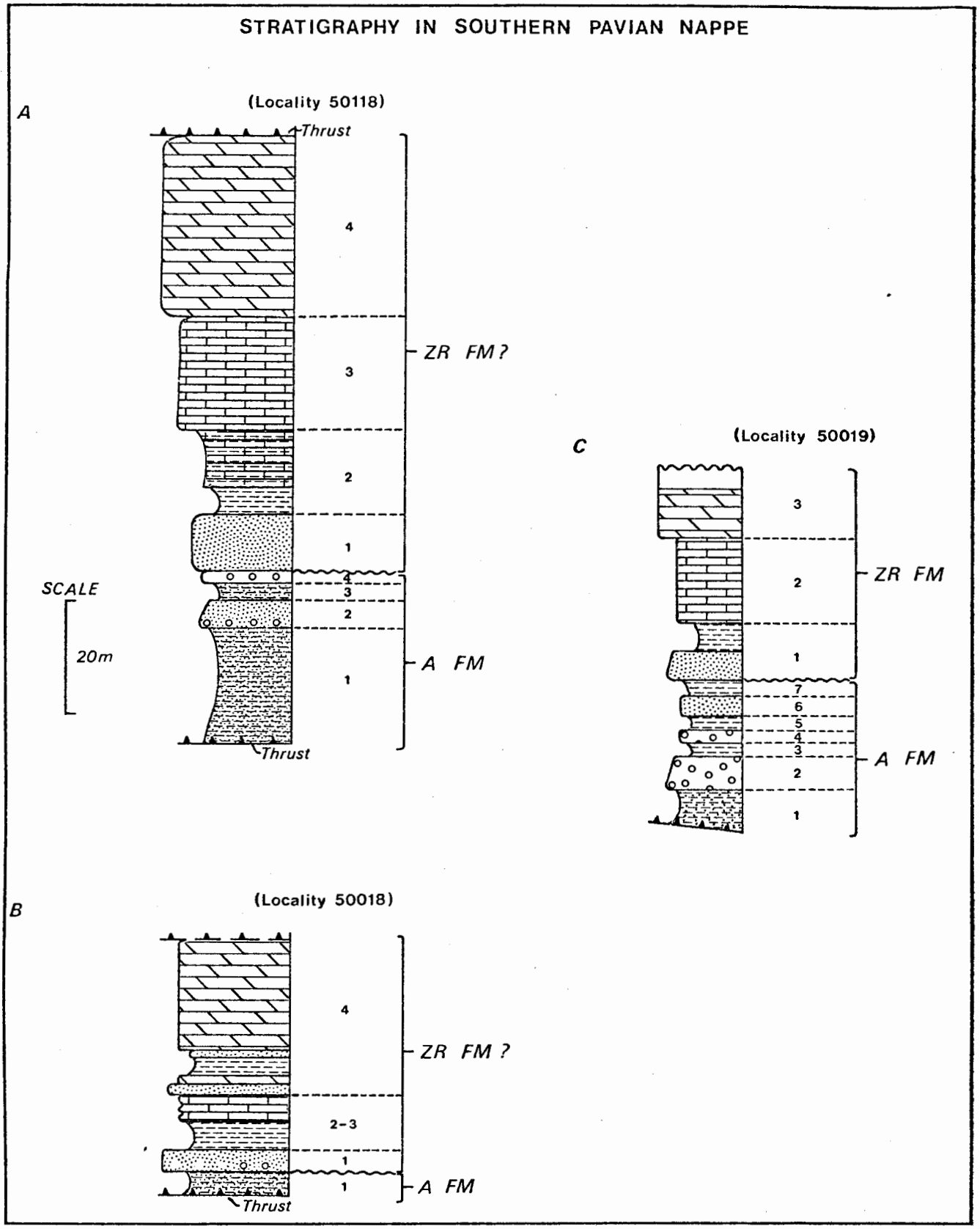

Figure 19. Three local stratigraphic columns from the Southern Pavian nappe on the farm Büllsport, showing the division of the nappe into a lower clastic unit (Aubschlucht Formation) and an upper unit probably corresponding to part of the Zebra River Formation.

River Formation. The lower formation is unlike any other lithostratigraphic unit within the Naukluft complex and is accordingly assigned the new provisional name of the Aubschlucht Formation, after the deep canyon of the Aub River on Büllsport (cf. Korn & Martin, Pl. 1) in which it is best exposed. It is evident from comparisons of the local sequences immediately beneath the upper (?Zebra River) formation that the Aubschlucht Formation is not characterised by much lateral continuity of lithology (Fig. 19). This feature may be ascribed either to very rapid lateral facies change or to an erosional disconformity resulting in different parts of the Aubschlucht Formation being overlain by the same basal quartzite of the upper unit.

b. Lithology

The rock types of the Aubschlucht Formation are reddish-purple siltstones (Beds 1 and 3 of section A, and bed 1 of sections B and C; Fig. 19), reddish-brown to greenish-brown shales (Beds 3, 5 and 7 of section C, Fig. 19), reddish quartzite (Bed 6 of section C), and characteristic coarse quartz-pebble conglomerates (Bed 4 of section A, and beds 2 and 4 of section C, Fig. 19) which also contain conspicuous clasts of pinkish K-felspar and deep red jasper. The conglomerate and conglomeratic sandstone (Bed 2) in section A of Fig. 19 contains numerous small angular clasts of granitoid material, and in all sections the quartzitic component is distinctly arkosic.

In some thin sections (CH 110, CH 113), lithic clasts of fine-grained volcanic material similar to that from the Tsabisis Formation are seen, but it is uncertain whether this provides a firm basis for conclusions about the relative age of the Tsabisis and Aubschlucht Formations. In the same sections, many quartz clasts have an internal microstructure of elongate subgrains (mylonitic fabric ?) although the grains themselves are rounded and subspherical in shape. Clasts of biotitic and chloritic schist are also present. This observation points to the derivation of the Aubschlucht Formation from a mixed terrain of granitoid and low-grade metamorphic rocks.

Where the Aubschlucht Formation is little deformed, the original clastic texture of the quartzitic rocks is very well preserved and all grains are seen

to be coated by a fine layer of hematite which is quite distinct from the interstitial phyllosilicate matrix and which gives the Aubschlucht rocks their ubiquitous reddish colouration. This feature, the arkosic composition and the coarsely-bedded nature of the Aubschlucht deposits, suggests that they were deposited in a continental, non-marine environment.

The overlying lithologies, in contrast, clearly belong to a different sedimentary environment. Starting with a well-bedded clean white orthoquartzite which is only locally pebbly (Section B, Fig. 19), it passes upwards through a thin zone of fissile green shales and thence into a sequence of black limestone locally with a basal marly division (Section A, Fig. 19). This limestone is remarkable for containing abundant minute zoned dolomitic structures unlike oolites in having highly elongate or subcylindrical shapes or alternatively a "flaky" or discoidal habit; they are probably oncolites. The limestone is overlain by a thick, massive, dark-grey dolomite generally characterised by abundant cherty inclusions or beds (e.g. bed 4 in section A, Fig. 19).

3. Relationships to adjacent units

The formations of the S. Pavian nappe overlie the Büllsport Formation above a tectonic contact and are in turn overlain by the Noab Formation at a higher thrust contact. These thrusts merge westwards so that the S. Pavian Formations wedge out completely.

4. Depositional environment

It is supposed from the rather meagre available evidence that the Aubschlucht Formation was deposited very rapidly, probably by fluviatile processes, in a shallow basin located above sea-level. Subsidence and marine transgression probably led to some local reworking of Aubschlucht material to form the clean basal quartzite of the overlying unit, and thereafter a regime of first fine pelitic, and later shallow-water carbonate, deposition was established.

5. Correlation and age of the S. Pavian formations

The former "Southern facies of the Pavian Series" was originally correlated as a whole with the "Zebra Series" (Korn & Martin, 1959) but the stratigraphic sequence then in use for the latter (*op.cit.*, p.1059) is unrecognisable in comparison with that defined here (Fig. 18). At present, it is proposed on lithological grounds that only the upper part of the S. Pavian nappe sequence might correlate with the Zebra River Formation. This correlation is based mainly on the similarity of the uppermost S. Pavian dark cherty dolomite with the lower cherty dolomite of the Tsams Member, and the possibility that the basal quartzite of the upper S. Pavian division may be a more mature or distal facies of the basal Ubusis Member quartzite. If this is accepted, then beds 2-3 of the upper S. Pavian sequence could also be interpreted as a more distal limestone-rich facies of the upper Ubusis siltstones. Otherwise, there is simply no part of the Zebra River sequence which bears quite as close a resemblance as this.

Münch (1975, and personal communication), however, proposes that the entire S. Pavian sequence be correlated with the middle and upper Zebra River Formation on the basis that the jasper-bearing Aubschlucht conglomerates are equivalent to the conglomerate bed in the Lemoenputs Member (Fig. 18) which is also observed to contain minute amounts of red jasper. If this were accepted, then the upper S. Pavian black limestone might correlate with the Lemoenputs limestone and the cherty dolomite might represent a facies of the Onis Member dolomite. Whereas the alternative interpretation excludes the Aubschlucht Formation and regards the upper S. Pavian as a more distal facies of the Ubusis and Tsams Members, this interpretation requires that the Aubschlucht Formation be a thicker, proximal facies of the lower Lemoenputs Member, and the upper S. Pavian be simultaneously a more limestone-rich distal facies of the upper Lemoenputs Member. In the writer's opinion, this is sufficient reason for its rejection if problems of tectonic reconstruction of the S. Pavian and Zebra River basins (cf. Chapter V) are also taken into account.

Korn & Martin's (1959) correlation of the upper S. Pavian dolomite with the white dolomite of the newly defined Tsabisis Formation cannot be maintained since there is absolutely no point of lithological comparison, either in detail or in general, between the stratigraphic sequences of the N. Pavian and S. Pavian nappes (cf. Figs. 10 & 19). The finite strain state of the rocks in both nappes, and tectonic reconstruction of nappe emplacement appear to support the view that the S. Pavian sequences were deposited after, or possibly during, a major deformation episode (D_2) in which the whole N. Pavian nappe was involved.

Regarding S. Pavian correlation with formations outside the Naukluft nappe complex, the identification of the upper division as a facies of the Kuibis Formation seems quite secure (G.J.B. Germs, personal communication). The Aubschlucht Formation, however, presents a real problem, since the units to which it bears most lithological resemblance are the pre-Nama Kamtsas and Blaubeker Formations as found in the region immediately north-east of the Naukluft complex (Annex. I). On purely lithological grounds it seems quite reasonable to regard the Kamtsas and Kuibis Formations of the Slangpoort area as being more distal facies representatives of the Aubschlucht and lower Zebra River Formations respectively.

The consequences of this interpretation for the stratigraphy of the southern margin of the Damara belt are radical, since it is implied that the Kamtsas Formation is younger than all units of the N. Pavian nappe and younger than the Noab and Büllsport Formations also. Accepting the correlation of the latter with lower Swakop Group marbles (Martin 1974), it is therefore also implied that *the Kamtsas Formation is younger than a major part of the Swakop Group* and is probably to be interpreted as a molasse facies of major early orogenic episodes in the Damara belt. The correlation of the Aubschlucht Formation with the Kamtsas Formation, over a distance of only 25 km, accordingly challenges the correlation, across the Khomas ridge province of the Damara belt, of the Kamtsas Formation and the Nosib Group (Martin, 1965).

The dating of the Zebra River and Aubschlucht Formations is crucial for placing a minimum age on early major thrusting episodes in the southern part of the Damara orogenic belt. On palaeontological grounds (Germs, 1974), it appears that the Kuibis Formation was deposited during the very latest part of the Precambrian, and an age between 600 Myr and 570 Myr (the conventional age of the lower Cambrian boundary; Harland, 1975) seems likely. Since the shelly fossils which establish an immediate infra-Cambrian age for the Kuibis Formation have not yet been discovered in appropriate lithologies of the Zebra River Formation, and since the latter is a basin edge facies of the former, it is possible that the age of the Zebra River Formation marginally exceeds that of the bulk of the Kuibis Formation so that an age closer to 600 Myr is favoured.

Because there is no difference in deformation intensity between the Aubschlucht and Zebra River Formations in the S. Pavian nappe, and only the possibility of slight disconformity, the age difference between them is probably very slight. Similarly the angular unconformity between the Kamtsas and Kuibis Formations is greatest in the west but generally they have a disconformable or paraconformable contact. In view of the evidence in intense tectonic activity in the Naukluft complex prior to deposition of the Zebra River Formation at least (Chapter V), this relationship is not intelligible if, as present Kamtsas-Nosib correlation implies, there is an approximate 400 Myr age difference between the Kamtsas and Kuibis beds.

CHAPTER IV

STRUCTURAL GEOMETRY OF THE NAUKLUFT COMPLEX

A. INTRODUCTION

1. General remarks

Korn & Martin's (1959) model of the structural geometry and mechanics of rock deformation in the Naukluft nappe complex is based on a concept of stratigraphic relationships and sedimentary environments which has since been radically revised (cf. Hartnady, 1974; Martin, 1974; Chapter III of this work). The Naukluft complex consists of a heterogeneous assemblage of sedimentary and low rank metasedimentary formations representative of environments ranging from moderately deep-water marine (e.g. Remhoogte Formation greywackes), through shallow marine (e.g. Blässkranz and Zebra River Formations) and tidal flat zones (e.g. Noab and Büllsport Formations) to probable local fluviatile conditions. Even where completely preserved, sequences of a specific facies are very thin. In the absence of datable fossils, except for some poorly known stromatolitic and oncolitic forms, the time interval spanned by the various formations can only be guessed, but probably ranges over 400 Myr (i.e. from -1000 to -600 Myr), although much of that period is represented by hiatuses between deposition of the major units.

The main problem of Naukluft tectonics is to explain how these varied formations were assembled in one major tectonic unit, with very little independent evidence of their relative age other than that which can be gleaned from internal structural relationships and from lithological correlation with similar units in less-deformed zones outside of the nappe complex.

2. Methods of structural analysis

The Naukluft complex was originally mapped without the aid of serviceable topographic maps and up to the present time the only available geological

map of the Naukluft complex was a partly diagrammatic one at a scale close to 1 : 200 000 (Korn & Martin, 1959, Pl. 1). In this project, therefore, a systematic re-mapping of the terrain was essential, especially when initial field investigations revealed a far greater lithological and structural complexity than was previously supposed. Mapping was carried out on overlays to aerial photographs at a scale of 1 : 36 000 (Job 294) and the data was transferred to preliminary 1 : 50 000 topographic maps (Sheets 2316CC, 2316CD, 2416AA, 2416AB, 2416AC, minor part of 2416AD) with a contour interval of 10 m. For the final map, individual 1 : 50 000 sheets were reduced and combined at a scale of 1 : 100 000 (Annex. 1).

In the course of field and photogeological mapping, particular attention was paid to the accurate tracing of lithological boundaries and major thrust-fault structures through the mountainous Naukluft terrain. The rugged and highly dissected geomorphology, with abundant stream confluences and other clearly recognisable topographic features, facilitated a relatively accurate manual transfer of location data from aerial photograph to map. It does, however, make rapid systematic structural mapping of the complex on a regular traverse basis generally impossible. Therefore the main aim of field structural investigation was to achieve a detailed sampling of structural geometry from a number of pre-selected small areas which prior photogeological investigation had shown to be particularly difficult to interpret or otherwise important.

To achieve a moderately close-spaced uniform sampling of structural orientation data over the entire Naukluft complex is a task involving several man-years of field work. In order to ensure that the data collected during the present investigation formed a permanent base for the extension of structural analysis towards that objective, so that an accurate quantitative geometric model of Naukluft structure could ultimately be "built", a computerised data filing system was designed and tested in the course of field-work. This system, named PRUDE for the Precambrian Research Unit Tectonic Data-base (Hartnady & Vajner, 1975; cf. Appendix Chapter A-I), enables precisely classified structural orientation data and the precise data

of location of the measurement sites, to be stored in files with a common simple structure which facilitates rapid retrieval for plotting or statistical processing.

In the sampling of structural data from individual sites, special attention was paid to the measurement of bedding orientations where possible (to map the rotational component of finite strain in the complex), the measurement of rock cleavage orientations (to map the trajectories of the XY principal plane of finite strain) and the measurement of mineral and grain elongation lineations (to map the trajectories of the X principal axis of finite strain). Quantitative measurement of strain ellipsoid ratios was not, however, accorded priority because of limited distribution of suitable material, apparently extreme heterogeneity of the deformation pattern even on a local scale and the need to achieve an adequate understanding of large-scale tectonostratigraphic relationships first.

The heterogeneous deformation in the Naukluft Formations is reflected in a sometimes considerable "within-site" variability of orientation data for a particular fabric element, most obviously for folded bedding but also for rock cleavage which may change orientation from one part of an outcrop to another due, not to later folding, but to variable degree of development in the course of a continuous rotational deformation (Ramsay & Graham, 1970). In order to compute vector mean orientations and "best-fit" axes of rotation for fabric elements displaying this variability, a program based on vector-statistical methods outlined by Watson (1966) was written to process data stored in the PRUDE system. If multiple measurements of individual fabric elements are made at an outcrop as a matter of conventional practice, this program can in principle be used within the PRUDE system to produce automatically a reduced orientation data set from which the usual sources of error and imprecision have been largely removed. In the Naukluft complex, where dips of important planar fabric elements such as the principal cleavage are generally low or subhorizontal, this methodology is valuable in the detection of late, very low amplitude deformations.

B. STRUCTURAL GEOMETRY

1. Shape of the nappe complex and definition of the constituent nappes

The shape of the Naukluft nappe complex, as defined by the outcrop trace of the Unconformity Dolomite zone, is that of a shallow oval basin. The highest part of the nappe sole is at an altitude of 1750 m, in the south-west on Urikos, whereas at the north-east end of the complex the maximum altitude of the Unconformity Dolomite zone is just 1680 m above mean sea-level. In a longitudinal section, therefore, the base of the nappe complex is at a greater altitude where it is underlain by at least 300 m of the Nama Group and at a lesser altitude where the Unconformity Dolomite all but overlaps onto pre-Nama basement; a feature which is surprising if the former gravity-slumping model of Naukluft development (Korn & Martin, 1959) were correct. In a transverse section from south-east to north-west across the complex, the lowest part of the nappe front is exposed at about 1400 m on Büllsport, whereas the lowest exposure at the rear of the complex is situated at about 1240 m in the Tsondab River valley on Zais. This implies a $0{,}5^{o}$ average *north-westward* dip of the nappe sole in the central segment of the complex. In fact, along the south-eastern nappe front between Naukluft and Büllsport the north-westward dip of the nappe sole actually reaches a maximum of about 10^{o}, as measured by structure contours on the Unconformity Dolomite trace.

It does not seem possible to distinguish a separate toe region to the Naukluft complex simply on the basis of these steeper basal dips in the south-east, although they do coincide with a zone of more steeply dipping imbricate structure within the nappes. Instead it will be argued that the entire Naukluft complex represents the transitional zone between the main body and the toe of a nappe structure much larger than that which is presently preserved and that prior to post-orogenic uplift the base of this larger nappe dipped consistently in a north-westward direction. The present south-eastward

dip of rear margin of the Naukluft complex is largely the result of post-emplacement uplift and local deformation (cf. Korn & Martin, 1959, p.1055, Fig. 4, profile f) of the nappe base, since the metamorphic grade of Naukluft pelites is quite incompatible with the original hypothesis of no change in relative height between the Nauchas Highlands and the Naukluft basin (*op.cit.*, p.1073).

Formerly no clear distinction was drawn between lithostratigraphic and tectonic units (nappes) in the Naukluft complex. This, however, has now become essential because the new mapping shows that the main tectonic discontinuities (overthrusts) truncate major lithostratigraphic boundaries. Hence the older stratigraphic nomenclature (Korn & Martin, 1959) is preserved for the principal nappe structures, while a new nomenclature is established for Naukluft lithostratigraphy.

The location of the principal Naukluft overthrusts is illustrated in Fig. 20, which has been considerably simplified from the map (Annex. I). Five major nappes are distinguished, three of which immediately overlie the Unconformity Dolomite along extensive segments of the nappe complex perimeter. These lower tectonic units of the Naukluft complex are, from north to south,

the *Northern Pavian nappe*
the *Eastern Dassie nappe*
and the *Western Dassie nappe*

The remaining two major nappes are the *Southern Pavian nappe*, which occurs as a narrow wedge partly overlying the western Dassie nappe and has a presumed extension to the north-west in the dolomitic inlier surrounded by the Northern Pavian nappe and the *Kudu nappe*, which overlies the Northern Pavian nappe mainly over most of the northern region of the Naukluft complex.

When arranged in simple tectonic sequence, on the basis of superposition relationships along the major contacts these five nappes stack as follows :

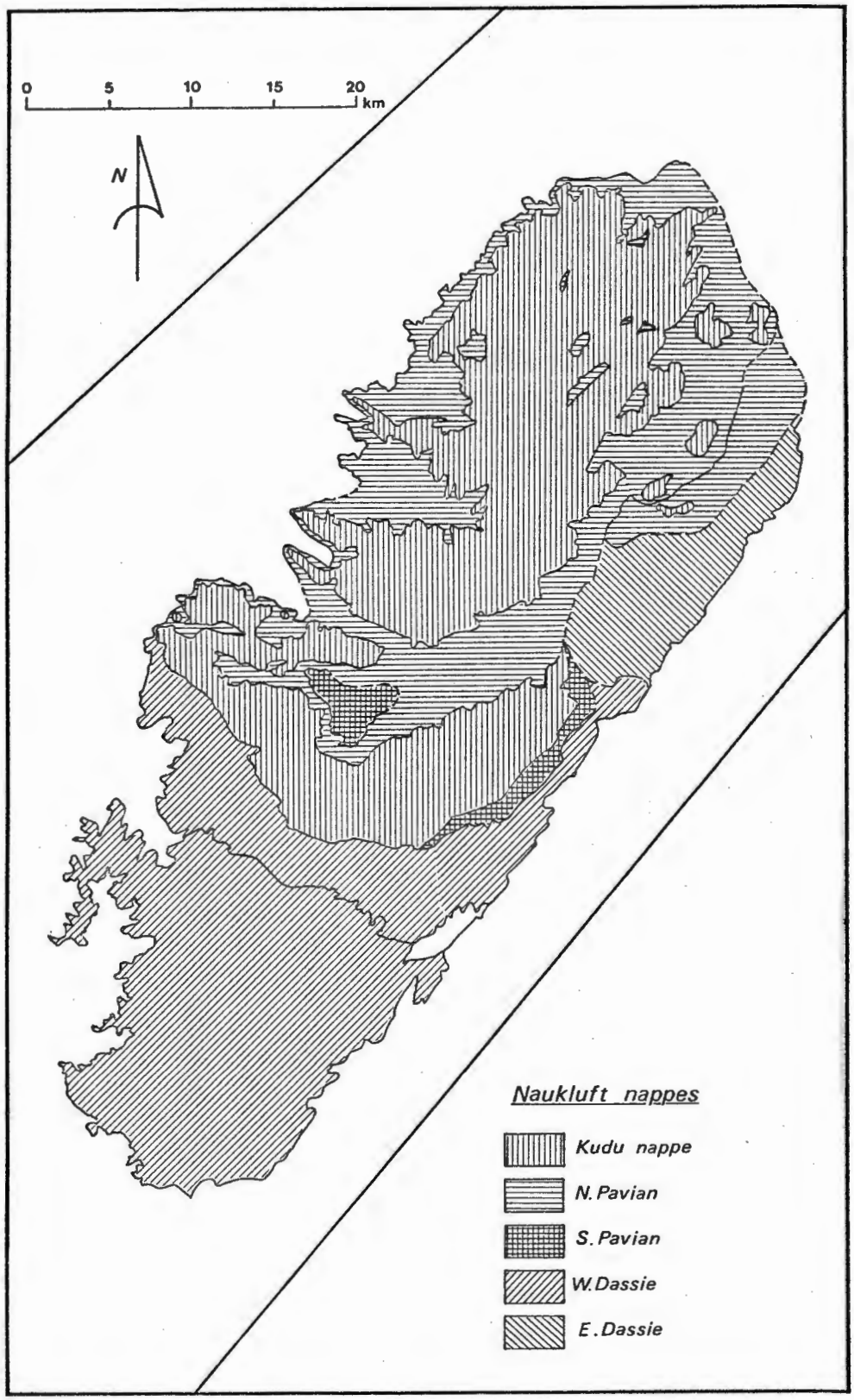

Figure 20. The five major nappe units of the Naukluft complex. Note the trace of a conspicuous unconformity within the W. Dassie nappe, separating the Büllsport and Zebra River Formations and also the wedge-shaped fragment of phyllitic rocks at its south-eastern end, which can be interpreted as part of the Nama substratum "captured" by imbrication processes near the nappe toe.

5. Kudu nappe
4. Northern Pavian nappe
3. Southern Pavian nappe
2. Western Dassie nappe
1. Eastern Dassie nappe

This sequence is locally reversed where, for example, secondary thrusting has emplaced parts of the N. Pavian nappe over parts of the Kudu nappe on Blässkranz and Tsabisis. These apparently minor phenomena are related to an even larger division of the Naukluft complex into two parts, consisting of tectonic units 4 + 5 and 1 + 2 + 3 respectively. The boundary between these northern and southern divisions of the Naukluft complex is a low-angle overthrust with an arcuate outcrop trace. Its northeast-striking segment in the east separates the Northern Pavian and Eastern Dassie nappes. When traced south-westwards to the Tsondab River this major thrust structure appears to splay into four separate discontinuities, with much of the displacement between the combined Northern Pavian and Kudu block and its substratum apparently being transferred to lower thrust surfaces at the base of the Southern Pavian and Western Dassie nappes respectively. At this point, the Kudu nappe replaces the Northern Pavian nappe above the principal boundary and rests on the Southern Pavian nappe. Where the same boundary re-appears down-dip in the tectonic window west of Blässkranz, the Northern Pavian nappe immediately overlies the contact. Along its western segment, the boundary between the northern and southern divisions of the Naukluft complex swings through a great arc into a northwest-striking orientation. Here the Kudu nappe overlies the Western Dassie nappe directly, although at a larger scale than Fig. 20 it is possible to show that there is a thin layer of pelitic schist along this contact which may correspond to a much-attenuated Northern Pavian unit (cf. Annex. I).

In Korn & Martin's (1959) interpretation of the large-scale nappe structure, the distinction between the Eastern and Western Dassie nappes was not clearly drawn, although they certainly recognised and drew attention to the main features of the boundary between these units in the front ranges

north-east of Büllsport (*op.cit.*, Fig. 13). Furthermore, in their interpretation the Western Dassie nappe consisted of two tectonic units, the older of which was the nappe of the "Zebra series". In the present interpretation, this "Zebra nappe" does not exist since the contact between the Büllsport Formation and the Zebra River Formation is shown to be an erosional unconformity along which only minor tectonic relative displacement has occurred.

The base of the W. Dassie nappe east of Büllsport is truncated in a downward-facing orientation by the main sole thrust of the Naukluft complex. It is most probable that this truncated thrust re-appears within the complex on Naukluft about 15 km to the south-west. Here it overlies a local wedge of deformed pelitic material which is correlated with a part of the Zebra River Formation. Farther south-westwards, however, it is displaced downwards by later imbrication and disappears from view once more. The abovementioned wedge which lies between this thrust and the Unconformity Dolomite zone is not formally assigned to any of the 5 major nappes in the Naukluft complex (cf. Fig. 20).

The distribution of the major lithostratigraphic units described in Chapter III between these five major nappe structures is illustrated in Table 3 . It is notable that members of the Zebra Formation are common to all three of the lower southern nappes, although the probable Zebra River equivalents in the E. Dassie nappe are very restricted. Furthermore, although the facies of these rocks and those in the upper part of the S. Pavian nappe is undoubtedly characteristic of the Zebra River Formation, the local differences in either sequence make the correlation somewhat problematic. It is also notable that the only lithostratigraphic units common to both the northern and southern divisions of the Naukluft complex are the Noab and Büllsport Formations which are almost certainly correlative as different facies of the same major sedimentary unit (cf. Chapter III; Section B). This unit occurs at three distinct structural levels within the nappe complex (nappes 1, 2 and 5). However, the nappe topology is such that a path can be traced from one structural level of the Noab-Büllsport

TABLE 3

Tectonic and Stratigraphic units of the Naukluft complex

Tectonic unit	Lithostratigraphic unit	
Kudu nappe	Klipbokrivier Formation	
	~~ Noab Formation	
Northern Pavian nappe	Tsabisis Formation	
	Blässkranz Formation	
	~~ Remhoogte Formation	
Southern Pavian nappe	Zebra River Formation (?)	
	~~?– ——— ? ——— ? ——— ? ——— ? ——— Aubschlucht Formation	
Western Dassie nappe	Onis Member	ZEBRA RIVER FORMATION
	~~ Lemoenputs Member	
	Tsams Member	
	Ubusis Member	
	Neuras Member	
	~~ Büllsport Formation	
Eastern Dassie nappe	Zebra River Formation (?)	
	~~ Büllsport Formation	

═══ Tectonic boundary

——— Conformable contact

~~~ Erosional unconformity
~~~

assemblage to another without passing through any other formation (except perhaps the thin strip of phyllite intercalated between the Kudu nappe and Western Dassie nappe along their northwest-striking contact).

The explanation of this last-mentioned fact lies at the core of the problems of structural geometry and kinematic evolution in the Naukluft complex.

2. Structure of the North-west and Northern areas

The areas in which structural data sites are concentrated are illustrated in Fig. 21 , relative to the SWA metric coordinate system which ranges from X = 195 000 m to X = 275 000 m, Y = 55 000 m to Y = 100 000 m. Five partly overlapping regions have been distinguished : North-west (NW), North (N), Central (C), South-east (SE), South-central (SC), West (W) and South-west (SW). In the PRUDE data files, the first part of the locality number (LOCALE), identifying each orientation measurement and its location, contains a numerically-coded reference to the data region, as follows:

NW area - 121011xxxx
N area - 121012xxxx
C area - 121013xxxx
SE area - 121014xxxx
SC area - 121015xxxx
W area - 121016xxxx
SW area - 121017xxxx

In references to particular data sites, the first five digits (project code) of the LOCALE identifier are usually omitted. Hence, reference to locality 10012, for example, means data site 12 in the NW area complete details of which can be obtained by consulting the PRUDE files for data bearing the full LOCALE number 1210110012.

The most important structural features of the NW and N areas concern the relationship between the Naukluft complex and the underlying deformed Nama Group, in the NW area and the relationship between the Northern Pavian

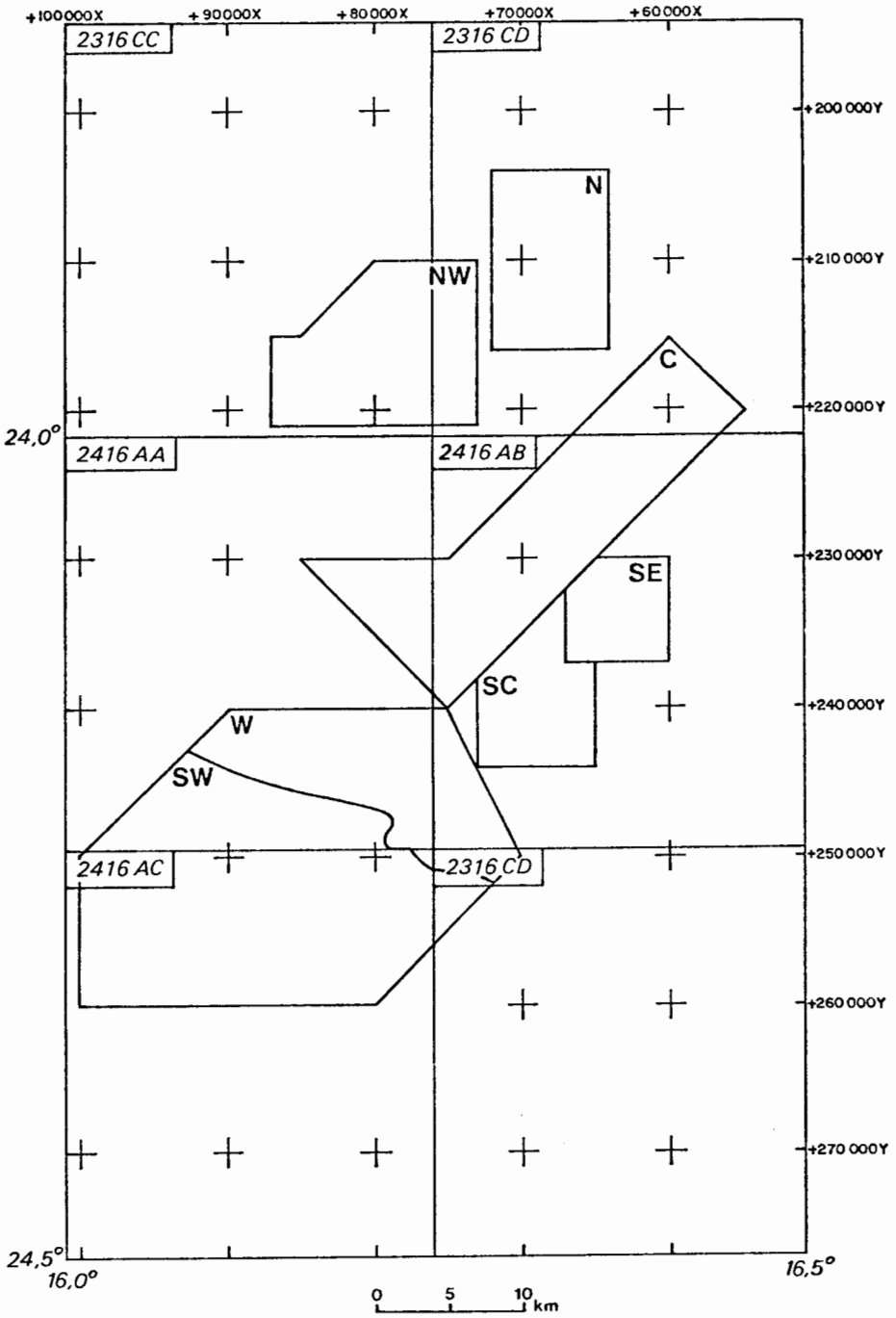

Figure 21. Diagram defining the boundaries of the seven principal data regions: 1 - North-western (NW); 2 - Northern (N); 3 - Central (C); 4 - South-eastern (SE); 5 - South-central (SC); 6 - Western (W); and 7 - South-western (SW).

and Kudu nappes in the North area.

a. Internal structure of the Kuibis Formation near Abbabis

A wide area of the Kuibis Formation is exposed in the hills north-east of the confluence of the Tsondab and Noab Rivers (Annex. I) and the deformation and partial dolomitization of Kuibis black limestone along the ridge summits shows that the base of the nappe complex lay close to this level before its erosion. A small outlier of the Naukluft complex is preserved at 1350 m in the west of the area, which is therefore convenient for studying the emplacement-related deformation of the Nama Group.

(i) Major structures

The Kuibis Formation here displays three distinct cycles of limestone deposition, each cycle beginning with a more pelitic zone, the basal cycle commencing with an arkosic quartzite and thin-bedded dolomite unit (Plate 25). The same three cycles are present south of the Naukluft complex in the Zaris Mountains where the entire Kuibis sequence is much thicker (cf. Korn & Martin, 1959, Pl.2). The most conspicuous major structure in the Abbabis area is a northwest-trending zone of foliated and sheared limestone with steep (50^{o} - 70^{o}) north-easterly dips (Fig.22), south-westwards of which the Kuibis sequence is preserved relatively intact, but north-eastwards of which that sequence is highly disturbed and apparently incomplete. The existence of a major basement depression in the Tsondab Valley region (Korn & Martin, 1959, p.1054) may be related to the preservation of the Kuibis sequence in the south-west.

Within the shear belt, at locality 10009, northwest-plunging asymmetric Z-folds may indicate it represents the overturned limb of a larger antiformal structure. Broad synformal structures separated by a tighter antiform converge on this structure from the south-west (Fig. 22). The gently curving patterns of the hinge-zone traces may indicate that earlier northeast-striking fold structures (F_1) are deformed by a later northwest-striking zone of simple shear, but no positive evidence of mesoscopic fold

superposition could be found close to the shear belt itself. It is, however, notable that on a macroscopic scale there is late gentle folding of an early tectonic cleavage near-parallel to bedding in the close vicinity of the shear belt.

(ii) Minor structures

Planar fabric elements

Even where bedding (SS; BED) and large-scale stratigraphy is well preserved, the internal deformation of the Kuibis Formation is greater than might appear from a distance (cf. the internal folding in the limestone units of Plate 25). On a mesoscopic scale, bedding in the limestones is folded into southeast-vergent asymmetric folds (e.g. Plate 26) and a well-developed cleavage (S_1; CLE) is superimposed across bedding at most localities. This is usually defined by a grain and inclusion-shaped fabric in the Kuibis limestones, but elsewhere it is a pressure-solution structure causing a new tectonic layering to develop across the original sedimentary bedding. The pressure-solution zones are defined by concentrations of "insolubles" and by zones of limonitic iron-oxide staining and disappearance of disseminated graphite (by oxidation). In areas of locally intense deformation it is macroscopically impossible to distinguish original bedding from pressure-solution cleavage except on the basis of the last-mentioned phenomena. The field identification "bedding cleavage" (S_1; BCL) covers cases of uncertainty where the dihedral angle between these fabric elements may be very small. This may imply a large amount of simple shear strain parallel to the plane of sedimentary anisotropy in the Kuibis sequence, but in most sites it appears to record a considerable component of extensional strain (reflected in thin section by the tectonic disruption and boudinage of paper-thin shale layers) parallel to bedding in the limestones. This apparently indicates that the Kuibis sequence may have been compressed along a subvertical axis between its basement and the overriding nappe complex during the latter's emplacement. The mechanism implies that the Kuibis Formation was simultaneously being squeezed out of a tectonic orifice

immediately beneath the nappe toe.

Although the orientation of S_1 varies considerably, secondary cleavages S_1 are rarely observed. A later "fracture cleavage" (S_2; FRC - 268/64) is observed in highly deformed marly shales at locality 10039, immediately beneath the nappe base, to be axial-planar to a type 3 interference fold structure (Ramsay, 1967). This structure (Plate 27) is found close to the Unconformity Dolomite zone where the deformed Kuibis sequence is relatively thin and reflects a possible two-phase deformation history in the Kuibis Formation which may be related to the shear belt structure described above. The first deformation (D_1) is evident in the tight recumbent folds which have axial-planes near parallel to the sedimentary bedding and/or bedding cleavage (Plate 28). The second deformation (D_2) folds are relatively open structures, but in discrete zones such as the north-west striking shear belt, D_2 structures may be found which are indistinguishable in style from D_1 folds.

While the late folds illustrated in Plate 27 , have northward-dipping axial planes and therefore the same vergence as the early structures on which they are superimposed, other D_2 folds observed near the base of the Kuibis sequence have southeastward-dipping axial planes. A particularly good example occurs at the same outcrop as the D_1 fold illustrated in Plate 28. The existence of D_2 folds with opposite vergence to D_1, i.e. late "backfolds", raises the question of possible thickening of the Kuibis sequence during D_2, partially reversing the prior tectonic thinning which occurred during D_1.

Linear fabric elements

The most conspicuous linear structures in the Kuibis sequence are the fold axes of the D_1 generation (L_1; FAX) and the kinematically equivalent lineation (L_{1B}; ISL) defined by the intersection of bedding and tectonic cleavage. In local marly zones within the Kuibis limestone, a lineation represented by the elongation of thin phyllite layers has been assumed kinematically equivalent to a mineral elongation (L_{1X}; MEL) parallel to the major principal axis of finite strain.

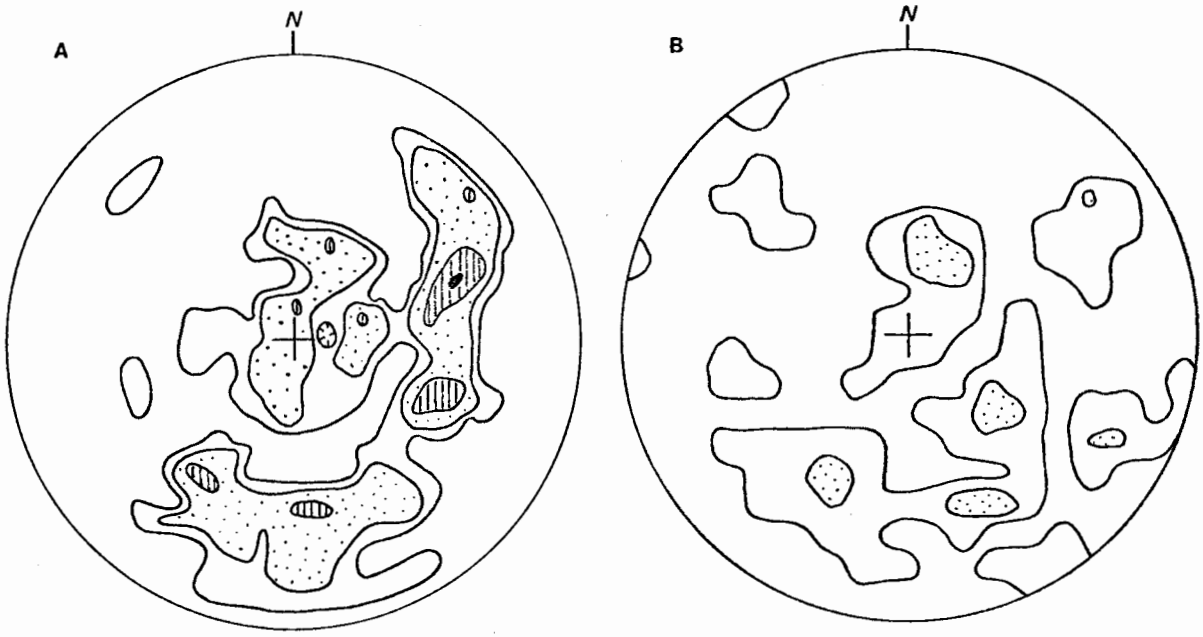

Figure 23. Orientation diagrams for SS and S_1 in the Nama Group of the NW area. A. 57 poles to SS; contours 1-2-5-10 %.
B. 43 poles to S_1; contours 1-5 %.

Statistical data processing

The orientation diagrams (Fig. 23) for the main planar fabric elements (SS and S_1) show their geometrical variability. The variable orientation of SS is due to the combination of D_1 and D_2 deformations, whereas that of S_1 is due to a combination of inhomogeneous deformation during D_1 and later D_2 folding.

For the purposes of statistically reducing the S_1 data to extract kinematically significant directions for D_1 and D_2, they were divided into four geographical groups or subareas. Data subareas A and B are from the block south-west of the prominent shear belt, while subareas C and D represent data site clusters from immediately north-east of the belt and from the Remhoogte Pass area, respectively (cf. Table 4).

In subarea A, the significant feature of S_1 geometry is the relatively large north-westward dip (53^o) of the hemispherical vector mean (HVM) cleavage orientation. Since the cleavage represents the XY principal plane of strain, this shows that its development cannot be simply related to simple shear parallel to the subhorizontal base of the overlying nappe complex, but must have included a compressional component acting subparallel to the bedding. The mean axis of rotation (B - corresponding to the direction of the eigenvector associated with the least eigenvalue of the data dispersion matrix, cf. Watson, 1966) of S_1 is probably related to D_1 inhomogeneous simple shear accompanying Naukluft nappe emplacement from an azimuth of 330^o approximately and not to the later D_2 episode.

In subarea A, cleavage (S_1; CLE) is easily distinguishable in the field from bedding, but as the shear zone bounding subarea B is approached the dominant fabric element in the field is "bedding cleavage" (S_1 ; BCL). The significant change in the strike of S_1 between subareas A and B is immediately obvious. The north-westerly or south-easterly trend of B for S_1 also contrasts with the south-westerly trend of B for subarea A.

The north-westerly dip of the HVM for bedding in subarea C contrasts with the 23^o south-westerly dip of the HVM for S_1, but the latter

TABLE 4

FABRIC STATISTICAL PARAMETERS FOR THE NAMA GROUP STRUCTURES IN THE NW AREA

UNIT/LOCALE[1]	FABELT[2]	TYCODE[3]	N[4]	HVM[5]	K_s[6]	L_B[7]	C_s[8]	Class[9]
NAMA area A	SS	BED	4	277/12	0,70	014/07	5,35	C - G
" "	S_1	CLE	9	228/53	1,13	244/20	3,44	C - G
NAMA area B	S_1	CLE	3	248/53	0,16	311/21	5,65	G
" "	S_1	BCL	5	304/55	0,36	113/15	4,86	G
NAMA area C	SS	BED	17	197/13	7,40	-	1,90	C
" "	S_1	BCL	4	114/23	3,68	-	5,60	C
NAMA areas A-C	SS	BED	22	203/11	6,85	-	2,09	C
" "	S_1	BCL	9	036/05	0,12	119/05	3,94	G
" "	S_1	CLE	14	225/39	0,99	249/19	2,19	G - C
" "	S_1	FAP	3	320/24	0,29	319/00	7,58	G
NAMA area D	SS	BED	16	195/45	0,11	295/45	4,15	G
" "	S_1	BCL	10	227/60	2,21	-	1,26	C

Area A - stations 10025 - 10035
Area B - stations 10002 - 10009
Area C - stations 10010 - 10024
Area D - stations 10036 - 10041

GENERAL NOTES CONCERNING TABLES 4 - 10

1 UNIT/LOCALE - column specifies lithostratigraphic unit and data station numbers where appropriate.

2 FABELT - fabric element

3 TYCODE - structure type code

4 N - number of data in set

5 HVM - hemispherical vector mean defined as the eigenvector corresponding to the maximum eigenvalue of the correlation tensor (Watson, 1966; Woodcock, 1977). It is expressed here as a strike and dip value for the planar fabric element

6 K_s - a fabric shape parameter defined by Woodcock (1977).

7 L_B - the pole to the girdle of best-fit through the orientation data, defined as the eigenvector corresponding to the minimum eigenvalue of the orientation tensor. It is expressed here as a trend/plunge value for data sets with a K_s value which is less than 2,0.

8 C_s - is a fabric strength parameter defined by Woodcock (1977) which approaches zero for subrandom fabrics and increases with increasing fabric strength.

9 Class - is a column indicating a fabric shape classification based on the K_s parameter C = cluster ($K_s > 2,0$); C - G = cluster transitional to girdle ($2,0 > K_s > 1,0$); G - C = girdle transitional to cluster ($1,0 > K_s > 0,5$); G = girdle ($K_s < 0,5$).

even more with the north-easterly dip of S_1 in subarea B. This shows that, north-east of the shear belt, the S_1 pattern is that of a major synform with a gently dipping NE limb and a more steeply dipping SW limb. The shear belt itself would form the complementary antiform in this interpretation, which would relate the deformation of S_1 to the D_2 folding episode. The fact that the cleavage generally dips 23° south-westward close to the base of the overlying nappe complex which has a maximum south-westerly dip of 5° is further evidence that there is no simple kinematic relationship between deformation of the Kuibis sequence and emplacement of the Naukluft nappes.

In treating the data from subareas A, B and C together for the purposes of statistical reduction, it is notable that the general north-westerly dip of SS in the deformed Kuibis Formation and the steeper north-westerly dip of S_1 are derived despite the general south-easterly dip of the Kuibis basal unconformity and the Unconformity Dolomite zone at the base of the Naukluft nappes. Both features are incompatible with the concept of Kuibis deformation by simple shear parallel to the regional bedding orientation combined with some degree of flattening along the normal to the nappe base. Instead they favour a significant degree of subhorizontal shortening in the Kuibis sequence above a *decollement* zone situated close to its base.

b. Internal structure of the Northern Pavian nappe

In the NW and N areas, the Northern Pavian nappe is comprised of the Remhoogte Formation alone. The latter, however, is a complex unit lithologically and structurally and certainly requires further detailed study. At present, it seems most probable that it has been pieced together tectonically as a large-scale *melange*. Field evidence for this point of view is clearly exposed in the region between Remhoogte and Stolzenfels (cf. Annex. I), where the Remhoogte Formation is composed of diverse tectonic elements. The lithological variability of the Remhoogte phyllites from highly crenulated varieties intensively veined by quartz to slaty varieties in which finely layered bedding remains well-preserved, can be related either to a pattern of extremely inhomogeneous deformation or to a subdivision of the Remhoogte

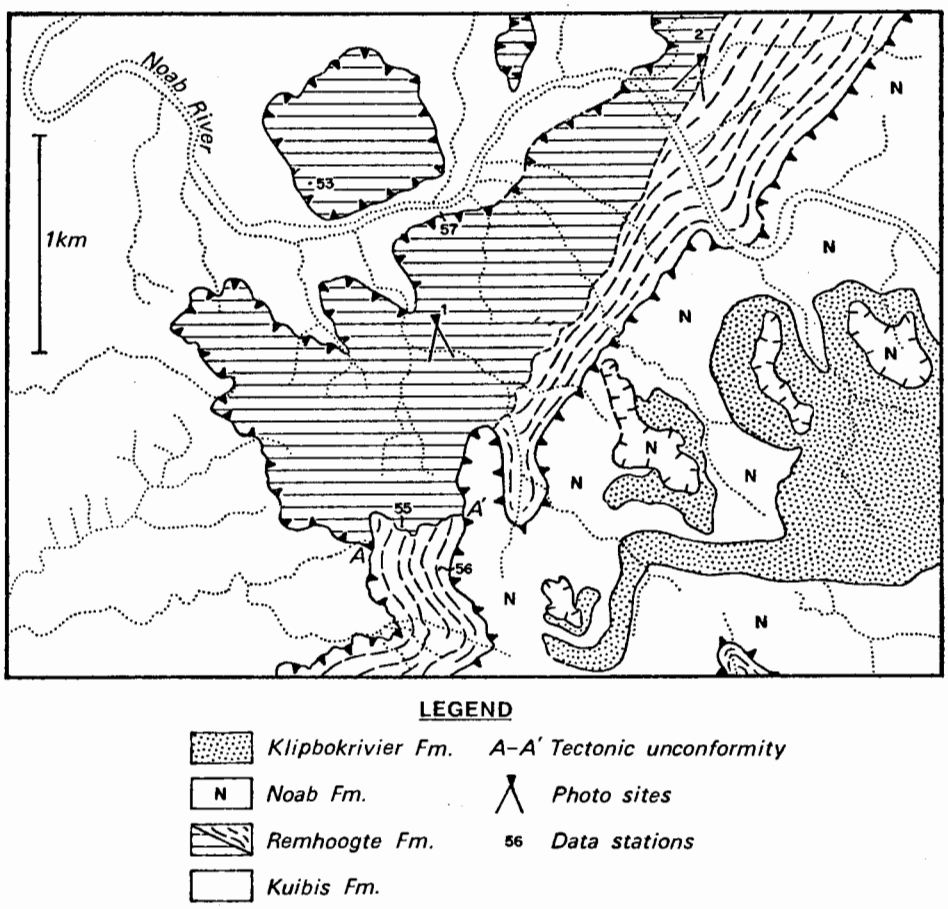

Figure 24. Detail map of critical area on boundary of farms Stolzenfels and Remhoogte, illustrating the internal structure of the N. Pavian and Kudu nappes.

Formation into two distinct phyllite units of different age. As yet, the available evidence does not allow a definite preference between these alternatives.

(i) Tectonic accretion phenomena in the Remhoogte Formation

In an area south of the Noab River gorge near the Remhoogte-Stolzenfels boundary (Fig. 24), a contact (A-A') cutting transversely across the exposed Northern Pavian nappe zone, clearly visible on the aerial photographs, is unusual in that it apparently links the trace of the Unconformity Dolomite zone with the trace of the Kudu nappe basal overthrust. In the field, it is marked by a thin dolomite zone, practically identical to the main Unconformity Dolomite at the base of the Naukluft nappe complex.

At locality 10057 (cf. Fig. 24), the subhorizontal Unconformity Dolomite, here about 1 m thick, divides a zone of cleaved chloritic *shale* in the Kuibis Formation (possibly a lower Schwarzrand facies) from a unit of highly deformed dark limestone locally transformed to greyish, fine-grained marble (Plate 29). The distinctive limestone passes upward into a marly zone of characteristic appearance (Plates 9 and 10). Irregular boudinaged layers, pellets and flakes of phyllite material in a calcite matrix show a complex array of tension gashes which are locally filled by fibrous calcite (Plate 9). The fractures are generally normal to and their internal fibres parallel to, a lineation (L_{1X}) defined by the general elongation of the phyllite fragments, having a measured orientation close to 125/05 (locality 10053). Locally the phyllitic marl zone is separated from an overlying limestone by a layer of boudinaged grey dolomite (Plate 10). If it was originally continuous, the boudinage of this rigid dolomite layer reflects bedding-parallel extensional strains of over 100 per cent, since the distance between individual dolomite boudins, which are about 1 m across, is greater than the boudin length in the L_{1X} direction. Apart from some minor fracturing and associated calcite veining, (cf. Plate 10), the dolomite boudins are not internally much deformed, thus reflecting the great ductility contrast which existed between this rock type and its surroundings during deformation.

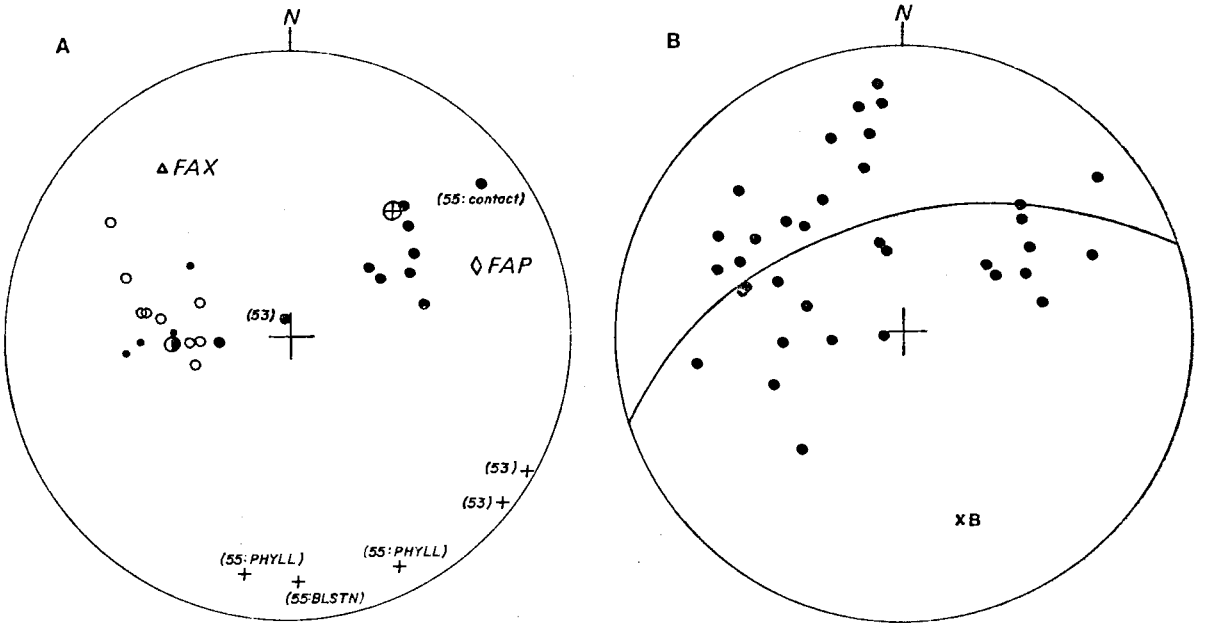

Figure 25. Orientation diagrams for fabric elements in the "exotic" unit of the Remhoogte Formation on the Stolzenfels-Remhoogte boundary.
A. Fabric elements from localities 10053, 10055, 10056, showing difference in orientation between S_1 measured in phyllite (open circles) and bituminous limestone (closed circles) at locality 10055 (Fig. 24).

Symbols :
- • SS in Noab Formation at 10056
- ○ S_1; PHF in Remhoogte Formation phyllite
- ● S_1; CLE in Remhoogte exotic unit
- ◑ S_1; MYF in Noab Formation at 10056
- ⊕ S_1; FRC in Noab Formation at 10056
- \+ L_{1X}; MEL in Remhoogte units

(FAP) axial plane of 10055 fold (Plate 30)
(FAX) axis of 10055 fold (Plate 30)

B. 35 poles to S_1 in Remhoogte exotic unit with computed best-fit girdle and B_{S_1} axis (B).

In the limestones the strain ellipsoid appears to be orientated with its X and Y principal axes parallel to original bedding, but in the marly zones (cf. lower left of Plate 10) a small dihedral angle between cleavage and bedding is generally observed and this invariably "faces" south-eastward (i.e. the cleavage dips more steeply north-westwards than the near horizontal bedding). Deformation of this carbonate sequence can therefore be partly related to simple shear due to traction near the base of the Naukluft nappe complex, but the relative magnitude of the bedding-parallel extensional strain component and the virtual absence of local zones of compensatory bedding-parallel shortening (i.e. no observed "shear folding") suggests that pure-shear flattening or "squeezing" of the sequence beneath the overriding nappes was the dominant deformation process.

The generally subhorizontal cleavage (S_1; CLE) in this unit changes suddenly to a dominantly south-westward dipping orientation near the contact trace A-A' (Fig. 24), suggesting a later (D_2) antiform here. At locality 10055, the contact itself dips 75° toward azimuth 231°, while S_1 foliation dips range between 30° - 50°. Between localities 10055 and 10056, however, the contact itself assumes a subhorizontal orientation and is approximately parallel to the cleavage in the *underlying* sequence. In detail (Plate 30), the contact between the deformed marl zone and the steeply dipping "Unconformity Dolomite" - type layer shows occasional fold structures. Orientations of the fold axial-plane (FAP) and fold-axis (FAX) for the illustrated example are represented in the accompanying orientation diagram (Fig. 25A).

The large-scale structural relationships of the contact zone and its surroundings are illustrated in the cross-sectional sketches (Figs.26 and 27) which have been traced directly from photographs taken at localities 1 and 2 respectively (cf. Fig. 24), the camera axis bisecting the V symbol used to identify the latter. The closer view (Fig. 26) shows the changing orientation of the contact zone and the way in which it steps up from the Unconformity Dolomite zone (which is below the camera level to the right of the field of view) to make contact with the Kudu nappe base in the centre of the field of view (point A' in Fig. 24). The distant view mainly

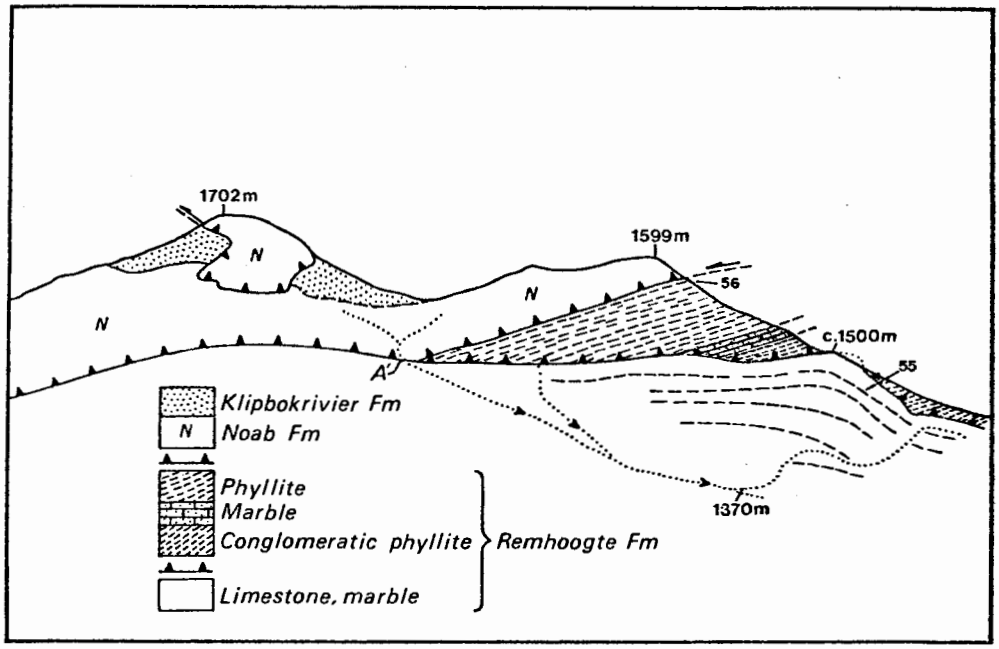

Figure 26. Sketch of photographic view from point 1 in Fig. 24, showing the southern contact of the exotic limestone unit within the Remhoogte Formation, along which a thin zone of "Unconformity Dolomite" is developed. Localities on the mountainside of data sites 10055 and 10056 are shown, as well as point A' of Fig. 24.

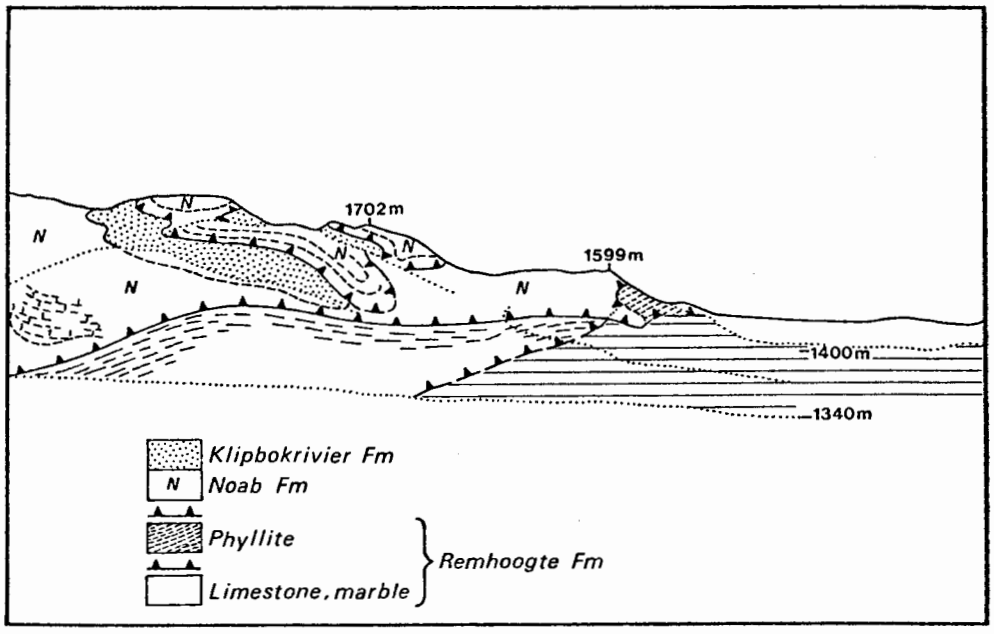

Figure 27. Sketch of photographic view from point 2 in Fig. 24, showing relationship between eastern contact of Exotic limestone unit and the base of the Kudu nappe. Relationships between the Noab Formation (blank) and the Klipbokrivier Formation (stippled) within the Kudu nappe are also visible.

illustrates the relationship of large-scale folding and imbricate structure in the Kudu nappe to the feature under discussion.

The major discordance of lithology and of tectonic cleavage orientation between the upper part of the Northern Pavian nappe and the sequence below the contact A-A' is particularly evident in Fig. 27 . Below locality 10056 and south-west of 10055 (Fig.24), the Remhoogte Formation is divisible into three sub-units in which lithological boundaries and planar fabric elements are sub-parallel to each other and to the base of the overlying Kudu nappe. The lowermost part of the Remhoogte formation is a zone of conglomeratic phyllite (Plate 31) which contains large pebbles and boulders of granitic gneiss but which is particularly conspicuous for large boudinaged quartz veins (cf. Plate 31) that locally form pseudo-conglomeratic layers parallel to the principal tectonic foliation. The latter (S_1; PHF) is evidently a compound structure comprising two microscopically distinguishable sub-fabrics (s_1 and s_2). Overlying this unit is a highly deformed zone of dark marble passing gradationally upwards into a thicker zone of fine-grained phyllite. The contacts between these zones are sharply truncated at the " Unconformity Dolomite" zone along the contact A-A' (Fig. 26).

It is notable that there is no obvious deformation of the upper sequence, no drag or traction structures (apart from a very low amplitude flexuring of the phyllitic foliation) which can definitely be related to movement along this tectonic discontinuity. In other words, while the development of a tectonic fabric in the lower carbonate sequence is clearly connected to deformation involving considerable relative movement along this boundary discontinuity, the upper sequence and the overlying Kudu nappe remained effectively rigid and undeformed.

The difference in orientation between the main tectonic foliation (S_1 ; PHF) in the upper Remhoogte phyllitic sequence and the cleavage (S_1 ; CLE) in the lower Remhoogte carbonate sequence (cf. orientation diagram of Fig. 25) is associated with an almost orthogonal relationship between the B axes defining the late open folding of these fabric elements.

The existence of a tectonic unit, about 5 x 2 km in areal extent and almost 200 m thick at its maximum point, which appears to have been incorporated into the Northern Pavian nappe at a relatively late stage in its tectonic evolution, has three important consequences for the interpretation of Naukluft nappe tectonics.

Firstly, it conclusively contradicts the former interpretation of the emplacement sequence of the major nappes (Korn & Martin, 1959). There can have been no major relative movement between the Kudu and Northern Pavian nappes after the formation of the A-A' discontinuity, since detailed relationships at point A' (Plate 32) show that the bedding in the Noab dolomites and the mylonitic marble zone below the latter is sharply truncated by the thin "Unconformity Dolomite" layer which elsewhere separates the two major divisions of the Remhoogte Formation. This is related to movement between the upper and lower parts of the Northern Pavian nappe, with the former moving south or south-eastward over the latter (cf. the downward-facing "flow folds" of Plate 30) and this in turn, pre-dates the slight folding of the upper "Unconformity Dolomite" and the subsequent formation of the planar, undeformed Unconformity Dolomite zone at the base of the Northern Pavian nappe. This sequence of events is unambiguous evidence for the *earlier formation of the higher overthrusts*, so that the upper Kudu nappe was transported into its present position in "piggyback mode" (Elliott,1976a) by the lower Northern Pavian nappe.

Secondly, the strain pattern as reflected qualitatively by the intensity and orientation of cleavages and lineations shows that the Kudu and the upper part of the Northern Pavian nappe were transported together as a rigid body over a much more ductile substratum. This too contradicts the general model of large-scale "plastic flow" of the nappe complex over a relatively rigid basement (Korn & Martin, 1959). The deformed lower part of the Northern Pavian nappe can be correlated with the Kuibis Formation, in particular with the upper part of the Schwarzkalk Limestone Member as the

latter passes laterally into the lower green shale facies of the Schwarzrand Formation (Germs, 1972). It would therefore appear that, during this phase of nappe emplacement, the ductile substratum corresponded with a major part of the Kuibis Formation. Since the autochthonous Kuibis Formation is apparently much less deformed than the overlying lower Remhoogte unit, it would further appear that during the last phase of nappe emplacement the ductile layer had become restricted to the 1 m-thick main Unconformity Dolomite zone.

Finally, the drumlin-like shape of the tectonic unit described above seems to reinforce the analogy between the horizontal tectonic movement of large rock sheets and the movement of glaciers. The processes by which the 200 m-high "drumlin" of deformed limestone became accreted to the base of the overriding nappe complex deserves further more detailed study.

(ii) Phyllite fabrics in the Remhoogte Formation.

An important aspect of the main part of the Remhoogte Formation concerns the perceptible differences between the fabrics of two different varieties of phyllite.

The northern Remhoogte Formation displays a slightly higher degree of metamorphism (probable lower greenschist facies) than the central or southern parts of the Northern Pavian nappe and the northernmost phyllite occurrences show the apparent growth of minute crystals of biotite/stilpnomelane along a principal foliation formed by crenulation and pressure solution of an early phengite-chlorite fabric. These s_2 foliation planes are locally marked by a conspicuous iron-oxide staining and locally oxidised chlorite may be mistaken for biotite. Farther south, phyllites with a single, well-developed cleavage (s_1) contain porphyroblasts of chlorite with pressure-solution and pressure-shadow phenomena showing that the growth of the chlorite was synkinematic with the s_1 deformation. The crenulation cleavage of the s_2 variety is found where the Northern Pavian nappe is thin and where samples have been collected close to the base of the overlying Kudu nappe. The phyllites with a well-preserved sedimentary layering and cleavage of the s_1 variety are found well

away from the base of the Kudu nappe where the Northern Pavian nappe is thick.

The differences between the Type I phyllite fabric, which shows original sedimentary layering and a single "slaty" cleavage and the Type II phyllite, which shows two penetrative planar fabrics both of tectonic origin, can possibly be mapped systematically in the field, with the Type I variety forming the southern and lower parts of the Remhoogte Formation and the Type II variety occurring mainly on the northern and upper parts. This possibility has, however, not yet been fully investigated and no zone of contact or transition between the phyllite types has been located.

In the field, the main cleavage in both Type I and Type II phyllites was regarded as the first generation-planar fabric element - S_1, and assigned the structure type code PHF (for "phyllite foliation"). The existence of an overprinted, phengite+chlorite fabric in Type II phyllite is really only apparent on microscopic examination. The widespread development in this rock type of syntectonic quartz veins which have been boudinaged or folded during the development of the main phyllitic foliation, is nevertheless a conspicuous characteristic. Microscopically, these veins which are present on scales ranging from a few tens of microns up to several metres, appear to have formed originally during or just after the development of the early s_1 fabric; some contain minute folds to which the s_2 crenulation cleavage, is axial-planar (cf. Fig.11). In these fold hinges and in areas of extensional necking between microboudins, the deformed quartz has a characteristic subgrain mosaic microstructure, probably indicative of a particular dislocation creep mechanism of quartz deformation.

Since "wet" quartzite deforming by dislocation creep at temperatures close to 400°C, apparently requires a deviatoric stress exceeding 200 MPa for steady-state plastic flow to occur at a strain-rate greater than 10^{-14} s^{-1}, (Heard, 1976), these features are important to the dynamic analysis of early nappe emplacement in the Naukluft complex.

Siliceous lamellae parallel to s_2 in the intensely deformed Remhoogte phyllites generally show a well-recrystallised microstructure (cf. CH38)

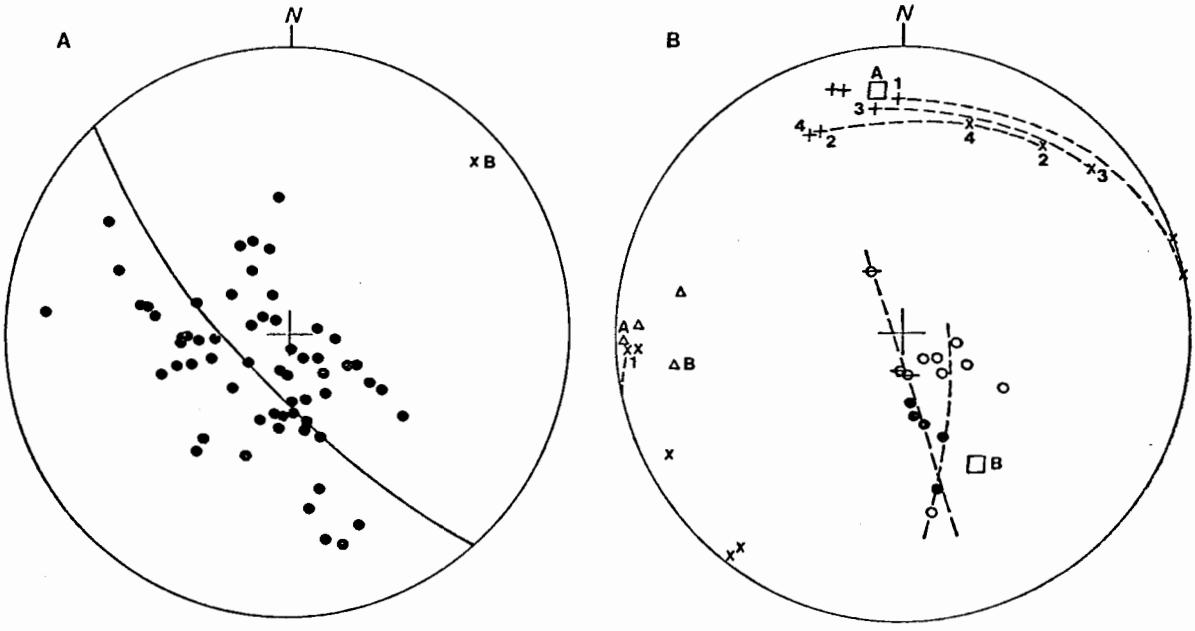

Figure 28. Orientation diagrams for main part of the Remhoogte Formation in the N and NW areas.

A. 60 poles to S_1 with computed best-fit girdle and B_{S_1} axis (B)

B. Fabric elements at localities 10052, 10070, 10072 near Remhoogte Pass, illustrating variation in angle between L_{1X} and L_{1B} lineations (cf. linked pairs 1-4).

Symbols : ○ ● ⊖ S_1 at 10052, 10070, 10072 respectively
+ L_{1X}; MEL
× L_{1B}; ISL
□ S_2
△ L_2

of fine (c.30 μm) grains with straight or gently curving boundaries meeting in equilibrium 120° triple junction (cf. Fig.12). The rise in temperature leading to the formation of unoriented biotite/stilpnomelane is therefore interpreted as having occurred after production of the s_2 fabric.
The s_2 foliation close to the shear zone at the base of the Kudu nappe and the s_1 phyllite cleavage lower in the tectonic sequence are folded and micro-crenulated by a later structure (s_3 or s_2 respectively) which is apparently associated with large-scale imbrication of the Kudu nappe observed most conspicuously in the Remhoogte Pass region.

In a few outcrops (e.g. 10067, 10072), the main S_1 cleavage is very planar and lacks signs of later crenulation and has accordingly been assigned the structure type code SLC (for slaty cleavage). In some quartzitic parts of the Remhoogte Formation, the S_1 fabric element is typed simply as CLE (for cleavage of unspecific sort). Comparing the main geometrical characteristics of S_1 in the NW and N Remhoogte Formation (Table 5), the differences between the S_1 fabrics in the lower "exotic" limestone and marl units of the Remhoogte Formation and the main part of this unit are immediately apparent on their respective hemispherical vector mean (HVM) orientations and B_{S_1} axes of rotation. The S_1 orientation diagram (Fig.25B) for the Remhoogte "exotics" (Fig. 24) shows a diffuse (C_s = 1,7) cluster transitional to a girdle (K_s = 1,1). Despite the small sample size (N = 35) the structural heterogeneity of these units is obvious and a more detailed investigation into the reasons for the very variable orientation of S_1 is probably warranted in future. The overlying main part of the Remhoogte Formation, from which a larger S_1 orientation sample was obtained, shows a weak clustering of poles (Fig.28A) with a poorly defined girdle pattern (K_s = 1,8) which is nevertheless indicative of greater geometric homogeneity.

The HMV orientation of the dominant phyllitic foliation (S_1; PHF) contrasts, in strike direction, with the orientation of SLC and CLE types at a minority of data sites. It reflects the generally shallow to subhorizontal orientation of S_1 in the Remhoogte Pass region, from which most of the data

TABLE 5

FABRIC STATISTICAL PARAMETERS FOR THE REMHOOGTE FORMATION STRUCTURES IN THE NW AND N AREAS

UNIT/LOCALE	FABELT	TYCODE	N	HVM	K_s	L_B	C_s	Class
RHB*	S_1	all	35	056/35	1,12	163/33	(1,67)	C - G
RH**	S_1	all	60	307/12	1,79	046/12	2,46	C - G
RH	S_1	PHF	48	342/13	3,25	-	2,48	C
RH	S_1	SLC	8	243/25	3,42	-	4,32	C
RH	S_1	CLE	4	246/57	0,58	278/39	6,71	G - C

* RHB - "exotic" units at base of Remhoogte Formation in NW + N areas

** RH - Remhoogte Formation, excluding RHB units

TABLE 6

FABRIC STATISTICAL PARAMETERS FOR THE KUDU NAPPE STRUCTURES IN THE NW AND N AREAS

UNIT/LOCALE		FABELT	TYCODE	N	HVM	K_s	L_B	C_s	Class
NO	(all)	SS	BED	59	040/17	1,59	212/02	2,54	C - G
NO	10056	"	"	4	006/38	1,58	132/33	5,59	C - G
NO	10064	"	"	6	165/18	0,57	313/10	5,01	G - C
NO	10068	"	"	4	056/33	0,26	058/01	5,01	G
NO	20031	"	"	3	046/55	1,05	099/49	8,91	C - G
KBR	(all)	"	"	7	032/19	0,87	067/11	7,32	G - C

NO - Noab Formation

KBR - Klipbokrivier Formation

was derived and the overall shallow north-easterly to north-north-easterly dip of the principal fabric element there. Where S_1 has a "slaty" character, its HVM orientation is closer to the overall HVM orientation of S_1 in the Remhoogte Formation of the Central area about the Tsondab River (247/36; cf Table 8).

This may point to a correlation between S_1 orientation and type, in that the phyllite variety appears to have flatter and the slaty variety somewhat steeper, dips: it could be related to transition from more intensely deformed to less intensely deformed pelite in a kinematic model of sub-horizontal inhomogeneous simple shear beneath the dolomitic Kudu nappe.

Indications of inhomogeneous finite strain are seen in the pattern of the two early lineations (L_{1X}; MEL and L_{1B}; ISL) associated with the slaty and less crenulated variety of phyllitic foliation in the Remhoogte Pass area. Within a restricted area at locality 10072, the rate angle of the lineation (L_{1B}) formed by the intersection of SS and S_1 relative to the lineation or "grain" (L_{1X}) formed by the elongation of metamorphic mineral aggregate and particularly minute chlorite porphyroblasts, in the plane of s_1 varies from 90^o down to only 38^o (cf., linked lineation pairs 1 to 4 in Fig. 28B). Data from nearby localities 10070 and 10052 which have similar pelite fabrics are included in the latter orientation diagram. The early fold style, the nature of the SS/S_1 intersection lineation and indications of L_{1X}, reflecting the principal extension direction, are illustrated in Plate 33 .

While it appears that some of the variability of S_1 orientation may be due to inhomogeneous finite strain patterns produced during the main cleavage-forming deformation episode, some later folding of S_1 is also obvious at some localities where the axial-plane orientations of minor folds in S_1 (S_2 ; FAP) or of distinct crenulation cleavages (S_2; CRC) are measureable. From the few data available it appears that these generally have steep to moderate southerly or westerly dips and that associated minor fold axes (L_2 ; FAX) or crenulations (L_2; CRC) have very variable trends (Fig. 29A).

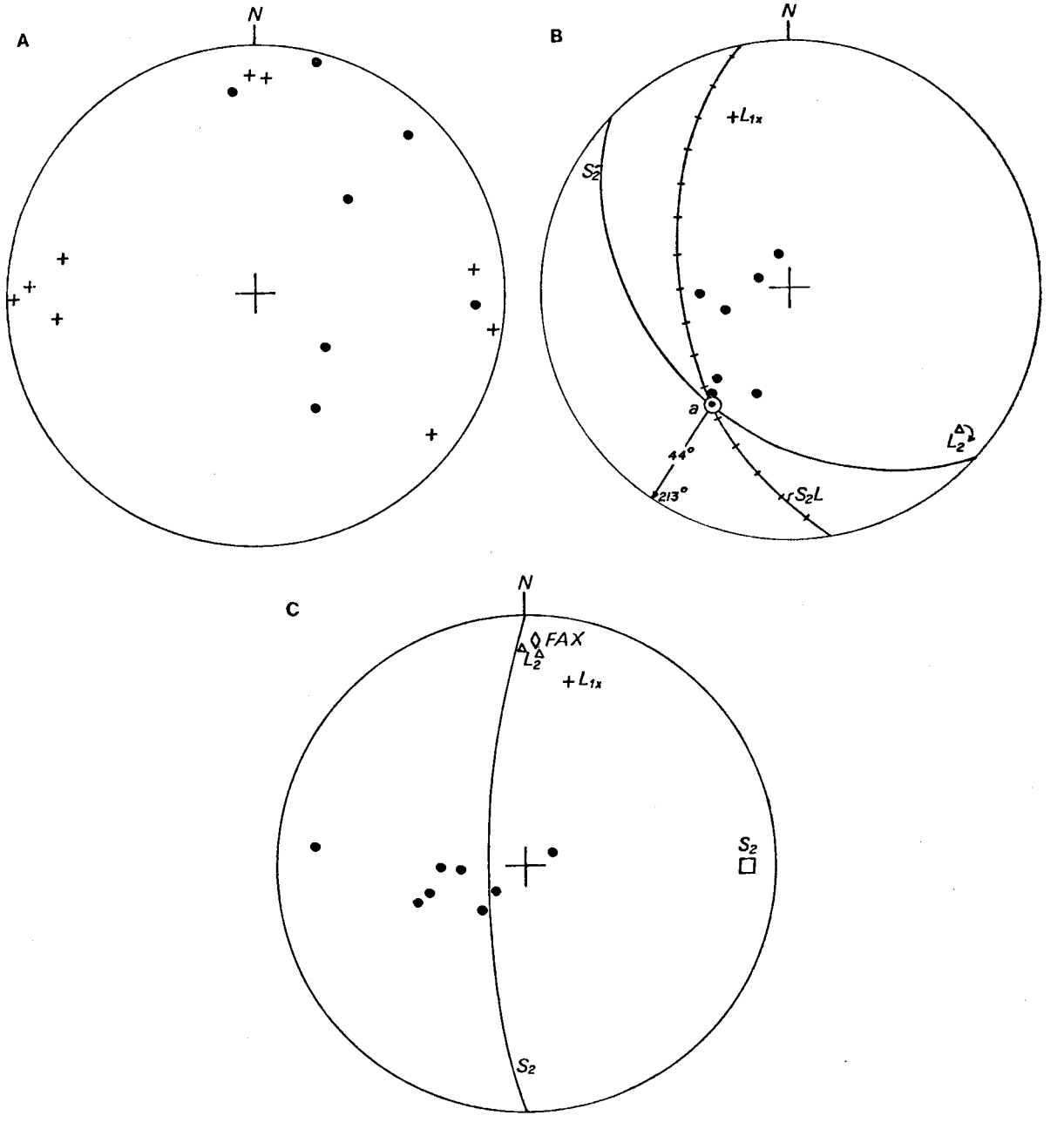

Figure 29. Orientation diagrams illustrating late (i.e. post-S_1) deformation of the Remhoogte Formation in the N and NW areas.

A. 7 poles to S_2; CRC & FAP (dots) and 9 poles to L_2; CRL (crosses)
B. Deformation of L_{1X} lineation (S_{2L} = plane of dispersion) by late fold (S_2 = axial plane) at locality 10061. Kinematic "a" direction defined by intersection of these planes trends 213° with 44° plunge. S_1 orientations (dots) and fold axis (L_2) with asymmetry sense shown.
C. Deformation of S_1 and orientation of late fold fabric elements between localities 20033-20036 (N area) in Remhoogte Formation. Dots represent orientations of S_1 ; PHF.

At locality 10061 in the Noab River gorge near Stolzenfels-Remhoogte boundary, the south-westerly dipping S_2 fold axial-planes appear as discrete shear surfaces with a spacing of about 10 cm (Plate 34). The orientation diagram here (Fig.29B) illustrates the attitude of S_2, L_2 and several poles to the folded S_1 foliation. In addition, the representative orientation of the mineral lineation L_{1X}; MEL is shown as well as the (directly measured) orientation of the plane (S_2L - 170/55) in which the L_{1X} lineation is dispersed as a result of folding about L_2. The intersection of S_2 and S_2L (marked "a" in the diagram) can be interpreted as the shear direction of the later deformation and its orientation (213/44) directly down-dip of the S_2 surface is consistent with this. The style of the folds in S_2 indicates dextral rotation about L_2 (130/11), so that the narrow south-westerly dipping limb zones appear more deformed than the wider north-easterly dipping limbs. The phyllites at this locality are of the Type II variety and therefore the mesoscopic S_1 fabric is composed of S_1 and S_2 subfabrics as described above. The contrast in general appearance between phyllite type is evident in a comparison of Plates 33 and 34.

Farther north, on Noab at localities 20033-360, a major antiformal structure causes the Remhoogte phyllites to appear in a small inlier beneath the Kudu nappe. Field and photogeological evidence suggests that this antiform may be bounded on the east by a long fault, the trace of which trends slightly east of north. The orientation diagram (Fig. 29C) shows the folding of S_1 about shallow north-plunging axes marked on a mesoscopic scale by a "pencil-like" intersection lineation (L_2; PEN). Also shown are the axial orientation of an early fold (L_1; FAX) observed at location 20036 and the orientation of the early mineral lineation at 20035. Whereas the minimum angle between L_{1B} and L_{1X} at site 10070 is about 40°, the angle between the equivalent structures at localities 20035-6 is only 20°. If it is assumed that early intersection lineations and field axes originally formed at right angles to the principal stretch direction and subsequently were rotated towards the direction with increasing finite strain, then it is possible to interpret the Type II phyllites of the latter area as more intensely deformed than and transitional from the Type I phyllites of the more southerly Remhoogte Pass

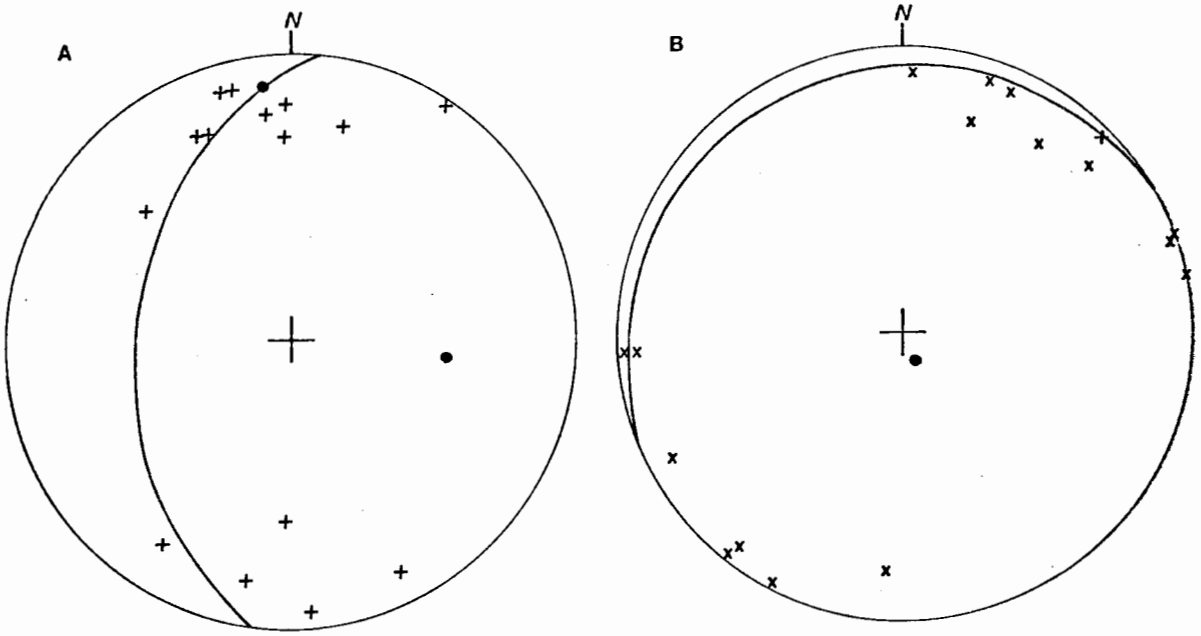

Figure 30. Orientation diagrams for linear structures in the Remhoogte Formation of the N and NW areas.

A. 15 L_{1X} poles with computed best-fit girdle and HVM orientation (great circle with associated heavy dot) and pole to this plane of preferred dispersion(isolated dot).

B. 16 L_{1B}; ISL & L_1; FAX poles with associated pole and great circle of preferred dispersion (dot and girdle).

area.

The deformation of early linear structures on Noab has not yet been analysed in detail. It is, however, interesting to note that, on processing by the VECSTA routine, relatively small sample (N = 14) of L_{1X}; MEL structures from the entire NW and N areas yields a HVM orientation of 354/11 and is preferentially dispersed in a plane orientated at 186/46 (Fig.30A). The shape and strength parameters of the orientation tensor (Woodcock, 1977) are K_s = 1,82 and C_s = 2,49 respectively, indicating that the sparse available data define a weak cluster barely transitional to a girdle pattern. Despite this *caveat* on the significance of the dispersion plane, its similarity in orientation to that actually measured at 10061 is perhaps significant. Its hypothetical intersection with the S_2; CRC plane measured at 20034 has a very shallow 7^o northward rake on the S_2 plane and this may indicate that the kinematic "a" direction of simple shear (assuming that this is the appropriate fold-forming deformation model) was subhorizontal. In view of the close spatial association of this late antiform with the fault structures on the east and the widespread pattern of arcuate fold axial trends in the NW and N areas (Fig. 31), this observation may support the hypothesis that the fractures are strike-slip faults which formed during the later, post-S_1 episode.

c. Internal structure of the Kudu nappe

The Kudu nappe in the northern and north-western areas is comprised of two quite distinct lithostratigraphic units; the lower Noab Formation and the upper Klipbokrivier Formation. Lithological differences and the consequent ductility contrasts between these different units are expressed in differences of structural styles and fabric development.

(i) Noab Formation structure

The most impressive large-scale features of the Noab Formation in these areas are the huge, apparently recumbent synclinal structures which are often cored by Klipbokrivier pelites (cf. Plates 35 & 36). The largest

of these structures is that below Grenzberg (1856 m) on Noab, which is well exposed and accessible from the main Remhoogte Pass road. The lower limb of this large structure is complicated by several subsidiary synclines and anticlines which are easily traced by mapping of the Noab-Klipbokrivier contact (cf. Fig.31). The larger structure apparently extends north-eastward into two more deeply eroded structures in which the Klipbokrivier Formation is preserved only as thin strips of strongly cleaved pelite. The hinge zones of similar, but smaller structures situated west of the Grenzberg syncline are illustrated in Figs. 26 & 27 which also show the Remhoogte accretion phenomena.

A significant feature of the synclinal hinge zones is that the complete passage from the normal lower limb to an inverted upper limb is rarely seen. Instead it generally appears that the upper limbs are not inverted and that the apparent hinge zones are at, or close to, the loci of major faults (cf. Plate 35). As the large synclines are part of a larger scale imbricate structure consisting of low-angle faults and appear to have developed by traction along fault surfaces only after the latter were formed, this explains why intervening anticlines of equivalent magnitude are not seen.

The absence of penetrative deformation fabrics over wide areas of the Noab Formation is also remarkable. A major lithological component of the Noab is the sandy dolomite in which abundantly scattered grains of sub-spherical and very well-rounded quartz grains are found. Evidence of microscopic deformation structures in thin sections of this rock type (CH 36 and CH 40) suggests that the quartz component of the rock was slightly more ductile than the surrounding dolomite when the Noab structures originated; some strained quartz grains showing undulose extinction patterns appear to have been slightly indented by adjacent dolomite grains. In general, however, the finite tectonic strain recorded by the quartz and dolomite clasts in the sandy dolomites is minimal. Though no intensive R_f/ϕ studies (Dunnet & Siddans, 1971) have been carried out to substantiate this, it is in most places evident that there is scarcely any or only a very minor component of

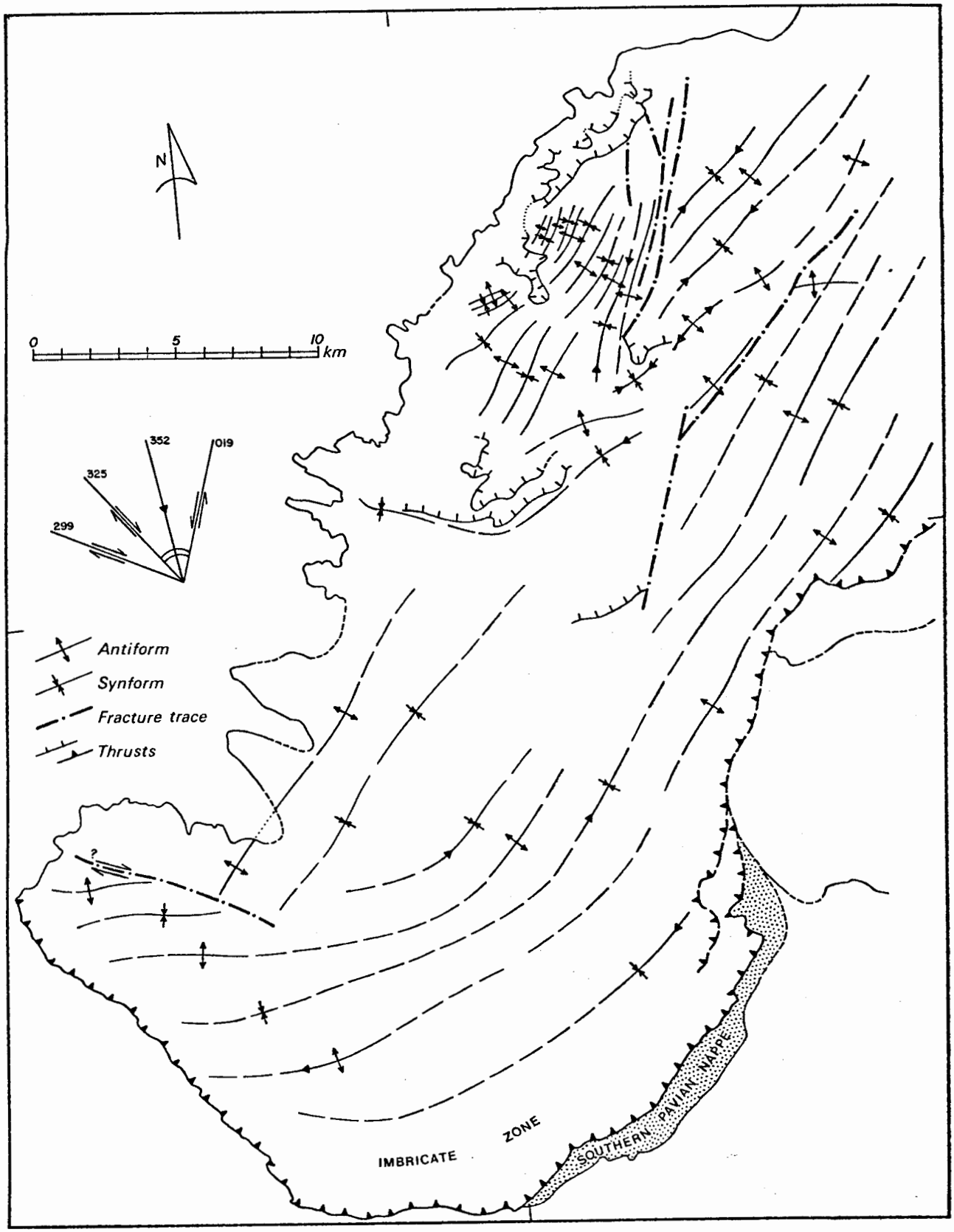

Figure 31. Diagram of fold trends in the N and NW areas of the Naukluft nappe complex, drawn from aerial photographs and reduced version of the accompanying 1 : 100 000 map (Annex. I).

grain shape and preferred orientation resulting from penetrative ductile flow in Noab dolomites. Where ductile deformation is most evident, namely in the zone of marble and phyllite which forms the basal *decollement* of the Kudu nappe, in areas close to the hinge zones of the major synclines and in narrow shear zones closely associated with the latter, the principal fabric element in the Noab is often a pressure solution foliation (S_1; PSF) of characteristic appearance (cf. Plates 37 to 42). The limited distribution of ductile deformation fabrics on the Noab dolomite is reflected in the relatively small sample of S_1 orientation measurements since at most sites the only visible penetrative planar element was sedimentary bedding.

In many parts of the Noab massive dolomite outcrop, it is even scarcely possible to obtain orientation measurements of the bedding fabric (SS; BED) because of the homogeneous composition of dolomite. This fact discouraged a closer and more systematic sampling of the dolomite structure. The general orientation diagram (Fig.32A) shows slight evidence of triclinic symmetry, although it is dominated by a partial girdle of poles normal to a south-westerly trending axis, possibly reflecting a sample site bias in the region north-east of the Grenzberg syncline where structural features of this orientation are dominant. If structural sampling were extended to areas further south or south-east where east-west structural trends are photogeologically evident (Fig. 31) the abundance of orientation data having strike values in the ranges 90° - 180° and 270° - 360° would certainly increase. As it is, the data having these anomolous strikes come mainly from a region south-west of the Grenzberg syncline, including localities 10056 and 10064-66.

At sites 10056 and 10064, the bedding orientations define axes of rotation (B_{SS}) with orientations of 132/33 and 313/10 respectively (Table 6). Both sites are situated close to the base of the Kudu nappe near to its north-western margin where some late folding and imbrication of the Kudu-N. Pavian contact is evident. It is therefore possible that this anomalous mesoscopic folding is not coeval with the main macroscopic folding, but this has yet to be fully investigated. The principal early linear structures, namely minor fold axes (L_1; FAX) and intersection lineations

(L_{1B}; ISL), scatter as the south-western and north-eastern quadrants of the orientation diagram (Fig.32A).

The diagram (Fig.32B) for S_1 fabric elements of all types shows poles plunging into all quadrants. The HVM orientation for the available data (N=31) is 059/21, but with a fabric strength parameter, C_s, of only 1,56 its significance is very weak. It does, however, point to the common occurrence of south-easterly dipping S_1 orientations and is close to the HVM orientation of S_1 in the "exotic" basal Remhoogte carbonate unit (Table 5). Being close to the HVM orientation of 040/17 for SS in the Noab Formation, it does not reflect the common field observation that SS usually dips more steeply south-eastwards than S_1 foliation in the basal Kudu nappe marble zone, where the latter is flat-lying over a wide area in the northern part of the nappe complex.

The latter phenomenon was described and illustrated by Korn & Martin (1959,p.1070 & Fig.18) as truncation of downward-facing imbrication at the base of the Kudu nappe, due supposedly to frictional ablation of the apices of early recumbent folds in the Noab Formation. No field evidence exists to support this point of view and in several places it is clear that the fabric element thus truncated is sedimentary bedding alone with no trace of parallel tectonic cleavage. On the contrary, at some sites (eg., 10068) it is obvious that the S_1 fabric is upward-facing and diverges smoothly in orientation when traced away from the mylonitic basal marble zone. Where the S_1 structure in the mylonite marble (S_1; MYF) is subhorizontal or dips gently south-eastward, the S_1 cleavage (S_1; PSF) in dolomite or dolomitic limestone only a few metres above may dip north-westward at angles close to 60°, there being a continuous gradation in structure-type and orientation between the end members as reflected in Plates 37 and 39 . Even within local north-west dipping shear zones as at locality 10074, the S_1 fabric associated with a lower degree of finite strain dips more steeply than that associated with a higher degree of finite strain. (cf. Plates 41 and 42).

Part of the variable orientation of S_1 reflected in the diagram and in the poorly-defined (shape parameter K_S=1,17) tendency towards a girdle normal

to an axis at 227/05, is therefore due to finite strain variation about the basal Kudu *decollement* resulting from inhomogeneous decreasing shear away from the thrust surface. Some of the steeper south-easterly dips in S_1 are due to late flexural-slip folding, sometimes of backfold or box style, of laminated marble in the thrust zone; this confined late folding is evident at locality 20008, for example and reflected in the S_1 data from that site. There is no corresponding large-scale deformation of the thrust zone or S_1 fabrics generally into such orientations. The essential point, though, is that the S_1 orientation diagram (Fig.32B) in no way supports the inaccurate schematic representation of Kudu nappe structure, figured by Korn & Martin (1959, Fig. 18), as large-scale downward-facing plastic flow structures.

(ii) Klipbokrivier Formation structure

Some lithological aspects of Klipbokrivier deformation have been briefly mentioned and illustrated in Chapter III (cf. Plates 7 & 8). According to Korn & Martin (1959, p.1070) the tectonics of the former "Klipbok series" is important for two reasons: Firstly because its sedimentation shows an "intimate relationship" to the deformation of the underlying dolomitic part of the Kudu nappe and secondly because its deformation, as shown by pebble elongation, "differs radically from the deformation found below the Kudu nappe". In the present project, the first contention is accepted but the second is rejected.

The bedding orientation (Fig.33A) in those parts of the Klipbokrivier outcrop which were sampled does not vary much from 032/19, but the data define a transitional girdle normal to a pole at 067/11 (Table 6). The HVM orientation of the small sample (N=5) of bedding-cleavage intersection lineations (L_{1B};ISL) is close at 040/06. A larger sample (N=33) of stretch lineations (L_{1X}), including pebble elongation in the carbonate breccia unit and mineral alignment in carbonate and pelitic rocks, shows a HVM orientation at 002/05. This data shows a tendency to be slightly dispersed in a plane with orientation 210/10 (Fig.33B), which is tolerably close to the HVM orientation of the S_1 foliations at 257/05.

These statistics and the relevant fabric diagrams (Fig. 33)

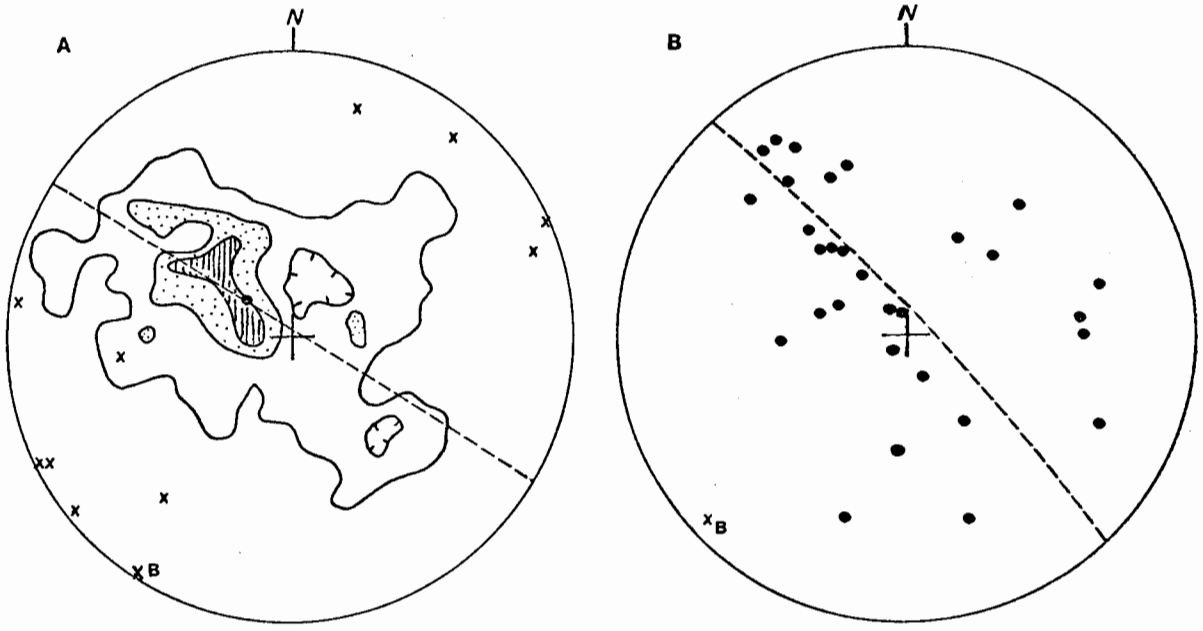

Figure 32. Orientation diagrams for the Noab Formation in the N and NW areas.

A. 59 poles to SS (contours 1-5-10%) and 10 L_{1B}; ISL & L_1; FAX poles (crosses). Also represented are SS mean orientation (dot) and computed best-fit girdle with pole (marked B).

B. 31 poles to S_1 with computed best-fit girdle and pole (xB).

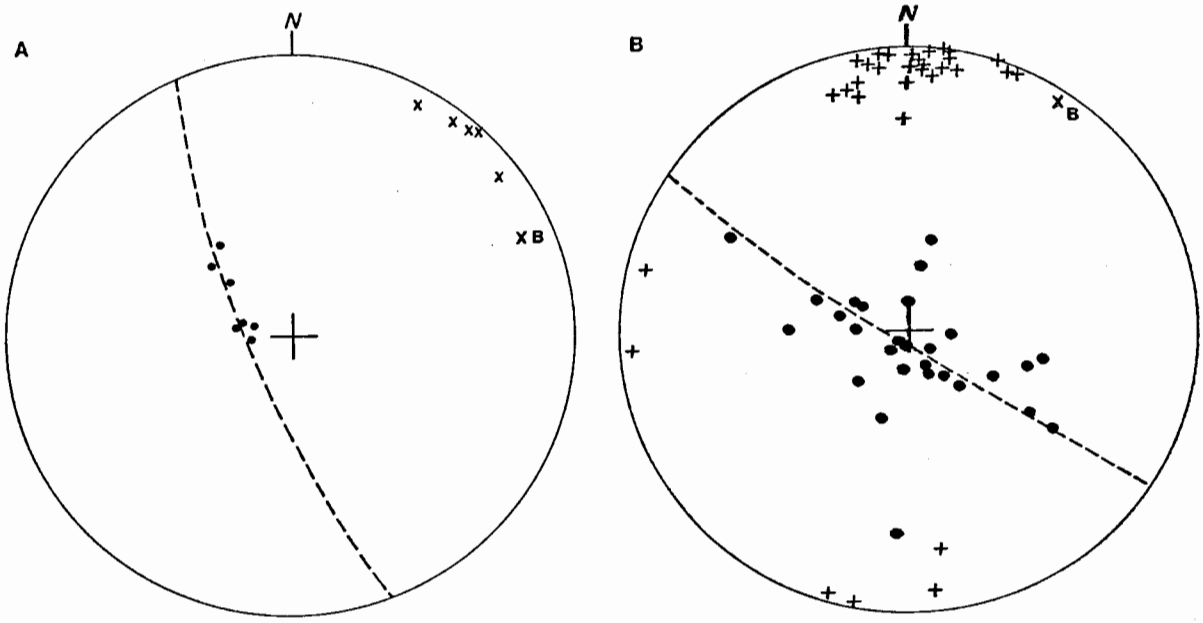

Figure 33. Orientation diagrams for the Klipbokrivier Formation.

A. 7 poles to SS (dots) and 5 L_{1B}; ISL poles with computed best-fit girdle and pole (B) to SS data.

B. 29 poles to S_1 (dots) and 33 L_{1X}; MEL & PEL poles (crosses) with computed best-fit girdle and pole (B) to S_1 data.

positively exclude the previous interpretation of deformation relationships between the Klipbokrivier Formation in the Kudu nappe and the underlying N. Pavian nappe (Korn & Martin, Fig. 15). Firstly, it is apparent that the pebbles are not "elongated in *b*" if the *b* kinematic axis is defined by the axis of rotation of bedding (B_{SS}), but the orientation data for S_1 are dispersed about a girdle with a pole at 033/04 which is intermediate between B_{SS} and L_{1X}. It is therefore locally probable that the L_{1X} lineation is subparallel to later folds in S_1. Secondly, the HVM orientation of L_{1X} in the Klipbokrivier Formation (002/05) is not significantly different from the L_{1X} HVM in the Remhoogte Formation of the N and NW areas (354/11). Neither is it significantly different from the HVM orientations of L_{1X} in the lower formations of the Northern Pavian nappe in the C area (cf. Section 3 below) which are 001/34 in the Remhoogte Formation and 356/24 in the Blässkranz Formation.

The problem of quantitative strain determinations in the Klipbokrivier breccias is difficult because the rocks include limestone and dolomite fragments of extreme angularity and very variable in size and initial orientation. However, it is possible to obtain some idea of the minimum extensions along certain directions in the rock by measurements on dolomite fragments which have fractured first and then been extended in pieces by ductile flow of the surrounding limestone component. Voids between the extended dolomite fragments have been filled by crystalline white calcite. A preliminary set of measurements in the XY plane, combined with a constant volume assumption to give the compressive strain component for which no direct data could be obtained, gives the following average values for the principal quadratic extensions in the rock: $\lambda_1 = 2{,}49$; $\lambda_2 = 1{,}29$; and $\lambda_3 = 0{,}31$. Even though this records the strain subsequent to the fracturing of the dolomite fragments, it seems likely that this may be very close to the total strain in the rock. It can be seen that the strain is of a flattening (oblate ellipsoid) type.

3. Structure of the Central (C) area

a. Internal structure of the N. Pavian nappe

In the C area, the Northern Pavian nappe is easily differentiated into three principal stratigraphic units (cf. Chapter 3) the distribution of which is illustrated on the 1:100 000 map (Annex. I). Over most of the western part of the C area, exposures are limited to the mountain slopes around the Tsondab River valley, but on the east (Fig.34) the escarpment zone between Blässkranz and Tsabisis supplies an almost continuously exposed section across the nappe.

There is a major difference in the N. Pavian nappe structure between the west and east areas. In the west the N. Pavian nappe is exposed in a large, gentle antiformal structure capped by the massive, thick and intact dolomite-plate of the Kudu nappe. In the east it is exposed as a northward-dipping imbricate zone overlain by the massive Kudu nappe on the north and itself overlying the imbricate eastern Dassie nappe on the south. The lower contact of the N. Pavian nappe in the west is exposed between Blässkranz and Arbeid Adelt separating the nappe from a massive, yet imbricated dolomite unit, previously correlated with the upper dolomite of the Southern Pavian series (Korn & Martin, 1959).

With regard to its internal structure, the most important features of the N. Pavian nappe are :

(1) the unconformity between the Remhoogte Formation and the Blässkranz Formation;

(2) the orientation pattern of S_1 cleavage in the nappe;

and (3) the imbricate structure of the nappe and its upper contact zone in the Tsabisis area.

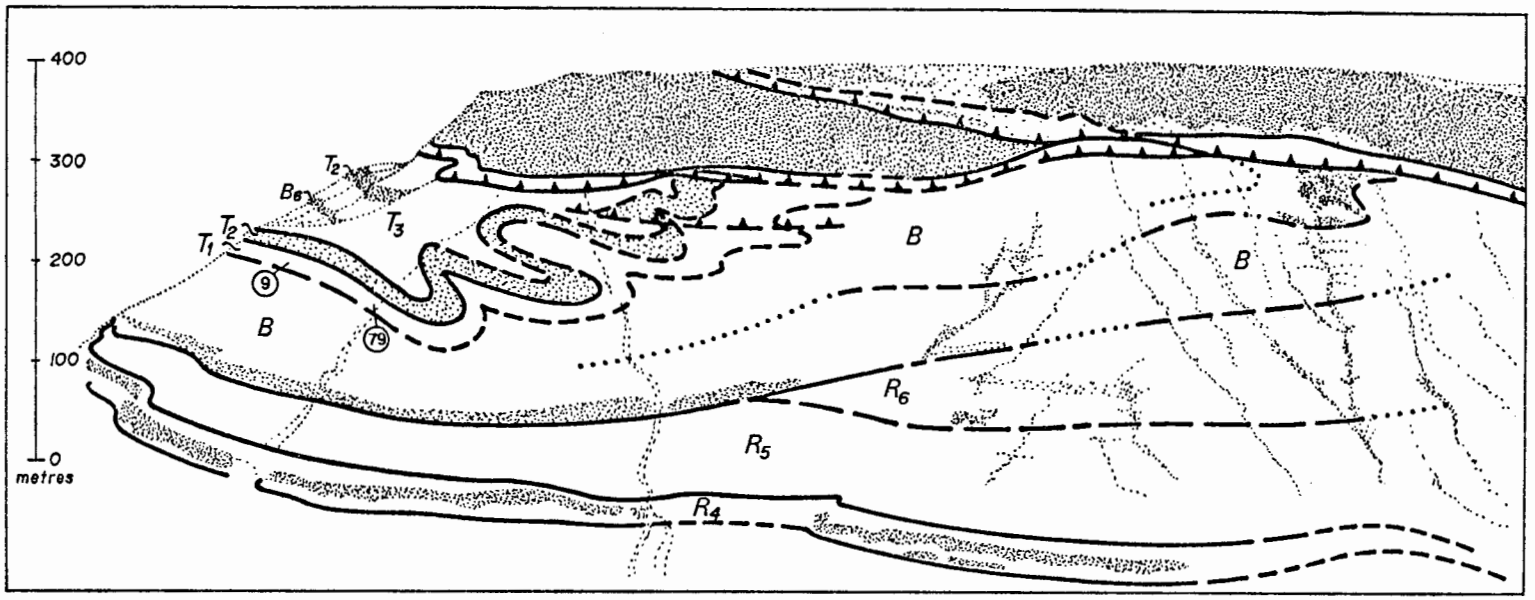

Figure 35. Sketch of panoramic photograph showing structure and stratigraphy along the section line A-A' in Fig. 34. The important features are the clear unconformity between Remhoogte lithostratigraphy (R_4 - R_6, after Fig. 10) and the overlying Blässkranz Formation (B), and the spectacular truncation of the folded Tsabisis Formation stratigraphy (T_1 - T_3) at the base of the massive dolomitic Kudu nappe.

(i) The Remhoogte-Blässkranz Formation unconformity

This important structural feature is exposed best on the northern side of the Tsondab River on the farm Blässkranz. West of the Tsondab on Arbeid Adelt, a conspicuous low-angle structural discordance is visible between the Blässkranz Formation and a prominent dark limestone near the top of the Remhoogte Formation and farther east around locations 30027-29, the Remhoogte limestone is succeeded by a 15 m sequence of "papery" phyllites containing disrupted layers of limestone and dolomite overlain in turn by a laminated quartzite unit. The latter rock type is exposed along a ~1 km segment of the mountain slope and wedges out eastward and westward beneath the Blässkranz Formation. It re-appears much farther westward, in the valley between Tsubgaus and Tsabisis, in the north-eastern corner of the Blässkranz farm. Here a north-south striking segment of the mountain face beneath the Kudu Plateau exposes a 400 m section through the Kudu and N. Pavian nappes, normal to the general structural trend. An accurate representation of structure along the section A - A' in Fig. 34 is given in Fig. 35 , which has been traced directly from a photographic panorama taken from locality 30057 on the opposite ridge. The ~15° angular unconformity between the phyllite-limestone-phyllite-quartzite sequence in the Remhoogte Formation is most obvious in this section.

The section also illustrates the spectacular overturned-to-recumbent folding of a prominent white dolomite layer in the Tsabisis Formation and more importantly, its truncation at the thin marble zone below the dolomitic Kudu nappe. Like folds in the same unit are exposed in the valley profiles of the southern mountain faces on the farm Blässkranz (cf. Plate 43 ; and Korn & Martin, 1959, Pl. 8A). The folds shown in Plate 43 correspond to those illustrated in Profiles d and e of Korn & Martin's (1959) Plate 8A. Truncation of Tsabisis dolomite at the base of the Kudu nappe is also seen in the extreme south-west of Blässkranz (cf. *op. cit.*, Profile g).

It should be noted, in passing, that although Korn & Martin's profiles of this region (*op.cit.*, Pl. 8A) give an adequate representation of

TABLE 7

FABRIC STATISTICAL PARAMETERS FOR THE N. PAVIAN NAPPE BEDDING (SS) STRUCTURES IN THE C AREA

UNIT/LOCALE		FABELT	TYCODE	N	HVM	K_s	L_B	C_s	Class
RH		SS	BED	72	244/20	2,26	(342/20)	1,65	C
BK		"	"	14	249/18	1,87	062/02	3,99	C - G
TSB		"	"	33	231/27	1,36	041/05	3,18	C - G
NO		"	"	23	169/17	2,96	(195/08)	3,57	C
RH	30031	SS	BED	4	195/23	1,55	238/16	5,56	C - G
RH	30034	"	"	3	181/16	2,41	-	6,33	C
RH	30046	"	"	7	117/80	0,34	293/19	4,66	G
RH	30050	"	"	8	270/24	0,42	030/21	6,32	G
RH	30052	"	"	5	270/26	0,97	012/25	5,70	G
RH	30055	"	"	11	010/25	0,36	027/08	4,00	G
RH	30056	"	"	6	203/58	0,29	014/14	5,02	G
RH	30057	"	"	10	211/39	0,47	319/38	2,40	G
RH	30059	"	"	4	189/34	2,03	-	6,63	C
RH	30069	"	"	5	301/39	6,96	-	4,92	C
BK	30029	"	"	5	242/22	2,60	-	6,51	C
BK	30038	"	"	4	240/20	7.19	-	6,64	C
TSB	30015	"	"	3	241/27	1,30	032/14	11,22	C - G
TSB	30040	"	"	5	234/20	4,65	-	6,62	C
TSB	30043	"	"	4	256/19	6,05	-	5,30	C
TSB	30079	"	"	3	232/49	4,74	-	8,11	C
NO	30041	"	"	6	173/21	46,22	-	5,14	C
NO	30044	"	"	3	244/10	2,84	-	5,98	C
NO	30045	"	"	4	061/18	1,62	088/08	9,90	C - G
NO	30071	"	"	8	170/30	3,28	-	5,37	C

RH - Remhoogte Formation
BK - Blässkranz Formation
TSB - Tsabisis Formation
NO - Noab Formation

structural style in the N. Pavian nappe, the structures shown in the overlying Kudu nappe are in the writer's opinion, not an accurate representation; downward-facing recumbent folds are not a large-scale feature of the Kudu nappe here. Furthermore, their lithostratigraphic divisions in the N. Pavian nappe miss the volcaniclastic zone below the white dolomite marker, and hence overlook the distinctive boundary between the Blässkranz and Tsabisis Formations. The mapping of the white dolomite in the northern parts of profiles f and g is also incorrect.

The orientation diagram (Fig.36A) for all sedimentary bedding measurements from all units in the C area shows no well-defined girdle pattern but is dominated by a diffuse cluster striking about 245° and dipping 35°. The dominance of north-westward dips in the sample reflects a bias in sampling on the northern side of the Tsondab valley and is not an intrinsic feature of the SS fabric in the central part of the nappe complex. The tabulated SS fabric statistics for each formation separately (Table 7) reveal a basic difference in HVM orientation between the Remhoogte (RH), Blässkranz (BK) and Tsabisis (TSB) Formations, on the one hand, and the Noab Formation (NO) on the other.

The mean SS orientations for the three N. Pavian units are similar, but there is a difference in the orientation of the computed axis of rotation (B_{SS}) which may be related to the unconformity described above. Fabric data for the Blässkranz and Tsabisis Formation describe weak clusters transitional to girdles (K_s ~1,50) with girdle axes plunging very shallowly (2 - 5°) to the north-east or east-north-east, whereas data for the Remhoogte Formation describes a diffuse cluster with poles scattered in all four quadrants. The best-fit girdle axis to the Remhoogte data plunges north-west (342/20) in stark contrast to the Blässkranz and Tsabisis axes, although HVM orientations for SS in the three formations are not significantly different.

The surprising features of the orientation diagram of intersection lineations (L_{1B}; ISL or PEN) and early minor fold axes (L_1; FAX) is the abundance of north-westerly trends in the sample which is dominated by data from the Remhoogte Formation (N = 37 out of 42). Orientation tensor treatment

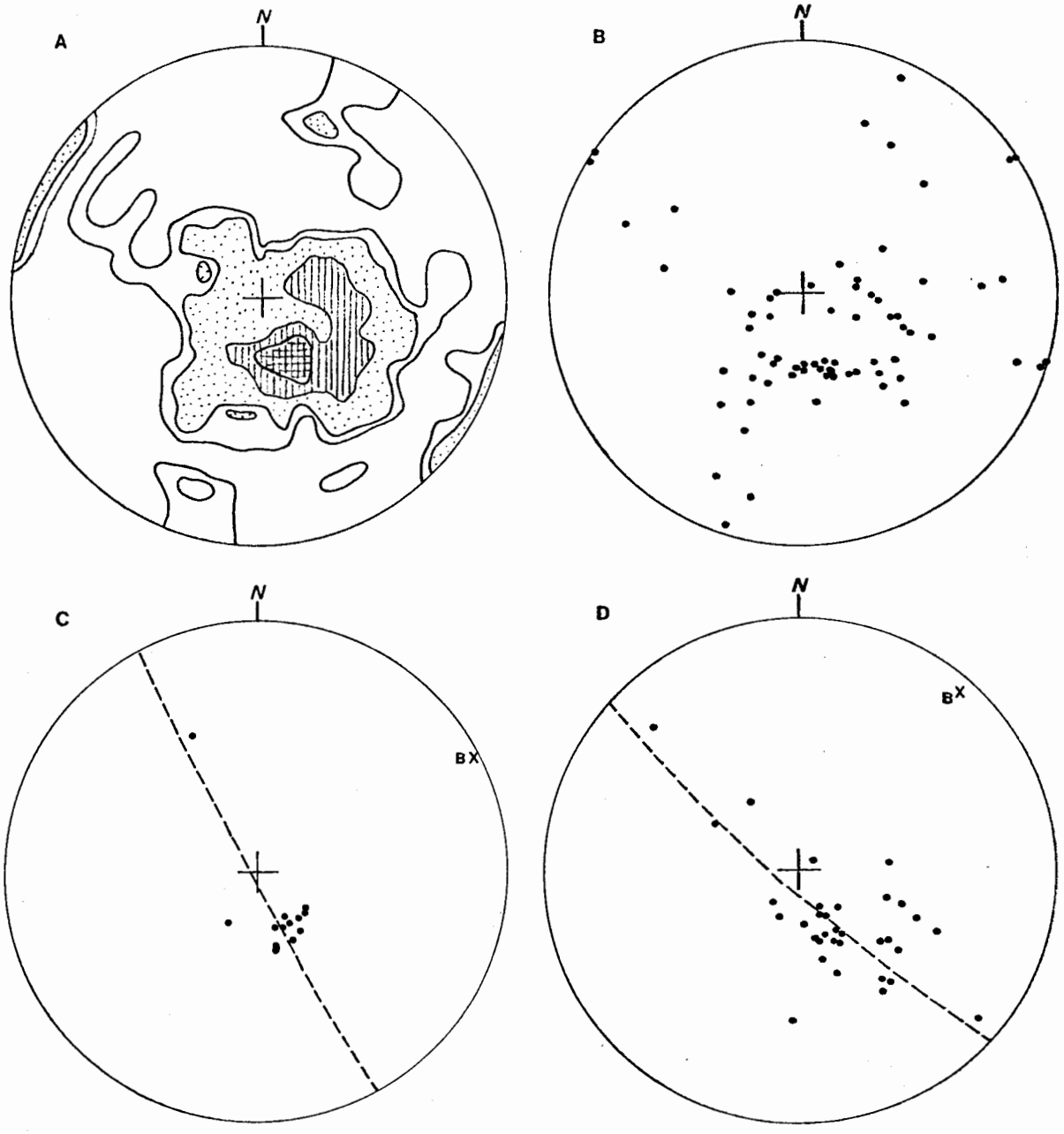

Figure 36. Orientation diagrams for bedding structures in the formations of the N. Pavian nappe in the C area.

A. 150 poles to SS and S_1; BCL (contours at 0,5-1-5-10%) in all lithostratigraphic units.

B. 72 poles to SS in the Remhoogte Formation.

C. 14 poles to SS in the Blässkranz Formation, with computed best-fit girdle and pole (B).

D. 33 poles to SS in the Tsabisis Formation, with computed best-fit girdle and pole (B).

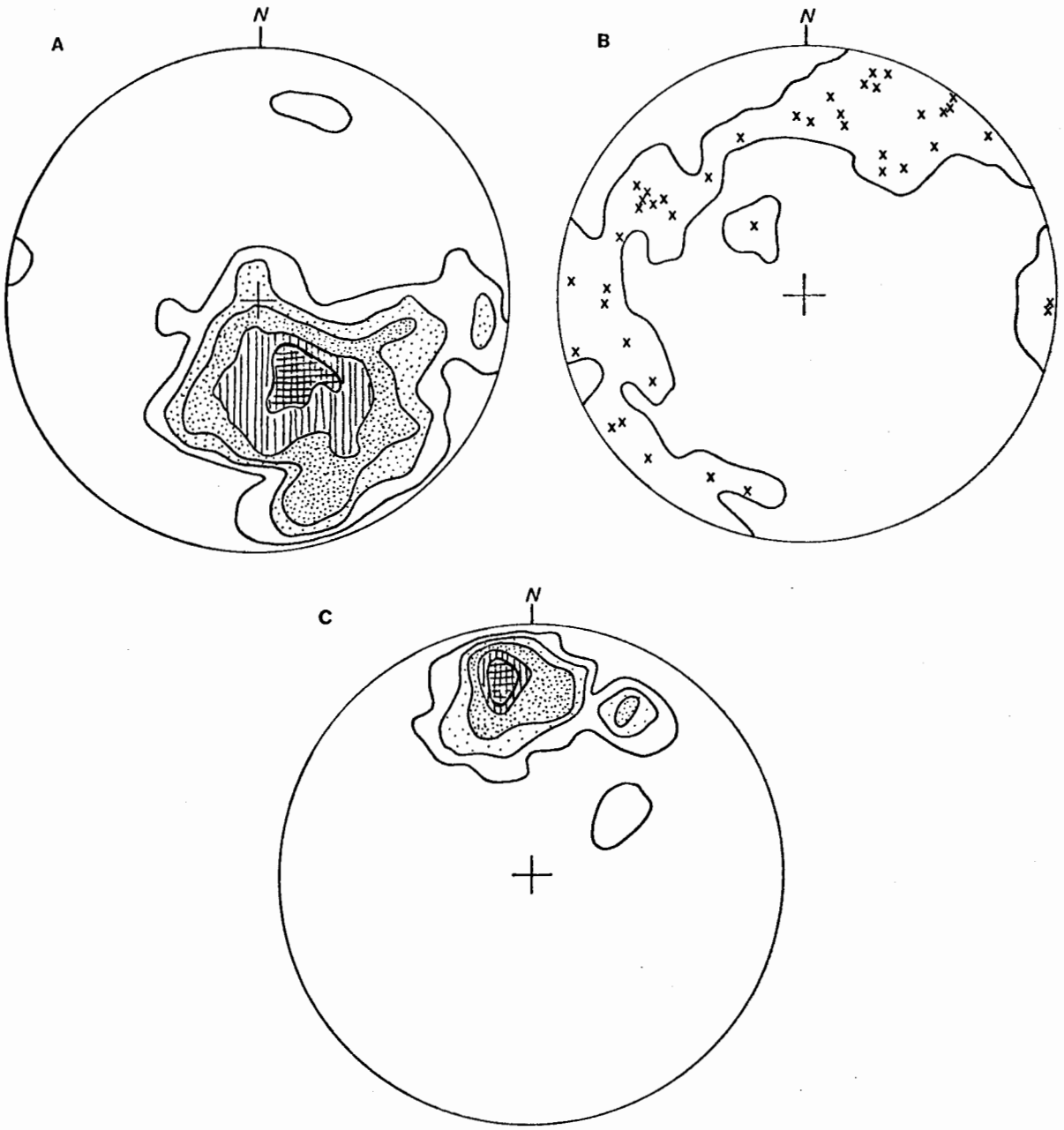

Figure 37. Orientation diagrams for S_1 and L_1 in the N. Pavian nappe of the C area.

A. 171 poles to S_1, including S_1; BCL (contours at 0,25-1-2-5-10%).

B. 42 poles to L_{1B}; ISL and L_1; FAX with 1% data contour.

C. 39 poles to L_{1X}; MEL & PEL (contours at 1-5-10-20-25%).

by VECSTA of 35 L_{1B} measurements showed that the HVM orientation of the early intersection lineation sample is 357/28 and that the data define a diffuse girdle (K_s = 0,20 and C_s = 2,52) or dispersion plane with an orientation of 239/31. The latter is close to the HVM orientation of all SS data and all S_1 data in the Remhoogte Formation, indicating that it may not be explained by latter folding of the S_1 cleavage. That the bedding/cleavage intersection lineation may vary considerably in orientation where the S_1 orientation remains constant is shown by the S_1 and L_{1B} data for the single Remhoogte Formation locality 10069; here the S_1 data define a clear cluster (K_s = 6,39) with the orientation 301/39, but the L_{1B} data range between the extremes of 338/32 and 138/37.

The same variability of L_{1B} orientation within S_1 observed in the Remhoogte phyllites of the N and NW areas (cf. Fig.28B) is therefore also present in the C area. With the additional observations that there is an unconformity between the Remhoogte and Blässkranz Formations within the N. Pavian nappe and that the S_1 cleavage is continuous across the unconformity and though locally different in character, is the same fabric element in both units, it is possible to suggest that the relatively large variation in L_{1B} orientation is due to the superimposition of the S_1 fabric upon older gentle folds within the Remhoogte Formation which pre-date the Blässkranz erosional unconformity. The alternative explanation of inhomogeneous stretching along the principal extension direction (X) in S_1 also remains feasible.

(ii) S_1 orientation and structure type patterns

The S_1 structure type in the N. Pavian nappe varies with rock type and position in the nappe sequence. A field distinction can generally be made in the pelitic rocks between a very planar slaty cleavage (SLC) and a phyllitic foliation (PHF) which is usually mildly crenulated on a mesoscopic or microscopic scale. In some pelitic greywackes, however, this distinction is impossible to make and the S_1 structure type is identified in the data files simply as cleavage (CLE) in a general sense. This structure type

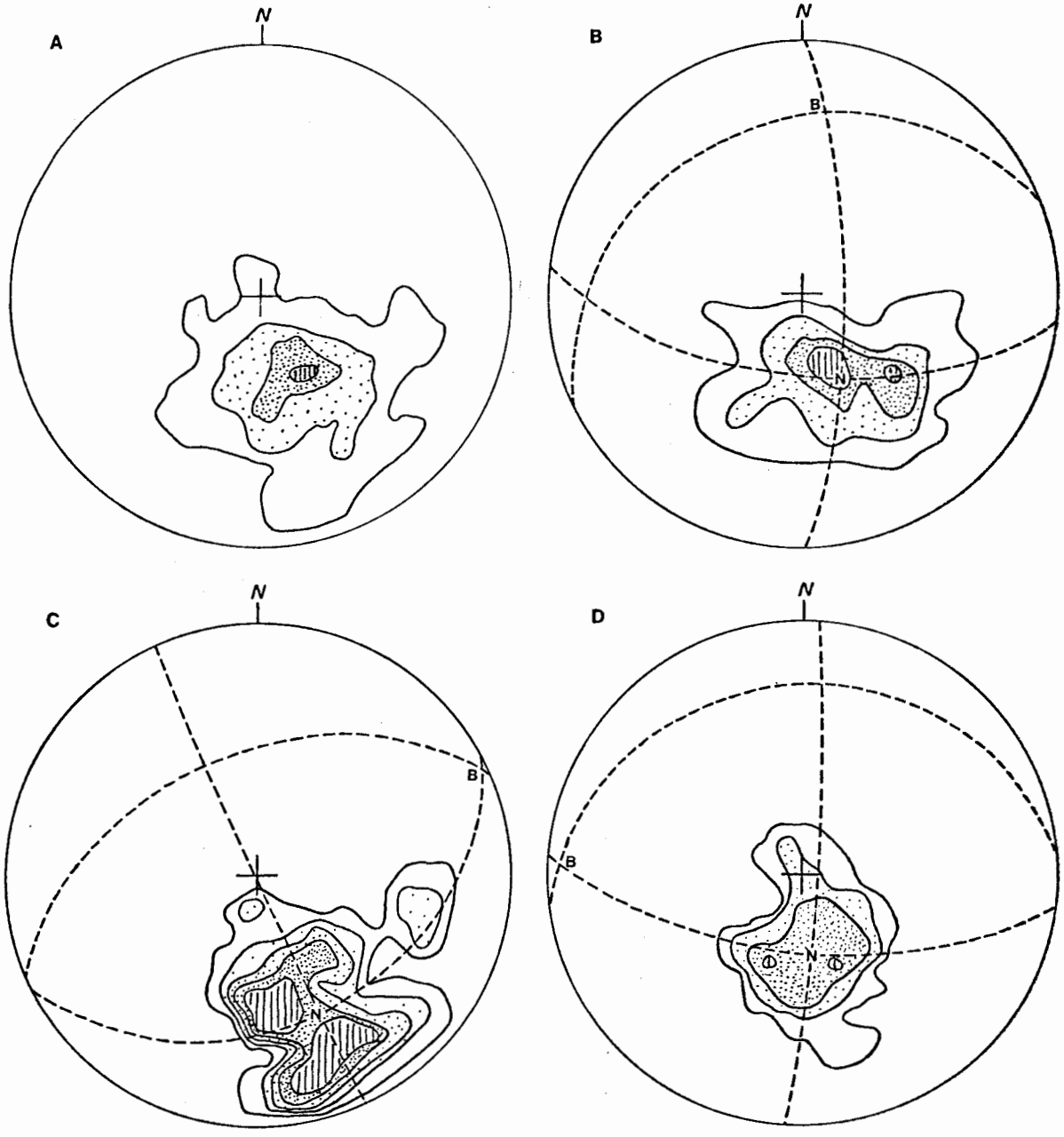

Figure 38. Orientation diagrams for S_1 structure types in the N. Pavian nappe of the C area.

A. 150 poles to S_1 types CLE, SLC and PHF (contours at 1-5-10-15%).

B. 78 poles to S_1; CLE (contours at 1-5-10-15%).

C. 44 poles to S_1; SLC (contours at 1-3-5-7-10%).

D. 28 poles to S_1; PHF (contours at 1-5-10-20%).

Diagrams B-D show orthogonal symmetry planes where N represents HVM orientation of planar structure and B represents pole to best-fit girdle, corresponding to the maximum and minimum eigenvectors of the orientation tensor.

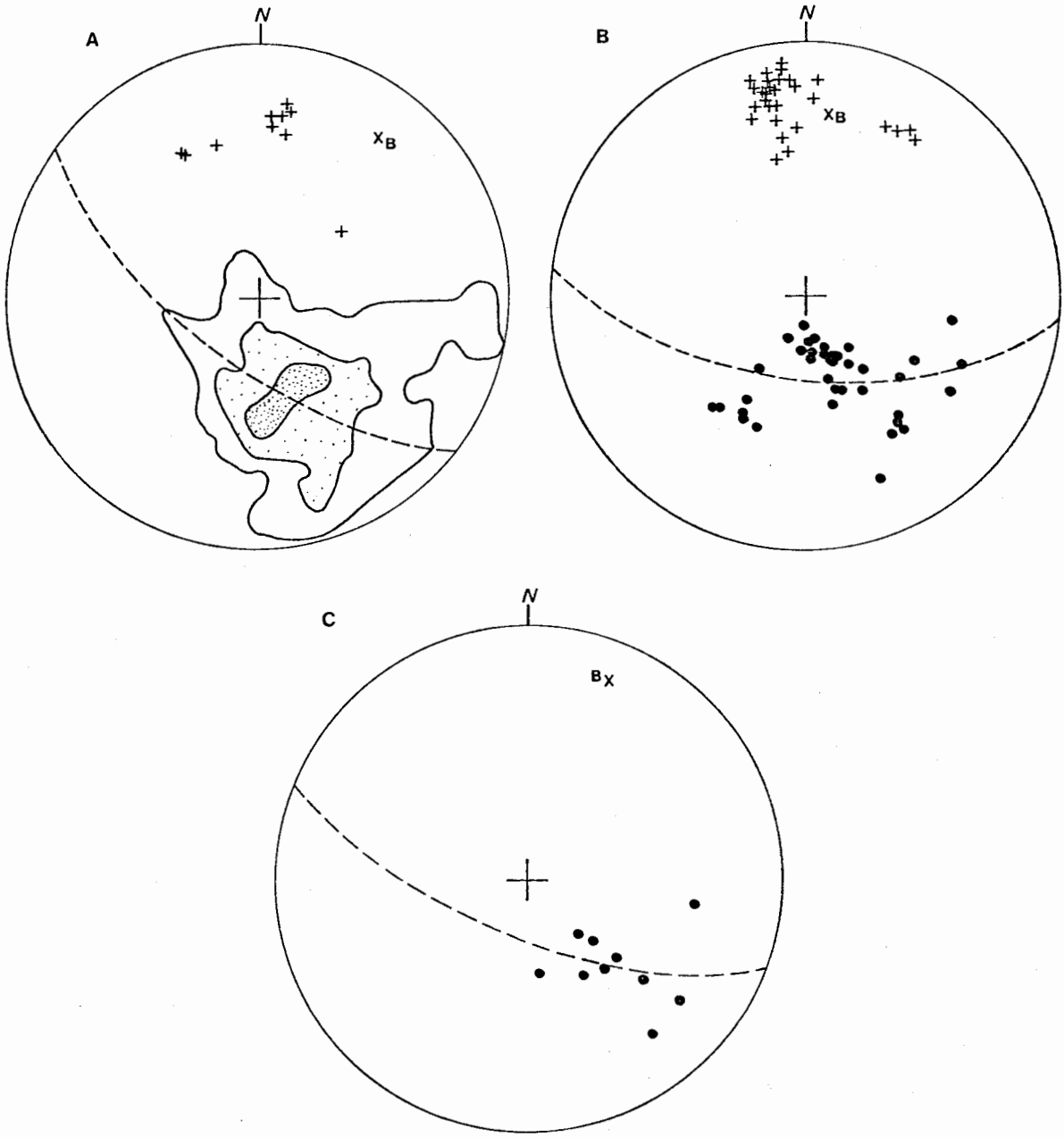

Figure 39. Orientation diagrams for S_1 and L_{1X} in lithostratigraphic units of the N. Pavian nappe in the C area.

A. 119 poles to S_1 in the Remhoogte Formation (contours at 1-5-10%) and 10 poles to L_{1X}. Computed best-fit girdle and pole B to S_1 data are also shown.

B. 38 poles to S_1 (dots) and 29 poles to L_{1X} (+ crosses), in the Blässkranz Formation also showing computed best-fit girdle and pole (B) to S_1 data.

C. 10 poles to S_1 in the Tsabisis Formation, with best-fit girdle and pole (B).

TABLE 8

FABRIC STATISTICAL PARAMETERS FOR THE N. PAVIAN NAPPE CLEAVAGE (S_1) STRUCTURES IN THE C AREA

UNIT/LOCALE	FABELT	TYCODE	N	HVM	K_s	L_B	C_s	Class
all	S_1	PHF,CLE, SLC	150	249/35	2,28	(039/19)	2,66	C
"	S_1	CLE	78	246/31	2,34	(006/27)	3,24	C
"	S_1	SLC	44	247/50	10,12	-	2,60	C
"	S_1	PHF	28	263/25	3,85	(273/05)	3,59	C
RH	S_1	CLE	40	242/32	2,73	(010/26)	3,20	C
RH	S_1	SLC	40	249/51	11,22	-	2,58	C
RH	S_1	PHF	28	263/25	3,85	(273/05)	3,59	C
RH	S_1	BCL	6	233/34	0,85	037/10	6,51	G - C
RH	S_1	FRC	5	192/70	0,86	009/08	3,00	G - C
RH	S_1	all	119	247/36	5,53	(036/21)	2,51	C
BK	S_1	all	38	250/30	2,31	(006/28)	3,04	C
TSB	S_1	all	10	224/43	2,84	(022/19)	3,45	C
RH 30069	S_1	CLE	3	271/39	3,26	-	6,43	C
RH 30030	S_1	"	4	239/24	1,35	058/01	6,79	C - G
RH 30048	S_1	"	3	282/29	4,68	-	7,05	C
RH 30049	S_1	"	8	272/14	0,70	006/14	4,74	G - C
RH 30054	S_1	"	4	258/48	2,60	-	6,21	C
RH 30057	S_1	"	5	231/41	1,42	341/40	5,39	C - G
RH 30058	S_1	"	7	223/43	3,20	-	6,74	C
RH 30060	S_1	"	4	211/38	1,58	245/24	7,18	C - G
BK 30070	S_1	"	7	298/42	6,04	-	5,19	C
BK 30003	S_1	"	4	251/33	5,17	-	7,16	C
BK 30067	S_1	CLE	7	268/16	6,67	-	6,45	C
BK 30068	S_1	"	8	242/22	6,09	-	6,86	C
BK 30064	S_1	"	4	234/54	3,70	-	8,52	C
RH 30031	S_1	SLC	8	259/45	7,85	-	5,45	C
RH 30036	S_1	SLC	5	246/35	3,61	-	3,86	C
RH 30061	S_1	"	4	259/74	0,90	335/73	10,59	G - C
RH 30062	S_1	"	4	250/74	5,36	-	6,33	C
RH 30063	S_1	"	5	244/59	3,86	-	6,83	C
RH 30065	S_1	"	4	230/66	4,60	-	4,67	C
RH 30046	S_1	"	5	267/34	1,49	272/03	5,05	C - G
RH 30010	S_1	"	3	192/56	2,07	(277/56)	7,59	C
RH 30069	S_1	PHF	8	286/31	4,88	-	5,49	C
RH 30027	S_1	"	6	294/20	0,83	059/02	6,51	G - C
RH 30028	S_1	"	3	260/33	15,79	-	6,11	C
RH 30035	S_1	"	3	261/33	3,19	-	5,94	C
RH 30037	S_1	"	8	241/21	0,96	262/08	4,35	G - C

RH - Remhoogte Formation
BK - Blässkranz Formation
TSB - Tsabisis Formation
NO - Noab Formation

identification is also used for nondescript S_1 in other rock types such as quartzite, limestone and carbonate breccia.

In contrast to the N and NW areas, slaty cleavage predominates over phyllitic foliation in the data sample, probably reflecting the slight decrease in metamorphic grade southwards. The orientation diagrams (Fig. 38) illustrate graphically the differences between S_1 fabrics of CLE, SLC and PHF types. Statistically (Table 8) the HVM orientation difference between the SLC and PHF types, 247/50 and 263/25, is significant. The slaty cleavage type generally has a steeper dip than the phyllitic foliation. This is related also to geographic position, since it is observed that the shallow-dipping PHF structure is dominant in the west and north of the C area whereas the steeply dipping SLC structure is dominant in the south and east of the same. This fact is important to the kinematic interpretation of deformation in the N. Pavian nappe with specific reference to the question of the "traineau ecraseur" mechanism suggested by Korn & Martin (1959, p.1076). It is also significant in this connection to note that the average northwestward dip of the S_1 cleavage (all types included) is not less than 30° - 35° (Table 8).

(iii) Imbricate structure in the Tsabisis area

Lithostratigraphic mapping of Remhoogte, Blässkranz, Tsabisis and Noab Formations on the farms Tsabisis and Tsabisis Oos shows clearly that there is a major imbrication of the N. Pavian and Kudu nappe together in this region. The most spectacular structure associated with this is the thrust fault at the head of the valley between Tsabisis and farm Blässkranz, which has resulted in the displacement of the Remhoogte Formation over the Noab Formation for a distance of 2-4 km (cf. Fig.34). Above this major thrust, there is a smaller scale imbrication of the Remhoogte and Blässkranz Formations. A similar but more complex "schuppen" structure in the Blässkranz and Tsabisis Formations is seen in the extreme north-east of the C area, along the boundary between farms Tsabisis-Oos and Bloedrivier and is recognised by the four-fold repetition of the distinctive carbonate breccia-volcaniclastic zone - white

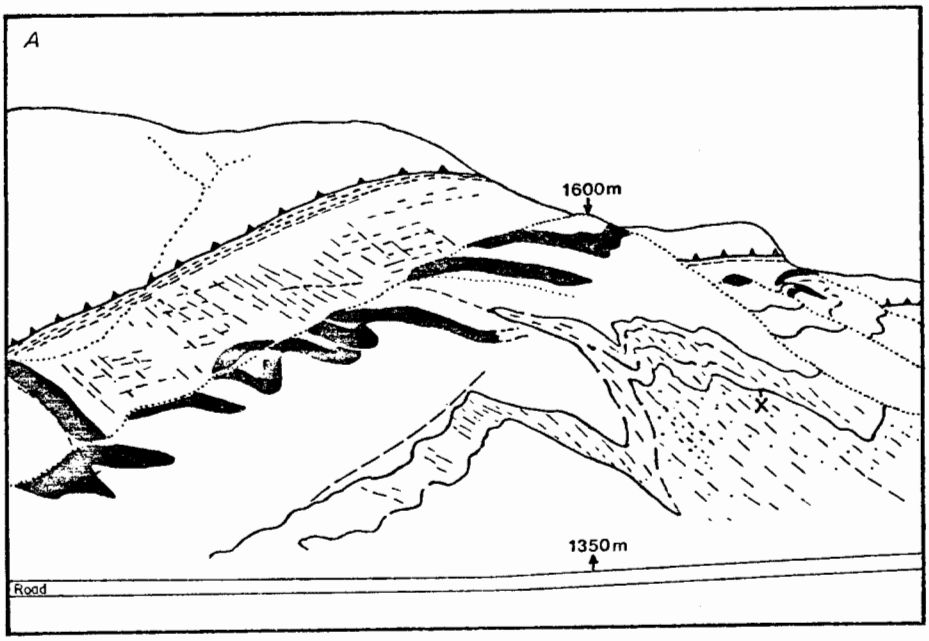
A
1600m
1350m
Road

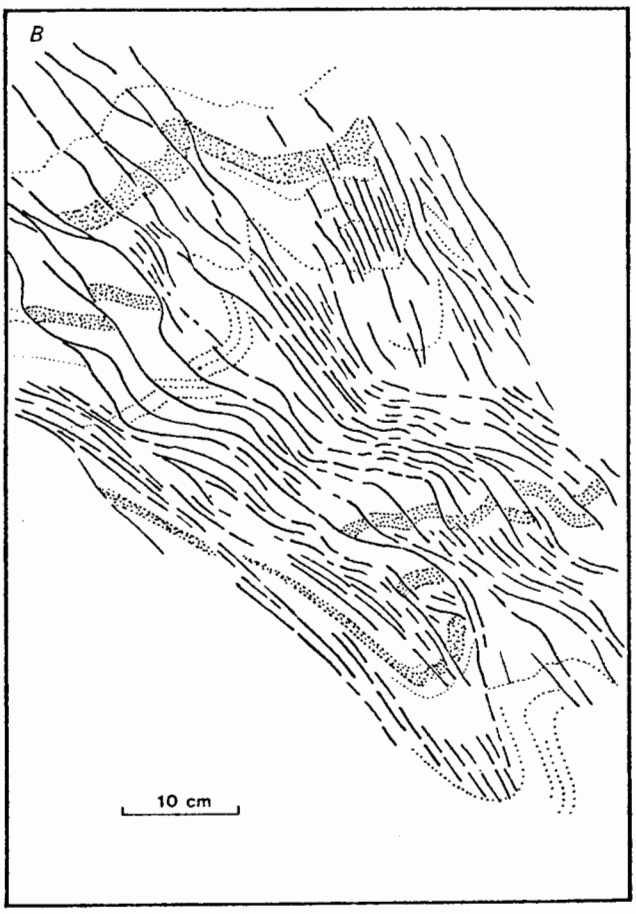
B
10 cm

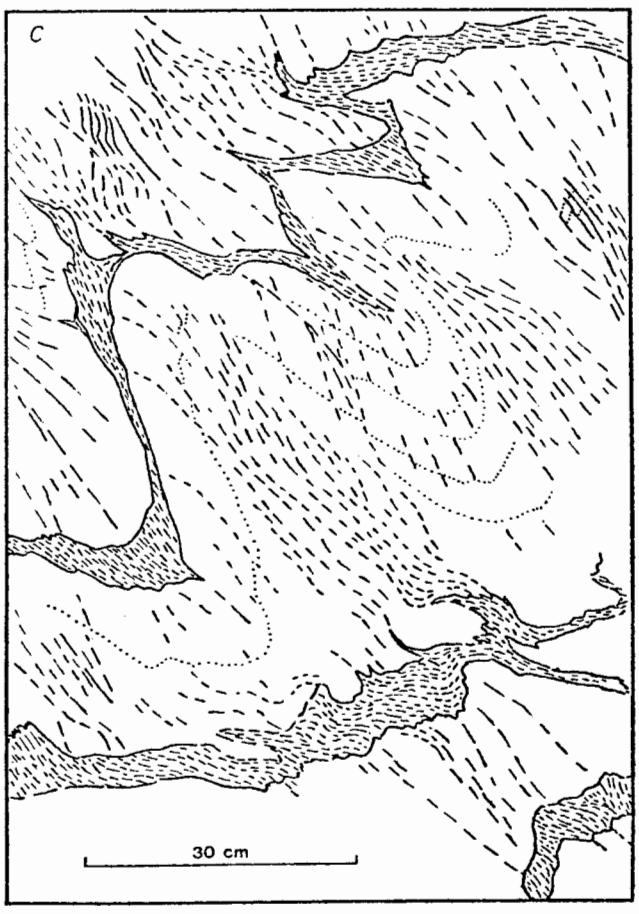
C
30 cm

dolomite sequence (Fig. 34). This may be related to a new unexposed larger thrust in the Remhoogte Formation on Bloedrivier, or could have originated during the earlier overthrusting of the Kudu nappe which has been removed by erosion here but is preserved on a large late open synform just to the south-east of the "schuppen" zone.

Imbrication of the Tsabisis white dolomite is also obvious in the mountain face immediately south-west of Pavianskopf (Plate 44 and Fig.40), where it is associated with spectacular plastic deformation - (phenomena in the underlying Blässkranz limestone unit (Plates 45 - 46). The imbricate zone here is separated from the Kudu nappe overthrust by a thick zone of cleaved purple slate and there is no definite evidence that it can be related to drag at the overlying nappe base.

b. Relationships between the Kudu and N. Pavian nappes

Over most of the C area the bedding fabric in the Noab dolomites (cf. Fig. 41A) is approximately parallel to the sub-horizontal base of the Kudu nappe. As in the areas farther north the latter is marked by a zone of marble and/or purple phyllite which is generally much more intensely deformed than the pelitic or carbonate units which it most commonly overlies. Naturally the contrast between this zone and the overlying, practically undeformed Noab dolomite is extreme.

The marble-phyllite zone in the C area is generally thicker than its northern equivalent and minor recumbent isoclinal folds are also more frequently encountered (Plates 47 and 48). There are perceptible differences in structural style which may be gauged by comparison with illustrations from locality 10068 (Plates 32 and 39).

Major tectonic discontinuities between the internal structure of the marble zone and the underlying N. Pavian nappe have already been described, but local tectonic discontinuities are also evident between the marble zone and overlying bedded dolomites. The best example is seen around localities 10069-71 near the boundary between Zais and Blässkranz, where there is a

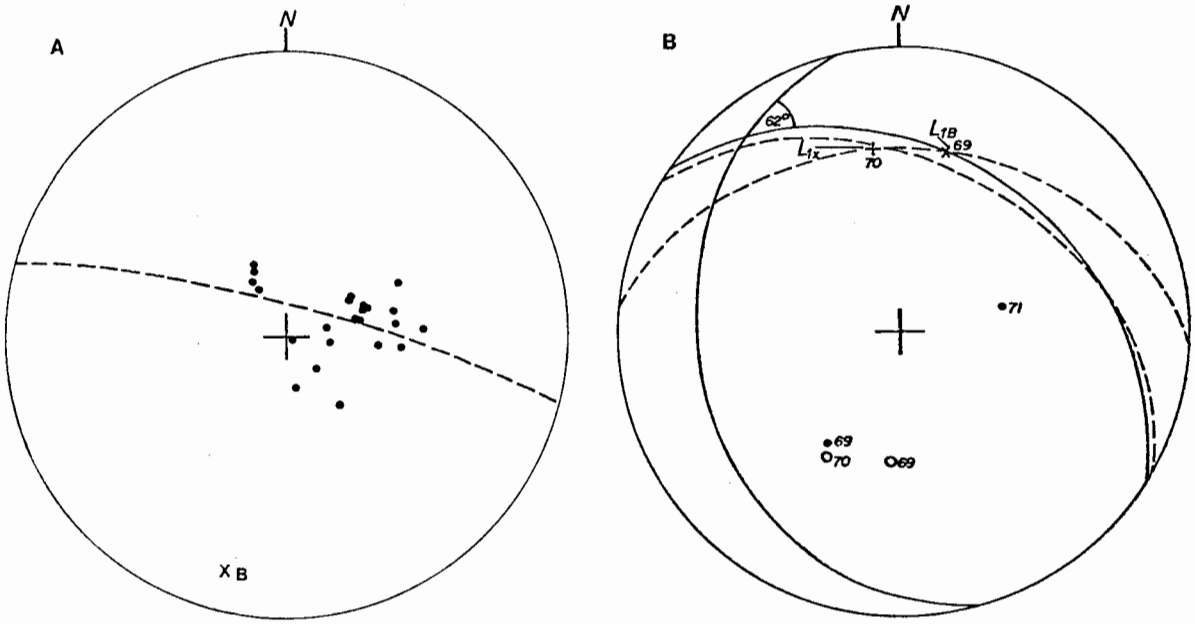

Figure 41. Orientation diagrams for the Noab Formation (Kudu nappe) in the C area.

A. 23 poles to SS with computed best-fit girdle and pole (B).

B. Attitudes of SS (solid dot and continuous great circle) and S_1 (open dot and dashed great circle) between closely spaced data sites at the boundary between the Kudu nappe (site 30071) and the N. Pavian nappe (30069-70). Note the 62° dihedral angle between SS orientations in the different nappes. The nappe contact is subparallel to S_1 in the N. Pavian nappe.

~60° discordance between SS in the Kudu nappe and subparallel SS and S_1 in the underlying N. Pavian nappe (Fig41B).

These structural discontinuities and the internal fabric of the intervening marble zone leave no room for doubt that the Kudu nappe has been extensively thrust over the N. Pavian nappe and the fact that the thrust plane rises south-eastwards through the N. Pavian stratigraphic sequence supports the view that this overthrusting produced an inversion of the original succession, contrary to Korn & Martin's (1959) hypothesis of no major stratigraphic inversion. The two local areas where the N. Pavian nappe actually *overlies* parts of the Kudu nappe are therefore especially important. These are in the south-east and east of the C area, near Pavianskopf and Tsabisis respectively.

The Pavianskopf area was previously interpreted differently as involving a three-way contact between the N. Pavian, Kudu and S. Pavian series just west of Pavianskopf (Korn & Martin, 1959, Pl. 1). Detailed mapping has, however, shown that the N. Pavian and S. Pavian nappes are not in contact (cf. Annex. I), but are separated by a massive dolomite wedge which is continuous with the frontal part of the Kudu nappe. In contrast to the previous interpretation, therefore, a three-way contact between the N. Pavian Kudu and E. Dassie nappes is obscured by recent alluvial deposits just east of Pavianskopf.

c. Relationships between the N. Pavian and Dassie nappes

It has been argued before (Korn & Martin, 1959, Chapter III of this work) that the Noab and Büllsport Formations are to be correlated on lithological grounds; consequently N. Pavian-Dassie nappe relationships are kinematically important because the N. Pavian nappe is presently sandwiched between the Noab and Büllsport Formations.

The long contact between the N. Pavian and E. Dassie nappe is exposed only over a ~2 km segment on Tsabisis where the S_1 foliation in the Remhoogte Formation (N. Pavian nappe) appears to be concordant with bedding in the

northern part of the Büllsport Formation (E. Dassie nappe). This would have given rise to the previous view (Korn & Martin, 1959) that the former followed the latter in conformable stratigraphic sequence. On a larger scale, however, it seems evident that the contact cuts across photo-geologically-mapped structural divisions in the E. Dassie nappe, although this remains to be confirmed by more detailed fieldwork. Furthermore, the large-scale mapping (cf. Annex. I) in this area suggests that the imbrication of the N. Pavian and Kudu nappes north-west of the contact may be related to displacement of the N. Pavian and Kudu nappes together over the E. Dassie nappe. In the Tsabisis area the overthrust displacement is at least 6-7 km, if it is assumed that the displacement vector is approximately normal to the strike of the N. Pavian - E. Dassie contact.

If the Noab and Büllsport Formations are to be correlated then it is necessary to suppose, on grounds of structural geometry, that the Kudu and E. Dassie nappes formerly were joined as a single larger nappe which was thrust as a unit over the N. Pavian formations and that the present N. Pavian-E. Dassie contacts and the associated N. Pavian-Kudu imbrication originated during a later distinct kinematic episode.

In the west of the Naukluft complex, in a relatively inaccessible mountainous area, a thin strip of greenish phyllite (interpreted as belonging to the Remhoogte Formation) separates the Kudu and W. Dassie nappes (Annex. I). This sliver of the N. Pavian nappe separates the highly imbricated Büllsport Formation from the relatively undeformed Noab Formation. The displacement of N. Pavian and Kudu nappes over the W. Dassie nappe may be large (>10 km) if the displacement vector trends approximately parallel to the thrust trace, as the orientation of the mineral lineation in the phyllite-marble zone at locality 60024 suggests.

4. Structure of the South-eastern and South-central (SC) areas

The SE and SC areas, including structural data sites bearing the LOCALE

codes 121014 and 121015 respectively, cover four main nappe units; namely, the Eastern Dassie nappe, the Western Dassie nappe, the Southern Pavian nappe and the south-eastern part of the Kudu nappe. The latter three units all come into contact with the first mentioned although only the contact with the Western Dassie nappe is well-exposed in the mountains around the trig. point Sieg east of the Tsondab valley on Büllsport. Contacts of the E. Dassie nappe with the S. Pavian, Kudu (and thereafter also the N. Pavian nappe) are obscured by alluvial and other recent deposits in the main river valley. The structural surface separating these upper nappes from the E. Dassie nappe in the SE area is evidently a major tectonic discontinuity, probably equal in importance to the overthrust at the base of the Kudu nappe in the N, NW and C areas and the sole of the entire Naukluft nappe complex.

a. Structure of the E. Dassie nappe

The E. Dassie nappe is composed almost entirely of Büllsport Formation rocks, dominantly purple slates or phyllite in the south-east and dolomite-calcareous quartzite association in the north-west. The contact between these two facies is sharp and locally appears to be a surface of tectonic discordance, but in the absence of more positive evidence for large relative displacement it has not been mapped as such (cf. Annex. I). The main slate-dolomite contact does, however, allow the subdivision of the E. Dassie nappe into a number of subordinate imbricate zones, bounded by "major" thrusts which are marked by the westward extension of long tongues of phyllite slate into the dolomite-quartzite terrain. The major thrust units are in turn broken up into a spectacular imbricate structure by numerous more steeply dipping minor thrusts (cf. Plates 49 - 51) which in places produce small displacements of the dolomite-slate contact. It is generally not possible to trace either the major or minor imbricate thrusts farther eastward into the slate terrain and the bulk strain produced by brittle imbrication in the dolomitic rocks appears to have been taken up near the boundary by pervasive ductile deformation in the pelite rocks.

The structural data sites in the SE area are heavily biased towards the

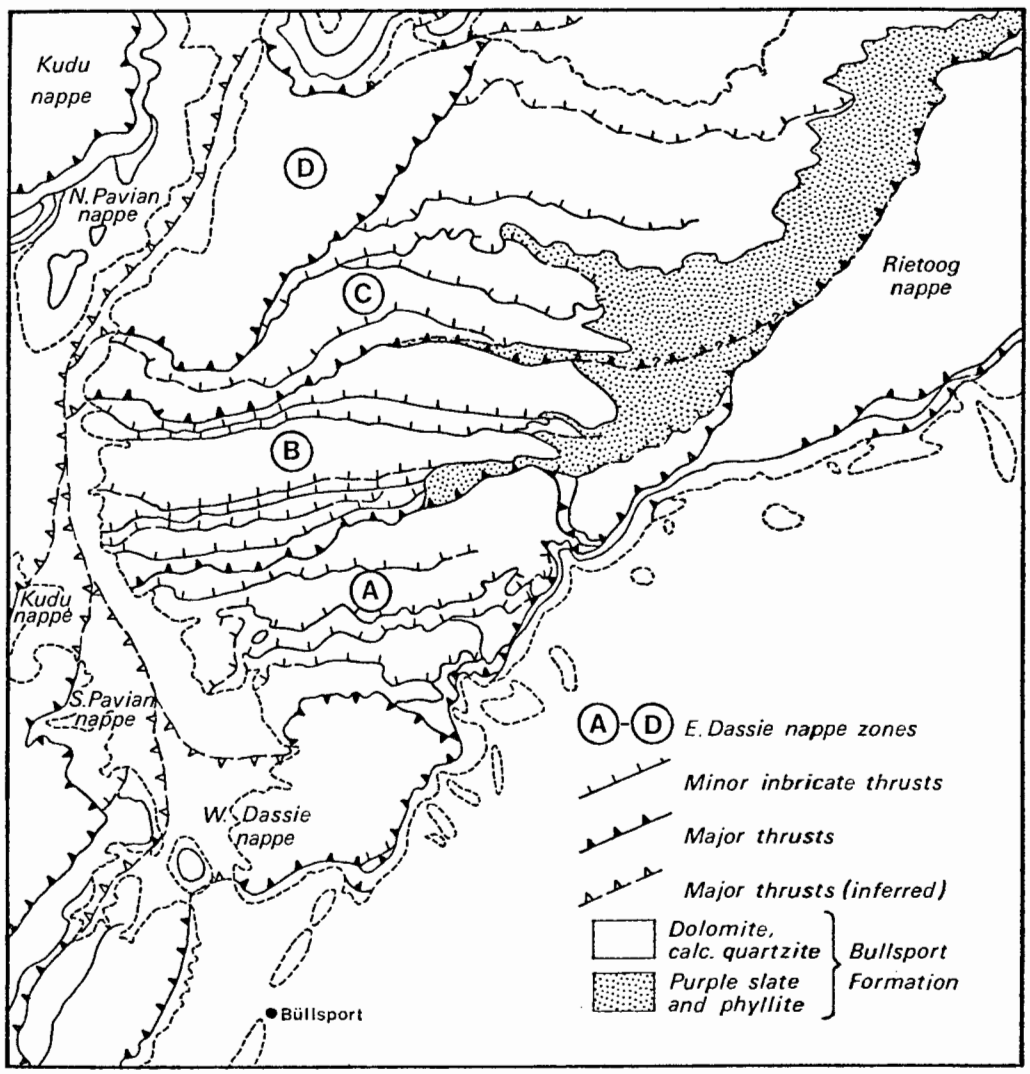

Figure 42. Map of the imbricate structure in the E. Dassie nappe between Büllsport and Tsabisis, showing the definition of zones A–D bounded by comparatively major thrust surfaces.

well-exposed dolomite-quartzite terrain where sedimentary bedding (SS; BED) is the dominant fabric element. As in the N and NW areas of much less imbricated Noab Formation it is remarkable how little penetrative ductile deformation of Büllspoort dolomites has occurred outside of the narrow marble zones which are a feature of the major (but not the minor) imbricate thrusts. Therefore S_1 fabric data is rarely obtained in the western parts of the E. Dassie nappe. In the eastern slates, however, S_1 is the dominant fabric element and it may be folded with the development of the locally penetrative "fracture cleavage" (S_2; FRC). Locality 40028 in this terrain, is one of the rare sites where evidence of three generations of tectonite fabric was found; namely S_1, S_2 axial-planar to a fold (L_2;FAX) in S_1, and an apparently later microscopic crenulation (L_3;CRL). The axial orientations of L_2 and L_3 on S_1 are 210/30 and 327/17 respectively and the latter may be controlled by a pre-existing mineral lineation (L_{1X};MEL) anisotropy in S_1.

The dolomitic part of the E. Dassie nappe can be subdivided as outlined above into four zones, A to D from north to south, separated by major thrust surfaces (Fig. 42). The orientation diagram from SS;BED (Fig.43A) represents a data sample drawn mainly from the southern zones A and B. VECSTA processing of this sample reveals an HVM orientation of 250/46 and a girdle pattern ($K_s = 1,06$) about the axis 267/17 (Table 9); the HVM orientation is fairly representative of the overall dip of the individual imbricate wedges in zones A and B and the girdle axis reflects the general westward plunge of the E. Dassie nappe structures beneath the N. Pavian and Kudu nappes south-west of the Tsondab valley.

The south zone A of the E. Dassie nappe contains none of the purple slate and phyllite seen farther north-east and in terms of the Büllsport Formation (Dassie zones) stratigraphy outlined by Korn & Martin (1959), it consists mainly of the upper lithological members (i.e. the so-called " chert-banded white dolomites", interbedded dolomite and fine-grained calcareous quartzite). This zone is overlain on the south by the southward-dipping marble zone at the base of the W. Dassie nappe and on the south-east it is underlain by the

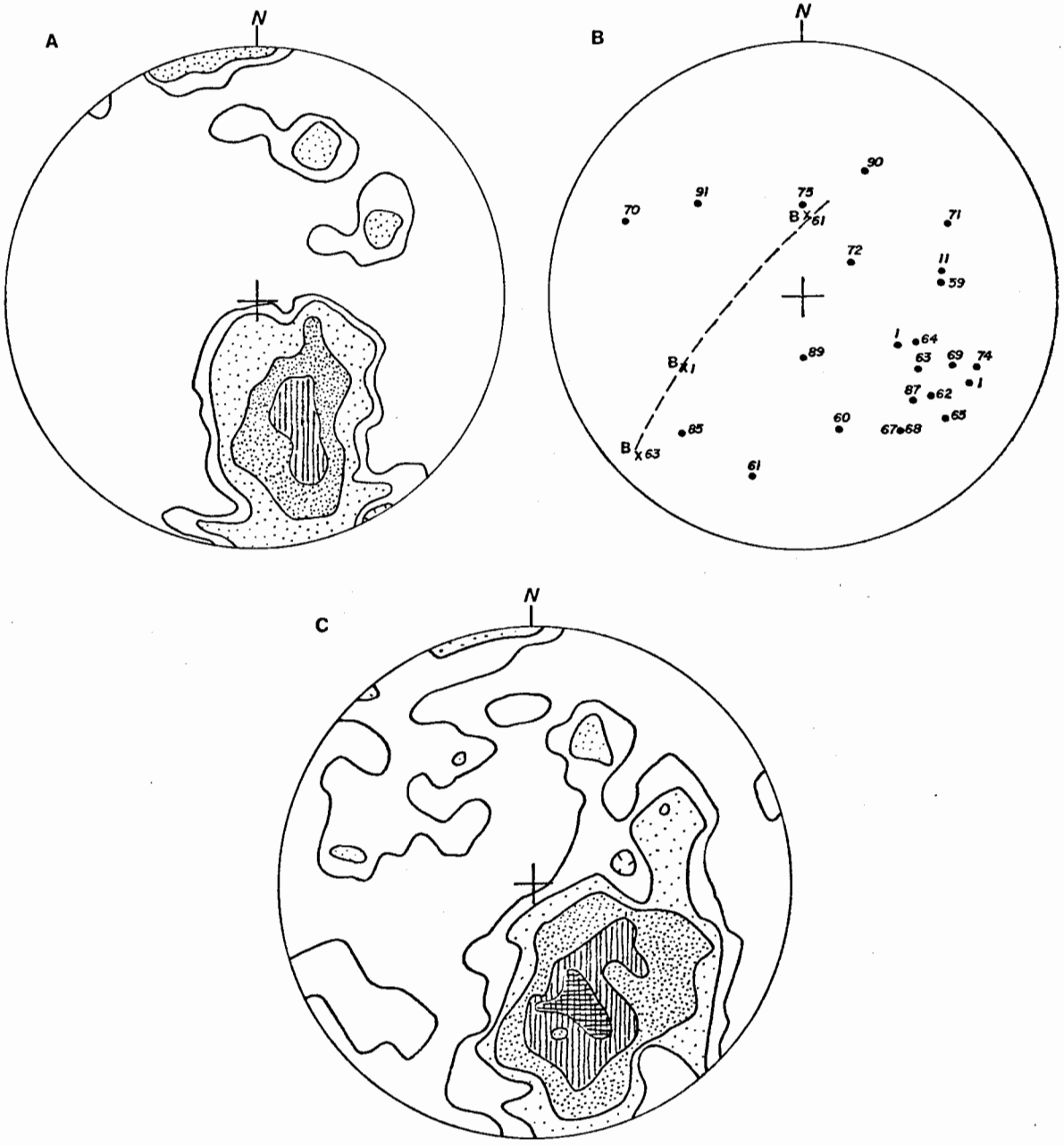

Figure 43. Orientation diagrams for SS in the Büllsport Formation of the SE area, east of the Tsondab Valley.

A. 108 poles to SS in the E. Dassie nappe (contours at 0,5-1-5-10%). B. SS data (HVM orientations) for individual numbered sites in the W. Dassie nappe of the SE area (Sieg sheet) and B_{SS} axis orientations for girdle-distributed data from sites 40001, 40061 and 40063. Data sites 40070-40075 and 40090-91 are from the northern part of the Sieg sheet.

C. 186 poles to SS and S_1; BCL from both E.Dassie and W. Dassie nappes of the SE area (contours at 0,25-1-2-5-7%)

TABLE 9

FABRIC STATISTICAL PARAMETERS FOR THE E.DASSIE (E.D.), W. DASSIE (W.D.), S. PAVIAN (S.P.) AND KUDU NAPPE BEDDING (SS) STRUCTURES IN THE SE AND SC AREAS

UNIT/LOCALE		FABELT	TYCODE	N	HVM	K_s	L_B	C_s	Class
E.D.		SS	BED	108	250/46	1,06	267/17	3,12	C - G
W.D. (SE)		"	"	77	222/50	14,51	-	1,40	C
W.D. (SC)		"	"	90	200/30	1,17	248/23	1,61	C - G
W.D.		"	"	167	215/40	2,11	-	1,44	C
S.P.		"	"	35	240/33	0,87	029/18	2,23	G - C
KUDU		"	"	60	241/38	2,28	-	2,22	C
E.D.	40004	SS	BED	8	229/39	1,70	237/07	6,97	C - G
	40007	"	"	3	218/33	0,13	236/11	8,19	G
	40015	"	"	4	098/63	1,56	261/29	3,96	C - G
	40031	"	"	4	232/43	0,17	278/35	4,72	G
	40047	"	"	3	207/31	2,01	-	5,87	C
	40049	"	"	4	271/39	0,89	286/12	6,04	G - C
	40076	"	"	4	248/36	4,85	-	8,11	C
	40077	"	"	8	244/34	0,60	280/21	4,77	G - C
	40078	"	"	4	257/31	6,10	-	5,86	C
	40079	"	"	4	257/42	4,70	-	7,19	C
	40080	"	"	4	250/51	3,24	-	4,86	C
	40081	"	"	7	246/59	1,30	060/10	4,64	C - G
	40082	"	"	6	257/69	3,20	-	6,35	C
W.D.	40001	SS	BED	3	209/62	0,90	240/44	6,41	G - C
	40002	"	"	4	211/36	1,06	013/3	5,17	C - G
	40060	"	"	6	255/46	8,88	-	4,85	C
	40061	"	"	10	286/64	0,39	003/64	4,59	G
	40062	"	"	4	219/55	4,79	-	4,02	C
	40063	"	"	7	215/44	0,69	229/12	6,96	G - C
	40064	"	"	4	205/39	2,53	-	5,07	C
	40065	"	"	4	223/63	15,18	-	5,87	C
	40067	"	"	4	235/55	1,45	037/24	7,32	C - G
	40068	"	"	4	235/55	2,12	-	6,47	C
	40070	"	"	4	024/65	2,02	-	4,27	C
	40071	"	"	4	155/53	1,07	334/03	8,50	C - G
	40074	"	"	4	204/62	2,83	-	5,64	C
	40091	"	"	5	041/46	9,64	-	3,76	C
	50013	"	"	3	236/42	4,03	-	4,78	C
	50014	"	"	10	121/32	0,20	244/28	3,27	G
	50078	"	"	4	215/37	2,59	-	5,62	C
	50079	"	"	7	185/24	0,32	216/13	4,83	G
	50113	"	"	6	102/31	1,57	225/27	4,87	C - G
	50114	"	"	5	061/58	1,44	235/11	6,06	C - G
	50115	"	"	12	256/41	0,55	297/29	3,46	G - C
	50138	"	"	11	168/48	0,41	191/24	3,68	G
	50140	"	"	6	207/43	4,77	-	6,10	C
S.P.	50024	SS	BED	7	354/47	3,40	-	3,73	C
	50034	"	"	4	224/35	8,38	-	5,94	C
	50040	"	"	3	248/44	1,81	037/26	6,77	C - G
	50042	"	"	3	234/48	1,84	339/47	7,53	C - G
KUDU	50056	SS	BED	3	252/39	1,03	065/06	9,20	C - G
	50105	"	"	5	192/46	0,65	263/45	4,88	G - C
	50119	"	"	3	103/15	0,17	235/12	6,25	G
	50128	"	"	4	260/34	5,33	-	6,76	C
	50133	"	"	4	241/39	6,44	-	6,43	C
	50134	"	"	5	282/37	9,64	-	5,20	C

Unconformity Dolomite which separates it from the then westward extension of the Rietoog nappe (Münch, 1975). Along the south-east margin of zone A, a sequence of basal coarse-grained quartzite preceded by interbedded dark dolomite shale and quartzite was originally correlated with the "Zebra Series" (Korn & Martin, 1959). It appears to overlie the upper Büllsport Formation (?pseudo) conformably and has been involved in the imbrication structure. Within zone A, the intensity of deformation appears to decrease eastwards, as reflected by generally shallower dips from west to east and by the fact that at least one imbricate thrust zone dies out eastward into a relatively open fold structure. In general, the bedding structure in zone A defines a large open antiform.

In contrast, zone B is one of uniformly northward-dipping bedding, although it is notable that there is a progressive steepening of the structure from south to north. At the western end of the major thrust separating zones B and C, the SS structure is almost vertical, but flattens eastward as indicated by the spacing of the northern minor thrusts.

In zone C, the significant new phenomenon is the truncation of some imbricate minor thrusts at the base of imbrications higher in the sequence. It is also apparent photogeologically that the three northern minor thrusts in this zone are truncated (upwards, in view of the westerly plunge of structure) by the major thrust at the base of zone D.

The latter zone consists of a thick relatively intact plate of dolomite which in part was formerly regarded as belonging to the "Southern Pavian Series" (Korn & Martin, 1959). The difficulty with the previous interpretation of the latter in the Pavianskopf region has already been mentioned. In the writer's opinion, the zone D dolomites are in fact quite unlike the open S. Pavian nappe dolomite which is generally dark and rich in irregularly-shaped chert bodies. Much of zone D could, however, be regarded as more closely related to the Noab Formation dolomites and since the dolomite body around Pavianskopf has been shown to belong structurally to the Kudu nappe, it is possible that the same may apply to zone D of the E. Dassie nappe.

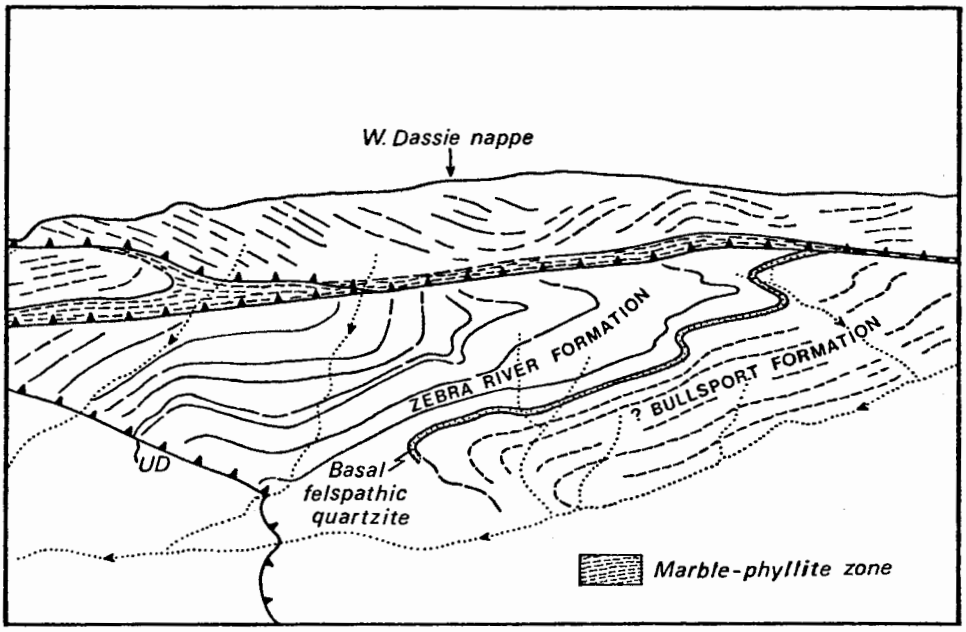

Figure 46. Sketch traced from Plate 52 showing the section of the mountain slopes immediately north-east of Sieg (Fig. 45). The truncation of lithostratigraphy in the Zebra River Formation at the basal thrust and marble zone of the W. Dassie nappe is clearly visible and the later truncation of both at the Unconformity Dolomite zone (UD) is traced at the left of the sketch.

b. Structure of the W. Dassie nappe

The W. Dassie nappe is the lowermost of the imbricate pile magnificently exposed west of the Tsondab valley on Büllsport (cf. Fig. 44). Parts of the nappe were previously assigned to the "Kudu Series" (Korn & Martin, 1959, Pl.1) but there is no justification for this on lithological grounds since the sedimentary facies throughout is that of the Büllsport Formation rather than the Noab Formation. For purposes of structural description, it is convenient here to consider three parts of the W. Dassie nappe; namely, the exposures east of the Tsondab Valley, the Büllenkopf exposures and the segment immediately west of the Tsondab Valley.

The "axial unconformity" between the W. Dassie nappe in the mountains around the trig. point Sieg (Fig. 45) and the underlying zone A of the E. Dassie nappe was noted previously (Korn & Martin, 1959). The truncation of lithostratigraphy in zone A (Plate 52 and Fig. 46) has also been figured before (*op.cit.*, Fig. 13). In the accompanying maps (Fig.45 and Annex. I), a comparison of the traces of minor thrust surfaces in zone A and the overlying Sieg zone shows an apparent 90^{o} discordance about the nappe contact.

The fabric data for SS BED in the W. Dassie nappe of the SE area (Table 9 and Fig.43B) reveals only that there is a 30^{o} difference in the strike from the E. Dassie HVM orientation (222/50 compared with 250/46, respectively). Although the W. Dassie SS fabric shape parameter indicates a distinct cluster pattern (K_s=14,5), the strength parameter shows it to be a diffuse one (C_s=1,40).

The mainly dolomitic W. Dassie nappe (SE area) differs conspicuously from the underlying dolomitic parts of the E. Dassie nappe in that marble zones with penetrative deformation fabrics separate individual imbricate zones and also floor the base of the entire nappe. The S_1 structure type in these zones is mainly described as a "mylonitic foliation" (S_1;MYF) and is a fabric element of major importance in the units presently lying above the E. Dassie nappe (Table 10). In the Sieg sheet, the HVM orientation of S_1 (183/25) corresponds well with the north-south trends of mapped thrust traces.

The orientation data sample (Fig. 47) defines a partial girdle about an axis orientated 260/24. At two individual data sites (40059, 40062), S_1 orientation data define local B_{S_1} axes which differ appreciably from the overall B_{S_1} orientation (Table 10).

A clearer pattern of SS deformation in the Sieg sheet emerges when the local data variability is reduced by plotting only HVM orientations from sites where multiple ($N \geq 3$) measurements were made (Table 9). The corresponding orientation diagram (Fig.43D) shows a pole cluster in the south-east quadrant as expected, but a pattern of crossed girdles is now apparent. When this pattern is related to the geographical location of the data sites, it is clear that the girdle of north-east and north-westward plunging poles is defined entirely by data drawn from the northern part of the Sieg sheet, whereas the girdle of south-east to south-westward plunging poles is defined entirely by data drawn from the southern part of the sheet. This feature can be explained by noting that it is possible to produce the northern girdle from the southern by a simple rotation about the B_{S_1} axis defined by the S_1 fabric (Table 10 and Fig. 47). The analysis therefore indicates that, after the deformational episode which distorted the SS fabric from its original orientation (as represented still in the E. Dassie nappe) and which enhanced the S_1 fabric in the W. Dassie imbricate thrust zones, a further deformation of the nappe occurred so that its present structure is one of a large, open synform plunging westward at about 24°.

Clear later folding of S_1 in a marble zone is in fact observed at locality 10066 with the development of a locally penetrative "fracture cleavage" (S_2;FRC) and associated intersection lineation (L_2;ISL). The orientation of S_2 (063/84) may indicate a "backfolding" component to this deformation.

The Sieg sheet is separated from the main exposure of the W. Dassie nappe by the Tsondab Valley, but the intervening small prominence of Büllenkopf provides a remarkable section through its lower part. The upper capping to Büllenkopf consists of well-bedded dolomite dipping at 40° with little trace of internal penetrative deformation. This well-preserved sedimentary

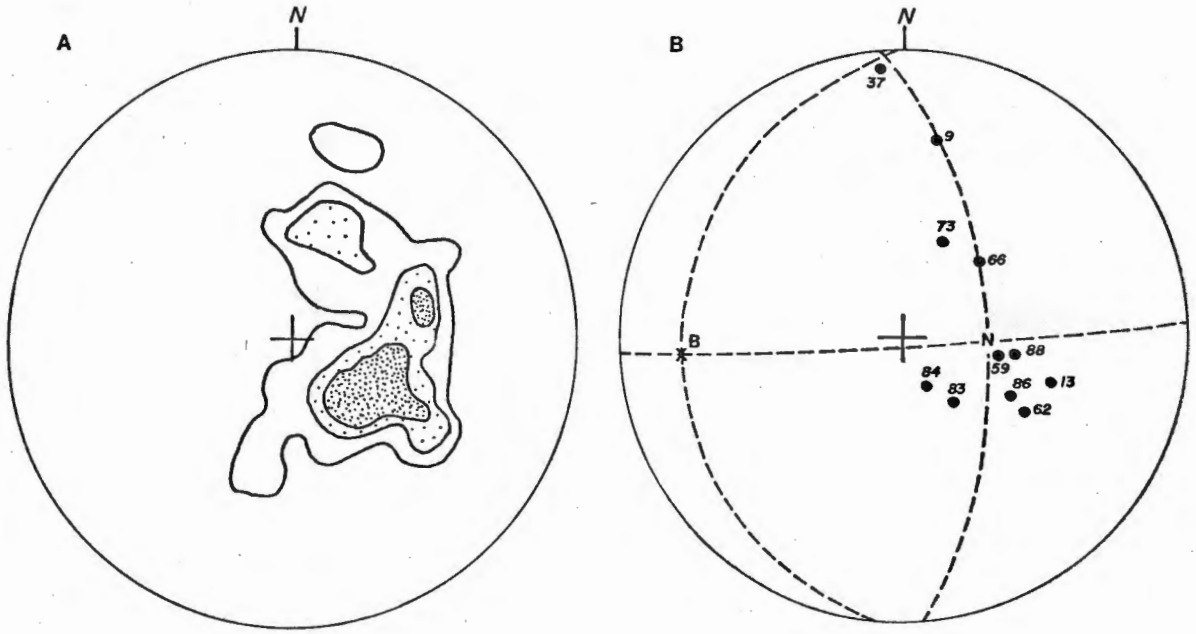

Figure 47. Orientation diagrams for S_1 in the W. Dassie nappe of the SE area (Sieg sheet).

A. 35 poles to S_1; MYF (contours at 1-5-10%).

B. S_1; MYF data (HVM orientations) for individual numbered sites in the Sieg sheet with orthogonal symmetry planes where N represents the HVM orientation of the total data sample and B represents the computed best-fit axis of rotation.

structure is truncated abruptly at the top of a zone of intensely deformed marble with subordinate phyllite. Locally the basal marble zone contains large lensoid bodies of massive dolomite, rather like giant boudins.

The S_1 foliation in the marble zone is south-west-dipping but has been deformed in large late open folds (Table 10 & Fig.48A). Within S_1 tight to isoclinal folds (Plates 53-56) have rather variable axial orientations. The asymmetry of these structures shows that the marble zone encompasses a larger fold structure as, viewed in profile facing west, structures near the northern base of the zone are Z-shaped whereas near the southern top of the zone they are S-shaped. A zone of minor M-folds several metres thick is seen near the inferred hinge trace of this structure (Plates 54 & 55). This region of the marble zone is remarkable also for including an example of a Type 3 interference pattern (Plate 56), showing that the early deformation in the zone comprises two geometrically distinct phases.

Regions near the top of the marble zone where early fold structures are tightest (Plate 53) have evidently experienced considerable layer-parallel extension subsequent to the first folding as evidenced by abundant boudinage phenomena (Plate 57). This is also evident in overlying less deformed enclaves of mixed marble and phyllite where the original sedimentary layering is still preserved and extension of relatively brittle shaly layers in much more ductile limestone has given rise to much "chocolate tablet" boudinage (seen in section in Plate 58).

Later folding of these boudinaged layers (Plates 59 & 60) has resulted locally in the formation of unusual cuspate phenomena (Plate 61) on the boundaries of shortened former boudins due to the same ductility contrast effects. The axial orientation of the later folding is also variable. One representative example of a late minor fold (L_2; FAX) has a west-south-westerly trend (Fig.48A) but the overall axis of late rotation defined by all Büllenkopf S_1 data is 154/03 (Table 10); the fabric shape parameter K_s for the data is, however, sufficiently large for the computed B_{S_1} to be ignored.

South-west of Büllenkopf (Fig.45), the W. Dassie nappe is divided into three sub-units by two conspicuous thrust zones. The northern thrust is

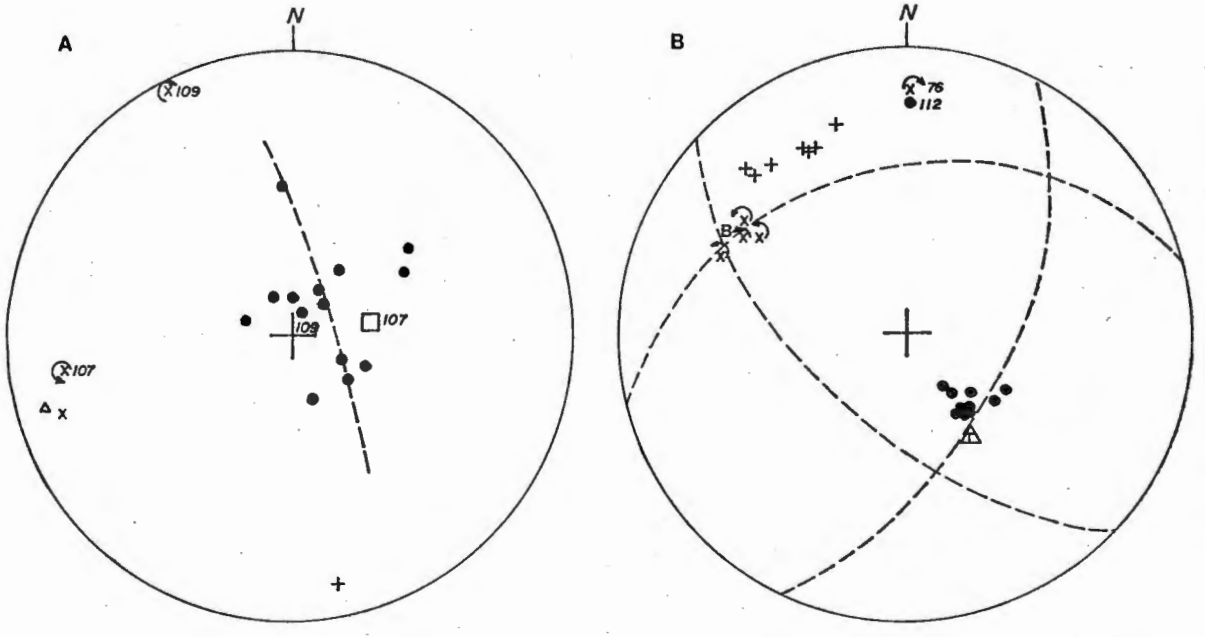

Figure 48. Orientation diagrams for data from Büllenkopf and the Tsondab tributary valley ("Polizeischlucht") to the immediate south-west (cf. Fig. 45).

A. Büllenkopf data, showing mild deformation of S_1 about south-west plunging axes.

Symbols :
- • - S_1
- □ - S_1 FAP
- x - L_1 FAX
- \+ - L_1 MEL
- △ - L_2 FAX

B. "Polizeischlucht" region: data from sites 50075-77, 111-112, 115-116, with orthogonal symmetry planes for SS data (N=12) from locality 50115. T symbol in triangle represents orientation of thrust fault illustrated in Plates 65 and 66.

Other symbols :
- • - S_1
- \+ - L_{1X}
- B - L_{1B}

In both diagrams, asymmetry of minor folds is indicated by screw symbol about fold axis.

situated at the base of a purple phyllite which in turn underlies a thick marble layer. The latter appears to be the westerly extension of the Büllenkopf marble and to have formed a ductile boundary shear layer at the base of the overlying S. Pavian nappe. Within a mixed marble and phyllite zone at the base of the northern thrust are numerous examples of folding in these finely layered rocks (Plates 62-64). Fold style varies considerably from open to near isoclinal over a few decimetres (cf. Plate 62) and nearly complete transposition of the early layering (SS) into a new foliation (S_1) occurs across sharp boundary zones of very high strain gradients (cf. Plate 63). Complex patterns of interference folding are also evident in this zone (Plate 64).

Early minor folds here trend west-north-west and also northwards. Their variable pitch in the S_1 plane appears to be due to inhomogeneous strain, namely variable amounts of rotation of early-formed folds into the principal extension direction defined by the L_{1X} lineation; asymmetry of the fold structures, recorded by rotation symbols in the fabric diagram for the area (Fig.48B), is consistent with this interpretation.

The southern thrust in the W. Dassie nappe pile immediately south-west of Büllenkopf has a very different character. It is not marked by the development of plastically deformed marbles, only a 10 cm zone of cataclasite (Plate 65), separating massive undeformed dolomite from truncated and chevron-folded Middle Büllsport Formation quartzites and slaty shales (Plate 66). In this respect it is similar to some of the minor imbricate thrusts found in the E. Dassie nappe. Along tectonically lower minor thrusts farther south-west in the W. Dassie nappe, however, there is further development of marble phyllite zones with complex internal deformation structures (Plate 67).

On a large scale, the W. Dassie nappe SS fabric in the SC area describes a diffuse girdle about a pole at 248/23 (Fig.49A & Table 9). The HVM orientation of SS (200/30) is interesting in that, even more than the thrust traces in the area (Fig.45), it reflects the late distortion of Büllsport Formation sedimentary structure into nearly north-south strikes. The HVM orientation of the sample (N = 19) of early fold axes (L_1; FAX)

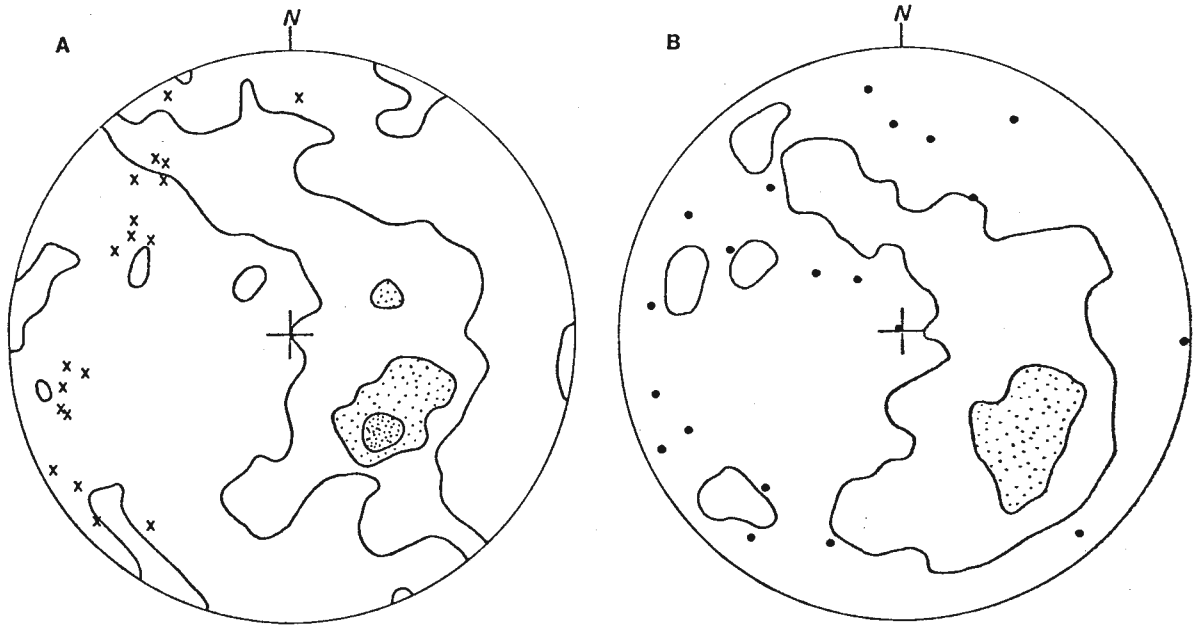

Figure 49. Orientation diagrams for SS and L_1 FAX in the W.Dassie nappe.
A. 91 poles to SS (contours at 1-5-10%) and 19 L_1 FAX poles (crosses) in the W. Dassie nappe of the SC area (i.e. west of Tsondab).
B. 168 poles to SS (contours at 1-5%, with data outside 1% contour shown as dots) from W.Dassie nappe of SC and SE areas combined.

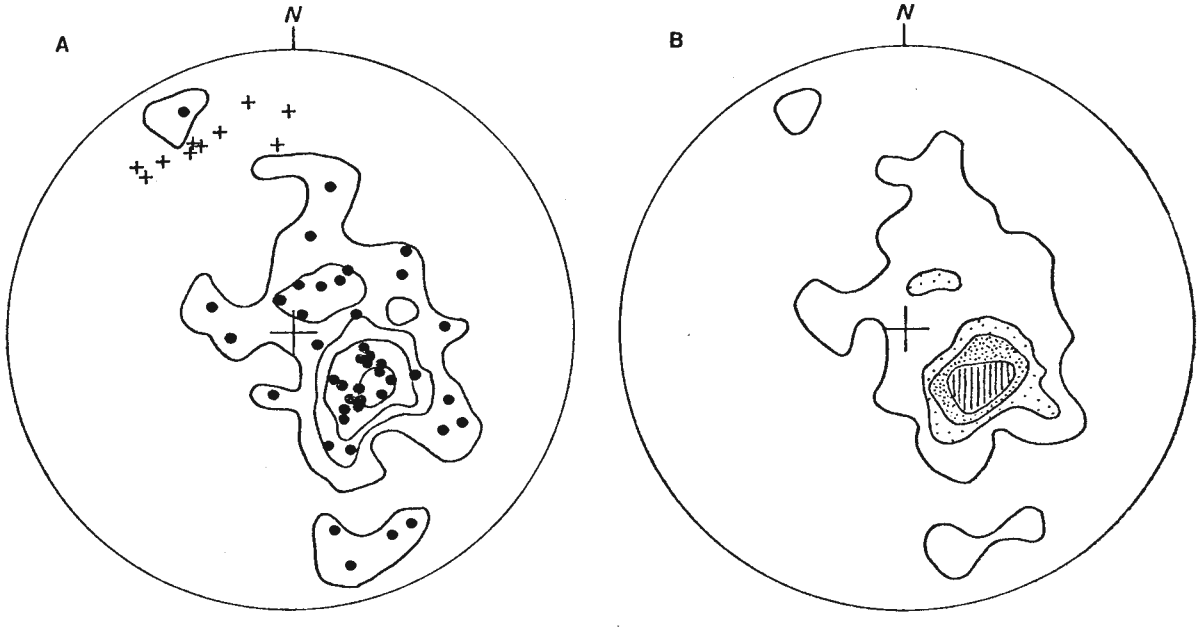

Figure 50. Orientation diagrams for S_1 and L_{1X} in the W.Dassie nappe.
A. 70 poles to S_1 (contours at 1-5-10-20%, with 44 poles to S_1 MYF shown as dots) and 11 L_{1X} MEL poles in the W.Dassie nappe of the SC area. B. 104 poles to S_1 (contours at 1-5-10-15%) in the W.Dassie nappe of the SC and SE areas combined.

is at 282/25 (Fig. 49A), but the data are obviously dispersed in a plane of orientation 208/26, not significantly different from the S_1 ; MYF mean orientation of 210/22 (Table 10). This dispersion of early fold axes in the main foliation plane is responsible for the deviation of the SS fabric from ideal monoclinic symmetry. When W. Dassie bedding data for the SC and SE areas are combined (Fig.49B), the data describe a very diffuse cluster about a mean orientation of 215/40.

The girdle pattern for all S_1 data from the SC area is well defined about a south-west trending axis of shallow plunge (Fig.50A). The data sample for the mylonitic foliation in the marble zones alone shows that the Büllenkopf occurrence has been deformed into an unusual orientation (Table 10), but the differences in attitude, shape and strength between the fabrics in the SC and SE areas are relatively slight. The combined S_1 data for the W. Dassie nappe in both areas has an HVM orientation of 201/23, and the poles define a weak cluster transitional to a girdle about an axis of rotation at 253/18 (Fig.50B & Table 10). The early mineral elongation lineation L_{1X} has a mean orientation of 337/23 in the SC area marble and phyllite zones. Although the data are dispersed in a plane of orientation 195/34 (Fig.50A) and some therefore have nearly northerly trends, it would appear that L_{1X} has a significantly more north-westerly trend in the southern part of the Naukluft nappe complex (cf. Section 2.c.(ii) above) and it is inferred that this is related to progressive changes in the orientation of the slip vector of the nappe relative to its basement during the emplacement history.

c. Structure of S. Pavian nappe

The S. Pavian nappe is an anomalous tectonic wedge consisting of a lower conglomerate and arenaceous unit (Aubschlucht Formation) and an upper carbonate and pelite unit (correlated with the lower members of the Zebra River Formation). It is remarkable that, although the S. Pavian nappe is bounded above and below by thick marble-phyllite zones of the Kudu and W. Dassie nappes respectively, it shows little evidence of severe internal

TABLE 10

FABRIC STATISTICAL PARAMETERS FOR THE W. DASSIE (W.D.) AND KUDU KAPPE CLEAVAGE (S_1) STRUCTURES IN THE SE AND SC AREAS

UNIT/LOCALE	FABELT	TYCODE	N	HVM	K_s	L_B	C_s	Class
W.D. (SE)	S_1	MYF	34	183/25	1,41	260/24	3,35	C – G
(SC)	"	"	44	210/22	1,32	247/14	2,73	C – G
W.D.B (SC)	"	"	11	140/13	2,30	(154/03)	3,42	C
W.D.	"	"	78	197/22	1,49	253/19	2,84	C – G
W.D.	"	(all)	104	201/23	1,56	253/18	3,04	C – G
KUDU	"	"	56	236/48	2,71	–	1,63	C
W.D. 40059	S_1	MYF	11	191/29	1,51	295/28	4,95	C – G
40062	"	"	4	211/43	1,41	019/11	7,29	C – G
40066	"	"	6	138/30	2,13	–	3,92	C
40073	"	"	4	115/29	6,18	–	5,05	C
40083	"	"	4	231/24	2,26	–	7,88	C
W.D. 50070	S_1	MYF	4	135/19	3,22	–	6,26	C
50110	"	"	4	124/18	0,34	165/12	6,31	G
W.D. 50011	S_1	MYF	10	251/64	0,11	253/04	2,66	G
50023	"	"	3	209/53	7,84	–	6,39	C
50111	"	"	4	231/27	4,15	–	9,50	C
50112	"	"	4	228/22	3,15	–	7,60	C
50139	"	"	4	198/23	3,77	–	8,03	C
KUDU 50005	S_1	MYF	6	(347/42)	0,82	(077/42)	1,00	G – C
50033	"	"	4	065/26	1,09	200/19	6,90	C – G
50120	"	"	6	127/37	0,11	273/22	5,01	G
50124	"	"	8	245/45	0,70	293/37	7,18	G – C
50126	"	"	4	235/45	5,28	–	4,65	C
50131	"	"	4	226/66	1,15	230/07	7,44	C – G
50135	"	"	5	174/63	2,67	–	6,02	C

W.D.B. (SC) – Bullenkopf area data from stations 50069, 50070, 50108-50110.

penetrative deformation except locally in more ductile limestone-pelite zones of the upper carbonate unit. In the underlying arenaceous Aubschlucht Formation original clastic sedimentary structure is well preserved and microscopically there is little evidence of grain suturing or intragranular deformation (CH 110).

The relative lack of deformation in the lower part of the S. Pavian nappe can be ascribed to the protective shield of strong dolomite which caps the sequence.

The original profiles of the S. Pavian nappe (Korn & Martin, 1959, Fig. 11) imply that this top dolomite has been thinned by ductile deformation on an overturned southern limb of the anticline, but this hypothesis is not sustained in the present work. The S. Pavian sequence is not overturned along any significant length of the lower contact except locally east of the 1817 m summit (Fig. 45). Elsewhere there is a pronounced truncation of a normal sedimentary sequence in the S. Pavian nappe at the basal thrust. The unconformity between the top massive dolomite and underlying blue limestones shown in profile g (*op.cit.*, Fig. 11) could not be substantiated in this work for lack of exposure in the critical area, but some disharmonic folding is present here between the layered and massive parts of the sequence and could account for this observation. The S. Pavian nappe is crossed by minor imbricate thrusts which splay in a westerly direction from the basal thrust (Fig. 45) and some minor folding is closely associated with these thrust traces.

The principal fabric elements in the S. Pavian nappe are bedding (SS) and a local bedding-parallel cleavage in marly limestones. The SS poles define a diffuse girdle about an axis of rotation at 029/18 (Table 9), which emphasizes the contrast in structure as well as lithology between the S. Pavian nappe, on the one hand, and the W. Dassie and Kudu nappes on the other.

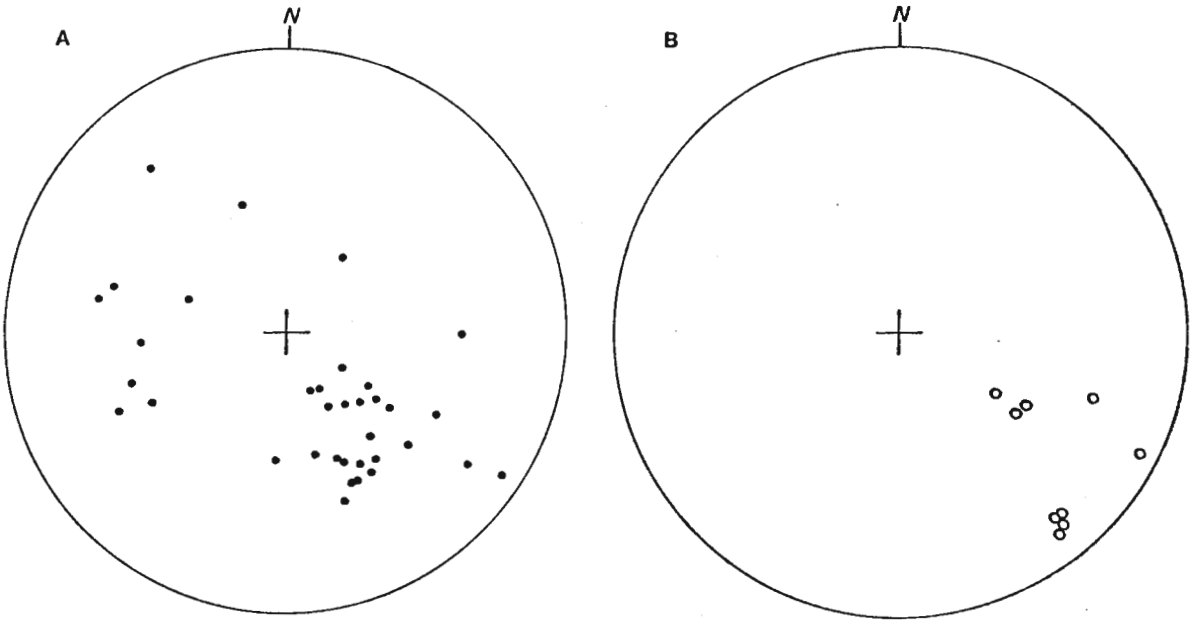

Figure 51. Orientation diagrams for the S.Pavian nappe.

A. 35 poles to SS.
B. 10 poles to S_1.

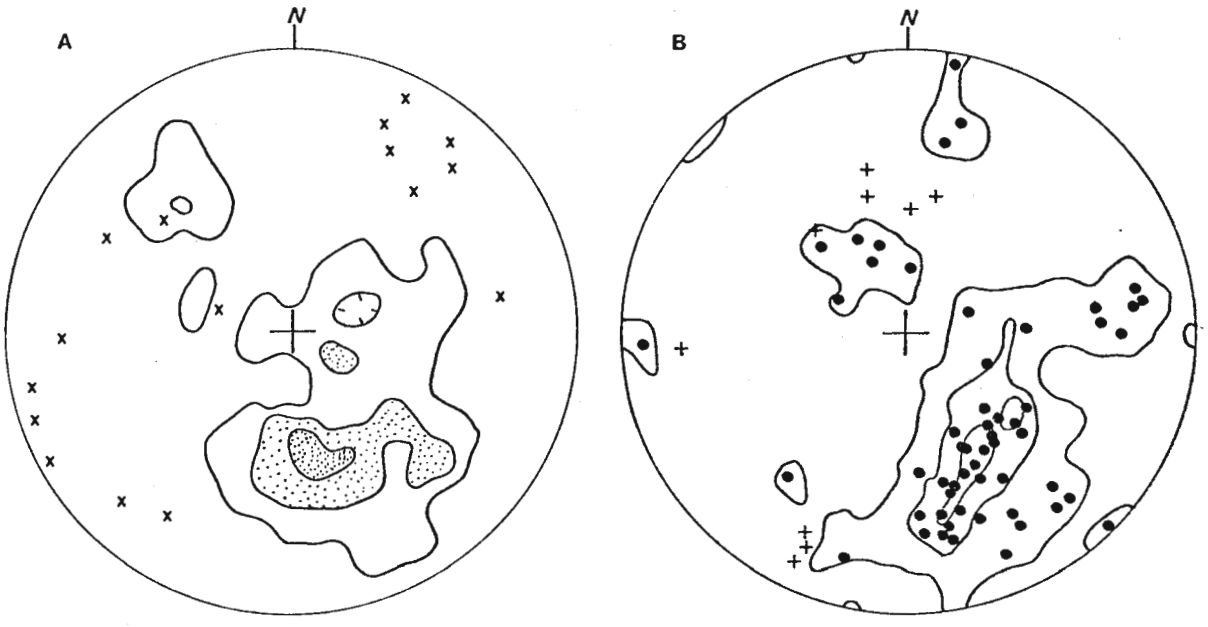

Figure 52. Orientation diagrams for the Kudu nappe in the SC area.

A. 60 poles to SS (contours at 1-5-10%) and 16 L_{1B} ISL & L_1 FAX poles (crosses).

B. 82 poles to S_1 (contours at 1-5-10%) with 56 poles to S_1 MYF (shown as dots) and 9 L_{1X} poles (crosses).

d. Structure of the Kudu nappe

The imbricate structure of the Kudu nappe toe in the region immediately west of the Tsondab valley is well defined by the pattern of minor thrusts which splay westwards from the basal thrust and marble zone (cf. Annex. I and Fig. 45). The mapping of the basal thrust northwards to the main road near Pavianskopf is important, because in the previous interpretation (Korn & Martin, 1959, Pl. 1), it was linked directly with the contact between the Kudu and N. Pavian nappes which is exposed in the southern cliffs of Blässkranz. It is, however, clear in the field (cf. Fig. 45) that the latter contact is truncated at its eastern end and that a thick plate of typical Noab Formation dolomite separates it from the basal thrust between the Kudu and S. Pavian nappes. The subordinate but relatively major thrust which truncates the Kudu-N. Pavian contact south of Pavianskopf appears to diminish in displacement westwards and beyond the 1902 m summit (Fig. 45) it becomes difficult to trace, partly because of residual soil cover on the summit plateau.

As the SS fabric indicates (Fig.52A), there is a general north-westward dip of bedding at about 40^{o}, and the total data sample does not strictly define any girdle pattern (Table 9), which reflects the lack of major folding in this part of the Kudu nappe. The sole exception is a large synclinal structure observed just south-east of the 1902 m summit mentioned above (Fig. 45), but the rugged terrain inhibited data collection here. On a smaller scale, there is some minor folding as the fabric diagram for L_1 structures (Fig. 52) and the SS statistics for a few individual Kudu nappe data sites (Table 9) indicate. The L_1 lineations are dispersed in a rough north-westerly dipping girdle and once again it appears that the north-westerly trending fold axes are located only in the basal marble zone of the nappe, while those with south-westerly and north-easterly trends and shallow plunges occur in both the less and more deformed zones.

The total S_1 fabric from the Kudu nappe (Fig.52B) actually shows less symmetry than the SS fabric, which again is a reflection of the difference between the plastically deformed marble zones, in which S_1 is almost exclusively developed, and the undeformed dolomite imbrications in which perfectly planar bedding structures are exceptionally well preserved. There is a tendency for the S_1 poles to be dispersed about an axis of rotation trending west-north-west (cf. Fig.52B and data statistics for localities 50120, 50124 in Table 10). The total data sample for the mylonitic carbonate foliation (S_1 ; MYF) shows no distinct girdle pattern and a HVM orientation of 236/48 (Table 10). The latter is important in that it appears to exclude an origin for S_1 by simple shear alone on the subhorizontal basal thrust. Together with the mean 38^o back-rotation of bedding in the Kudu nappe toe, it indicates a significant component of horizontal shortening and vertical thickening of the nappe.

The available L_{1X} data is sparse and obviously affected by the above-mentioned late folding of S_1 (Fig. 52B), but the major concentration of poles has a northerly or north-north-westerly trend in common with L_{1X} in the N. Pavian nappe.

5. Structure of the Western and South-western areas

a. Relationship between the Western Dassie nappe and the Zebra River Formation

For interpreting the tectonic evolution of the Naukluft complex and for relating the present study to the Damara-Nama correlation problem, the relationship between the Büllsport Formation and the Zebra River Formation is probably the single most important aspect of nappe tectonostratigraphy. The major part of the contact zone between these formations is remarkable because the trend of its surface trace is almost normal to the trend of the nappe front and because it obviously separates regions of vastly different tectonic style and orientation.

As the new mapping indicates (cf. Annex. I), the Büllsport Formation is intensely imbricated (Plate 68) and individual lithostratigraphic zones cannot be traced laterally for any great distance. In contrast, the Zebra River Formation is subdivided into at least six members which are laterally persistent everywhere except in the easternmost outcrops of the formation. The imbrication and associated folding of the Büllsport Formation has north-westerly axial trends, whereas the fold axes of relatively open Zebra River structures (Plate 69) trend in a north-easterly direction. This feature was formerly described as an "axial unconformity" (Korn & Martin, 1959) and an expression of the "great freedom which distinguishes the Naukluft folding from that of other folded belts"(*op.cit.*, p.1067). The northeast-striking structures were considered to be older than those striking north-west and the lowest slices of the Dassie nappe "to have even intruded the Zebra series."

This former view of contact relationships is not supported by the present work. The formerly undifferentiated surface of contact between the two formations is divisible into two distinct parts (cf. Annex. I). The northwest-trending segment follows the lithological boundaries in the overlying Zebra River sequence, the Ubusis clastic member being a particularly useful marker zone. The Neuras sequence of intercalated dolomite and calcareous quartzite, which is thickest in the north-west, wedges out south-eastwards.

This segment of the contact was formerly represented (cf. Korn & Martin, 1959, Fig. 2) as a thrust zone dipping steeply north-eastward. The present mapping shows it to have gentle to moderate south-westerly dips almost everywhere. The Zebra River Formation overlies the Büllsport Formation and the contact itself is an erosional unconformity locally marked by a conglomerate at the base of the Ubusis Member (e.g. locality 70051 on Naukluft) containing chert pebbles derived from Büllsport dolomites. The basal Ubusis quartzite is generally coarse and arkosic, indicating that material from an eroded granitic massif was also being transported into the basin at this time.

This conspicuous unconformity truncates several of the imbricate thrust slices in the Western Dassie nappe. The intervention of the Neuras Member in the north-west complicates the interpretation of the contact zone here, since it is lithologically very similar to parts of the Büllsport Formation. In the south-east segment, however, where the Neuras Member is either absent or very thin and the contact zone is deeply dissected by the Naukluft stream, northward-dipping thrust zones marked by highly deformed marble-phyllite layers are overlain without deflection by subhorizontal Ubusis quartzites and shales (Plate 70).

In stark contrast to the structural geometry of the northwest-trending segment, the northeast-trending trace of the contact, which is well exposed in the cliff sections on Naukluft, is a subhorizontal to gently dipping overthrust defining the base of the western Dassie nappe. The most important feature of the Zebra River contact zone occurs at the junction of these two segments where it is clearly apparent that *the unconformity segment is deformed above and truncated by the overthrust segment of the contact* (Fig. 53). The thrust-plane trace can be mapped south-westwards beneath a tectonic wedge of imbricated Tsams Member dolomite, identifiable as such by the characteristic middle zone of flaggy calcareous quartzite. Beyond this it is lost in a complex zone of later tectonic imbrication and partly obscured by an erosional unconformity at the base of the overlying Onis Member.

The north-western end of the unconformity segment of the contact is also

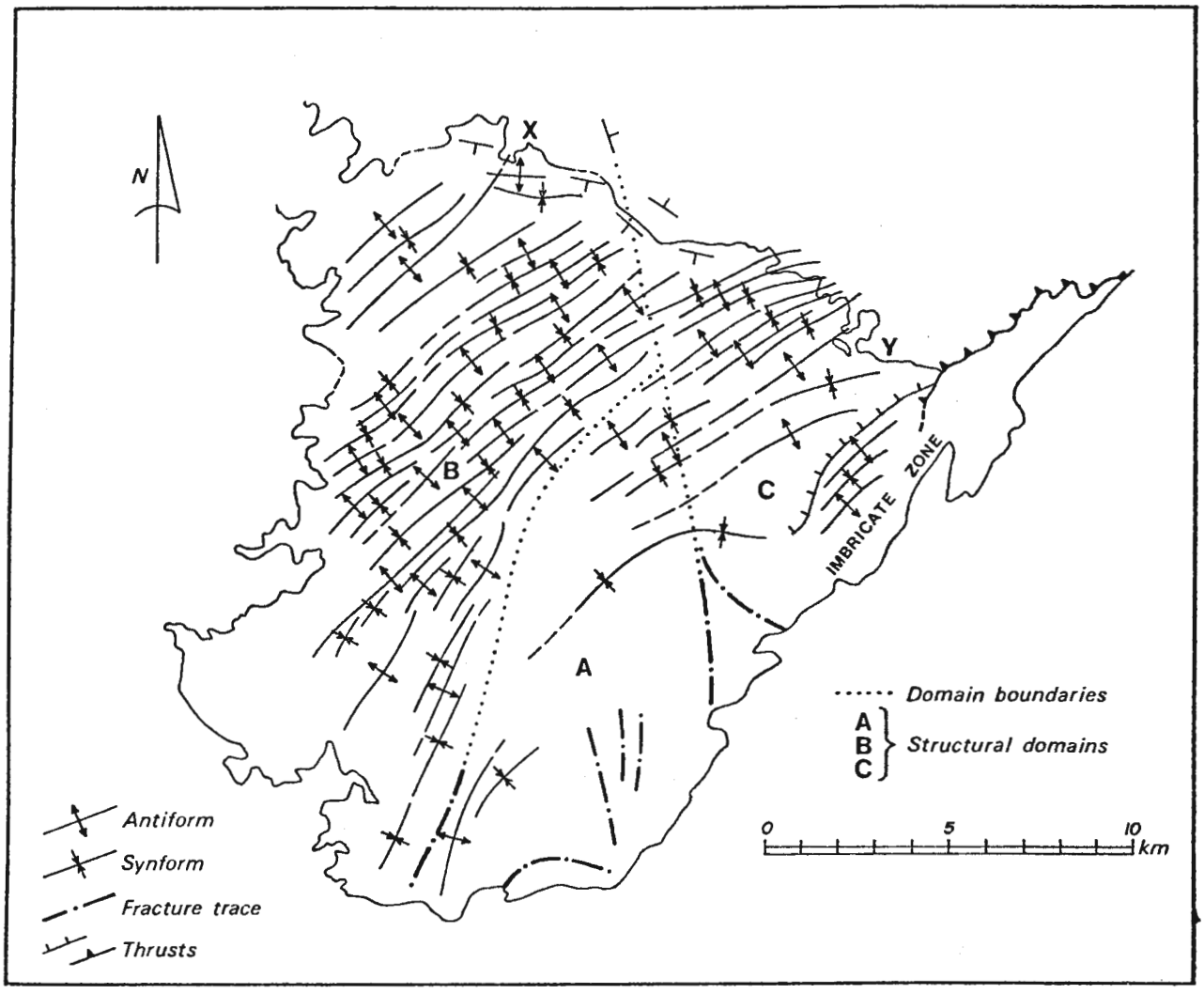

Figure 53. Diagram of fold trends in the Zebra River Formation, also illustrating its subdivision into structural domains A, B and C.

exceptional. The Ubusis Member has a near-vertical orientation and is locally overturned towards the south-west. The internal structure of the basal Neuras Member, however, is unusually complex (cf. Fig.54 redrawn from a composite panoramic photograph). The Büllsport Formation in the north of the mountain section is a massive dolomite, overlain in the central part of the section by a probable lower division of the Neuras Member (Ne_1). A sharp apparent truncation of the bedding in the Ne_1 unit at its subvertical northern contact with the massive Büllsport dolomite is presently interpreted as a feature related to burial of rugged, tectonically created topography on the surface of the dolomite which is intensely imbricated just north of this point (cf. Annex. I). The overlying unit of a similar, interbedded dolomite-arenite succession (Ne_2) overlaps the above-mentioned contact and is also distinctly unconformable upon the lower Ne_1 sequence. This evidently reflects continuing vertical tectonic movements of an oscillatory nature during Neuras deposition. Finally, in the southern part of the mountain section, the Ubusis Member (U) commencing with its distinctive arkosic basal zone, is here in unconformable contact with all three of the above-mentioned stratigraphic units in a unique narrow zone of complex convergent structure (cf. Fig. 54).

The detailed tectonostratigraphic relationships seen in this area constitute evidence for rather special tectonic and environmental conditions during the deposition of the lowermost Zebra River units. The well-bedded Neuras sequences give the impression of a relatively high degree of sedimentological maturity, with fine, well-rounded quartz grains being the only siliciclastic material available for deposition. That sediments of this nature were deposited in a mobile zone so as to bury conspicuous topographic prominences on the underlying dolomites, seems most paradoxical. The most likely explanation is that the Neuras beds were deposited at the *subsiding* leading edge of a large dolomite nappe at a time when rugged islands of imbricated dolomite constituted the only nearby land exposures. The silica grains were probably derived by sedimentary re-cycling of the well-rounded quartz in the Noab and Büllsport Formations. It is probable that a great hiatus exists between the Neuras and the Ubusis Members of the Zebra River

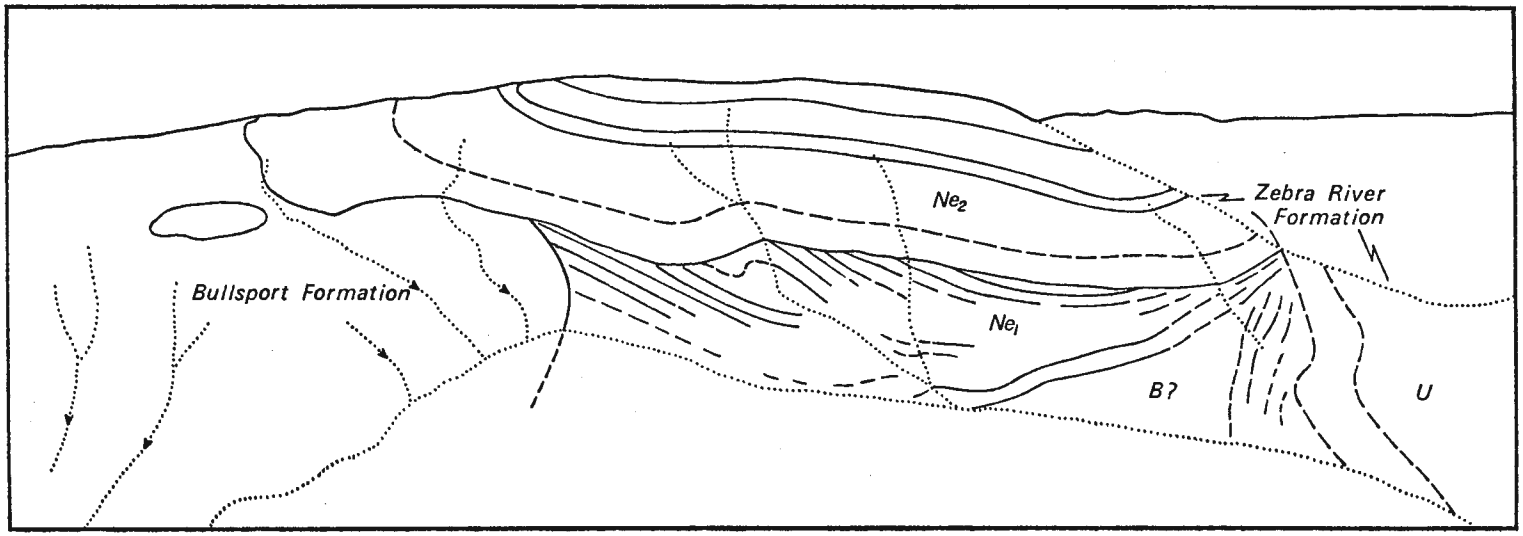

Figure 54. Sketch traced from photographic panorama of contact relationships between the Büllsport Formation (B) and the Zebra River Formation, the latter including two divisions of the Neuras Member (Ne_1 and Ne_2) and the basal part of the Ubusis Member (U). Location of contact is near point X in Fig. 53.

Formation, for with the sedimentation of the basal arkose of the latter unit a large provenance of granitic basement rocks must have been exposed to rapid erosion.

b. Internal structure of the Zebra River Formation

As already noted, the structure of the Zebra River Formation is radically different from that of the north-eastern part of the Naukluft complex. In general, three large domains, designated A, B and C (Fig. 53) can be distinguished. The southern domain A, is the least deformed. Structurally it consists of a shallow, basin-like syncline defined mainly by the outcrops of the Lemoenputs and Onis Members (cf. Annex. I). The south-eastern limb of this structure is magnificently exposed in the cliffs of the Johann-Albrecht-Felsen (Korn & Martin, 1959, Pl. 1) and their north-easterly extensions, which reveal the complete Zebra River succession. Broadly, the whole sequence appears quite conformable. There is some slight imbrication of the contact between the Neuras and Ubusis Members, best seen in the southern cliffs, but photogeologically the most conspicuous structures are fractures with a general north-south trend which appear to splay out southwards from a point close to the boundary between the north-western and eastern domains (B and C, respectively).

The boundary between domains A and B is a narrow zone of partly *en echelon* anticlines, trending north-eastward and emphasised by the exposure of Tsams dolomite within an extensive area of Lemoenputs shale. Domain B is a region of slightly asymmetric large-scale chevron folds, prominently involving the laminated or well-bedded dolomite-calcareous quartzite sequence of the Tsams Member. The more massive dolomite unit of the Onis Member is deformed into less acute folds and there is therefore some structural disharmony between the two dolomite members accommodated by shear within the more ductile Lemoenputs sequence. No evidence, however, exists of major horizontal relative movement between these two layers; a point that needs emphasis because of the erosional unconformity at the base of the Onis Member in domain C, which on superficial appearance could be mistaken for a tectonic discontinuity. In domain B, as in domain A, the entire Zebra River sequence

is conformable, although the sharp boundaries between the main carbonate and clastic lithologies evidently reflect significant depositional hiatuses or non-sequences.

The difference in tectonic style between domains A and B is best represented in a structural cross-section (A-B on Annex. II) with no vertical exaggeration, as the contrast between a very gently folded, almost undeformed domain A and the openly folded domain B. Alternatively, the representation of anticlinal and synclinal hinge-zone traces in the Zebra River sequence (cf. Fig. 53) also shows the north-westward increase in fold density. Comparison of this accurate representation of fold trends with the previous schematic representation of folding in the "Zebra series" indicates that the folding has a trend which is more north-easterly than east-northeasterly, as formerly represented, with the exception of locally complex subdomains in the northern part of domain A and the eastern part of domain C. The fold trends are practically orthogonal to the trend of the basal contact of the Zebra River sequence and the "axial unconformity" at this zone is therefore emphasised even more.

The western boundary of domain C is a diffuse zone trending slightly west of north from its southern segment which aligns with the two major fracture zones in the Onis Member. In the north it is reflected in the south-westward dipping boundary between the Tsams and Lemoenputs Members in a region where the outcrops of these two units are unusually extensive (cf. Annex. I) and it also aligns with a prominent deflection of the base of the Zebra River Formation. This in turn is located above a photogeologically conspicuous zone of convergent minor thrust planes in the Büllsport Formation in which the latter are deflected into more northerly trends. The geometric pattern of this structure suggests that it was formed by a component of right-lateral motion with some relative uplift of the western block. This is also visible in the sympathetic right-lateral deflection of the hinge zone in the large domain A syncline of Onis dolomites and can be related to eastward tightening of this structure and its progressive imbrication in the same direction.

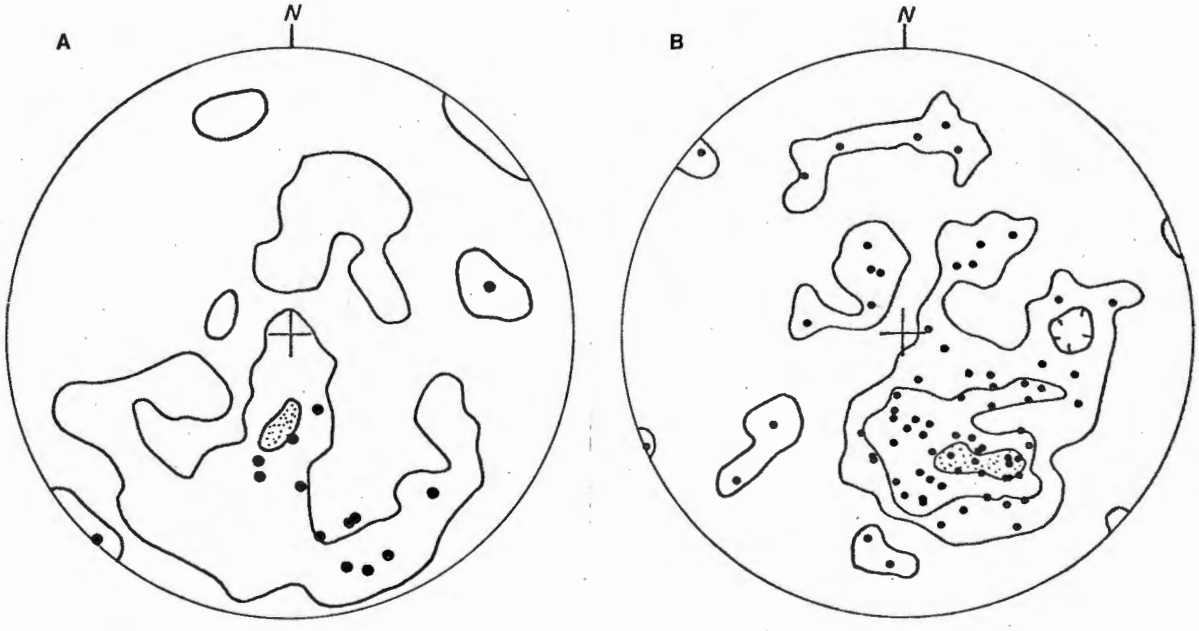

Figure 55. Orientation diagrams for the W and SW areas.

A. 36 poles to SS (contours at 1-10%) and 14 poles to S_1 in the Büllsport Formation of the W. area.

B. 77 poles to SS (contours at 1-5-10%) in the Zebra River Formation of the SW area.

The imbricate zone in the eastern part of domain C is related primarily to the development of the main overthrust at the base of the Büllsport Formation in the Western Dassie nappe. The lithological unit immediately below this overthrust, a 150 m-thick wedge of cleaved, phyllitic green shale with local lenses of conglomerate and grey dolomite, is somewhat uncertainly correlated with the Lemoenputs Member, but can also be interpreted as a part of the autochthonous or para-autochthonous Schwarzrand Formation which was tectonically incorporated in, or accreted to, the toe of the nappe complex in the final stages of its emplacement. The Lemoenputs shale, which rarely exceeds 30 m in thickness, cannot actually be traced continuously from its type area into this zone of deformed pelite, as strongly imbricated slices of the underlying Tsams dolomite intervene. In the triangular area west of the intersection between the unconformity and thrust segments of the Büllsport-Zebra River contact, the internal structure of the Zebra River Formation is extraordinarily complicated. Close to the plane of the unconformity the lower Zebra River beds have been folded into a near-vertical orientation and below them partly chaotic slices of Tsams dolomite mark the south-westward extension of the main Western Dassie overthrust. The latter is transected by a later thrust zone at the base of the deformed Lemoenputs (?Schwarzrand) pelites.

Within the fault-bounded mass of rock lying south of this secondary thrust an erosional unconformity is exposed at several localities at the base of the Onis dolomite and oolitic black limestone member (Fig. 56). The contact between steeply dipping Tsams dolomite and gently dipping basal Onis limestone is most abrupt and occasionally marked by a thin sedimentary breccia of dolomite fragments. The state and shape of oolitic layers in nearby Onis limestones shows that there has been minimal tectonic movement along this discordant contact and thereby confirms its erosional character. This pre-Onis deformation of the lower part of the Zebra River Formation can also be seen in exposures in the western wall of the gorge on Naukluft (cf. Annex. I) north of the imbricate zone. There is an exposure of the unconformity in the frontal mountain range near the Naukluft-Neu Onis boundary, south-westward of which the lower and upper parts of the Zebra River Formation in domain C

rapidly become (pseudo-) conformable.

The pre-Onis deformation of the lower part of the Zebra River sequence can be related to movement and tractional effects along the basal overthrust of the Western Dassie nappe. This episode of deformation probably coincided with uplift in the tectonic hinterland and the consequent deposition of clastic detritus in the Lemoenputs Member, as a relatively thin, compressed sequence above rigid dolomitic lower units on the hanging-wall side of the overthrust and as a much thicker, more rapidly accumulated sequence on the footwall side which is now represented by the lower Schwarzrand shale facies or the northward-thickening tongues of green shale in the upper part of the Schwarzkalk Limestone Member of the Kuibis Formation.

The subsequent shallow-water deposition of limestone and dolomite (of probable diagenetic origin?) in the Onis Member, partly overlapping the imbricate thrust zone which evidently formed a locally rugged topographic ridge in the Zebra River basin, probably reflects subsidence in the tectonic hinterland, shore-line transgression and a cessation or slowing of movement on the Western Dassie overthrust.

The south-westward disappearance of the latter is therefore due partly to its burial beneath the Onis Member during this interval. Renewal of movement along the Western Dassie overthrust, resulting in post-Onis displacement along a family of minor imbricate thrust surfaces in the Naukluft area, is also responsible for displacing the original Western Dassie overthrust to a level below that of the present Unconformity Dolomite zone.

The main structural differences between domain C and the combined domains A and B were apparently established during this post-Onis episode of deformation. Simultaneous ductile deformation in the phyllitic zone beneath the Western Dassie nappe and further movement along the principal dislocation at the base of the Büllsport Formation, caused post-Onis folding and further local imbrication of the entire Zebra River sequence close to the thrust. There is also a north-south striking fault which is well exposed in the mountainside near the Onis-Naukluft boundary and shows a ~50 m displacement of the Zebra River stratigraphy (downthrow to east), cannot be traced into the

upper black limestone of the Onis Member, although it is responsible for a major vertical displacement of the lower massive dolomite. The conspicuous fracture zones farther south-west, forming the boundary between domains A and C, have only minor associated vertical displacements but transect all Zebra River units up to and including the upper Onis limestones. The north-south faulting episode therefore commenced during and was active after the deposition of the Onis carbonates. That it preceded the formation of the present basal sliding surface of the Naukluft complex and the Unconformity Dolomite is shown by the fact that the Unconformity Dolomite zone transects the fractures sharply and clearly.

While these fractures do not extend into the autochthonous Nama rocks, the western boundary of domain C, they can be extended northwards along the apparent shear zone which divides the Büllsport Formation of the Western Dassie nappe into two distinct tectonic domains. This probably indicates *reactivation* of the right-lateral shear zone during the post-Onis deformation episode, the zone itself having been formed earlier in the Naukluft deformation history. The folding and local imbrication of the contact between the basal clastic Ubusis Member and the middle carbonate Tsams Member, which is mapped parallel to the basal Zebra River unconformity from Naukluft to Die Valle, is not reflected in obvious structures within the Büllsport Formation away from the unconformity. Some structures appear to curve into approximate parallelism with the imbrication in the more massive underlying dolomites, but this tendency is not nearly as evident as it was formerly represented schematically (Korn & Martin, 1959, Pl. 1).

CHAPTER V

KINEMATIC AND DYNAMIC ANALYSIS OF NAUKLUFT NAPPE EMPLACEMENT

A. ASPECTS OF NAUKLUFT KINEMATICS

1. Role of unconformities in defining deformation episodes

In other parts of the Damara orogenic belt, various folding or deformation *phases* have been defined on the basis of fabric overprinting relationships (e.g., De Waal, 1966; Hälbich, 1970). Structures indicative of polyphase deformation are found in the Naukluft nappe complex, but are confined to regions of anomalously high finite strain, such as the mylonitic marble zones at the base of the Kudu nappe, or the Remhoogte phyllites in the Northern Pavian nappe. It is accordingly difficult to relate these structures, which have developed in a pattern of extremely inhomogeneous deformation, to a regionally coherent kinematic history of distinct phases of deformation.

The erosional unconformities found within the nappe complex, however, can clearly be related to an episodic deformation history, but the distinction between *deformation episodes*, defined on a stratigraphic basis such as this and *deformation phases*, defined by the successive development of tectonic fabrics, should not be overlooked. For example, it is theoretically possible (and is actually the case in the Naukluft complex) that two similar formations separated by a large angular unconformity each might show the same single tectonic cleavage and lineation set. Interpreted purely on fabric grounds, these two formations have been subjected to a single *phase* of deformation even though the presence of a large unconformity indicates two distinct deformation *episodes*, pre- and post-unconformity respectively. It is alternatively possible in some lithologies that fabric elements related to two distinct phases of deformation, e.g. a late crenulation cleavage super-

imposed on an early slaty cleavage in low-grade meta-pelites, can have formed during a single continuous deformation episode due to a combination of boundary conditions of rotational progressive deformation and continuously changing, finite strain-related mechanical properties (e.g., anisotropy) in the rock.

In the present account of Naukluft kinematics, therefore, it should be clearly understood that the five deformation episodes (D_1-D_5) described are defined by tectonostratigraphic field relationships. In most outcrops within the nappe complex, the rock fabric on a mesoscopic scale records only one principal deformation phase, but the unconformity relationships show that this principal deformation phase has a different age in the various lithostratigraphic units. Once deformed, the older units either remained relatively rigid during the later deformation episodes or the later strain increments were superimposed on the earlier fabrics in such a way that the pre-existing cleavage and lineation structures were further enhanced instead of being overprinted. Outcrops located close to the main tectonic discontinuities, i.e., overthrusts or *decollements*, generally show more complex deformation patterns (cf. Plates 56 & 64) and here the problem is reversed since it is by no means clear that these polyphase structures formed during more than one deformation episode.

2. Correlation of deformation episodes

The correlation of deformation episodes across a major part of the Naukluft complex is based on observations at nine critical locations (Fig. 57). The features at these locations and their interrelationships are described as follows:

Locality 1. At this locality, an unconformity at the base of the Blässkranz Formation is the main evidence for the earliest (D_1) episode of deformation. The Blässkranz and overlying Tsabisis Formations were folded to some extent in a later episode (D_2), which was related to their overthrusting by the Noab Formation in the Kudu nappe;

Locality 2. The D_2 overthrust surface at the base of the Kudu nappe is itself folded and imbricated near locality 2, during a third episode of

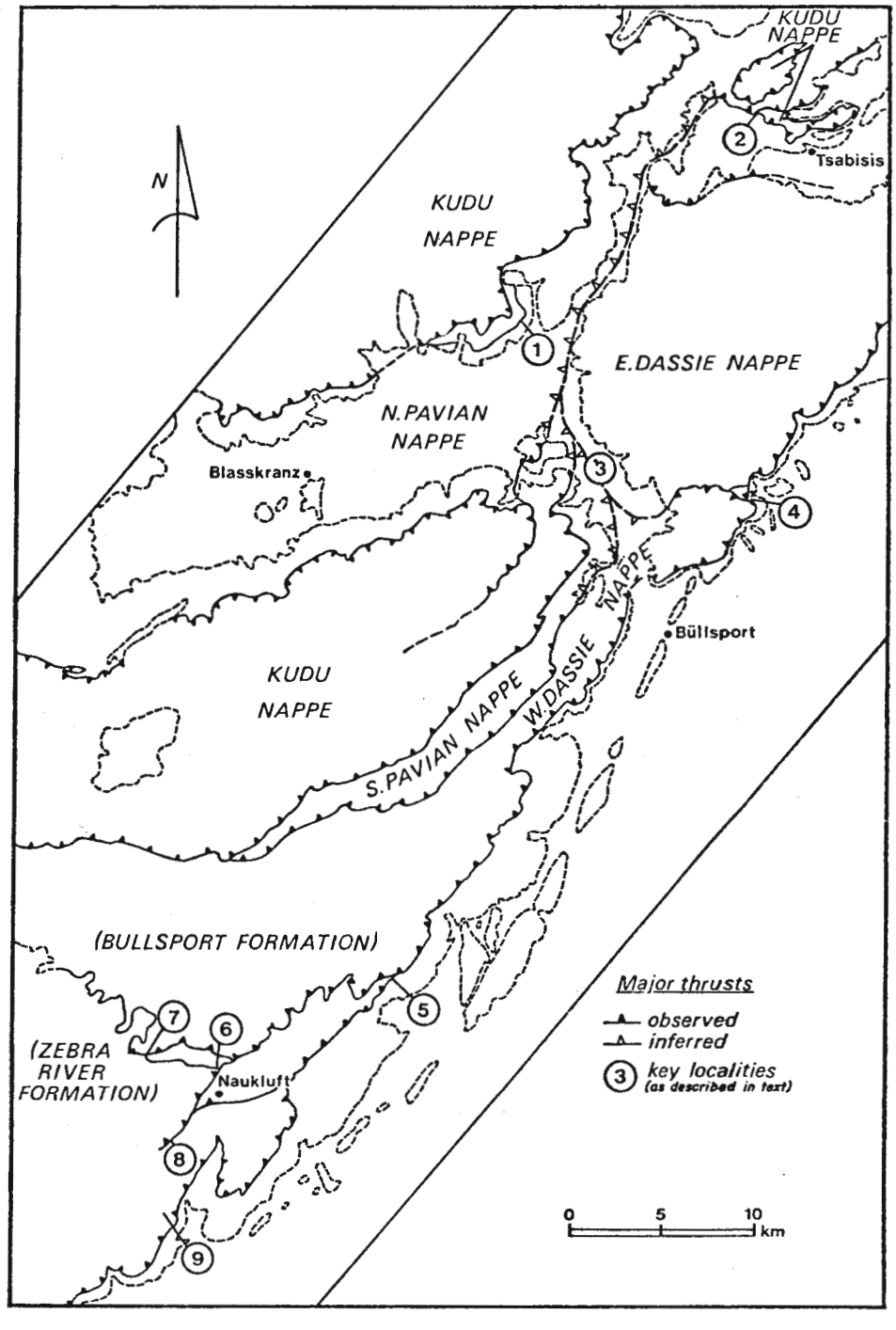

Figure 57. Sketch map of the nine localities critical to kinematic interpretation of Naukluft nappe evolution.

deformation (D_3 - for evidence of this refer forward to locality 9) which is related to thrusting of the Northern Pavian and Kudu nappes together over the Büllsport Formation in the Eastern Dassie nappe;

Locality 3. Further evidence of major D_3 displacement of the overthrust between the Kudu and Northern Pavian nappes is seen at this locality where the tectonic sequence is locally reversed by displacement of part of the Northern Pavian sequence over a slice of Noab Formation. The latter has in turn been thrust over the formations of the Southern Pavian nappe, which has also been displaced farther southward by thrusting over the Büllsport Formation in the Western Dassie nappe. Although it is possible in geometric principle to interpret the contact between the Kudu and Southern Pavian nappes as a D_2 overthrust, on stratigraphic grounds (i.e., the lack of correlation between lithologies in the Northern and Southern Pavian nappes) the preferred interpretation is that the three splayed thrust surfaces seen near this locality reflect a serial migration of the main D_3 thrust-surface southwards and tectonically downwards during the course of relative movement between the Kudu and Dassie nappes;

Locality 4. The D_3 overthrust below the Western Dassie nappe at this locality is observed to truncate sedimentary structure in an underlying formation (cf. Plate 52 and Fig. 46) which bears a close lithological resemblance to both the Zebra River Formation and the Kuibis Formation in the underlying Rietoog nappe, thus helping to establish that deposition of these units pre-dated the D_3 episode. At this locality, the D_3 overthrust is in turn truncated, in a downward-facing orientation, by the principal dislocation at the base of the Naukluft nappe complex, thereby definitely establishing that the latter structure was formed at a late post-D_3 stage;

Locality 5. The overthrust surface at the base of the Western Dassie nappe reappears within the Naukluft complex at this location, where it overlies a thick deformed pelitic sequence which is correlated with part of the Zebra River Formation, but which technically belongs to none of the five major nappes defined in the introduction to this chapter;

Locality 6. Tracing this conspicuous overthrust westward, it is observed to truncate overlying, vertically dipping strata of the basal clastic member of the Zebra River Formation. As at locality 4 above, this relationship establishes that the D_3 overthrust at the base of the Western Dassie nappe post-dates deposition of the lower part of the Zebra River Formation;

Locality 7. When the truncated basal beds of the Zebra River sequence are traced north-westwards to this locality, they are seen to overlie different tectonic and lithological slices in the Büllsport Formation of the Western Dassie nappe along a conspicuous local and regional unconformity. The surface of a minor imbricate thrust in the Western Dassie nappe is truncated by the erosion surface here (cf. Plate 70), indicating that a major part of the Dassie nappe imbrication may pre-date the D_3 episode and may therefore have formed during D_2, when it is supposed that the now distinct Dassie nappes were part of the frontal or toe region of the larger Kudu nappe;

Locality 8. Traced south-westwards from locality 6 above, the D_3 overthrust at the base of the Western Dassie nappe splays into a complex of minor imbricate slices in the lower Zebra River Formation. At locality 8, this complex of subsidiary D_3 structures is overlain unconformably by Onis Member limestone and dolomite at an erosional sedimentary contact locally marked by sedimentary carbonate breccia. This relationship establishes that deposition of the upper part of the Zebra River Formation post-dates the D_3 episode, but it has here been folded and locally imbricated in a subsequent deformation episode D_4;

Locality 9. At this locality the stratigraphic units of the lower Zebra River Formation are truncated at the sole overthrust of the Naukluft nappe complex and a fault causing internal displacement of the lower Zebra River Formation is also truncated. The base of the overlying Onis Member is less displaced than lower units, which may be explained by syndepositional growth of the fault. Related fault structures farther south-west, which cut obliquely across the main D_4 synform in the Onis Member but which were probably formed synchronously with the latter, are also truncated at the level of the Unconformity Dolomite. Hence it is inferred that the latter's

formation, and the final emplacement of the nappe complex into its present position, constituted a tectonic episode (D_5) which was distinctly later than the D_4 folding and thrusting in the Zebra River Formation.

This interpretation of the kinematic evolution of the Naukluft nappes in terms of five distinct deformation episodes, D_1 through D_5, has a critical link between localities 3 and 5 above which emphasises the great importance of the nappe geometry in the Tsondab valley between Büllsport and Blässkranz. The major problem of tectonic interpretation has been to link the clearly episodic, three-stage evolution of the central and Northern Naukluft, as represented at localities 1 to 3, with the episodic three-stage evolution of the southern Naukluft, as represented at localities 5 to 9. The suggested solution lies in the recognition of a major tectonic discontinuity between localities 3 and 4, separating the compound pile of the W. Dassie, S. Pavian and Kudu nappes from the underlying E. Dassie nappe, and the postulated western extension of this same thrust in the Naukluft complex between localities 5 and 6. Between localities 2 and 3, the thrust is clearly associated with the third deformation episode in the central area, whereas between localities 5 and 6 it is associated with the second deformation episode (i.e. post-lower Zebra River) in the south-western area.

3. Kinematic Reconstruction of nappe emplacement

Having outlined a sequence of five episodes of deformation, culminating in the final emplacement of the Naukluft nappe complex, which differs appreciably from the previous model of Naukluft tectonics (Korn & Martin, 1959), it is now necessary to attempt a reconstruction of the pre-deformation geometry of the Naukluft formations. The method adopted is to proceed from the last deformation (D_5) to the first (D_1) systematically reversing displacements on major thrusts and horizontal strains acquired in imbrication or ductile flow.

a. The D_5 and D_4 episodes

The last two deformation episodes are grouped as one for the purposes of establishing the post-D_3 configuration of the Naukluft complex. In effect, the D_4-related shortening across the Zebra River Formation is disregarded as relatively insignificant.

It is assumed that, since the Zebra River Formation can be correlated with the underlying Kuibis Formation, and the D_5 episode involved rigid-body displacement of the nappe complex on the thin, highly ductile Unconformity Dolomite zone, the Naukluft complex should be rigidly displaced north-westwards until the south-eastern edge of the Zebra River Formation is just past the north-westernmost occurrences of the Kuibis Formation. The approximate azimuth of this reversed displacement is obtained from several features of structural geometry that can be related to the D_4 or D_5 deformation episodes. They are:

(i) the normal to average strike of the vertical or slightly overturned, thick quartzite formation in the basal Schwarzrand beds below the south-eastern nappe front (Korn & Martin, 1959);

(ii) the normal to the average strike of S_1 cleavage in the Kuibis Formation underlying the Naukluft complex (cf. Chapter IV, Section 2);

(iii) the average normal to the bundle of fold hinge traces in the Zebra River Formation (cf. Chapter IV, Section 5, Fig. 53);

(iv) the average trend of linear structures in the Unconformity dolomite zone (e.g., local basal groove structures) and stretch lineations (L_{1X}) or fibre orientations in calcite tension gashes in the deformed Kuibis limestones.

All are consistent in indicating that the approximate azimuth of reverse displacement for the D_4 and D_5 episodes is 305°.

The conservatively estimated total length of the displacement vector along this azimuth is 35 km (Fig. 58). Hence prior to D_4 , a point X, situated on longitude 16,25°E at the southern apex of the Kudu nappe was

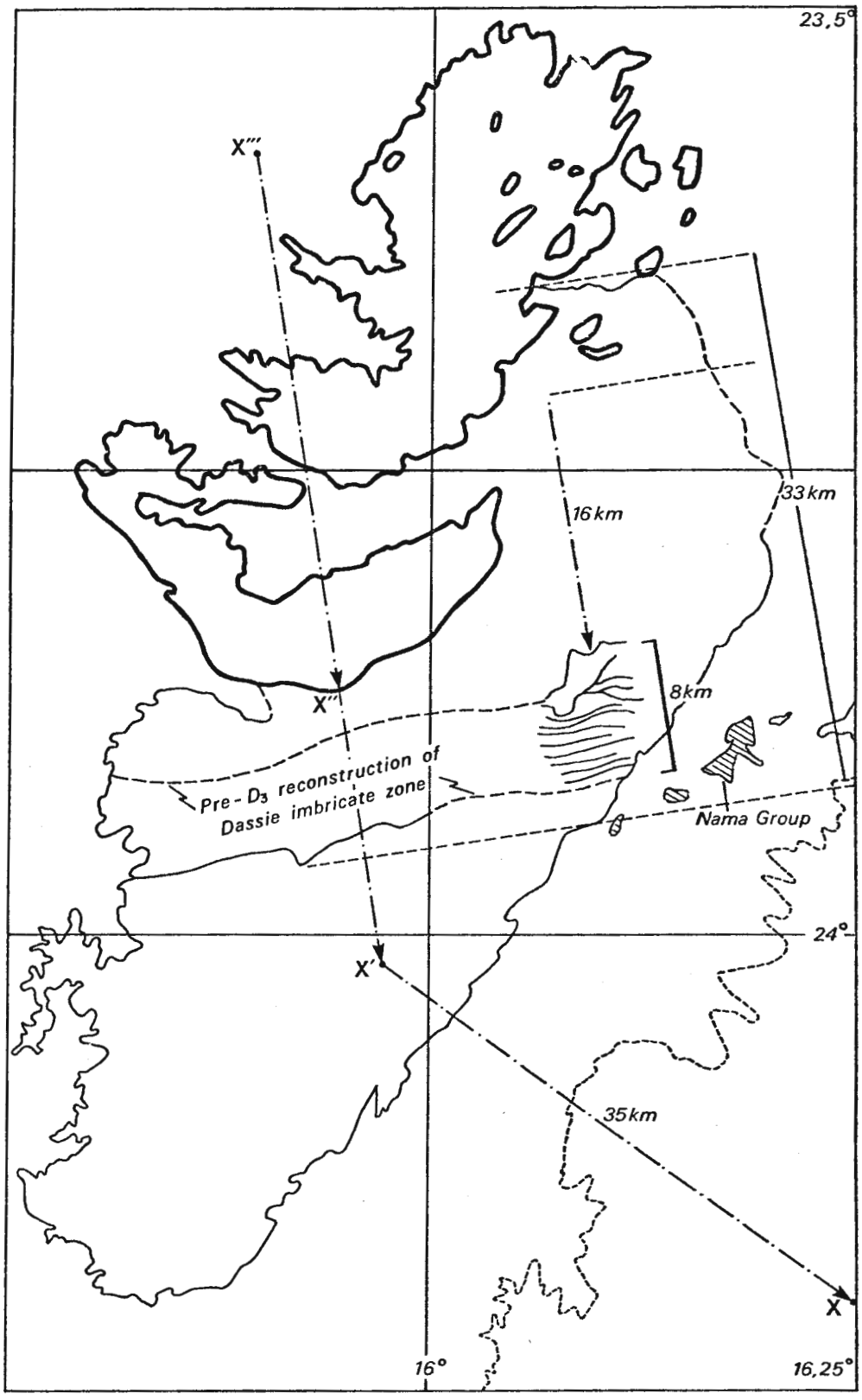

Figure 58. Reconstruction of Naukluft nappe emplacement, showing displacement vectors to reference point X, part outline of Naukluft complex in present position (dashed line), outline of Naukluft complex in pre-D_4 position (thin line), outline of Kudu nappe in pre-D_3 position (thick line) and locations of north-westernmost Kuibis Formation outliers (hachured).

located at point X' near lat. 24,02°S, long. 15,97°E (Fig. 58). It is perhaps significant that in this position the Naukluft complex covers the Nauchas massif of basement rocks almost entirely and that its north-western edge is situated close to the present locus of the Areb mylonite belt near lat. 23,75°S, long. 16°E.

b. The D_3 episode

This deformation involves three important features of the Naukluft complex, which are:

(i) the large-scale imbrication of the W. Dassie, S. Pavian, Kudu and N. Pavian nappes in the Büllsport region and their joint displacement over the E. Dassie nappe, including the problem of S. Pavian nappe emplacement and that of relating the S. Pavian carbonate facies to the Zebra River and Kuibis Formations;

(ii) the large-scale arcuate structure of the W. Dassie and southern Kudu nappes;

(iii) the large-scale ductile deformation of the N. Pavian nappe in the Blässkranz region.

In the attempt to estimate the length and azimuth of a D_3 displacement vector to point X' of Fig. 58 , the abovementioned aspects are discussed in turn.

(i) The S. Pavian emplacement problem

The S. Pavian nappe is bounded entirely by major dislocation zones, having a total length of 15 km and a maximum width of 1,5 km, and has a maximum vertical exposure of about 400 m in the Aub River valley on Büllsport. The lower tectonic contact of the nappe dips more steeply north-westward than the upper tectonic contact, which leads to the inference of an antiformal structure reinforced by the convergence of the upper and lower contacts towards the south-west (cf. Korn & Martin, 1959, Fig. 11, Profiles a & b). In the region of the convergence, however, there is little

indication of such a fold structure in the tectonic foliation of the upper and lower marble and phyllite zones which mark the contacts. It is also clear from mapping of lithological marker zones along the southern contact of the S. Pavian nappe, that it truncates the internal stratigraphy of the nappe (cf. Chapter IV, Section 4(c)). The S. Pavian nappe was therefore not emplaced as a result of folding of the Kudu nappe front, but was thrust together with the overlying Kudu nappe over the W. Dassie nappe.

This thrusting episode must have occurred after the W. Dassie and Kudu nappe together had been thrust over the S. Pavian nappe, since the Büllsport and Noab Formations are simply different facies of the same major stratigraphic unit. The minimum total displacement involved in overthrusting of the W. Dassie by the S. Pavian can be estimated at just over 8 km, if it is assumed that the displacement vector had a trend normal to the trace of the W. Dassie contact north of beacon Sieg (cf. Fig. 45 and region west of point Z' in Fig. 59A) and that points Y and Z' (Fig.59A) were previously colinear.

The minimum total displacement of the earlier D_3 thrusting of the combined W. Dassie and Kudu nappes over the S. Pavian nappe can be similarly estimated by assuming that points Z and Z' (Fig.59A) were formerly colinear along the extension of the thrust trace west of Z'; point Z on Naukluft is in the place at which the Zebra River Formation unconformity in the W. Dassie nappe is truncated *above* the major D_3 thrust, and point Z' is the place at which the stratigraphy in the Zebra River equivalents of the E. Dassie nappe is truncated *below* the same thrust. The reverse displacement vector length thus derived is about 14 km and its azimuth is 353°.

A minimum total displacement of about 22 km resulted from the compound earlier and later D_3 thrusting, D_{3a} and D_{3b} respectively, where the D_{3b} episode produced a duplication of the main D_3 thrust (as represented between Z and Z' in Fig.59A) along the trace Y-Y' in Fig. 59A. Although this figure corresponds well with an independent estimate of the total horizontal shortening in the underlying E. Dassie nappe due to D_3-related imbrication (see Section 4 below), it may be an overestimate. The slightly different attitude of L_{1X} fabrics in the Kudu and W. Dassie nappes could in-

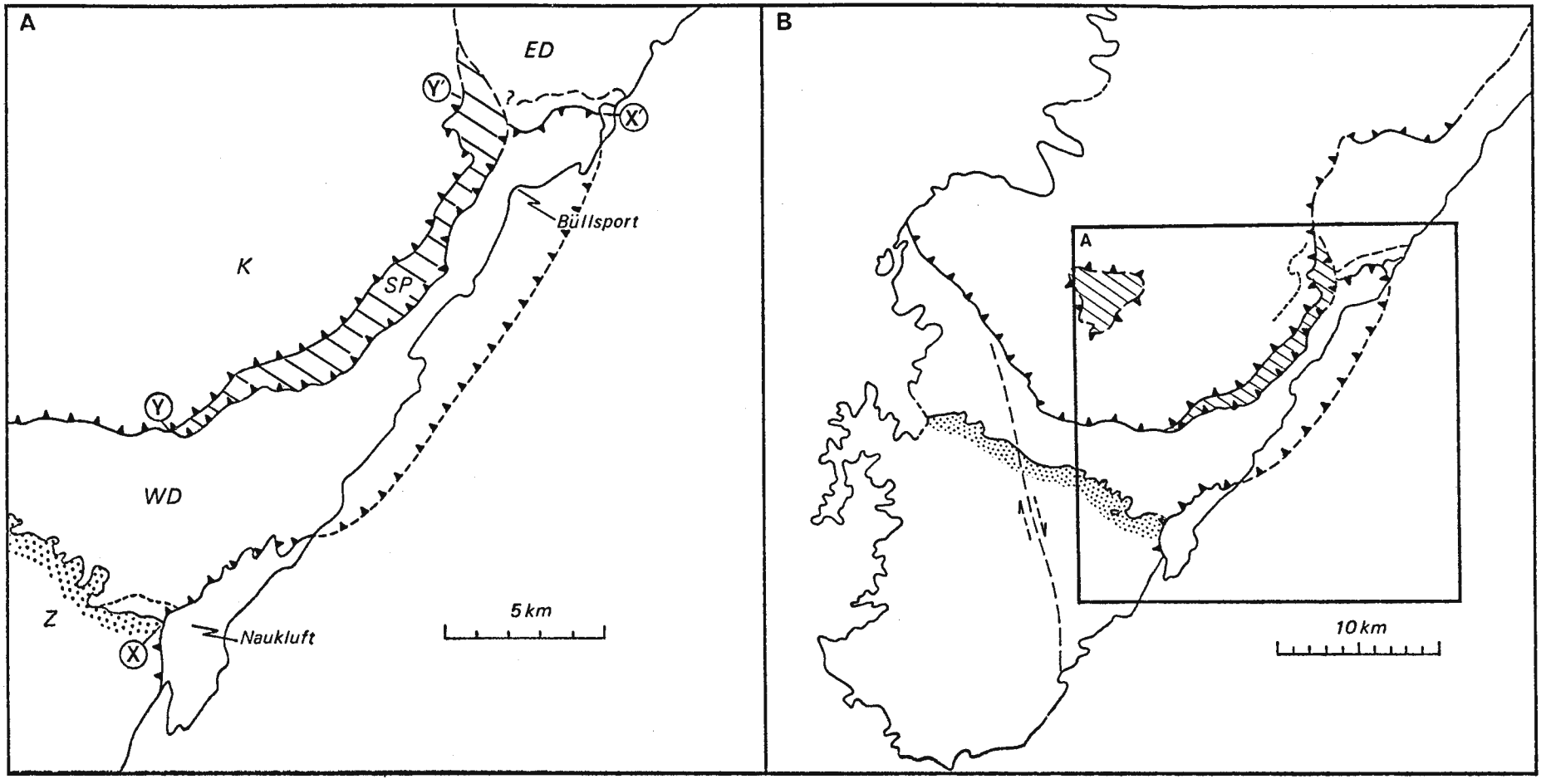

Figure 59. Sketch maps relating to the problem of S. Pavian nappe emplacement and the nature of the D_3 deformation episode.

dicate that the displacement vector for D_{3b} may have been aligned closer to 335° than to 350° (Chapter IV, Section B. 4.b). The effect of the latter assumption is to reduce the calculated D_{3b} thrust displacements to about 4 km only.

An important palaeogeographic implication of this kinematic model of S. Pavian nappe evolution is that the Zebra River Formation in the W. Dassie nappe was situated northwards of the Zebra River equivalents in the S. Pavian nappe, which further implies that, from north to south, the basal Zebra River sediments (excluding the Neuras Member?) originally overlapped an unconformable contact between already imbricated and deformed Büllsport Formation and an undeformed Aubschlucht Formation. Hence despite the fact that the S. Pavian units have been thrust southwards over the Büllsport Formation in the W. and E. Dassie nappes, the depositional basin of the Aubschlucht Formation in particular was originally located south of the original Büllsport basin and was probably formed in the fore of the D_2 thrust front.

The major D_3 features illustrated in Fig. 59 A are placed in their larger context in Fig. 59 B which emphasizes the strongly arcuate form of the main thrust surfaces, particularly the D_{3b} surface at the base of the Kudu nappe in the west and the S. Pavian nappe in the east. It also shows the dextral transcurrent structure which affects both the Büllsport and Zebra River Formations in the W. Dassie nappe and which was probably initiated during D_3, being subparallel to the approximate D_3 displacement vector.

(ii) Origin of the arcuate nappes

The arcuate nature of the deformation trends in the Naukluft complex, particularly in the Kudu and W. Dassie nappes, has been regarded as evidence that nappe deformation was due to "plastic flow under the influence of gravity" (Korn & Martin, 1959, p.1047). The trends are supposed to "delineate a cascading movement" which is "plainly controlled by the shape of the basin", but it is evident that they formed principally during the D_3 episode and are therefore not related immediately to the emplacement of the nappe complex in its present position in the northern Nama sedimentary basin.

Several possible modes of overthrust emplacement leading to formation of an arcuate overthrust belt have been listed and illustrated by Grubbs & Van der Voo (1976, Fig. 3). Korn & Martin's model has elements both of radial emplacement off a rising highland and of divergent emplacement due to constraining effects of the foreland margin and other topographic features (e.g. the Nama basin shape). It is also possible to suppose that differential southward displacement of the Kudu and W. Dassie nappes was related to steeper basin slope angles along the hinge of the nappe arc (cf. Korn & Martin, 1959, p.1072). The hypothesis of post-thrusting "oroclinal bending" (Grubbs & Van der Voo, 1976) can be rejected because it is incompatible with the D_3 and D_4 nappe history of the Büllsport region.

The preferred hypothesis of this work is that of the southward thrusting of an originally arcuate frontal edge (*op.cit.*, p.325). In this case, the edge was defined by the southern facies boundary of the thick massively bedded Noab dolomites and it is postulated that this acted as a practically rigid indenter against its foreland during the D_3, more specifically the D_{3b} episode. In some respects, the mechanism has an experimental analogue in the finite element experiment CE4E, discussed below in Appendix Chapter A-II in which a central particle fifty times more viscous than the surrounding matrix remains virtually undeformed during pure shear deformation of the whole system while the matrix in the immediate vicinity of the particle experienced highly rotational incremental strains. Although not shown in the strain intensity plot (Fig AII-9) for experiment CE4E, the principal extension directions in the zone of contact strain adjacent to the particle-matrix interface are approximately parallel to the latter; in effect, the less ductile particle indents the surrounding more ductile matrix. Recent experimental data on the mechanical properties of dolomite, discussed briefly later in this Chapter, show that the assumption of a ductility ratio of about 50 between dolomite and other Naukluft lithologies, such as shale and limestone, is quite reasonable.

(iii) Ductile deformation in the N. Pavian nappe

Deformation in the N. Pavian nappe was formerly explained by the "traineau ecraseur" or "crushing sledge" mechanism, whereby the great load of the moving Kudu nappe produced intense cleavage development and stretching in the general direction of flow (Korn & Martin, 1959); but the structural pattern of the southern part of the N. Pavian nappe does not support this hypothesis. While it is locally observed that the cleavage in N. Pavian pelitic and carbonate rocks converges and becomes more flatly orientated close to the marble-phyllite shear zone at the base of the Kudu nappe, this effect is generally restricted to within a few metres or tens of metres at most below the nappe sole. Farther downwards, in the Tsondab valley exposures, the cleavage reflects a lesser strain intensity and adopts a slightly steeper orientation. Locally, however, the carbonate breccias of the Blässkranz Formation are almost undeformed. In the lowermost phyllitic units of the Remhoogte suite there is a definite increase in strain intensity, reflected in the transposition and virtual obliteration of much of the original sedimentary layering and the cleavage again becomes subhorizontally orientated; and this might indicate major drag or traction toward the base of the N. Pavian nappe. It is also partly explained by the evidently more complex structural history of the Remhoogte suite (i.e. the D_1 episode of deformation which preceded deposition of the Blässkranz Formation).

Deformation increases southwards in the Tsondab valley exposures of the Blässkranz and Tsabisis Formations, but the cleavage does not adopt flatter orientations; instead it steepens against the imbricated dolomite thrust sheets of the Dassie nappe. Near Pavianskopf, the white marker dolomite of the Tsabisis Formation is intensely imbricated itself, close to the sheared contact at which the N. Pavian nappe has locally been thrust over a southern part of the Kudu nappe (Plate 44). These observations suggest that the major deformation of the N. Pavian nappe, at least of the upper Blässkranz and Tsabisis Formations, was produced during the D_3 episode, when the Kudu-N. Pavian nappe contact was deformed and imbricated and not during the D_2 episode when the Kudu nappe was thrust over the N. Pavian nappe.

It is therefore postulated that during the D_3 episode the underthrusting rigid dolomite of the E. Dassie and southern Kudu nappes acted as a block against which the relatively ductile N. Pavian rocks piled up. In other words, the underthrusting southern dolomite nappes were indenting the N. Pavian nappe, thus effectively scraping it off the base of the overthrusting northern Kudu nappe. This mechanism is the counterpart of the foreland indentation described above.

There is a distinct westwards increase in the intensity of N.Pavian deformation along the northern contact with the Dassie nappes, culminating in the reduction of the N. Pavian nappe to a thin strip of schist separating the Kudu and W. Dassie nappes. This can perhaps be correlated with an observable westwards thickening of the Zebra River Formation which must have formed a great part of the overburden on the frontal part of the combined Dassie-Kudu nappe during the early stages of the D_3 episode.

(iv) Displacement vector for D_3 thrusting

The problem of calculating a unique displacement vector for the D_3 thrusting is complicated by the inhomogeneous ductile deformation of the N. Pavian nappe and by the local imbrication of the N. Pavian and Kudu nappes in the Tsabisis region. (cf. Chapter IV, Section B.3.a(iii)). The likewise complicating, variable relative displacement of the W. Dassie nappe due to its postulated indentation by the Kudu nappe is illustrated in Fig. 60 on the assumption that the W. and E. Dassie nappes were previously united and deformed during D_2 along a rectilinear trend close to the present attitude of E. Dassie imbrication.

As the reference point X (Fig. 58) chosen for displacement vector calculations is situated at the leading edge of the effectively rigid Kudu dolomite nappe, these problems are largely circumvented. In the synoptic diagram (Fig. 58), this point is shown as having been displaced about 16 km along azimuth 170^{o} from X'' to X' during D_3. The vector is based on a rough calculation of D_3 shortening in the E. Dassie nappe (see Section 4 below), which has since been revised downward slightly. It is, however,

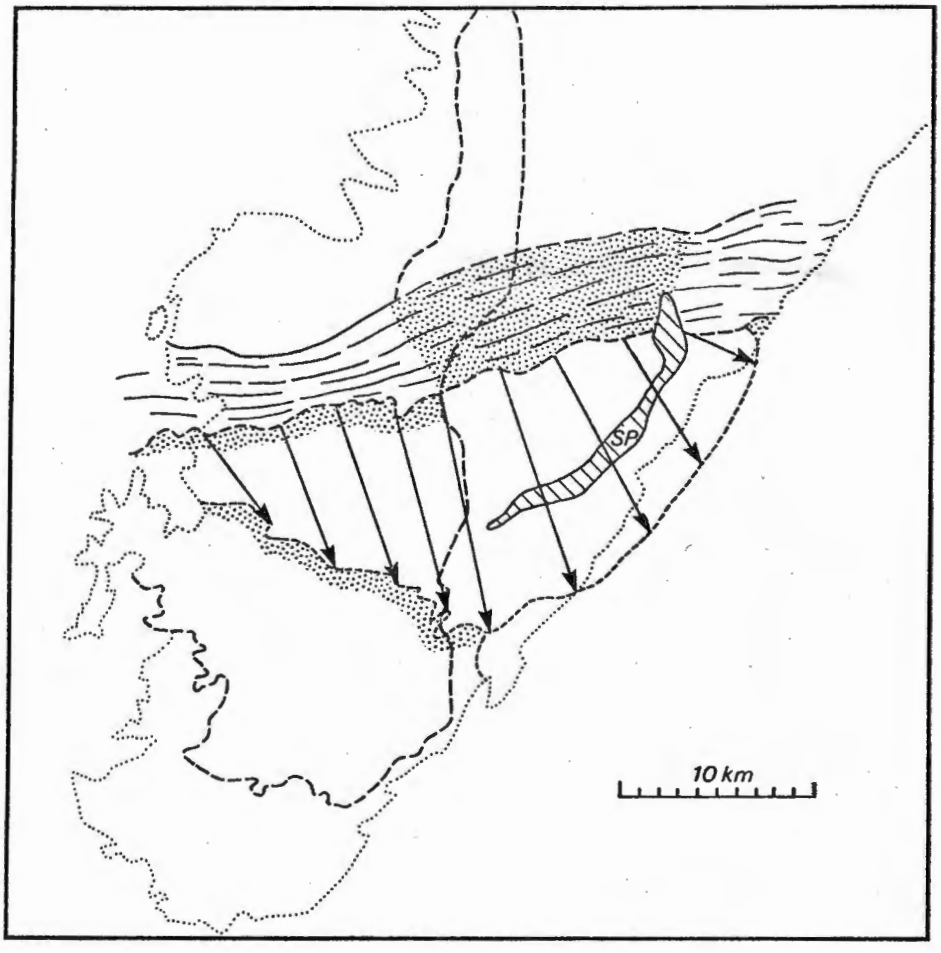

Figure 60. Schematic illustration of postulated pre-D_3 configuration of imbrication and fold trends in the combined W. and E. Dassie nappe and displacement vectors for the deformed Büllsport-Zebra River Formation contact. Dotted outline is trace of Naukluft complex perimeter. Dashed line in south-west represents Zebra River Formation rotated into its pre-D_3 position so that fold and imbrication trends in the underlying Büllsport Formation line up with those farther east in the E. Dassie nappe. Dashed outline in north represents rotated eastern part of W. Dassie nappe, and stippled zone between W. and E. Dassie zones is the provenance of the D_3-deformed eastern W. Dassie nappe. The present relative position of the S. Pavian nappe is indicated (hachured area).

slightly less than the value derived in the analysis of S.Pavian nappe emplacement (see (i) above) and is therefore accepted as a convenient compromise.

c. The D_2 and D_1 episodes

Prior to the D_3 episode, the preceding reconstruction suggests that the Kudu and both Dassie nappes were united in a single plate-like body occupying the positions indicated in Fig. 58 . At this stage the Kudu-Dassie plate had already been thrust over the stratigraphically younger Blässkranz and Tsabisis Formations, as clearly indicated by the well-exposed truncation phenomena at the Kudu nappe sole. Reversal of this deformation therefore entails shifting the leading edge of the Dassie nappes north-north-westwards beyond the sub-nappe limit of the Blässkranz Formation. Since it has been inferred also that the Remhoogte Formation is stratigraphically younger than the Noab and Büllsport Formations, a further shift of the dolomite nappes beyond the exposed limits of the Remhoogte Formation is also indicated. Deformation by D_1 folding of the Remhoogte Formation has been ignored in this calculation which again is a conservative minimum for the total displacement.

The azimuth of 350° has again been chosen for the reverse displacement vector X'' - X''' (Fig. 58) since it corresponds approximately with the mean trend of all L_{1X} lineations in the N. Pavian and Kudu nappes. The resultant vector length after restoration of the Kudu nappe on the basis of the above assumptions is about 33 km (Fig. 58).

d. Resultant total displacement and provenance of nappe units

In the above kinematic model, displacement of the reference point X is accomplished in two geometrically distinct phases : an early phase for which the resultant minimum vector is 170°, 49 km and a late phase for which the resultant minimum vector is 125°, 35 km. The resultant by vector addition (X''' - X in Fig. 58) is 151°, 78 km.

When the total displacement vector of Fig. 58 is placed in regional context, it is remarkable that reference point X is shown to have been

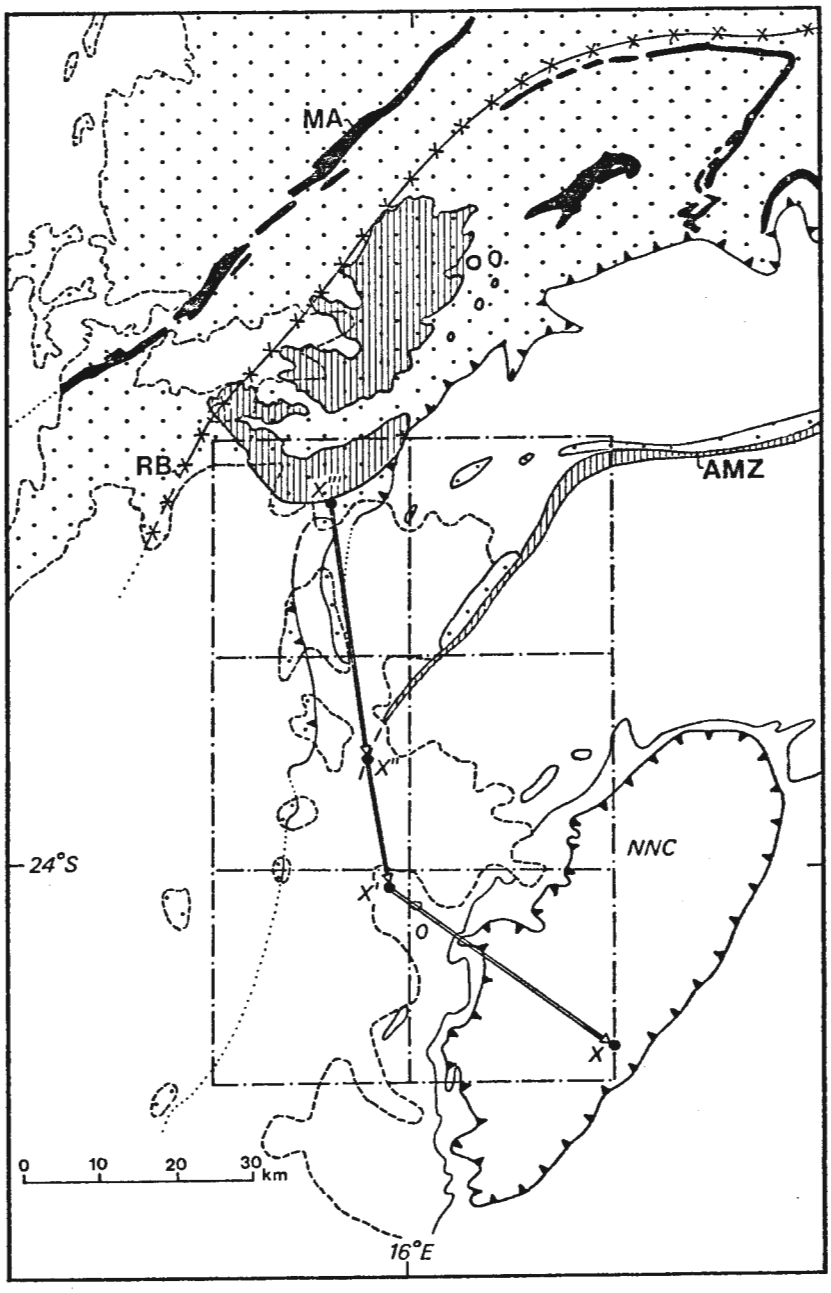

Figure 61. Diagram relating the total displacement vector for Naukluft reference point X (Fig. 58) to the major tectonic features of the southwestern Damara belt.

originally situated near the base of the Damara sequence south of Rostock (Fig. 61). The original provenance of the Noab Formation is thus identified as the region between Rostock and Natas Mine and the provenance of the Büllsport Formation appears to have been the present Gaub Valley schist terrain west and north-west of the Probeer Formation (Martin, 1974), an obvious Büllsport correlate.

The basin of deposition of N. Pavian formations seems to have straddled both the Gaub Valley and the Nauchas highlands terrains, while the main part of the original Zebra River basin is situated farther south-west. Between Noab and Zebra River times a progressive south-westward migration of depositional axes seems to have occurred.

4. Some aspects of brittle and ductile deformation kinematics

a. Imbrication of the Dassie Nappe

(i) Possible relation of bedding dip to bulk finite strain

Excellent exposure of the W. Dassie nappe on Büllsport and Die Valle (cf. Plate 68), and of the E. Dassie nappe in the Tsondab River valley on Büllsport and Blässkranz, show that the Büllsport Formation has been deformed into a northward-dipping stack of thrust slices or imbrications, yet the rocks within each individual slice are almost undeformed. In the E. Dassie nappe, the imbrications are separated by thin zones of largely brittle faulting (cf. Plates 65 - 66). In the W. Dassie nappe, however, the zones between individual rigid imbrications are wider and usually consist of intensely-deformed marble or mixed marble-phyllite with numerous boudinage and fold structures indicative of ductile flow of rock in the zone. If the brittle-ductile transition in rock is correlated directly with confining pressure, it seems clear that the W. Dassie nappe was more intensely deformed at deeper levels than the E. Dassie nappe.

It is also clear from the large-scale structural geometry of the E. Dassie nappe that the western part is more deformed than the eastern part, and even within the latter it is evident that the intensity of imbrication

(and therefore of bulk strain in the tectonic unit) increases westwards. Concomitant with the westward or south-westward increase in the number of thrust slices in the E. Dassie nappe is a general increase in the dip of bedding within the imbrications. To the north-east the bedding in the dolomite and quartzite unit dips at low angles or is subhorizontal, while the dips observed close to the Tsondab River valley generally exceed 45^{o} and locally are vertical.

These observations suggest that bedding dip within the effectively rigid imbrications can be used as an approximate index of bulk longitudinal shortening strain in the E. Dassie nappe. The elaboration of an idealised kinematic model of horizontal shortening in a rigid layer surrounded by a ductile medium throws further light on the process responsible for deformation of the E. Dassie nappe, which tectonostratigraphic evidence relates to the D_3 episode.

(ii) Kinematic model

In the idealised two-dimensional model of imbrication tectonics adopted here, it is assumed that the centroid of each individual imbrication is constrained by the larger scale boundary conditions to remain on a horizontal line. The process of imbrication can then be conveniently decomposed into two "phases", although it is not implied that these stages occur successively in discrete time intervals; the decomposition is a purely formal one distinguishing processes which take place concurrently. These stages are firstly "*back-rotation*" and secondly *shortening* (Fig. 62).

The model oversimplifies nature in another respect because it postulates that the imbrication process begins with the production of a series of equally spaced incipient thrust faults with equal spacing L in a uniform horizontal layer of thickness T. The angle between the bedding (originally horizontal) and the planar thrust fractures is represented as α (Fig. 62A). In reality, whatever the initial geometry of the rigid brittle layer, the development of imbrication by listric (not planar) thrust-faulting is likely to proceed serially from one side of the system to the other (Price, 1977). As long as attention remains focussed on a small part of the imbricate system,

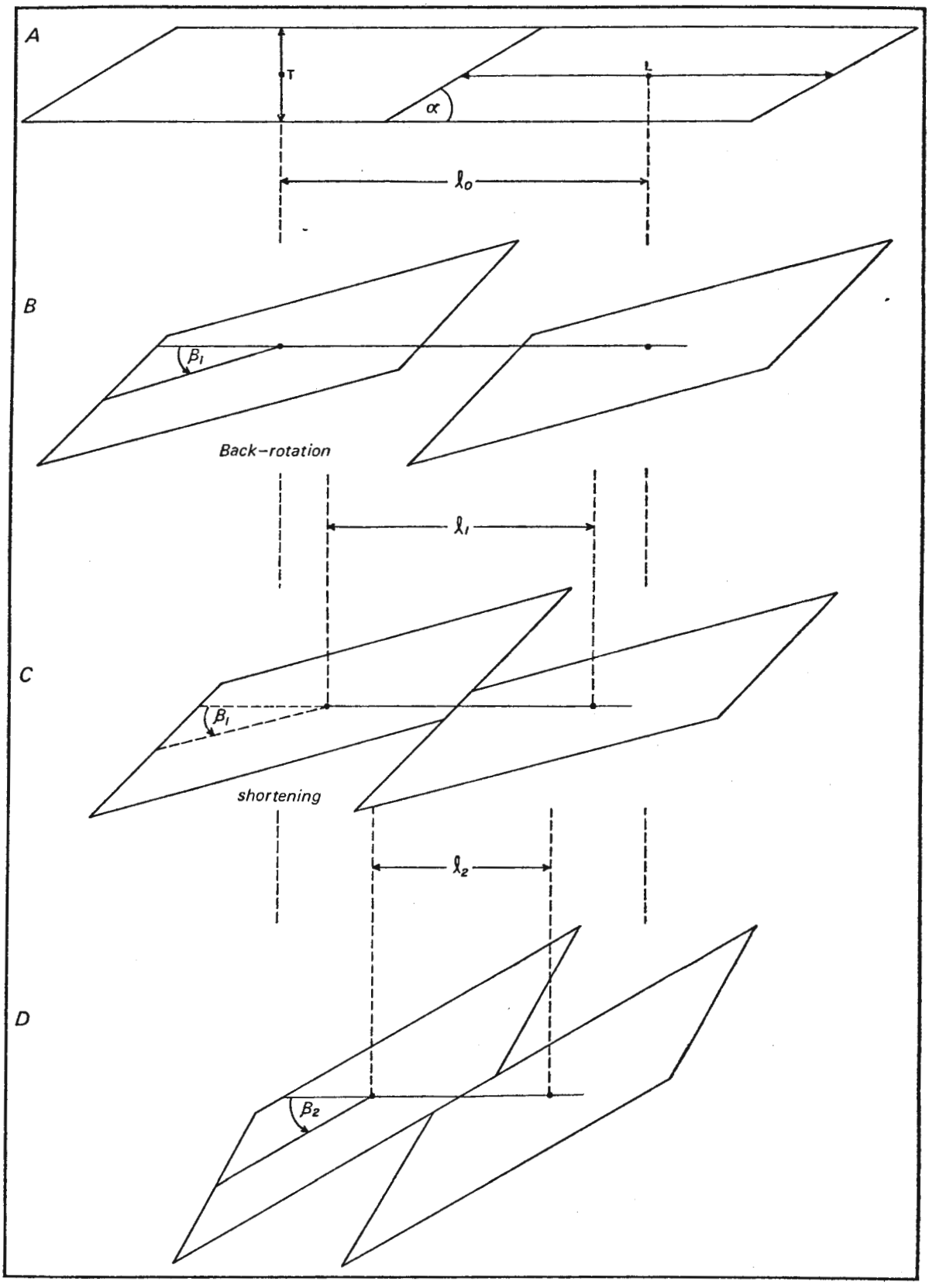

Figure 62. Idealised model of the imbrication process, showing the initial configuration of imbrications of particular T/L ratio (A), the "back-rotation" phase (B), the shortening phase (C), and the overriding phase (D), when the imbrication centroids are referred to a horizontal line.

bounded by three thrust faults, this limitation is not serious.

In the "back-rotation" phase (Fig.62B) each imbrication is envisaged as rotating by an angle β about its centroid. This angle therefore becomes the new bedding dip. The shortening phase (Fig.62C) closes the gap which is thereby developed along the horizontal line connecting the imbrication centroids.

At the starting configuration, an obvious geometric constraint is that must equal or exceed $(\tan^{-1}(T/L)$; alternatively expressed, the ratio (T/L) cannot exceed tan(α), so that if α is measured at 30°, for example, then the imbrication thickness-to-length ratio must have been equal to or less than 0,58. In practice, it is most probable that the value of (T/L) will be less than 0,5 $\tan^{-1}(T/L)$.

The back-rotation phase of the imbrication process is accompanied by a dilatation, represented by the appearance of a gap between the imbrications and the shortening phase can be envisaged as the restorative collapse of the deforming system to its original volume.

In the course of progressive or incremental deformation of the system by successive cycles of back-rotation and shortening, displacement will initially take place on the thrust-plane oblique to bedding, but once an angle β defined by the formula

$$\beta = \tan^{-1}\left\{\frac{(T/L)\ \tan(\alpha)}{\tan(\alpha)-(T/L)}\right\}$$

is reached, the displacement is assumed to become concentrated along the former upper and lower boundaries of the imbricate layer so that the surrounding highly ductile material is effectively replaced along these contacts. Thus two stages in the process of deformation by rigid-body imbrication are distinguished which do occupy discrete time-intervals. In the first or rising stage the imbrications move on the thrusts and in the second or overriding stage the imbrications move on surfaces parallel to bedding (Fig.62D).

During the rising stage, the relationship between shortening e_x along the (horizontal) line connecting the imbrication centroids and the angles α

and β is given by the following equation:

$$e_x = 1 - \left\{\frac{\sin(\alpha)}{\sin(\alpha)\cos(\beta) + \cos(\alpha)\sin(\beta)}\right\}$$

During the overriding stage, the shortening e_x is governed only by the angle β and the ratio (T/L) according to the following relationship

$$e_x = 1 - \left\{\frac{(T/L)}{\sin(\beta)}\right\}$$

In these equations, e_x is defined as the longitudinal strain or ratio between the change in length and the original length (dl/l_0).

These relations can be combined on a single graph relating e_x and β, with two sets of curves representing different values of α and (T/L) for the rising and overriding stages respectively (Fig.63). If the values of α and (T/L) are known for an imbricate system, and the bedding dip angle β is measured, the shortening strain e_x can be estimated from this graph. The angle α is generally a measureable variable in the field if the imbrication process was arrested during the rising stage (e.g., Plate 49 illustrates an angle of 30^o between bedding and the thrust plane). For systems with low (T/L) ratios in which the transition from the rising stage to the overriding stage is reached at relatively low values of β and e_x, the angle α may not be directly observable. If the leading edges of the imbrications have been extensively eroded, both α and (T/L) may have to be estimated indirectly. In this respect, the imbrication thickness T is generally recoverable while the imbrication length observed is a minimum so that (T/L) is usually over-estimated. For a given β value, this would result in under-estimation of the shortening e_x, if the imbrication is observed (i.e., through parallelism of bedding and major movement zones) to have passed into the overriding stage.

The angle β, strictly defined, is the angle through which bedding has been rotated away from the line connecting imbrication centroids. In the model it has been assumed (cf. Fig.62) that the latter remains horizontal, so that β is the uncorrected dip of bedding. If, however, the centroid line has itself been rotated (most probably in a "forward" sense in the majority of

imbricate systems) the "raw" bedding-dip values measured in the field obviously require correction by this rotation, if it can be observed or estimated, before the shortening along the centroid line can be determined using the above theory. In this connection, it can be noted that the term "back-rotation" is used to emphasize that the rotation of bedding during imbrication is opposite in sense to the rotation associated with ductile shear deformation in overthrust zones. The process of imbrication not only involves significant shortening, but also thickening of the imbricated sequence.

(iii) Application to E. Dassie nappe imbrication

In both the western and eastern parts of the E. Dassie nappe, the imbricated units are bounded below by a subhorizontal plane and to a first approximation the thickness of individual imbrications is the same. The centroids of the imbrications therefore lie approximately along a subhorizontal line in any section drawn across strike of the imbricate zone. These large-scale aspects of structural geometry in the E. Dassie nappe allow the theory relating bedding dip to shortening strain, developed in the previous section, to be applied in this case without correction for other rotations.

The well-exposed portion of the E. Dassie nappe bordering the Tsondab River contains a number of thrust-planes showing that the angle α is close to 30° (cf. Plate 49). These exposures, representative of thrusts arrested during the rising stage of their motion, are not found in the immediate vicinity of the Tsondab Valley, but farther north-eastward on Spitskop Suidwes. In the eastern valley side, the exposed thrust planes are parallel to bedding in the undeformed dolomitic imbrications, indicating that they had passed into the overriding stage before deformation ceased. In some cases, these surfaces are recognisable as thrusts only because they can be traced continuously from exposures farther north-eastward which show clear angular discordances; in others, the repetition of the characteristic clastic zone in the Büllsport Formation provides evidence for the existence of otherwise inconspicuous thrusts.

Since the E. Dassie nappe has been extensively eroded after deformation

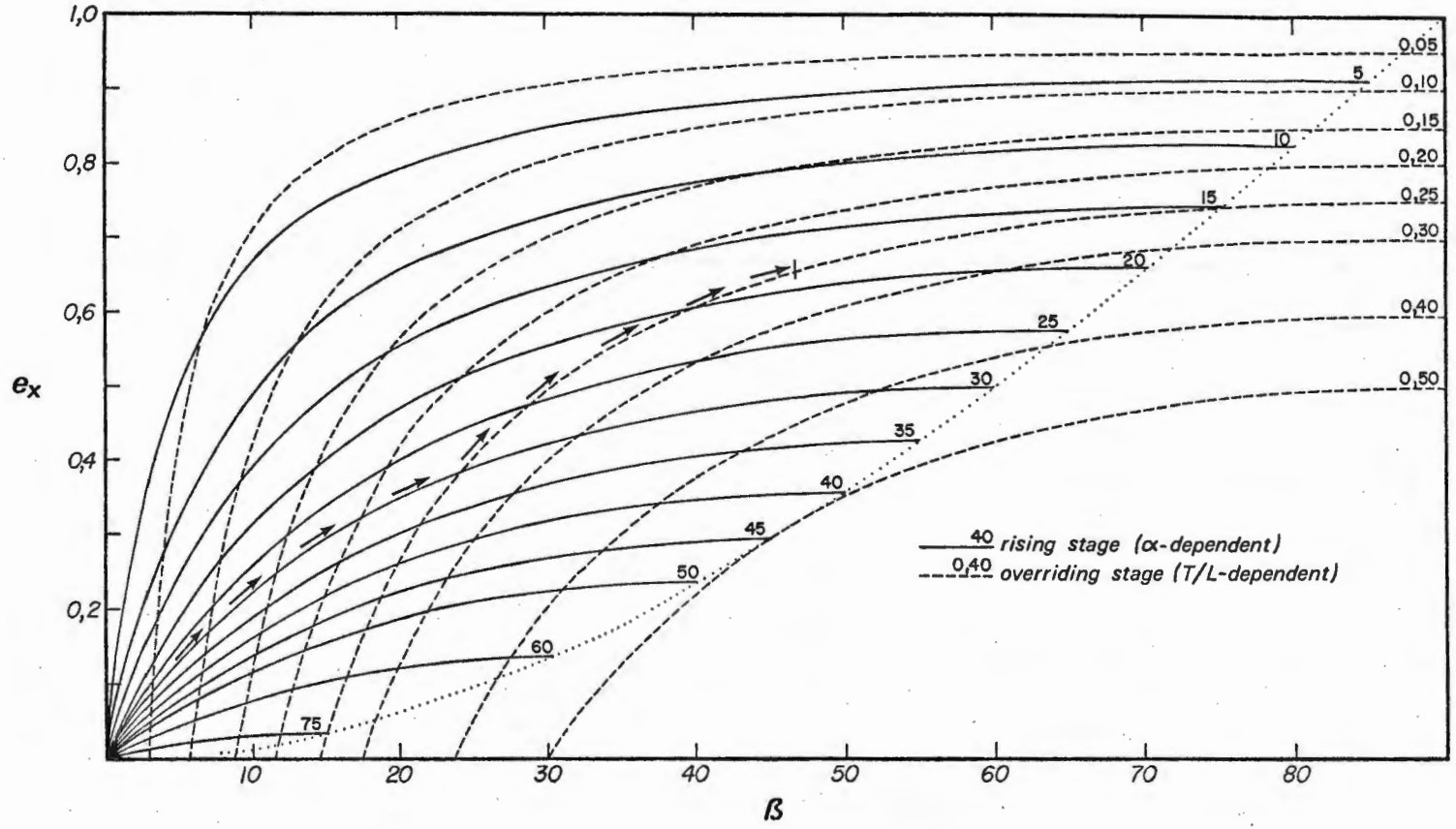

Figure 63. Graph relating shortening e_x along the centroid reference line (assumed horizontal) to the bedding dip β, as governed by (i) the thrust angle α in the rising stage of motion (solid lines, for α-values at 5° intervals between 5° and 75°) and (ii) the thickness/length ratio T/L in the overriding stage of motion (dashed lines, for T/L-values at 0,05 intervals between 0,05 and 0,30 and 0,10 intervals up to 0,50). Arrowed lines represent probable deformation path in E. Dassie nappe during imbrication.

the estimation of the original average (T/L) ratio for the imbricate zone is difficult, but was certainly not more than 0,25 as generally observed in the present valley exposures. The HVM orientation of SS measurements from data sites in zones A and B of the E. Dassie nappe, HVM is 250/46. In conjunction with the above-mentioned estimates of α and (T/L), this average dip indicates that the minimum shortening in these parts of the imbricate zone is about 0,65 or 65 per cent (Fig. 63).

The present width of the E. Dassie imbricate zone is about 8 km, therefore the original width of the zone prior to shortening by the above amount was about 23 km; in other words, the northernmost imbrication has been displaced about 15 km southwards relative to the southernmost imbrication. As outlined in a preceding section, this deformation is correlated with the D_3 thrusting episode.

b. Polyphase folding in thrust-related marble zones

In a previous discussion of folding within *decollement* zones (Kehle, 1970), it has been noted that systematic and random variations in the generally rectilinear shear field may be caused by changes in the regional concavity or convexity of the *decollement* zone, thickness variations in both the upper plate and the *decollement* zone, local obstructions to motion, and other possible factors. "This means a single deformation event could contribute several structural patterns. Rocks folded in one locale could be transported to areas where different patterns originate. New structures would be superimposed on old. This could easily be interpreted as the result of two or more distinct stages of deformation, when in reality the complex structures result from a single continuing process" (*op.cit.*, p.1665).

The recognition of refolded isoclinal folds within the sheared marble-phyllite zone below the S. Pavian nappe (Plates 56 & 64) and between imbricated thrust slices in the W. Dassie nappe (Plate 67) naturally raises the question : are they the product of intermittent and hence unpredictable perturbations of the continuous flow field, or can they be systematically

related to the distinct deformation episodes recognised within the Naukluft complex on the independent basis of large-scale tectonostratigraphic relationships? Specifically, did the initial formation of *decollement*-confined isoclinal folds coincide with the D_2 episode of tectonic transport of the Kudu nappe and did the subsequent refolding of these folds coincide with the D_3 episode?

The fact that refolding relationships appear to be most abundant near the base of the S. Pavian nappe suggests a positive answer to these questions. It is in this area that large-scale D_3 deformation of the D_2 *decollement* zone is most spectacularly displayed and it therefore seems natural to relate the development of minor refolding structures to the larger phenomenon. It remains possible, however, that this impression is due to inadequate regional sampling of the Kudu nappe *decollement* zone and that similar minor folding may yet be found in areas where the *decollement* zone itself shows no later large-scale rotation or imbrication.

The morphology of the recumbent isoclinal folds observed within the Kudu nappe *decollement* zone is similar to those observed in foliated or banded ice in the base or margins of glaciers and ice-caps (Hudleston, 1976). Since the analogy between nappe transport of rock and glacier transport of ice is often drawn, it is interesting to examine the mechanisms by which the latter structures may be produced. In Hudleston's (1976) model, bedrock ridges or troughs acting as obstacles to flow at the glacier base produce initial low-amplitude sinusoidal deflections of the flow lines. An abrupt change of glacier thickness or surface slope changes the velocity vector at points within the glacier. A necessary condition for recumbent folding is that "some material points on a band move on new particle paths that are higher than those of points that were originally nearer to the glacier margin on the same band" (*op.cit.*, p.1690). The layering (banding) is taken to parallel to the particle paths under the old steady-state conditions. A material point on a higher particle path is subject to a larger displacement because of the velocity gradient near the base of the glacier, which in turn is a consequence of the approximate relationship

$\tau = -\rho g(h-y)\tan\alpha$, where ρ is the density, g is gravitational acceleration, h is the height of the surface above a reference horizontal axis, y is the height above the axis at which the stress τ is estimated, and α is the surface slope (Hudleston, 1976, equation 2).

Favourable conditions for recumbent folding of a layer deflected at a basal ridge are created when glacier thickness decreases and the surface slope is simultaneously steeper than the basal slope on the lee side of the ridge, or when the surface slope increases while the glacier thickness over the apex of the ridge remains constant (cf. Hudleston, 1976, Fig. 7A). In the former case, it is conceivable that erosional ablation near the toe of a moving rock sheet decreasing its thickness and simultaneously increasing its local surface slope by scarp retreat processes, could produce recumbent folding conditions at basal obstacles in the *decollement* zone. As noted by Hudleston (1976), these folds would be "seeded" at the obstacle during the episode of (erosional?) thickness and/or surface slope change, and would begin to appear and develop fully only when the rock of the *decollement* zone had flowed some distance beyond the initial source of the disturbance.

Quantitative application of this theory to the development of recumbent fold structures in the Kudu nappe *decollement* zone is at present limited by insufficient knowledge of several of the factors involved, such as original thickness of the Kudu nappe and pressure-temperature conditions at its base (which affect the rheology of the *decollement* zone), and by the difficulty of deducing surface slope conditions at the time of nappe movement.

B. DYNAMIC INTERPRETATION OF NAUKLUFT NAPPE EMPLACEMENT

In view of the reputation of the Naukluft nappe complex as a classic example of gravitational gliding tectonics, some consideration of the D_1-D_5 kinematic model in a dynamic context, i.e. one in which the displacements are related to the action of specific body or surface forces, is inescapable. For this purpose a knowledge of the rock material properties and boundary conditions during deformation are required (cf. Appendix Chapter A-II).

as sound dynamic interpretation cannot be based on structural geometry and kinematics alone.

The rock types of the Naukluft complex show a great mechanical inhomogeneity, ranging from very strong dolomite to very weak marbles and metapelites (Korn & Martin, 1959) judged simply on the relative basis of their variable tectonic response. It also seems likely, judging from the variable attitudes of strain-related S_1 and L_{1X} fabrics in different parts of the complex, that the boundary conditions of deformation also changed between D_1 and D_5. The following discussion is therefore intended as a very tentative introduction to a difficult subject. It is founded mainly on the observation that there are strikingly obvious differences between the successive generations of major *decollement* surface in the nappe complex (Hartnady, 1974, p.87), from which it may be inferred that the early emplacement (D_1 - D_3) of the Kudu and Dassie nappes took place at deeper crustal levels than the final emplacement (D_4-D_5) of the Naukluft complex as a whole. This, together with observations of stratigraphic inversion, establishes a new boundary condition for Naukluft emplacement which is considered to be absolutely fatal to the previous gravity sliding model (Korn & Martin, 1959) based on the assumption that the Unconformity Dolomite was a stratigraphic unit separating discrete levels of deformation like a plane bed might separate individual large-scale slump sheets.

1. Evidence of the mechanical state of thrust surfaces during D_2 and D_3

In Chapter IV, evidence has been produced to show that large-scale ductile flow has occurred in certain rock units of the Naukluft complex, particularly in the Remhoogte Formation of the N. Pavian nappe and in the marble-phyllite zones of the basal Kudu nappe and the W. Dassie nappe. Evidence has also been produced to show that this deformation involved a pressure-solution mechanism as well as an intra-crystalline plastic flow mechanism. Photographic evidence of the formation of foliation by pressure-solution is presented in Plates 37-42 , drawn mainly from dolomite or dolomitic limestone units close to major thrust zones or nappe boundaries.

Evidence of deformation by plastic flow mechanisms is to be seen mainly in photographs and sketches drawn from minor fold structures in the marble-phyllite zones. The preservation of the continuity of differently coloured layers of marble, despite major changes in their orthogonal thickness from the limbs to the hinge-zones of Class 3 isoclinal folds, shows that pressure-solution was not a significant contributor to their deformation. In some layers within the marble-phyllite zones, loss of continuity of the early layering and the apparent "transposition" of the latter into a new layered structure (cf. Plate 63) does however, appear to indicate an important localised component of pressure-solution deformation, and the abundant formation of (usually fibrous) calcite veins in boudinaged phyllite layers (cf. Plate 58) also points to the activity of solution-transfer of material during deformation.

The above observations are important for assessing the mechanical state of the marble-phyllite zones and the regimes of temperature, confining pressure, deviatoric stress, pore-fluid pressure and strain rate that were operative during their deformation. The remarkable co-existence of pressure-solution and crystal-plastic-flow textures, in a complex which is otherwise dominated by the brittle fracture and large-scale cataclastic deformation of effectively rigid "plates" of strong dolomitic rock, is important because new experimental data (e.g. Heard, 1976; Rutter, 1976), combined with a clearer modern understanding of the submicroscopic mechanisms of rock deformation, place constraints on the conditions under which such a co-existence of deformation textures is possible.

a. Estimation of temperature and confining pressure

The deformation map for calcite of 100 μm grain size (Rutter, 1976, Fig. 8), shows that the boundary between the pressure-solution and dislocation creep fields is located between temperatures of 300 - 450°C, and between deviatoric stress values of approximately 10 - 100 MPa at strain-rates between 10^{-13} - 10^{-12} s^{-1}. If the strain-rate during penecontemporaneous pressure-solution and plastic flow of the Dassie and Kudu nappe marble zones

was slower at about 10^{-14} s^{-1}, the map indicates that the Coble creep (grain-boundary diffusion) mechanism of plastic flow will have been operative at a temperature of about 450°C at a deviatoric stress level between 1 and 10 MPa. Observations made in the course of petrographic examination of the Remhoogte phyllites and the marble-phyllite zones seem to indicate that temperatures during and after the deformation of these rocks did not exceed 400°C, although the presence of biotite/stilpnomelane and the relatively large size of the chlorite porphyroblasts in the northern Remhoogte phyllites, point to temperatures close to 400°C in the lower greenschist facies. In the relatively undeformed sandy dolomites of the overlying Noab Formation, on the other hand, no firm evidence has yet been seen of the occurrence of the reactions of dolomite + quartz or dolomite + K-felspar to form talc + calcite or phlogopite + calcite respectively, which at low pressures and high H_2O activities are expected to occur near 400°C (Winkler, 1976).

The formation of the marble zone does however, pose the problem of metamorphic dedolomitisation by a number of reactions involving as solid phases, dolomite, quartz, K-felspar, white mica (phengite), chlorite and phlogopite (biotite) and the fluid phases, H_2O and CO_2. Dedolomitisation, involving the transformation of dolomite to calcite by its reaction with surrounding solid and fluid phases, would immediately result in a major reduction in strength or equivalent viscosity of the rock (Heard, 1976). At a temperature of about 400°C and a constant strain-rate between 10^{-13}–10^{-14} s^{-1}, the equivalent viscosity of a quartzose dolomite could be reduced by almost two orders of magnitude from about 10^{22} Pa.s to about 10^{20} Pa.s if the dedolomitisation reaction to talc + calcite occurred: this would involve a fall in the steady-state flow stress for the rock from about 1000 MPa (which is unrealistically high and shows that dolomite at 400°C is practically undeformable in plastic flow) to about 20 MPa (cf. Heard, 1976, Fig. 6). Future detailed analysis of the phyllosilicate phases present in the marble-phyllite zones may show that they formed by a metamorphic dedolomitisation process along zones of contact or interbedding of carbonate and silicate rocks and that this was in turn responsible for a massive reduction in their strength and the consequent concentration of very high strains within them. This hypo-

thesis is suggested in opposition to the former view of the zones as "laminated limestones" (Korn & Martin, 1959) of primary sedimentary origin. If the it can be confirmed, it will further substantiate the view that deformation of the Naukluft nappe complex took place at a temperature and confining pressure that was higher than previously supposed.

The truncation of a conspicuous marble-phyllite zone by an erosional unconformity at the base of the Zebra River Formation in the W. Dassie nappe, appears to show that rocks which were undergoing deformation at temperatures close to 400°C during the D_2 kinematic episode, had been rapidly uplifted and eroded before the D_3 kinematic episode commenced. Because of observations such as this which testify to rapid vertical movements associated with the large-scale horizontal displacements during nappe evolution, it is difficult to postulate a definite relationship between temperature and confining pressure or depth. Depending upon the rate and sense of vertical movement, the ambient temperature at any particular depth or pressure might be lower or higher than that which would be predicted on the basis of reasonable heat flow assumptions and conduction theory. In nappe emplacement, tectonic advection of heat is probably more important and more effective than simple conduction so that during phases of rapid relative uplift near-surface temperatures are anomalously high, whereas during phases of relatively rapid depression they are anomalously low. The slight changes in temperature and pressure associated with such fluctuations may be related to the local transition from pressure-solution modes to crystal plastic modes of deformation in the same region of rock at different times.

Pressure-solution usually implies the channelling or infiltration of active fluids along zones of relatively high permeability and if these fluids are largely derived by metamorphic dehydration or decarbonation reactions at greater depth, this also introduces the possibility of localised temperature increase due to convective transfer of heat by large quantities of moving fluid. The *apparent* (not necessarily real) higher grade of metamorphism of the marble-phyllite zones compared to the surrounding less-deformed rocks may be related to this phenomenon. Viscous dissipation (or "shear-strain heating") is another

factor which, through thermal feedback, may have caused the local temperatures within the marble-phyllite shear zones to have exceeded those in the surroundings.

The above-mentioned factors all complicate the assignment of a definite value for the confining pressure during the earlier episodes of Naukluft deformation. Nevertheless, the good development of ductile folding and metamorphic cleavages in the lower parts of the nappe complex shows that confining pressure was high enough then to suppress cataclastic modes of deformation almost completely. In the absence of a good metamorphic geobarometer, it can be estimated only by relating the likely temperature conditions of 350-400°C to a reasonable geothermal gradient and then assuming a probable depth-temperature relationship. Assuming a gradient of 25°C km^{-1} entails syntectonic burial of the northern part of the Naukluft complex to depths of 14-16 km which, with a linear pressure-depth relation of about 27,5 MPa km^{-1}, further entails a confining pressure of about 400 MPa.

b. Estimation of strain rate and deviatoric shear stress

Estimation of the D_2 or D_3 strain-rates operative in the marble-phyllite zones, requires that the total finite strains be known and also the time-period over which those strains accumulated; neither can actually be measured directly. It is, however, possible to obtain an indirect estimate of the total shear strain in the basal marble-phyllite zone of the Kudu nappe by assuming, from field observation, that the minimum horizontal displacement of about 33 km (cf. Section B above) was distributed through a shear zone with an average width of 30 m. The value of the shear strain γ thus obtained is 1100. If the rate of nappe emplacement was about 3 cm yr^{-1}, so that this displacement was completed in about 10^6 yr or 3×10^{13} s, the derived rate of shear strain in the zone is about 4×10^{-11} s^{-1}. Following Heard (1976), the equivalent viscosity of marble deforming in extension at a strain rate close to 10^{-11} s^{-1} and temperature of 350-400°C is about 2×10^{18} Pa.s and the steady-state differential flow stress in the marble is about 50 MPa (*op. cit.*, Fig. 6). At the same temperature and shear stress, the equivalent

viscosities predicted for dry quartzite and dolomite by the steady-state dislocation creep flow law exceed 10^{27} and 10^{30} Pa.s respectively. Even for wet quartzite, the predicted equivalent viscosity under the same stress-temperature conditions exceeds 10^{22} Pa.s, corresponding to a wet quartzite/marble ductility contrast of at least 1000.

These experimental and theoretical considerations suggest that large-scale deformation outside the marble-phyllite zones cannot have resulted from "frictional stresses" or viscous drag in the zone during nappe movement; the ductility contrast between these zones and their surroundings was far too great to permit large-scale operation of any such mechanism. The results of computer experiments performed under different boundary conditions (cf. Appendix Chapter A-II), show that where the ductility contrast between viscous media reaches values of only 50, the less ductile medium behaves as if it were effectively rigid and almost all the bulk strain in the inhomogeneous system becomes concentrated in the more ductile material.

The ductility contrast between the marble-phyllite zones and the immediately underlying siliceous rocks is most evident where the Kudu nappe overlies the Tsabisis Formation in the Northern Pavian nappe. The foliation and fold structures in the nappe contact zone (cf. Plates 47-48) imply very large deformation in the marble-phyllite rocks, but fine-grained quartzites in the Tsabisis Formation only a few metres below are essentially undeformed, with perfect preservation of original sedimentary grain shapes and fine sedimentary bedding structures. The interbedded purple shales and volcaniclastics are slightly deformed ($\lambda_1/\lambda_3 \simeq 3$) and show an incipient slaty cleavage (cf. Plate 19). These observations may be partly explained by the presence of the middle Tsabisis white dolomite as a protective rigid shield intervening between the basal Kudu shear zone and these fine-grained quartzites and shales. Nevertheless, if the above estimates of a 10^{-11} s^{-1} strain-rate and a 50 MPa shear stress in the marble-phyllite zone are correct, a subhorizontal shear stress of about the same magnitude should have been transmitted to its substratum. The undeformed nature of the Tsabisis quartzites then suggests that these rocks were able to support this

level of differential stress during the overthrusting episode (<1 Myr?) without undergoing steady-state flow at a geologically observable rate (i.e. $>10^{-14}$ s^{-1}).

The shear stress of 50 MPa estimated from Heard's (1976) experimental results and the assumption of a relatively rapid rate of emplacement of the Kudu nappe during the (D_1-) D_2 episodes may be excessive. The maximum long term shear strength of rock is usually supposed to be about 25 MPa (cf. Elliott, 1976a, b) and it is suggested that the maximum long-term average regional shear stress for an entire thrust sheet is of the order of 10 MPa. The imbrication of the Kudu and Dassie dolomite nappes in the frontal region of the complex, for which the D_2 episode was partly responsible, is however evidence that deviatoric shear stresses in the nappes did reach values close to, or just in excess of 25 MPa.

c. Relation between shear stress, nappe thickness and surface slope

It has been demonstrated for a gravity spreading model of thrust motion (Elliott, 1976a) that the shear stress τ acting on the base of a thrust sheet is

$$\tau = \rho g H \alpha$$

where ρ is the density, H the local thickness of the sheet, α is the surface slope and g the gravitational acceleration. The basal shear stress τ is an average value calculated over a distance along the base several times the local thickness H of the sheet. A typical value of 5 MPa for τ has been estimated along a sole thrust in the Canadian Rockies.

If a similar value is assumed for the D_1-D_2 shear stress at the base of the Kudu nappe, difficulties arise with the interpretation of deformation structures in the marble-phyllite decollement zones. At a differential flow stress of 5 MPa and a temperature of 400°C, the experimental results of Heard (1976) indicate that the maximum attainable strain-rate in dislocation creep is about 10^{-17} s^{-1}. Rutter's (1976) deformation maps for calcite indicate a maximum strain-rate of about 10^{-16} s^{-1} in grain-boundary

diffusion creep, (grain size 100 μm) and about 10^{-14} s^{-1} for a flow mechanism involving pressure-solution. With a strain rate of only 10^{-16} s^{-1} a 33 km displacement about a 30 m-thick ductile shear zone would require at least 300 Gyr to produce! Even at a 10^{-14} s^{-1} strain-rate in pressure-solution creep, the time required for deformation would be 3000 Myr which is manifestly absurd since the rocks involved are less than 1000 Myr old and deformation was certainly complete before -500 Myr. In fact the maximum time-span available for the entire Naukluft deformation history is at most about 150 Myr (i.e., from about -650 to -500 Myr) which implies that strain-rates within features such as the major marble-phyllite zones cannot possibly have been less than 10^{-13} s^{-1}. This in turn implies that flow stresses therein cannot have been less than 20 MPa (Heard, 1976).

It should however, be noted that flow by diffusional creep mechanisms such as Coble or pressure-solution creep is strongly grain size dependent so that the equivalent strain rates for calcite with an average grain diameter of 10 μm are approximately 1000 times faster than those quoted above (Rutter, 1976). The evidence of most of the isoclinal folds in finely layered marble is nevertheless interpreted as contradicting the suggestion of dominant diffusional creep mechanisms in their formation, so that even though the grain size in these marbles is closer to 10 μm than to 100 μm a dislocation creep mechanism involving high stress levels to produce realistic strain rates is preferred. This problem could be resolved in the future by detailed petrofabric and electron microscopic work on the marbles.

In the gravity spreading model (Elliott, 1976a), basal shear stresses in the range 20-50 MPa require that the local thickness of the thrust sheet should be in the range 10-15 km and that the average surface slope in the direction of overthrusting should be in the range 5-10°. The thickness estimate for the Kudu nappe in the D_1-D_2 interval is compatible with the metamorphic state of the underlying Remhoogte Formation. From the sedimentary history of the Blässkranz and Tsabisis Formations it is known that in this interval the frontal region of the Kudu nappe was situated close to a shoreline and just below sea-level. The total width of the Kudu nappe (i.e.,

including the present Dassie nappe as its frontal zone) is shown by kinematic reconstruction to have been at least 50 km, without taking into account possible erosion of the frontal zone in the D_2-D_3 interval. An average surface slope of, say, 7,5° implies that over a distance of 50 km the surface of the nappe rose from sea-level to altitudes over 6000 m.

d. Summary

The evidence of deformation textures related to the D_2 episode may constitute the major argument against the simple down-slope gravity gliding model (Korn & Martin, 1959) for the Naukluft nappe complex. Assuming the validity of extrapolating from recent experimental data on the flow behaviour of calcite and marble (Heard, 1976; Rutter, 1976), the relatively high stress, plastic flow structures found within the Naukluft marble zones cannot possibly have formed in an environment of thin-skinned superficial tectonics. They show that superincumbent loads of the order of 10-15 km, corresponding to confining pressures of 300-450 MPa, were necessary both to suppress cataclastic flow and generate the deviatoric stresses to drive shear flow. The same thick cover to the moving Kudu nappe also provided the overlying "blanket" enabling temperatures close to 400°C to be reached within and below the decollement zones, although it is still an open question whether this occurred through simple thermal conduction or whether processes related to the deformation, such as the convective transfer of heat along shear zones by fluids or the viscous dissipation of heat in zones of high strain rate and stress, were responsible.

2. Origin and mechanical state of the Unconformity Dolomite

The Unconformity Dolomite was described by Korn & Martin (1959, p.1063) as "probably the most unusual structure" in the Naukluft area. Identified by a yellowish-brown dolomite band lying in a smooth plane and showing "no trace of folding or serious disturbance of any kind" (*op.cit.*, p.1064), it

separates intensely deformed formations : the Kuibis and lower Schwarzrand Formations of the Nama Group below, and various units of the Naukluft nappe complex above. Korn & Martin (1959) considered the unaffected dolomite sandwiched between an upper and a lower folded series to represent a "double unconformity". They believed that the lower contact of this dolomite marked an unconformity between the Schwarzrand Formation of the Nama Group and the Zebra River Formation of the Naukluft complex. The upper contact of the thin dolomite layer they regarded as a surface of *decollement* along which the overlying units had been completely sheared off.

The "sparsely jointed" nature of the dolomite layer in places where it rests upon black limestone was noted by Korn & Martin (1959, p.1064). The lack of close-spaced tectonic jointing in this rock, which is intercalated between rock units that are generally intensely fractured was emphasized by the writer (Hartnady, 1974, p.86) as being a significant indicator of the mechanical state of the material during nappe emplacement.

As the Unconformity Dolomite was the subject of a concurrent thesis project by H.G. Münch (cf. Münch, 1975), a more detailed investigation of it was avoided in this work though a few samples were collected for routine petrographic examination. Münch (1975) has subsequently proposed a "dynamometamorphic" hypothesis for the origin of this rock, according to which it is a cataclastically formed tectonic breccia in its outer layers grading into a central dolomitic "blastomylonite". The purpose of the following section is a brief critical review of the available evidence since the implications of "cataclastic" mechanisms for frictional shear stresses along the Naukluft sole thrust and of "mylonitisation" in dolomite for other factors such as temperature, confining pressure and strain rate seem to be incompatible with most probable tectonic models of Naukluft emplacement.

a. Some macroscopic and microscopic features

The Unconformity Dolomite (i.e., the so-called "Central Blastomylonite" of Münch, 1975) generally has an isotropic granular texture in which idio-

morphic or subidiomorphic dolomite crystals ranging in diameter from about 1 cm to 1 mm are homogeneously distributed (Plate 74). Locally, however, a distinct textural layering is observed which is seen to be deformed into rare near-isoclinal folds, generally of Ramsay Class 3 (Plate 73). The rock often appears to have narrow gradational contact zones with overlying or underlying carbonate units, but in some places the lower contact especially is remarkably sharp on a plane, almost polished surface (Plates 71-72). Near the Naukluft sole thrust, material identical to or very similar to the Unconformity Dolomite is found in narrow planar veins and irregular apophyses which penetrate either the overlying or the underlying units (Plate 29); in one place a vein of "Unconformity Dolomite" can be seen several hundred metres above the nappe sole in the E. Dassie unit.

Microscopically the rock is seen to consist of about 75 per cent dolomite with a minor proportion of calcite (Münch, 1975). The next in abundance, locally exceeding 20 per cent, is albite-oligoclase in characteristically twinned, subidiomorphic to idiomorphic crystals having interlocking grain contacts with the surrounding dolomite. The Unconformity Dolomite is in most cases really a dolomite-albite rock. Other characteristic minerals found in minor proportions are hematite, opaque ore (mainly pyrite?), chlorite and tourmaline, with some xenomorphic quartz (Münch, 1975).

In some thin sections (e.g., CH75), numerous idiomorphic dolomite rhombs are observed to have a well-developed zonal growth structure, defined by inclusion trails parallel to the crystal edges. The latter are frequently coated with a fine layer of iron-oxide (?goethite). Several crystals show more than one such iron-oxide coating, separated by clear overgrowths of calcite or dolomite.

Sporadic "porphyroclasts" or xenolithic fragments of diverse rock types, ranging in size from 1 cm to 50 cm are commonly encountered in the Unconformity Dolomite (Münch, 1975). It is highly significant that some of these xenoliths have been derived from basement granitoid rocks which now appear at surface from beneath the Kuibis Formation at a distance of at least 30 km from their discovery sites at the nappe front on Büllsport. The most remarkable of these

fragments, and one which speaks volumes for the mechanical state of the Unconformity Dolomite during nappe transport, is illustrated in Plate 74, from locality 50011 on Büllsport. This, together with similar pieces of rock nearby, is a "jigsaw" fragment of a larger granitoid block which had been tectonically transported for at least 30 - 35 km from the north-west before being fractured, probably hydraulically, in the proto-Unconformity Dolomite close to its present resting-place.

b. Interpretation

The tectonic location of the Unconformity Dolomite, its internal flow structures, the preservation of sharply angular exotic fragments within the thin layer, and finally its occurrence in veins in the surrounding "wallrock" all point to its having had an extremely weak and fluid mechanical constitution during the last stages of Naukluft nappe emplacement (D_5). In some respects the Unconformity Dolomite resembles the *cornieules* of the Western Alps or the *rauhwackes* of the Eastern Alps, which are dolomitic rocks that formed discontinuous cushions of high ductility underneath major nappes, such as the *Schistes Lustres* (cf. Warrak, 1974). The Alpine *cornieules* in their present state pose the same problem as the Unconformity Dolomite, for they are brittle and could not have acted so incompetently or as tectonic lubricators (*op.cit.*, p.230). They likewise show "sedimentary" features to some geologists and tectonic breccia features to others.

Warrak (1974) has recently shown that the *cornieules* in a part of the French Alps originated by replacement of a mixed dolomite and gypsum-anhydrite evaporite unit, with the highly mobile gypsum having constituted the lubricating cushion for nappe movement. Subsequent replacement of the gypsum by calcite, the calcite by dolomite, and then later partial de-dolomitisation and iron-oxide staining all contributed to change the nature of the original parental material almost completely.

In view of the evaporitic associations of the Noab and Büllsport Formations in the Naukluft nappe pile, a similar origin for the Unconformity Dolomite is not improbable, but because of the complex history of deformation

preceding the final D_5 rigid-plate nappe emplacement episode to which the Unconformity Dolomite is directly related, it remains doubtful whether that source for an evaporitic starting material can be invoked. A possible alternative hypothesis of *in situ* evaporite formation at the base of a moving nappe is accordingly outlined below.

The key postulates of this hypothesis are : firstly, a locally inverted thermal gradient at the base of a hotter nappe moving over a cold sub-stratum, and secondly, the presence of relatively porous, semi-consolidated pelitic units in the substratum through which a sea-water brine can infiltrate at an adequate rate. As there is a distinct inverted discontinuity of metamorphic grade across the Unconformity Dolomite in the north-west of the Naukluft complex, and as newly deposited pelitic units occurred in the Zebra River, Kuibis and Schwarzrand Formations during the D_4 - D_5 tectonic interval, the above conditions are considered to have been fulfilled.

It is proposed in the model that the tectonically advected heat source in the overlying nappe sets up a brine circulation system in the substratum, slowly drawing sea-water up into the overthrust surface by infiltration from the ocean through the pelitic layers and rapidly expelling a CO_2-rich solution upwards along the overthrust back into the oceanic reservoir. At the overthrust surface, the following coupled hydrothermal reactions occur involving the subjacent pelitic rock (illite + quartz), the suprajacent carbonates (dolomite) and the NaCl-rich brine:

$$8 \text{ illite} + 4 \text{ quartz} + 4 Na^+ + 4 Cl^- = 6 \text{ muscovite} + 4 \text{ albite} + 4 H^+ + 4 Cl^-$$

$$1 \text{ dolomite} + 4 H^+ + 4 Cl^- = CaCl_2 + MgCl_2 + 2 CO_2 + 2 H_2O.$$

The net result is that a thin layer of Ca- and Mg- (possibly also Na-) halides is formed along the overthrust surface to lubricate the nappe's continued movement. At the end of nappe movement or cooling of the heat source, increasing pCO_2 can be expected to drive the second reaction in reverse, resulting in ultimate dolomitisation of the halide layer so formed.

The hypothesis explains the fold structures seen in the Unconformity Dolomite (Plate 73) as *salt* flow structures and potentially combines features

of true lubrication and of effective stress reduction by fluid overpressure (Hubbert & Rubey, 1959). According to modern experimental and theoretical models of dolomite rheology (Heard, 1976), the formation of such flow folds is impossible at temperatures much below 500°C. At a temperature of only 100°C, however, halite can deform at the relatively fast strain rate of 10^{-12} s^{-1} under a steady-state flow stress of less than 5 MPa, having an effective viscosity in those circumstances of only 10^{18} Pa.s (*op.cit.*, Fig. 5, p.182).

3. Analysis of the relative importance of gravitational and longitudinal compressive forces in Naukluft nappe tectonics

In the preceding sections, the gravity gliding model of Naukluft tectonics has been rejected as inappropriate, but an aspect of the newer gravity spreading theory has been used in connection with the estimation of basal shear stresses for the Kudu nappe, and the calculation of the thrust sheet thickness and surface slope that is necessary to drive flow by dislocation creep in the basal marble zones. In this section, a further quantitative development of gravity spreading theory (Elliott, 1976a) is used to evaluate the possible role of superimposed longitudinal compressive stresses.

The high strength of the dolomitic rock making up the (presently preserved) bulk of the Kudu nappe, makes it necessary to assume that the relatively high basal shear stresses were related to gravity-spreading alone. The basal dolomite layer of the Kudu nappe was certainly capable of acting in the long term as an efficient "stress-guide" transmitting any longitudinal compressive surface force applied to its north-western end. A quantitative theory relating a uniform compression applied to one end of a rectangular elastic body (length L and thickness H), dying out at the other end and balanced by a shearing stress along its base, has been developed by Hafner (1951). The supplementary stress system set up by the subhorizontal push is in static equilibrium and can be added to the down-surface slope stress system to obtain a further equilibrium result (cf. Elliott, 1976a, p.956, equation 8). If the horizontal push C is expressed as the

ratio k of the down-surface slope compressive normal stress, so that

$$k = C/\rho g H \cos(\alpha),$$

and it is assumed that maximum shear stress within the thrust sheet reaches the value of the rock strength only along the thrust at depth H at the end where the compression C is applied, an equation is obtained which relates the maximum shear stress τ_m (i.e. rock strength), to the surface slope α, the thrust sheet thickness H at the compressed end, the length/thickness ratio L/H and the ratio of compressive to gravitational stresses k. This equation (Elliott, 1976a)

$$\left\{\frac{\tau_m}{\rho g H \cos(\alpha)}\right\}^2 = \left(\frac{k}{2}\right)^2 + \left\{\tan(\alpha) + \frac{kH}{L}\right\}^2$$

has been solved for a given value of α (i.e., 3^o) for values of τ_m between 2-50 MPa and for k-values of 0,1 and 1,0 in a graph of H versus (L/H). Values of 2700 kg m^{-3} and 9,8 m s^{-2} were prescribed for ρ and g respectively. In this graph (Fig. 64), two stippled fields are indicated; the lower one, centred on H = 1,5 km and (L/H) = 30, represents the dimensions of the Naukluft nappe complex as presently preserved, and the upper field, centred below H = 15 km and about (L/H) = 5, represents the inferred dimensions of the Kudu nappe during the D_1-D_2 episodes.

The graph shows that a maximum basal shear stress τ_m of about 30 MPa (corresponding to a dislocation creep strain rate of 10^{-12} s^{-1} at about 400^oC) is reached for Kudu nappe thickness greater than 13 km if the ratio k is only 0,1. In other words, in the Kudu nappe field the gravitational forces effectively overwhelm the possible longitudinal compressive forces even if a relatively high rock strength or a "hard" sliding law is assumed. If the initial ratio of compressive to gravitational stresses is assumed to have been closer to 1,0 during the Kudu nappe emplacement, it is evident from the graph that a rock strength between 30-50 MPa is exceeded at much shallower depths (<5 km) for a thrust sheet with (L/H) in the range 5-30. Under these circumstances, one might imagine that a large sheet would collapse into a sequence of smaller thrust sheets at its compressed end and

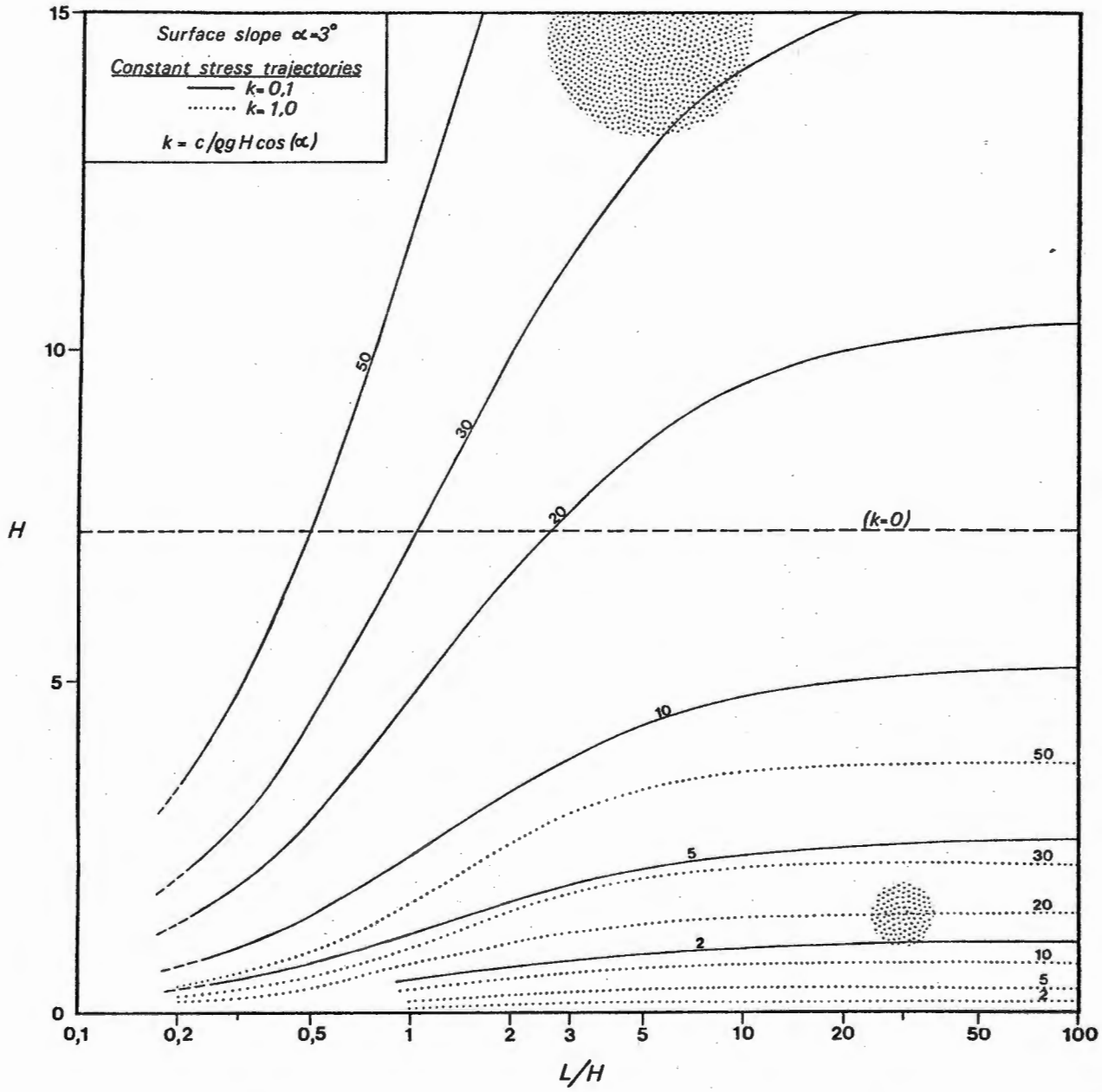

Figure 64. Graph relating nappe thickness H to nappe length/thickness ratio L/H, in which curves of constant basal shear stress τ and constant ratio k of compressive to gravitational stresses are plotted following an equation derived by Elliott (1976a). Dotted lines represent curves for $k = 0,1$ and different τ_m values as annotated; solid lines represent curves for $k = 1$ (equal compressive and gravitational stresses) and different τ_m values as annotated. In the limit $k = 0$, the curves are horizontal and the dashed line represents an example where $k = 0$ and $\tau_m = 10$ MPa.

would thicken by internal deformation at that end, thereby simultaneously reducing the ratio k and increasing the surface slope α.

The influence of the variable α in the above equation has been examined quantitatively for a maximum shear stress τ_m of 10 MPa and surface slopes α of 1^o, 5^o and 10^o, for the same k ratios 0,1 and 1,0. Changing α has little effect on the k = 1,0 trajectory, but lowers the k = 0,1 trajectory considerably, thus illustrating that steeper surface slopes significantly extend the field in which gravitational forces are dominant.

The present dimensions of the whole Naukluft nappe complex (cf. Fig. 64) do not correspond with the field of dominant gravitational forces (k<0,1) for a 3^o surface slope, unless it is assumed that the cohesion of its basal sliding-plane was very low, i.e., about 2 MPa. This issue concerns the interpretation of the Unconformity Dolomite layer and structures in the immediately underlying Kuibis limestones. The problem can be minimised by assuming that the nappe complex thickness prior to Karoo-age erosion may have been as much as 5 km, and the surface slope during the final phases of its emplacement may have been close to 10^o. In these circumstances, a cohesive resistance of about 20 MPa could be overcome largely by gravitationally induced stresses.

Until the very low grade metamorphic history of the Naukluft complex becomes better known, particularly in respect of geobarometry, it is not worth pursuing this type of theoretical analysis in more detail. The present brief excursion into the subject does, however, show that (contrary to intuitive expectation) the early Naukluft deformation may have more to do with gravity (spreading) tectonics than the late Naukluft deformation.

In the writer's opinion, longitudinal compressive forces were probably important at all stages in the development of the Naukluft nappe complex. The sequence of tectonic and sedimentary episodes showing that the complex was generally moving from deeper to higher crustal levels, implies that the nappes constituted a system that was gaining gravitational potential energy. This gain in potential energy may have occurred as a result of the expense of gravitational potential elsewhere in a still larger system, comprising most of the Khomas Ridge province in the Damara belt. Two possible

sources can be identified, one crustal and one lithospheric. It is, for example, possible that uplift related to the extensive granitic magmatism of the central Damara belt may have lead to an increase in regional surface slope over the whole Khomas Ridge province, resulting in a regional loss of potential energy by gravitational spreading there with a local gain in a "toe" region of which the Naukluft complex formed a part.

Alternatively, the gravitational sliding into the mantle of a slab of dense oceanic lithosphere attached to the north-western margin of the Kalahari craton prior to its collision with the Congo craton, could have formed the larger system on a scale which is energetically capable of driving both the above-mentioned secondary crustal system and the tertiary local Naukluft system (cf. Fig. 66 B). The possible relationship of the Naukluft complex to its orogenic hinterland is accordingly explored in the following Chapter.

CHAPTER VI

GEODYNAMIC INTERPRETATION OF THE DAMARA OROGENY

A. INTRODUCTION

1. The asthenolith hypothesis

It has recently been proposed that the ultimate cause of the Damara orogeny is the intrusion of a high-temperature body into the lithosphere (Martin, and Porada, 1977). The temperature field which this asthenolith induced and its subsequent cooling to form an eclogite "sinker", are postulated as the principal causes of Damaran metamorphism and orogenic activity respectively. The asthenolith hypothesis also postulates that the site of the Damara orogenic belt was controlled by a pre-existing Rehoboth-Irumide structural trend in the crust. It is, however, not clear what the influence of anisotropy in a 40 km-thick continental crust, or in the underlying lithosphere, upon the behaviour of presumably much larger, partially-molten asthenospheric bodies could be. The nature of the boundary forces that a weaker asthenosphere can exert on a relatively strong lithosphere is also a possible contentious issue. A realistic quantitative analysis might show that the asthenolith hypothesis requires additional superimposed tensional or compressive stresses in the lithosphere, in order to be able to do any work in rifting or orogenically deforming the latter. Since the asthenolith hypothesis, as presently understood, is a largely qualitative concept and has not been applied successfully to any Phanerozoic orogenic belt, a detailed critique is not possible. There is but slight justification for its application to the Damara belt.

Most modern geodynamic analysis points to a major importance of lithospheric body forces in driving large-scale convective motions in the Earth's outer shells (Harper, 1975; Forsyth & Uyeda, 1975; Solomon, Sleep & Richardson, 1975). An alternative geodynamic hypothesis for the Damara belt may be con-

structed by assuming Orowan-Elsasser convection in the mantle, with the negative bouyancy force of sinking slabs of oceanic lithosphere as the primary driving mechanism. In this model, asthenoliths appear at divergent or constructive plate boundaries, in oceanic crust, but are not responsible for orogenic deformation and large-scale dynamo-thermal metamorphism in the continents. The latter phenomena are restricted to zones of plate convergence.

2. Some geophysical aspects of modern geodynamic theory

In choosing between the Orowan-Elsasser convection model and the opposing Rayleigh-Benard convection model, the determinative factor is the rheological constitution of upper mantle rock, including the importance of dislocation creep processes (Kohlstedt, Goetze & Durham, 1976) and the role of thermal feedback resulting from the P- and T-dependence of the effective viscosity (Froidevaux & Schubert, 1975). The geophysical model preferred here is one in which the presence of an asthenosphere, or layer of low effective viscosity, is related to a fundamental law of rock mechanics, namely the steady-state dislocation creep law, $\dot{\varepsilon} \propto \exp\left[-(E^*+PV^*)/kT\right]\tau^n$, (Weertman, 1970) and is not imposed by some *ad hoc* assumption about partial melting in the upper mantle. The quantitative basis of the model is outlined by Froidevaux & Schubert (1975) and its implications for the thermal and mechanical structure of oceanic lithosphere have also been elaborated (Froidevaux *et al.*, 1976; Schubert *et al.*, 1976). The extension of this model to earlier geological periods has not yet been undertaken. The controlling variable in this respect is surface heat flow, for which a present representative value of about 45 mW m^{-2} has been assumed for continental shield areas (Froidevaux *et al.*, 1976). In the Precambrian this value will have been higher due to the greater concentration of radio-active heat sources in the Earth.

At present heat escapes from the Earth at a rate slightly more than 10^{21} J yr^{-1} (Lee & Uyeda, 1965) equivalent to a power of 30 000 MW. A small proportion of this energy budget is used in deforming the lithosphere, mainly along orogenic zones. Higher heat production in the past means that more energy was available for driving orogenic processes, but its quantitative magnitude is

constrained by realistic models of the bulk composition of the Earth. Of the two principal models of planetary composition, the average chondrite model (Birch, 1965) predicts that global heat production will have been about 3½ x its present value about 3000 Myr ago, whereas the Wasserburg model (Wasserburg *et al.*, 1964) predicts a lesser value of about twice the present heat production.

While attempts have recently been made to translate higher past rates of heat production into geothermal gradients (cf. Lambert, 1976), few have come to grips with the core of the problem, which is to determine the relative proportions of geothermal energy lost by conduction through the lithosphere to heat lost by hydrothermal convective processes near oceanic ridges plus that advectively transported in the cooling and thickening oceanic lithosphere (Parker & Oldenburg, 1973). Revised estimates of heat loss from the Earth (Williams &Von Herzen, 1974) suggest that almost 40 percent of the Earth's internal energy, about 5×10^{20} J yr^{-1}, is released in the process of oceanic lithosphere formation.

Since the cooler oceanic lithosphere is denser than the underlying, hotter asthenosphere by about 50 kg m^{-3}, there is a natural tendency for it to sink back into the mantle. The lithosphere, however, is also very much stronger than the asthenosphere because of the near-surface temperature-dependence of effective viscosity, as described by the dislocation creep law. The estimated effective viscosity of the lithospheric upper mantle is close to 10^{25} Pa s. (Lliboutry, 1974), whereas asthenosphere viscosity is only about 10^{20} Pa s. (Froidevaux & Schubert, 1975). The high strength of the oceanic lithosphere, combined with its thickness (c. 100 km) and gravitational confinement at the surface of a spherical body, dictates the Orowan-Elsasser convection mode in which large plates of "floating", but denser lithosphere move relatively rapidly in a horizontal direction towards localised linear trench zones where subduction takes place.

In this model, the internal heat energy convectively released in the course of oceanic lithosphere formation is related to the lithosphere-asthenosphere density contrast, which in turn is the fundamental cause of the convective or, strictly speaking, the advective motion of plates. The present-day ratio of heat transfer by advection to heat transfer by conduction in the

lithosphere-asthenosphere system is relatively high. In the geological past, when the total internal energy budget was higher, this ratio will be higher too. The existence of thermal boundary layer (i.e. oceanic plate) motions at the present time quite simply implies that the Earth's total heat production exceeds that which can be released by conduction through upper mantle rock types. In Precambrian times, therefore, there will have been a greater, not lesser, degree of thermal boundary layer movement.

Since the decay of the heat-producing isotopes in the Earth exponential, all calculations based on reasonable compositional models show that the global thermal regime in the period of interest to Damaran geodynamics, i.e. from -1000 Myr to -500 Myr will not have been significantly different from the present. The total global heat loss will then have been about $1{,}5 \times 10^{21}$ J yr^{-1}, of which at least 6×10^{20} J yr^{-1} will have been released by cooling oceanic lithosphere plates. There seems to be no sound physical reason for assuming that this occurred in some mode other than Orowan-Elsasser advection.

It is, moreover, possible that the present rate of internal heat loss by conduction, namely 8×10^{20} J yr^{-1} (Williams & Von Herzen, 1974), is a permanent upper limit and that all present and previous excess heat production in the Earth has been released to the hydrosphere-atmosphere system and ultimately radiated to outer space, by convective motions in the lithosphere-asthenosphere system. This suggests a method of estimating the global extent of plate tectonic activity in past geological time. At present, the rate of advective transfer of heat away from the oceanic ridges is about 5×10^{20} J yr^{-1} (Williams & Von Herzen, 1974) and the total length of such oceanic ridge is about 5×10^{4} km (Forsyth & Uyeda, 1975). Therefore, each one kilometre length of spreading ridge is responsible, on average, for the release of 10^{16} J yr^{-1}. Assuming that the thermal and mechanical structure of oceanic ridges is governed only by the gross physical properties of upper mantle rock and has thus not changed significantly in the course of Earth history, but that the total length of oceanic ridge has been exponentially decreasing in proportion to the exponential decay of radio-active heat sources, it is possible to calculate the probable total ridge length in, for example, Late-Precambrian times. With a global

heat loss of $1,5 \times 10^{21}$ J yr^{-1}, of which 8×10^{20} J yr^{-1} is advectively transferred, total oceanic ridge length will have been about 7×10^4 km.

It has been suggested that plate motion in the past may also have been faster to accommodate the greater energy release, (Burke, Dewey & Kidd, 1976), but theoretical calculations suggest that asthenosphere viscosity is maintained at a constant value close to 10^{20} Pa s by self-adjustment of asthenosphere depth and temperature (Froidevaux *et al.*, 1976), due to thermal feedback. It has also been shown that there is a definite terminal velocity close to 8,0 cm yr^{-1} for the descent of oceanic slabs into the mantle (Forsyth & Uyeda, 1975), which is probably governed by Stoke's law relating velocity of free fall of a body in a viscous medium to the viscosity of that medium (Christoffel & Calhaem, 1973). There are strong arguments against the concept of significantly faster convective motions in the more distant geological past. Instead, it seems more probable that total ridge length was greater, which in turn implies greater total trench length. In a spherical surface of constant area, however, *greater total* ridge and trench length, implies a larger number of smaller oceanic plates (assuming their approximate equidimensional geometry) and hence *shorter individual* ridge or trench segments.

The previous vertical extent of the lithosphere-asthenosphere system is probably more important in controlling the character of Precambrian tectonic regimes, particularly the depth and thickness of the asthenosphere. In the solid-state mechanical model of the asthenosphere (Froidevaux & Schubert, 1975), it is a zone in which effective viscosity reaches a self-adjusting minimum where the effects of T-dependent viscosity decrease and P-dependent viscosity increase are balanced. The depth of the minimum is governed mainly by the activation volume V^*, which is related to the diffusion process allowing dislocation climb and recovery and for which a most likely value of 0,02 nm^3 has been suggested (Froidevaux *et al.*, 1976). Because numerical simulation experiments relating variable surface heat flow to asthenosphere depth in the solid-state model have not yet been carried out, it is still not possible to make precise predictions about the effect of increased global heat production on asthenosphere depth (or conversely, lithosphere thickness). Much also depends

on the actual vertical and horizontal distribution of radiogenic elements in the crust and upper mantle (Pollack & Chapman, 1977).

In general, it can be intuitively assumed that greater heat flow in the past and attendant higher geothermal gradients, imply lesser depths to the base of the lithosphere. Thinner lithosphere and a better developed asthenosphere are conditions that would have facilitated plate motion and continental drift in Precambrian times. At present, continental shield lithosphere areas are thickening to depths in excess of 300 km and are developing substantial "viscous anchors" (Pollack & Chapman, 1977), the effect of which is to significantly retard continental plate motions (Forsyth & Uyeda, 1975; Solomon *et al.*, 1975). In the long-term geological future, it can be expected that plate motions will diminish and eventually cease. Quantitatively, however, the rate of such change is slow (and decreasing) and has been so for the past 1000 Myr. Since the thickness of lithosphere plates affects their flexural rigidity and strength, it is an important parameter governing the tectonic style of deformation. Thinner lithosphere naturally seems more susceptible to tensional disruption and flexure.

This is a further argument against the application of an *ad hoc* asthenolith hypothesis, which does not involve large-scale horizontal movements, to the Damara orogenic belt. In Late-Precambrian times as at the present, asthenolith intrusion will have been the result and not the cause, of continental separation; in contrast to the present, however, the thermal and mechanical structure of the lithosphere-asthenosphere system in Late-Precambrian times will have facilitated large-scale horizontal separation of formerly continuous continental masses.

Although much remains to be learned about the character of modern geodynamic regimes and the tectonics of the lithosphere-asthenosphere system, there is an emerging consensus that the system may be a relatively shallow one, comprising only the outer 600 km or so of the Earth; that a large proportion of the Earth's heat is transferred to the surface by dominantly horizontal advection motions, of the type originally suggested by Orowan (1965) and Elsasser (1969); that the principal driving force for these motions is the pull by sink-

ing slabs of oceanic lithosphere; and that mantle drag, which was previously postulated as the major driving force for continental drift, is instead a force which significantly retards plate motion, particularly beneath continental plates. There is a further emerging consensus, arising from experimental and theoretical work on the steady-state flow of mantle rocks, that the asthenosphere is essentially a solid-state phenomenon (Froidevaux & Schubert, 1975), which does not require any significant degree of partial-melting, except very close to oceanic ridges at depths less than 70 km. These new concepts, together with a clearer distinction between the surface relative motion of lithosphere plates and the absolute motion of those plates with respect to the rigid deep mantle or mesosphere (Solomon & Sleep, 1974; Minster *et al.*, 1974), constitute a radical departure from traditional notions of mantle convection and continental drift. It is inconceivable that they should not have a profound effect on Precambrian geotectonic interpretations.

The development of quantitative models based on experimental and theoretical studies, which allow precise predictions to be made about relationships between motions, driving forces, strain-rates, stresses, geothermal gradients, surface heat flow and lithosphere-asthenosphere parameters (thicknesses, depths, viscosities, thermal conductivities, etc.), is still in its infancy (eg. Froidevaux & Schubert, 1975; Pollack & Chapman, 1977). It is already clear, though, that these factors have complex and sometimes unexpected inter-relationships, due to phenomena such as thermal feedback. The extrapolation of these models back to earlier geological eras is a logical further development as more geophysical and petrological data become available.

It should be noted that an aspect of modern plate tectonic interpretation is the tendency to avoid postulating "deep and speculative mechanisms" (Parker & Oldenburg, 1973) for observed processes particularly those involving convective heat-transport and anomalous near-surface geothermal regimes. The asthenolithic masses beneath spreading ridges, for example, are definitely not related to the rising limbs of deep mantle convection cells, even if the latter exist, which is doubtful. Likewise, the hypothesis of *deep seated* "mantle upwelling" as a primary cause of Precambrian tectonothermal events is also

arguably in the category of speculative mechanisms for which there is little or no experimental and theoretical support.

In conclusion, therefore, it is argued that the asthenolith hypothesis is ultimately irrelevant as an explanation of Damaran orogenesis and that it rests on insecure geophysical foundations. By placing the ultimate cause of the orogenic activity in the deep mantle, it in fact conveniently defers the task of rational explanation: the problem of explaining the Damara orogenesis is subtly transformed into the larger problem of justifying and explaining the existence of quasi-metaphysical entities of which direct knowledge is, in principle, unobtainable.

On the basis of the simplicity principle, that no unnecessary theoretical processes should be invoked as long as observable ones can successfully explain past changes, an alternative model is outlined in the following section. This model is based on the general concept that all observed phenomena of the Khomas Ridge province can be successfully explained in terms of modern plate tectonic theory and that there are several little-understood or as yet unobserved features of the province which can be clarified or predicted by the model.

B. A REALISTIC MODEL FOR THE DAMARA OROGENY

1. Major indications for plate tectonics

The formulation and elaboration of a large-scale plate tectonic model for the Damara orogenic belt is prompted by three important major features which are exclusive to the Khomas Ridge province. These features are:

(1) the existence of an extraordinary thick and voluminous sequence of "eugeosynclinal" schists in the Khomas Trough, the origin and provenance of which still poses serious problems;

(2) the existence at and near the base of the schist sequence, of mafic to ultramafic rocks of probable ophiolitic affinity;

(3) the large-scale and local tectonic structure of Khomas Ridge zones KR-II and KR-III, from which extensive underthrusting ("subduction") of the north-western margin of the Kalahari craton can be inferred.

Characteristic of the last-mentioned major feature are pervasive plastic and cataclastic deformations of the Damaran cover and basement together, at relatively low temperatures and significant crustal shortening and thickening which is reflected even today in the topography and gravity field of the Khomas Ridge. Much of this deformation has previously gone unrecognised because of its extreme intensity, although the paradoxical fact was originally noted by Gevers (1934) that the structural complexity of the low- to medium-grade southern part of the Damara belt is greater than the high-grade central zone in western Damaraland. The essential structural feature of Khomas Ridge zones KR-II and KR-III is a well-developed tectonic schistosity, dipping north-westward at an average angle of about 30° where it has not been re-folded. This schistosity thoroughly overprints and obliterates ("transposes") original sedimentary structures in the schists and from the evidence of quartz vein relationships north of Windhoek (Hälbich, 1970) probably obscures an earlier generation of tectonic structure as well.

The folding, thrusting, schistosity development in the southern Damaran cover rocks and the formation of major mylonite gneiss belts in the sub-Damaran basement indicate the existence of powerful deviatoric stresses in a relatively localised segment of the crust. It is evident that the boundary conditions of the deforming system were such that these deviatoric stresses diminished quite rapidly northwards, since relatively weak, fine-grained sedimentary rocks in zone KR-IV were, in general, less deformed than strong, coarse-grained plutonic igneous rocks in zone KR-II. Metamorphic evidence indicates that the rocks presently exposed in zone KR-II were more deeply buried than rocks now at the surface in zone KR-IV (Hoffer & Puhan, 1975; Haack & Hoffer, 1976), but were simultaneously held at much lower temperatures (Fig. 65 , after Haack, 1976). Since the combination of higher confining pressure and lower temperature generally operates to strengthen crustal rocks, the apparent relative weakness of granitoid rocks in zone KR-II is rendered even more anomalous by this finding.

The general conclusion which is drawn from the above observations is that the driving force for orogenic deformation and crustal thickening in zone KR-II was located within or very close to this zone and that the associated boundary

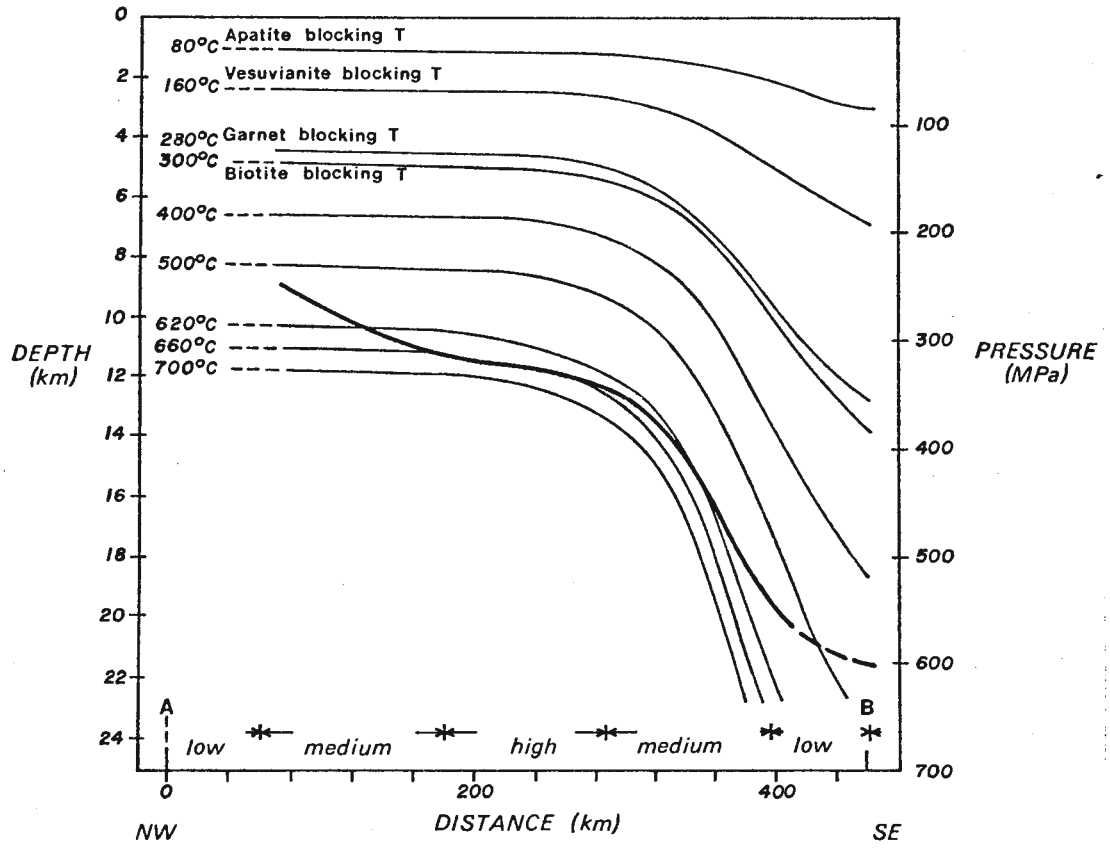

Figure 65. Model of temperature versus depth to present erosion surface (thick line) at peak of Damaran post-tectonic metamorphism about 550 Myr before present (traced from Haack, 1976). The major feature of the Damaran metamorphic pattern is its geobarometric asymmetry, with the low-grade zone in the south (to the right in the figure) showing the highest equilibration pressures up to and possibly exceeding 600 MPa when temperatures did not exceed about 500°C. The model indicates that the maximum post-metamorphic uplift has occurred along the southern margin of the Damara belt, and not as might intuitively have been expected in the central granite zone.

shear stresses were relaxed by steady-state plastic or quasi-viscous flow in zone KR-III. Support for this concept is obtained from local finite-strain measurements in the northern parts of zone KR-II (Hälbich, 1970) and the observation that the most intense development of folded and boudinaged quartz veins in the Damara belt occurs in the southern part of zone KR-III, structurally beneath the Matchless Amphibolite and above the KR-II/KR-III boundary. These show that zone KR-III behaved as a weak and ductile boundary layer or slip zone.

As in the case of a similar observation in the Naukluft nappe complex, it is once again significant to note that most extensional quartz-vein structures were formed *early* and not late, in the tectonic history of the Khomas Ridge province and that these structures were *subsequently* deformed by intracrystalline plastic flow mechanisms, as shown microscopically by characteristic recovery structures. This clearly implies that, during the course of their tectonic evolution, the rocks were being transported from a regime where temperatures and confining pressures were relatively low and pore fluid pressures were high, to one in which temperature and confining pressures were higher and pore fluid pressures were low. These features are therefore a probable indication of subduction.

In the model which is proposed here, the immediate driving force of the subduction process is considered to have been a sinking slab of oceanic lithosphere formerly contiguous with the north-western margin of the Kalahari craton and therefore situated directly subjacent to zone KR-II. The degree of deformation and crustal thickening in the latter indicates that the slab must have been sizeable and accordingly possessed of a considerable negative bouyancy.

Remnants of this former oceanic slab are considered to be extant in the mafic to ultramafic ophiolitic rocks of zones KR-II and KR-III, the most conspicuous of which is the Matchless Amphibolite situated centrally in the latter zone. It is however, further postulated that a large, if not the greater proportion of the enormous mass of schist in the Khomas Trough is indirectly derived from the subducted slab: a minor part in the south, as the tectonically accreted oceanic Layer 1 sedimentary cover of the slab,

analogous to the Franciscan complex of California; a major part in the north, as a volcanogenic sedimentary pile ultimately derived by partial melting of oceanic Layer 2, analogous to the Otago schists of New Zealand or the Great Valley sequence of California. If this hypothesis is correct, it may be possible to use mass-balance calculations in estimating the width of oceanic crust formerly separating the Kalahari and Congo cratons. This possibility is explored in the following section.

2. Implications of plate theory to the interpretation of the Khomas schists

a. The Khomas schists

The Khomas schists (now renamed the Kuiseb Formation) form the bulk of the material filling the "eugeosynclinal" part of the Damara orogenic belt (Martin, 1965; Clifford, 1967). In places they overlie, in other places they interfinger with, the lower marble and quartzite formations of the Damara Supergroup. They are most massively developed in the southern part of the Damara orogen, within a major trough or synclinorium which underlies the Khomas Highlands.

Gevers (1931b, p.81) originally recorded that:

> "On account of the great uniformity of rock types and the absence of variety and marker beds, it is impossible to make out the detail of the tectonic structure of this part of the Khomas Highlands and to arrive at a reliable estimate of the thickness of the rocks of this group.....The thickness, however, must be an enormous one, running into tens of thousands of metres. In the Windhoek area between the Auas Mountains and Okahandja where the tectonic structure is very simple, the figure of 30 000 metres does not seem to be excessive."

In underestimating the effects of deformation in the apparently simple synclinal form of the Khomas Trough, this original thickness estimate of 30 km is certainly excessive. Martin (1965, Table V) placed an uncertain estimate of 10 000 metres for the maximum thickness of the Khomas schists in the Windhoek district. It would appear however, that a figure of 10 km should rather be considered as a minimum. Martin (*op.cit.*, p.41) considered that these rocks "must originally have been illite-bearing shales, arenaceous shales and grey-

wackes, making a typical eugeosynclinal assemblage."

b. The structure of the Khomas Trough

A structural section across the Khomas Trough along a line between Windhoek and Okahandja given in Fig. 66A which has been traced with very little modification directly from Hälbich (1970, Plate XV). In this section, the different styles of deformation in the northern and southern parts of the Khomas Highlands are represented and in particular the way in which early upright folds in the northern zone KR-IV become overturned and overprinted by the effects of much more intense later deformation in the southern zone of KR-II. In this deformation pattern the X-Y principal plane of strain in the Khomas schist becomes progressively flatter towards the south as the intensity of strain (as evidenced by the X/Z ratio of ellipsoidal objects) becomes greater. This deformation pattern is alone very strong, if not conclusive, evidence of considerable subduction of crustal material along the southern margin of the Damara orogen. Fig. 66A should also convey some idea of the difficulty of stratigraphic reconstruction and thickness estimation in the Khomas metasediments. Fig. 66B represents a section across a modern continental margin, that of Guatamala, where subduction of oceanic crust is known to be occurring. This section has been traced, again with very little modification, from Seely, Vail & Walton (1974, Fig. 12) after having been brought to the same scale. The figures have been aligned on the right, along the line of first occurrence of granite. It must be emphasized that the originals of these figures both attempted to represent the crustal substructure without vertical exaggeration. Hence there is no distortion of angular relationships in either section.

Bearing in mind that Fig. 66A represents a crustal section from which 10-20 km of overburden have been removed following post-orogenic uplift (Haack & Hoffer, 1976) and that both the schist body in this section and the granitic continental crust by which it is bounded on the south (left), have been severely deformed in collision, the resemblance which it bears to Fig. 66B is very remarkable. This similarity of sections drawn from two entirely independent sources supports the suggestion that the Khomas schists represented a "flysch apron" fringing a wide volcano-plutonic orogen of the cordilleran type (Dewey &

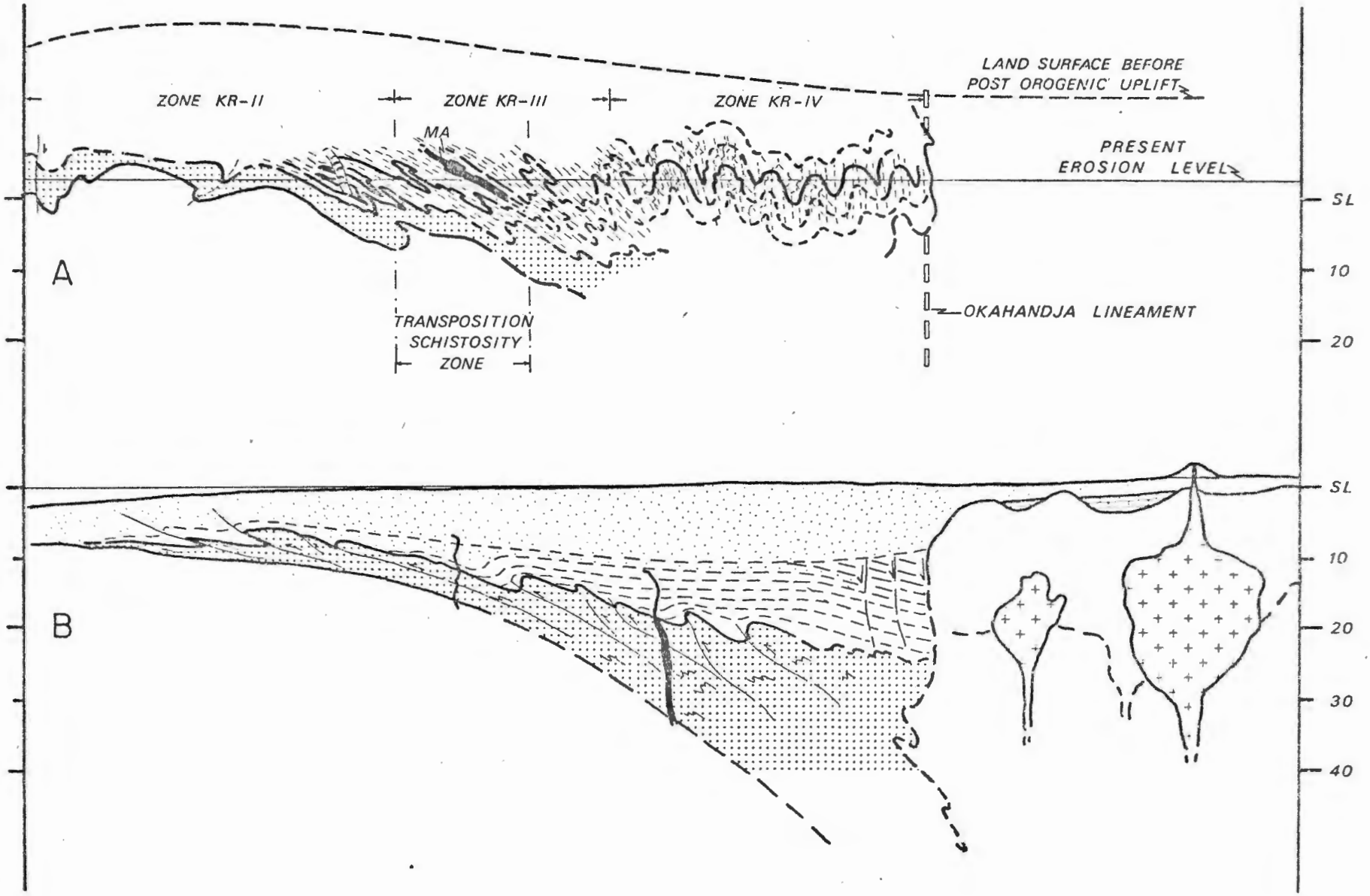
LAND SURFACE BEFORE
POST OROGENIC UPLIFT
ZONE KR-II
ZONE KR-III
ZONE KR-IV
MA
PRESENT
EROSION LEVEL
SL
10
20
A
TRANSPOSITION
SCHISTOSITY
ZONE
OKAHANDJA LINEAMENT
SL
10
20
30
40
B

Bird, 1970) and inspired the present effort to develop a quantitative model for the origin of the Khomas schist body.

c. Composition of the Khomas schist

In discussing the results of chemical analyses of Khomas schist (Clifford, 1967; Hoffer & Puhan, 1975) one point should be made at the outset. The object of sampling the Khomas metasediments has never been to determine their average composition. In one case, (Clifford, 1967) the object was to gather fresh material for the K-Ar isotopic dating of biotite; in another (Hoffer & Puhan, 1975), to gather fresh material for the detailed mineralogical study of metamorphic phases, in particular the Al_2SiO_5 polymorphs. In the first case, the immediate objective in the field will have been to seek out best exposed and preserved material and this is likely to have biased the sampling in favour of more siliceous and calcareous varieties of schist. In the second case, the immediate objective will have been to seek out or select material in which critical metamorphic reactions, involving mostly aluminous minerals, are best displayed and this is likely to have biased the sampling in favour of more pelitic and aluminous varieties of the schist. That these assumptions of bias are very probably true, is borne out by a comparison of Columns 1 and 2 in Table 12. There are significant discrepancies between SiO_2, Al_2O_3 and CaO along the lines indicated above.

However, it is reasonable to assume that Column 3 of the table, which represents the oxide means of analyses from both abovementioned sources, is a good approximation to the average composition of the great body of Khomas schist. This, of course, will remain an assumption until there is a conscious effort to sample the mass of Khomas schist on a sound probability basis and to determine the mean abundances and variances of major and trace elements in the samples so gathered. The present lack of just such an effort is a serious deficiency affecting all programmes of geological research in the Damara belt, both economic and academic. The Khomas schist may appear to be a very large mass of uninteresting and monotonously uniform material, but its importance lies precisely in its very extensiveness and homogeneity. One of the truly major questions of the Damara orogen is: how did such a large and homogeneous

TABLE 12

COMPOSITION OF THE KHOMAS SCHIST

	1	2	3	4	5	6	7
SiO_2	63,78	59,03	61,28	60,76	66,7	68,1	58,17
TiO_2	0,75	0,97	0,87	0,81	0,5	0,7	0,80
Al_2O_3	13,01	18,30	15,79	16,73	15,0	15,4	17,26
Fe_2O_3	1,37	4,76	3,15	2,53	4,5	1,0	3,07
FeO	3,68	4,44	4,08	3,58	-	3,4	4,17
MnO	0,09	0,09	0,09	0,07	0,07	0,2	-
MgO	3,22	3,94	3,60	2,49	2,3	1,8	3,23
CaO	4,28	0,75	2,42	1,74	4,2	2,3	0,93
Na_2O	2,31	1,00	1,62	1,82	3,6	2,6	3,21
K_2O	2,94	3,32	3,14	3,41	3,2	2,2	1,61
P_2O_5	0,19	-	(0,19)	0,14	-	0,2	0,20
H_2O^{tot}	1,53	2,84	2,22	3,43	-	2,1	1,24
	97,15	99,44	98,45	97,51	100,07	100,0	99,89

COLUMN	EXPLANATION
1.	Oxide means of 9 analyses of Khomas schist given by Clifford (1967, p.80).
2.	Oxide means of 10 analyses of Khomas metapelite given by Hoffer & Puhan (1975, p.119).
3.	Oxide means of 19 analyses from 1 and 2 above combined.
4.	Average pelite from Shaw (1956, p.928).
5.	Estimated composition of the Canadian Precambrian Shield (Shaw *et al.*, 1967).
6.	Average of 30 greywacke sediments compiled by G.W.Tyrrell (from Pettijohn, 1949, p.250).
7.	Average of 1775 Cenozoic andesites from Chayes (1969).

body originate?

Comparison between the "average" Khomas schist (Column 3) and Shaw's average pelite (Column 4) reveals interesting differences between the iron oxides and magnesia. The Khomas schist apparently contains about 1 per cent more Fe_2O_3 + FeO and 1 per cent more MgO. Otherwise the columns are closely comparable. Comparison between the Khomas schist and the estimated composition of a typical Precambrian shield (Column 5) points up to the same differences even more markedly. There are also slight differences between SiO_2, and CaO and Na_2O here. If a region having the bulk composition illustrated in Column 5 were to be eroded to form a sedimentary deposit having the bulk composition of Column 3, then the differences regarding CaO and Na_2O are easily explained when the effects of hydration and solution, which result in the leaching of sodium and calcium, are taken into account in the weathering and transport processes. Enrichment of iron and magnesium, however, remains a problem. The Khomas schists are often considered to be a metamorphosed flysch-type greywacke deposit, so a comparison between them and an average greywacke (Column 6) is warranted. First, though, it is interesting to note that the average greywacke is very similar in major element composition to the Precambrian Shield (Column 5), except perhaps for leaching of the alkali elements. Compared to the average greywacke, the Khomas schist is somewhat less siliceous and once more, its unusual iron and magnesium content is emphasised.

What is the explanation for this apparent anomaly? One which suggests itself, because of the flysch-like and probable turbiditic nature of the Khomas metasediments, is that these rocks were derived rather rapidly, with very little secondary compositional modification (except for alkali leaching), from a source having the composition of a basic intermediate igneous rock. For the purpose of testing this suggestion, the chemical composition of an average andesite is represented in Column 7 of Table 12.

As expected, there is a very close compositional similarity between the Khomas schist and the average andesite, except with respect to the alkali elements where leaching effects during weathering and transport are likely to have played an important role. This similarity leads to the hypothesis that the

sediments of the Khomas trough were derived by rapid erosion of a volcanic provenance of andesitic composition. Attention may now be turned to the problem of locating this provenance.

d. Source of the Khomas schist

"The great volume of the Khomas schists poses a problem: where is the source area of these sediments?" (Martin, 1965, p.41). Because the sedimentary structures have been largely obliterated by deformation and metamorphism, Martin considered that the rocks do not offer any clues.

With the given compositional constraints in mind, this question may be reconsidered. A possible source in the Kamanjab and Grootfontein inliers of pre-Damara basement, in the northern part of the geosyncline and the Rehoboth inlier of pre-Damara basement at the southern margin has been proposed considering that the "area or areas from which the erosion products were derived must have been extensive and must have undergone rapid erosion of the pre-Damara basement" (Martin, 1965, p.41). Although both the Kamanjab and Rehoboth inliers contain some intermediate to basic volcanic rocks, their proportions do not appear to be sufficient to account for the compositional peculiarities of the Khomas schist. Furthermore, the Kamanjab inlier is relatively remote and by Khomas times was largely covered by Tsumeb Group formations. It cannot therefore be considered as a significant contributor of sediment to the Khomas Trough in the southern part of the Damara belt. The Rehoboth inlier, moreover, appears to be areally too small even when its extensions to the southwest are considered. Most of the uplift and deep erosion of the Rehoboth inlier has evidently occurred in post-Khomas times (Haack & Hoffer, 1976). That the Rehoboth inlier did shed some sediment northward into the Khomas Trough may be evident from the increasing prominence of arenaceous units such as the Auas Formation as one approaches the southern margin of the trough (Martin, 1965, p.42).

The Abbabis inlier, exposed in the very centre of the so-called "eugeosyncline", was not considered as a potential source of clastic detritus in Khomas times, obviously because of its apparent areal insignificance (cf. Martin,

1965, p.7, Fig.2). Following a suggestion by Martin (*op.cit.*, p.6), it has recently been shown that other anticlines in the central Damara belt also contain cores of pre-Damara basement and that the Abbabis inlier or "geanticline" has a considerable extension south-westwards into the flats of the Namib Desert (Jacob, Burger & Kröner, 1977). It is probable, then, that the central zone of the Damara belt must be considered as a potential provenance for Khomas Trough sediments. The pre-Damara rocks of the Abbabis inlier are, however, mainly highly silicic granites and it is evident that in Khomas times they were not exposed to deep erosion. The problem of the Khomas schist provenance therefore remains.

It is, of course, possible that the material in the Khomas Trough was brought into the depositional trough from the north-east by a great river or rivers draining a highly-uplifted area in Central Africa, but this would be an arbitrary *ad hoc* explanation. Instead, it is proposed here that the andesitic volcanic provenance from which the proto-sediment of Khomas schists was derived was situated close at hand in the region of the Abbabis Swell and that it may be related by the early dioritic members of the Salem granite suite (Smith, 1965), which outcrop abundantly in the region just south of Karibib. It is postulated that the emplacement of these dioritic rocks as subvolcanic intrusions into the lower part of the Khomas Subgroup was effectively synchronous with the deposition of higher parts of the latter, i.e. the Kuiseb Formation. Isotopic evidence in support of this contention, showing that certain early members of the Salem granite suite may have an age range between 700 Myr and 800 Myr, is presently emerging (Hawkesworth *et al.*, 1977; Kröner *et al.*, 1977; Jacob *et al.*, 1977).

e. Presentation of the quantitative model

The Khomas Trough has the geometry of a wedge-shaped or triangular prism having a width of about 90 km, an exposed length of about 300 km and an estimated present depth of about 15 km. The total volume of Khomas schist contained within this prism is thus 202,5 x 10^{12} m^3 (Fig.66A). Alternatively one kilometre length of the Khomas Trough at present contains 675 x 10^9 m^3 of material. We may conservatively estimate the original dimensions of the Khomas basin, prior to post-orogenic uplift as having a width of about 120 km and a depth of about

25 km. A one kilometre length of the basin will have contained 1500 x 10^9 m^3 of material (Fig. 66B). This calculation suggests that an amount of Khomas schist approximately equal to that still preserved has been removed by erosion and is probably now largely distributed between the stratigraphic units of the Mulden and Nama Groups and to a lesser extent, the lower units of the Karoo Supergroup in SWA.

Field observation (Jacob, 1974; Blaine, 1977) indicates that, during Khomas deposition, large relative vertical movements were taking place about the Okahandja Lineament. In Fig. 66B the fault zone at the inland boundary of the Guatamalan coastal plain basin is suggested as a modern analogue of the Okahandja Lineament at this time and in this example the andesitic volcanism in the uplifted cordillera farther inland may be equated with the early Salem magmatic episode, now represented only be deeply-eroded intrusives. The Salem suite was formerly considered to be derived by anatexis of Khomas schists (Smith, 1965; Miller, 1974), but this hypothesis is not supported by preliminary investigations of initial Sr-isotope ratios (Hawkesworth *et al.*, 1977). It is instead suggested by the present writer that the Salem suite will be found to show geochemical and isotopic characters of a typically calc-alkaline orogenic igneous province. In this case, the appropriate petrological model for its derivation may be similar or identical to that proposed on recent experimental grounds by Ringwood (1974), namely the two-stage (or even multi-stage) model of which the first stage is the generation of oceanic crust at a spreading ridge and the second stage is the partial melting of that crust at depths exceeding 100 km in a subduction zone.

In the comparative sections of Fig. 66 the locus of the proposed subduction zone is perfectly clear. The large-scale and detailed structure of the Khomas Trough allows for no other interpretation except north-westward subduction at a trench zone situated close to the present southern margin of zone KR-II.

Early uplift of the Abbabis Swell relative to the Khomas Trough can be related to the mechanism of dynamic uplift by compositional contamination of the lithosphere with andesite magma originating in a subduction zone (Gough, 1973).

In this model a cordilleran mountain belt is uplifted and supported essentially by compositional contamination of the lithospheric column with about 16% andesite which is received continuously through its base. It is estimated (*op. cit.*, p.40) that each kilometre length of the Andes needs 4500 cubic kilometres ($4{,}5 \times 10^{12}$ m^3) of andesite to contaminate a column 200 km wide and 140 km high. By assuming that a certain fixed proportion (20%) of oceanic crustal Layer 2 becomes fused in the subduction zone, it has been computed that 3800 km of oceanic slab must have passed beneath the Andean cordilleran column in order to raise that mountain chain to its present height (Gough, 1973).

Clearly, a similar calculation is possible using the volumetric data for the Khomas schist. The first point to note is that the original volume of schist calculated for each kilometre segment of the Khomas Trough (about $1{,}5 \times 10^{12}$ m^3) is the same order as the volume of andesitic magma presently suggested to contaminate a one-kilometre segment of the sub-Andean lithosphere ($4{,}5 \times 10^{12}$ m^3; Gough, 1973). A straightforward calculation on precisely the basis of the Gough model suggests that at least 1200 km of oceanic crust must have been "processed" to yield this amount of andesitic material.

The further assumption behind this calculation is that this material was not detained at depth within the uplifted zone, by being accreted at the base of the granitic crust for example. The andesite magma generated in the subduction zone at depth beneath the Abbabis Swell is here supposed to have passed through the overlying lithosphere, perhaps assisted by hydraulic over-pressure within the cover sequence at or near to the top of the lithospheric column. The precise location of the andesitic component within the lithospheric column is not important to the dynamic uplift mechanism, since isostatic compensation results in the same downward displacement of an equivalent mass of denser subcrustal material wherever the andesite is emplaced.

It is further postulated that this material was rapidly subjected to processes of surface erosion and transport, without major chemical weathering and alteration, except for leaching of alkali elements. The reasons for this are probably twofold. Firstly, the dynamic uplift of the Abbabis Swell contemporaneous with the calc-alkaline orogenic magmatism implies a high erosion

potential for material near the top of the column. Secondly, it is well known from modern zones of andesitic magmatism that the principal product of andesite volcanoes is not lava, but overwhelming volumes of unconsolidated tephra and volcaniclastic debris; the Rittman "explosion index" of such volcanoes is high and the proportion of actual andesitic lava is sometimes trivial. It is accordingly suggested that the rapidly eroded andesitic detritus was carried directly down the regional topographic slope by juvenile mountain streams or perhaps through the agency of major mud- or debris-flows (lahars) across a narrow piedmont coastal plain onto a relatively steeply sloping trench inner wall, where it may have been subjected to further south-eastward distribution by submarine turbidity flow mechanisms. This model for the origin and deposition of the enormous volume of schist in the Khomas Trough can be expressed in formal mathematical terms using six simple equations. Firstly, the Khomas depositional basin is modelled as a triangular wedge, tapering away from a fault-bounded margin at which maximum subsidence has occurred. The volume of sediment V in a unit section of this wedge is therefore expressed as:

$$V = \tfrac{1}{2}.W^2.\tan\alpha \qquad (1).$$

where W is the horizontal width of the wedge and α is the dihedral angle formed at its leading edge. The maximum thickness D of the sediment in wedge is expressed as:

$$D = W.\tan\alpha \qquad (2).$$

In selecting W and α as the observational variables, consideration was given to the possibility of estimating them from surface field evidence. The equation relating the length of subducted oceanic slab L to the sediment volume V, via the Ringwood and Gough models is:

$$L = V / (P_m.P_s.T) \qquad (3).$$

The variables in the denominator on the right-hand side are: the thickness of the fusible basaltic layer in the oceanic crust, T; a proportionality constant P_m reflecting the degree of partial fusion of this layer; and a proportionality constant P_s reflecting the actual amount of initially-formed magma that is finally deposited as andesitic greywacke sediment in the basin.

TABLE 13

QUANTITATIVE MODELS OF KHOMAS TROUGH EVOLUTION

Data Group	Variable/Units	Models KT1	KT2	KT3	KT4	KT5	KT6
1	W / km	90	100	120	120	120	120
	a / degrees	9,5	11,3	11,8	11,8	11,8	11,8
	D / km	15	20	25	25	25	25
	T / km	6	6	6	6	6	6
	P_m / -	0,2	0,2	0,2	0,1	0,05	0,05
	Ps / -	1,0	1,0	1,0	0,5	0,75	0,75
	U / cm yr^{-1}	5,0	5,0	5,0	5,0	5,0	5,0
2	V / km^3	675	1000	1500	1500	1500	1500
	L / km	560	833	1250	5000	6667	6667
	I / Myr	11	17	25	100	133	100*
	M / $x^3 10^{-5} km^{-3} yr^{-1}$	6,0	6,0	6,0	3,0	1,5	2,0
	S / mm yr^{-1}	1,4	1,2	1,0	0,25	0,19	0,25*

From these equations and variables, three further quantities of interest can be calculated. The time interval I over which the subduction process operates is related to slab length L and slab relative velocity normal to the trench U by the equation:

$$I = L / U \qquad (4).$$

Magma production rates in a unit segment of the subduction zone are expressed as:

$$M = V / P_s.I \qquad (5).$$

Finally, the average rate of sedimentation S in the deepest part of the trough is obtained from the equation:

$$S = D / I \qquad (6).$$

The object of including these derived quantities in the model is to ensure realism by comparison with the same quantities actually measured for analogues of the Khomas sequence.

Application of the mathematical model to the Khomas Trough is illustrated in Table 13. The columns of the Table represent quantitatively different versions of the basic model, obtained by varying the structural geometry of the original Khomas basin (models KT1-KT3) or by varying kinematic or other quantities related to the volcanogenic sediment production (models KT3-KT6). The rows of the Table are divided into two main groups. Group 1 data in the upper portion "assumed" or observed variables, while Group 2 in the lower portion are the derived variables, which are original sediment volume V, length of oceanic slab subducted L, time-interval for the subduction process I, magma production rate M and average sedimentation rate in the basin axis S.

Six possible models are presented in Table 13. Since the present object of the exercise is mainly to obtain an estimate of the length of oceanic slab that may have been consumed, the models are ordered from left to right with increasing L values. Realistic constraints on the models are provided by recent estimates of magma production rates in the Andes and elsewhere (e.g. Francis & Rundle, 1976) and by recent sedimentation rate statistics of stratal units which closely resemble the Khomas sequence and which are found in Mesozoic-

Cenozoic orogenic belts (Spencer, 1974).

In the Central Andes, it has been shown that, over the past 10 Myr, the likely maximum rate of magma production for extrusive andesites, rhyolitic ignimbrites and granitic batholithic material combined is nearly 2×10^{-5} km^3 yr^{-1} in one-kilometre segment transverse to the length of the Andean mountain chain (Francis & Rundle, 1976). This represents just less than 5% of the total volume of oceanic *crust* which passes beneath the Andes at the eastern Pacific trench zones each year, about $4,8 \times 10^{-4}$ km^3 for each one-kilometre length of plate margin. However, since this figure is inadequate to account for the crustal thickening of about 30 km that has occurred in the Andes since the Jurassic (D.E. James, in Francis & Rundle, 1976), it can be suggested that a significant proportion of the magma generated in the subduction zone did not rise near to surface but contributed to crustal underplating, Gough (1973) suggested that andesite equivalent to 20% by volume of the consumed oceanic crust was added to the lithospheric column.

It should, in passing, be emphasised that the present model simply assumes that there is a specific functional relationship between volume of consumed oceanic crust and calc-alkaline magma generation, but the precise petrological mechanisms implicit in this relationship are not important as such. In other words, it is of no particular concern if the mechanism of magma generation is less direct than simple partial fusion of the basaltic layer.

Stratal units with thickness of 10 km or more are exceptional in Mesozoic-Cenozoic orogenic belts, but are reported from the Hellenides, Borneo and parts of the Circum - Pacific belts (Spencer, 1974, p.776). Rates of accumulation of stratal units in these orogens vary up to a maximum of 2,5 mm yr^{-1} reported for 5 km thick Quaternary clastics from Papua - New Guinea, but rates between 0,1 mm yr^{-1} and 1 mm yr^{-1} must be considered the normal maximum rates at which strata in the Mesozoic-Cenozoic orogenic belts accumulated. Some examples of thick sedimentary accumulations, together with their rates of accumulation, from the data analysed by Spencer (1974) are as follows:

(1) a 16 km greywacke-shale-radiolarite unit of Palaeocene age from Borneo accumulated at 0,25 mm yr^{-1};

(2) a 14,5 clastic-shale-coal/lignite unit of Pliocene age from the same area accumulated at 1,5 mm yr^{-1};

(3) a 12 km shale-clastics unit of Miocene-Pliocene age from Papua-New Guinea accumulated at 0,6 mm yr^{-1};

(4) a 10 km clastic-shale unit of Oligocene age from S.W. Japan accumulated at 0,4 mm yr^{-1};

(5) a 10 km clastic-shale-volcanics unit of Oligocene age from Alaska accumulated at 0,25 mm yr^{-1}; and

(6) a 10 km shale-volcanics unit of Lower Cretaceous age from Colombia accumulated at 0,25 mm yr^{-1}.

All these examples may, in some way, be regarded as Phanerozoic analogues of the Khomas deposits. It is indeed significant that they are all associated with orogenic belts of the "cordilleran" type (Dewey & Bird, 1970).

Quantities derived for the models KT1 and KT2 of Table 13 in which very conservative estimates of the original Khomas Trough volume are made and in which the Gough (1973) assumption of a 20% partial melting of 6 km thick oceanic basalt layer is made, indicate that the process of generation was completed within 10 - 20 Myr and imply magma production and sedimentation rates that are probably too high. With the preferred value for Trough volume V (1500^3km), the quantities I, M and S become more realistic as the partial melting proportion P_m and the proportion of calc-alkaline magma that is ultimately converted to sediment P_s are decreased (cf. models KT3 and KT4). Models KT5 and KT6 are considered to be most realistic. The protolith of the Khomas schist body was probably generated over a time span of 100 - 150 Myr, between the dates of about -800 Myr and -650 Myr according to emerging geochronological evidence. Magma generation rates at the time are assumed to have been similar to those estimated for the Central Andes at the present time, i.e. around 2 x 10^{-5} km^3 yr^{-1} (Francis & Rundle, 1976) and the average sedimentation rate in the axis of the trough may have been close to 0,25 mm yr^{-1} (cf. Spencer, 1974).

The length of slab consumed in the models KT5 and KT6 exceeds 6500 km and this estimate is controlled mainly by the assumption that not more than 5% of subducted oceanic crust ultimately contributes to the generation of orogenic

calc-alkaline magma (cf. Francis & Rundle, 1976).

In the present state of knowledge of the Khomas schist, the above calculations have no more than order-of-magnitude significance. The model outlined above attempts to reconcile the large-scale structural geometry of the Khomas Trough, with as yet meagre quantitative data on the gross composition of the rocks contained within it and illustrates how these features can be related to a realistic petrogenetic model for the generation of calc-alkaline rocks. Its primary function at this stage is to draw attention to the obvious but neglected fact that the Khomas schists are an exceptional crustal unit. If the hypothesis outlined in this section is correct, they represent a major opportunity for studying an important stage in the process by which a small proportion of the upper mantle is permanently converted to continental crust.

3. The Matchless Amphibolite: a possible ophiolite

a. Brief review

The thin zone, about 2 km wide, of mafic rocks which extends about 375 km along strike of the Damara orogen from the Namib into the Kalahari (Fig. 67) was first noted by Reuning (1923). Segments of the amphibolite belt were described by de Kock (1934, p.86) and Gevers (1934, p.238-239), the latter noting the presence of chloritic serpentinite near Windhoek. Martin (1965, p.41) described it as a "conspicuous belt of amphibolites and several lenses of serpentinite". At Matchless Mine, the belt comprises two prominent bands of amphibolite, a wider northern band called the "Friedenau Amphibolite" and a thinner southern band called the "Matchless Amphibolite" (Hälbich, 1970). Noting that the Friedenau Amphibolite was the most consistent of the lensoid bands in the amphibolite zone, Hälbich (*op.cit.*, p.60) extended the name to cover the belt as a whole.

The possibility that the amphibolite belt may be an ophiolite complex defining line of suture between two plates which collided in late Precambrian or Cambrian times was first raised by Hartnady (1973), following a qualitative study of ERTS (LANDSAT) imagery of the region (Hartnady, 1974). The photo-

geological expression of the amphibolite belt was then called the "Friedenau Line". However, the term "Matchless Amphibolite Belt" has gained much wider currency among the economic geologists prospecting the feature for iron-copper mineralisation (cf. Viljoen, Viljoen, Grootenboer & Longshaw, 1975) and the unit is now formally known as the Matchless Member of the Kuiseb Formation.

Kröner (1974c)disputed the interpretation of the Matchless Belt as an ophiolite complex, maintaining that pillow structures described by Viljoen (in Anhaeusser & Button, 1974) are really boudinage phenomena and that the Matchless Belt is conformably intercalated in the surrounding Khomas flysch-type metasediments.

Near Windhoek, three different types of amphibolite have been recognised (Finnemore, 1975), *viz.*, calcium-enriched "epidote amphibolite", a "porphyroblastic amphibolite" and magnesium-rich "chlorite-amphibole schist", as well as ultrabasic talc schist. The "porphyroblastic" variety is a relatively coarse-grained amphibolite type resembling a meta-gabbro (Gevers, 1934). Systematic changes in the major and trace element geochemistry of the Matchless rocks are suggestive of the presence of a differentiated suite following the trend for normal tholeiites and picrites (Finnemore, 1975). Metasomatic alteration is considered to be responsible for the departure of the epidote amphibolites from the expected trend and medium-grade metamorphism complicates the use of Pearce & Cann's (1973) method for classifying basaltic rocks according to tectonic setting. Finnemore (*op.cit.*, p.38) also disputes an "ophiolite origin" for the belt on the grounds of a "lack of rock types typically associated with ophiolite complexes".

Martin (1975b,p.95), too, states quite categorically that, in the "ensialic" Damara belt, there "are no ophiolitic masses which could be interpreted as obducted wedges of oceanic crust". However, he also considers (*op. cit.*, p.96) that the amphibolite layers of the Matchless Belt are "in all probability metamorphosed submarine basaltic volcanics", and that the iron-copper sulphide ore deposits occurring in close proximity to the belt "probably belong to the large group of submarine hydrothermal deposits associated with submarine volcanism in most geosynclines".

Goldberg (1976), in an account of the recently discovered Otjihase copper deposit, also notes that it seems "the Otjihase ore derives its origin in deep water having been deposited during volcanic activity together with volcanic rocks, aquagene tuffs and pelagic shales".

b. Comments on the definition of an "ophiolite"

In attempting to interpret the Matchless Amphibolite it is essential in the first place to define precisely what is meant by the term "ophiolite". For this, the definition provided by the 1972 Penrose Ophiolite Symposium (Geotimes, December 1972) and a recent discussion by Gass, Smith & Vine (1975) will suffice.

"Ophiolite" is a *non-genetic* term which serves simply to describe a commonly occurring rock association found in both young and old mountain belts. It is related to the terms "greenstone", "roches vertes" and "Steinmann Trinity". An ophiolite suite or complex is characterised by the presence of three or more of the following rock types in association: serpentinite, dunite, peridotite, pyroxenite, gabbro, basic lava (often pillowed) and radiolarian chert, with flysch being a commonly associated sediment but not part of the actual assemblage which the term describes.

The idealised and complete ophiolite assemblage consists of all the above rock types in a structural/stratigraphic succession which is considered to reflect the well-known geophysical layered structure of the oceanic crust. But this last consideration is a matter of interpretation, which perhaps should not enter into the usage and meaning of the purely descriptive term ophiolite. The two real problems with the application of the term ophiolite to any candidate feature are simply (i) shearing and (ii) metamorphism. Ophiolite associations are usually found in belts of highly deformed rock, hence the ideal, complete ophiolite succession is rather rare. They commonly occur in various states of tectonic dismemberment, in some cases in *mèlanges* in which all or some of the abovementioned components (and some others) are chaotically mixed together.

New data from oceanic exploration suggest that the processes accompanying oceanic crust formation at spreading ridges include complex deformations and

major metamorphism. The simple model of the oceanic crust as a Troodos-type igneous complex may not be globally applicable and is probably not representative of the uppermost Layer 1/ Layer 2 boundary region, which is the part most likely to be sheared off and preserved in an intercontinental suture zone. At DSDP site 334, for example, the drillhole penetrated first a 60 m-thick surface layer of basalt and then a complex sequence of gabbro, olivine gabbro, serpentinized peridotite and breccias consisting of the latter three rock types *with some sedimentary matrix*. Up to 30% of the plutonic sequence drilled consists of sedimentary breccia. It is suggested that tectonic processes at oceanic ridges during the construction of new crust often result in the surface exposure of a kind of plutonic melange, perhaps formed along the rift valley fault or transform fault scarps, which are subsequently buried by basaltic eruptions (Hyndman & Drury, 1976). It is accordingly evident from actual observation that the "ideal" oceanic crustal sequence of sediment - pillow basalt - diabasic dykes - plutonics may be a far-from-realistic description. To argue that the Matchless amphibolite sequence cannot be a tectonic fragment of oceanic crust because, in its original pre-tectonic and pre-metamorphic constitution, it does not appear to exactly match a purely hypothetical ideal, is therefore not rational.

In its general character the Matchless Member is clearly ophiolitic, containing at various points along its length, coarse-grained chromite- and magnetite-bearing ultramafic rocks of evident cumulate origin (Gevers, 1934), differentiated intrusive gabbroic and extrusive basaltic members of tholeiitic affinity (Finnemore, 1975), meta-volcanic rocks with structures and textures indicative of submarine eruption (Kröner, 1976b,1977) and local Fe-Cu-Ag-metalliferous volcanogenic meta-sediments (Viljoen *et al.*, 1975; Goldberg, 1976). This varied assemblage is contained within a single continuous thin zone, but any randomly selected segment of the zone will normally show only one or two of the abovementioned aspects.

The most relevant comparison of the Matchless amphibolite assemblage is not with an idealised, hypothetical, oceanic crustal model, but with similar bodies in Mesozoic-Cenozoic orogenic belts. Interbedding of the Matchless rocks

with surrounding Kuiseb formation flysch does not exclude their interpretation as ophiolites (cf. Kröner, 1974c,1976b). Ophiolitic rocks interstratified with flysch deposits that formed along a continental margin are also known from coastal southern Alaska (Tysdal, Case, Winkler & Clark, 1977). Even in this young belt the precise origin of the ophiolites is controversial, but this question does not alter the main points which are relevant to the present work; namely that the probable Alaskan analogues of the Matchless amphibolite and related bodies originally formed at a continental margin and that they are presently situated within a major trench and volcanic arc system at which oceanic subduction is active. The lithological resemblances between the rock types present in both localities are striking and their structural setting is very similar.

c. Tectonic setting

The Matchless lineament is not the only zone of mafic to ultramafic rock in the southern part of the Damara belt. It is merely the longest and most continuous unit of several serpentinitic amphibolite zones (Höhewarte, Aris, Townlands, Choaberib and others) found in this region (see Fig. 67, after Gevers, 1934; De Waal, 1966; Hälbich, 1970). Only the larger of these bodies can be represented on a small-scale map. It can, however, be seen that the Matchless lineament marks a boundary between a marginal zone of the Khomas geosyncline in which bodies of mafic and ultramafic rock are relatively abundant and an internal zone in which they are absent. The entire southern zone in which these rocks occur is one of intense penetrative deformation and polyphase southward-vergent recumbent folding (Hälbich, 1970). Tectonic strains $\sqrt{\lambda_1/\lambda_3}$ exceeding 20 have been measured close to the Choaberib amphibolite (Hälbich, 1970) and it is probable that severe thrusting (Guj, 1969) has caused multiple repetition of a single stratigraphic zone of mafic rocks. The alternative hypothesis of three (or more) distinct stratigraphic levels of mafic volcanism has yet to be proven or disproven by rigorous analysis of structural geometry.

The Matchless Amphibolite itself lies in a tectonised zone forming a slab dipping north-westwards at an average angle of 30°. The proposal that it marks a transform fault (Wynne-Edwards, 1976) fails to recognise that notwithstanding its almost rectilinear strike, it is a shallow-dipping body. Without exception

all minor deformation structures within this zone of shallow north-westward dip show that the hanging-wall has been displaced a considerable distance south-eastwards over the foot-wall parallel to the trend of a strongly developed north-west plunging lineation. The precise magnitude of this displacement is still arguable in the absence of suitable strain markers, but with an assumed average shear strain γ equal at least to 4, distributed over a zone about 25 km thick, an estimate of 100 km or more is quite reasonable. The structural geometry of bedding, schistosities and quartz veins in a section across the KR-III/KR-IV boundary in the Windhoek-Okahandja region points clearly to the "transposition" character of the main foliation in the zone surrounding the Matchless Amphibolite (Hälbich, 1970). Strongly boudinaged quartz veins, some up to several metres in width, are a characteristic feature of this zone, particularly the foot-wall regions of the Matchless Amphibolite. This generation of veins may be traced northward away from the Matchless lineament, through a zone in which they are folded but not boudinaged, into a region in which they are generally planar and undeformed. Here they can be clearly seen to post-date a subvertical metamorphic banding cleavage (Hälbich, 1970), which is roughly axial-planar to large open synforms in bedding in the northern part of the Khomas geosyncline. The southward increase in intensity of deformation in the Khomas geosyncline results not only in the pronounced change of orientation of this s_1 cleavage but also in its almost complete overprinting by a second schistosity s_2.

The implication of these observations of minor structure and fabric development require more detailed study and elaboration, since they appear to provide a concrete clue to the deformation path (Elliott, 1972) followed by the rock mass surrounding the Matchless Amphibolite in zone KR-III. Boudinage of folded syn-tectonic quartz veins is especially significant. Firstly, it implies early syn-tectonic hydraulic fracturing of deformed and dewatered geosynclinal sediments, at high crustal levels and ambient temperatures less than 250°C so that quartz dissolved from the deforming rock mass at deeper levels was abundantly deposited in the dilatant fractures. Secondly, it implies subsequent downward migration of the rock mass into a different tectonic regime in which plastic buckling of the early formed quartz veins was possible. While there remains no detailed petrofabric study of these rocks, it seems likely

that higher temperature dislocation creep mechanisms were involved at this stage. Thirdly, it shows that directions of original shortening were rotated through the surface of no infinitesimal longitudinal strain (Ramsay, 1967). Very strongly elongated early folds of so-called "intrafolial" style (Turner & Weiss, 1963) are observed not only in quartz veins but also in early lithological layering (?bedding) where the latter is still preserved. Here too the implication, that an early phase of layer-parallel extension, is clear.

With these observations in mind, it is reasonable to assume a kinematic model of progressive simple shear for zone KR-III, in which the orientation of the shear-plane was originally oblique to bedding. The original dihedral angle between bedding and the shear zone is important in determining the subsequent history of bedding-parallel strain. It must have been less than 45°, otherwise no layer-parallel shortening phase will have occurred, but must have been significantly greater than 0°, otherwise layer-parallel extensions will have commenced only at very high shear strains. In a plane-strain shear zone dipping at 15° relative to the original bedding orientation, for example, bedding-parallel longitudinal strain will pass from the compressive phase into the extensional phase at shear strain γ between 3,5 and 4,0 when a line on the bedding surface trending parallel to the shear direction will have been shortened to about one quarter of its original length. The line will be extended to its original length when the shear strain γ reaches 7,5. At this stage if the bedding was originally horizontal it will dip at 30° in the same direction as the shear zone; in other words, complete inversion of the original stratigraphy will have occurred.

In this respect it is significant to recall the observation that the Matchless amphibolites sampled near Windhoek show an inverted differentiation trend, with more ultramafic varieties forming the hanging-wall and more differentiated varieties lying close to the foot-wall (Finnemore, 1975).

It therefore seems clear, from the available structural evidence that the Matchless Amphibolite is located within a zone of the most severe tectonic deformation in the entire Damara orogenic belt, that this zone has the form of a shallow-dipping slab and that the hanging-wall of the slab has been displaced upward over the foot-wall by an amount of the order of 100 km.

CHAPTER VII

CONCLUSIONS

A. Regional Relationships

1. The Naukluft nappe complex is situated within the marginal zone of a tectonically distinct southern province of the Damara orogenic belt centred about a physiographically prominent chain of mountain ranges called the Khomas Ridge.

2. The Khomas Ridge province can be divided into four parallel tectonic zones, labelled KR-I to KR-IV from south to north, each of which on the basis of a recent research review and a LANDSAT analysis is seen to be structurally and stratigraphically distinct, although precise relationships across zone boundaries have yet to be clarified. The northern boundary of the entire Khomas Ridge province is a conspicuous tectonic discontinuity now called the Okahandja Lineament. The southern boundary is a diffuse one situated close to an important stratigraphic unconformity within the northern Nama Group.

3. The Naukluft Mountains/Kharubeam Hills zone (KR-I) is bounded on the north by the Areb mylonite belt, initially identified in the course of this project as a possible root zone of the Naukluft nappe complex which stratigraphically and structurally displays characteristics of both zones KR-I and KR-II.

B. Stratigraphy

1. The stratigraphy of the Naukluft nappe complex has been totally revised and eight lithostratigraphic formations have been defined according to formal stratotype principles as far as is possible in a tectonically disrupted complex. These eight units, in assumed order from oldest to youngest, are:

(i) Noab Formation
(ii) Büllsport Formation
(iii) Remhoogte Formation
(iv) Klipbokrivier Formation
(v) Blässkranz Formation
(vi) Tsabisis Formation
(vii) Aubschlucht Formation
(viii) Zebra River Formation

2. The dolomitic Noab and Büllsport Formations are the beach bar and tidal flat facies, respectively, of a Persian Gulf-type *sabkha* complex facing the open sea to the north and grading southwards into a terrigeneous clastic facies. It is tentatively concluded that they may represent a link between the Klein Aub Formation of zone KR-I and the Duruchaus Formation of zone KR-II, as well as correlating quite obviously with lower southern units of the Swakop Group in the Damara sequence (Martin, 1974).

3. The mainly phyllitic Remhoogte Formation shows the greatest degree of internal structural complexity and the highest degree of metamorphism (lower greenschist facies), and is accordingly the least amenable to formal lithostratigraphic definition. In some respects it resembles a very large scale tectonic *melange* complex.

4. The Blässkranz Formation overlies the Remhoogte Formation unconformably and contains carbonate breccias of olistostromic, of sedimentary slump origin which apparently formed in the course of several "stick-slip-slide" cycles above a zone of active faulting. These submarine slides were probable precursors to the later southward overthrusting of the Kudu nappe.

5. The Tsabisis Formation includes a unique lower division of felsic volcaniclastic rocks, evidently derived from a volcanic source of a highly explosive type. Together the conformable Blässkranz and Tsabisis Formations comprise a lithological association with marked resemblance to sequences elsewhere known, or inferred, to have formed in subduction zones between colliding continental plates.

6. The Aubschlucht Formation in the enigmatic S. Pavian nappe contains reddish, coarse-grained, arkosic quartzites and conglomerates probably deposited in a fluviatile environment in which clastic particles became thinly coated with fine hematite. It is unique in the Naukluft complex, but is very tentatively correlated with the immediately pre-Nama Kamtsas Formation of zone KR-I. Together with the correlation of the Büllsport and Klein Aub Formations tentatively proposed in paragraph B.2 above, this represents a serious challenge to existing models of Damara belt stratigraphy which associate the Kamtsas Formation with the north Damaran Nosib Group.

7. The Zebra River Formation is a northern basin edge facies of the Kuibis Formation in the Nama Group which is conspicuously unconformable upon the Büllsport Formation. It is subdivided into five members which, from oldest to youngest, are:

(i) Neuras Member
(ii) Ubusis Member
(iii) Tsams Member
(iv) Lemoenputs Member
(v) Onis Member

Their mapping in the south-western Naukluft complex illustrates the major difference in structural style across the Büllsport-Zebra River unconformity.

C. Naukluft structural geology

1. Five major nappe units are distinguished in the Naukluft complex, and are stacked in large-scale imbricate sequence from north to south, highest to lowest, as follows:

(v) Kudu nappe
(iv) N. Pavian nappe
(iii) S. Pavian nappe
(ii) W. Dassie nappe
(i) E. Dassie nappe

2. Nappe boundaries do not in general coincide with the boundaries between lithostratigraphic units, but cut across them spectacularly in places.

3. The earliest recognisable, important tectonic episode (D_1) in the Naukluft complex is the pre-Blässkranz deformation of the Remhoogte Formation, which is also reflected in the more complex character of S_1 phyllitic fabrics in this unit and the more complex orientation patterns of L_1 fabrics.

4. The major tectonic episode of the northern Naukluft complex was the D_2 thrusting of the Kudu nappe over the Remhoogte, Blässkranz and Tsabisis Formations. At this stage, the Kudu nappe comprised both the massive Noab dolomites and the well-bedded Büllsport dolomites which had become imbricated at the leading edge of the nappe.

5. The Aubschlucht Formation may then have been deposited in a sediment-choked foredeep trough, and the basal members of the Zebra River Formation were laid down in a subsequent marine transgression, disconformably on the Aubschlucht beds, but with a pronounced unconformity on the D_2-imbricated Büllsport dolomites in the Kudu nappe front.

6. Southward nappe translation recommenced in the D_3 episode with the detachment of the Remhoogte, Blässkranz and Tsabisis Formations from their original substratum to form the N. Pavian nappe, the extensive large-scale imbrication of the frontal zones of the original Kudu and N. Pavian nappes to form the E. Dassie and W. Dassie nappes, and the deformation of the lower members of the Zebra River Formation in the W. Dassie and S. Pavian nappes.

7. The upper members of the Zebra River Formation were deposited with locally disconformable and unconformable contacts on the lower Zebra River units and were folded during the subsequent D_4 episode.

8. Structures of all pre-existing episodes were truncated at the basal overthrust surface of the Naukluft nappe complex when it was finally emplaced in its present position, overlying the lower Nama Group, during the D_5 episode.

9. A minimum total displacement vector of 78 km from azimuth 331^{o} is

estimated for a reference point in the frontal zone of the Naukluft nappe complex, this being the resultant of displacements of 49 km from azimuth 350° during D_1-D_3, and 35 km from azimuth 305° during D_4-D_5. This places the tectonic provenance of the Kudu nappe in the Naukluft complex well north of the Areb mylonite zone in the northern part of zone KR-II.

10. The arcuate form of the imbricate frontal zone in the south-central part of the Naukluft complex and much of the relatively steeply dipping deformation in the frontal part of the N. Pavian nappe is due to indentation of its surroundings by the massive central dolomite of the Kudu nappe. This reflects, on the largest scale, the extreme contrast in ductility between the dolomites and other lithological components of the nappe complex.

D. Nappe dynamics

1. The evidence of the formation of 10-30 m thick marble zones containing isoclinal, intrafolial and locally refolded fold structures along the main D_2 overthrust surfaces is interpreted, on the basis of recent experimental and theoretical studies, as indicating relatively high basal shear stresses of between 25-50 MPa during Kudu nappe emplacement at a temperature close to 400°C and a possible confining pressure of 400 MPa. A 33 km nappe displacement can have occurred over a period of only 1 Myr at a reasonable strain rate, in the *decollement* zone, of about 4×10^{-11} s^{-1}. The maximum time-span available for Naukluft deformation (about 150 Myr) places a minimum limit of about 10^{-13} s^{-1} on the strain rate and 20 MPa on the shear stress in the Kudu nappe marble zones, according to modern experimental data.

2. In contrast, the D_5-related sole thrust of the Naukluft complex, now containing the remarkable Unconformity Dolomite, was very effectively lubricated by a material similar to that which has also given rise to the Alpine *rauhwackes* or *cornieules*, so that basal shear stress in this phase of nappe emplacement did not exceed about 5 MPa. It is tentatively postulated that the (halide?) precursor to the Unconformity Dolomite was not

derived from pre-existing sedimentary evaporite deposits, but formed *in situ* by very low-grade hydrothermal metamorphic reactions between the dolomite nappe complex and its cooler pelitic substratum.

3. Although the simple gravity gliding theory of Naukluft nappe emplacement is ruled out by the geometrical boundary conditions implied by paragraphs D. 1 and D. 2 above, a preliminary analysis of nappe dynamics in terms of the modern theory of gravitational spreading shows that gravitational forces, due to a significant southward surface slope away from the axis of the Khomas Ridge province in zone KR-II, can have effectively overwhelmed the possible contribution of longitudinal compressive forces during Kudu nappe emplacement even if a "hard" sliding law and a relatively high basal shear stress is assumed. Gravitational forces are likely to have been dominant during the D_5 emplacement of the whole Naukluft complex only if the cohesion of the basal sliding surface was very low, as implied in paragraph D. 2 above.

E. Damara belt geodynamics

1. It is postulated, on the grounds of large-scale structural geometry and composition, that the extensive schist infilling of the Khomas Trough was derived by rapid erosion of a youthful andesitic volcanic provenance, and that model calculations with volumetric data can be used to estimate the lateral extent of oceanic crustal subduction necessary to produce such a thick continental margin deposit. These calculations lead to estimates of the former extent of oceanic crust between the Okahandja Lineament and the Naukluft nappe complex in the range 530-6667 km, with the most acceptable "compromise" model (KT4) yielding an estimate of 5000 km.

2. The distribution of the larger mafic and ultramafic "ophiolites" of the Khomas Ridge in tectonic zones KR-II and KR-III is compatible with the model of the Khomas Trough as a convergent continental margin, but the question of whether or not these bodies actually represent obducted oceanic crust has yet to be resolved. The conspicuous Matchless Amphibolite which is centrally situated in zone KR-III is, over almost all of its length,

the effective northern terminator of the Damaran "ophiolite" occurrences.

3. The tectonic setting of the Matchless Amphibolite, and the structural style of the surrounding schists in zone KR-III is indicative of extensive southward translation of zone KR-IV relative to zone KR-II, above a shallow (30^{o}) northward-dipping zone of simple shear. Zone KR-III is interpreted as a 10-20 km thick slab of distributed boundary layer shear between the northern overriding plate and the southern underthrusting Kalahari craton.

4. The large-scale orogenic attributes of the Khomas Ridge province as noted in paragraphs E. 1 - E. 3 are reconcilable with the conclusions drawn for the stratigraphic and tectonic development of the Naukluft nappe complex in paragraphs B. 2 - D. 3, but much more clarity has yet to be achieved about the accurate timing and correlation of depositional, deformational and also metamorphic events in the southern marginal zones of the Damara orogenic belt.

5. The Naukluft complex should be regarded as a relatively unmetamorphosed and undeformed representative of the stratigraphic and structural complication which is likely to be encountered in a detailed analysis of any part of the more northerly zone KR-II and future researchers in that terrain should be on guard against the possibility of major unrecognised stratigraphic inversion.

REFERENCES

Annhaeusser, C.R. & Button, A., 1974 - A review of southern African stratiform ore deposits - their position in time and space. *Econ. Geol. Res. Unit, Univ. Witwatersrand, Inf. Circ.* 85, p.

Atwater, T., 1970 - Implications of plate tectonics for the Cenozoic tectonics of western North America. *Geol. Soc. Amer. Bull.*, 81, 3513-3536.

Bailey, E.B., 1910 - Recumbent folds in the schists of the Scottish Highlands. *Q. Jl geol. Soc. Lond.*, 66, 586-620.

Beloussov, V.V., 1962 - *Basic Problems in Geotectonics*. Mc Graw Hill, N.Y., 809 p.

Bertrand, M., 1884 - "Rapports de Structure des Alpes de Glaris & du Bassin Houllier du Nord" *Geol. Soc. France Bull. ser. 3*, v.xii, 318 p.

Bickle, M.J. & Coward, M.P., 1977 - A major thrust in the southern Damara belt, Namibia. *20th ann. Rep. res. Inst. afr. Geol., Univ. Leeds*, 8-17 .

Birch, F., 1965 - Speculations on the Earth's thermal history. *Geol. Soc. Amer. Bull.*, 76, 133-153.

Blaine, J.L., 1977 - Tectonic evolution of the Waldau Ridge structure and the Okahandja Lineament in part of the Central Damara Orogen, west of Okahandja, South West Africa. *Bull. Precambr. Res. Unit, Univ. Cape Town*, 21 95p.

Botha, B.J.V., Gunter, C.J., Koornhof, J.C., Schoeman, P.J., Tordiffe, E.A.W. & Van Reenen, D.D., 1974 - Die Sisteem Damara in die Gebied tussen Uis en Kaap Kruis. *Ann. geol. Surv. S. Afr.*, 9, (for 1971-2), 57-67 .

Bott, M.H.P. & Dean, D.S., 1972 - Stress systems at young continental margins *Nature Phys. Sci.*, 235, 23-25.

Bouillé, F., 1976 - A model of scientific data bank and its applications to geological data. *Computers & Geosciences*, 2, 279-291 .

Bowen, R.W. & Botbol, J.M., 1975 - The Geologic Retrieval and Synopsis Program (GRASP). *U.S. Geol. Surv. Prof. Paper*, 966, 87 p.

Bullard, E.C., Everett, J.E. & Smith, A.G., 1965 - The fit of the continents around the Atlantic. *Phil. Trans. R. Soc. Lond. A*, 258, 41-51 .

Burger, A.J., Clifford, T.N. & Miller, R. McG., 1976 - Zircon U-Pb ages of the Franzfontein granitic suite, northern South West Africa. *Precambrian Research*, 3, 415-431 .

_____, & Coertze, F.J., 1973 - Radiometric age measurements on rocks from Southern Africa to the end of 1971 - *Geol. Surv. S. Afr. Bull.* 58, 46 p.

Burger, A.J. & Coertze, F.J., 1975 - Addendum to Bulletin 58 : Age determinations - April 1972 to March, 1974. *Ann. geol. Surv. S. Afr.*, 10, (for 1973-4), 135-141.

Burke, K., Dewey, J.F. & Kidd, W.S.F., 1976 - Dominance of horizontal movements, arc and microcontinental collisions during the later permobile regimes. In: Windley, B.F. (ed.), *The Early History of the Earth.* Wiley, London, 113-129.

Cahen, L., 1970 - Igneous activity and mineralization episodes in the evolution of the Kibaride and Katangide orogenic belts of Central Africa. In: Clifford, T.N. & Gass, I.G. (eds.), *African Magmatism and Tectonics : A volume in honour of W.Q. Kennedy FRS.* Oliver & Boyd, Edinburgh, 1-26.

Chayes, F., 1969 - The chemical composition of Cenozoic andesite. *Proc. Andesite Conference. Oreg. Dept. Geol. Min. Ind. Bull.*, 65, 1-11.

Christoffel, D.A. & Calhaem, I., 1973 - Upper mantle viscosity determined from Stokes's law. *Nature*, 243, 51-52 .

Clemmey, H., 1977 - Aspects of stratigraphy, sedimentology and ore genesis on the Zambian Copperbelt with special reference to Rokana Mines (Ph.D. thesis, Abstract) - *20th ann. Rep. res. Inst. afr. Geol., Univ. Leeds*, 20-21 .

Clifford, T.N., 1967 - "The Damaran Episode in the Upper Proterozoic - Lower Palaeozoic structural history of Southern Africa." - *Geol. Soc. Amer., Spec. Paper No. 92*, 100 p.

_____, Rex, D.C. & Snelling, N.J., 1967 - Radiometric age data for the Urungwe and Miami granites of Rhodesia. *Earth Planet. Sci. Lett.*, 2, 5-12.

_____, Martin, H. & Nicolaysen, L.O., 1972 - A proposed joint Göttingen-South African Geodynamics Project in the Damara Orogen. *Unpublished manuscript of S.A. Committee for the International Union of Geological Sciences (SACUGS)*, 4 p.

Cloos, H., Korn, H. & Martin, H., 1937 - Das Naukluftgebirge in Südwestafrika. *Geol. Rdsch.*, 28.

Cloud, P.E., Jr & Semikhatov, M.A., 1969 - Proterozoic stromatolite zonation. *Amer. J. Sci.*, 267, 1017-1061.

_____, & Wright, L.A., Williams, E.G., Diehl, P. & Walter, M.R., 1974 - Giant stromatolites and associated vertical tubes from the Upper Proterozoic Noonday Dolomite, Death Valley region, Eastern California. *Geol. Soc. Amer. Bull.*, 85, 1869-1882.

Collet, L.W., 1935 - *The structure of the Alps.* Arnold, London.

De Beer, J.H., Gough, D.I. & Van Zijl, J.S.V., 1975 - An electrical conductivity anomaly and rifting in Southern Africa. *Nature*, 225, 678-680.

_____, van Zijl, J.S.V., Huyssen, R.M.J., Hugo, P.L.V., Joubert, S.J. & Meyer, R., 1976 - A magnetometer array study in South-West Africa, Botswana and Rhodesia. *Geophys. J.R. astr. Soc.* 45, 1-17 .

Debelmas, J. & Kerckhove, C., 1973 - Large gravity nappes in the French-Italian and French-Swiss Alps. In: De Jongh, K.A. & Scholten, R. (eds.), *Gravity and Tectonics*, Wiley Intersci. N.Y., 189-200.

De Kock, W.P., 1934 - The geology of Western Rehoboth : An explanation of Sheet F. 33-W-3 (Rehoboth). *S.W.A. Dept. of Mines, Mem. 1, Windhoek*, 148 p.

Dennis, J.G., 1967 - *International Tectonic Dictionary : English Terminology*. Amer. Assoc. Petroleum Geologists, Tulsa, 196 p.

De Sitter, L.U., 1956 - *Structural Geology*. McGraw-Hill, Tokyo, 522 p.

De Villiers, J. & Simpson, E.S.W., 1974 - Late-Precambrian tectonic patterns in south-western Africa. *Bull. Precambr. Res. Unit, Univ. Cape Town*, 15, 141-152.

De Waal, S.A., 1966 - *The Alberta Complex, a metamorphosed layered intrusion, north of Nauchas, South West Africa, the surrounding granites and repeated folding in the younger Damara System.* Unpubl. D.Sc. Thesis, University of Pretoria, 207 p.

Dewey, J., 1975 - Finite plate implications : Some implications for the evolution of rock masses at plate margins. In: Ostrom, J.H. & Orville, P.M. (eds.), *Tectonics and Mountain Ranges : The Rodgers Volume*, Amer. J. Sci., 275-A, 260-284.

_____, & Bird, J.M., 1970 - Mountain belts and the new global tectonics. *J. Geophys. Res.*, 75, 2625-2647.

_____, Pitman, W.C., Ryan, W.B.F. & Bonnin, J., 1973 - Plate tectonics and the evolution of the Alpine System. *Geol. Soc. Amer. Bull.*, 84, 3137-3180.

Dieterich, J.H. & Onat, E.T., 1969 - Slow finite deformation of viscous solids *J. Geophys. Res.*, 74, (8), 2081-2088.

Douglas, A., 1970 - Finite elements for geological modelling. *Nature*, 226, 630-631.

Dunnet, D. & Siddans, A.W.B., 1971 - Non-random sedimentary fabrics and their modification by strain. *Tectonophysics*, 12, 307-325.

Elliott, D., 1972 - Deformation paths in structural geology. *Geol. Soc. Amer., Bull.* 83, 2621-2638.

_____, 1973 - Diffusion flow laws in metamorphic rocks. *Geol. Soc. Amer. Bull.*, 84, 2645-2664.

_____, 1976a - The motion of thrust sheets. *J. Geophys. Res.* 81, 949-963.

_____, 1976b - The energy balance and deformation mechanisms of thrust sheets. *Phil. Trans. R. Soc. Lond. A.283*, 289-312.

Elsasser, W.M., 1969 - Pattern of convection creep in the Earth's mantle. In: Argon, A.S. (ed.), *Physics of Strength and Plasticity*, M.I.T. Press, Cambridge, Mass. 367-375.

Emery, K.O., Uchupi, E., Bourin, C.O., Phillips, J. & Simpson, E.S.W., 1975 - Continental margin off Western Africa. Cape St. Francis (South Africa) to Walvis Ridge (South West Africa). *Bull. Amer. Assoc. Petrol. Geol.*, 59, 3-59.

Evans, G., Murray, J.W., Biggs, H.E.J., Bate, R. & Bush, P.R., 1973 - The oceanography, ecology, sedimentology and geomorphology of parts of the Trucial Coast barrier island complex, Persian Gulf. In: Purser, B.H. (ed.) *The Persian Gulf*, Springer-Verlag, Berlin, 233-277.

Faupel, J., 1974 - Geologisch-mineralogische Untersuchungen am Donkerhoek-Granit (Karibib-District, Südwestafrika). *Göttinger Arb. Geol. Paläont.* 15, 95 p.

Finnemore, S.H., 1975 - Major and trace element studies on units of the Matchless Amphibolite belt, Windhoek district, S.W.A. In: *Geokongres 75 : Mineralization in Metamorphic Terranes* Abstracts volume, Univ. Stellenbosch, 36-39.

Forsyth, D. & Uyeda, S., 1975 - On the relative importance of the driving forces of plate motion. *Geophys. J.R. astr. Soc.*, 43, 163-200.

Francis, P.W. & Rundle, C.C., 1976 - Rates of production of the main magma types in the central Andes. *Geol. Soc. Amer. Bull.*, 87, 474-480.

Frets, D.C., 1969 - Geology and structure of the Huab-Welwitschia area South West Africa. *Bull. Precambr. Res. Unit, Univ. Cape Town*, 5, 235p.

Frey, M., 1973 - Progressive niedriggradige Metamorphose glaukonitführender Horizonte in den Helvetischen Alpen. *Contr. Mineral. Petrol.* 39, 185-218 .

Froidevaux, C. & Schubert, G., 1975 - Plate motion and structure of the continental asthenosphere: A realistic model of the upper mantle. *J. Geophys. Res.*, 80, 2553-2564 .

_____, C., Schubert, G. & Yuen, D.A., 1976 - Thermal and mechanical structure of the upper mantle : A comparison between continental and oceanic models. *Tectonophysics*, 37, 233-246 .

Fuller, A.O., 1972 - Possible fracture zones and rifts in Southern Africa. In: Shagam, R. *et.al.* (eds.), *Studies in Earth and Space Sciences*. Geol. Soc. Amer. Mem. 132, 159-172 .

Gass, I.G., Smith, A.G. & Vine, F.J., 1975 - Origin and emplacement of ophiolites. In: *Geodynamics Today : A review of the Earth's dynamic processes*, R. Soc., London, 55-64.

Gay, N.C., 1968a - The motion of rigid particles embedded in a viscous fluid during pure shear deformation of the fluid. *Tectonophysics 5, (2)*, 81-88.

Gay, N.C., 1968b - Pure shear and simple shear deformation of inhomogeneous viscous fluids. I : Theory. *Tectonophysics, 5, (3),* 211-234.

Geodynamics project in South Africa, The, 1975 - *Interim report on the South African National Programme presented to the Inter-Union Commission on Geodynamics.* C.S.I.R. Pretoria, 22 p.

Geotimes, 1972 - GSA Penrose Field Conference : ophiolites. *Geotimes, 17,* 24-25.

Germs,G.J.B.,1972 - The stratigraphy and palaeontology of the lower Nama group South West Africa. *Bull. Precambr. Res. Unit, Univ. Cape Town, 12,* 250 p.

_____, 1974 - The Nama Group in South West Africa and its relationship to the Pan-African geosyncline. *J. Geol., 82,* 301-317.

_____, 1975 - Silicification structures from the Upper Otavi Group and the significance of chert in this unit. *Trans. geol. Soc. S.Afr., 78,* 67-70.

Gevers, T.W., 1931a - An ancient tillite in South West Africa. *Trans. geol. Soc. S. Afr., 34,* 1-17.

_____, 1931b - *The Fundamental Complex of Western Damaraland, South West Africa.* Unpubl. D.Sc. thesis, Univ. Cape Town,163 p.

_____, 1934 - The geology of the Windhoek district in South West Africa. *Trans. geol. Soc. S.Afr., 37,* 221.251.

_____, 1963 - Geology along the northwestern margin of the Khomas Highlands between Otjimbingwe-Karibib and Okahandja, South West Africa. *Trans. geol. Soc. S.Afr., LXVI,* 199-251.

Gignoux, M., 1948 - La tectonique d'ecoulement par gravite et la structure des Alpes : *Soc. Geol. France Bull. 18,* 739-671.

Glaessner, M.F., 1969 - Trace fossils from the Precambrian and basal Cambrian. *Lethaia, 2,* 369-393.

Goldberg, I., 1976 - A preliminary account of the Otjihase copper deposit, South West Africa. *Econ. Geol., 71,* 384-390.

Goudie, A., 1972 - Climate, weathering, crust formation, dunes and fluvial features of the Central Namib Desert, near Gobabeb, South West Africa. *Madoqua, series II,* 1 (54-62), 15-31.

Gough, D.I., 1973 - Dynamic uplift of Andean mountains and island areas. *Nature Physical Science, 242,* 39-41.

Grubbs, K.L. & Van der Voo, R., 1976 - Structural deformation of the Idaho-Wyoming overthrust belt (U.S.A.) determined by Triassic palaeomagnetism. *Tectonophysics, 33,* 321-336.

Guj, P., 1969 - Structural geology of the Auas Mountains, Windhoek District, South West Africa. *Ann. geol. Surv. S.Afr., 6 (for 1967),* 55-62.

Guj, P., 1970 - The Damara mobile belt in the south-western Kaokoveld South West Africa. *Bull. Precambr. Res. Unit, Univ. Cape Town, 8,* 168 p.

_____, 1974 - A revision of the Damara stratigraphy along the southern margin of the Kamanjab inlier, South West Africa. *Bull. Precambr. Res. Unit, Univ. Cape Town, 15,* 167-176.

Haack, U., 1976 - Rekonstruktion der Abkühlungsgeschichte des Damara-Orogens in Südwest-Afrika mit Hilfe von Spaltspuren-Altern. *Geol. Rdsch., 65,* 967-1002.

_____ & Hoffer, E., 1976 - K/Ar ages of biotites from the Damara-orogen, South West Africa. *Trans. geol. Soc. S.Afr., 79,* 213-216.

Haarman, E., 1930 - *Die Oszillationstheorie.* Enke, Stuttgart, 260 p.

Hafner, W., 1951 - Stress distributions and faulting. *Geol. Soc. Amer. Bull., 62,* 373-398.

Hälbich, I.W., 1970 - *The geology of the Western Windhoek and Rehoboth Districts: A stratigraphic - structural analysis of the Damara System.* Unpubl. D.Sc. thesis, Univ. Stellenbosch, 199 p.

Handley, J.R.F., 1965 - General geological succession on the Farm Klein Aub 350, and environs, Rehoboth district, South West Africa. *Trans. geol. Soc. S.Afr., 68,* 211-224.

Harland, W.B., 1975 - The two geological time scales. *Nature, 253,* 505-507.

Harper, J.F., 1975 - On the driving forces of plate tectonics. *Geophys. J.R. Astron. Soc., 40,* 465-474.

Hartnady, C.J.H., 1973 - *A new model for the Damaran Orogeny.* Unpubl. Ms. to S.A. Committee for IUGS, 4 p.

_____, 1974 - Structural investigations in the Naukluft Mountains : A preliminary report. *Ann. Rep. Precambr. Res. Unit, Univ. Cape Town, 10-11,* 83-88.

_____, 1975a - Progress Report on the Naukluft Mountains Project. *Ann. Rep. Precambr. Res. Unit, Univ. Cape Town, 12,* 47-55.

_____, 1975b - An ERTS-1 view of the southwestern part of the Damaran mobile belt (abstract). *Ann. Rep. Precambr. Res. Unit, Univ. Cape Town, 12,* 60.

_____, 1976 - Tectonic development of the Naukluft nappe complex. *Ann. Rep. Precambr. Res. Unit, Univ. Cape Town, 13,* 33-36.

_____ & Vajner, V., 1975 - Formulation of a tectonic data-base. In: *Geokongres 75 : Mineralization in Metamorphic Terranes.* Abstracts volume, Univ. Stellenbosch, 50-53.

Hawkesworth, C.J., Miller, R. McG. & Roddick, J.C., 1977 - Geochronology on the Damarides, South West Africa. *9th Colloquium Afr. Geol., Univ. Göttingen Abstracts, 44.*

Heard, H.C., 1976 - Comparison of the flow properties of rocks at crustal conditions. *Phil. Trans. R. Soc. Lond.* A.283, 173-186.

Hedberg, R.M., 1975 - *Stratigraphy of the Ovamboland Basin, South West Africa.* Unpubl. Ph.D. thesis, Harvard Univ.

Hobbs, B.E., 1971 - The analysis of strain in folded layers. *Tectonophysics, 11,* 329-375.

Hoffer, E., 1975 - Die zeitliche Beziehung zwischen Tektogenese und Metamorphose : Ein Beitrag zur Rekonstruktion der thermischen Geschichte des Damara-Orogens. In: Martin, H., (reporter) *Stoffbestand, Tektonik, Metamorphose und Granitbildung im Damara-Orogen,* Bericht des Sonderforschungsbereiches 48 : Projektbereich B. Georg-August-Univ., Göttingen, 170-183.

_____, & Puhan, D., 1975 - Isoreaktionsgrade in den Metapeliten des Damara-Orogens. In: Martin, H., (reporter), *Stoffbestand, Tektonik, Metamorphose und Granitbildung im Damara-Orogen,* Bericht des Sonderforschungsbereiches 48 : Projektbereich B. Georg-August-Univ., Göttingen, 111-151.

Hoffman, K.H., 1972 - *Geological report on area north-east of Rosh Pinah in South West Africa.* Unpubl. Honours Project, Univ. Cape Town, 27 p.

Holmes, A., 1965 - *Principles of Physical Geology.* Nelson, London, 1288 p.

Hubbert, M.K. & Rubey, W.W., 1959 - Role of fluid pressure in mechanics of overthrust faulting : 1. Mechanics of fluid-filled porous solids and its application to overthrust faulting. *Geol. Soc. Amer. Bull.,* 70, 115-166.

Hudleston, P.J., 1976 - Recumbent folding in the base of the Barnes Ice Cap, Baffin Island, Northwest Territories, Canada. *Geol. Soc. Amer. Bull.,* 87, 1684-1692.

Hugo, P.J. & Schalk, K.E.L., 1974 - The isotopic ages of certain granites and acid lavas in the Rehoboth and Maltahöhe Districts, South West Africa. *Ann. geol. Surv. S. Afr.,* 9, (for 1971-2), 103-105.

Hyndman, R.D. & Drury, M.J., 1976 - The physical properties of oceanic basement rocks from deep drilling on the Mid-Atlantic Ridge. *J. Geophys. Res.,* 81, 4042-4060.

Jacob, R.E., 1974 - Geology and metamorphic petrology of part of the Damara orogen along the lower Swakop river, South West Africa. *Bull. Precambr. Res. Unit, Univ. Cape Town,* 17, 185 p.

_____, Burger, A.J. & Kröner, A., 1977 - Areal extent and preliminary ages of pre-Damara basement in the central Damara belt of South West Africa. *9th Colloquium Afr. Geol., Univ. Göttingen, Abstracts, 48.*

Kaiser, E., 1926 - *Die Diamantenwüste Südwestafrikas.* Mit Beitragen von W. Beetz, J. Böhm, R. Martin, R. Rauff, M. Storz, E. Stromer, W. Weissermel, und K. Willman. Dietrich Reimer, Berlin. 2 vol.

Kasch, K.W., 1976 - A preliminary report on the geology of the southern margin of the Damara orogen around Omitara, South West Africa. *Ann. Rep. Precambr. Res. Unit, Univ. Cape Town, 13,* 102-138.

Kehle, R.O., 1970 - Analysis of gravity sliding and orogenic translation. *Geol. Soc. Amer. Bull. 81,* 1641-1664.

Kindle, C.H. & Whittington, H.B., 1958 - Stratigraphy of the Cow Head region, Western Newfoundland. *Geol. Soc. Amer. Bull., 69,* 315-342.

King, C. & Knopoff, L., 1968 - Stress drop in earthquakes. *Bull. Seism. Soc. Amer., 58,* 249-257.

Kleywegt, R.J., 1967 - *The gravity survey of South West Africa.* Unpubl. Ph.D. thesis, Univ. Natal

Kohlstedt, D.L., Goetze, C. & Durham, W.B., 1976 - Experimental deformation of single crystal olivine with application to flow in the mantle. In: Strens, R.G.J. (ed.), *The Physics and Chemistry of Minerals and Rocks.* John Wiley, New York, 35-50.

Korn, H. & Martin, H., 1951 - The seismicity of South West Africa. *Trans. geol. Soc. S. Afr., 54,* 85-88.

_____, & Martin, H., 1959 - Gravity tectonics in the Naukluft Mountains of South West Africa. *Geol. Soc. Amer. Bull. 70,* 1047-1078.

Kröner, A., 1971 - Late-Precambrian correlation and the relationship between the Damara and Nama Systems of South West Africa. *Geol. Rdsch. 60,* 1513-1523.

_____, 1974a - Editorial comments concerning the present confusion over lithostratigraphic nomenclature and a proposal for a new Damara terminology. *Bull. Precambr. Res. Unit, Univ. Cape Town, 15,* 139-140.

_____, 1974b - The Gariep Group: Part I - Late Precambrian formations in the western Richtersveld, northern Cape Province. *Bull. Precambr. Res. Unit, Univ. Cape Town, 13,* 115 p.

_____, 1974c - Note on the alleged occurrence of pillow lavas in the southern Damara Belt. In: Kröner, A. (ed.), *Contributions to the Precambrian geology of Southern Africa : A volume in honour of John de Villiers,* Bull. Precambr. Res. Unit, Univ. Cape Town, 15, 177-181.

_____, 1974d - Report on Mixtite Field Excursion in South Africa, South West Africa and Angola. *Ann. Rep. Precambr. Res. Unit, Univ. Cape Town, 10-11,* 93-97.

_____, 1976a - Geochronology. *Ann. Rep. Precambr. Res. Unit, Univ. Cape Town, 13,* 139-143.

Kröner, A., 1976b - Preliminary report on geological investigations of portions of the Matchless amphibolite belt and environs. *Ann. Rep. Precambr. Res. Unit, Univ. Cape Town,* 13, 37-41.

_____, 1977 - Precambrian mobile belts of southern and eastern Africa - ancient sutures or sites of ensialic mobility? A case for crustal evolution towards plate tectonics. *Tectonophysics,* 40, 101-135.

_____, Halpern, M., Clauer, N., Hawkesworth, C.J. & Jacob, R.E., 1977 - Timing of polymetamorphism and deformation in the Pan-African Damara belt of Namibia as deduced from near Rb-Sr chronologic data. *9th Colloquiem Afr. Geol., Univ., Göttingen, Abstracts, 52-53.*

_____, & Jackson, M.P.A., 1974 - Geological reconnaissance of the coast between Lüderitz and Marble Point, South West Africa. *Bull. Precambr. Res. Unit, Univ. Cape Town,* 15, 79-103.

_____, & Rankama, K., 1972 - Late Precambrian glaciogenic sedimentary rocks in Southern Africa : A compilation with definitions and correlations. *Bull. Precambr. Res. Unit, Univ. Cape Town,* 11, 1-37.

Kuhn, T.S., 1970 - *The structure of scientific revolutions.* 2nd ed. Chicago Univ. Press, 210 p.

Kupfer, D.H., 1960 - Thrust faulting and chaos structure, Silurian Hills, San Bernadino County, California. *Geol. Soc. Amer. Bull.,* 71, 181-214.

Lambert, R. St. J., 1976 - Archean thermal regions, crustal and upper mantle temperatures, and a progressive evolutionary model for the Earth. In: Windley, B.F. (ed.), *The Early History of the Earth.* Wiley, London, 363-373.

Larson, R.L. & Ladd, J.W., 1973 - Evidence for the opening of the South Atlantic in the Early Cretaceous. *Nature,* 246, 209-212.

Lee, W.H.K. & Uyeda, S., 1965 - Review of heat flow data. In: Lee, W.H.K. (ed.), *Terrestrial heat flow,* Geophys. Monogr. No. 8, Amer. Geophys. Union, Washington D.C., 87-190.

Le Fort, P., 1975 - Himalayas : The collided range. Present knowledge of the continental arc. In: Ostrom, J.H. & Orville, P.M. (eds.), *Tectonics and Mountain Ranges; The Rodgers Volume,* Amer. J.Sci., 275-A, 1-44.

Lemoine, M., 1973 - About gravity-gliding tectonics in the Western Alps. In: De Jong, K.A. & Scholten, R. (eds.), *Gravity and Tectonics,* Wiley Intersci, N.Y., 201-216.

Lepersonne, J., 1974 - Notice explicative de la Carte géologique du Zäire au 1/2.000.000. *Rep. Zäire, Dept. Mines, Div. Géol.*

Le Pichon, X., 1968 - Sea-floor spreading and continental drift. *J. Geophys. Res.,* 73, 3661-3697.

_____, Francheteau, J. & Bonnin, J., 1973 - *Plate Tectonics.* Elsevier, Amsterdam, 300 p.

Lliboutry, L., 1974 - Rheological properties of lithosphere. *Tectonophysics*, *24*, 13-29.

Longwell, C.R., 1951 - Megabreccia developed downslope from large faults. *Amer. J. Sci.*, *249*, 343-355.

Loudon, T.V., 1964 - Computer analysis of orientation data in structural geology. *Tech. Rep. Geog. Branch Off. Naval Res.*, O.N.R. Task No. 389-135, Contr. No. 1228(26), No. 13, 1-130.

Mabbutt, J.A., 1955 - Erosion surfaces in Namaqualand and ages of surface deposits in the south-western Kalahari. *Trans. geol. Soc. S. Afr.*, *58*, 13-30.

Mahtab, M.A., Bolstad, D.D., Alldredge, J.R. & Shanley, R.J., 1972 - Analysis of fracture orientations for input to structural models of discontinuous rock. *U.S. Bureau of Mines, Rep. Invest. 7669*, 76 p.

Martin, H., 1953 - Notes on the Dwyka succession and on some pre-Dwyka valleys in South West Africa. *Trans. geol. Soc. S. Afr.*, *56*, 37-41.

_____, 1965 - *Precambrian Geology of S.W.A. and Namaqualand.* Precambr. Res. Unit, Rustica Press, Wynberg, C.P.

_____, 1974 - Damara rocks as nappes on the Naukluft mountains, South West Africa. In: Kröner, A. (ed.), *Contributions to the Precambrian geology of Southern Africa.* Bull. Precambr. Res. Unit, Univ. Cape Town, 15, 153-165.

_____, 1975a - Structural and palaeogeographical evidence for an Upper Palaeozoic sea between Southern Africa and South America. In: Campbell, K.S.W. (ed.), *Gondwana Geology : Papers presented at the Third Gondwana Symposium, Canberra, Australia, 1973.* Austral. Nat. Univ. Press, 37-51.

_____, 1975b - The mineralization of the ensialic Damara orogenic belt. In: *Geokongress 75 : Mineralization in Metamorphic Terranes*, Abstracts volume, Univ. Stellenbosch, 95-98.

_____, & Porada, H., 1977 - The intracratonic branch of the Damara orogen in South West Africa. I. Discussion of geodynamic models. *Precambr. Res.*, *5*, 311-338.

_____, & Wilcewski, N., 1970 - Palaeoecology, conditions of deposition and the Palaeogeography of the marine Dwyka Beds of South West Africa. In: *I.U.G.S. 2nd Gondwana Symposium, C.S.I.R. Pretoria*, 225-232.

McElhinny, M.W. & McWilliams, M.O., 1977 - Precambrian geodynamics - a palaeomagnetic view. *Tectonophysics*, *40*, 137-159.

McKenzie, D.P. & Parker, R.L., 1967 - The North Pacific, an example of tectonics on a sphere. *Nature*, *216*, 1276-1280.

McLachlan, I.R. & Anderson, A., 1975 - The Age and stratigraphic relationship of the glacial sediments in Southern Africa. In: Campbell, K.S.W. (ed.), *Gondwana Geology : Papers presented at the Third Gondwana Symposium, Canberra, Australia, 1973.* Austral. Nat. Univ. Press, 415-422.

Miller, R. Mc G., 1972 - *The geology of a portion of southern Damaraland, South West Africa, with particular reference to the petrogenesis of the Salem granites.* Unpubl. Ph.D. thesis, Univ. Cape Town.

_____, 1974 - The stratigraphic significance of the Naauwpoort Formation of east central Damaraland, South West Africa. *Trans. geol. Soc. S. Afr.*, *77*, 363-367.

Minster, J.B., Jordan, T.H., Molnar, P. & Haines, E., 1974 - Numerical modelling of instantaneous plate tectonics. *Geophys. J. R. astr. Soc.*, *36*, 541-576.

Mitchell, A.H. & Reading, H.G., 1969 - Continental margins, geosynclines and ocean-floor spreading. *J. Geol.*, *77*, 629-646.

Morgan, W.J., 1968 - Rises, trenches, great faults and crustal blocks. *J. Geophys. Res.*, *73*, 1959-1982.

Münch, H.G., 1975 - Die Geologie des Naukluft-Deckensystems, Südwestafrika (Vorläufiger Bericht). *N. Jb. Geol. Paläont. Mh.*, *1975*, 657-663.

Nash, C.R., 1971 - Metamorphic petrology of the SJ area Swakopmund district South West Africa. *Bull. Precambr. Res. Unit, Univ. Cape Town*, *9*, 77 p.

Naylor, M.A. & Harle, T.J., 1976 - Palaeogeographic significance of rocks and structures beneath the Vourinos ophiolite, Northern Greece. *Jl. geol. Soc. Lond.*, *132*, 667-675.

Nicolaysen, L.O., 1962 - Stratigraphic interpretation of age measurements in Southern Africa. In: *Petrologic Studies : A Volume in honour of A.F. Buddington*, Geol. Soc. Amer., 569-598 p.

Nieberding, F., 1976 - Die Grenze der zentralen Granitzone südwestlich Otjimbingwe (Karibib-District, Südwestafrika) : Intrusionsverband, Tektonik, Petrographie. *Göttinger Arb. Geol. Paläont.* *19*, 78 p.

Orowan, E., 1965 - Convection in a non-Newtonian mantle, continental drift, and mountain building. In: *A symposium on continental drift*, Phil. Trans. R. Soc. Lond., A.258, 284-313.

Parker, R.C. & Oldenburg, D.W., 1973 - Thermal model of ocean ridges. *Nature phys. Sci.*, *242*, 137-139.

Pearce, J.A. & Cann, J.R., 1973 - Tectonic setting of basic volcanic rocks determined using trace element analyses. *Earth Planet. Sci. Lett.*, *19*, 290-300.

Perkins, W.J. & Hammond, B.J., 1975 - Computer-aided thought in biomedical research. *Nature*, *256*, 171-175.

Pettijohn, F.J., 1949 - *Sedimentary rocks (1st ed.)* Harper, New York, 526 p.

Pollack, H.N. & Chapman, D.S., 1977 - On the regional variation of heat flow, geotherms and lithospheric thickness. *Tectonophysics, 38,* 279-296.

Porada, H., 1973 - Tektonisches Verhalten und geologische Bedeutung von Kalksilikatfels-Lagen und -Spindeln im Damara-Orogen Südwest-Afrikas. *Geol. Rdsch., 62,* 918-938.

_____, Schmidt, A.E. & Wittig, R., 1972 - *Die Tektonik der geologischen Fazieseinheiten im Damara-Orogen.* Bericht des Sonderforschungsbereichs 48 der DFG (unveröffentl.), 135-152, Göttingen.

_____, & Wittig, R., 1975 - Zur Tektonik des südlichen Damara-Belts. In: Martin, H. (reporter). *Stoffbestand, Tektonik, Metamorphose und Granitbildung im Damara-Orogen, Bericht des Sonderforschungsbereiches 48 : Projektbereich B.* Georg-August-Univ., Göttingen, 51-70.

_____, & Wittig, R., 1976 - Das Chausib-Turbiditbecken an Südrand des Damara-Orogens, Südwest-Afrika. *Geol. Rdsch., 65,* 1002-1019.

Price, N.J., 1977 - Aspects of gravity tectonics and the development of listric faults. *Jl geol. Soc. Lond. 133,* 311-327.

Purser, B.H. & Evans, G., 1973 - Regional sedimentation along the Trucial Coast, S.E. Persian Gulf. In: Purser, B.H. (ed.), *The Persian Gulf,* Springer-Verlag Berlin, 211-231.

Ramsay, C.R. & Ridgway, J., 1977 - Metamorphic patterns in Zambia and their bearing on problems of Zambian tectonic history. *Precambr. Res., 4,* 321-337.

Ramsay, J.G., 1967 - *Folding and Fracturing of Rocks.* McGraw-Hill, New York, 568 p.

_____, 1969 - The measurement of strain and displacement in orogenic belts. In: Kent, P.E., Satterthwaite, G.E. & Spencer, A.M. (eds.), *Time and Place in Orogeny,* Geol. Soc. Lond., Spec. Publ. 3, 43-79.

_____, 1976 - Displacement and strain. *Phil. Trans. R. Soc. Lond. A.283,* 3-25.

_____, & Graham, R.H., 1970 - Strain variation in shear belts. *Can. J. Earth Sci. 7, (3),* 786-813.

Reeves, C., 1977 - The delineation of crustal provinces in southern Africa from a compilation of gravity data. *20th Ann. Rep. Res. Inst. Afr. Geol., Univ. Leeds,* 36-41.

_____, & Hutchins, D.G., 1975 - Crustal structures in central southern Africa. *Nature, 254,* 408-410.

Reuning, E., 1923 - *Geologische Uebersichtskarte des mittleren Teils von Südwestafrika.* Scharfes Druckereien, Wetzlar.

Ringwood, A.E., 1974 - The petrological evolution of island arc systems. *Jl geol. Soc. Lond., 130,* 183-204.

Roering, C., 1961 - The mode of emplacement of certain Li- and Be- bearing pegmatites in the Karibib District, South West Africa. *Econ. Geol. Res. Unit, Univ. Witwatersrand, Inf. Circ*, 4, 38 p.

Rutter, E.H., 1976 - The kinetics of rock deformation by pressure solution. *Phil. Trans. R. Soc. Lond.* A.283, 203-219.

SACS, 1971 - South African Code of Stratigraphic terminology and nomenclature. *Trans. geol. Soc. S. Afr.*, 74, 111-129.

Schalk, K.E.L., 1973 - Some late Precambrian formations in central South West Africa. *Ann. geol. Surv. S. Afr.*, 8 *(for 1970)*, 29-47.

Scholz, C.H., Koczynski, T.A. & Hutchins, D.G., 1976 - Evidence for incipient rifting in Southern Africa. *Geophys. J.R. astr. Soc.* 44, 135-144.

Schubert, G., Froidevaux, C. & Yuen, D.A., 1976 - Oceanic lithosphere and asthenosphere : Thermal and mechanical structure. *J. Geophys. Res.*, 81, 3525-3540.

Seely, D.R., Vail, P.R. & Walton, G.G., 1974 - Trench slope model. In: Burk, C.A. & Drake, C.L. (eds.), *The Geology of Continental Margins.* Springer, New York, 179-196.

Selby, M.J., 1976 - Some thoughts on the geomorphology of the Central Namib Desert. *Bull. Desert-Ecological Res. Unit (August, 1976)*, 5-6.

Shaw, D.M., 1956 - Geochemistry of pelitic rocks. III: Major elements and general geochemistry. *Geol. Soc. Amer. Bull.*, 67, 919-934.

_____, Reilly, G.A., Muysson, J.R., Pattenden, G.E. & Campbell, F.E., 1967 - An estimate of the chemical composition of the Canadian Precambrian Shield. *Can. J. Earth Sci.*, 5, 829-853.

Shimazaki, K., 1974 - Pre-seismic crustal deformation caused by an underthrusting oceanic plate, in eastern Hokkaido, Japan. *Phys. Earth Planet. Interiors*, 8, 148-157.

Shinn, E.A., 1973 - Sedimentary accretion along the leeward, SE coast of Qatar Peninsular, Persian Gulf. In: Purser, B.H. (ed.), *The Persian Gulf*, Springer-Verlag Berlin, 199-209.

Smith, D.A.M., 1965 - The geology of the area around the Khan and Swakop Rivers in South West Africa. *Geol. Surv. S. Afr., S.W.A. Series, Mem.* 3, 113 p.

Smoluchowski, M.S., 1909 - Some remarks on the mechanics of overthrusts: *Geol. Mag., new ser., dec. V., v. VI*, 204-205.

Solomon, S.C. & Sleep, N.H., 1974 - Some simple physical models for absolute plate motions. *J. Geophys. Res.*, 79, 2557-2567.

_____, Sleep, N.H., & Richardson, R.M., 1975 - On the forces driving plate tectonics : Inferences from absolute plate velocities and intraplate stress. *Geophys. J.R. astr. Soc.*, 42, 769-801.

Spencer, A.M., 1974 - The Data for Orogenic Studies Questionnaire. In: Spencer, A.M. (ed.), *Mesozoic-Cenozoic Orogenic Belts : Data for Orogenic Studies*. Geol. Soc. Lond., Spec. Publ. No. 4, 787-802.

Spreitzer, H., 1966 - Beobachtungen zur Geomorphologie der Zentralen Namib und ihrer Randgebiete. *J. Scient. Soc. S.W.A., 20.*

Stanley, S.M., 1976 - Fossil data and the Precambrian-Cambrian evolutionary transition. *Amer. J. Sci., 276,* 56-76.

Starkey, J., 1970 - A computer programme to prepare orientation diagrams. In: Paulitsch, P. (ed.), *Experimental and natural rock deformation.* Springer-Verlag, Berlin, 51-74.

Stephansson, O. & Berner, H., 1971 - The finite element method in tectonic processes. *Phys. Earth Planet. Interiors, 4, (4),* 301-321.

Sutton, J., 1976 - Introductory Remarks to "A Discussion on global tectonics in Proterozoic times". *Phil. Trans. R. soc. Lond. A.280,* 399-403.

Temple, P.G., 1968 - Mechanics of large-scale gravity sliding in the Greek Peloponnesos. *Geol. Soc. Amer. Bull., 79,* 687-700.

Toens, P.D., 1975 - The Geology of part of the Southern Foreland of the Damara Orogenic Belt in South West Africa and Botswana. *Geol. Rdsch., 64,* 175-192.

Törnbohm, A.E., 1896 - Grunddragen af det centrala Skandinaviens bergbyggnad. *K. Sv. Vet. Akad. Handl., v. 28(5),* 201 p.

Tucker, M.E., 1976 - Quartz replaced anhydrite nodules ("Bristol Diamonds") from the Triassic of the Bristol district. *Geol. Mag. 113,* 569-574.

Turner, F.J. & Weiss, L.E., 1963 - *Structural Analysis of Metamorphic Tectonites.* McGraw-Hill, New York.

Tysdal, R.G., Case, J.E., Winkler, G.R. & Clark, S.H.B., 1977 - Sheeted dykes, gabbro and pillow basalt in flysch of coastal Southern Alaska. *Geology, 5,* 377-383.

Van Bemmelen, R.W., 1933 - The Undation theory of Development of the Earth's Crust. *Trans. Int. Geol. Congress, Washington, 2.*

Vegter, J.R., 1953 - *Underground water supplies in the crystalline complex of the Kenhardt District, C.P. and the water supply of Walvis Bay.* Unpubl. M.Sc. thesis Univ. Pretoria.

Viljoen, R.P., Viljoen, M.J., Grootenboer, J. & Longshaw, T.R., 1975 - ERTS-1 Imagery : An appraisal of applications in geology and mineral exploration. *Minerals Sci. Engng., 7,* 132-168.

von Groote-Bidlingmaier, M., 1974 - Tektonik und Metamorphose im Grenzbereich Damara-Prädamara, südwestlich Windhoek (Südwestafrika). *Göttinger Arb. Geol. Paläont. 14,* 80 p.

Warrak, M., 1974 - The petrography and origin of dedolomitized, veined or brecciated carbonate rocks, the "cornieules", in the Frejus region, French Alps. *Jl. geol. Soc. Lond.*, *130*, 229-247.

Wasserburg, G.J., Macdonald, G.J.F., Hoyle, F. & Fowler, W.A., 1964 - Relative contributions of uranium, thorium and potassium to heat production in the Earth. *Science*, *143*, 465-467.

Watson, G.S., 1966 - Statistics of orientation data. *J. Geol.*, *74*, 786-797.

Watson, J.V., 1976 - Vertical movements in Proterozoic structural provinces. *Phil. Trans. R. Soc. Lond.*, *A.280*, 629-640.

Watters, B.R., 1974 - Stratigraphy, igneous petrology and evolution of the Sinclair Group in southern South West Africa. *Bull. Precambr. Res. Unit, Univ. Cape Town*, *16*, 235 p.

_____, 1976 - Possible late Precambrian subduction zone in South West Africa. *Nature*, *259*, 471-473.

Weber, K., 1972a - Notes on determination of illite crystallinity. *N. Jb. Miner. Mh.*, *6*, 267-276.

_____, 1972b - Crystallinity of illite in slates and other criteria of weak metamorphism in the northeastern Rheinisches Schiefergebirge. *N. Jb. Geol. Paläont. Abh.* *141*, 333-363.

Weertman, J., 1970 - The creep strength of the earth's mantle. *Rev. Geophys. Space Phys.*, *8*, 145-168.

Weiss, L.E., 1959 - Structural analysis of the Basement System at Turoka, Kenya. *Overseas Geol. & Min. Resources*, *7*, 3-35.

Williams, D.L. & von Herzen, R.P., 1974 - Heat loss from the Earth : New estimate. *Geology*, *2*, 327-328.

Wilson, J.T., 1965 - A new class of faults and their bearing on continental drift. *Nature*, *207*, 343-347.

Winkler, H.J.F., 1976 - *Petrogenesis of Metamorphic Rocks (Fourth Edition)*. Springer-Verlag, New York, 334 p.

Woodcock, N.H., 1977 - Specification of fabric shapes using an eigenvalue method. *Geol. Soc. Amer. Bull.* *88*, 1231-1236.

Wynne-Edwards, H., 1976 - Proterozoic ensialic orogenesis; the millipede model of ductile plate tectonics. *Amer. J. Sci.*, *276*, 927-953.

_____, Laurin, A.F., Sharma, K.N.M., Nandi, A.A., Kehlenbreck, M.M. & Franconi, A., 1970 - Computerized geological mapping in the Grenville Province Quebec. *Can. Jl Earth Sci.*, *7*, 1357-1373.

P L A T E S

1 - 74

Plate 1. View of nappe front and Tsondab Valley at Büllsport, showing Büllenkopf hill and the Kudu plateau with its summit erosion bevel in the far distance.

Plate 2. Interbedding of fine-grained calcareous quartzite and dolomite in Noab Formation, also showing pattern of graben microfaulting. (Locality 50057)

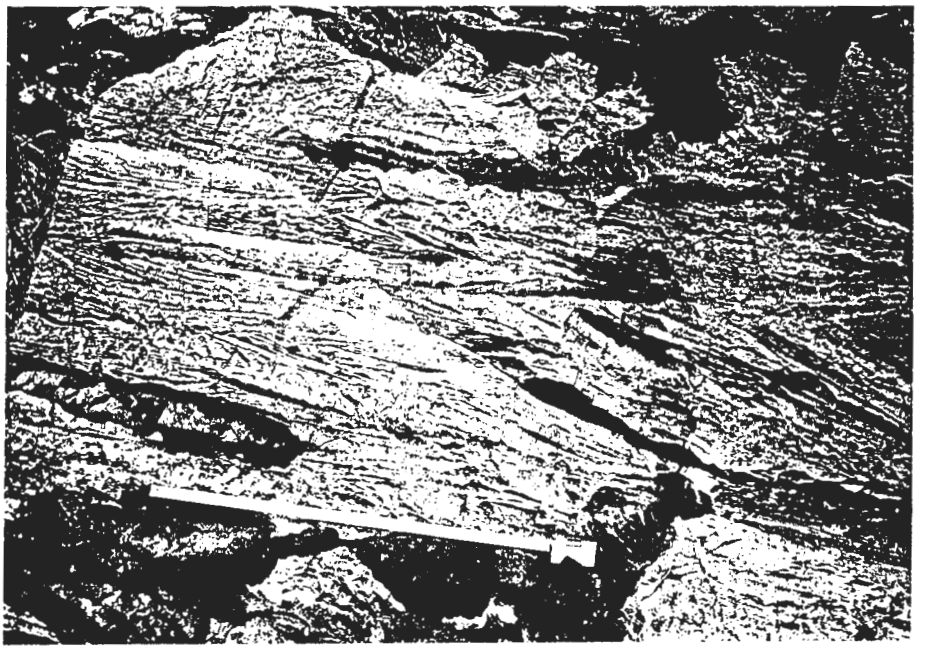

Plate 3. Cross-bedding (partly herringbone) and chert lenses in dolomite of the Noab Formation. (Locality 50059)

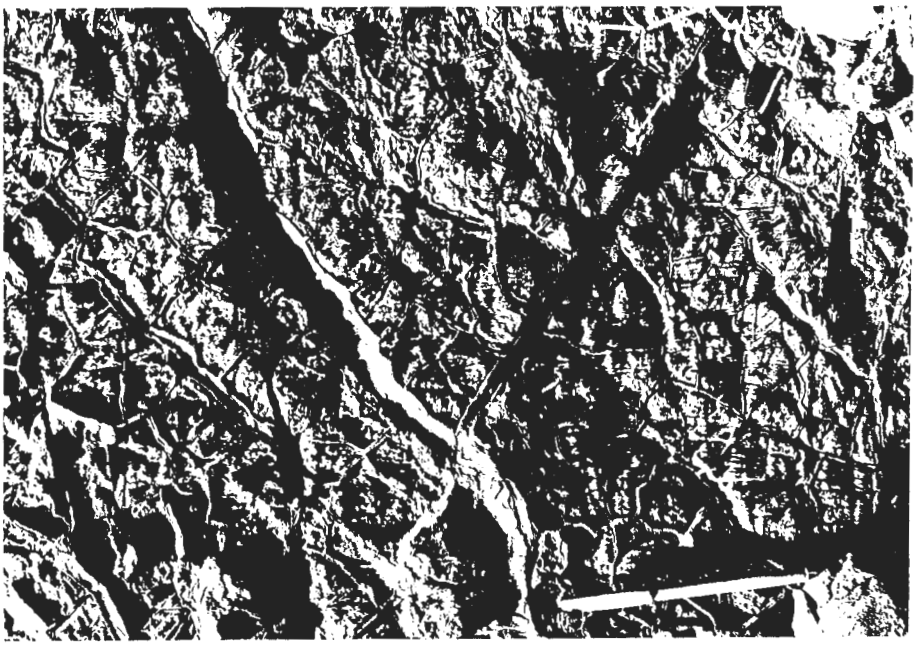

Plate 4. Polygonal dessication cracks on bedding surface in Noab dolomite. (Locality 10064)

Plate 5. "Posed" photograph of sedimentary structures including ripple-marks and synaeresis cracks in middle clastic member of the Büllsport Formation. (Locality 40063)

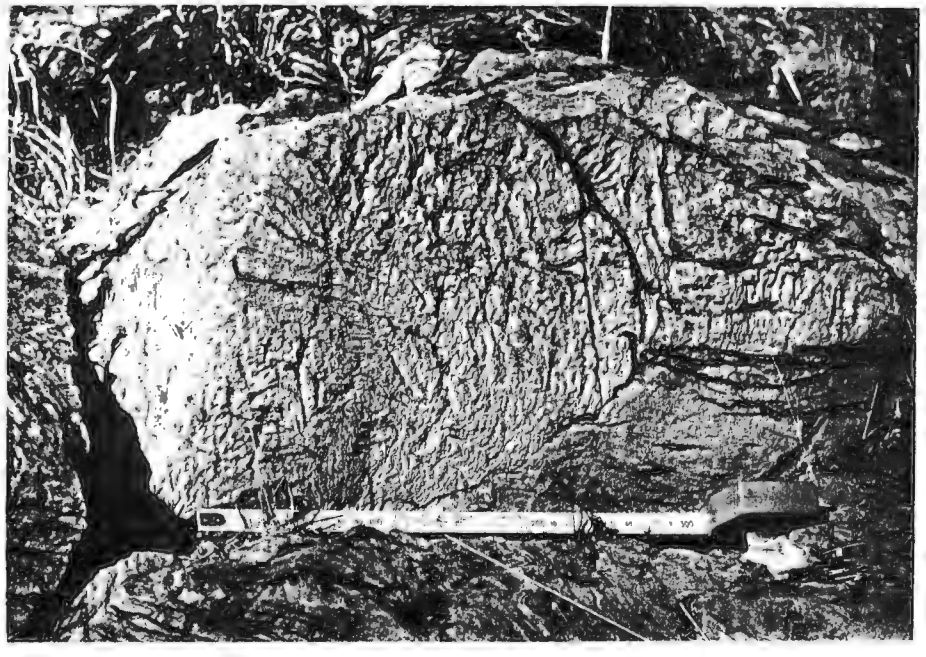

Plate 6. Cauliflower-shaped stromatolite in dolomite of the upper Büllsport Formation. (Locality 50116)

Plate 7. Large dolomite boulders in carbonate breccia of the Klipbokrivier Formation. Black limestone clasts have been strongly flattened in zone between dolomite blocks. (Locality 20057)

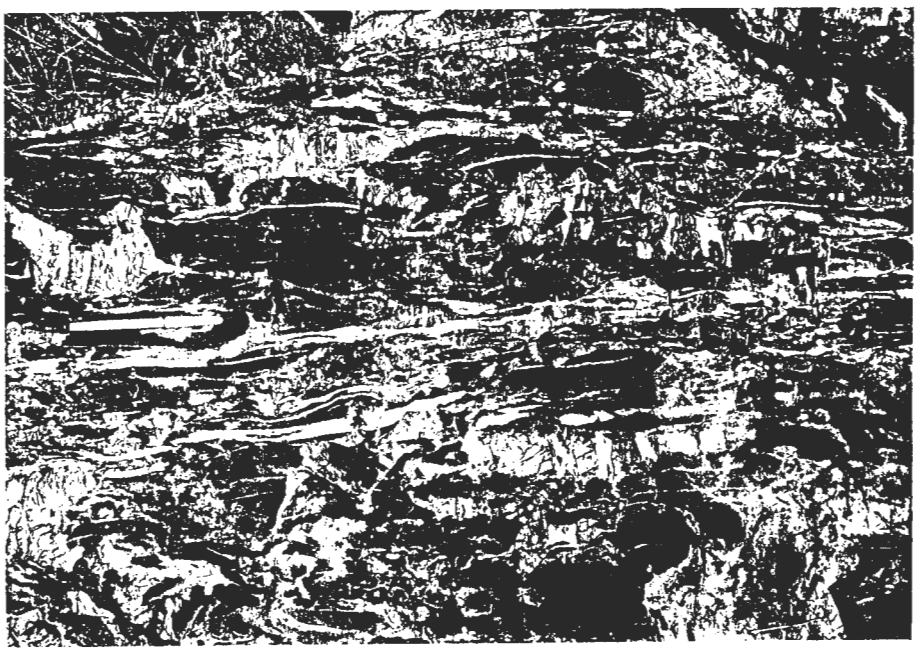

Plate 8. Boudinaged dolomite clasts and stretched black limestone clasts in highly-deformed Klipbokrivier breccia. Streaky calcite veining normal to foliation surface is parallel to principal stretch direction and white calcite fills spaces between dolomite fragments. (Locality 20056).

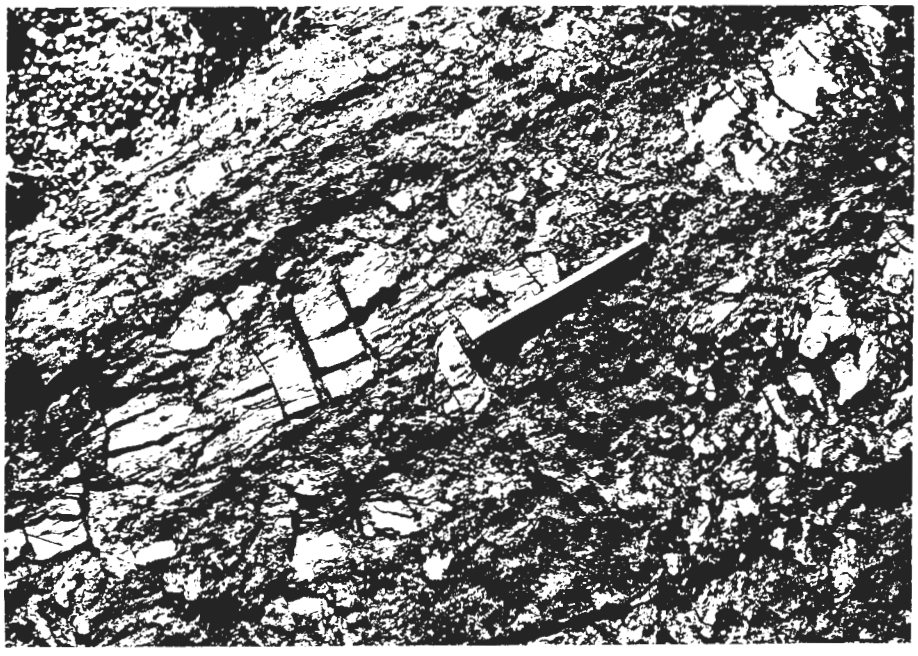

Plate 9. Irregular "chocolate tablet" boudinage in thin phyllite layers within marly limestone of the lower Remhoogte "exotic" unit. (near Locality 10055)

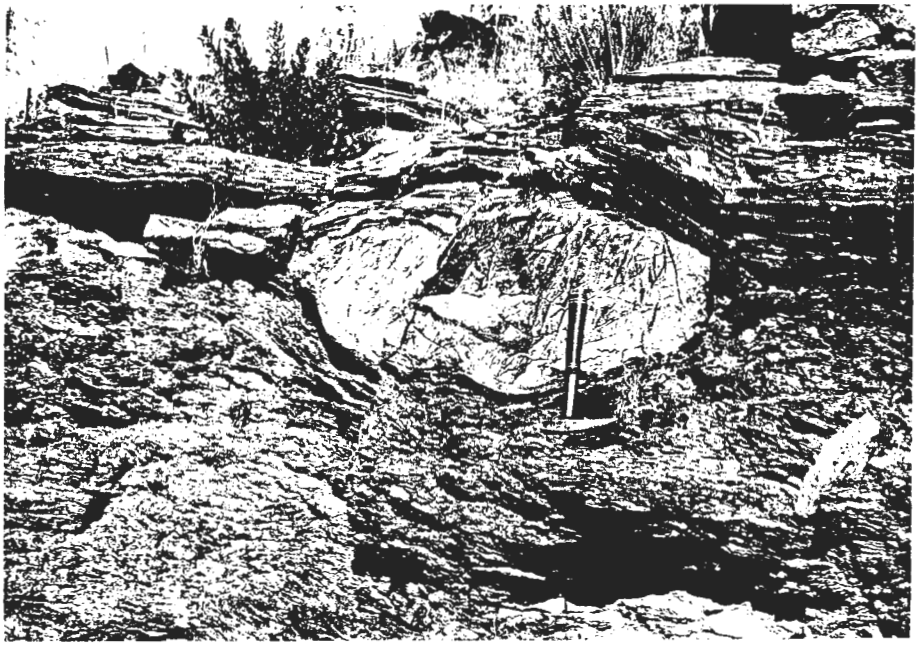

Plate 10. Boudinaged dolomite layer between marl and black limestone of the lower Remhoogte Formation. (near Locality 10055)

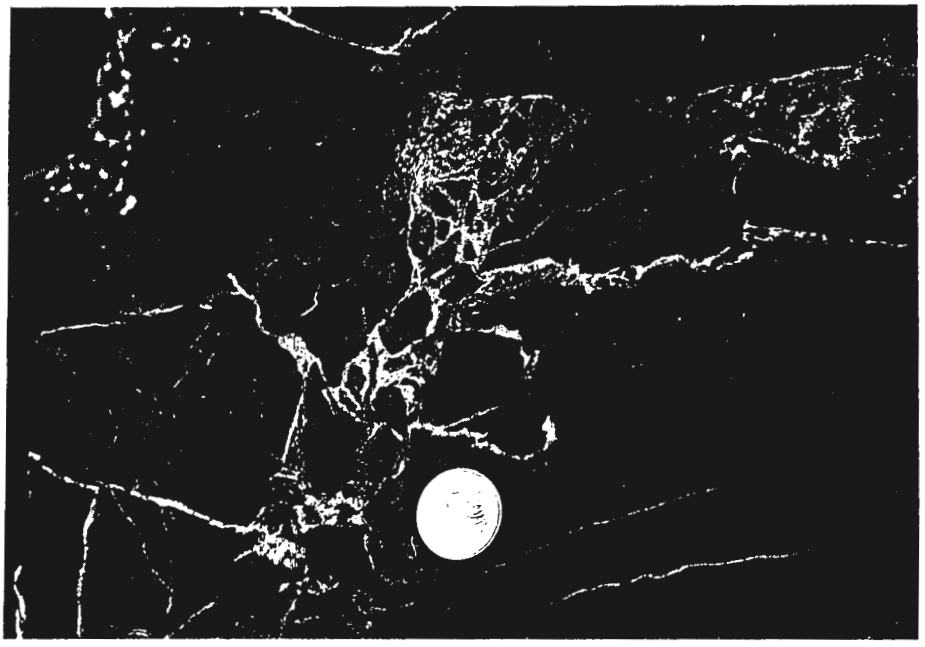

Plate 11. Detail view of crack pattern in large block of black limestone within the Blässkranz carbonate breccia. Coin diameter is 2 cm. (Locality 30022)

Plate 12. Structure of Blässkranz breccia adjacent to large fragmented block of black limestone. Clast beneath coin shows three cracks arrested at an early stage of their development. (Locality 30022)

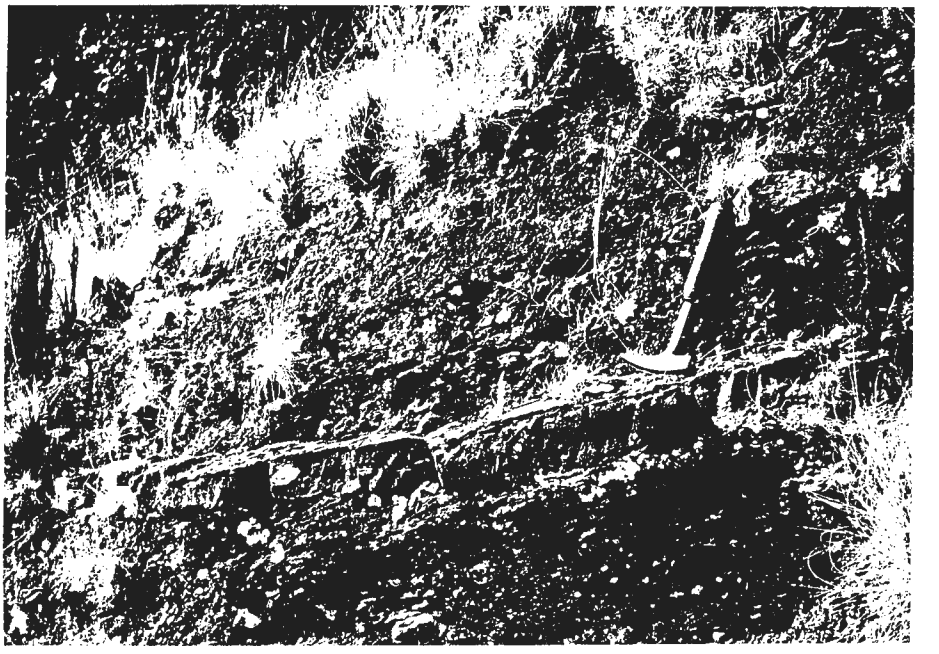

Plate 13. Bedding structure within the Blässkranz breccia showing layer of finer carbonate-cemented breccia in coarser breccia with a phyllitic matrix. (Locality 30029)

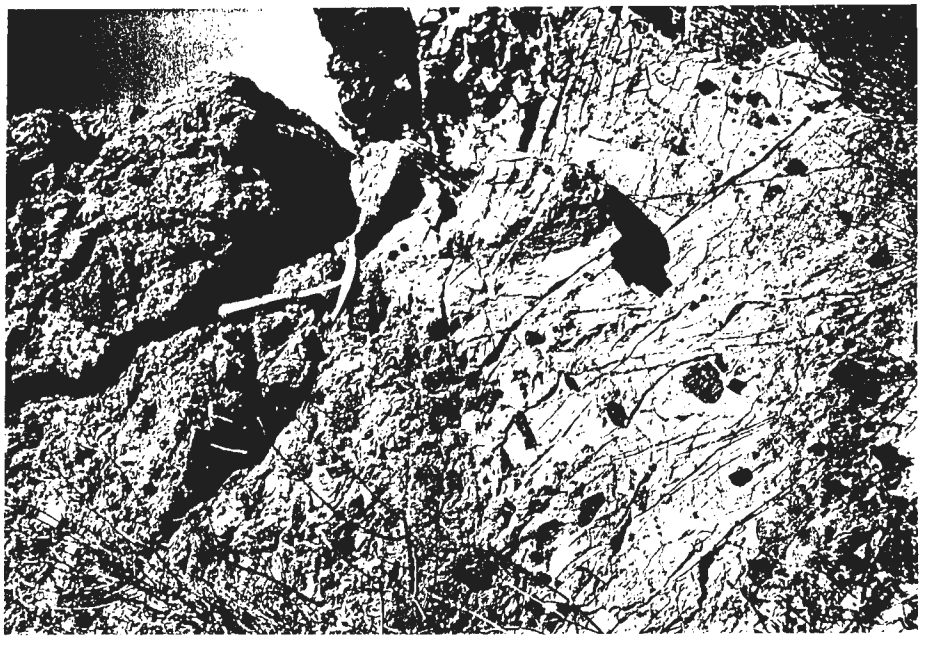

Plate 14. Basal zone of the Blässkranz Formation in the far eastern part of the Naukluft Complex. (Locality 30011)

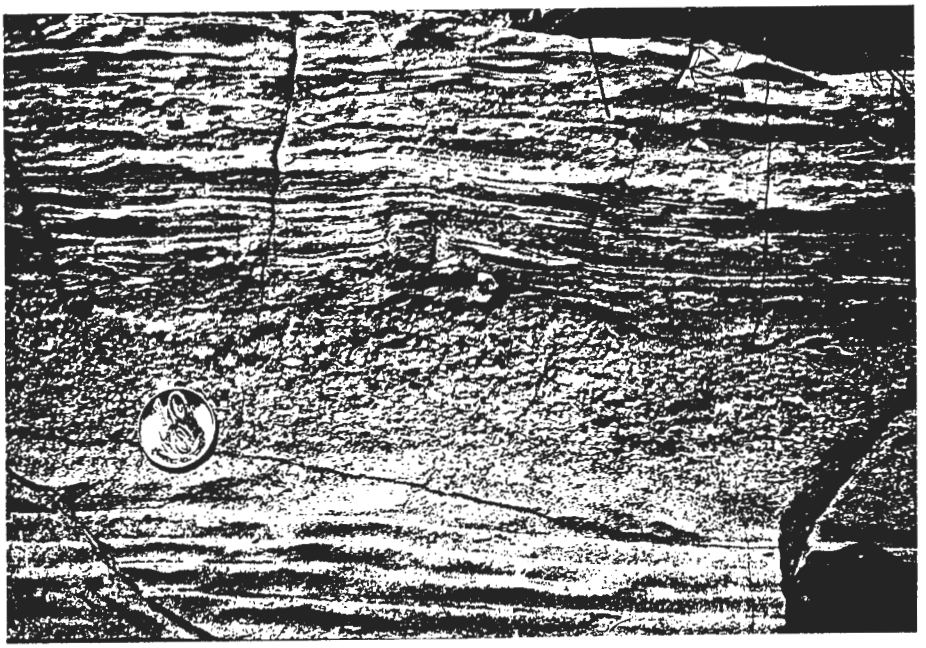

Plate 15. Detail of sedimentary structure in fine-grained basal units of the Blässkranz Formation showing apparent dropstone phenomena. Coin diameter for scale is 2 cm. (Locality 30011)

Plate 16. Structure of layer of volcaniclastic microbreccia between calcareous quartzite beds. Coin diameter for scale is 2,5 cm. (Locality 30079)

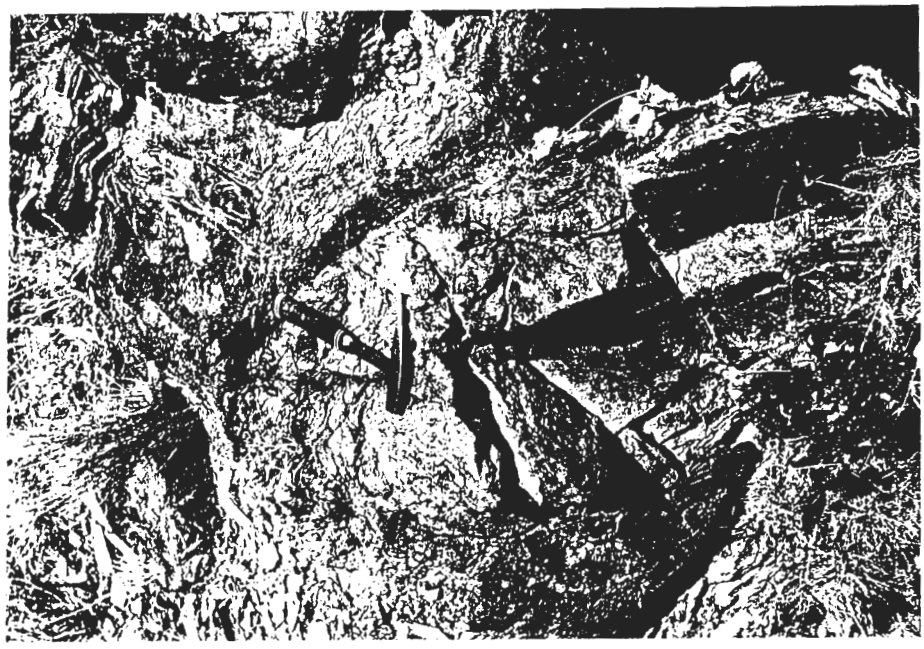

Plate 17. Granitoid boulder in lower purple shale of the Tsabisis Formation. (Locality 30009).

Plate 18. Brecciated microgranitic layer and rounded boulder of same in overlying calcareous quartzite bed. Coin on boulder is 2,5 cm in diameter. In upper right of photograph the microbreccia layer illustrated in plate 16 is also seen. (Locality 30079)

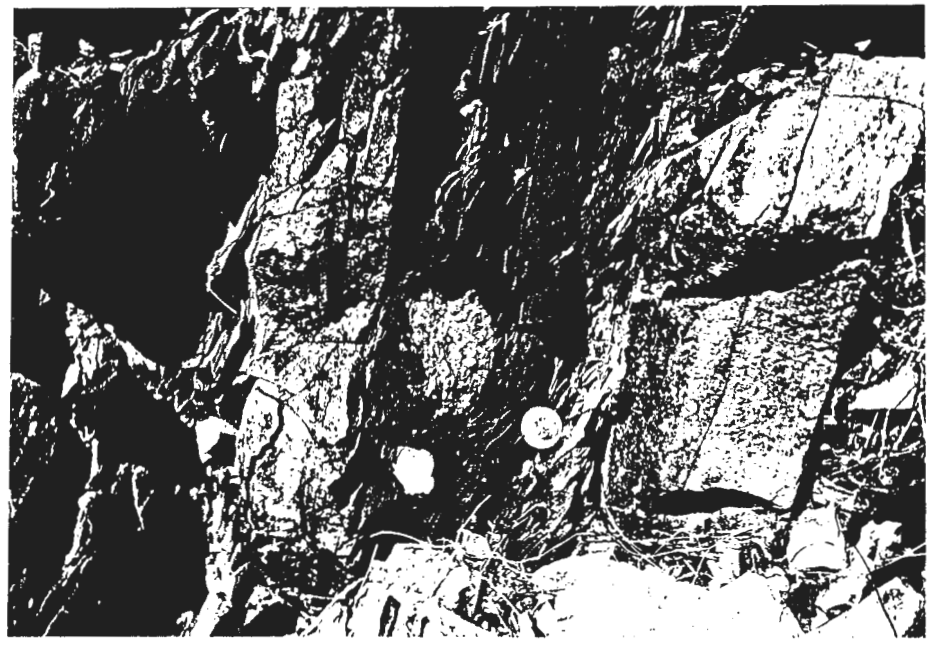

Plate 19. Large clasts of white quartz and granite in fine-grained purple shale of Tsabisis Formation. (Locality 30009)

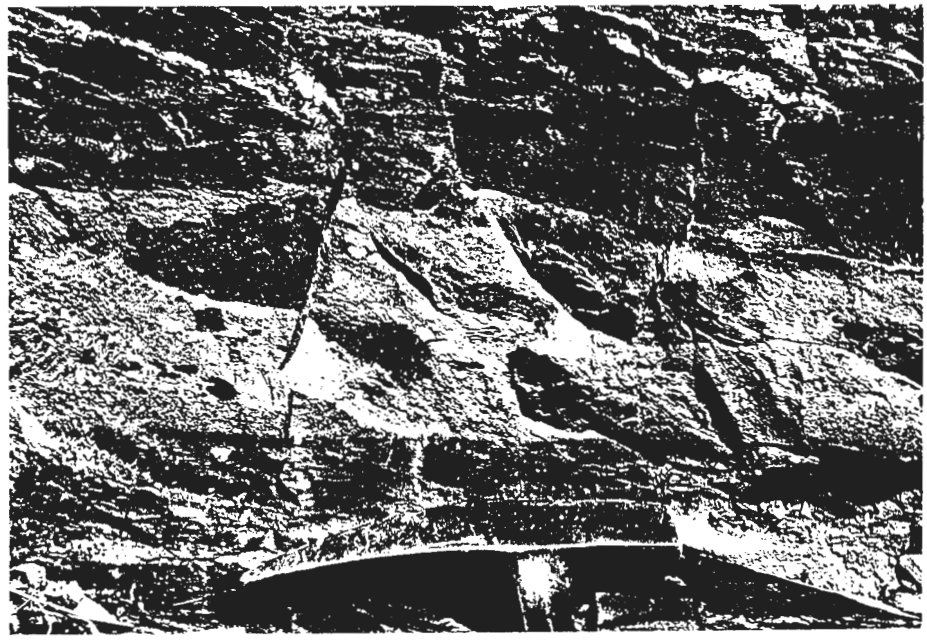

Plate 20. Detail view of lapilli tuff layer in Tsabisis Formation. (Locality 30079)

Plate 21. View of 1837 m summit along south-eastern nappe front near the Ubusis-Onis boundary. Sole thrust of Naukluft nappe complex is located along base of the vertical dolomite cliffs (Neuras Member). Highly sheared black limestone of the Kuibis Formation occurs between the underlying Schwarzrand shales and the nappe complex. The clastic Ubusis Member and the lower Tsams Member are visible at the top of the section.

Plate 22. View upward towards 1846 m summit near locality 7001Q on farm Ubusis (now part of Naukluft Mountain Zebra Park), showing thick dolomite of the Tsams Member separated by middle calcareous quartzite unit and overlain by clastic Lemoenputs Member with prominent black limestone layer near top of section.

Plate 23. View of Lemoenputs Member in section near locality 70010 showing conspicuous double marker layers of conglomerate below and black limestone above. The Lemoenputs succession is underlain by thick partly stromatolitic Tsams dolomite and overlain by massive Onis dolomite.

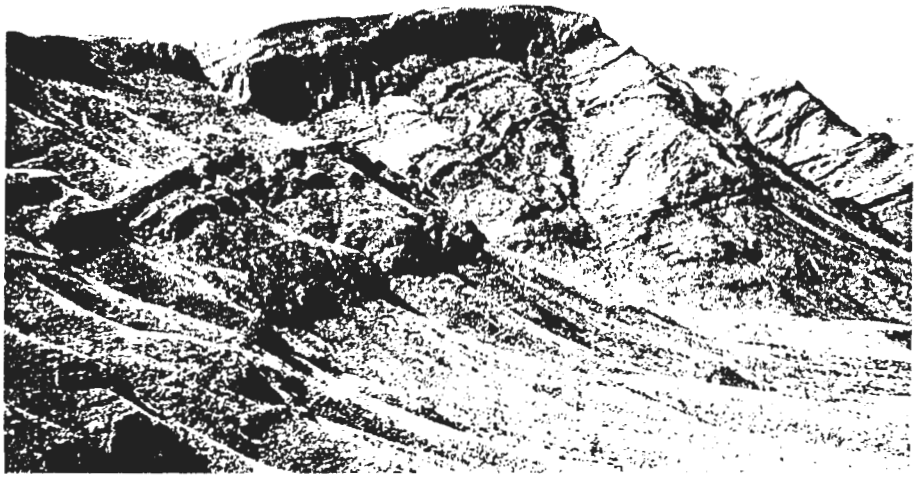

Plate 24. View from locality 70010 of 1905 m summit in southernmost corner of former farm Naukluft (now part of Naukluft Mountain Zebra Park), showing complete succession of the Zebra River Formation.

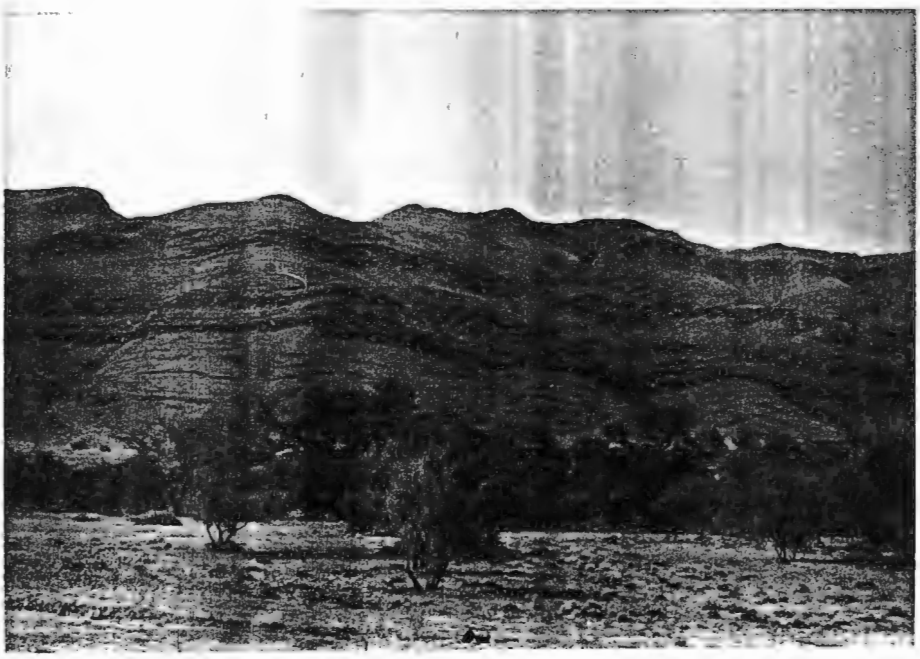

Plate 25. View of Kuibis Formation from Tsondab Valley near Zais Farmhouse, illustrating three-fold clastic carbonate succession.

Plate 26. D_1 minor folds in Kuibis limestone. (Locality 10003)

Plate 27. Fold interference pattern (Ramsay Type 3) in upper Kuibis Formation just below base of Naukluft nappe complex. (Locality 10041)

Plate 28. Near isoclinal minor D_1 fold in Kuibis limestone. (Locality 10011)

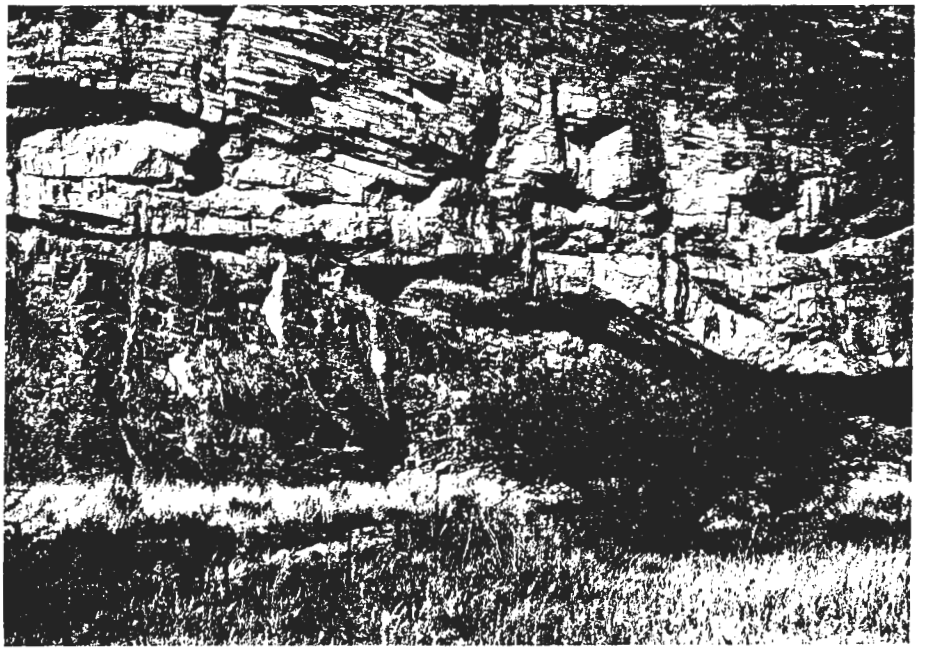

Plate 29. Base of Naukluft nappe complex overlying poorly cleaved Schwarzrand shales on left cut by "dykes" of unconformity dolomite leading from thin sill of same approximately in the horizontal centre of plate. (Locality 10057)

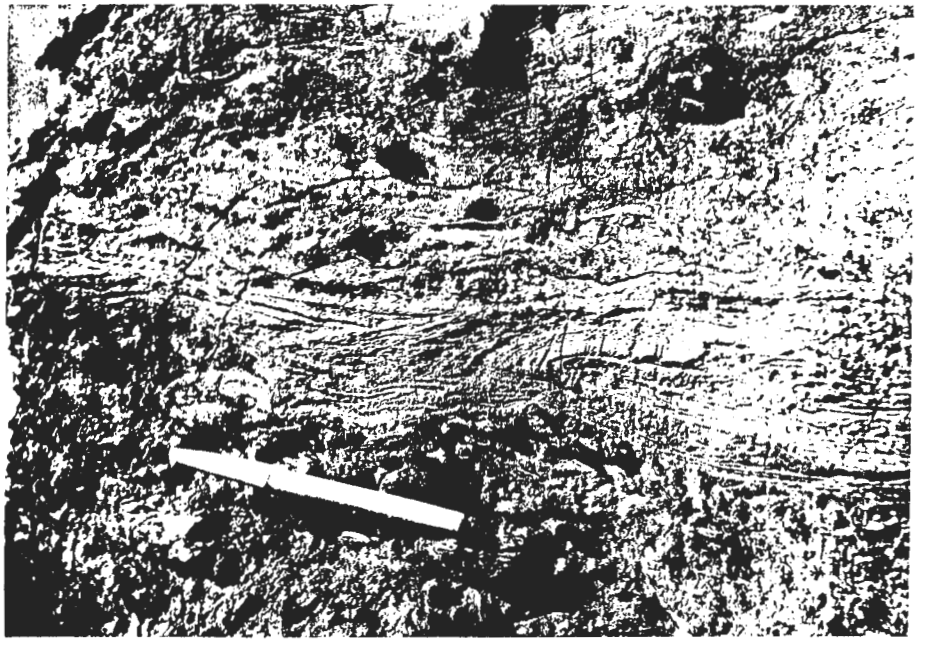

Plate 30. Downward facing minor folding in basal parts of steeply dipping unconformity dolomite zone at locality 10055.

Plate 31. "Boulder shales" in Remhoogte Formation formed by tectonic disruption and boudinage of quartz veins. (Locality 10055)

Plate 32. Thin layer of unconformity dolomite separating dolomitic Kudu nappe from lower Remhoogte "exotic" unit near localities 10055-56 (point A/ in Fig. 24).

Plate 33. Recumbent folding and cleavage development in Type 1 phyllite of the Remhoogte Formation (near Locality 10070)

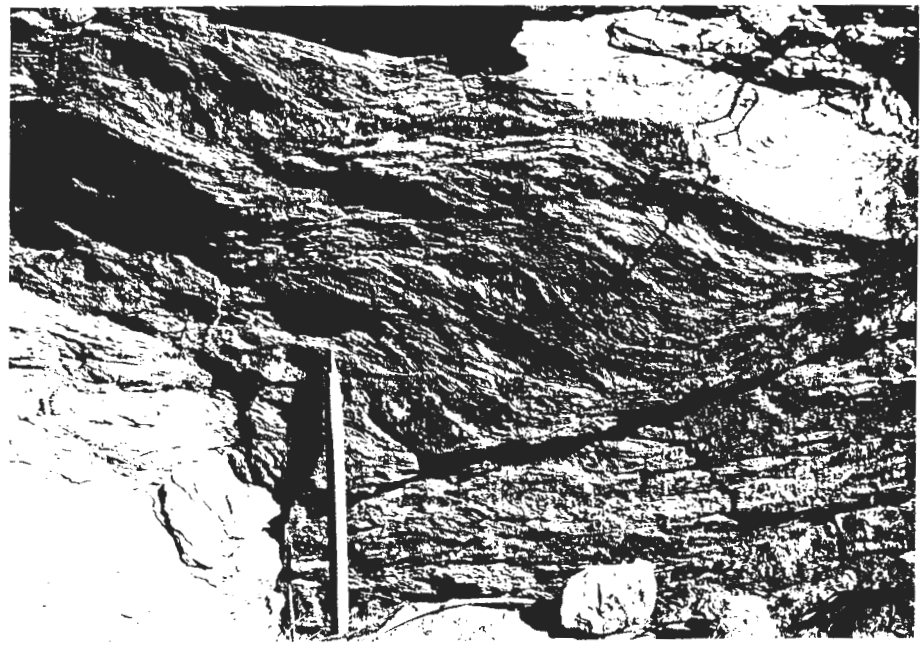

Plate 34. Late crenulation (S_2) of S_1 phyllitic foliation in Type 2 Remhoogte phyllites also illustrating deformation of L_1 lineation. (Locality 10061)

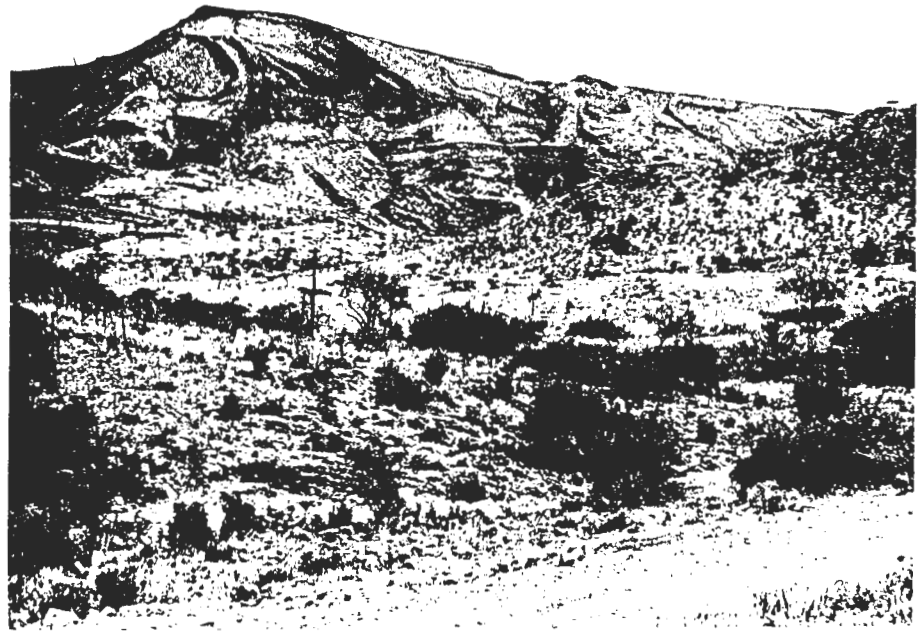

Plate 35. View from Remhoogte Pass road towards locality 10052 showing Keitzub Mountain structure. Klipbokrivier pelites are poorly exposed in core of the recumbent syncline and a discontinuity between overturned dolomite beds in the hinge zone and layers in the upper limb is evident.

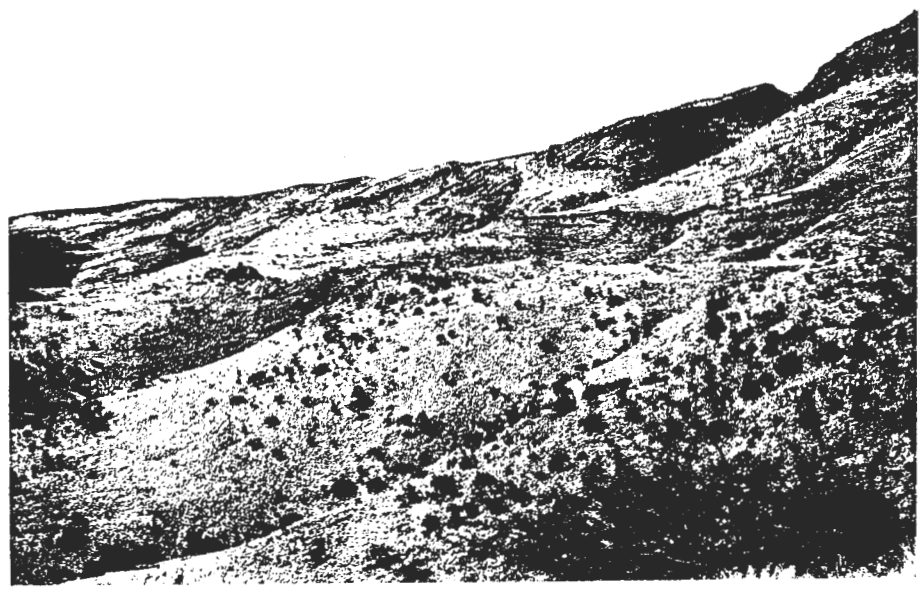

Plate 36. View eastward from locality 10052 showing detail of multiple folding of a thin dolomite layer in the hinge zone of the larger Keitzub structure.

Plate 37. A gentle minor syncline in layered dolomitic limestone underlain by massive dolomite. S_1 cleavage (orientation - 252/58) apparently formed by pressure solution processes is etched in dolomitic limestone. (Locality 10062)

Plate 38. Detail of pressure solution cleavage axial-planar to a recumbent fold in dolomitic limestone layers at the base of the Kudu nappe. (Locality 10068)

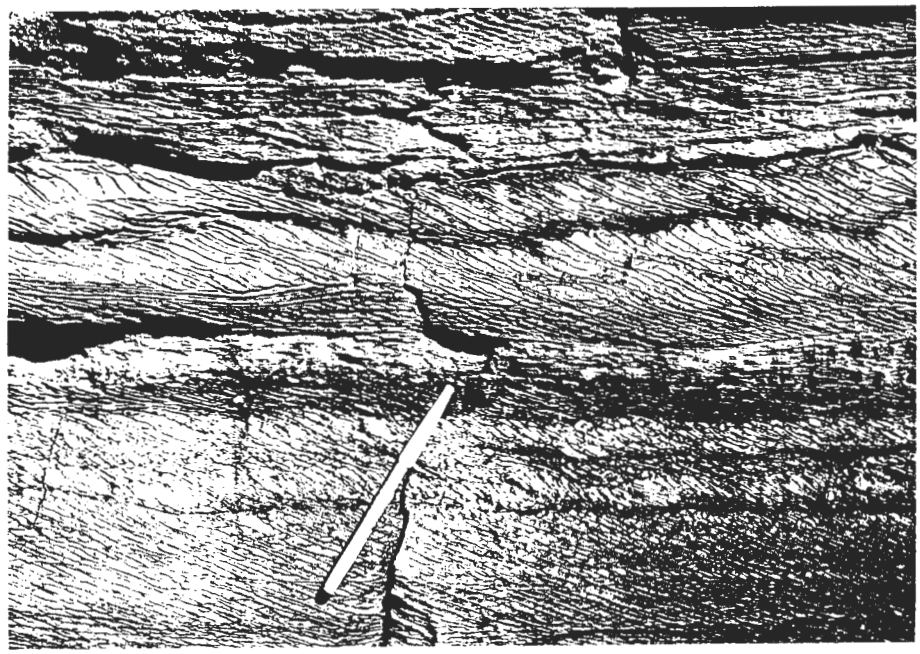

Plate 39. Relationship between sedimentary bedding and pressure solution cleavage in dolomitic limestone close to the base of the Kudu nappe. Layers in upper left of plate show the effects of boudinage and small cusp-like structures have developed on the upper and lower surfaces of some less ductile dolomitic layers. (Locality 10068)

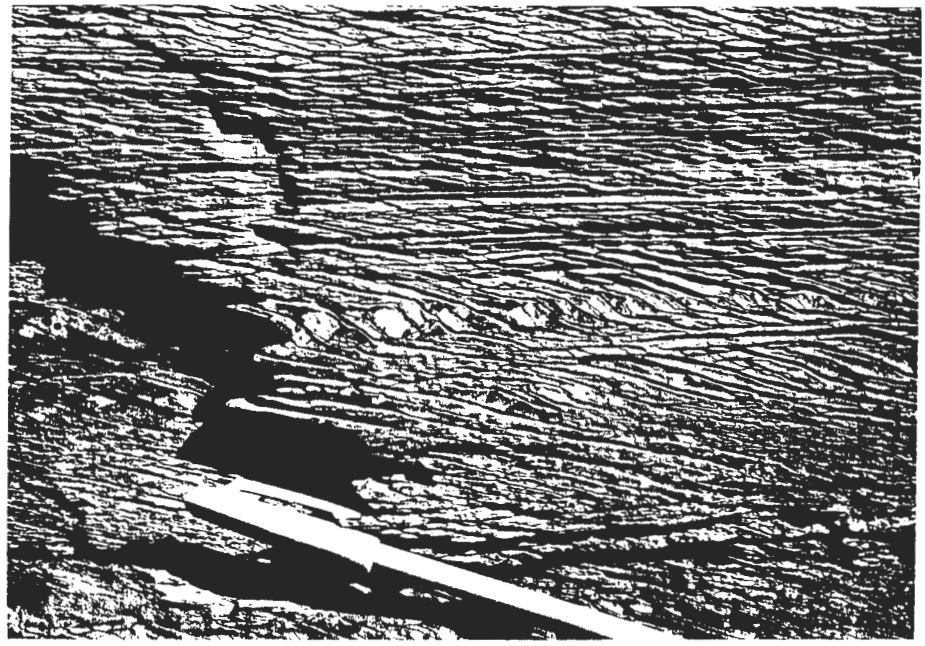

Plate 40. Close-up of pressure solution cleavage at locality 10068 showing apparent rotation and displacement of bedding within microlithons in middle layer within the plate.

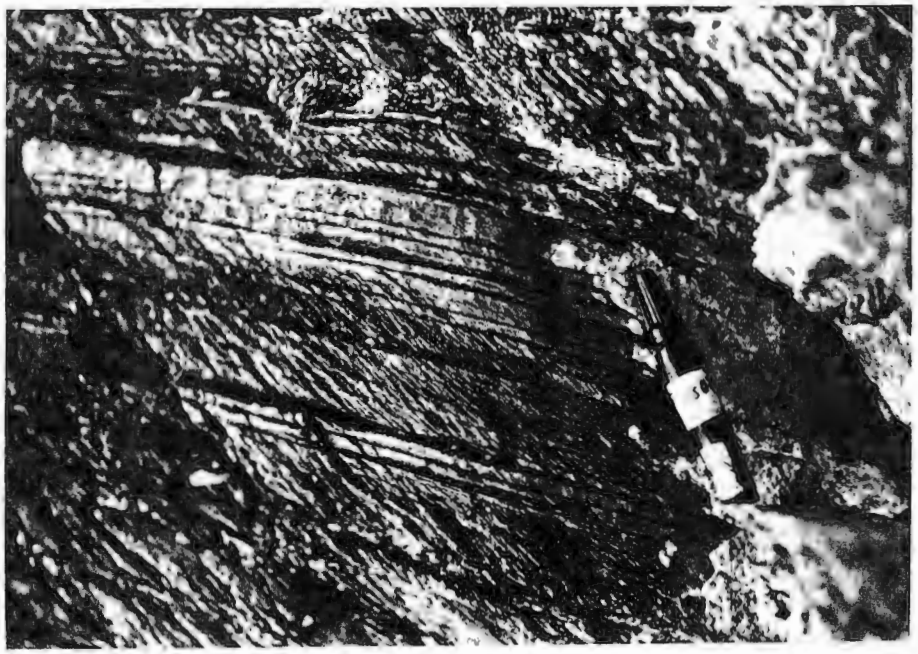

Plate 41. Detail of bedding and pressure solution cleavage in marginal parts of shear zone at locality 20074 (S_1 orientation - 206/63).

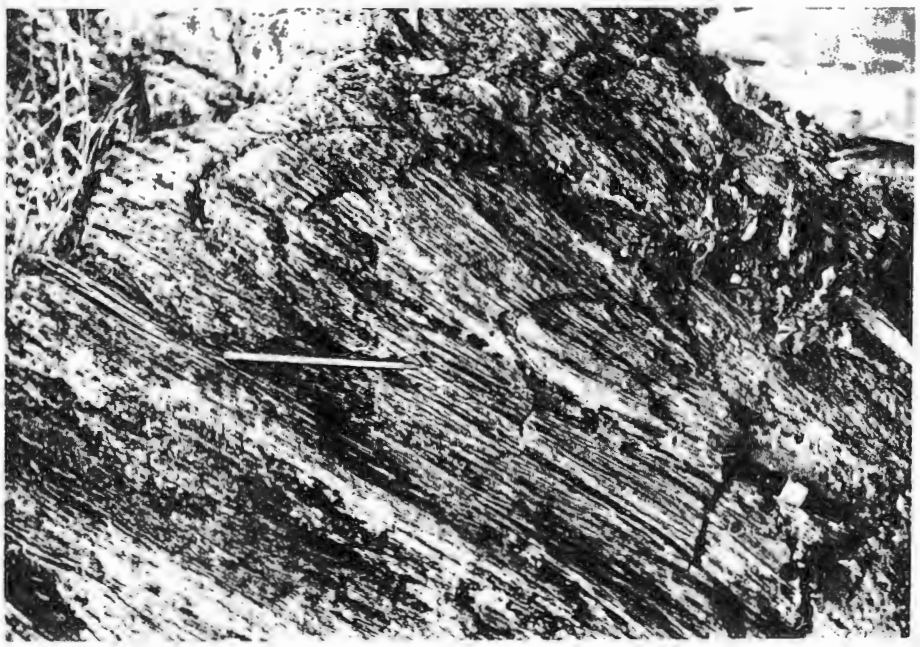

Plate 42. Detail of fold with axial-planar pressure solution foliation in central parts of shear zone at locality 20074 (S_1 orientation - 180/51.

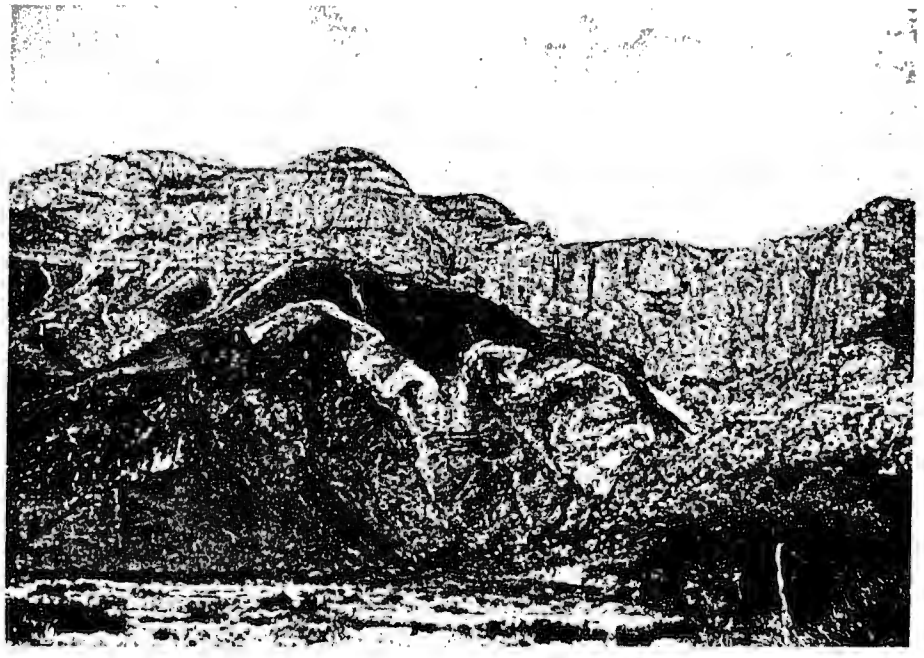

Plate 43. Folding in Tsabisis dolomite (N. Pavian nappe) below thick undeformed Noab dolomites. At upper left a very slight angular discordance between bedding in the Noab Formation and the base of the Kudu nappe is apparent.

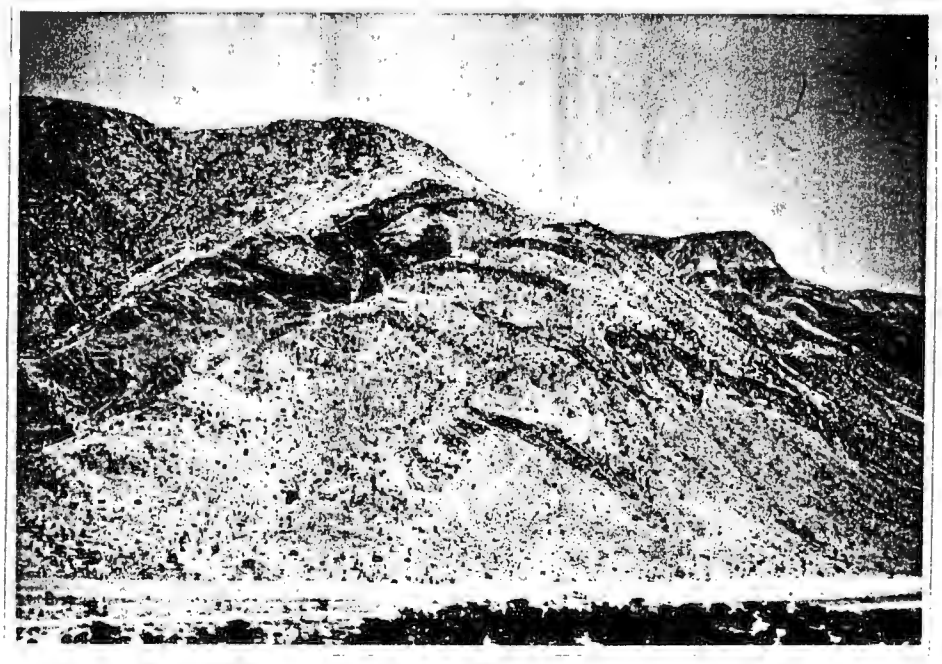

Plate 44. Imbrication in Tsabisis dolomite and folding in Blässkranz limestone beneath Kudu nappe west of Pavianskopf (Plate includes locality 30006 at point X).

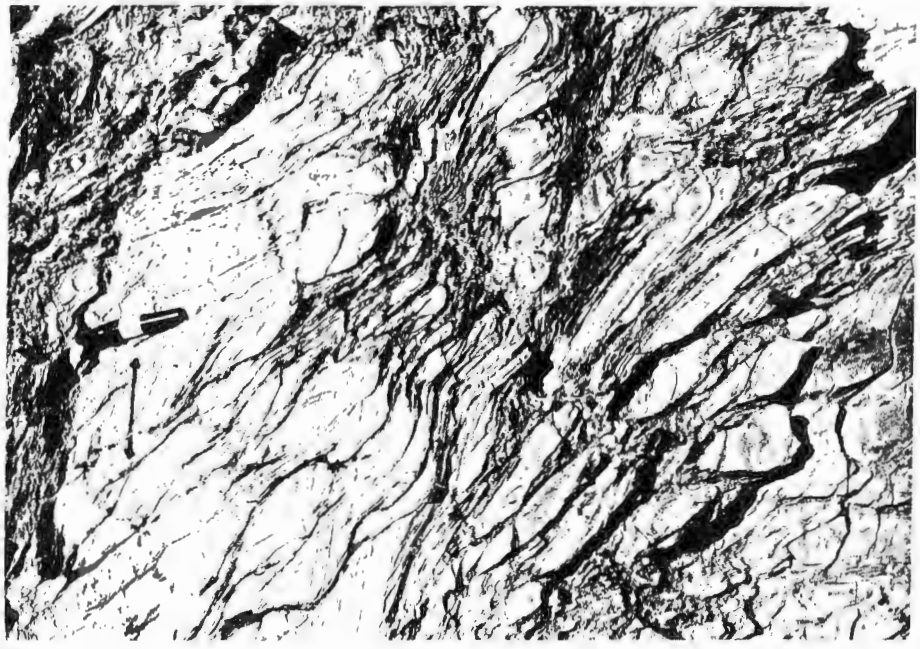

Plate 45. Minor folding and cleavage development in Blässkranz limestone. (Locality 30006)

Plate 46. Minor folding and cleavage development in Blässkranz limestone. (Locality 30006)

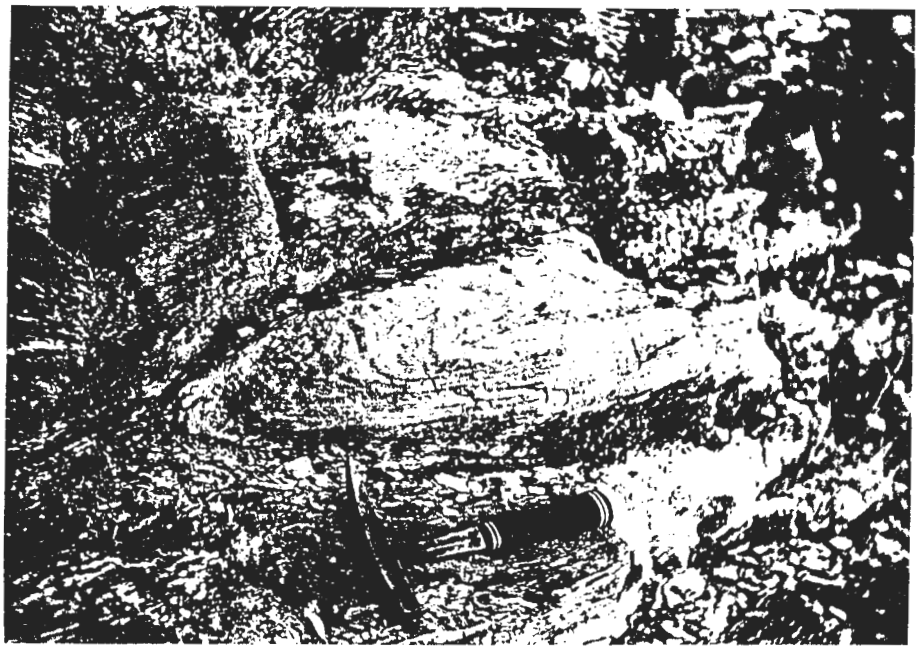

Plate 47. Minor fold in marble-phyllite zone at base of Kudu nappe on Tsabisis Oos. (Locality 30021)

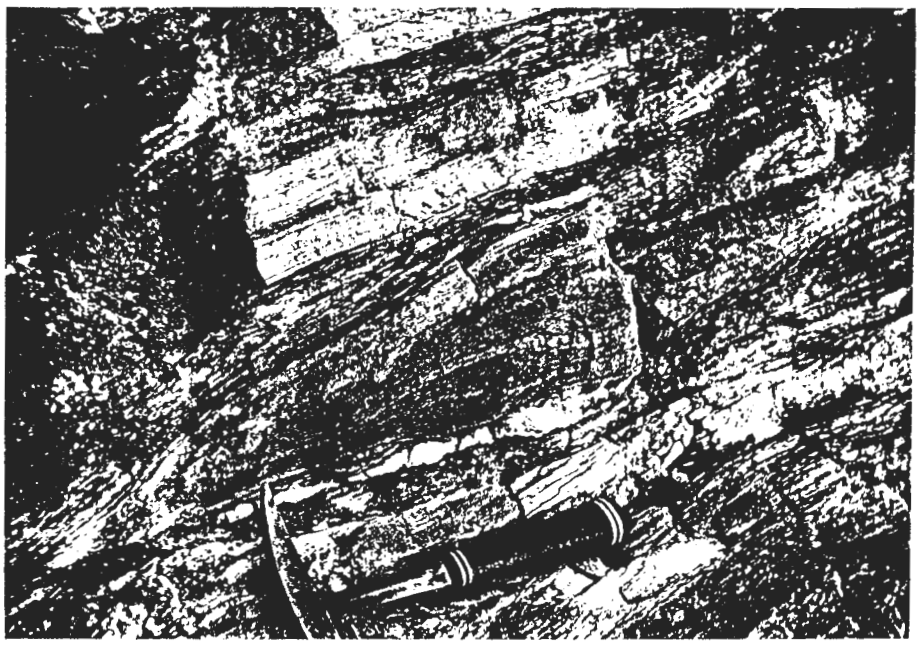

Plate 48. Isoclinal minor folds at base of Kudu nappe with pressure solution cleavage developed in the thickened lower limb of the fold above a conspicuous calcite vein. (Locality 30021)

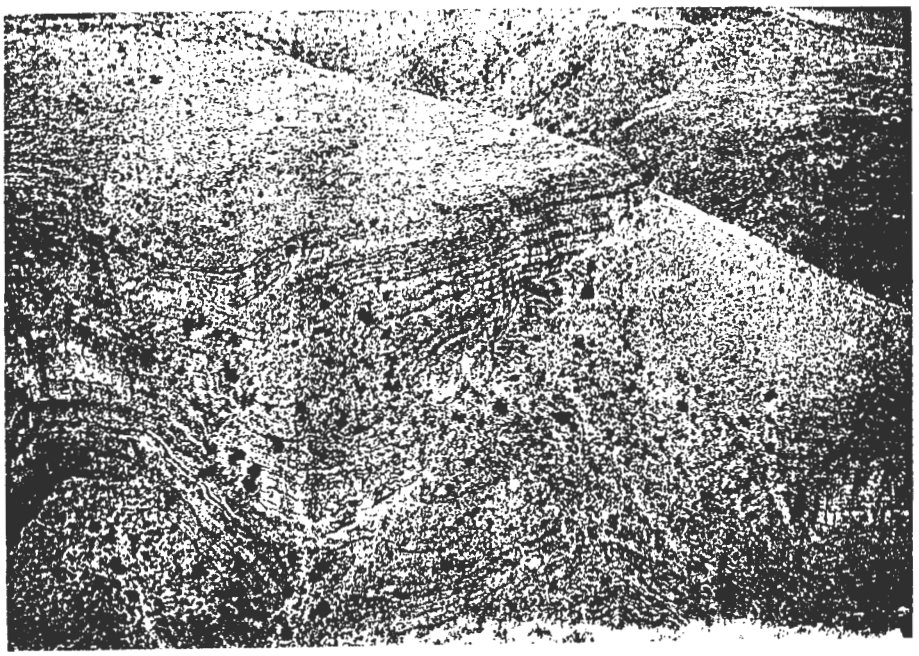

Plate 49. Anticline and thrust exposed in slopes south of locality 40027, upper Büllsport Formation. (View from locality 40056)

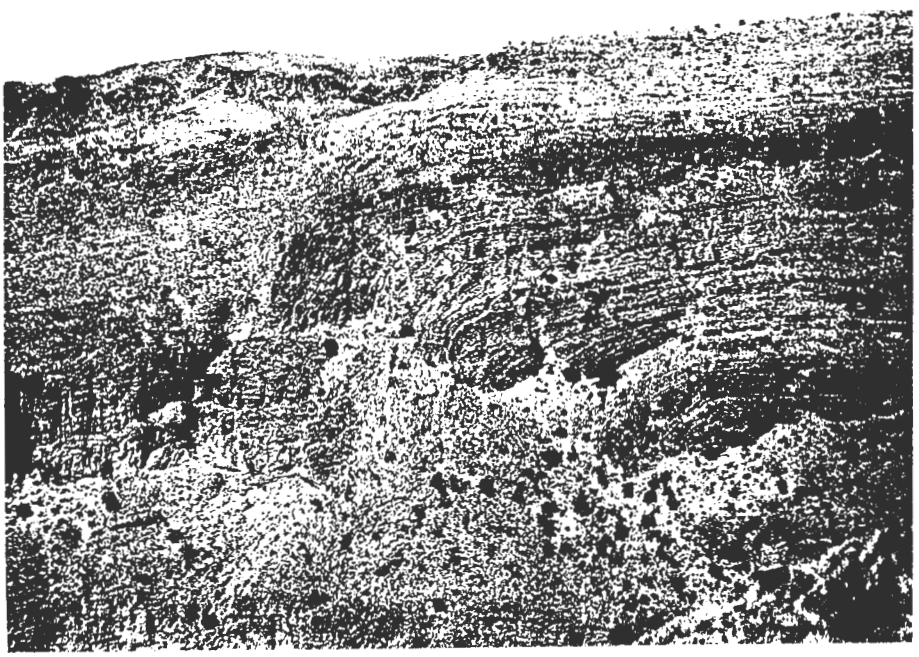

Plate 50. Monoclinal fold and thrust in upper Büllsport Formation west of locality 40019.

Plate 51. Truncated syncline in Büllsport Formation above low-angle thrust exposed in ridge below locality 40056. (View from locality 40027)

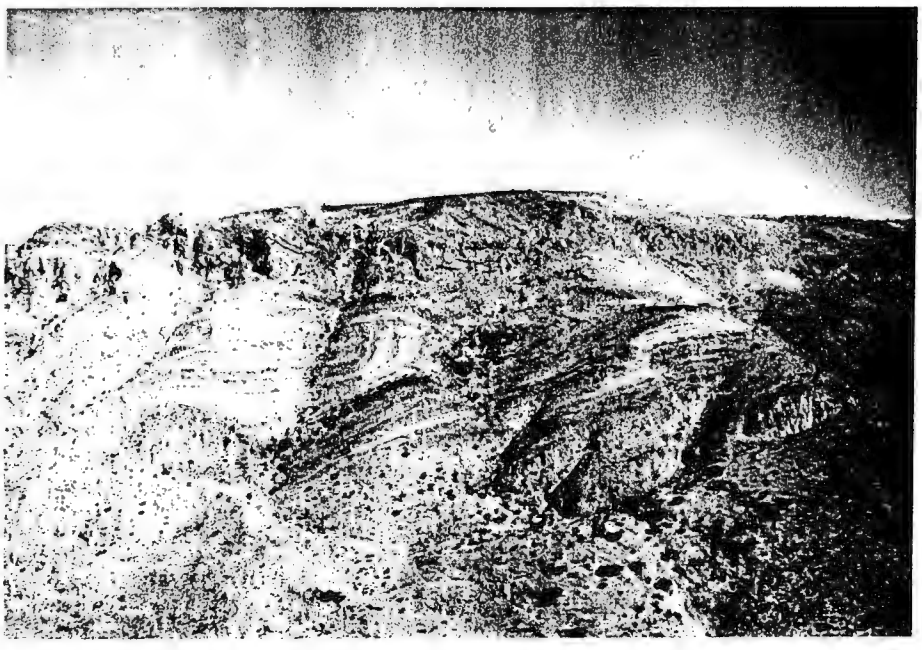

Plate 52 View of slopes east of trig. beacon Sieg showing truncation structures at base of E. Dassie nappe. (View from locality 40004)

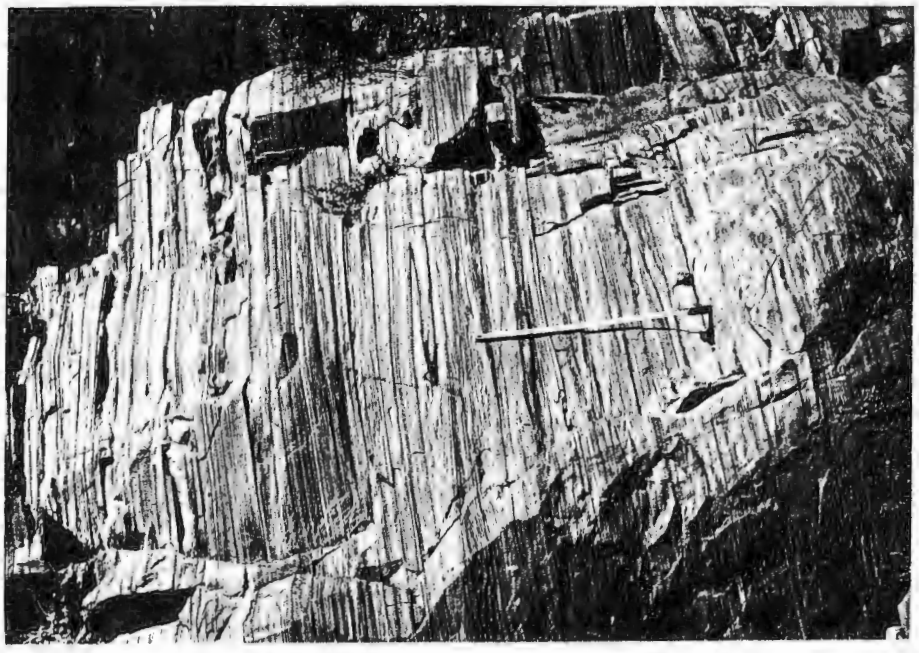

Plate 53. Structures in marble zone at base of Büllenkopf, W. Dassie nappe. Note irregularly deformed calcite veining left of scale tip and that although minor Z-folds are predominant rare minor S-folds are also seen, e.g. immediately to right of scale. (Locality 50108)

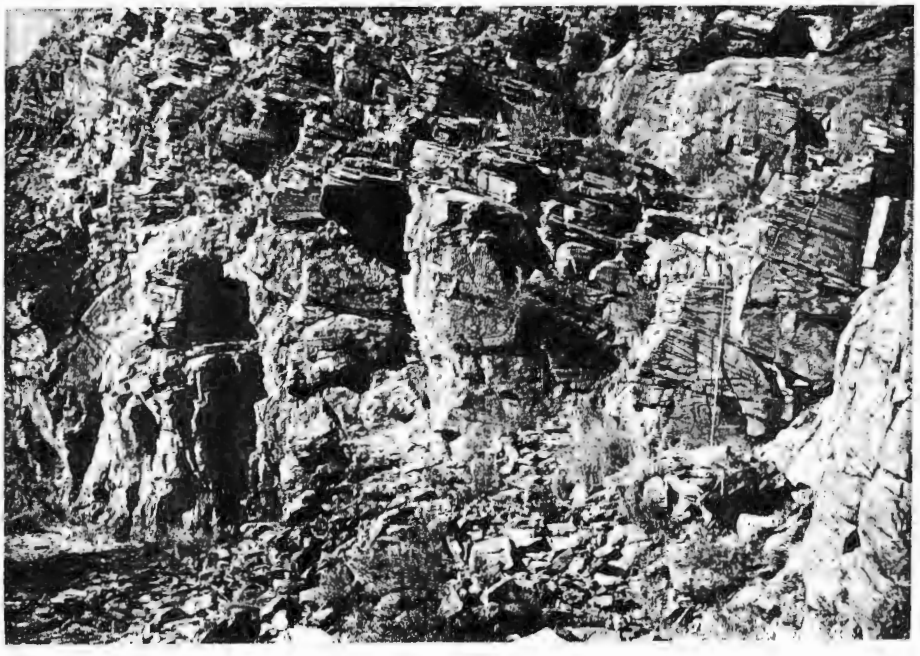

Plate 54. Downward facing folds in marble zone below Büllenkopf. Scale on right is 2 m long. (Locality 50108)

Plate 55. Detail of fold in plate 54. (Locality 50108)

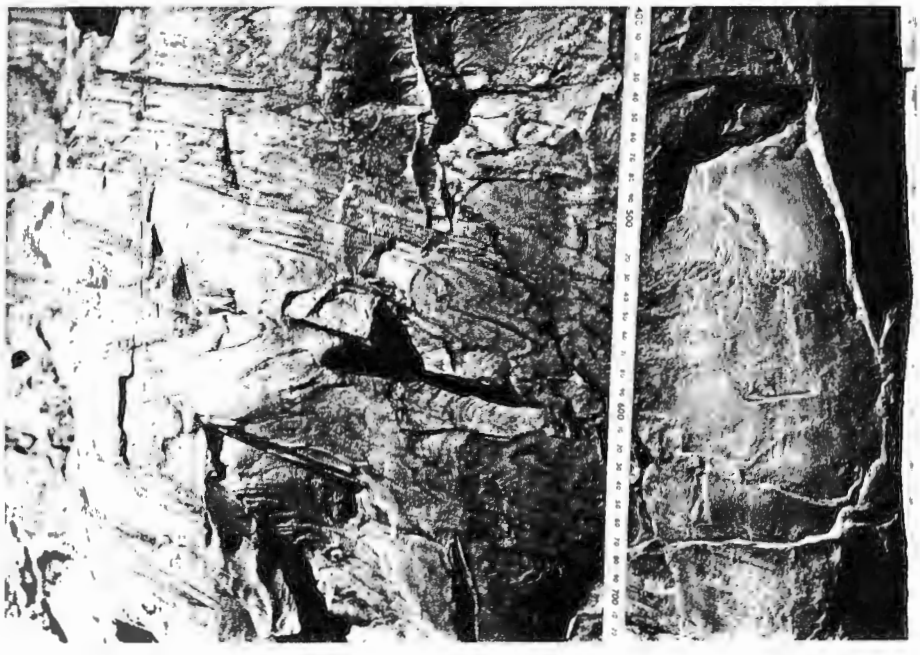

Plate 56. Fold interference pattern (Ramsay Type 3) in Büllenkopf marble zone. (Locality 50108)

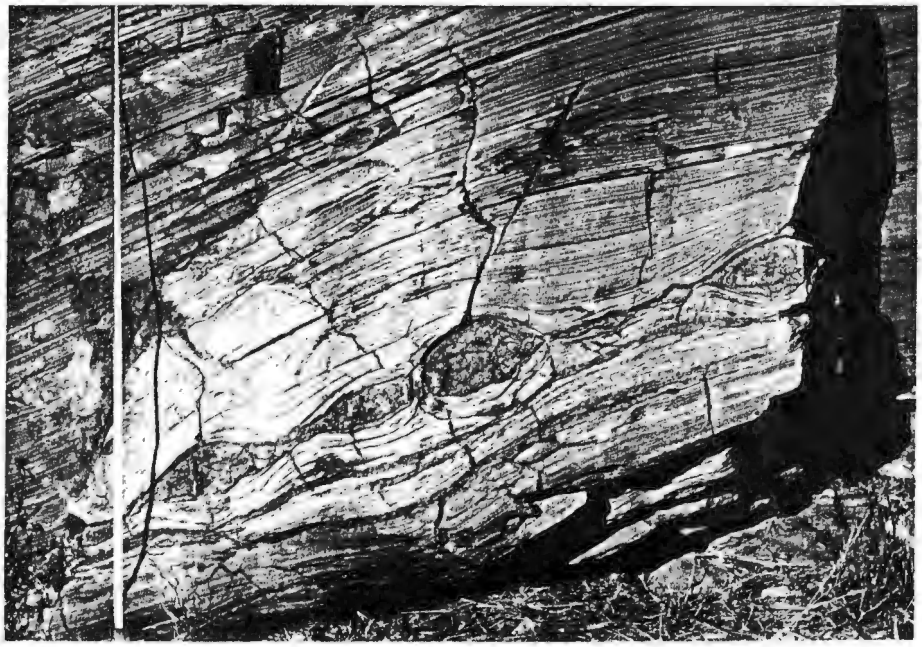

Plate 57. Boudinage of dolomite layer in Büllenkopf marble zone. (Locality 50108)

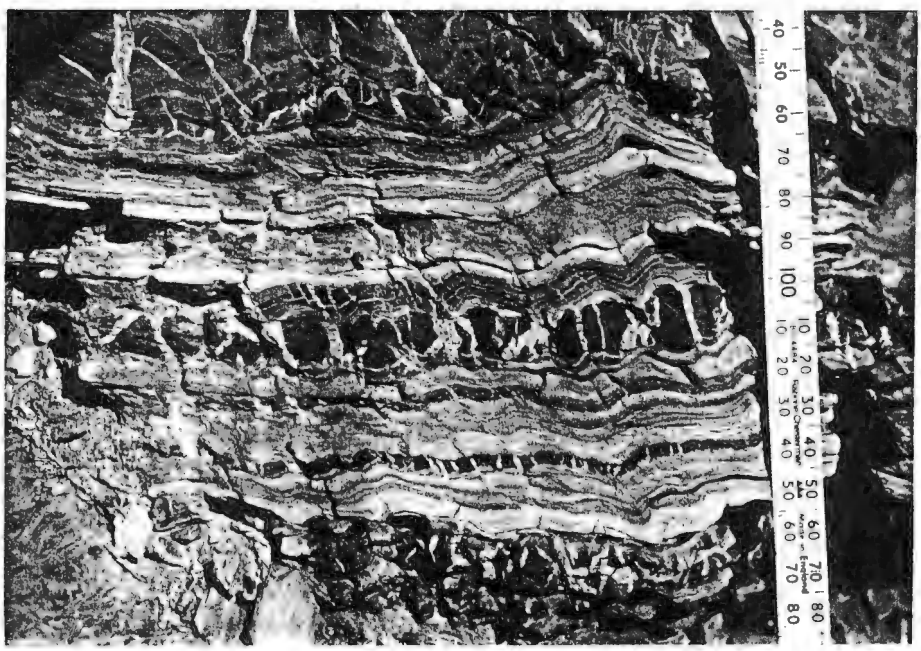

Plate 58. Boudinage of less ductile phyllite layers in marble with calcite veining in spaces between phyllite fragments. (Locality 50107)

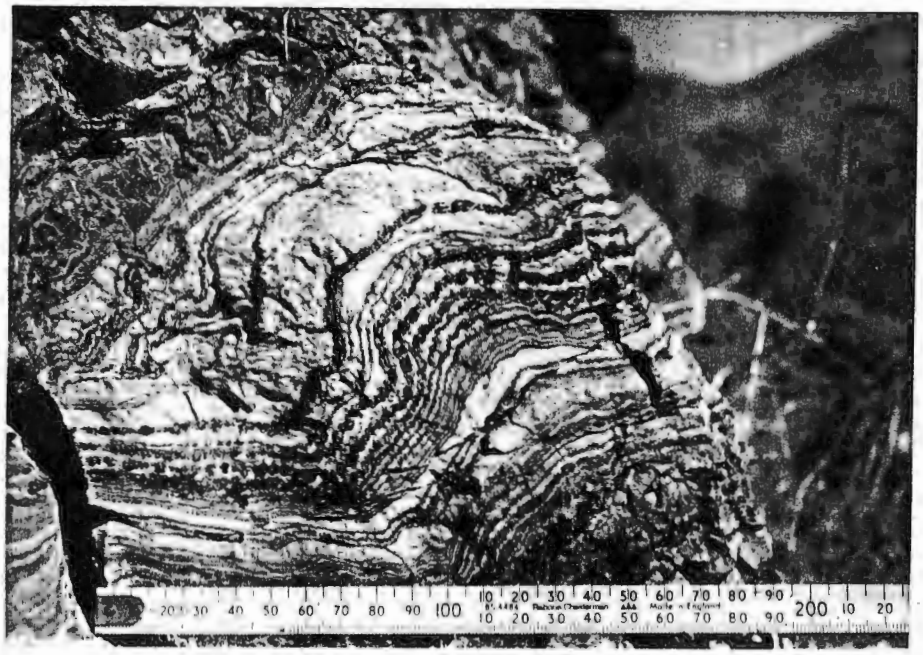

Plate 59. Late folding of previously boudinaged phyllite layers in marble. (Locality 50107)

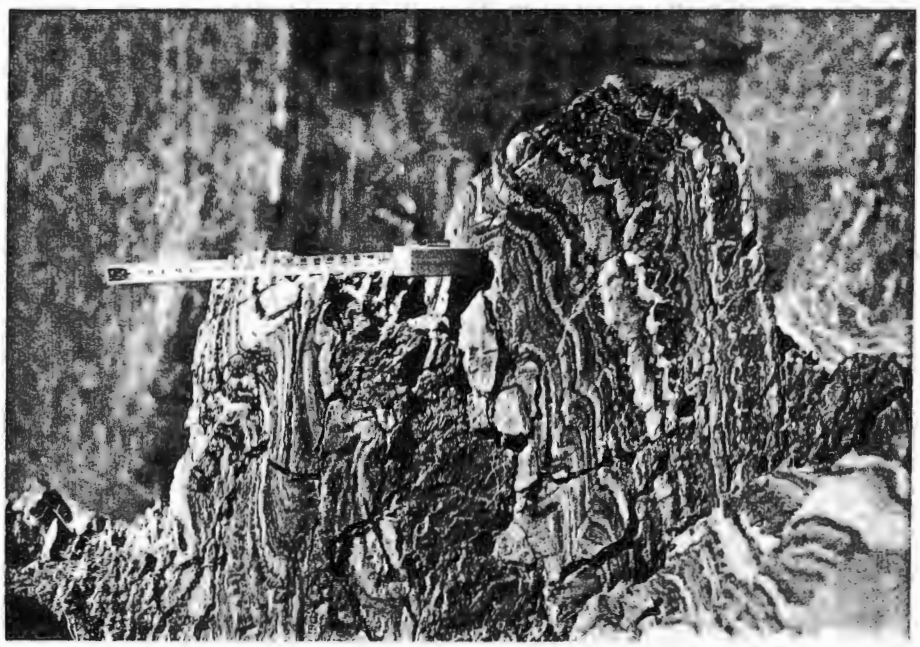

Plate 60. Cusp and fold structures reflecting ductility contrast between phyllite and marble. (Locality 50107)

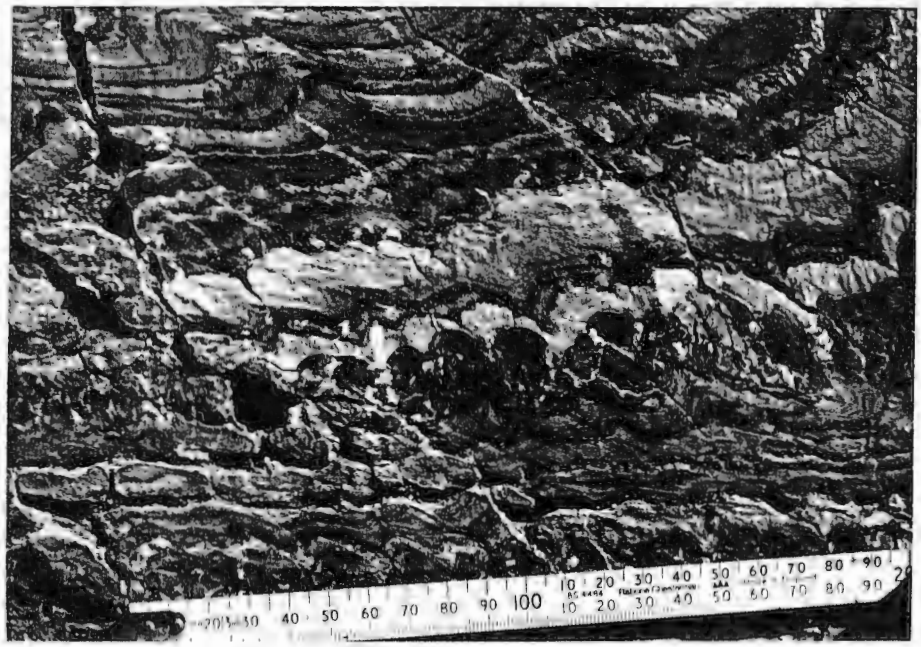

Plate 61. Detail of part of Plate 60.

Plate 62. Folds of variable style in marble zone. (Locality 50076)

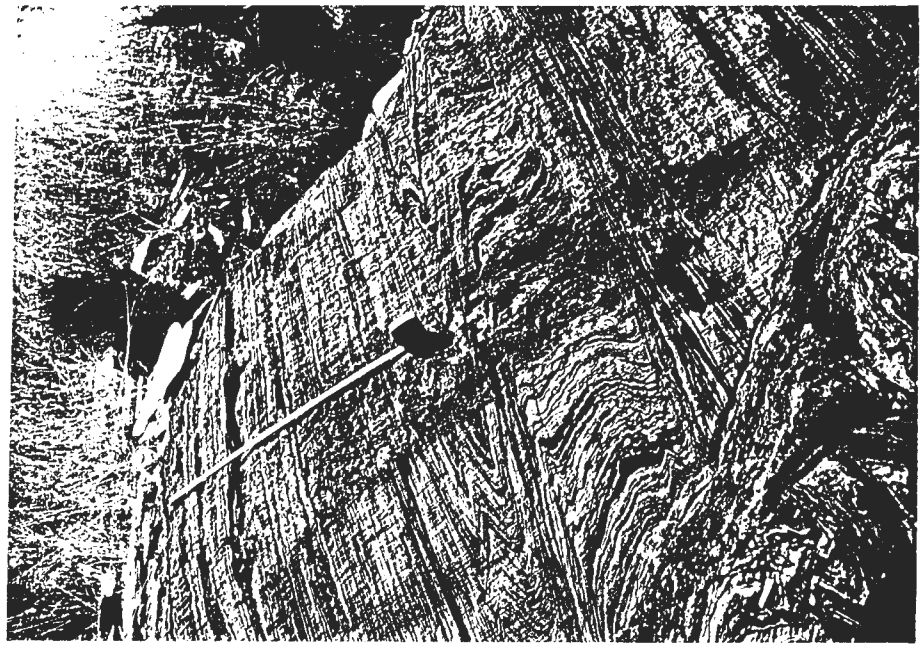

Plate 63. Tight folding and transposition of early layering in marble zone. (Locality 50076)

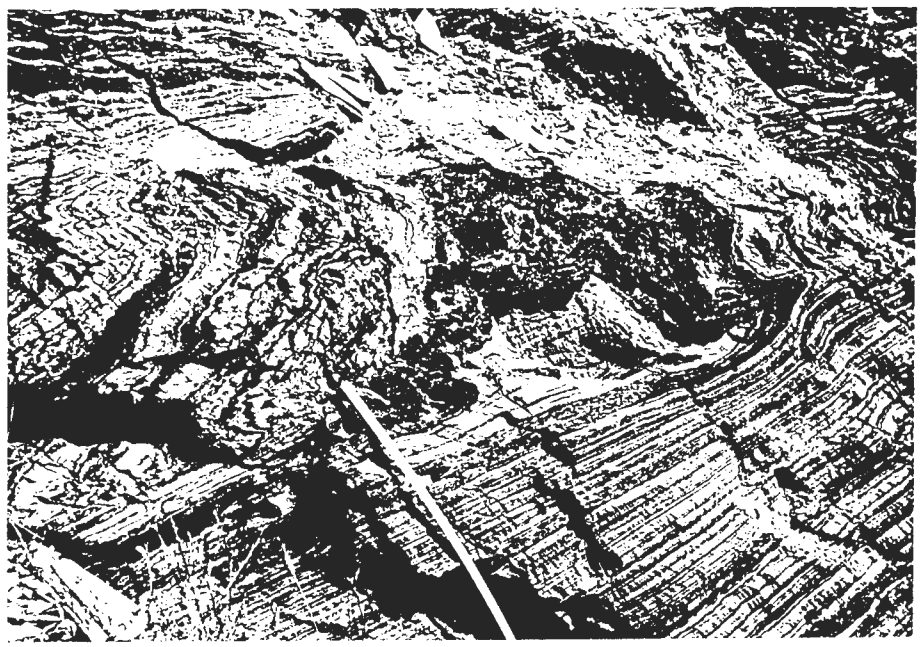

Plate 64. Fold interference pattern in thin marble and phyllite layers. (Locality 50076)

Plate 65. 10 cm thick breccia zone along thrust surface between lower Büllsport dolomite and middle Büllsport clastic unit. (Locality 50115)

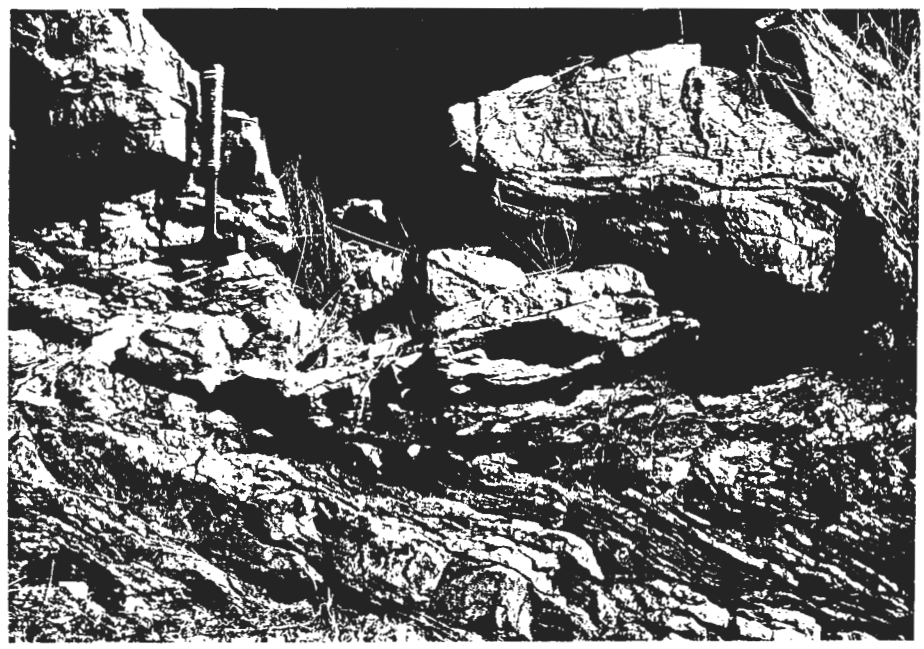

Plate 66. Folding in middle Büllsport quartzite-phyllite sequence below minor thrust surface. (Locality 50115)

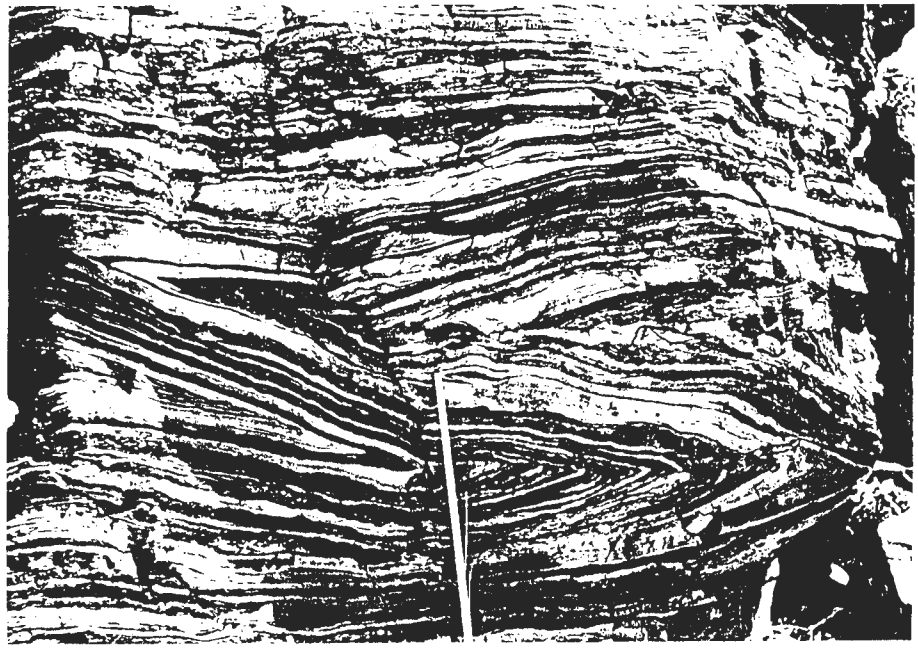

Plate 67. Tight minor S-fold of chevron style with incongruous minor S-fold on overturned limb immediately right of scale tip, marble zone in W. Dassie nappe. (Locality 50139)

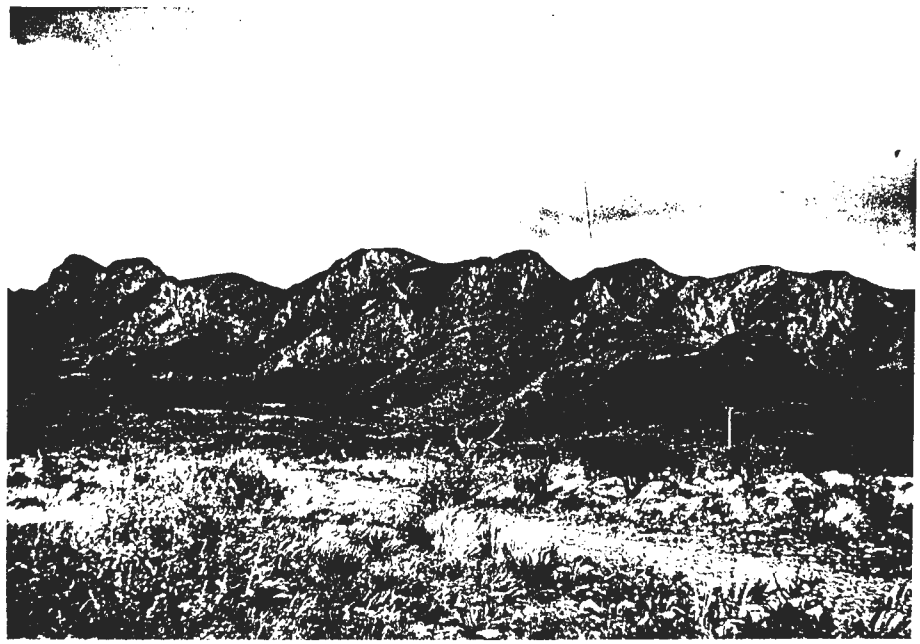

Plate 68. View of major imbrication structures above horizontal Unconformity Dolomite in westernmost cliffs of W. Dassie nappe, farm Die Valle.

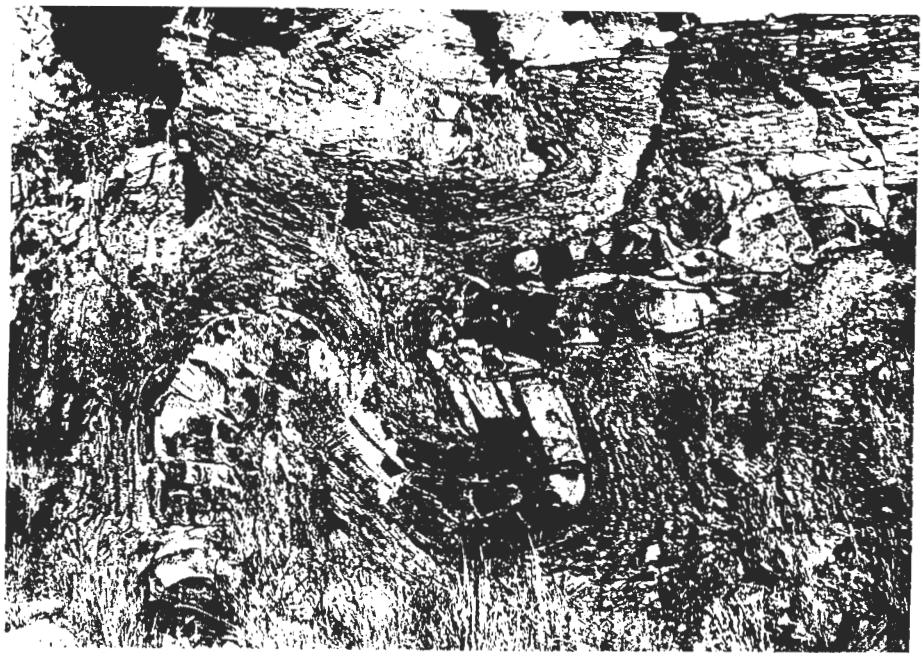

Plate 69. Style of minor folding in sandstone layers within shale of lower Zebra River Formation. (Locality 70001)

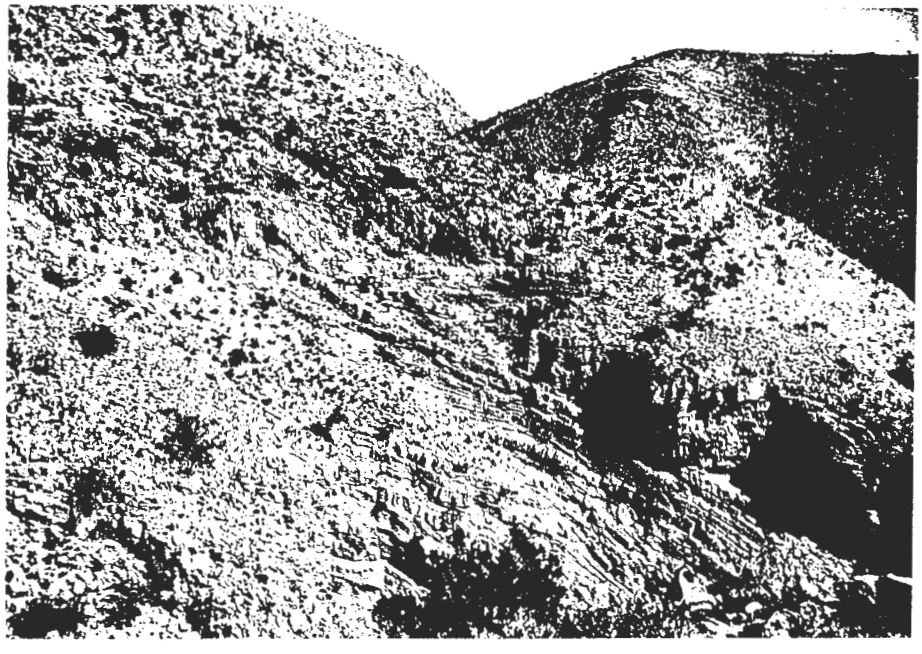

Plate 70. Unconformity between subhorizontal Zebra River Formation at upper left of plate and highly deformed Büllsport Formation at lower right. (Near Locality 60017)

Plate 71 View of northwest dipping unconformity dolomite in nappe front on Naukluft. Figure on right gives scale (below Locality 70034)

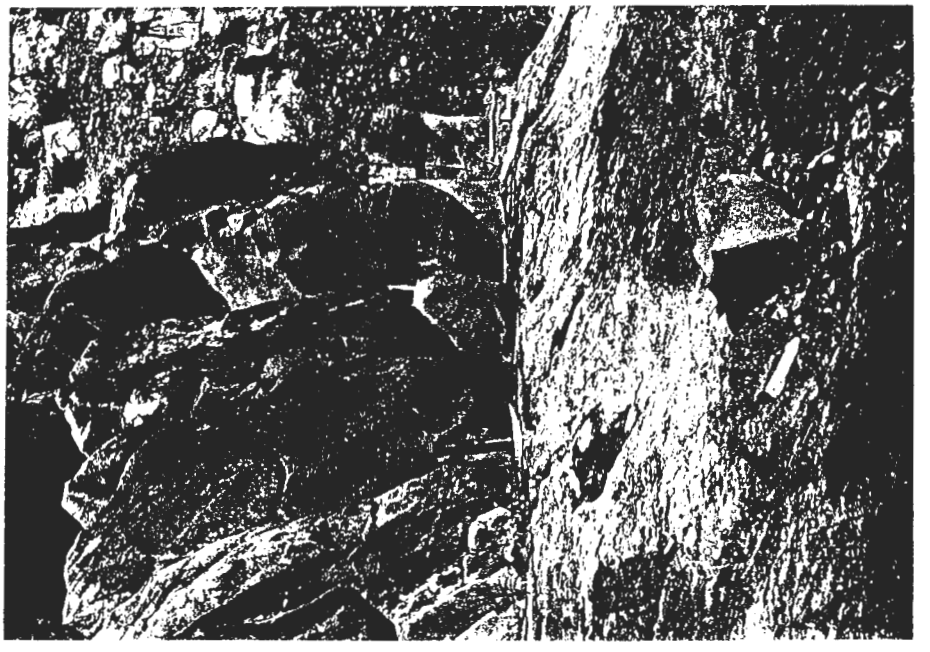

Plate 72. Close-up of Unconformity Dolomite in Plate 71 illustrating smooth basal surface.

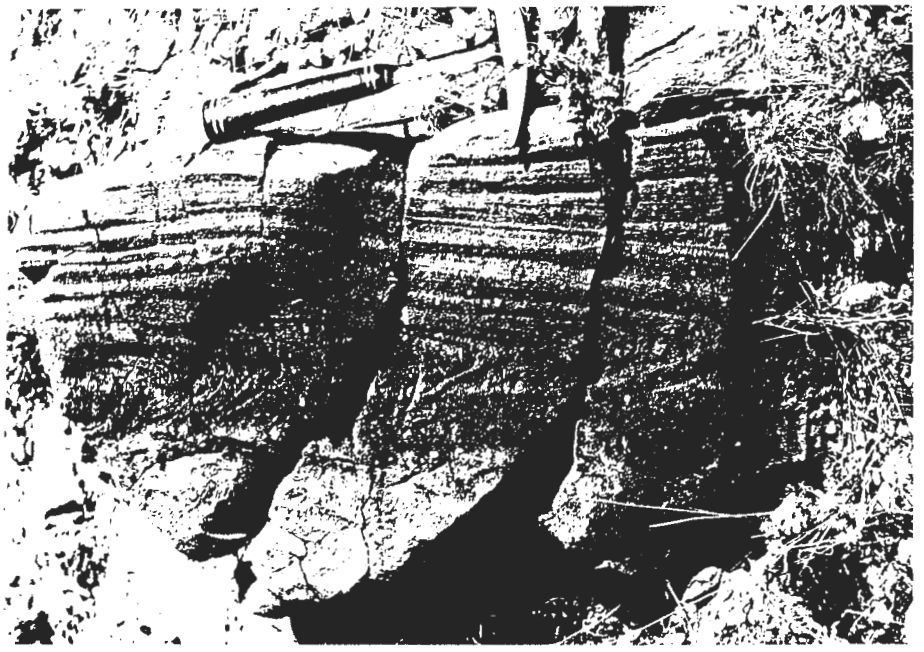

Plate 73. Minor fold in Unconformity Dolomite fragment found below nappe front near locality 40004.

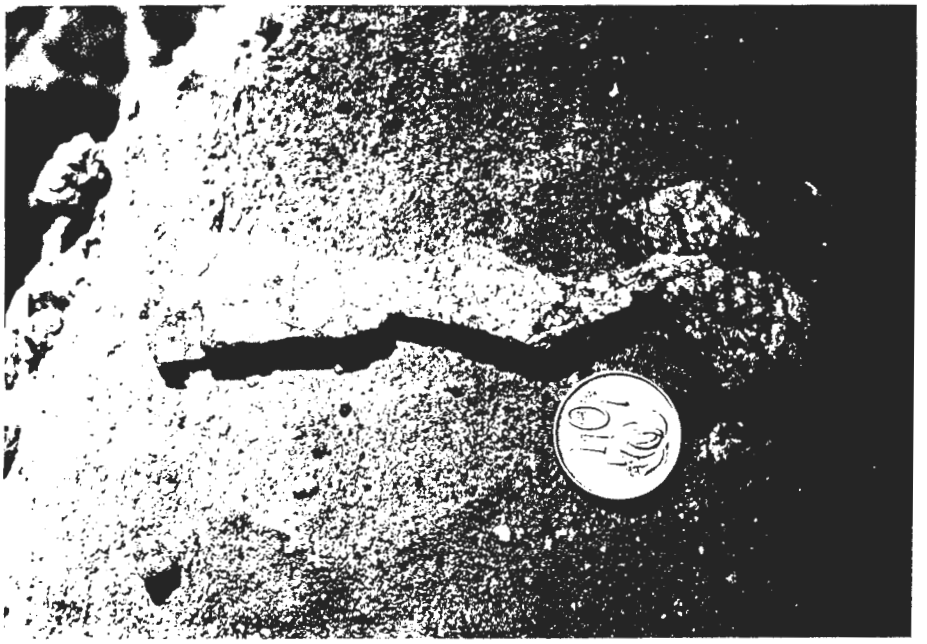

Plate 74. Curiously shaped granitoid "xenolith" in Unconformity Dolomite from nappe front on Büllsport. Coin diameter is 2 cm. (Locality 50011)

THE STRUCTURAL GEOLOGY OF THE NAUKLUFT NAPPE COMPLEX AND ITS RELATIONSHIP TO THE DAMARA OROGENIC BELT, SOUTH WEST AFRICA/NAMIBIA

APPENDIX VOLUME

CHRISTOPHER JOHN HUBERT HARTNADY

Appendix to

thesis submitted in fulfilment of the requirements for the degree of Doctor of Philosophy in the Faculty of Science of the University of Cape Town.

1978

APPENDIX CONTENTS

CHAPTER A-I

THE PRECAMBRIAN RESEARCH UNIT TECTONIC DATABASE - PRUDE

A INTRODUCTION

B PURPOSE OF THE PRUDE SYSTEM

C DATABASE DESIGN AND STRUCTURE

1 Computer system for structural data - a brief review

2 Design of the PRUDE system

3 Structure of records in PRUDE data files

D BRIEF DESCRIPTION OF THE PRUDE SYSTEM

1 PRUDE+PRGFILE

2 PRUDE+RELFILE

3 PRUDE+ABS

4 Functions of PRUDE programmes

REFERENCES - A-I

(29 pages, 3 figures, 1 table)

KEY TO CODES USED IN THE NAUKLUFT ORIENTATION DATA FILE

(4 pages)

THE NAUKLUFT ORIENTATION DATA FILE

(35 pages)

THE NAUKLUFT LOCATION DATA FILE

(11 pages)

CHAPTER A-II

DYNAMIC ANALYSIS OF SLOW FINITE DEFORMATION IN INHOMOGENEOUS VISCOUS SOLIDS: A CONTRIBUTION TO THE THEORY OF CONGLOMERATE DEFORMATION

A THE CONTINUUM MECHANICS APPROACH TO STRUCTURAL GEOLOGY

1 Introduction

2 Constitutive equations for crustal rock

B THE FINITE-ELEMENT METHOD

1 Evolution and general principles

2 Outline of the present technique

C APPLICATION OF THE FINITE-ELEMENT METHOD

1 Brief review of tectonic applications

2 Application to aspects of conglomerate deformation theory

3 Results of computer experiment series CE4

4 Discussion of the results

REFERENCES - A-II

(34 pages, 12 figures, 5 tables)

CHAPTER A-I

THE *P*RECAMBRIAN *R*ESEARCH *U*NIT TECTONIC *D*ATA/BAS*E* - PRUDE[1]

> "Without observations and measurement, without data there would be no geology. And yet these humble servants of the science have received remarkably little attention. Only a small part of these data are being published. The bulk remain in notebooks and are, for all practical purposes, lost to the geological community. In geology, it is easier to find a publisher for the most irrelevant ideas than it is to publish a table of good data."
>
> (Hubaux, 1973, p.159)

A. INTRODUCTION

Modern structural geology is being transformed into a quantitative science in which the importance of mathematical theory and experimental method is steadily increasing. The upsurge of interest in mechanical theory, exemplified in the continuum mechanics approach to structural geology (cf. Hobbs, 1971; Ramsay, 1976) and advances in experimental and modelling technology expecially in relation to the mechanical behaviour of rocks *as materials* (cf. Paterson, 1976) is evidence of this trend. A problem remains, however, in the proper application of the results of theoretical and experimental studies to some of the major problems of structural geology encountered in the field. This presupposes that quantities assumed by or derived from theory and experiment can be measured in the field.

Tectonic geology begins in the field with the precise description of

[1] *Prude*, n. Woman of extreme (esp. affected) propriety in conduct or speech.
(Concise Oxford Dictionary of Current English 1964)

structural geometry (Turner & Weiss, 1963) in terms of data of location, dimension and orientation. This data is clearly capable of being related quantitatively to similar data measured in model systems of either the "analogue" type (i.e. plasticine experiments, etc.) or the "digital" type (i.e. computer simulation studies). At the present time, most comparisons of experimental or computer models with real geological examples are qualititative. In the future, however, it is likely that realistic modelling will be possible in which the complicated geometry boundary conditions and material properties of a computer simulation study by the finite element method (cf. Chapter A-II) for example, are matched, in as precise a manner as possible, with equivalent quantities measured or inferred for an actual large- or small-scale rock structure.

The data system described in this chapter anticipates this development. It aims to show how the basic quantitative data from the geometric analysis of rock structure can be stored, handled and accumulated prior to the stage of quantitative kinematic or dynamic analysis in computer file structures which can later be used to store, handle and accumulate the same types of data derived from laboratory, but more especially from computer simulation experiments. The PRUDE system is therefore ultimately intended as a practical bridge between field structural geology and theoretical/experimental tectonophysics.

B. PURPOSE OF THE PRUDE SYSTEM

Apart from this rather fundamental, long-range objective, there are other reasons for the design and implementation of a tectonic data base system in the Precambrian Research Unit at the University of Cape Town. These revolve mainly about the Unit's participation in the South African National Geodynamics Programme (Geodynamics Project in South Africa, 1975). This involves basic structural analysis of fairly extensive areas within highly deformed and metamorphosed terrains of the Namaqua Metamorphic Complex and the Damara orogenic belt. Since the work in some study strips is carried out by a number of individual participants, not all from the same institution, it was felt that a formal computer-

based system for tectonic data storage, retrieval and processing had become a practical necessity. It was especially felt that:

(i) Geometric data acquired in an on-going project involving a number of successive participants or contributors should meet high and well-defined standards of objectivity and reproducibility;

(ii) Data acquired by a participant during an early stage of the project should be readily accessible, bare of any interpretation whatsoever, to other participants in the same or later stages of the project;

(iii) Fast, convenient and mathematically-sound methods should be available to all project participants for the standard analysis, processing and display of vector and tensor tectonic data and should ideally be supplemented as work proceeds by more sophisticated techniques of kinematic strain modelling as these are developed;

(iv) An intensive programme of tectonic research such as the Geodynamics Project should be concerned as much to develop and disseminate new methodologies for advanced tectonic analysis, as well as more efficient means for the communication of primary data between participants at different institutions, as with more substantive questions.

In this last respect, it should be noted that the PRUDE system is envisaged not only as a tool for assisting and improving the analysis and interpretation of tectonic data, but also as an effective medium for data communication and publication.

With large-scale projects such as the Geodynamics Programme (and, one might add, projects in mineral exploration or the tectonic analysis of an individual mine, as well as rock mechanics projects for large underground or open-cast excavations) there are, at the present time, many reasons of economy and convenience for resorting to computer-based systems for the handling of geological field data. Some of these are that large volumes of data may be speedily processed - and if necessary, be reprocessed again and again - without undue effort or tedium ; that data stored permanently in this tractable form has a cumulative value, increasing in significance with successive additions; and that a greater and more modern variety of modes of presentation - graphical

and tabular - may be conveniently employed in its dissemination. The capabilities now provided by third-generation computers and their associated software are, as Gordon and Hutchinson (1974) have stated, "essential to any scientific programme requiring interpretation of and instantaneous interaction with, large volumes of data". Speed of computer-based data processing is many orders of magnitude greater than manual data-processing, which in certain respects enables methods of data interpretation to be employed which would previously have been unthinkable because of the sheer volume of calculation required. Thus the use of the computer may extend the scope of data interpretation into entirely new realms.

One aspect of geometrical analysis in structural geology that has given some cause for concern is the tendency of orientation data measured in the field to become divorced from the precise location of measurement in the course of conventional quasi-statistical data-processing operations, such as the plotting and contouring of equal-area Schmidt orientation diagrams (cf. Turner & Weiss, 1963). In geomorphological research the same concern has led to the development of so-called "spatial analysis" techniques (Chorley, 1972). The PRUDE system has been designed with view to the eventual incorporation of spatial-analytical methods in tectonic geology, although this is not an immediate objective.

The various purposes of the PRUDE tectonic data-base system may therefore be summarised as follows:

(1) To encourage and facilitate the acquisition of high-quality field orientation data, which are precisely measured and accurately located in space;
(2) To facilitate the storage, processing and reduction of such data within the framework of an on-going project;
(3) To assist moves towards the establishment of a standardised system for recording and objectively classifying field structural data;
(4) To provide a practical computer-based system whereby properly classified structural orientation and location data may be permanently stored on completion of the project in which it was required, in a form in which it can be rapidly searched, retrieved, reprocessed

or disseminated for the benefit of future research;

(5) To provide a practical computer-based system which enables field orientation and/or location data to be easily processed by routines for the quantitative kinematic modelling of rock deformations (i.e. "unstraining" programmes) or to be realistically correlated with the results of future quantitative theoretical modelling routines.

The last-mentioned purpose of the PRUDE system is perhaps the most important.

C. DATA BASE DESIGN AND STRUCTURE

Previous work towards the development of computer-based systems for the recording, storage and retrieval of structural field data has usually been done in the context of state geological surveys of large areas, where a large number of differently experienced workers are involved and the need arises to maintain consistency between and order within data collected by them. The PRUDE system, however, has been developed in the context of structural research in terrains which may be either well-surveyed or totally unsurveyed. The prime objective is to promote the development of realistic and precise models of structural geometry over a wide range of possible scales and the application of quantitative methods for modelling the kinematic evolution of structures in deformed rocks. The present system therefore contrasts strongly with a number of other computer-based systems for handling geological field data that have been developed recently.

1. Computer systems for structural data: a brief review

In recent years, a number of "computerised field mapping systems" have been publicised in the geological literature. Prominent examples are systems described by Wynne-Edwards *et al.*, (1970), Berner *et al.*, (1972, 1975), Platou (1971, 1975) Roddick & Hutchinson (1972), Gaál & Suokonautio (1973) and Reinhardt & Jackson (1973). The subject of computer-based geological data systems was briefly reviewed from the general standpoint by Hubaux (1973) and

more specifically the requirements for and descriptions of successful field data systems have been dealt with generally by Hutchinson (1974), Gordon & Martin (1974a, b), Gordon (1975), McRitchie (1975) and Hruška (1976) for example. Important contributions to the subject of computer-based systems for geological data have been made in the volumes : "Computer use in Projects of the Geological Survey of Canada" (Gordon & Hutchinson, eds. 1974), "Computer-based Systems for Geological Field Data" (Hutchinson, ed., 1975) and "Capture, Management and Display of Geological Data : with special emphasis on Energy and Mineral Resources" (Merriam, 1976).

Most of the geological field data systems mentioned above (e.g. Wynne-Edwards *et al.*, 1970; Berner *et al.*,1972; Platou, 1971 and Gaal & Suokonautio 1973) are designed specifically for project work in a specific type of terrain, such as a granite-gneiss complex and are based on some form of "input document" dictated by the terrain character and the project objectives. This formalised field sheet prescribes the type of observations that are to be recorded at each outcrop. In other words, the implicit "geological object" which is being described is the "outcrop". In defining data files, it is imperative to choose basic units of description, each of which corresponds to a single record in the file, that are quite distinct and capable of clear definition (Hubaux, 1973). In most contexts, the "outcrop" is an extremely complex entity, which is not always distinct and hardly capable of clear definition. Data input documents constructed on this basis are often themselves complex, thus complicating subsequent data management and sometimes burdened with numerous irrelevancies, such as "state of weathering of the outcrop" (cf. Wynne-Edwards *et al.*, 1970).

Systems such as these are usually described as the *ad hoc* type (Williams, 1975), in contrast to *generalised* systems, the design philosophy of which is quite different. A generalised system, in simple terms, is one which can handle almost any kind of data. Prominent examples of generalised systems for geological data management are G-EXEC (Jeffery & Gill, 1975, 1976) and GRASP (Botbol & Bowen, 1975; Bowen & Botbol, 1975). The objectives which have been spelled out for the G-EXEC system are that it should:

(i)be *generalised*;

(ii) be *portable* (i.e. run on almost any kind of large- or medium-sized computer);

(iii) be *integrated* through all the phases of data management, data analysis and data display;

(iv) be *amenable to extension* by programmers;

(v) *handle "current project" and "archival" data* with equal ease.

(Jeffery & Gill, 1975)

The fundamental characteristics that G-EXEC and GRASP have in common are:

(i) they have a *modular design*;

(ii) they have been *written in a high-level computer language*, namely FORTRAN IV.

Modular design, which means that the system is made of relatively short individual programme segments or subroutines, each of which has a specific function, allows easy building of new programmes and simple improvement or updating of individual programme modules as the system matures and develops. The fact that the systems are written in FORTRAN IV means that they can be implemented on any computer that has a FORTRAN compiler. Thus the future extensibility and portability of these systems is assured.

Generalisation is achieved in both systems by adoption of the matrix as the standard form for data-base files. In matrix form, the file *records* (i.e. the items or objects to be described) are the rows and the attributes of each record are the columns. In computer terminology, each column of the matrix is called a *field*. The matrix form for data-base files dictates that all records in an individual file must contain the same fields and that each field must be of the same length and type throughout all records in the file. This is sometimes called "fixed field" structure. *Field length* is measured in *words*, corresponding to a given number of binary *bits* (usually 32 or 36) and *field type* may be alphameric, alphanumeric, real-numeric or integer-numeric. In both G-EXEC and GRASP, the number, length, type and meaning of fields in a data file can be defined ahead of time to the system, thus allowing the system to operate on any kind of data file as long as it is in standard matrix form.

2. Design of the PRUDE system

a. Brief history

A process of experimentation with an *ad hoc*-type geological field data system which began during 1973 and acquaintance with the NASA Apollo data-base which was used as a model for a geochemical data-base in the University of Cape Town Department of Geochemistry (Duncan & Willis, 1975), culminated during 1974 with the design of a file format for tectonic data. By mid-1975, almost all PRUDE system programmes had been written, a process which was facilitated by the fact that fairly simple modifications to routines written for the above-mentioned geochemical data-base enabled their adaptation to the intended tectonic data system. The PRUDE data system has been effectively operational since late-1975, (cf. Hartnady & Vajner, 1975) and has been used in the course of a number of projects (Vajner, 1976; Moore, 1977; Blaine, 1977; Van Bever Donker, in preparation) apart from the Naukluft investigation. This use of the system by geologists with little or no computer experience has enabled aspects of data entry and editing procedures to be improved or streamlined. Much remains to be done, however, to lower the barrier to effective use of the computer by such users.

b. Logical structure of the data files

The clear distinction between the *logical structure* of data files and the *physical structure* of the same has recently been identified as one of the major trends in the evolution of data-base management software (Engles, 1972). This distinction is associated with the concept of "data independence", which has been defined as "the capability by which an application programme is insulated from the various aspects of data-base design and implementation" (*op.cit.*, p.52). The concepts of "data independence" and "generalisation", as described in the previous section, are effectively the same.

The massive pre-occupation with complicated pre-determined numerical or alphanumerical coding schemes which characterises many earlier attempts at designing computer-based geological field data systems (e.g. Wynne-Edwards *et*

al., 1970; Berner *et al.*, 1972; Gaal & Suokonautio, 1973) arises mainly out of a failure to make this distinction and can be seen as an attempt to artificially impose the physical structure of the computer onto the logical structure of conventional geological activity. To the extent that this is true, these systems have met with traditional resistance.

At an early stage in the design of the PRUDE system, this potential pitfall was encountered and subsequently conscious attempts were made to avoid it. In the PRUDE system, there is a minimum of *pre-determined* coding. The user is largely free to specify his own codes and to change these as his needs require. This already reflects a large degree of data independence. The ultimate foundation of this data independence however, is the standard matrix form of the data files, a feature which PRUDE shares with the G-EXEC and GRASP systems.

In specifying the logical structure of PRUDE data files, quite independently of any consideration as to how the data would be physically stored in the computer, three fundamental questions were asked:

(i) What is the basic item of an individual data file?
(ii) What are the fundamental characteristics of an item of tectonic data?
(iii) What is the common current convention in the recording of structural field data?

In answer to the first question, the fundamental decision was made that the basic item of the tectonic data files should be the individual structural measurement made by the field geologist. As Hubaux (1973) has pointed out, in building geological data files it is preferable by far to adopt a man-made object as the basic unit of description, rather than natural geological objects which are not so easy to define. The individual structural measurement, for example of the orientation of a bedding surface, is itself a distinct and clearly-defined entity.

In answer to the second question, it was recognised that there are two classes of quantitative measurement made in the course of the geometric analysis of rock structure; namely, measurements of *orientation* and measurements of *location* (Turner & Weiss, 1963). It was accordingly decided that these two

classes of measurement should be stored separately in different files, following the principle that a data file should preferably be a collection of observations on *one kind* of geological object (Hubaux, 1973). It was, however, appreciated that, on a more fundamental level, measurements of orientation and location belong to the same class of mathematical entity. They are *both vector quantities* in spaces defined by three-dimensional orthogonal reference-frames. Both therefore require the measurement of three components for their complete specification.

The core fields of both the location and orientation data files are given over to the description of these vector components. In the orientation data file, the components of an orientation vector are described in the traditional polar form familiar to geologists (e.g. trend, plunge and length of a lineation vector). In the location data file, the components of a location vector are described in the Cartesian form familiar to both geologists and surveyors.

In addition to the three *core fields*, which constitute the essential single quantitative measurement in each record of the data file, it was necessary to include *supplementary fields* which describe the measurement in terms of a few important attributes. This means that each record of the data file is essentially self-describing, provided that the significance of the supplementary fields and the meaning of the valuesor codes within them is established. The position and significance of the supplementary fields is established in the PRUDE system by convention, but within reasonably wide limits the meaning of values and codes used in these fields remains at the discretion of the individual user of the system.

In establishing the position and significance of the supplementary fields in the PRUDE data files, an attempt was made to answer the third fundamental question asked above. Essentially, it was initially decided to model the PRUDE orientation data file on a common field note-book format used by structural geologists (cf. Turner & Weiss, 1963, p.86). It was subsequently realised that this basic file design could be used without change for the location data file as well. The supplementary fields in each file are organised into two categories:

Principal descriptor fields			Core fields			Subordinate descriptor fields			
LOCALE	FABELT	TYCODE	STR	DPL	SIZE	TAG	LITHCO	METHOD	REFER
1210110001	SI	GNB	.1680+03	.5000+02	.1000+00	0	AMPHBL	CCL	77P001
1210110002	SS	BED	.5400+02	.1100+02	.1000+00	0	QTZITE	CCL	77P001
1210110003	LI	FAX	.1580+03	.2100+02	.1000+00	1	BLSTN	CCL	77P001
1210110003	LI	FAX	.1000+02	.0000	.1000+00	0	BLSTN	CCL	77P001
1210110003	SI	FAP	.3200+03	.5700+02	.1000+00	1	BLSTN	CCL	77P001
1210110003	SI	FAP	.1000+02	.2000+01	.1000+00	0	BLSTN	CCL	77P001
1210110004	SI	BCL	.8400+02	.3200+02	.1000+00	0	BLSTN	CCL	77P001
1210110005	LIX	MEL	.3110+03	.3300+02	.1000+00	0	PELITE	CCL	77P001
1210110005	SI	CLE	.2480+03	.6000+02	.1000+00	0	QTZITE	CCL	77P001
1210110005	SI	CLE	.2130+03	.4100+02	.1000+00	0	QTZITE	CCL	77P001
1210110005	SI	CLE	.2580+03	.6200+02	.1000+00	0	QTZITE	CCL	77P001
1210110005	SI	CLE	.2540+03	.6500+02	.1000+00	0	QTZITE	CCL	77P001
1210110005	S2	CFC	.2170+03	.2900+02	.1000+00	0	QTZITE	CCL	77P001
1210110006	SI	CLE	.2910+03	.4200+02	.1000+00	0	BLSTN	CCL	77P001
1210110007	SI	CLE	.2480+03	.2700+02	.1000+00	0	BLSTN	CCL	77P001
1210110007	S2	TEVF	.7300+02	.7300+02	.1000+00	0	BLSTN	CCL	77P001
1210110008	SI	CLE	.1470+03	.5000+02	.1000+00	0	BLSTN	CCL	77P001
1210110009	LIB	ISL	.3140+03	.2900+02	.1000+00	0	BLSTN	GCS	77P001
1210110009	SI	BCL	.3080+03	.6900+02	.1000+00	0	BLSTN	CCL	77P001
1210110009	SI	BCL	.3060+03	.4500+02	.1000+00	0	BLSTN	CCL	77P001
1210110009	SI	BCL	.3010+03	.5300+02	.1000+00	0	BLSTN	CCL	77P001
1210110009	SI	BCL	.2960+03	.6100+02	.1000+00	0	BLSTN	CCL	77P001
1210110010	SS	BED	.2670+03	.1800+02	.1000+00	0	BLSTN	CCL	77P001
1210110011	SS	BED	.1550+03	.4800+02	.1000+00	0	BLSTN	CCL	77P001
1210110011	SS	BED	.1710+03	.4800+02	.1000+00	0	BLSTN	CCL	77P001
1210110011	SS	BED	.1620+03	.4300+02	.1000+00	0	BLSTN	CCL	77P001
1210110011	SS	BED	.2000+03	.2000+02	.1000+00	0	BLSTN	CCL	77P001
1210110011	SS	BED	.1720+03	.2100+02	.1000+00	0	BLSTN	CCL	77P001
1210110011	SS	BED	.1710+03	.3600+02	.1000+00	0	BLSTN	CCL	77P001
1210110011	SI	FRC	.2140+03	.6700+02	.1000+00	0	BLSTN	CCL	77P001
1210110012	SS	BED	.2050+03	.4700+02	.1000+00	0	BLSTN	CCL	77P001
1210110013	SS	BED	.5000+01	.3100+02	.1000+00	0	BLSTN	CCL	77P001
1210110014	LI	FAX	.1000+02	.0000	.1000+00	0	BLSTN	CCL	77P001
1210110014	LI	FAX	.5000+01	.1000+02	.1000+00	0	BLSTN	CCL	77P001
1210110014	L2	FAX	.6200+02	.1800+02	.1000+00	0	BLSTN	CCL	77P001
1210110014	SS	BED	.2610+03	.7600+02	.1000+00	0	BLSTN	CCL	77P001
1210110014	SS	BED	.2650+03	.5500+02	.1000+00	0	BLSTN	CCL	77P001
1210110014	SI	FAP	.3150+03	.1630+02	.1000+00	0	BLSTN	CCL	77P001
1210110014	S2	FAP	.4800+02	.5400+02	.1000+00	0	BLSTN	GCS	77P001
1210110015	SS	BED	.2940+03	.1700+02	.1000+00	0	BLSTN	CCL	77P001
1210110016	SS	BED	.8000+01	.1300+02	.1000+00	0	BLSTN	CCL	77P001
1210110017	SS	BED	.6800+02	.1000+02	.1000+00	0	BLSTN	CCL	77P001
1210110018	SS	BED	.0000	.0000	.1000+00	0	BLSTN	CCL	77P001
1210110019	SS	BED	.0000	.0000	.1000+00	0	BLSTN	CCL	77P001
1210110020	SI	CLE	.9200+02	.2100+02	.1000+00	0	BLSTN	CCL	77P001
1210110021	SS	BED	.0000	.0000	.1000+00	0	BLSTN	CCL	77P001
1210110022	SI	CLE	.1060+03	.2600+02	.1000+00	0	BLSTN	CCL	77P001
1210110023	SI	BCL	.9900+02	.2500+02	.1000+00	0	MARL	CCL	77P001
1210110024	LIX	MEL	.1220+03	.5000+01	.1000+00	0	MARL	CCL	77P001
1210110024	SI	BCL	.1160+03	.2900+02	.1000+00	0	MARL	CCL	77P001

LOCALE	IDENTIFICATION	X	Y	Z	TAG	SHEET	METHOD	REFER
1210110001		.2169250+06	.8617500+05	.1200000+04	25	2316CC	MANPLT	77P001
1210110002		.2171500+06	.8620000+05	.1220000+04	25	2316CC	MANPLT	77P001
1210110003		.2173000+06	.8620000+05	.1260000+04	25	2316CC	MANPLT	77P001
1210110004		.2174250+06	.8617500+05	.1310000+04	25	2316CC	MANPLT	77P001
1210110005		.2177500+06	.8602500+05	.1355000+04	25	2316CC	MANPLT	77P001
1210110006		.2166500+06	.8507500+05	.1300000+04	25	2316CC	MANPLT	77P001
1210110007		.2164500+06	.8517500+05	.1300000+04	25	2316CC	MANPLT	77P001
1210110008		.2161250+06	.8512500+05	.1750000+04	25	2316CC	MANPLT	77P001
1210110009		.2179500+06	.8505000+05	.1220000+04	25	2316CC	MANPLT	77P001
1210110010		.2176500+06	.8455000+05	.1200000+04	25	2316CC	MANPLT	77P001
1210110011		.2171000+06	.8485000+05	.1200000+04	25	2316CC	MANPLT	77P001
1210110012		.2170000+06	.8487500+05	.1230000+04	25	2316CC	MANPLT	77P001
1210110013		.2170250+06	.8467500+05	.1245000+04	25	2316CC	MANPLT	77P001
1210110014		.2169250+06	.8460000+05	.1280000+04	25	2316CC	MANPLT	77P001
1210110015		.2169500+06	.8450000+05	.1290000+04	25	2316CC	MANPLT	77P001
1210110016		.2169000+06	.8437500+05	.1300000+04	25	2316CC	MANPLT	77P001
1210110017		.2169750+06	.8430000+05	.1300000+04	25	2316CC	MANPLT	77P001
1210110018		.2171500+06	.8440000+05	.1295000+04	25	2316CC	MANPLT	77P001
1210110019		.2169250+06	.8387500+05	.1340000+04	25	2316CC	MANPLT	77P001
1210110020		.2168750+06	.6360000+05	.1370000+04	25	2316CC	MANPLT	77P001
1210110021		.2166250+06	.6372500+05	.1360000+04	25	2316CC	MANPLT	77P001
1210110022		.2165500+06	.6342500+05	.1370000+04	25	2316CC	MANPLT	77P001
1210110023		.2168500+06	.8327500+05	.1425000+04	25	2316CC	MANPLT	77P001
1210110024		.2169750+06	.8315000+05	.1435000+04	25	2316CC	MANPLT	77P001
1210110025		.2184250+06	.8677500+05	.1160000+04	25	2316CC	MANPLT	77P001
1210110026		.2186250+06	.8675000+05	.1160000+04	25	2316CC	MANPLT	77P001
1210110027		.2187750+06	.8650000+05	.1180000+04	25	2316CC	MANPLT	77P001
1210110028		.2189500+06	.8640000+05	.1175000+04	25	2316CC	MANPLT	77P001
1210110029		.2190000+06	.8622500+05	.1190000+04	25	2316CC	MANPLT	77P001
1210110030		.2191750+06	.8595000+05	.1200000+04	25	2316CC	MANPLT	77P001
1210110031		.2193250+06	.8595000+05	.1230000+04	25	2316CC	MANPLT	77P001
1210110032		.2196500+06	.8595000+05	.1265000+04	25	2316CC	MANPLT	77P001
1210110033		.2198750+06	.8595000+05	.1290000+04	25	2316CC	MANPLT	77P001
1210110034		.2200250+06	.8597500+05	.1330000+04	25	2316CC	MANPLT	77P001
1210110035		.2203750+05	.8585000+05	.1440000+04	25	2316CC	MANPLT	77P001
1210110036		.2160750+06	.7867500+05	.1260000+04	25	2316CC	MANPLT	77P001
1210110037		.2161500+06	.7865000+05	.1280000+04	25	2316CC	MANPLT	77P001
1210110038		.2161250+06	.7857500+05	.1260000+04	25	2316CC	MANPLT	77P001
1210110039		.2167500+06	.7840000+05	.1285000+04	25	2316CC	MANPLT	77P001
1210110040		.2163500+06	.7647500+05	.1290000+04	25	2316CC	MANPLT	77P001
1210110041		.2164250+06	.7820000+05	.1300000+04	25	2316CC	MANPLT	77P001
1210110042		.2172750+06	.7745000+05	.1330000+04	25	2316CC	MANPLT	77P001
1210110043		.2172000+06	.7755000+05	.1400000+04	25	2316CC	MANPLT	77P001
1210110044		.2171500+06	.7765000+05	.1410000+04	25	2316CC	MANPLT	77P001
1210110045		.2173000+06	.7767500+05	.1420000+04	25	2316CC	MANPLT	77P001
1210110046		.2175000+06	.7775000+05	.1430000+04	25	2316CC	MANPLT	77P001
1210110047		.2177500+06	.7785000+05	.1420000+04	25	2316CC	MANPLT	77P001
1210110048		.2180000+06	.7772500+05	.1380000+04	25	2316CC	MANPLT	77P001
1210110049		.2181500+06	.7775000+05	.1380000+04	25	2316CC	MANPLT	77P001
1210110050		.2182250+06	.7772500+05	.1385000+04	25	2316CC	MANPLT	77P001

Figure AI-1. The structure of records in the PRUDE orientation and location data files.

(i) principle descriptor fields;

(ii) subordinate descriptor fields.

The principle descriptor fields, of which there are three, precede the core fields in each record. The four subordinate descriptor fields follow the core fields (Fig. 1*). The significance of the fields in the PRUDE orientation and data files is outlined in the following section.

In all of these fundamental design decisions, the main concern was to establish a logical correspondence between the structure of information obtained by the geologist (and generally initially recorded more or less systematically in a field note-book) and the structure of data systematically organised in a computer. This procedure has been formally identified as "file organisation" (Engles, 1972). "Data organisation", on the other hand, is concerned with establishing correspondence between the structure of the data and the structure of *storage* (Fig. 2). Here the *physical structure* of the storage device largely dictates the nature of the correspondence established.

The explicit distinction between file organisation and data organisation and the implicit distinction between the logical structure and the physical structure of the data-base, has been considered to be of fundamental importance in the design of the PRUDE system, even though at the present stage of its development the logical and physical structures of the files are practically identical. This, however, is merely a question of programming convenience and also reflects the fact that the present volume of data handled is not very large. It could therefore be considered as the infantile phase of the PRUDE system. The logical structure of the PRUDE files entails a fairly large degree of data redundancy, which simply means that the files could in principle be considerably compressed without any loss of information content by restructuring them according to principles derived from modern information theory. In so doing, however, they would certainly become completely unfamiliar to the user-geologist.

In future, as the amount of archived data in the PRUDE system grows and as the need arises to re-process or retrieve this archived data, it will un-

---

* Note: Figure and table numbers in text are abbreviated so that e.g. Fig. 1 refers to Fig. A I-1, Table 2 refers to Table A I-2, etc.

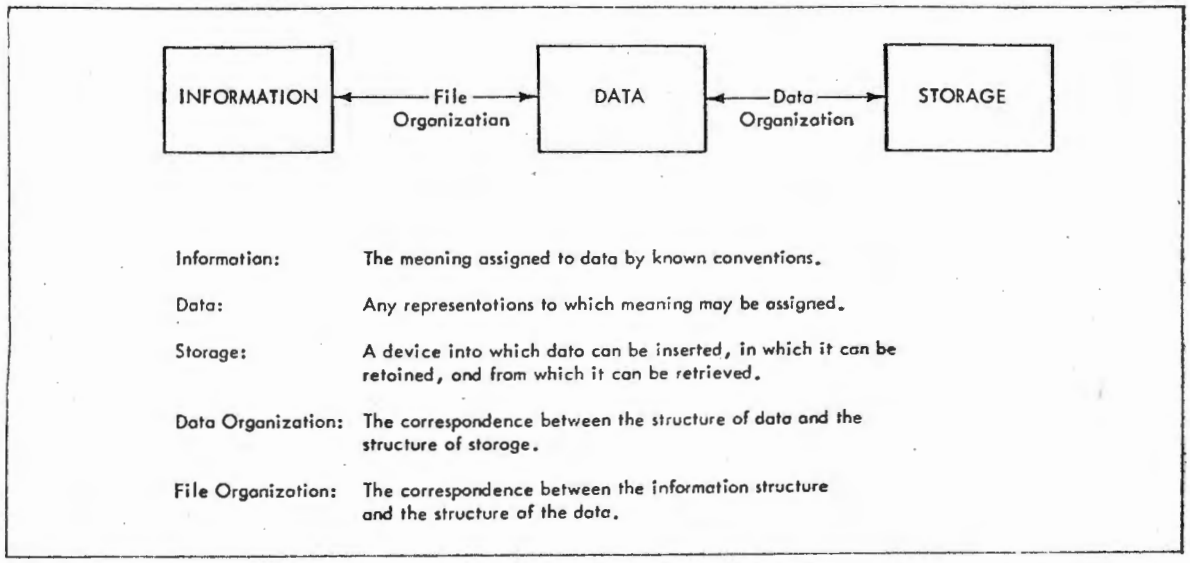

Figure AI-2. Illustration of the difference between file organization and data organization (after Engles, 1972).

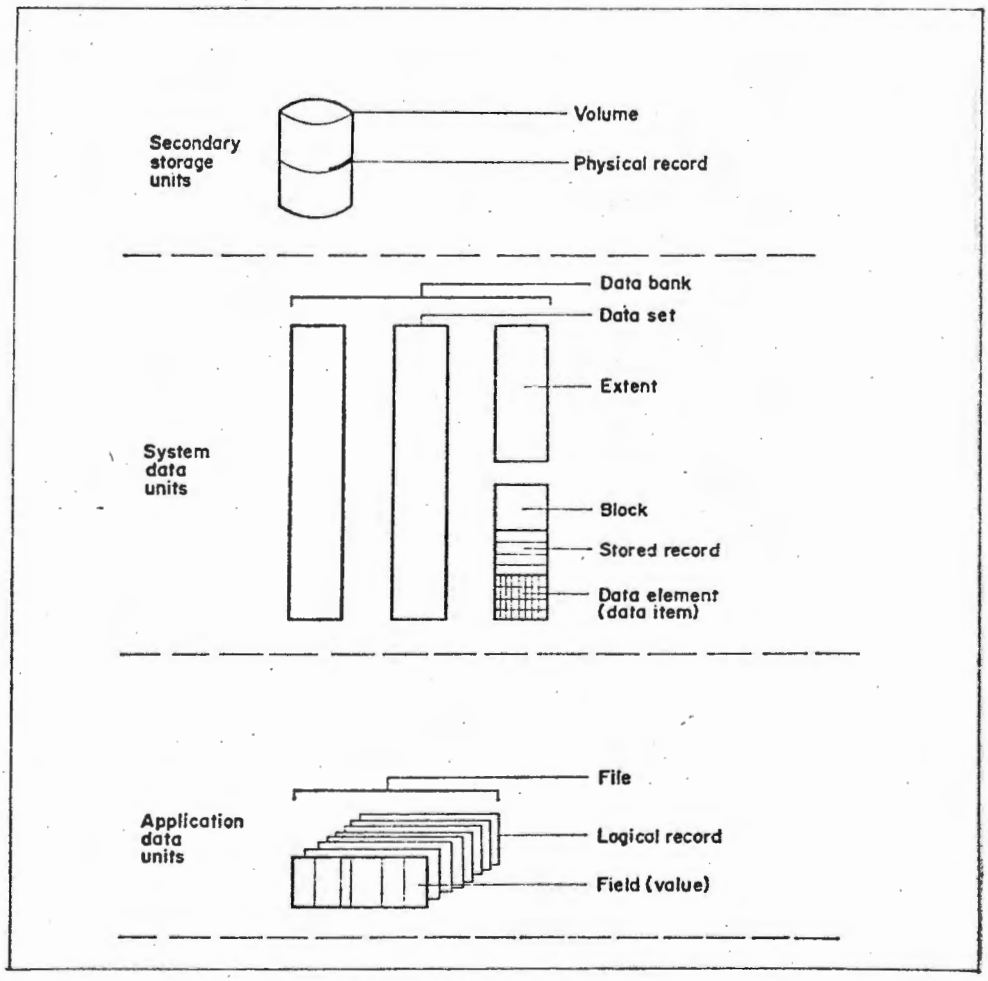

Figure AI-3. Illustration of concepts of storage, system data units and application data units (after Engles, 1972).

doubtedly become necessary to resort to methods of physically compressing the stored data, mainly for practical reasons of speed and economy. This development, however, should be completely invisible to the general user of the system and could, for example, be achieved by the insertion of a set of "transparent" routines which in fact operate on a complex chained or link-listed data structure while maintaining the appearance of the familiar simple structure for the benefit of the user. The intention always has been that the system should be user-orientated and should not require levels of computer understanding that the average geologist could not easily acquire.

c. Physical structure of the data files and storage

Although this will certainly change, it is appropriate to give a brief outline of the present physical basis of the PRUDE system, as this is relevant to understanding some of the usage of existing systems programmes.

The principle units into which the data-base is logically subdivided, namely fields, logical records and files (from lowest to highest in the hierarchy), have already been described (Fig. 1). These have been called "application data units" (Engles, 1972). "System data units", on the other hand, refer to subdivisions of the physical data-base and are (in the same hierarchical order) data elements, stored records, blocks, extents, data sets and data banks (Fig. 3). In the present PRUDE system, each data element in a storage device corresponds to an actual field in a logical record. The stored records correspond exactly with the logical records.

Storage is defined as "a device into which data can be inserted, in which it can be retained and from which it can be retrieved" (Engles, 1972). In computer science, there is a distinction between "central memory", in which data is temporarily stored for actual processing and *secondary storage*, which are devices for permanent or semi-permanent storage of data. The major unit of secondary storage is the *volume* and the basic unit is the *physical record* (Fig. 3). Magnetic tape reels and disc packs are examples of volumes. Physical records are recorded between gaps on tape or address markers on a sector of disc. Access to records on tape is sequential, whereas to records on disc

is described as "random". The PRUDE system makes use of both modes of secondary storage.

Most of the PRUDE data loading, validation, updating and retrieval operations are performed on data files in random-access disc storage. This storage is provided as a normal service in the existing computer configuration by a number of permanently mounted disc packs. Occasionally, PRUDE files thus stored may be temporarily "unloaded" or rolled-off onto magnetic tape reels when not in active use and when the disc space that they occupy is required by other users. This temporary transferrence of PRUDE files is generally transparent to the user. The PRUDE system, however, also provides routines for preserving "back-up" copies of PRUDE files on private magnetic tape reels, or for transferring PRUDE files from one computer installation to another.

In addition, the PRUDE system provides routines for storing PRUDE files on magnetic tape in a special format using the NTRAN subroutine in the UNIVAC 1100 series system. PRUDE files stored in this way are written in binary code to tape in blocks of 2000 records (except for the last block in each file which may contain fewer records). Several PRUDE files may be thus stored in one volume (tape) each between end-of-file (EOF) marks, as a special PRUDE routine exists to enable the tape to be moved forward or backward over NTRAN-written EOF marks.

The blocked magnetic tape mode can, in fact be considered to be the principle PRUDE storage mode for archived data especially, or even for current project data which is not being actively analysed or processed. A special retrieval routine exists in the PRUDE system which enables direct selection of data from tape storage and thus only the most relevant data need be brought into disc storage for active analysis. This allows more efficient and economical usage of the disc storage facilities. It should be noted, in this context, that "retrieval" of selected data from tape storage to disc storage actually means that the selected data is *copied* from tape to disc, but the tape storage remains unaffected. At the conclusion of disc processing, such retrieved data is simply deleted.

3. Structure of records in PRUDE data files

The master orientation and location data files have a logical structure in which each record is composed of ten fields, which are made up as follows:

(i) three principle descriptor fields;
(ii) three core numeric fields;
(iii) four subordinate descriptor fields.

In addition to the master data files, there is a dictionary file which provides definitions of the alphanumeric or numeric codes used in the descriptor fields.

a. Orientation data files

The ten fields into which an orientation data record is divided are code-named as follows:

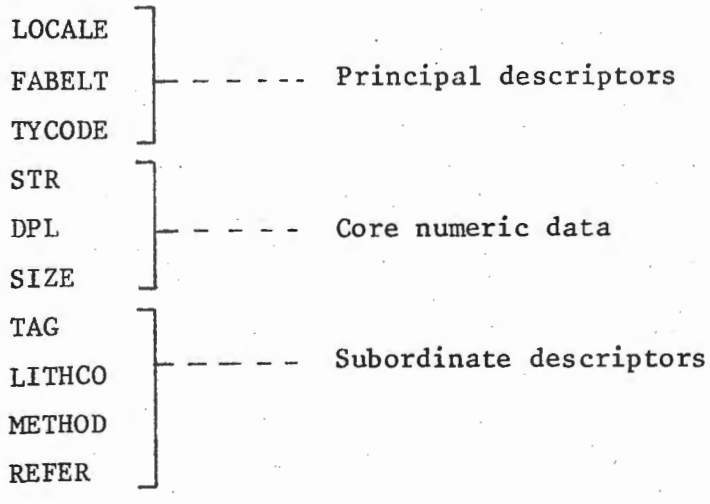

(i) LOCALE field

This field serves a dual purpose. It firstly contains a code to the regional geographic and geological setting of the project and secondly it represents a locality identifier, i.e. a unique number identifying the "station" at which the measurement following in the core fields was made. LOCALE is a one-word field of integer-numeric type. In the PRUDE files, it is represented as a

ten-digit number. The first five digits of this number are used as the regional code, which is also a project identifier unique to each data set in the PRUDE bank and the last five digits are used as measurement station identifiers.

For example, the regional code of the Naukluft project is 12101. This code is assigned to the user according to Precambrian Research Unit conventions. The first digit, 1, indicates a PRU project. The second digit, 2, indicates the country in which the project was carried out; in this case SWA/Namibia. The third digit, 1, indicates the geological terrain in which the project was situated, namely the Damara orogenic belt. The fourth and fifth digits indicate that this was the first project in that terrain to make use of PRUDE facilities and also defines the specific area.

Complete LOCALE values are integer numbers such as 1210110013 or 1210140056, for example. The last five digits are structural station numbers which the PRUDE user is free to use in any convenient way. In the present example, it will be noted that the writer has used the sixth digit to code local regions or sub-areas within the project area.

The LOCALE field is used to link the orientation data file with the location data file in which the precise geographic co-ordinates of the measurement locality are stored.

(ii) FABELT and TYCODE fields

The purpose of these fields is classification of the measured structure. FABELT is an abbreviation for "fabric element" and TYCODE is a shortened form of "structure type code".

It is intended that the fabric element descriptor should firstly inform whether the following orientation measurement refers to a planar or a linear structure. The conventional rule in this respect is that the fabric element code for planar structures commences with the character "S", whereas the code for linear structures commences with character "L". There is also a specific provision in the PRUDE data listing routines for indicating that no measurable fabric elements were observed at a particular locality by coding the six-character string ØØbbbb (zero-zero-blanks x 4). Apart for this last implicit

restriction, the user is free to define his own individual codes for fabric elements (or perhaps for identifying measurements which do not actually refer to the fabric element orientations, but are related to them in some way, such as components of a measured finite strain tensor, for example). Coding "S" or "L" as the first character of the FABELT code is only important in that it affects the interpretation of the numerical values in the STR and DPL fields.

Like FABELT, TYCODE is a one-word field of alphanumeric type represented by a six-character string. Here the user again has complete freedom of choice to define his own mnemonic or other types of codes to describe the type of structure. In the present, example "SLC" refers to slaty cleavage, for instance and "PHF" to phyllitic foliation. Up till now, no attempt has been made to prescribe codes to users, but obviously questions of standardisation and objectivity of description are likely to become important as PRUDE usage continues.

(iii) STR and DPL fields

In the orientation data files, these fields contain the essential quantitative measurement of structure attitude. The numerical value in the field is, however, interpreted in two possible ways. STR is an acronym for "strike and trend" and DPL is an acronym for "dip or plunge". Thus, in order to interpret the value in these fields, it must be known whether the measurement refers to a planar or linear structure : hence the convention used in the FABELT field, that planar structures are coded with a leading "S" and linear structures are coded with a leading "L".

Unambiguous numerical expression of linear orientation measurement presents no problems. For example, a STR value of 345 and a DPL value of 23, for a fabric element identified as L2, indicates that the structure in question is a (second-phase) lineation and that it trends towards the azimuth 345^{o} and an angle of plunge equal to 23^{o}. In adopting a wholly numerical expression for strike-and-dip measurements of planar structures, it is necessary to formulate a clear convention. The one presently adopted by the writer in using PRUDE system is a simple "right-hand" rule, namely that the dip direction is to the right-hand side as the specified strike azimuth is faced. This rule, however,

is not inherent in the PRUDE system itself (although it is inherent in some applications programmes which interpret or analyse PRUDE data files). Some users of the present PRUDE system have, in fact, used other conventions (for example, specifying dip direction and dip instead of strike and dip for planar structures). In these cases, it has been extremely simple matter to write a short transgeneration programme which converts from one data convention to another. This is just another illustration of the flexibility of PRUDE.

(iv) SIZE field

Strike-and-dip or trend-and-plunge are special geological forms of the polar representation of vector quantities. The size or length of the vector quantity is the implicit third dimension in these representations. This is usually taken as unit dimension, but in some cases (cf. Kröner, 1968) geologists have, for "statistical" purposes, chosen to weight measurements differently according to the size of the structure to which they referred. In the present example, since most field orientation measurements have been made directly on the planar or linear structure with a compass-clinometer device about 10 cm long, this has been taken as the "size" of the measured vector. The value 0,1000+00 in the Naukluft data file listing is scientific notation (FORTRAN E-field representation) for 0,1 m.

It is, in principle, possible to envisage other ways in which orientation data might be acquired which would necessitate different size specifications to accurately reflect the measured quantity. For example, if a fold-axis orientation was computed from photogrammetrically measured location data taken from two widely spaced points on a hinge line in some conspicuous stratigraphic marker unit, the true "size" of the measurement would obviously be the length of the vector connecting the two points and this could amount to several tens or hundreds, or even thousands of metres. The PRUDE data system, in fact, anticipates the day in which the deployment of such precision photogrammetric methods for mapping large-scale structures becomes commonplace. The data-handling capabilities provided by PRUDE are essential to any such future development.

(v) TAG field

This is a one-word field of integer-numeric type, represented by three digits (i.e. with a range from 0 to 999). At present it is reserved for "tagging" data from a given measurement locality in order to divide it into distinct subsets. For example, if a structural station is defined at a particular outcrop of complex structural geometry, the tag field can be used to define "substations" at different parts of the outcrop, if the distance between these is not resolvable at the mapping scale.

It is likely that there are other uses to which the TAG field can be put and in general any possible use can be considered quite legitimate as long as it is clearly defined and preferably the same from station to station.

(vi) LITHCO field

This is a one-word field of alphanumeric type, used to specify the lithology in which the structural measurement was made. This field has a special structure designed to allow for a hierarchical system of rock-type coding. For example, a system may be imagined in which a sedimentary rock of unspecified character is represented by the six-character code 3ØØØØØ, sedimentary rock of clastic character by the code 31ØØØØ and a sedimentary rock of chemical nature (e.g. banded iron-formation) by the code 32ØØØØ. One may further imagine that the lower levels of the code hierarchy (i.e. the remaining four characters on the right) are used to further subdivide the clastic-sedimentary and chemical-sedimentary classes according to other physical or mineralogical criteria in similar systematically hierarchical fashion.

The section of the retrieval programme which operates on this field allows for selection to any desired depth of the LITHCO hierarchy, simply by specifying trailing blank characters for the depths of the hierarchy within which no specific type selections are required. As an example, all data measured in clastic sedimentary rocks, regardless of physical type or mineralogy, can in principle be retrieved by the specification of the code 31bbbb (three-one-blanks x 4).

It is important to note that this structure of the LITHCO field imposes one

restriction on the type of code that may be used: that is, *a code which includes the blank character(s) between alphanumerics* (e.g. ABCbb1) *is prohibited*, since the levels of the code hierarchy lower than the first blank character in the code are in principle inaccessible to any retrieval operation.

In the present work, the hierarchical rock-type coding facility has not been used and simple mnemonic codes for rock types are employed (e.g. DOLOM for dolomite, QTZITE for quartzite and so on).

(vii) METHOD field

This one-word field of alphanumeric type is used to indicate the method by which the numerical data in the STR, DPL and SIZE fields was obtained. In the present example, only two codes are used; namely, CCL for compass-clinometer measurement and GCS for graphical (Schmidt net) construction from primary compass-clinometer data. As mentioned above in connection with the SIZE field, digital photogrammetric technology has reached a stage where its application to precise geometric analysis of geological structure is imminent and the METHOD field (as well as the PRUDE concept generally) anticipates the diversification in the methodology of structural analysis which this development will certainly entail.

(viii) REFER field

The REFER field is used as a kind of compressed "bibliographic" code. The two leading numerical characters in this one-word alphanumeric field (e.g. 77PØØ1) refer to the year in which the data was either acquired or made public in some form. The third character refers to the category of the data, i.e. either published or declared public in some way (P), unpublished and private (C for "closed"), or unpublished in thesis (T). The last three characters of the code indicate the person who compiled the data file and any literature reference to data publication that might exist.

b. Location data files

The ten fields into which a location data record is divided are code-named as follows:

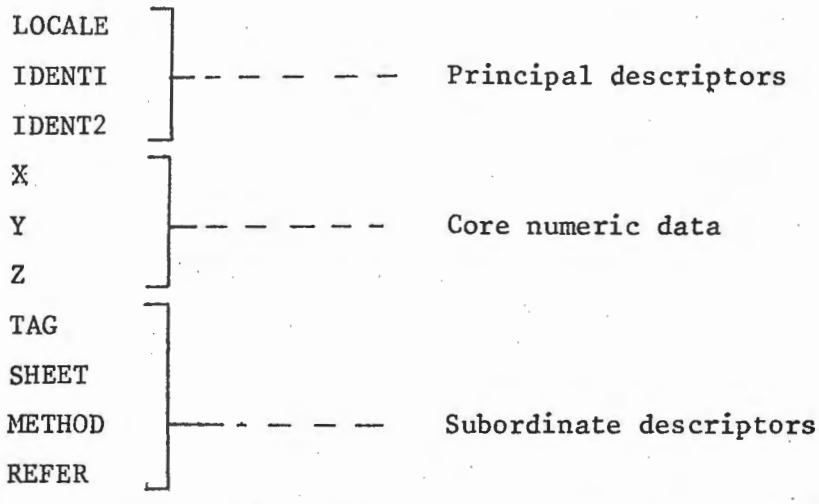

The attributes of data elements corresponding to these fields are the same as for the orientation data file, even though most of the fields are used to different purpose. This identity of physical structure facilitates programme construction for the PRUDE system.

(i) LOCALE field

See section C.3a(i) of this Chapter.

(ii) IDENT1 and IDENT2 fields

These fields can be used to classify location data. In the present example, where all location data refer to structural measurement stations, no such classification has been applied. In principle, however, it is possible that future acquisition of location data by photogrammetric methods (e.g. spot locations along a conspicuous contact between two formations) might necessitate this. For the purposes of quantitative contact-tracing in this way, these fields can be used to specify the formations which are in contact with each other. For example, a digitized contact between a dolomitic and a quartzitic formation could be coded as DOLOM1 QTZTE1.

Once again the flexibility of the PRUDE system and its anticipation of future methodological developments is emphasised. In the above example, simple rules and conventions for spot location (digital) tracing along contacts would allow the PRUDE location file to form the nucleus of a system for automatic or semi-automatic structural cartography. This is, in fact, already possible using the PRUDE programme TDBXYMAP.

(iii) X, Y and Z fields

These fields contain the essential quantitative location measurement. In the present example the South West African Co-ordinate System is used and the X and Y data refer to measurements in this metric grid. The Z data refer elevation above sea-level, again in metres.

(iv) TAG field

At present this integer numeric field is used simply to indicate the approximate precision of X, Y location measurements. It is possible that it can be used for other purposes to suit the individual user.

(v) SHEET field

This field indicates the topocadastral map sheet on which the specified location actually falls. It therefore provides a guide to the geographical area from which it comes. The system of labelling 1 : 50 000 topocadastral sheet in use in South Africa and South West Africa/Namibia is illustrated in Fig.21*. Because the SHEET field has the same hierarchical coding structure described for the LITHCO field in a previous section of this chapter, the SHEET field may be used to select data from an area for which only approximate latitudes and longitudes are known. For example, specifying only the selection code 2416bb (two-four-one-six-blanks x 2) would enable all data falling within the degree-square bounded by latitudes 24°S and 25°S and longitudes 16°E and 17°E to be retrieved for processing.

(vi) METHOD field

This field specifies the method by which the location data was obtained. Remarks similar to those made in connection with the METHOD field in the orientation data file apply here. At present the only code used in this field is MANPLT, indicating that the measurements of location data were made by manually plotting and measuring structural data sites on available survey sheets.

(vii) REFER field

See section C.3a(viii) of this Chapter.

---

* Chapter 4

D. BRIEF DESCRIPTION OF THE PRUDE SYSTEM

The system at present operates in a UNIVAC 1106 configuration at the Computer Centre, University of Cape Town. It is composed of three disc files : (1) the source file, PRUDE*PRGFILE;

(2) the relocatable file, PRUDE*RELFILE;

(3) the absolute file, PRUDE*ABS

1. PRUDE*PRGFILE

This file contains the source versions of all PRUDE programmes and subroutines. These are the "elements" of the file and are listed as follows:

INFORM	(P)
UNFORM	(P)
UNLOCA	(P)
TDBADD	(P)
REFORM/ORIENT	(P)
TDBLIST	(P)
TDBSORT	(P)
TSORTLIST	(P)
TDBSELECT	(P)
ALPHA	(S)
ATYPE	(S)
INMERC	(S)
RNMERC	(S)
TDBLOCKTAPE	(P)
TDBSELECT/TAPE	(P)
TDBUNBLOCK	(P)
LOCORLINK	(P)
TMOVETAPE	(P)
TDBFORTAPE	(P)
TDBMTCOPY	(P)
TDBXYMAP	(P)
BASEMAP	(S)

There are 21 elements, comprising 16 programmes (P) and 5 subroutines (S). The full source listings of all programmes and subroutines are obtainable from the Precambrian Research Unit. All programmes and subroutines have been quite extensively annotated, using comment statements interspersed in the

FORTRAN text. Further description of each programme is given below in section D.4.

The source programmes are all written in UNIVAC FORTRAN V. Almost all of them can be adapted easily to any other computer system similar to the UNIVAC 1106. The programmes TBLOCKTAPE, TDBSELECT/TAPE and TDBUNBLOCK involve calls to a system subroutine NTRAN for input/output (I/O) buffering allowing time-saving parallel processing of I/O units and the central processing unit (CPU). This facility might not be available on some other systems. Nevertheless, the existence of the PRUDE source programmes in a high-level language such as FORTRAN implies a high degree of portability, i.e. the system is not machine-dependent, but can be adapted for use on a wide variety of computers.

2. PRUDE*RELFILE

This file contains the relocatable versions of all twenty-one PRUDE programmes and subroutines. Relocatables are produced from the sources by the FORTRAN compiler, which effectively translates the FORTRAN text into machine-code (binary).

3. PRUDE*ABS.

This file contains the absolute versions of the sixteen PRUDE programmes as its elements. These are listed in Table 1, with details of their storage requirements, i.e. how much of the central memory they occupy, expressed in words decimal. The absolute versions represent the executable machine-code, in which the relocatables of PRUDE*RELFILE have been combined with various UNIVAC systems routines to form the working programmes. Some of the programmes, namely TDBSORT, TSORTLIST, TDBSELECT, TDBSELECT/TAPE and TDBXYMAP call on subroutines from special systems libraries such as SORT*LIB, UTIL*LIB and CALCOMP*SUBR.

TABLE AI-1

PRUDE * ABS programs

Name	Storage (words decimal)		
	IBANK	DBANK	TOTAL
INFORM	4824	3104	7928
UNFORM	4842	2029	6871
UNLOCA	4614	2016	6630
TDBADD	4517	2086	6603
REFORM/ORIENT	4890	2076	6966
TDBLIST	4989	2150	7139
TDBSORT	10234	19957	30191
TSORTLIST	10366	20035	30402
TDBSELECT	6667	7020	13687
TBLOCKTAPE	5589	22388	27977
TDBSELECT/TAPE	7125	27281	34406
TDBUNBLOCK	4433	22308	26741
LOCORLINK	4888	2100	6988
TMOVETAPE	5250	2299	7549
TDBFORTAPE	2985	1946	4931
TDBMTCOPY	5285	22304	27589
TDBXYMAP	6851	9766	16617

IBANK - instruction

DBANK - data bank

4. Functions of PRUDE programmes

Each PRUDE programme has a specific function to fulfil. These may be briefly outlined as follows:

a. INFORM

The function of this programme is to transform structural orientation data punched in a specific format on cards into an expanded format similar to that of the data-base files and at the same time to produce a check-listing of the re-formatted data so that it can easily be scrutinized for errors. The programme itself has some error-detecting operations.

b. UNFORM

This programme takes the re-formatted data produced by INFORM, assumed now to have been checked and corrected where necessary and produces a file of unformatted data records as described in Section C of this Chapter.

c. UNLOCA

This programme produces a similar file of unformatted data records from structural location data punched in a specific format on cards. Because of the character and format of the card-punched location data, no re-formatting programme such as INFORM is used for the purpose of check-listing the data. Introduction of such check-lists, in this case simply of the card-images, is more easily obtained using the Element processor (∂ELT command in the UNIVAC system).

d. TDBADD

The function of this programme is the expansion of an existing data file by the simple addition of another file of similar, new data.

e. REFORM/ORIENT

To facilitate editing of database files this programme is used to transform unformatted orientation data into the same format as the temporary data records produced by the programme INFORM.

f. TDBLIST

This programme lists all or part of the data which exists, in unformatted form, in a PRUDE-type file. It operates either on orientation data files or location data files, according to the option specified at execution by the user.

g. TDBSORT

This programme sorts orientation data files or location data files on any one or more of the ten fields making up each record of the files. The data may be sorted hierarchically on any combination of the fields arranged in any order. The sorted and thus re-constructed data file is copied to a user-specified new file.

h. TSORTLIST

This programme combines the functions of TDBLIST and TDBSORT. The re-structured data file may, or may not be copied to a new file according to the requirements of the user.

i. TDBSELECT and TDBSELECT/TAPE

These programmes allow the selection and copying of data records from a file, according to variable specifications supplied by the user. Selections are possible on any one of, or any combination of, the ten PRUDE fields. TDBSELECT operates on PRUDE files in disc storage, while TDBSELECT/TAPE operates on PRUDE files created by NTRAN on magnetic tape.

j. TBLOCKTAPE

The function of this programme is to create "blocked" data files on magnetic tape using the NTRAN processor. These files can thereafter be accessed in selective mode by TDBSELECT/TAPE, or in non-selective mode by

combination of TDBUNBLOCK with a listing programme (TDBLIST or TSORTLIST).

k. TDBUNBLOCK

This programme is the effective "inverse" of TBLOCKTAPE, in that it creates PRUDE files in disc storage from blocked PRUDE files stored on magnetic tape.

l. LOCORLINK

This programme allows for the linking of PRUDE orientation data files and PRUDE location data files. The linking field is the first field on each record, namely that called LOCALE. LOCORLINK scans selected data records that have been sorted on this field, notes all the different values of the LOCALE field and combines these into a file of values automatically formatted as input to a subsequent selection operation. For example, if the first set of selected data records was drawn from the orientation data file, this subsequent selection will perhaps operate on the location data file to obtain the geographic coordinates associated with each orientation measurement.

m. TMOVETAPE

This is a utility programme which enables two NTRAN-created files to be stored in the same magnetic tape reel. It is necessary since the UNIVAC system ∂MOVE command does not recognise NTRAN-created end-of-file (EOF) marks.

n. TDBFORTAPE

The function of this utility routine is to copy an unblocked PRUDE data file from disc to tape or from tape to tape. It would be used for example, in preserving back-up copies of files or for disseminating the data through the medium of magnetic tape.

o. TDBMTCOPY

This utility routine copies a blocked PRUDE data file from one magnetic tape to another.

p. TDBXYMAP

This programme allows for accurate graphical presentation of location data, via the CALCOMP plotting facility at any desired scale.

REFERENCES - A-I

Berner, H., Ekström, T., Lilljequist, R., Stephansson, O.& Wikström, A., 1972 - GEOMAP - A data system for geological mapping. *24th Inter. Geol. Congress, Section 16,* 3-11.

_____, Ekström, T., Lilljequist, R., Stephansson, O. & Wikström, A., 1975 - GEOMAP. In: Hutchison, W.W., (ed.), *Computer-based systems for geological field data.* Geol. Surv. Can., Paper 74-63, 8-18.

Blaine, J.L., 1977 - *Tectonic evolution of the Waldau Ridge structure and the Okahandja Lineament in part of the Central Damara Orogen, west of Okahandja, South West Africa.* Unpubl. M.Sc. thesis, Univ. Cape Town, 95 p.

Botbol, J.M. & Bowen, R.W., 1975 - Geological Retrieval and Storage Program (GRASP). In: Hutchison, W.W., (ed.), *Computer-based systems for geological field data.* Geol. Surv. Can., Paper 74-63, 89-93.

Bouillé, F., 1976 - A model of scientific data bank and its applications to geological data. *Computers & Geosciences, 2,* 279-291.

Bowen, R.W. & Botbol, J.M., 1975 - The Geological Retrieval and Synopsis Program (GRASP) - *U.S. Geol. Surv. Prof. Paper, 966,* 87 p.

Chorley, R.J., 1972 - Spatial analysis in geomorphology. In: Chorley, R.J. (ed.), *Spatial Analysis in Geomorphology,* Methuen, London, 3-64.

Duncan, A.R. & Willis, J.P., 1975 - Formulation and operation of a geochemical database. *Geokongres 75 : Mineralization in Metamorphic Terranes.* Abstracts Vol., Univ. Stellenbosch, 32-35.

Engles, R.W., 1972 - A tutorial on data-base organisation. *Ann. Rev. Automatic Programming, 7,* 1-64.

Gaál, G. & Suokonautio, V., 1973 - An automatic data processing system for explorational mapping in Precambrian terrain: GEOKU. *Geol. Surv. Finland Bull. 266,* 26 p.

Geodynamics project in South Africa, The 1975 - *Interim report on the South African National Programme presented to the Inter-Union Commission on Geodynamics.* C.S.I.R., Pretoria, 22 p.

Gordon, T.M., 1975 - Computer-based field data files in the Regional and Economic Geology Division. In: Hutchison, W.W. (ed.), *Computer-based systems for geological field data.* Geol. Surv. Can., Paper 74-63, 29-31.

_____, & Hutchison, W.W., eds., 1974 - Computer use in Projects of the Geological Survey of Canada. *Geol. Surv. Can., Paper 74-60,* 108 p.

Gordon, T. & Martin, G., 1974a - Computer-based data management in the Geological Survey of Canada - a preliminary appraisal. In: Gordon, T. & Hutchison, W.W. (eds.), *Computer use in Projects of the Geological Survey of Canada.* Geol. Surv. Can., Paper 74-60, 7-14.

_____, & Martin, G., 1974b - File management systems and geological field data. In: Gordon, T. & Hutchison, W.W., (eds.), *Computer use in Projects of the Geological Survey of Canada.* Geol. Surv. Can., Paper. 74-60, 23-28.

Hartnady, C.J.H. & Vajner, V., 1975 - Formulation of a tectonic data-base. In: *Geokongres 75 : Mineralization in Metamorphic Terranes.* Abstracts Vol., Univ. Stellenbosch, 50-53.

Hruška, J., 1976 - Current data-management systems : problems of application in economic geology. *Computers & Geosciences, 2,* 299-304.

Hobbs, B.E., 1971 - The analysis of strain in folded layers. *Tectonophysics, 11,* 329-375.

Hubaux, A., 1973 - A new geological tool - the data. *Earth Science Reviews, 9,* 159-196.

Hutchison, W.W., 1974 - Towards computer based "systems" for recording, storage, retrieval, analysis and presentation of geological field data in the Geological Survey of Canada. In: Gordon, T. & Hutchison, W.W. (eds.), *Computer use in Projects of the Geological Survey of Canada.* Geol. Surv. Can., Paper 74-60, 1-5.

_____, W.W., (ed.), 1975 - Computer-based systems for Geological Field Data. *Geol. Surv. Can., Paper 74-60,* 100 p.

Jeffery, K.G. & Gill, E.M., 1975 - G-EXEC: a generalized FORTRAN system for data handling. In: Hutchison, W.W. (ed.), *Computer-based systems for geological field data.* Geol. Surv. Can., Paper 74-63, 59-61.

_____, K.G. & Gill, E.M., 1976 - The design philosophy of the G-EXEC system. *Computers & Geosciences, 2,* 345-346.

Kröner, A., 1968 - The gneiss-sediment relationships north-west of Vanrhynsdorp, Cape Province. *Bull. Precambr. Res. Unit, Univ. Cape Town, 3,* 233 p.

Loudon, T.V., 1964 - Computer analysis of orientation data in structural geology. *Tech. Rep. Geog. Branch Off. Naval Res.,* O.N.R. Task No. 389-135, Contr. No. 1228(26), No.13, 1-130.

Mahtab, M.A., Bolstad, D.D., Alldredge, J.R. & Shanley, R.J., 1972 - Analysis of fracture orientations for input to structural models of discontinuous rock. *U.S. Bureau of Mines, Rep. of invest., 7669,* 76 p.

McRitchie, W.D., 1975 - Selected geological field data systems in Canada: a brief description of their capabilities and objectives. In: Hutchison, W.W. (ed.), *Computer-based systems for geological field data.* Geol. Surv. Can., Paper 74-63, 21-28.

Merriam, D.F., (ed.), 1976 - Capture, management and display of geological data : with special emphasis on energy and mineral resources. *Computers & Geosciences, 2,* 279-376.

Moore, J.M., 1977 - The geology of Namiesberg Northern Cape. *Bull. Precambr. Res. Unit, Univ. Cape Town, 20,* 69 p.

Paterson, M.S., 1976 - Some current aspects of experimental rock deformation. *Phil. Trans. R. Soc. Lond. A.283,* 163-172.

Perkins, W.J. & Hammond, B.J., 1975 - Computer-aided thought in biomedical research. *Nature, 256,* 171-175.

Platou, S.W., 1971 - An electronic data processing system for geological field and laboratory data. The E.D.P. system Agto. *Grønlands Geol. Unders. Rept., 39,* 42 p.

_____, S.W., 1975 - Aarhus University System II. In: Hutchison, W.W. (ed.), *Computer-based systems for geological field data.* Geol. Surv. Can., Paper 74-63, 43-46.

Ramsay, J.G., 1976 - Displacement and strain. *Phil. Trans. R. Soc. Lond. A.283,* 3-25.

Reinhardt, E.W. & Jackson, G.D., 1973 - Use of a geological field data collecting form on Operation Bylot, North-central Baffin Island, 1968. *Geol. Surv. Can., Paper 73-35.*

Roddick, J.A. & Hutchison, W.W., 1972 - A computer-based system for geological field data on the Coast Mountains Project, British Columbia, Canada. *24th Inter. Geol. Congress, Section 16,* 36-46.

Starkey, J., 1970 - A computer programme to prepare orientation diagrams. In: Paulitsch, P. (ed.), *Experimental and natural rock deformation.* Springer-Verlag, Berlin, 51-74.

Turner, F.J. & Weiss, L.E., 1963 - *Structural Analysis of Metamorphic Tectonites.* McGraw-Hill, New York.

Vajner, V., 1976 - Progress report on the statistical evaluation of structural data from the Namaqua foreland, Northern Cape. *Ann. Rep. Precambr. Res. Unit, Univ. Cape Town, 13,* 7-18.

Watson, G.S., 1966 - Statistics of orientation data. *J. Geol., 74,* 786-797.

Williams, G.D., 1975 - Advantages of using a generalized system to manage geological data. In: Hutchison, W.W. (ed.), *Computer-based systems for geological field data.* Geol. Surv. Can., Paper 74-63, 84-88

Woodcock, N.H., 1977 - Specification of fabric shapes using an eigenvalue method. *Geol. Soc. Amer. Bull., 88,* 1231-1236.

Wynne-Edwards, H.R., Laurin, A.F., Sharma, K.N.M., Nandi, A.A., Kehlenbreck, M.M. & Franconi, A., 1970 - Computerized geological mapping in the Grenville Province Quebec. *Can. Jl Earth Sci., 7,* 1357-1373.

Yamamoto, K. & Nishiwaki, N., 1976 - Automatic analysis of geologic structure from dip-strike data. *Computers & Geosciences, 1,* 309-323.

KEY TO CODES USED IN NAUKLUFT ORIENTATION DATA FILE

A. FABELT codes

LS	-	Linear structure of sedimentary origin
L1	-	First generation tectonic linear structure
L1X	-	First generation tectonic linear structure parallel to X principal strain axis
L1B	-	First generation tectonic linear structure parallel to local fold axis or "b" kinematic direction
L2	-	Second generation tectonic linear structure
L3	-	Third generation tectonic linear structure
SF	-	Planar fracture structure
SS	-	Planar structure of sedimentary origin
S1	-	First generation tectonic planar structure
S2	-	Second generation tectonic planar structure
S2L	-	Plane of second tectonic generation defined by loci of deformed first generation linear structure

B. TYCODE codes (in alphabetical order)

BCL	-	Cleavage parallel or subparallel to sedimentary bedding
BDA	-	Long axis of tectonic boudin
BED	-	Sedimentary bedding
CLE	-	Tectonic cleavage of unspecified type
CRC	-	Crenulation cleavage
CRL	-	Crenulation lineation
DFLN	-	Deformed early lineation
FAP	-	Fold axial plane
FAULT	-	Fault plane
FAX	-	Fold axis
FOL	-	Tectonic foliation of unspecified type
FRC	-	"Fracture" or spaced cleavage

GNB - Gneissic layering

ISL - Intersection lineation defined by two planar structures

JNT - Joint or fracture structure

KINK - Kink-band

MEL - Mineral elongation lineation

MYF - "Mylonitic" foliation in marble

PEL - Pebble elongation

PEN - "Pencil"-like linear structure formed by two intersecting, spaced planar structure

PHF - Phyllitic foliation in meta-pelite

PSF - "Pressure solution" foliation in carbonate rock

RPM - Ripple-marking

SLC - Slaty cleavage in meta-pelite

TEV - Tension gash-vein

TEVF - Tension gash with fibrous vein filling

XBED - Cross-bed foreset strata

XBISL - Intersection of foreset with topset strata in cross-bedded rock

C. Table of FABELT codes with appropriate TYCODE qualifiers

FABELT	:	TYCODE qualifiers used
LS	:	RPM, XBISL
L1	:	FAX
L1B	:	BDA, ISL, PEN
L1X	:	MEL, PEL
L2	:	CRL, FAX, ISL, PEN
L3	:	CRL
SF	:	FAULT, JNT, TEV, TEVF
SS	:	BED, XBED
S1	:	BCL, CLE, FAP, FOL, FRC, GNB, MYF, PHF, PSF, SLC
S2	:	CRC, FAP, FRC, KINK
S2L	:	DFLN

D. LITHCO codes (in alphabetical order)

BLSGSH - Bituminous, dark limestone with thin green shale interbeds
BLSMAR - Bituminous, dark limestone partly transformed to marble
BLSTN - Bituminous, dark limestone
CONGL - Conglomerate
CONGLQ - Conglomeratic quartzite
CQTZTE - Calcareous quartzite
DOLBLS - Dolomite with interbedded bituminous dark limestone
DOLMAR - Dolomitic marble
DOLOM - Dolomite
DOLSH - Dolomite with thin shale interbeds
FELSIT - Felsitic volcanics
LSTBRE - Limestone or carbonate rock sedimentary breccia
MAFICV - Mafic volcanic rock
MARBLE - Marble
MARL - Marly, calcareous pelitic rock
MARPHY - Mixed marble and phyllite
PELITE - Pelitic rock of unspecific type
PHYLL - Phyllite
PHYSLT - Phyllitic slate
PSH - Purple (Hematitic) shale
QTZDOL - Quartzite (calcareous) with dolomite interbeds
QTZITE - Quartzite
QTZPSH - Quartzite with purple, hematitic shale interbeds
SHALE - Shale of unspecific type
SLATE - Slate
SLTSTN - Siltstone
UDOL - "Unconformity Dolomite".
VOLCLS - Volcaniclastic

E. METHOD codes

CCL - Compass-clinometer measurement

GCS - Orientation graphically constructed from other data at site.

NAUKLUFT ORIENTATION DATA FILE

LOCALE	FABELT	TYCODE	STR	DPL	SIZE	TAG	LITHCO	METHOD	REFER
1210110001	S1	GNB	.1680+03	.5000+02	.1000+00	0	AMPHBL	CCL	77P001
1210110002	SS	BED	.5400+02	.1100+02	.1000+00	0	QTZITE	CCL	77P001
1210110003	L1	FAX	.1580+03	.2100+02	.1000+00	1	BLSTN	CCL	77P001
1210110003	L1	FAX	.1000+02	.0000	.1000+00	0	BLSTN	CCL	77P001
1210110003	S1	FAP	.3200+03	.5700+02	.1000+00	1	BLSTN	CCL	77P001
1210110003	S1	FAP	.1000+02	.2000+01	.1000+00	0	BLSTN	CCL	77P001
1210110004	S1	BCL	.8400+02	.3200+02	.1000+00	0	BLSTN	CCL	77P001
1210110005	L1X	MEL	.3110+03	.3300+02	.1000+00	0	PELITE	CCL	77P001
1210110005	S1	CLE	.2480+03	.6000+02	.1000+00	0	QTZITE	CCL	77P001
1210110005	S1	CLE	.2130+03	.4100+02	.1000+00	0	QTZITE	CCL	77P001
1210110005	S1	CLE	.2580+03	.6200+02	.1000+00	0	QTZITE	CCL	77P001
1210110005	S1	CLE	.2540+03	.6500+02	.1000+00	0	QTZITE	CCL	77P001
1210110005	S2	CRC	.2170+03	.2900+02	.1000+00	0	QTZITE	CCL	77P001
1210110006	S1	CLE	.2910+03	.4200+02	.1000+00	0	BLSTN	CCL	77P001
1210110007	S1	CLE	.2480+03	.2700+02	.1000+00	0	BLSTN	CCL	77P001
1210110007	S2	TEVF	.7300+02	.7300+02	.1000+00	0	BLSTN	CCL	77P001
1210110008	S1	CLE	.1470+03	.5000+02	.1000+00	0	BLSTN	CCL	77P001
1210110009	LIB	ISL	.3140+03	.2900+02	.1000+00	0	BLSTN	GCS	77P001
1210110009	S1	BCL	.3080+03	.6900+02	.1000+00	0	BLSTN	CCL	77P001
1210110009	S1	BCL	.3060+03	.4500+02	.1000+00	0	BLSTN	CCL	77P001
1210110009	S1	BCL	.3010+03	.5300+02	.1000+00	0	BLSTN	CCL	77P001
1210110009	S1	BCL	.2960+03	.6100+02	.1000+00	0	BLSTN	CCL	77P001
1210110010	SS	BED	.2670+03	.1800+02	.1000+00	0	BLSTN	CCL	77P001
1210110011	SS	BED	.1550+03	.4800+02	.1000+00	0	BLSTN	CCL	77P001
1210110011	SS	BED	.1710+03	.4800+02	.1000+00	0	BLSTN	CCL	77P001
1210110011	SS	BED	.1620+03	.4300+02	.1000+00	0	BLSTN	CCL	77P001
1210110011	SS	BED	.2000+03	.2000+02	.1000+00	0	BLSTN	CCL	77P001
1210110011	SS	BED	.1720+03	.2100+02	.1000+00	0	BLSTN	CCL	77P001
1210110011	SS	BED	.1710+03	.3600+02	.1000+00	0	BLSTN	CCL	77P001
1210110011	S1	FRC	.2140+03	.6700+02	.1000+00	0	BLSTN	CCL	77P001
1210110012	SS	BED	.2050+03	.4700+02	.1000+00	0	BLSTN	CCL	77P001
1210110013	SS	BED	.5000+01	.3100+02	.1000+00	0	BLSTN	CCL	77P001
1210110014	L1	FAX	.1000+02	.0000	.1000+00	0	BLSTN	CCL	77P001
1210110014	L1	FAX	.5000+01	.1000+02	.1000+00	0	BLSTN	CCL	77P001
1210110014	L2	FAX	.6200+02	.1800+02	.1000+00	0	BLSTN	CCL	77P001
1210110014	SS	BED	.2610+03	.7800+02	.1000+00	0	BLSTN	CCL	77P001
1210110014	SS	BED	.2650+03	.5500+02	.1000+00	0	BLSTN	CCL	77P001
1210110014	S1	FAP	.3150+03	.1800+02	.1000+00	0	BLSTN	CCL	77P001
1210110014	S2	FAP	.4800+02	.5400+02	.1000+00	0	BLSTN	GCS	77P001
1210110015	SS	BED	.2940+03	.1700+02	.1000+00	0	BLSTN	CCL	77P001
1210110016	SS	BED	.8000+01	.1300+02	.1000+00	0	BLSTN	CCL	77P001
1210110017	SS	BED	.6800+02	.1000+02	.1000+00	0	BLSTN	CCL	77P001
1210110018	SS	BED	.0000	.0000	.1000+00	0	BLSTN	CCL	77P001
1210110019	SS	BED	.0000	.0000	.1000+00	0	BLSTN	CCL	77P001
1210110020	S1	CLE	.9200+02	.2100+02	.1000+00	0	BLSTN	CCL	77P001
1210110021	SS	BED	.0000	.0000	.1000+00	0	BLSTN	CCL	77P001
1210110022	S1	CLE	.1060+03	.2600+02	.1000+00	0	BLSTN	CCL	77P001
1210110023	S1	BCL	.9900+02	.2500+02	.1000+00	0	MARL	CCL	77P001
1210110024	L1X	MEL	.1220+03	.5000+01	.1000+00	0	MARL	CCL	77P001
1210110024	S1	BCL	.1160+03	.2900+02	.1000+00	0	MARL	CCL	77P001

LOCALE	FABELT	TYCODE	STR	DPL	SIZE	TAG	LITHCO	METHOD	REFER
1210110024	S1	BCL	.1290+03	.1300+02	.1000+00	0	MARL	CCL	77P001
1210110024	S1	BCL	.1200+03	.2500+02	.1000+00	0	MARL	CCL	77P001
1210110025	SS	BED	.2380+03	.1000+01	.1000+00	0	BLSTN	CCL	77P001
1210110026	SS	BED	.2400+03	.1300+02	.1000+00	0	BLSTN	CCL	77P001
1210110027	S1	CLE	.2240+03	.3400+02	.1000+00	0	BLSTN	CCL	77P001
1210110028	S1	CLE	.1860+03	.3300+02	.1000+00	0	BLSTN	CCL	77P001
1210110029	SS	BED	.2010+03	.4300+02	.1000+00	0	BLSTN	CCL	77P001
1210110030	S1	CLE	.2200+03	.3000+02	.1000+00	0	BLSTN	CCL	77P001
1210110031	S1	CLE	.2280+03	.4500+02	.1000+00	0	BLSTN	CCL	77P001
1210110032	S1	CLE	.2370+03	.5700+02	.1000+00	0	BLSTN	CCL	77P001
1210110033	L1B	ISL	.5500+02	.1800+02	.1000+00	1	BLSTN	GCS	77P001
1210110033	SS	BED	.3150+03	.1200+02	.1000+00	1	BLSTN	CCL	77P001
1210110033	S1	CLE	.2410+03	.8900+02	.1000+00	0	BLSTN	CCL	77P001
1210110033	S1	CLE	.2380+03	.8200+02	.1000+00	1	BLSTN	CCL	77P001
1210110034	S1	CLE	.2460+03	.5700+02	.1000+00	0	BLSTN	CCL	77P001
1210110035	S1	CLE	.2060+03	.6400+02	.1000+00	0	BLSTN	CCL	77P001
1210110036	L1B	ISL	.3080+03	.4300+02	.1000+00	2	BLSTN	CCL	77P001
1210110036	SS	BED	.1290+03	.6700+02	.1000+00	0	BLSTN	CCL	77P001
1210110036	SS	BED	.1440+03	.6200+02	.1000+00	2	BLSTN	CCL	77P001
1210110036	SS	BED	.1310+03	.6700+02	.1000+00	2	BLSTN	CCL	77P001
1210110036	SS	BED	.1820+03	.4700+02	.1000+00	0	BLSTN	CCL	77P001
1210110036	SS	BED	.1590+03	.5500+02	.1000+00	2	BLSTN	CCL	77P001
1210110036	SS	BED	.1560+03	.5300+02	.1000+00	0	BLSTN	CCL	77P001
1210110036	SS	BED	.1480+03	.7100+02	.1000+00	2	BLSTN	CCL	77P001
1210110036	SS	BED	.2860+03	.7700+02	.1000+00	2	BLSTN	CCL	77P001
1210110036	SS	BED	.2700+03	.6300+02	.1000+00	2	BLSTN	CCL	77P001
1210110036	SS	BED	.2680+03	.5100+02	.1000+00	2	BLSTN	CCL	77P001
1210110036	SS	BED	.2420+03	.4800+02	.1000+00	1	BLSTN	CCL	77P001
1210110036	SS	BED	.2380+03	.5600+02	.1000+00	1	BLSTN	CCL	77P001
1210110036	SS	BED	.2340+03	.5900+02	.1000+00	2	BLSTN	CCL	77P001
1210110036	SS	BED	.2300+03	.4400+02	.1000+00	2	BLSTN	CCL	77P001
1210110036	SS	BED	.2080+03	.4500+02	.1000+00	3	BLSTN	CCL	77P001
1210110036	SS	BED	.1970+03	.5300+02	.1000+00	2	BLSTN	CCL	77P001
1210110036	S1	FAP	.1460+03	.7000+02	.1000+00	2	BLSTN	CCL	77P001
1210110037	S1	CLE	.2490+03	.5300+02	.1000+00	0	BLSTN	CCL	77P001
1210110038	S1	BCL	.1450+03	.6500+02	.1000+00	0	BLSTN	CCL	77P001
1210110039	L2	ISL	.3050+03	.4300+02	.1000+00	0	MARL	CCL	77P001
1210110039	S1	BCL	.1630+03	.5500+02	.1000+00	0	MARL	CCL	77P001
1210110039	S2	FRC	.2680+03	.6400+02	.1000+00	0	MARL	CCL	77P001
1210110040	S1	CLE	.2450+03	.8500+02	.1000+00	0	MARL	CCL	77P001
1210110041	S1	BCL	.3450+03	.5000+02	.1000+00	1	MARL	CCL	77P001
1210110041	S1	BCL	.2990+03	.4700+02	.1000+00	1	MARL	CCL	77P001
1210110041	S1	BCL	.2840+03	.5700+02	.1000+00	2	MARL	CCL	77P001
1210110041	S1	BCL	.2780+03	.7000+02	.1000+00	2	MARL	CCL	77P001
1210110041	S1	BCL	.2750+03	.5100+02	.1000+00	2	MARL	CCL	77P001
1210110041	S1	BCL	.2540+03	.5600+02	.1000+00	0	MARL	CCL	77P001
1210110041	S1	BCL	.2460+03	.8000+02	.1000+00	0	MARL	CCL	77P001
1210110041	S1	BCL	.4700+02	.6700+02	.1000+00	1	MARL	CCL	77P001
1210110042	S1	PHF	.2860+03	.2500+02	.1000+00	0	PHYLL	CCL	77P001
1210110043	S1	CLE	.1600+02	.4800+02	.1000+00	0	BLSTN	CCL	77P001

LOCALE	FABELT	TYCODE	STR	DPL	SIZE	TAG	LITHCO	METHOD	REFER
1210110043	S1	CLE	.3570+03	.3400+02	.1000+00	0	BLSTN	CCL	77P001
1210110043	S1	CLE	.2200+02	.3900+02	.1000+00	0	BLSTN	CCL	77P001
1210110044	S1	CLE	.4100+02	.6500+02	.1000+00	0	BLSTN	CCL	77P001
1210110045	S1	CLE	.1900+02	.5800+02	.1000+00	0	BLSTN	CCL	77P001
1210110045	S1	CLE	.3300+02	.5200+02	.1000+00	0	BLSTN	CCL	77P001
1210110046	S1	CLE	.1400+02	.4800+02	.1000+00	0	BLSTN	CCL	77P001
1210110046	S1	CLE	.7700+02	.5000+02	.1000+00	0	BLSTN	CCL	77P001
1210110047	S1	CLE	.2400+02	.5200+02	.1000+00	0	BLSTN	CCL	77P001
1210110048	S1	CLE	.3390+03	.4000+02	.1000+00	0	BLSTN	CCL	77P001
1210110048	S1	CLE	.1400+02	.2800+02	.1000+00	0	BLSTN	CCL	77P001
1210110048	S1	CLE	.3510+03	.6200+02	.1000+00	0	BLSTN	CCL	77P001
1210110049	S1	CLE	.3100+03	.4500+02	.1000+00	0	BLSTN	CCL	77P001
1210110050	S1	CLE	.2800+02	.6200+02	.1000+00	0	BLSTN	CCL	77P001
1210110051	S1	PHF	.7000+02	.2900+02	.1000+00	0	PHYLL	CCL	77P001
1210110052	L1B	ISL	.2680+03	.7000+01	.1000+00	0	PHYLL	CCL	77P001
1210110052	L1B	ISL	.2430+03	.9000+01	.1000+00	0	PHYLL	CCL	77P001
1210110052	L1B	ISL	.2190+03	.1000+01	.1000+00	0	PHYLL	CCL	77P001
1210110052	L1B	ISL	.2190+03	.6000+01	.1000+00	0	PHYLL	CCL	77P001
1210110052	L1X	MEL	.3440+03	.1200+02	.1000+00	0	PHYLL	CCL	77P001
1210110052	L2	CRL	.2730+03	.9000+01	.1000+00	0	PHYLL	CCL	77P001
1210110052	L2	CRL	.2810+03	.2200+02	.1000+00	0	PHYLL	CCL	77P001
1210110052	S1	PHF	.1860+03	.1500+02	.1000+00	0	PHYLL	CCL	77P001
1210110052	S1	PHF	.2620+03	.5200+02	.1000+00	0	PHYLL	CCL	77P001
1210110052	S1	PHF	.2310+03	.8000+01	.1000+00	0	PHYLL	CCL	77P001
1210110052	S1	PHF	.2220+03	.1500+02	.1000+00	0	PHYLL	CCL	77P001
1210110052	S1	PHF	.2140+03	.1100+02	.1000+00	0	PHYLL	GCS	77P001
1210110052	S1	PHF	.2090+03	.3200+02	.1000+00	0	PHYLL	CCL	77P001
1210110052	S1	PHF	.2060+03	.1900+02	.1000+00	0	PHYLL	CCL	77P001
1210110053	L1X	MEL	.1280+03	.5000+01	.1000+00	0	BLSTN	CCL	77P001
1210110053	L1X	MEL	.1190+03	.4000+01	.1000+00	0	BLSTN	CCL	77P001
1210110053	S1	CLE	.3550+03	.5000+01	.1000+00	0	BLSTN	CCL	77P001
1210110054	S1	CLE	.4200+02	.5000+02	.1000+00	0	BLSTN	CCL	77P001
1210110055	L1	FAX	.3200+03	.3000+02	.1000+00	3	BLSTN	CCL	77P001
1210110055	L1X	MEL	.1540+03	.1000+02	.1000+00	0	PHYLL	CCL	77P001
1210110055	L1X	MEL	.1900+03	.1500+02	.1000+00	5	PHYLL	CCL	77P001
1210110055	L1X	MEL	.1770+03	.1500+02	.1000+00	1	BLSTN	CCL	77P001
1210110055	S1	CLE	.1370+03	.4800+02	.1000+00	1	BLSTN	CCL	77P001
1210110055	S1	CLE	.1320+03	.5100+02	.1000+00	2	BLSTN	CCL	77P001
1210110055	S1	CLE	.3550+03	.2000+02	.1000+00	5	BLSTN	CCL	77P001
1210110055	S1	CLE	.1670+03	.4100+02	.1000+00	2	BLSTN	CCL	77P001
1210110055	S1	CLE	.1530+03	.4000+02	.1000+00	2	BLSTN	CCL	77P001
1210110055	S1	CLE	.1480+03	.3200+02	.1000+00	2	BLSTN	CCL	77P001
1210110055	S1	CLE	.1460+03	.4500+02	.1000+00	1	BLSTN	CCL	77P001
1210110055	S1	CLE	.1410+03	.7500+02	.1000+00	3	BLSTN	CCL	77P001
1210110055	S1	CLE	.1400+03	.3100+02	.1000+00	2	BLSTN	CCL	77P001
1210110055	S1	FAP	.1580+03	.6000+02	.1000+00	3	BLSTN	CCL	77P001
1210110055	S1	PHF	.3560+03	.2500+02	.1000+00	0	PHYLL	CCL	77P001
1210110055	S1	PHF	.3420+03	.2800+02	.1000+00	0	PHYLL	CCL	77P001
1210110055	S1	PHF	.3200+02	.6300+02	.1000+00	5	PHYLL	CCL	77P001
1210110055	S1	PHF	.2100+02	.2700+02	.1000+00	0	PHYLL	CCL	77P001

LOCALE	FABELT	TYCODE	STR	DPL	SIZE	TAG	LITHCO	METHOD	REFER
1210110055	S1	PHF	.2100+02	.5200+02	.1000+00	5	PHYLL	CCL	77P001
1210110055	S1	PHF	.1100+02	.4200+02	.1000+00	4	PHYLL	CCL	77P001
1210110055	S1	PHF	.1100+02	.4100+02	.1000+00	4	PHYLL	CCL	77P001
1210110055	S1	PHF	.9000+01	.3800+02	.1000+00	5	PHYLL	CCL	77P001
1210110055	S1	PHF	.3560+03	.2900+02	.1000+00	4	PHYLL	CCL	77P001
1210110056	L1B	ISL	.1600+02	.1900+02	.1000+00	0	DOLOM	CCL	77P001
1210110056	SS	BED	.3600+02	.3500+02	.1000+00	0	DOLOM	CCL	77P001
1210110056	SS	BED	.2000+01	.3300+02	.1000+00	0	DOLOM	CCL	77P001
1210110056	SS	BED	.3580+03	.4200+02	.1000+00	0	DOLOM	CCL	77P001
1210110056	SS	BED	.3550+03	.4700+02	.1000+00	0	DOLOM	CCL	77P001
1210110056	S1	FRC	.1320+03	.4900+02	.1000+00	0	DOLOM	CCL	77P001
1210110056	S1	MYF	.3560+03	.3400+02	.1000+00	0	DOLOM	CCL	77P001
1210110057	S1	CLE	.2150+03	.3200+02	.1000+00	0	PELITE	CCL	77P001
1210110058	S1	CLE	.7100+02	.6200+02	.1000+00	0	BLSTN	CCL	77P001
1210110058	S1	CLE	.8100+02	.6000+02	.1000+00	0	BLSTN	CCL	77P001
1210110058	S1	CLE	.7900+02	.6900+02	.1000+00	0	BLSTN	CCL	77P001
1210110058	S1	CLE	.8500+02	.7000+02	.1000+00	0	BLSTN	CCL	77P001
1210110058	S1	CLE	.8400+02	.7600+02	.1000+00	0	BLSTN	CCL	77P001
1210110058	S1	FOL	.4400+02	.4700+02	.1000+00	1	MARBLE	CCL	77P001
1210110058	S1	FOL	.3600+02	.4500+02	.1000+00	2	DOLOMU	CCL	77P001
1210110058	S1	FOL	.7800+02	.2300+02	.1000+00	1	MARBLE	CCL	77P001
1210110058	S1	FOL	.7600+02	.2600+02	.1000+00	1	MARBLE	CCL	77P001
1210110058	S1	FOL	.5800+02	.4500+02	.1000+00	1	MARBLE	CCL	77P001
1210110058	S1	FOL	.4700+02	.4200+02	.1000+00	1	MARBLE	CCL	77P001
1210110058	S1	PHF	.4100+02	.8000+01	.1000+00	2	PHYLL	CCL	77P001
1210110059	L1X	PEL	.1750+03	.4000+01	.1000+00	0	PHYLL	CCL	77P001
1210110059	S1	PHF	.5600+02	.5000+01	.1000+00	0	PHYLL	CCL	77P001
1210110060	S1	CLE	.1980+03	.8500+02	.1000+00	0	BLSTN	CCL	77P001
1210110061	L2	CRL	.1300+03	.1100+02	.1000+00	1	PHYLL	CCL	77P001
1210110061	SF	JNT	.1500+02	.8800+02	.1000+00	0	PHYLL	CCL	77P001
1210110061	S1	PHF	.7400+02	.1200+02	.1000+00	0	PHYLL	CCL	77P001
1210110061	S1	PHF	.1900+02	.1000+02	.1000+00	0	PHYLL	CCL	77P001
1210110061	S1	PHF	.3430+03	.2200+02	.1000+00	1	PHYLL	CCL	77P001
1210110061	S1	PHF	.3080+03	.3800+02	.1000+00	0	PHYLL	CCL	77P001
1210110061	S1	PHF	.3070+03	.4300+02	.1000+00	0	PHYLL	CCL	77P001
1210110061	S1	PHF	.2870+03	.3600+02	.1000+00	0	PHYLL	CCL	77P001
1210110061	S1	PHF	.3580+03	.2900+02	.1000+00	0	PHYLL	CCL	77P001
1210110061	S2	FAP	.1340+03	.7700+02	.1000+00	0	PHYLL	CCL	77P001
1210110061	S2	FAP	.1350+03	.4500+02	.1000+00	2	PHYLL	CCL	77P001
1210110061	S2L	DFLN	.1700+03	.5500+02	.1000+00	2	PHYLL	CCL	77P001
1210110062	L1B	ISL	.7100+02	.1000+02	.1000+00	0	DOLOM	CCL	77P001
1210110062	SS	BED	.2260+03	.1800+02	.1000+00	0	DOLOM	CCL	77P001
1210110062	S1	PSF	.2520+03	.5800+02	.1000+00	0	DOLOM	CCL	77P001
1210110063	L1X	MEL	.3580+03	.3000+02	.1000+00	0	PHYLL	CCL	77P001
1210110063	S1	PHF	.2760+03	.2300+02	.1000+00	0	PHYLL	CCL	77P001
1210110063	S1	PHF	.2730+03	.2700+02	.1000+00	0	PHYLL	CCL	77P001
1210110063	S1	PHF	.2720+03	.2300+02	.1000+00	0	PHYLL	CCL	77P001
1210110063	S1	PHF	.2590+03	.4000+01	.1000+00	0	PHYLL	CCL	77P001
1210110063	S1	PHF	.2580+03	.2700+02	.1000+00	0	PHYLL	CCL	77P001
1210110063	S1	PHF	.2500+03	.1900+02	.1000+00	0	PHYLL	CCL	77P001

LOCALE	FABELT	TYCODE	STR	DPL	SIZE	TAG	LITHCO	METHOD	REFER
1210110064	SS	BED	.1540+03	.3800+02	.1000+00	0	DOLOM	CCL	77P001
1210110064	SS	BED	.1330+03	.5400+02	.1000+00	0	DOLOM	CCL	77P001
1210110064	SS	BED	.2830+03	.1300+02	.1000+00	0	DOLOM	CCL	77P001
1210110064	SS	BED	.2410+03	.1100+02	.1000+00	0	DOLOM	CCL	77P001
1210110064	SS	BED	.1750+03	.1000+02	.1000+00	0	DOLOM	CCL	77P001
1210110064	SS	BED	.1740+03	.2400+02	.1000+00	0	DOLOM	CCL	77P001
1210110065	L1	FAX	.2620+03	.4100+02	.1000+00	0	DOLOM	CCL	77P001
1210110065	L1B	ISL	.2480+03	.1700+02	.1000+00	3	SLATE	CCL	77P001
1210110065	L1B	ISL	.2500+03	.8000+01	.1000+00	2	SLATE	CCL	77P001
1210110065	SF	JNT	.3400+03	.4100+02	.1000+00	0	DOLOM	CCL	77P001
1210110065	SS	BED	.1240+03	.3600+02	.1000+00	1	DOLOM	CCL	77P001
1210110065	SS	BED	.1050+03	.4300+02	.1000+00	3	SLATE	CCL	77P001
1210110065	SI	FAP	.1660+03	.5800+02	.1000+00	0	DOLOM	CCL	77P001
1210110065	SI	SLC	.1810+03	.2000+02	.1000+00	3	SLATE	CCL	77P001
1210110065	SI	SLC	.1870+03	.1400+02	.1000+00	2	SLATE	CCL	77P001
1210110066	SF	JNT	.2460+03	.5800+02	.1000+00	0	DOLOM	CCL	77P001
1210110066	SS	BED	.1720+03	.2200+02	.1000+00	0	DOLOM	CCL	77P001
1210110067	L1B	ISL	.1900+02	.7000+01	.1000+00	1	PHYLL	CCL	77P001
1210110067	L1B	ISL	.2090+03	.2000+01	.1000+00	2	PHYLL	CCL	77P001
1210110067	L1B	ISL	.2400+02	.9000+01	.1000+00	0	PHYLL	CCL	77P001
1210110067	SI	SLC	.2090+03	.2800+02	.1000+00	1	PHYLL	CCL	77P001
1210110067	SI	SLC	.2010+03	.2200+02	.1000+00	2	PHYLL	CCL	77P001
1210110067	SI	SLC	.2340+03	.2000+02	.1000+00	0	PHYLL	CCL	77P001
1210110068	L1	FAX	.2300+03	.5000+01	.1000+00	3	DOLOM	CCL	77P001
1210110068	L1	FAX	.2420+03	.1000+01	.1000+00	3	DOLOM	CCL	77P001
1210110068	L1B	ISL	.6600+02	.2000+01	.1000+00	3	DOLOM	CCL	77P001
1210110068	L1B	ISL	.1850+03	.1800+02	.1000+00	0	PHYLL	CCL	77P001
1210110068	L1X	MEL	.3400+02	.3000+01	.1000+00	0	PHYLL	CCL	77P001
1210110068	L1X	MEL	.2100+03	.1700+02	.1000+00	1	PHYLL	CCL	77P001
1210110068	L1X	MEL	.1810+03	.3600+02	.1000+00	2	PHYLL	CCL	77P001
1210110068	L2	CRL	.9900+02	.5000+01	.1000+00	2	PHYLL	CCL	77P001
1210110068	L2	CRL	.8500+02	.1400+02	.1000+00	0	PHYLL	CCL	77P001
1210110068	SS	BED	.5800+02	.3100+02	.1000+00	3	DOLOM	CCL	77P001
1210110068	SS	BED	.4900+02	.4800+02	.1000+00	3	DOLOM	CCL	77P001
1210110068	SS	BED	.2410+03	.4700+02	.1000+00	3	DOLOM	CCL	77P001
1210110068	SS	BED	.6600+02	.3200+02	.1000+00	3	DOLOM	CCL	77P001
1210110068	SI	BCL	.5600+02	.7000+02	.1000+00	4	MARBLE	CCL	77P001
1210110068	SI	BCL	.5400+02	.2100+02	.1000+00	4	MARBLE	CCL	77P001
1210110068	SI	CLE	.2890+03	.5700+02	.1000+00	5	MARBLE	CCL	77P001
1210110068	SI	CLE	.2730+03	.3300+02	.1000+00	5	MARBLE	CCL	77P001
1210110068	SI	FOL	.8500+02	.6000+01	.1000+00	3	DOLOM	CCL	77P001
1210110068	SI	FOL	.6300+02	.8000+01	.1000+00	3	DOLOM	CCL	77P001
1210110068	SI	PHF	.8600+02	.4000+02	.1000+00	2	PHYLL	CCL	77P001
1210110068	SI	PHF	.7800+02	.2500+02	.1000+00	1	PHYLL	CCL	77P001
1210110068	SI	PHF	.6400+02	.2900+02	.1000+00	0	PHYLL	CCL	77P001
1210110068	SI	PHF	.3800+02	.1900+02	.1000+00	0	PHYLL	CCL	77P001
1210110068	SI	PSF	.2480+03	.1400+02	.1000+00	3	DOLOM	CCL	77P001
1210110068	S2	CRC	.1050+03	.8600+02	.1000+00	2	PHYLL	CCL	77P001
1210110069	SI	FOL	.3090+03	.5000+01	.1000+00	0	MARBLE	CCL	77P001
1210110069	S2	FRC	.8400+02	.8200+02	.1000+00	0	MARBLE	CCL	77P001

LOCALE	FABELT	TYCODE	STR	DPL	SIZE	TAG	LITHCO	METHOD	REFER
1210110070	L1	FAX	.7000+02	.1000+01	.1000+00	0	PHYLL	CCL	77P001
1210110070	L1B	ISL	.7100+02	.2000+01	.1000+00	0	PHYLL	CCL	77P001
1210110070	L1B	ISL	.1470+03	.5000+01	.1000+00	1	DOLOM	CCL	77P001
1210110070	L1B	ISL	.7800+02	.0000	.1000+00	0	PHYLL	CCL	77P001
1210110070	L1X	MEL	.3460+03	.1200+02	.1000+00	0	PHYLL	CCL	77P001
1210110070	SF	JNT	.1510+03	.8800+02	.1000+00	0	PHYLL	CCL	77P001
1210110070	SS	BED	.7500+02	.7000+01	.1000+00	0	PHYLL	GCS	77P001
1210110070	SS	BED	.7500+02	.4300+02	.1000+00	0	PHYLL	GCS	77P001
1210110070	S1	CLE	.3000+01	.2200+02	.1000+00	1	DOLOM	CCL	77P001
1210110070	S1	PHF	.6400+02	.2100+02	.1000+00	0	PHYLL	CCL	77P001
1210110070	S1	PHF	.2760+03	.1000+02	.1000+00	0	PHYLL	CCL	77P001
1210110070	S1	PHF	.2650+03	.1100+02	.1000+00	0	PHYLL	CCL	77P001
1210110071	S1	CLE	.3000+01	.2200+02	.1000+00	0	DOLOM	CCL	77P001
1210110072	L1B	ISL	.1700+02	.2400+02	.1000+00	5	PHYLL	CCL	77P001
1210110072	L1B	ISL	.4800+02	.1400+02	.1000+00	3	PHYLL	CCL	77P001
1210110072	L1B	ISL	.3600+02	.2000+02	.1000+00	1	PHYLL	CCL	77P001
1210110072	L1B	ISL	.2680+03	.3000+01	.1000+00	0	PHYLL	CCL	77P001
1210110072	L1X	MEL	.3350+03	.2300+02	.1000+00	5	PHYLL	CCL	77P001
1210110072	L1X	MEL	.3530+03	.2200+02	.1000+00	3	PHYLL	CCL	77P001
1210110072	L1X	MEL	.3380+03	.2400+02	.1000+00	1	PHYLL	CCL	77P001
1210110072	L1X	MEL	.3590+03	.1900+02	.1000+00	0	PHYLL	CCL	77P001
1210110072	L2	CRL	.2630+03	.2000+02	.1000+00	6	PHYLL	CCL	77P001
1210110072	L2	CRL	.2690+03	.2000+01	.1000+00	1	PHYLL	CCL	77P001
1210110072	S1	SLC	.2490+03	.3100+02	.1000+00	1	PHYLL	CCL	77P001
1210110072	S1	SLC	.2640+03	.1900+02	.1000+00	0	PHYLL	CCL	77P001
1210110072	S1	SLC	.2630+03	.2200+02	.1000+00	3	PHYLL	CCL	77P001
1210110072	S1	SLC	.2570+03	.2500+02	.1000+00	5	PHYLL	CCL	77P001
1210110072	S1	SLC	.2570+03	.4500+02	.1000+00	2	PHYLL	CCL	77P001
1210110072	S2	CRC	.2420+03	.4300+02	.1000+00	6	PHYLL	CCL	77P001
1210110072	S2	CRC	.8400+02	.7000+02	.1000+00	4	PHYLL	CCL	77P001
1210120001	L1X	PEL	.3340+03	.5800+02	.1000+00	0	VLCFEL	CCL	77P001
1210120001	S1	CLE	.2520+03	.6600+02	.1000+00	0	VLCFEL	CCL	77P001
1210120001	S1	CLE	.2570+03	.5100+02	.1000+00	0	VLCFEL	CCL	77P001
1210120001	S1	CLE	.2560+03	.6000+02	.1000+00	0	VLCFEL	CCL	77P001
1210120001	S2	FRC	.1930+03	.5300+02	.1000+00	0	VLCFEL	CCL	77P001
1210120002	SS	BED	.1530+03	.4500+02	.1000+00	0	VLCMAF	CCL	77P001
1210120003	S1	PHF	.2480+03	.6500+02	.1000+00	0	PHYLL	CCL	77P001
1210120004	L2	CRL	.2540+03	.9000+01	.1000+00	0	PHYLL	CCL	77P001
1210120004	S1	PHF	.2340+03	.4200+02	.1000+00	0	PHYLL	CCL	77P001
1210120004	S1	PHF	.2340+03	.3300+02	.1000+00	0	PHYLL	CCL	77P001
1210120004	S1	PHF	.2380+03	.3600+02	.1000+00	0	PHYLL	CCL	77P001
1210120004	S2	CRC	.6900+02	.8700+02	.1000+00	0	PHYLL	CCL	77P001
1210120005						0	DOLOMU		77P001
1210120006	SS	BED	.3490+03	.7500+02	.1000+00	0	DOLOM	CCL	77P001
1210120007	SS	BED	.1530+03	.6000+02	.1000+00	0	DOLOM	CCL	77P001
1210120008	L1	FAX	.2760+03	.5000+01	.1000+00	0	MARBLE	CCL	77P001
1210120008	L2	FAX	.1700+03	.3100+02	.1000+00	0	MARBLE	GCS	77P001
1210120008	S1	BCL	.7200+02	.5300+02	.1000+00	2	DOLOM	CCL	77P001
1210120008	S1	BCL	.1740+03	.5000+02	.1000+00	2	DOLOM	CCL	77P001
1210120008	S1	BCL	.1380+03	.3300+02	.1000+00	2	DOLOM	CCL	77P001

LOCALE	FABELT	TYCODE	STR	DPL	SIZE	TAG	LITHCO	METHOD	REFER
1210120008	S1	BCL	.1170+03	.3200+02	.1000+00	2	DOLOM	CCL	77P001
1210120008	S1	MYF	.2400+02	.2100+02	.1000+00	1	MARBLE	CCL	77P001
1210120008	S1	MYF	.5200+02	.5700+02	.1000+00	1	MARBLE	CCL	77P001
1210120008	S1	MYF	.5000+02	.3300+02	.1000+00	0	MARBLE	CCL	77P001
1210120008	S1	MYF	.4600+02	.3500+02	.1000+00	1	MARBLE	CCL	77P001
1210120008	S1	MYF	.4200+02	.6100+02	.1000+00	1	MARBLE	CCL	77P001
1210120008	S1	MYF	.6400+02	.5200+02	.1000+00	1	MARBLE	CCL	77P001
1210120008	S1	MYF	.5300+02	.7000+02	.1000+00	1	MARBLE	CCL	77P001
1210120009	S1	BCL	.5300+02	.3000+02	.1000+00	0	QTZITE	CCL	77P001
1210120010	S1	BCL	.1500+02	.2700+02	.1000+00	0	DOLOM	CCL	77P001
1210120011	SS	BED	.1700+02	.2100+02	.1000+00	0	DOLOM	CCL	77P001
1210120012	SS	BED	.2200+02	.4000+02	.1000+00	0	DOLOM	CCL	77P001
1210120013	SS	BED	.2400+02	.2400+02	.1000+00	0	DOLOM	CCL	77P001
1210120014	S1	BCL	.3210+03	.2800+02	.1000+00	0	DOLOM	CCL	77P001
1210120015	SS	BED	.9600+02	.3000+02	.1000+00	0	DOLOM	CCL	77P001
1210120016	SS	BED	.3220+03	.2500+02	.1000+00	0	DOLOM	CCL	77P001
1210120017	SF	JNT	.2720+03	.7200+02	.1000+00	0	DOLOM	CCL	77P001
1210120017	SS	BED	.1800+02	.1500+02	.1000+00	0	DOLOM	CCL	77P001
1210120017	SS	BED	.2700+02	.3400+02	.1000+00	0	DOLOM	CCL	77P001
1210120018	SS	BED	.5600+02	.3300+02	.1000+00	0	DOLOM	CCL	77P001
1210120019	S1	BCL	.4800+02	.4100+02	.1000+00	0	DOLOM	CCL	77P001
1210120020	SS	BED	.0000	.0000	.1000+00	0	DOLOM	CCL	77P001
1210120021	SF	JNT	.2260+03	.2900+02	.1000+00	0	DOLOM	CCL	77P001
1210120021	SF	JNT	.2000+01	.4500+02	.1000+00	0	DOLOM	CCL	77P001
1210120021	SS	BED	.2240+03	.4800+02	.1000+00	0	DOLOM	CCL	77P001
1210120021	SS	BED	.2120+03	.4700+02	.1000+00	0	DOLOM	CCL	77P001
1210120022	SS	BED	.5000+01	.1100+02	.1000+00	0	DOLOM	CCL	77P001
1210120023	SS	BED	.3300+02	.1600+02	.1000+00	0	DOLOM	CCL	77P001
1210120023	SS	BED	.5800+02	.3300+02	.1000+00	0	DOLOM	CCL	77P001
1210120024	SS	BED	.5100+02	.2500+02	.1000+00	0	DOLOM	CCL	77P001
1210120025	SS	BED	.0000	.0000	.1000+00	0	DOLOM	CCL	77P001
1210120026	SS	BED	.0000	.0000	.1000+00	0	DOLOM	CCL	77P001
1210120027	SF	JNT	.3240+03	.7200+02	.1000+00	0	DOLOM	CCL	77P001
1210120027	SS	BED	.3600+02	.2000+02	.1000+00	0	DOLOM	CCL	77P001
1210120028	SS	BED	.2200+02	.4300+02	.1000+00	0	DOLOM	CCL	77P001
1210120029	SS	BED	.4900+02	.3700+02	.1000+00	0	DOLOM	CCL	77P001
1210120030	SF	JNT	.2180+03	.6100+02	.1000+00	0	DOLOM	CCL	77P001
1210120030	SS	BED	.3200+02	.5700+02	.1000+00	0	DOLOM	CCL	77P001
1210120030	SS	BED	.4900+02	.3700+02	.1000+00	0	DOLOM	CCL	77P001
1210120031	SS	BED	.4100+02	.5300+02	.1000+00	0	DOLOM	CCL	77P001
1210120031	SS	BED	.5500+02	.5900+02	.1000+00	1	DOLOM	CCL	77P001
1210120031	SS	BED	.4200+02	.5500+02	.1000+00	0	DOLOM	CCL	77P001
1210120032	SS	BED	.5600+02	.3500+02	.1000+00	0	DOLOM	CCL	77P001
1210120033	SS	BED	.1600+02	.7200+02	.1000+00	0	DOLOM	CCL	77P001
1210120033	S1	PHF	.5000+01	.7400+02	.1000+00	0	PHYLL	CCL	77P001
1210120034	L2	PEN	.3000+01	.1500+02	.1000+00	0	PHYLL	CCL	77P001
1210120034	L2	PEN	.3590+03	.1300+02	.1000+00	0	PHYLL	CCL	77P001
1210120034	S1	PHF	.1690+03	.1000+02	.1000+00	0	PHYLL	CCL	77P001
1210120034	S1	PHF	.3420+03	.3700+02	.1000+00	0	PHYLL	CCL	77P001
1210120034	S1	PHF	.3190+03	.1300+02	.1000+00	0	PHYLL	CCL	77P001

LOCALE	FABELT	TYCODE	STR	DPL	SIZE	TAG	LITHCO	METHOD	REFER
1210120034	S2	CRC	.1830+03	.7800+02	.1000+00	0	PHYLL	CCL	77P001
1210120035	L1X	MEL	.1300+02	.2500+02	.1000+00	0	PHYLL	CCL	77P001
1210120035	S1	PHF	.3440+03	.3200+02	.1000+00	0	PHYLL	CCL	77P001
1210120035	S1	PHF	.3110+03	.2100+02	.1000+00	0	PHYLL	CCL	77P001
1210120035	S1	PHF	.3590+03	.2800+02	.1000+00	0	PHYLL	CCL	77P001
1210120036	L1	FAX	.2000+01	.9000+01	.1000+00	0	PHYLL	CCL	77P001
1210120036	S1	PHF	.3560+03	.2000+02	.1000+00	0	PHYLL	CCL	77P001
1210120037	SF	JNT	.2010+03	.9000+02	.1000+00	0	DOLOM	CCL	77P001
1210120037	SF	JNT	.3280+03	.9000+02	.1000+00	0	DOLOM	CCL	77P001
1210120037	SF	JNT	.2620+03	.9000+02	.1000+00	0	DOLOM	CCL	77P001
1210120037	SS	BED	.0000	.0000	.1000+00	0	DOLOM	CCL	77P001
1210120038	SF	JNT	.3510+03	.6900+02	.1000+00	0	DOLOM	CCL	77P001
1210120038	SS	BED	.8000+01	.1100+02	.1000+00	0	DOLOM	CCL	77P001
1210120039	SS	BED	.1200+02	.2900+02	.1000+00	0	DOLOM	CCL	77P001
1210120040	SS	BED	.3420+03	.1700+02	.1000+00	0	DOLOM	CCL	77P001
1210120041	SS	BED	.1100+02	.1500+02	.1000+00	0	SHALE	CCL	77P001
1210120041	SS	BED	.3530+03	.1100+02	.1000+00	0	SHALE	CCL	77P001
1210120041	SS	BED	.1600+02	.1100+02	.1000+00	0	SHALE	CCL	77P001
1210120041	SS	BED	.1600+02	.1400+02	.1000+00	0	SHALE	CCL	77P001
1210120042	SS	BED	.2300+02	.1000+02	.1000+00	0	DOLOM	CCL	77P001
1210120042	SS	BED	.3400+02	.3700+02	.1000+00	0	DOLOM	CCL	77P001
1210120043	SS	BED	.1400+02	.1000+02	.1000+00	0	DOLOM	CCL	77P001
1210120043	SS	BED	.2540+03	.2500+02	.1000+00	0	DOLOM	CCL	77P001
1210120044	SS	BED	.2600+02	.9000+01	.1000+00	0	DOLOM	CCL	77P001
1210120045	SF	FAULT	.2360+03	.6500+02	.1000+00	0	DOLOM	CCL	77P001
1210120046	SS	BED	.6400+02	.3200+02	.1000+00	0	DOLOM	CCL	77P001
1210120047	SS	BED	.5300+02	.3300+02	.1000+00	0	SHALE	CCL	77P001
1210120047	SS	BED	.4300+02	.3000+02	.1000+00	0	SHALE	CCL	77P001
1210120048	S1	CLE	.2740+03	.6100+02	.1000+00	0	DOLOM	CCL	77P001
1210120049	S1	CLE	.5900+02	.6400+02	.1000+00	0	DOLOM	CCL	77P001
1210120050	SS	BED	.6400+02	.1500+02	.1000+00	0	DOLOM	CCL	77P001
1210120051	S1	SLC	.2160+03	.5100+02	.1000+00	0	SLATE	CCL	77P001
1210120052	S1	PHF	.1000+01	.3400+02	.1000+00	1	PHYLL	CCL	77P001
1210120052	S1	SLC	.3000+02	.6000+02	.1000+00	0	PHYLL	CCL	77P001
1210120053	S1	PHF	.3050+03	.4000+01	.1000+00	0	PHYLL	CCL	77P001
1210120054	S1	SLC	.3100+02	.1700+02	.1000+00	0	SLATE	CCL	77P001
1210120055	L1X	MEL	.3520+03	.2000+01	.1000+00	1	LSTBRE	CCL	77P001
1210120055	L1X	MEL	.3000+01	.4000+01	.1000+00	0	LSTBRE	GCS	77P001
1210120055	S1	FOL	.2730+03	.4000+01	.1000+00	0	LSTBRE	CCL	77P001
1210120055	S1	FOL	.0000	.0000	.1000+00	1	LSTBRE	CCL	77P001
1210120056	L1X	MEL	.3590+03	.2500+02	.1000+00	0	LSTBRE	GCS	77P001
1210120056	S1	FOL	.2880+03	.2600+02	.1000+00	0	LSTBRE	CCL	77P001
1210120057	L1X	MEL	.1970+03	.3000+01	.1000+00	1	LSTBRE	CCL	77P001
1210120057	SF	JNT	.2720+03	.6700+02	.1000+00	0	LSTBRE	CCL	77P001
1210120057	S1	FOL	.2900+02	.1400+02	.1000+00	1	LSTBRE	CCL	77P001
1210120058	L1X	MEL	.9000+01	.3000+01	.1000+00	0	LSTBRE	CCL	77P001
1210120058	SF	JNT	.3150+03	.9000+02	.1000+00	0	LSTBRE	CCL	77P001
1210120058	S1	FOL	.2000+01	.1500+02	.1000+00	0	LSTBRE	CCL	77P001
1210120058	S1	FOL	.1800+02	.2000+02	.1000+00	0	LSTBRE	CCL	77P001
1210120059	L1X	MEL	.2000+01	.3000+01	.1000+00	3	LSTBRE	CCL	77P001

LOCALE	FABELT	TYCODE	STR	DPL	SIZE	TAG	LITHCO	METHOD	REFER
1210120059	L1X	MEL	.2840+03	.7000+01	.1000+00	3	LSTBRE	CCL	77P001
1210120059	L1X	MEL	.2000+01	.7000+01	.1000+00	3	LSTBRE	CCL	77P001
1210120059	L1X	MEL	.3550+03	.2000+01	.1000+00	0	LSTBRE	GCS	77P001
1210120059	L1X	MEL	.3550+03	.6000+01	.1000+00	3	LSTBRE	CCL	77P001
1210120059	L1X	PEL	.4000+01	.7000+01	.1000+00	2	LSTBRE	CCL	77P001
1210120059	L1X	PEL	.1000+01	.1200+02	.1000+00	2	LSTBRE	CCL	77P001
1210120059	L1X	PEL	.8000+01	.7000+01	.1000+00	2	LSTBRE	CCL	77P001
1210120059	L1X	PEL	.8000+01	.0000	.1000+00	4	LSTBRE	CCL	77P001
1210120059	L1X	PEL	.6000+01	.1000+02	.1000+00	4	LSTBRE	CCL	77P001
1210120059	L1X	PEL	.5000+01	.1000+01	.1000+00	4	LSTBRE	CCL	77P001
1210120059	L1X	PEL	.3570+03	.2000+01	.1000+00	0	LSTBRE	GCS	77P001
1210120059	L1X	PEL	.3540+03	.3000+01	.1000+00	0	LSTBRE	GCS	77P001
1210120059	L1X	PEL	.3540+03	.3000+01	.1000+00	0	LSTBRE	GCS	77P001
1210120059	L1X	PEL	.2670+03	.4000+01	.1000+00	4	LSTBRE	CCL	77P001
1210120059	L1X	PEL	.1920+03	.1000+01	.1000+00	0	LSTBRE	GCS	77P001
1210120059	L1X	PEL	.2300+02	.2000+01	.1000+00	4	LSTBRE	CCL	77P001
1210120059	L1X	PEL	.2200+02	.2000+01	.1000+00	3	LSTBRE	CCL	77P001
1210120059	L1X	PEL	.1900+02	.0000	.1000+00	2	LSTBRE	CCL	77P001
1210120059	L1X	PEL	.1100+02	.7000+01	.1000+00	2	LSTBRE	CCL	77P001
1210120059	L1X	PEL	.9000+01	.2000+01	.1000+00	4	LSTBRE	CCL	77P001
1210120059	S1	FOL	.2250+03	.8000+01	.1000+00	3	LSTBRE	GCS	77P001
1210120059	S1	FOL	.1860+03	.1200+02	.1000+00	0	LSTBRE	CCL	77P001
1210120059	S1	FOL	.2770+03	.1100+02	.1000+00	1	LSTBRE	CCL	77P001
1210120060	L1X	MEL	.1730+03	.2300+02	.1000+00	1	LSTBRE	CCL	77P001
1210120060	L1X	MEL	.1760+03	.7000+01	.1000+00	0	LSTBRE	GCS	77P001
1210120060	S1	FOL	.8800+02	.7000+01	.1000+00	0	LSTBRE	CCL	77P001
1210120060	S1	FOL	.1020+03	.2700+02	.1000+00	1	LSTBRE	CCL	77P001
1210120061	S1	SLC	.1900+02	.2700+02	.1000+00	0	SLATE	CCL	77P001
1210120062	S1	SLC	.3160+03	.2000+02	.1000+00	0	SLATE	CCL	77P001
1210120063	S1	SLC	.9900+02	.1900+02	.1000+00	0	SLATE	CCL	77P001
1210120064	S1	SLC	.2160+03	.4200+02	.1000+00	0	SLATE	CCL	77P001
1210120065	S1	SLC	.2100+03	.2800+02	.1000+00	0	SLATE	CCL	77P001
1210120066	L1B	ISL	.4100+02	.5000+01	.1000+00	0	SLATE	CCL	77P001
1210120066	L1X	MEL	.3490+03	.1600+02	.1000+00	0	SLATE	CCL	77P001
1210120066	S1	SLC	.2280+03	.2100+02	.1000+00	0	SLATE	CCL	77P001
1210120067	L1B	ISL	.3700+02	.7000+01	.1000+00	0	PELITE	CCL	77P001
1210120067	L1X	MEL	.3440+03	.1400+02	.1000+00	0	PELITE	CCL	77P001
1210120067	SS	BED	.4100+02	.2300+02	.1000+00	0	PELITE	CCL	77P001
1210120067	S1	CLE	.2460+03	.1400+02	.1000+00	0	PELITE	GCS	77P001
1210120068	L1B	ISL	.4900+02	.8000+01	.1000+00	0	PELITE	CCL	77P001
1210120068	L1X	MEL	.4000+01	.6000+01	.1000+00	0	PELITE	CCL	77P001
1210120068	S1	CLE	.3120+03	.7000+01	.1000+00	0	PELITE	GCS	77P001
1210120069	L1B	ISL	.4200+02	.3000+01	.1000+00	0	PELITE	CCL	77P001
1210120069	L1B	ISL	.2900+02	.7000+01	.1000+00	1	PELITE	CCL	77P001
1210120069	L1X	MEL	.3500+03	.1100+02	.1000+00	1	PELITE	CCL	77P001
1210120069	L1X	MEL	.3470+03	.1400+02	.1000+00	0	PELITE	CCL	77P001
1210120069	S1	CLE	.2460+03	.1100+02	.1000+00	1	PELITE	GCS	77P001
1210120069	S1	CLE	.2340+03	.1600+02	.1000+00	0	PELITE	CCL	77P001
1210120070	SS	BED	.2420+03	.3200+02	.1000+00	0	DOLOM	CCL	77P001
1210120071	L1	FAX	.3900+02	.1000+02	.1000+00	0	DOLOM	CCL	77P001

LOCALE	FABELT	TYCODE	STR	DPL	SIZE	TAG	LITHCO	METHOD	REFER
1210120071	SS	BED	.2200+02	.3700+02	.1000+00	0	DOLOM	CCL	77P001
1210120071	S1	FAP	.2370+03	.3000+02	.1000+00	0	DOLOM	GCS	77P001
1210120072	S1	SLC	.1980+03	.3500+02	.1000+00	0	SLATE	CCL	77P001
1210120073	S1	SLC	.1930+03	.3900+02	.1000+00	0	SLATE	CCL	77P001
1210120074	L1	FAX	.2170+03	.3000+02	.1000+00	1	DOLOM	CCL	77P001
1210120074	SF	JNT	.3000+01	.5200+02	.1000+00	2	DOLOM	CCL	77P001
1210120074	SS	BED	.1830+03	.1500+02	.1000+00	2	DOLOM	CCL	77P001
1210120074	SS	BED	.1360+03	.3200+02	.1000+00	0	DOLOM	CCL	77P001
1210120074	S1	MYF	.1800+03	.5100+02	.1000+00	1	DOLOM	CCL	77P001
1210120074	S1	PSF	.2060+03	.6300+02	.1000+00	0	DOLOM	CCL	77P001
1210120075	L1	FAX	.2410+03	.3000+01	.1000+00	0	DOLOM	CCL	77P001
1210130001	SS	BED	.2700+03	.5100+02	.1000+00	0	VOLCLS	CCL	77P001
1210130001	S1	CLE	.2620+03	.3200+02	.1000+00	0	VOLCLS	CCL	77P001
1210130003	SF	JNT	.2600+03	.7000+02	.1000+00	0	LSTBRE	CCL	77P001
1210130003	SF	JNT	.3300+03	.8500+02	.1000+00	0	LSTBRE	CCL	77P001
1210130003	SS	BED	.3010+03	.2000+02	.1000+00	0	LSTBRE	GCS	77P001
1210130003	SS	BED	.3010+03	.2000+02	.1000+00	0	LSTBRE	GCS	77P001
1210130003	S1	CLE	.2470+03	.3400+02	.1000+00	0	LSTBRE	CCL	77P001
1210130003	S1	CLE	.2540+03	.3700+02	.1000+00	0	LSTBRE	CCL	77P001
1210130003	S1	CLE	.2510+03	.3300+02	.1000+00	0	LSTBRE	CCL	77P001
1210130003	S1	CLE	.2540+03	.2900+02	.1000+00	0	LSTBRE	CCL	77P001
1210130004	SS	BED	.2700+02	.2900+02	.1000+00	0	DOLOM	CCL	77P001
1210130005	S1	BCL	.2470+03	.6900+02	.1000+00	0	BLSTN	CCL	77P001
1210130006	L1	FAX	.4800+02	.4000+01	.1000+00	0	BLSTN	CCL	77P001
1210130006	SS	BED	.2570+03	.2600+02	.1000+00	0	BLSTN	CCL	77P001
1210130006	S1	FAP	.2140+03	.5900+02	.1000+00	0	BLSTN	CCL	77P001
1210130007	L1	FAX	.3700+02	.2000+01	.1000+00	0	BLSTN	CCL	77P001
1210130008	S1	BCL	.2230+03	.3000+02	.1000+00	0	DOLOM	CCL	77P001
1210130009	SS	BED	.2190+03	.3700+02	.1000+00	0	VOLCLS	CCL	77P001
1210130009	S1	CLE	.2210+03	.5100+02	.1000+00	0	VOLCLS	CCL	77P001
1210130010	L1B	ISL	.2080+03	.1900+02	.1000+00	0	PELITE	CCL	77P001
1210130010	SS	BED	.1360+03	.1600+02	.1000+00	0	PELITE	CCL	77P001
1210130010	S1	SLC	.1990+03	.5600+02	.1000+00	0	PELITE	CCL	77P001
1210130010	S1	SLC	.1910+03	.5800+02	.1000+00	0	PELITE	CCL	77P001
1210130010	S1	SLC	.1860+03	.5500+02	.1000+00	0	PELITE	CCL	77P001
1210130011	L1B	ISL	.1970+03	.1900+02	.1000+00	0	LSTBRE	CCL	77P001
1210130011	SS	BED	.6500+02	.5000+02	.1000+00	0	LSTBRE	CCL	77P001
1210130011	S1	CLE	.1890+03	.5100+02	.1000+00	0	LSTBRE	CCL	77P001
1210130011	S1	CLE	.2030+03	.5900+02	.1000+00	0	LSTBRE	CCL	77P001
1210130012	S1	BCL	.1890+03	.5700+02	.1000+00	0	QTZITE	CCL	77P001
1210130013	SS	BED	.1750+03	.3000+02	.1000+00	0	QTZITE	CCL	77P001
1210130014	SS	BED	.1970+03	.3100+02	.1000+00	0	QTZITE	CCL	77P001
1210130014	SS	BED	.1980+03	.3700+02	.1000+00	0	QTZITE	CCL	77P001
1210130015	SS	BED	.2380+03	.2900+02	.1000+00	0	QTZITE	CCL	77P001
1210130015	SS	BED	.2450+03	.2400+02	.1000+00	0	QTZITE	CCL	77P001
1210130015	SS	BED	.2410+03	.2700+02	.1000+00	0	QTZITE	CCL	77P001
1210130016	SS	BED	.3010+03	.1300+02	.1000+00	0	QTZITE	CCL	77P001
1210130016	S1	TEV	.1060+03	.7100+02	.1000+00	0	QTZITE	CCL	77P001
1210130017	SS	BED	.2190+03	.8100+02	.1000+00	0	QTZITE	CCL	77P001
1210130018	SS	BED	.1450+03	.5000+01	.1000+00	0	DOLOM	CCL	77P001

LOCALE	FABELT	TYCODE	STR	DPL	SIZE	TAG	LITHCO	METHOD	REFER
1210130019	L1B	ISL	.3700+02	.6000+01	.1000+00	0	MARBLE	CCL	77P001
1210130019	S1	MYF	.2330+03	.8100+02	.1000+00	0	MARBLE	CCL	77P001
1210130019	S1	MYF	.2420+03	.3800+02	.1000+00	0	MARBLE	CCL	77P001
1210130020	S1	CLE	.2310+03	.3100+02	.1000+00	0	LSTBRE	CCL	77P001
1210130020	S1	CLE	.2380+03	.3700+02	.1000+00	0	LSTBRE	CCL	77P001
1210130021	L1	FAX	.4100+02	.2400+02	.1000+00	0	MARBLE	CCL	77P001
1210130021	S1	MYF	.2780+03	.2500+02	.1000+00	0	MARBLE	CCL	77P001
1210130022	S1	CLE	.2210+03	.4200+02	.1000+00	0	LSTBRE	CCL	77P001
1210130023	SS	BED	.2040+03	.5100+02	.1000+00	0	VOLCLS	CCL	77P001
1210130024	SS	BED	.2490+03	.3700+02	.1000+00	0	QTZITE	CCL	77P001
1210130026	SS	BED	.2170+03	.4300+02	.1000+00	0	QTZITE	CCL	73T001
1210130027	L2	CRL	.2610+03	.5000+01	.1000+00	0	PHYLL	CCL	77P001
1210130027	SF	JNT	.9600+02	.8500+02	.1000+00	0	PHYLL	CCL	77P001
1210130027	S1	PHF	.5000+02	.4000+01	.1000+00	0	PHYLL	CCL	77P001
1210130027	S1	PHF	.2570+03	.1000+02	.1000+00	0	PHYLL	CCL	77P001
1210130027	S1	PHF	.2500+03	.2300+02	.1000+00	0	PHYLL	CCL	77P001
1210130027	S1	PHF	.2440+03	.3300+02	.1000+00	0	PHYLL	CCL	77P001
1210130027	S1	PHF	.2430+03	.2800+02	.1000+00	0	PHYLL	CCL	77P001
1210130027	S1	PHF	.2340+03	.3000+02	.1000+00	0	PHYLL	CCL	77P001
1210130028	L1B	ISL	.2740+03	.6000+01	.1000+00	2	PHYLL	CCL	77P001
1210130028	SS	BED	.2540+03	.2700+02	.1000+00	2	PHYLL	CCL	77P001
1210130028	SS	BED	.2500+03	.2200+02	.1000+00	1	PHYLL	CCL	77P001
1210130028	S1	PHF	.2660+03	.3000+02	.1000+00	2	PHYLL	CCL	77P001
1210130028	S1	PHF	.2620+03	.3700+02	.1000+00	2	PHYLL	CCL	77P001
1210130028	S1	PHF	.2530+03	.3100+02	.1000+00	1	PHYLL	CCL	77P001
1210130028	S2	FRC	.8300+02	.4800+02	.1000+00	2	PHYLL	CCL	77P001
1210130029	L2	CCFIB	.5000+01	.7300+02	.1000+00	0	LSTBRE	GCS	77P001
1210130029	SS	BED	.2200+03	.2000+02	.1000+00	0	LSTBRE	CCL	77P001
1210130029	SS	BED	.2380+03	.2000+02	.1000+00	0	LSTBRE	CCL	77P001
1210130029	SS	BED	.2350+03	.2400+02	.1000+00	0	LSTBRE	CCL	77P001
1210130029	SS	BED	.2580+03	.2700+02	.1000+00	0	LSTBRE	CCL	77P001
1210130029	SS	BED	.2540+03	.2000+02	.1000+00	0	LSTBRE	CCL	77P001
1210130029	S2	TEV	.2600+03	.7400+02	.1000+00	0	LSTBRE	CCL	77P001
1210130030	S1	CLE	.2310+03	.2300+02	.1000+00	0	QTZITE	CCL	77P001
1210130030	S1	CLE	.2480+03	.1200+02	.1000+00	0	QTZITE	CCL	77P001
1210130030	S1	CLE	.2410+03	.3400+02	.1000+00	0	QTZITE	CCL	77P001
1210130030	S1	CLE	.2400+03	.2800+02	.1000+00	0	QTZITE	CCL	77P001
1210130030	S2	KINK	.2260+03	.5200+02	.1000+00	0	QTZITE	CCL	77P001
1210130031	L1B	ISL	.3040+03	.3200+02	.1000+00	4	PELITE	CCL	77P001
1210130031	L1B	ISL	.3010+03	.2900+02	.1000+00	4	PELITE	CCL	77P001
1210130031	L1B	ISL	.3000+03	.3800+02	.1000+00	4	PELITE	CCL	77P001
1210130031	L1B	ISL	.9300+02	.4000+01	.1000+00	2	PELITE	CCL	77P001
1210130031	SS	BED	.2140+03	.3700+02	.1000+00	4	PELITE	CCL	77P001
1210130031	SS	BED	.2030+03	.1800+02	.1000+00	3	PELITE	CCL	77P001
1210130031	SS	BED	.1850+03	.2500+02	.1000+00	3	PELITE	CCL	77P001
1210130031	SS	BED	.1620+03	.1800+02	.1000+00	3	PELITE	CCL	77P001
1210130031	S1	SLC	.2660+03	.4100+02	.1000+00	2	PELITE	CCL	77P001
1210130031	S1	SLC	.2650+03	.5000+02	.1000+00	1	PELITE	CCL	77P001
1210130031	S1	SLC	.2630+03	.4300+02	.1000+00	4	PELITE	CCL	77P001
1210130031	S1	SLC	.2610+03	.4700+02	.1000+00	4	PELITE	CCL	77P001

LOCALE	FABELT	TYCODE	STR	DPL	SIZE	TAG	LITHCO	METHOD	REFER
1210130031	S1	SLC	.2600+03	.4700+02	.1000+00	4	PELITE	CCL	77P001
1210130031	S1	SLC	.2590+03	.3700+02	.1000+00	4	PELITE	CCL	77P001
1210130031	S1	SLC	.2520+03	.5000+02	.1000+00	1	PELITE	CCL	77P001
1210130031	S1	SLC	.2460+03	.4800+02	.1000+00	1	PELITE	CCL	77P001
1210130032	L1B	ISL	.3200+03	.3900+02	.1000+00	0	LSTBRE	CCL	77P001
1210130032	L1X	PEL	.3330+03	.3600+02	.1000+00	0	LSTBRE	CCL	77P001
1210130032	L1X	PEL	.3450+03	.3700+02	.1000+00	0	LSTBRE	CCL	77P001
1210130032	SS	BED	.1460+03	.8900+02	.1000+00	0	LSTBRE	CCL	77P001
1210130032	SS	BED	.2500+03	.2600+02	.1000+00	0	LSTBRE	CCL	77P001
1210130032	S1	CLE	.2730+03	.4600+02	.1000+00	0	LSTBRE	CCL	77P001
1210130033	L1X	MEL	.3330+03	.3500+02	.1000+00	0	BLSMAR	CCL	77P001
1210130033	S1	BCL	.2220+03	.5300+02	.1000+00	0	BLSMAR	CCL	77P001
1210130033	S1	BCL	.2540+03	.1800+02	.1000+00	0	BLSMAR	CCL	77P001
1210130033	S1	BCL	.2360+03	.3300+02	.1000+00	0	BLSMAR	CCL	77P001
1210130033	S1	BCL	.2350+03	.2200+02	.1000+00	0	BLSMAR	CCL	77P001
1210130033	S1	BCL	.2330+03	.4400+02	.1000+00	0	BLSMAR	CCL	77P001
1210130033	S1	BCL	.2320+03	.3500+02	.1000+00	0	BLSMAR	CCL	77P001
1210130034	L1B	ISL	.2720+03	.2000+02	.1000+00	0	QTZITE	CCL	77P001
1210130034	SS	BED	.1800+03	.2300+02	.1000+00	0	QTZITE	CCL	77P001
1210130034	SS	BED	.1680+03	.1700+02	.1000+00	0	QTZITE	CCL	77P001
1210130034	SS	BED	.2060+03	.1000+02	.1000+00	0	QTZITE	CCL	77P001
1210130034	S1	CLE	.2220+03	.3700+02	.1000+00	0	QTZITE	CCL	77P001
1210130035	SS	BED	.2700+03	.2200+02	.1000+00	0	PHYLL	CCL	77P001
1210130035	S1	PHF	.2520+03	.3900+02	.1000+00	0	PHYLL	CCL	77P001
1210130035	S1	PHF	.2740+03	.3200+02	.1000+00	0	PHYLL	CCL	77P001
1210130035	S1	PHF	.2580+03	.2900+02	.1000+00	0	PHYLL	CCL	77P001
1210130036	L1B	ISL	.2680+03	.2000+02	.1000+00	0	PHYSLT	CCL	77P001
1210130036	L1B	ISL	.2360+03	.1000+02	.1000+00	0	PHYSLT	CCL	77P001
1210130036	L1B	ISL	.2870+03	.2200+02	.1000+00	0	PHYSLT	CCL	77P001
1210130036	SS	BED	.1250+03	.5000+01	.1000+00	0	PHYSLT	CCL	77P001
1210130036	S1	SLC	.2420+03	.3200+02	.1000+00	0	PHYSLT	CCL	77P001
1210130036	S1	SLC	.2220+03	.3600+02	.1000+00	0	PHYSLT	CCL	77P001
1210130036	S1	SLC	.2720+03	.1800+02	.1000+00	0	PHYSLT	CCL	77P001
1210130036	S1	SLC	.2570+03	.5600+02	.1000+00	0	PHYSLT	CCL	77P001
1210130036	S1	SLC	.2470+03	.3700+02	.1000+00	0	PHYSLT	CCL	77P001
1210130037	L1B	ISL	.9400+02	.4000+01	.1000+00	0	PHYLL	CCL	77P001
1210130037	S1	PHF	.2640+03	.1600+02	.1000+00	0	PHYLL	CCL	77P001
1210130037	S1	PHF	.2630+03	.4400+02	.1000+00	0	PHYLL	CCL	77P001
1210130037	S1	PHF	.2550+03	.6000+02	.1000+00	0	PHYLL	CCL	77P001
1210130037	S1	PHF	.2350+03	.1300+02	.1000+00	0	PHYLL	CCL	77P001
1210130037	S1	PHF	.2260+03	.2200+02	.1000+00	0	PHYLL	CCL	77P001
1210130037	S1	PHF	.2110+03	.2300+02	.1000+00	0	PHYLL	CCL	77P001
1210130037	S1	PHF	.2000+03	.1300+02	.1000+00	0	PHYLL	CCL	77P001
1210130037	S1	PHF	.9500+02	.5000+01	.1000+00	0	PHYLL	CCL	77P001
1210130037	S2	FRC	.7600+02	.6300+02	.1000+00	0	PHYLL	CCL	77P001
1210130038	SS	BED	.2290+03	.2000+02	.1000+00	0	LSTBRE	CCL	77P001
1210130038	SS	BED	.2440+03	.2500+02	.1000+00	0	LSTBRE	CCL	77P001
1210130038	SS	BED	.2400+03	.1700+02	.1000+00	0	LSTBRE	CCL	77P001
1210130038	SS	BED	.2470+03	.2000+02	.1000+00	0	LSTBRE	CCL	77P001
1210130039	SS	BED	.2170+03	.2000+02	.1000+00	0	LSTBRE	CCL	77P001

LOCALE	FABELT	TYCODE	STR	DPL	SIZE	TAG	LITHCO	METHOD	REFER
1210130048	S2	FRC	.2400+03	.4200+02	.1000+00	0	PELITE	CCL	77P001
1210130048	S2	FRC	.2250+03	.3300+02	.1000+00	0	PELITE	CCL	77P001
1210130049	S1	CLE	.2270+03	.3100+02	.1000+00	0	BLSMAR	CCL	77P001
1210130049	S1	CLE	.1890+03	.4100+02	.1000+00	0	BLSMAR	CCL	77P001
1210130049	S1	CLE	.3150+03	.2100+02	.1000+00	0	BLSMAR	CCL	77P001
1210130049	S1	CLE	.3000+03	.1500+02	.1000+00	0	BLSMAR	CCL	77P001
1210130049	S1	CLE	.2670+03	.1000+02	.1000+00	0	BLSMAR	CCL	77P001
1210130049	S1	CLE	.2410+03	.2400+02	.1000+00	0	BLSMAR	CCL	77P001
1210130049	S1	CLE	.3480+03	.2900+02	.1000+00	0	BLSMAR	CCL	77P001
1210130049	S1	CLE	.3330+03	.2000+02	.1000+00	0	BLSMAR	CCL	77P001
1210130049	S2	TEV	.4500+02	.5600+02	.1000+00	0	BLSMAR	CCL	77P001
1210130050	SS	BED	.3200+02	.9000+02	.1000+00	2	QTZITE	CCL	77P001
1210130050	SS	BED	.2770+03	.2600+02	.1000+00	1	QTZITE	CCL	77P001
1210130050	SS	BED	.2600+03	.2300+02	.1000+00	1	QTZITE	CCL	77P001
1210130050	SS	BED	.2560+03	.2500+02	.1000+00	1	QTZITE	CCL	77P001
1210130050	SS	BED	.2500+03	.2800+02	.1000+00	1	QTZITE	CCL	77P001
1210130050	SS	BED	.3000+03	.2300+02	.1000+00	1	QTZITE	CCL	77P001
1210130050	SS	BED	.2910+03	.2300+02	.1000+00	1	QTZITE	CCL	77P001
1210130050	SS	BED	.2910+03	.2300+02	.1000+00	2	QTZITE	CCL	77P001
1210130051	SS	BED	.2530+03	.3100+02	.1000+00	0	VOLCLS	CCL	77P001
1210130052	L1B	ISL	.1300+02	.3100+02	.1000+00	0	PELITE	CCL	77P001
1210130052	L1B	ISL	.1100+02	.2800+02	.1000+00	0	PELITE	CCL	77P001
1210130052	L1B	ISL	.7000+01	.2200+02	.1000+00	0	PELITE	CCL	77P001
1210130052	SS	BED	.2280+03	.4100+02	.1000+00	0	PELITE	CCL	77P001
1210130052	SS	BED	.2990+03	.3200+02	.1000+00	0	PELITE	CCL	77P001
1210130052	SS	BED	.2900+03	.2200+02	.1000+00	0	PELITE	CCL	77P001
1210130052	SS	BED	.2730+03	.2300+02	.1000+00	0	PELITE	CCL	77P001
1210130052	SS	BED	.2690+03	.2500+02	.1000+00	0	PELITE	CCL	77P001
1210130052	S1	FRC	.1900+03	.7400+02	.1000+00	0	PELITE	CCL	77P001
1210130052	S1	FRC	.1870+03	.8200+02	.1000+00	0	PELITE	CCL	77P001
1210130052	S1	FRC	.1770+03	.7400+02	.1000+00	0	PELITE	CCL	77P001
1210130053	SS	BED	.2510+03	.2600+02	.1000+00	0	BLSTN	CCL	77P001
1210130054	S1	CLE	.2700+03	.4700+02	.1000+00	0	PHYSLT	CCL	77P001
1210130054	S1	CLE	.2600+03	.4700+02	.1000+00	0	PHYSLT	CCL	77P001
1210130054	S1	CLE	.2520+03	.4500+02	.1000+00	0	PHYSLT	CCL	77P001
1210130054	S1	CLE	.2500+03	.5300+02	.1000+00	0	PHYSLT	CCL	77P001
1210130055	L1	FAX	.3200+02	.1600+02	.1000+00	1	QTZITE	CCL	77P001
1210130055	L1B	ISL	.3700+02	.1000+02	.1000+00	2	QTZITE	CCL	77P001
1210130055	SS	BED	.6000+01	.8000+01	.1000+00	2	QTZITE	CCL	77P001
1210130055	SS	BED	.2000+01	.2300+02	.1000+00	1	QTZITE	CCL	77P001
1210130055	SS	BED	.3420+03	.1800+02	.1000+00	2	QTZITE	CCL	77P001
1210130055	SS	BED	.3310+03	.1200+02	.1000+00	2	QTZITE	CCL	77P001
1210130055	SS	BED	.3300+03	.2000+02	.1000+00	2	QTZITE	CCL	77P001
1210130055	SS	BED	.2150+03	.1280+03	.1000+00	1	QTZITE	CCL	77P001
1210130055	SS	BED	.3400+02	.9000+02	.1000+00	1	QTZITE	CCL	77P001
1210130055	SS	BED	.2300+02	.6500+02	.1000+00	1	QTZITE	CCL	77P001
1210130055	SS	BED	.1800+02	.1350+03	.1000+00	1	QTZITE	CCL	77P001
1210130055	SS	BED	.1200+02	.4600+02	.1000+00	1	QTZITE	CCL	77P001
1210130055	SS	BED	.3570+03	.9000+01	.1000+00	2	QTZITE	CCL	77P001
1210130055	S1	FRC	.2150+03	.6900+02	.1000+00	2	QTZITE	CCL	77P001

LOCALE	FABELT	TYCODE	STR	DPL	SIZE	TAG	LITHCO	METHOD	REFER
1210130056	L1B	PEN	.1300+02	.1500+02	.1000+00	0	PELITE	CCL	77P001
1210130056	L1B	PEN	.1200+02	.7000+01	.1000+00	0	PELITE	CCL	77P001
1210130056	L1B	PEN	.1900+02	.1200+02	.1000+00	0	PELITE	CCL	77P001
1210130056	L1B	PEN	.1600+02	.2500+02	.1000+00	0	PELITE	CCL	77P001
1210130056	SS	BED	.1960+03	.8900+02	.1000+00	0	PELITE	CCL	77P001
1210130056	SS	BED	.1950+03	.9000+02	.1000+00	0	PELITE	CCL	77P001
1210130056	SS	BED	.2450+03	.2400+02	.1000+00	0	PELITE	CCL	77P001
1210130056	SS	BED	.2230+03	.3200+02	.1000+00	0	PELITE	CCL	77P001
1210130056	SS	BED	.1990+03	.3800+02	.1000+00	0	PELITE	CCL	77P001
1210130056	SS	BED	.1970+03	.7700+02	.1000+00	0	PELITE	CCL	77P001
1210130056	S1	FRC	.3010+03	.4000+01	.1000+00	0	PELITE	CCL	77P001
1210130057	L1	FAX	.2560+03	.2500+02	.1000+00	1	BLSTN	CCL	77P001
1210130057	SS	BED	.1170+03	.1320+03	.1000+00	2	BLSTN	CCL	77P001
1210130057	SS	BED	.1090+03	.6300+02	.1000+00	1	BLSTN	CCL	77P001
1210130057	SS	BED	.2400+03	.3000+02	.1000+00	2	BLSTN	CCL	77P001
1210130057	SS	BED	.2330+03	.3000+02	.1000+00	2	BLSTN	CCL	77P001
1210130057	SS	BED	.2270+03	.4900+02	.1000+00	1	BLSTN	CCL	77P001
1210130057	SS	BED	.2250+03	.3600+02	.1000+00	2	BLSTN	CCL	77P001
1210130057	SS	BED	.2200+03	.4200+02	.1000+00	2	BLSTN	CCL	77P001
1210130057	SS	BED	.1770+03	.6000+02	.1000+00	2	BLSTN	CCL	77P001
1210130057	SS	BED	.1750+03	.6900+02	.1000+00	2	BLSTN	CCL	77P001
1210130057	SS	BED	.1460+03	.9000+02	.1000+00	2	BLSTN	CCL	77P001
1210130057	S1	CLE	.2550+03	.3400+02	.1000+00	2	BLSTN	CCL	77P001
1210130057	S1	CLE	.2420+03	.4500+02	.1000+00	1	BLSTN	CCL	77P001
1210130057	S1	CLE	.2390+03	.4300+02	.1000+00	1	BLSTN	CCL	77P001
1210130057	S1	CLE	.2150+03	.4600+02	.1000+00	1	BLSTN	CCL	77P001
1210130057	S1	CLE	.2090+03	.4500+02	.1000+00	1	BLSTN	CCL	77P001
1210130058	L1X	PEL	.5000+01	.2700+02	.1000+00	1	LSTBRE	CCL	77P001
1210130058	L1X	PEL	.8000+01	.2800+02	.1000+00	2	LSTBRE	CCL	77P001
1210130058	L1X	PEL	.5000+01	.3100+02	.1000+00	2	LSTBRE	CCL	77P001
1210130058	L1X	PEL	.1000+02	.2500+02	.1000+00	1	LSTBRE	CCL	77P001
1210130058	L1X	PEL	.9000+01	.2300+02	.1000+00	1	LSTBRE	CCL	77P001
1210130058	L1X	PEL	.9000+01	.3300+02	.1000+00	2	LSTBRE	CCL	77P001
1210130058	S1	CLE	.2180+03	.4000+02	.1000+00	1	LSTBRE	CCL	77P001
1210130058	S1	CLE	.2250+03	.4000+02	.1000+00	1	LSTBRE	CCL	77P001
1210130058	S1	CLE	.2240+03	.4800+02	.1000+00	2	LSTBRE	CCL	77P001
1210130058	S1	CLE	.2230+03	.3600+02	.1000+00	1	LSTBRE	CCL	77P001
1210130058	S1	CLE	.2200+03	.4700+02	.1000+00	2	LSTBRE	CCL	77P001
1210130058	S1	CLE	.2270+03	.4600+02	.1000+00	2	LSTBRE	CCL	77P001
1210130058	S1	CLE	.2260+03	.4700+02	.1000+00	2	LSTBRE	CCL	77P001
1210130059	SS	BED	.1920+03	.3200+02	.1000+00	0	LSTBRE	CCL	77P001
1210130059	SS	BED	.1740+03	.4000+02	.1000+00	0	LSTBRE	CCL	77P001
1210130059	SS	BED	.1980+03	.3500+02	.1000+00	0	LSTBRE	CCL	77P001
1210130059	SS	BED	.1930+03	.3000+02	.1000+00	0	LSTBRE	CCL	77P001
1210130060	L1B	ISL	.1700+02	.8000+01	.1000+00	0	PELITE	CCL	77P001
1210130060	L1B	ISL	.1600+02	.1400+02	.1000+00	0	PELITE	CCL	77P001
1210130060	L1B	ISL	.2100+02	.7000+01	.1000+00	0	PELITE	CCL	77P001
1210130060	L1B	ISL	.1900+02	.1400+02	.1000+00	0	PELITE	CCL	77P001
1210130060	S1	CLE	.2110+03	.3800+02	.1000+00	0	PELITE	CCL	77P001
1210130060	S1	CLE	.1980+03	.3100+02	.1000+00	0	PELITE	CCL	77P001

LOCALE	FABELT	TYCODE	STR	DPL	SIZE	TAG	LITHCO	METHOD	REFER
1210130060	S1	CLE	.2190+03	.4200+02	.1000+00	0	PELITE	CCL	77P001
1210130060	S1	CLE	.2120+03	.4300+02	.1000+00	0	PELITE	CCL	77P001
1210130061	L1X	MEL	.5200+02	.5500+02	.1000+00	0	PHYSLT	CCL	77P001
1210130061	S1	SLC	.2530+03	.7300+02	.1000+00	0	PHYSLT	CCL	77P001
1210130061	S1	SLC	.2660+03	.7400+02	.1000+00	0	PHYSLT	CCL	77P001
1210130061	S1	SLC	.2610+03	.7400+02	.1000+00	0	PHYSLT	CCL	77P001
1210130061	S1	SLC	.2570+03	.7400+02	.1000+00	0	PHYSLT	CCL	77P001
1210130062	S1	SLC	.2450+03	.7000+02	.1000+00	0	PELITE	CCL	77P001
1210130062	S1	SLC	.2550+03	.7400+02	.1000+00	0	PELITE	CCL	77P001
1210130062	S1	SLC	.2520+03	.7600+02	.1000+00	0	PELITE	CCL	77P001
1210130062	S1	SLC	.2470+03	.7700+02	.1000+00	0	PELITE	CCL	77P001
1210130063	L1B	ISL	.3210+03	.6200+02	.1000+00	0	PELITE	CCL	77P001
1210130063	L2	ISL	.3400+02	.3800+02	.1000+00	0	PELITE	CCL	77P001
1210130063	L2	ISL	.3000+02	.3300+02	.1000+00	0	PELITE	CCL	77P001
1210130063	L2	ISL	.3000+02	.4000+02	.1000+00	0	PELITE	CCL	77P001
1210130063	L2	ISL	.1800+02	.3600+02	.1000+00	0	PELITE	CCL	77P001
1210130063	S1	SLC	.2460+03	.6400+02	.1000+00	0	PELITE	CCL	77P001
1210130063	S1	SLC	.2460+03	.5700+02	.1000+00	0	PELITE	CCL	77P001
1210130063	S1	SLC	.2400+03	.5600+02	.1000+00	0	PELITE	CCL	77P001
1210130063	S1	SLC	.2390+03	.5800+02	.1000+00	0	PELITE	CCL	77P001
1210130063	S1	SLC	.2480+03	.6100+02	.1000+00	0	PELITE	CCL	77P001
1210130063	S2	FRC	.7000+01	.5500+02	.1000+00	0	PELITE	CCL	77P001
1210130063	S2	FRC	.2700+02	.8800+02	.1000+00	0	PELITE	CCL	77P001
1210130063	S2	FRC	.2000+02	.7900+02	.1000+00	0	PELITE	CCL	77P001
1210130063	S2	FRC	.2800+02	.8700+02	.1000+00	0	PELITE	CCL	77P001
1210130064	L1X	PEL	.2600+02	.2800+02	.1000+00	0	LSTBRE	CCL	77P001
1210130064	L1X	PEL	.3300+02	.2400+02	.1000+00	0	LSTBRE	CCL	77P001
1210130064	L1X	PEL	.2900+02	.2700+02	.1000+00	0	LSTBRE	CCL	77P001
1210130064	L1X	PEL	.3500+02	.2700+02	.1000+00	0	LSTBRE	CCL	77P001
1210130064	S1	CLE	.2320+03	.5200+02	.1000+00	0	LSTBRE	CCL	77P001
1210130064	S1	CLE	.2330+03	.5300+02	.1000+00	0	LSTBRE	CCL	77P001
1210130064	S1	CLE	.2330+03	.5600+02	.1000+00	0	LSTBRE	CCL	77P001
1210130064	S1	CLE	.2360+03	.5600+02	.1000+00	0	LSTBRE	CCL	77P001
1210130065	S1	SLC	.2220+03	.6600+02	.1000+00	0	PHYSLT	CCL	77P001
1210130065	S1	SLC	.2310+03	.5700+02	.1000+00	0	PHYSLT	CCL	77P001
1210130065	S1	SLC	.2250+03	.7500+02	.1000+00	0	PHYSLT	CCL	77P001
1210130065	S1	SLC	.2440+03	.6500+02	.1000+00	0	PHYSLT	CCL	77P001
1210130067	L1X	PEL	.2000+01	.2400+02	.1000+00	2	LSTBRE	CCL	77P001
1210130067	L1X	PEL	.3430+03	.2900+02	.1000+00	1	LSTBRE	CCL	77P001
1210130067	L1X	PEL	.3000+01	.1700+02	.1000+00	2	LSTBRE	CCL	77P001
1210130067	L1X	PEL	.3500+03	.1600+02	.1000+00	2	LSTBRE	CCL	77P001
1210130067	L1X	PEL	.3500+03	.1800+02	.1000+00	1	LSTBRE	CCL	77P001
1210130067	L1X	PEL	.3480+03	.2000+02	.1000+00	1	LSTBRE	CCL	77P001
1210130067	L1X	PEL	.3460+03	.1500+02	.1000+00	1	LSTBRE	CCL	77P001
1210130067	L1X	PEL	.3560+03	.1600+02	.1000+00	2	LSTBRE	CCL	77P001
1210130067	L1X	PEL	.3540+03	.1100+02	.1000+00	1	LSTBRE	CCL	77P001
1210130067	L1X	PEL	.3540+03	.1200+02	.1000+00	1	LSTBRE	CCL	77P001
1210130067	L1X	PEL	.3530+03	.1600+02	.1000+00	1	LSTBRE	CCL	77P001
1210130067	L1X	PEL	.3510+03	.1900+02	.1000+00	1	LSTBRE	CCL	77P001
1210130067	SF	JNT	.2050+03	.8400+02	.1000+00	2	LSTBRE	CCL	77P001

LOCALE	FABELT	TYCODE	STR	DPL	SIZE	TAG	LITHCO	METHOD	REFER
1210130067	SF	JNT	.2500+03	.4600+02	.1000+00	1	LSTBRE	CCL	77P001
1210130067	S1	CLE	.2570+03	.1500+02	.1000+00	2	LSTBRE	CCL	77P001
1210130067	S1	CLE	.2890+03	.1500+02	.1000+00	2	LSTBRE	CCL	77P001
1210130067	S1	CLE	.2700+03	.1800+02	.1000+00	2	LSTBRE	CCL	77P001
1210130067	S1	CLE	.2670+03	.1600+02	.1000+00	1	LSTBRE	CCL	77P001
1210130067	S1	CLE	.2660+03	.1000+02	.1000+00	1	LSTBRE	CCL	77P001
1210130067	S1	CLE	.2640+03	.2100+02	.1000+00	1	LSTBRE	CCL	77P001
1210130067	S1	CLE	.2630+03	.1900+02	.1000+00	1	LSTBRE	CCL	77P001
1210130067	S2	FRC	.2950+03	.6800+02	.1000+00	2	LSTBRE	CCL	77P001
1210130067	S3	JNT	.2400+02	.8500+02	.1000+00	2	LSTBRE	CCL	77P001
1210130068	LIX	PEL	.3570+03	.1900+02	.1000+00	2	LSTBRE	CCL	77P001
1210130068	LIX	PEL	.3510+03	.2500+02	.1000+00	1	LSTBRE	CCL	77P001
1210130068	LIX	PEL	.3500+03	.1300+02	.1000+00	2	LSTBRE	CCL	77P001
1210130068	LIX	PEL	.3500+03	.2500+02	.1000+00	2	LSTBRE	CCL	77P001
1210130068	LIX	PEL	.3490+03	.2300+02	.1000+00	1	LSTBRE	CCL	77P001
1210130068	LIX	PEL	.3490+03	.2200+02	.1000+00	2	LSTBRE	CCL	77P001
1210130068	LIX	PEL	.3460+03	.1800+02	.1000+00	2	LSTBRE	CCL	77P001
1210130068	LIX	PEL	.3450+03	.2500+02	.1000+00	1	LSTBRE	CCL	77P001
1210130068	S1	CLE	.2500+03	.2000+02	.1000+00	2	LSTBRE	CCL	77P001
1210130068	S1	CLE	.2490+03	.1900+02	.1000+00	2	LSTBRE	CCL	77P001
1210130068	S1	CLE	.2470+03	.2300+02	.1000+00	2	LSTBRE	CCL	77P001
1210130068	S1	CLE	.2460+03	.2400+02	.1000+00	1	LSTBRE	CCL	77P001
1210130068	S1	CLE	.2430+03	.2200+02	.1000+00	2	LSTBRE	CCL	77P001
1210130068	S1	CLE	.2410+03	.2200+02	.1000+00	1	LSTBRE	CCL	77P001
1210130068	S1	CLE	.2370+03	.2700+02	.1000+00	1	LSTBRE	CCL	77P001
1210130068	S1	CLE	.2270+03	.2300+02	.1000+00	1	LSTBRE	CCL	77P001
1210130069	LIB	ISL	.3570+03	.2900+02	.1000+00	3	PELITE	CCL	77P001
1210130069	LIB	ISL	.3380+03	.3200+02	.1000+00	3	PELITE	CCL	77P001
1210130069	LIB	ISL	.3800+02	.3700+02	.1000+00	2	PELITE	CCL	77P001
1210130069	LIB	ISL	.3300+02	.4200+02	.1000+00	2	PELITE	CCL	77P001
1210130069	LIB	ISL	.2900+02	.3700+02	.1000+00	2	PELITE	CCL	77P001
1210130069	LIB	ISL	.2000+01	.3100+02	.1000+00	3	PELITE	CCL	77P001
1210130069	SS	BED	.2960+03	.3800+02	.1000+00	2	PELITE	CCL	77P001
1210130069	SS	BED	.2910+03	.3100+02	.1000+00	2	PELITE	CCL	77P001
1210130069	SS	BED	.3150+03	.3400+02	.1000+00	2	PELITE	CCL	77P001
1210130069	SS	BED	.3060+03	.4500+02	.1000+00	3	PELITE	GCS	77P001
1210130069	SS	BED	.2970+03	.4800+02	.1000+00	2	PELITE	CCL	77P001
1210130069	S1	CLE	.2650+03	.3700+02	.1000+00	2	PELITE	CCL	77P001
1210130069	S1	CLE	.2740+03	.3500+02	.1000+00	2	PELITE	CCL	77P001
1210130069	S1	CLE	.2730+03	.4600+02	.1000+00	3	PELITE	CCL	77P001
1210130069	S1	PHF	.2780+03	.2200+02	.1000+00	1	PHYLL	CCL	77P001
1210130069	S1	PHF	.2740+03	.4000+02	.1000+00	1	PHYLL	CCL	77P001
1210130069	S1	PHF	.2980+03	.3000+02	.1000+00	1	PHYLL	CCL	77P001
1210130069	S1	PHF	.2940+03	.3000+02	.1000+00	1	PHYLL	CCL	77P001
1210130069	S1	PHF	.2920+03	.3200+02	.1000+00	1	PHYLL	CCL	77P001
1210130069	S1	PHF	.2890+03	.3500+02	.1000+00	1	PHYLL	CCL	77P001
1210130069	S1	PHF	.2880+03	.2700+02	.1000+00	1	PHYLL	CCL	77P001
1210130069	S1	PHF	.2800+03	.3800+02	.1000+00	1	PHYLL	CCL	77P001
1210130069	S1	SLC	.2750+03	.3300+02	.1000+00	3	PELITE	CCL	77P001
1210130069	S1	SLC	.2690+03	.3500+02	.1000+00	3	PELITE	CCL	77P001

LOCALE	FABELT	TYCODE	STR	DPL	SIZE	TAG	LITHCO	METHOD	REFER
1210130070	L1X	PEL	.3570+03	.3500+02	.1000+00	0	LSTBRE	CCL	77P001
1210130070	L1X	PEL	.3540+03	.4300+02	.1000+00	0	LSTBRE	CCL	77P001
1210130070	L1X	PEL	.3520+03	.3800+02	.1000+00	0	LSTBRE	CCL	77P001
1210130070	L1X	PEL	.3510+03	.3100+02	.1000+00	0	LSTBRE	CCL	77P001
1210130070	L1X	PEL	.3480+03	.4500+02	.1000+00	0	LSTBRE	CCL	77P001
1210130070	S1	CLE	.2880+03	.4600+02	.1000+00	0	LSTBRE	CCL	77P001
1210130070	S1	CLE	.2960+03	.4400+02	.1000+00	0	LSTBRE	CCL	77P001
1210130070	S1	CLE	.2950+03	.4500+02	.1000+00	0	LSTBRE	CCL	77P001
1210130070	S1	CLE	.3070+03	.4700+02	.1000+00	0	LSTBRE	CCL	77P001
1210130070	S1	CLE	.3050+03	.4600+02	.1000+00	0	LSTBRE	CCL	77P001
1210130070	S1	CLE	.2990+03	.2800+02	.1000+00	0	LSTBRE	CCL	77P001
1210130070	S1	CLE	.2980+03	.3900+02	.1000+00	0	LSTBRE	CCL	77P001
1210130071	SS	BED	.1640+03	.2500+02	.1000+00	0	DOLOM	CCL	77P001
1210130071	SS	BED	.1630+03	.2400+02	.1000+00	0	DOLOM	CCL	77P001
1210130071	SS	BED	.1570+03	.3500+02	.1000+00	0	DOLOM	CCL	77P001
1210130071	SS	BED	.1520+03	.2100+02	.1000+00	0	DOLOM	CCL	77P001
1210130071	SS	BED	.1880+03	.3400+02	.1000+00	0	DOLOM	CCL	77P001
1210130071	SS	BED	.1790+03	.4000+02	.1000+00	0	DOLOM	CCL	77P001
1210130071	SS	BED	.1770+03	.3200+02	.1000+00	0	DOLOM	CCL	77P001
1210130071	SS	BED	.1700+03	.3200+02	.1000+00	0	DOLOM	CCL	77P001
1210130074	S1	FOL	.2100+03	.4300+02	.1000+00	0	BLSMAR	CCL	77P001
1210130075	L1B	ISL	.2360+03	.5000+01	.1000+00	0	SLATE	CCL	77P001
1210130075	S1	SLC	.2270+03	.2600+02	.1000+00	0	SLATE	CCL	77P001
1210130076	L1B	ISL	.2570+03	.5000+01	.1000+00	0	SLATE	CCL	77P001
1210130076	SS	BED	.5500+02	.2600+02	.1000+00	0	SLATE	CCL	77P001
1210130076	S1	SLC	.2220+03	.4100+02	.1000+00	0	SLATE	CCL	77P001
1210130076	S1	SLC	.2390+03	.3700+02	.1000+00	0	SLATE	CCL	77P001
1210130077	L1B	ISL	.2420+03	.3000+02	.1000+00	0	SLATE	CCL	77P001
1210130077	SS	BED	.2020+03	.4200+02	.1000+00	0	SLATE	GCS	77P001
1210130077	S1	SLC	.2300+03	.6800+02	.1000+00	0	SLATE	CCL	77P001
1210130078	L1	FAX	.2240+03	.9000+01	.1000+00	0	DOLOM	CCL	77P001
1210130078	SS	BED	.4400+02	.6900+02	.1000+00	0	DOLOM	CCL	77P001
1210130078	SS	BED	.2170+03	.3800+02	.1000+00	0	DOLOM	CCL	77P001
1210130078	S1	FAP	.2190+03	.6700+02	.1000+00	0	DOLOM	CCL	77P001
1210130079	SS	BED	.2320+03	.4700+02	.1000+00	0	VOLCLS	CCL	77P001
1210130079	SS	BED	.2300+03	.4900+02	.1000+00	0	VOLCLS	CCL	77P001
1210130079	SS	BED	.2350+03	.5100+02	.1000+00	0	VOLCLS	CCL	77P001
1210140001	SS	BED	.2000+03	.6000+02	.1000+00	0	DOLOM	CCL	77P001
1210140001	SS	BED	.2240+03	.7400+02	.1000+00	0	DOLOM	CCL	77P001
1210140001	SS	BED	.2030+03	.5500+02	.1000+00	0	DOLOM	CCL	77P001
1210140002	SS	BED	.2440+03	.1900+02	.1000+00	0	QTZITE	CCL	77P001
1210140002	SS	BED	.2110+03	.5200+02	.1000+00	0	QTZITE	CCL	77P001
1210140002	SS	BED	.2100+03	.2900+02	.1000+00	0	QTZITE	CCL	77P001
1210140002	SS	BED	.1990+03	.4600+02	.1000+00	0	QTZITE	CCL	77P001
1210140003	SS	BED	.5200+02	.7700+02	.1000+00	0	QTZITE	CCL	77P001
1210140004	SS	BED	.2230+03	.3300+02	.1000+00	1	QTZDOL	CCL	77P001
1210140004	SS	BED	.2270+03	.3800+02	.1000+00	1	QTZDOL	CCL	77P001
1210140004	SS	BED	.2250+03	.3300+02	.1000+00	1	QTZDOL	CCL	77P001
1210140004	SS	BED	.2350+03	.4100+02	.1000+00	2	QTZDOL	CCL	77P001
1210140004	SS	BED	.2310+03	.4500+02	.1000+00	2	QTZDOL	CCL	77P001

LOCALE	FABELT	TYCODE	STR	DPL	SIZE	TAG	LITHCO	METHOD	REFER
1210140004	SS	BED	.2290+03	.5000+02	.1000+00	1	QTZDOL	CCL	77P001
1210140004	SS	BED	.2290+03	.3900+02	.1000+00	1	QTZDOL	CCL	77P001
1210140004	SS	BED	.2280+03	.3000+02	.1000+00	1	QTZDOL	CCL	77P001
1210140005	SS	BED	.2910+03	.1400+02	.1000+00	0	QTZITE	CCL	77P001
1210140006	L1	FAX	.2310+03	.1400+02	.1000+00	0	DOLOM	CCL	77P001
1210140007	SF	FAULT	.4500+02	.6400+02	.1000+00	2	DOLOM	CCL	77P001
1210140007	SS	BED	.2360+03	.9000+02	.1000+00	1	DOLOM	CCL	77P001
1210140007	SS	BED	.2060+03	.2000+02	.1000+00	2	DOLOM	CCL	77P001
1210140007	SS	BED	.2050+03	.2300+02	.1000+00	2	DOLOM	CCL	77P001
1210140008	SS	BED	.2310+03	.3200+02	.1000+00	1	DOLOM	CCL	77P001
1210140008	SS	BED	.2400+03	.4900+02	.1000+00	2	QTZITE	CCL	77P001
1210140009	S1	MYF	.1010+03	.5800+02	.1000+00	0	MARBLE	CCL	77P001
1210140011	SS	BED	.1720+03	.4600+02	.1000+00	0	DOLOM	CCL	77P001
1210140012	SS	BED	.1420+03	.3100+02	.1000+00	0	DOLOM	CCL	77P001
1210140013	SS	BED	.2090+03	.3800+02	.1000+00	1	DOLOM	CCL	77P001
1210140013	S1	BCL	.1980+03	.4700+02	.1000+00	2	MARBLE	CCL	77P001
1210140014	SS	BED	.2440+03	.5900+02	.1000+00	0	DOLOM	CCL	77P001
1210140015	SS	BED	.8400+02	.6000+02	.1000+00	0	QTZPSH	CCL	77P001
1210140015	SS	BED	.1150+03	.5600+02	.1000+00	0	QTZPSH	CCL	77P001
1210140015	SS	BED	.1060+03	.5200+02	.1000+00	0	QTZPSH	CCL	77P001
1210140015	SS	BED	.8800+02	.8900+02	.1000+00	0	QTZPSH	CCL	77P001
1210140016	SS	BED	.1450+03	.5300+02	.1000+00	0	QTZPSH	CCL	77P001
1210140017	SS	BED	.1960+03	.2600+02	.1000+00	0	DOLOM	CCL	77P001
1210140018	SS	BED	.2270+03	.2000+02	.1000+00	0	QTZITE	CCL	77P001
1210140019	SS	BED	.2320+03	.1400+02	.1000+00	0	QTZDOL	CCL	77P001
1210140020	SS	BED	.2550+03	.6700+02	.1000+00	0	QTZDOL	CCL	77P001
1210140021	SS	BED	.2600+03	.9000+02	.1000+00	0	QTZITE	CCL	77P001
1210140022	SS	BED	.2530+03	.3400+02	.1000+00	0	QTZDOL	CCL	77P001
1210140022	SS	BED	.2590+03	.5300+02	.1000+00	0	QTZDOL	CCL	77P001
1210140023	SS	BED	.2520+03	.5200+02	.1000+00	0	QTZITE	CCL	77P001
1210140024	SS	BED	.2530+03	.3300+02	.1000+00	0	QTZITE	CCL	77P001
1210140025	SS	BED	.2280+03	.4500+02	.1000+00	0	QTZDOL	CCL	77P001
1210140026	SS	BED	.2970+03	.2500+02	.1000+00	0	DOLOM	CCL	77P001
1210140027	SS	BED	.2720+03	.4900+02	.1000+00	0	DOLOM	CCL	77P001
1210140028	L2	FAX	.2100+02	.3000+02	.1000+00	0	SLATE	CCL	77P001
1210140028	L3	CRL	.3270+03	.1700+02	.1000+00	0	SLATE	CCL	77P001
1210140028	S1	SLC	.2920+03	.3800+02	.1000+00	0	SLATE	CCL	77P001
1210140028	S2	FRC	.3510+03	.7000+02	.1000+00	0	SLATE	CCL	77P001
1210140029	L1B	ISL	.2620+03	.2000+01	.1000+00	0	SLATE	CCL	77P001
1210140029	SS	BED	.2610+03	.4600+02	.1000+00	0	SLATE	CCL	77P001
1210140029	S1	SLC	.2670+03	.6600+02	.1000+00	0	SLATE	CCL	77P001
1210140030	SS	BED	.2680+03	.1200+02	.1000+00	0	DOLOM	CCL	77P001
1210140031	SS	BED	.2700+03	.8200+02	.1000+00	0	DOLOM	CCL	77P001
1210140031	SS	BED	.2470+03	.5500+02	.1000+00	0	DOLOM	CCL	77P001
1210140031	SS	BED	.2120+03	.3000+02	.1000+00	0	DOLOM	CCL	77P001
1210140031	SS	BED	.1560+03	.4500+02	.1000+00	0	DOLOM	CCL	77P001
1210140032	SS	BED	.2400+03	.4900+02	.1000+00	0	DOLOM	CCL	77P001
1210140033	SS	BED	.2490+03	.4300+02	.1000+00	0	CQTZTE	CCL	77P001
1210140034	SS	BED	.2700+03	.4600+02	.1000+00	0	QTZITE	CCL	77P001
1210140035	SS	BED	.2620+03	.6100+02	.1000+00	0	QTZITE	CCL	77P001

LOCALE	FABELT	TYCODE	STR	DPL	SIZE	TAG	LITHCO	METHOD	REFER
1210140036	SS	BED	.2520+03	.8000+02	.1000+00	0	DOLOM	CCL	77P001
1210140037	L1	FAX	.2600+03	.1100+02	.1000+00	0	DOLOM	CCL	77P001
1210140037	S1	BCL	.8500+02	.8200+02	.1000+00	0	DOLOM	CCL	77P001
1210140037	S1	FAP	.2650+03	.9000+02	.1000+00	0	DOLOM	CCL	77P001
1210140038	SS	BED	.2530+03	.8200+02	.1000+00	0	QTZITE	CCL	77P001
1210140039	SS	BED	.7600+02	.8400+02	.1000+00	0	QTZPSH	CCL	77P001
1210140040	SS	BED	.2520+03	.8500+02	.1000+00	0	CQTZTE	CCL	77P001
1210140041	SS	BED	.2600+03	.6100+02	.1000+00	0	CQTZTE	CCL	77P001
1210140042	SS	BED	.2440+03	.6200+02	.1000+00	0	CQTZTE	CCL	77P001
1210140043	SS	BED	.2590+03	.7400+02	.1000+00	0	CQTZTE	CCL	77P001
1210140043	SS	BED	.2760+03	.7800+02	.1000+00	0	CQTZTE	CCL	77P001
1210140044	SS	BED	.2870+03	.8000+02	.1000+00	0	DOLOM	CCL	77P001
1210140045	SS	BED	.2750+03	.4300+02	.1000+00	0	CQTZTE	CCL	77P001
1210140046	S1	MYF	.2820+03	.3700+02	.1000+00	0	MARBLE	CCL	77P001
1210140047	SS	BED	.2070+03	.4000+02	.1000+00	0	DOLOM	CCL	77P001
1210140047	SS	BED	.1940+03	.2200+02	.1000+00	0	DOLOM	CCL	77P001
1210140047	SS	BED	.2160+03	.3300+02	.1000+00	0	DOLOM	CCL	77P001
1210140048	SS	BED	.2470+03	.3800+02	.1000+00	0	DOLOM	CCL	77P001
1210140049	SS	BED	.2720+03	.3800+02	.1000+00	0	DOLOM	CCL	77P001
1210140049	SS	BED	.2450+03	.2000+02	.1000+00	0	DOLOM	CCL	77P001
1210140049	SS	BED	.2790+03	.4300+02	.1000+00	0	DOLOM	CCL	77P001
1210140049	SS	BED	.2730+03	.5400+02	.1000+00	0	DOLOM	CCL	77P001
1210140050	SS	BED	.2700+03	.5700+02	.1000+00	0	QTZITE	CCL	77P001
1210140051	L1B	ISL	.5400+02	.3200+02	.1000+00	0	SLATE	GCS	77P001
1210140051	SS	BED	.2740+03	.4500+02	.1000+00	0	SLATE	CCL	77P001
1210140051	S1	SLC	.2630+03	.5300+02	.1000+00	0	SLATE	CCL	77P001
1210140052	SS	BED	.2520+03	.6300+02	.1000+00	0	QTZITE	CCL	77P001
1210140053	SS	BED	.2590+03	.6300+02	.1000+00	0	DOLOM	CCL	77P001
1210140054	SS	BED	.2550+03	.6200+02	.1000+00	0	QTZITE	CCL	77P001
1210140055	SS	BED	.2490+03	.1800+02	.1000+00	0	DOLOM	CCL	77P001
1210140056	SS	BED	.2430+03	.5800+02	.1000+00	0	QTZITE	CCL	77P001
1210140057	SS	BED	.2680+03	.6400+02	.1000+00	0	QTZPSH	CCL	77P001
1210140058	LS	RPM	.3210+03	.2500+02	.1000+00	0	QTZPSH	CCL	77P001
1210140058	SS	BED	.2670+03	.3300+02	.1000+00	0	QTZPSH	CCL	77P001
1210140059	L1B	ISL	.8000+01	.1600+02	.1000+00	1	MARBLE	CCL	77P001
1210140059	L1B	ISL	.7000+01	.1400+02	.1000+00	1	MARBLE	CCL	77P001
1210140059	L1B	ISL	.3550+03	.1400+02	.1000+00	1	MARBLE	CCL	77P001
1210140059	L1B	ISL	.3530+03	.1600+02	.1000+00	1	MARBLE	CCL	77P001
1210140059	L1B	ISL	.3460+03	.9000+01	.1000+00	1	MARBLE	CCL	77P001
1210140059	L1B	ISL	.2000+02	.1700+02	.1000+00	1	MARBLE	CCL	77P001
1210140059	SS	BED	.1760+03	.4600+02	.1000+00	2	DOLOM	CCL	77P001
1210140059	S1	MYF	.1530+03	.3500+02	.1000+00	1	MARBLE	CCL	77P001
1210140059	S1	MYF	.1630+03	.4000+02	.1000+00	1	MARBLE	CCL	77P001
1210140059	S1	MYF	.1620+03	.3700+02	.1000+00	1	MARBLE	CCL	77P001
1210140059	S1	MYF	.2190+03	.2900+02	.1000+00	1	MARBLE	CCL	77P001
1210140059	S1	MYF	.2180+03	.3200+02	.1000+00	1	MARBLE	CCL	77P001
1210140059	S1	MYF	.2160+03	.2800+02	.1000+00	1	MARBLE	CCL	77P001
1210140059	S1	MYF	.2080+03	.2700+02	.1000+00	1	MARBLE	CCL	77P001
1210140059	S1	MYF	.2070+03	.3500+02	.1000+00	1	MARBLE	CCL	77P001
1210140059	S1	MYF	.2000+03	.2500+02	.1000+00	1	MARBLE	CCL	77P001

LOCALE	FABELT	TYCODE	STR	DPL	SIZE	TAG	LITHCO	METHOD	REFER
1210140059	S1	MYF	.1940+03	.1700+02	.1000+00	1	MARBLE	CCL	77P001
1210140059	S1	MYF	.1790+03	.3500+02	.1000+00	1	MARBLE	CCL	77P001
1210140060	SS	BED	.2640+03	.4500+02	.1000+00	0	DOLOM	CCL	77P001
1210140060	SS	BED	.2620+03	.5500+02	.1000+00	0	DOLOM	CCL	77P001
1210140060	SS	BED	.2570+03	.3800+02	.1000+00	0	DOLOM	CCL	77P001
1210140060	SS	BED	.2560+03	.4000+02	.1000+00	0	DOLOM	CCL	77P001
1210140060	SS	BED	.2500+03	.4500+02	.1000+00	0	DOLOM	CCL	77P001
1210140060	SS	BED	.2440+03	.5400+02	.1000+00	0	DOLOM	CCL	77P001
1210140061	SS	BED	.2550+03	.7100+02	.1000+00	0	DOLOM	CCL	77P001
1210140061	SS	BED	.2470+03	.6200+02	.1000+00	0	DOLOM	CCL	77P001
1210140061	SS	BED	.3370+03	.7000+02	.1000+00	0	DOLOM	CCL	77P001
1210140061	SS	BED	.3360+03	.8300+02	.1000+00	0	DOLOM	CCL	77P001
1210140061	SS	BED	.3200+03	.7600+02	.1000+00	0	DOLOM	CCL	77P001
1210140061	SS	BED	.2900+03	.6600+02	.1000+00	0	DOLOM	CCL	77P001
1210140061	SS	BED	.2850+03	.5800+02	.1000+00	0	DOLOM	CCL	77P001
1210140061	SS	BED	.2780+03	.6700+02	.1000+00	0	DOLOM	CCL	77P001
1210140061	SS	BED	.2750+03	.5700+02	.1000+00	0	DOLOM	CCL	77P001
1210140061	SS	BED	.2620+03	.6800+02	.1000+00	0	DOLOM	CCL	77P001
1210140062	L1B	ISL	.3340+03	.4100+02	.1000+00	1	MARBLE	CCL	77P001
1210140062	L1B	ISL	.3330+03	.3600+02	.1000+00	1	MARBLE	CCL	77P001
1210140062	L1B	ISL	.3290+03	.4400+02	.1000+00	1	MARBLE	CCL	77P001
1210140062	L1B	ISL	.3240+03	.2800+02	.1000+00	1	MARBLE	CCL	77P001
1210140062	SS	BED	.2370+03	.5700+02	.1000+00	2	MARBLE	CCL	77P001
1210140062	SS	BED	.2180+03	.5100+02	.1000+00	2	MARBLE	CCL	77P001
1210140062	SS	BED	.2160+03	.6800+02	.1000+00	2	MARBLE	CCL	77P001
1210140062	SS	BED	.2020+03	.4500+02	.1000+00	2	MARBLE	CCL	77P001
1210140062	S1	MYF	.2180+03	.3200+02	.1000+00	1	MARBLE	CCL	77P001
1210140062	S1	MYF	.2110+03	.4900+02	.1000+00	1	MARBLE	CCL	77P001
1210140062	S1	MYF	.2100+03	.4600+02	.1000+00	1	MARBLE	CCL	77P001
1210140062	S1	MYF	.2070+03	.4400+02	.1000+00	1	MARBLE	CCL	77P001
1210140063	SS	BED	.2180+03	.5300+02	.1000+00	2	QTZPSH	CCL	77P001
1210140063	SS	BED	.2140+03	.4100+02	.1000+00	1	QTZPSH	CCL	77P001
1210140063	SS	BED	.2080+03	.4000+02	.1000+00	2	QTZPSH	CCL	77P001
1210140063	SS	BED	.1840+03	.1600+02	.1000+00	2	QTZPSH	CCL	77P001
1210140063	SS	BED	.2220+03	.5200+02	.1000+00	1	QTZPSH	CCL	77P001
1210140063	SS	BED	.2190+03	.5600+02	.1000+00	1	QTZPSH	CCL	77P001
1210140063	SS	BED	.2190+03	.4800+02	.1000+00	1	QTZPSH	CCL	77P001
1210140064	SS	BED	.1930+03	.4600+02	.1000+00	0	DOLOM	CCL	77P001
1210140064	SS	BED	.2240+03	.2800+02	.1000+00	0	DOLOM	CCL	77P001
1210140064	SS	BED	.2100+03	.4600+02	.1000+00	0	DOLOM	CCL	77P001
1210140064	SS	BED	.1990+03	.3600+02	.1000+00	0	DOLOM	CCL	77P001
1210140065	SS	BED	.2170+03	.6200+02	.1000+00	0	DOLOM	CCL	77P001
1210140065	SS	BED	.2270+03	.6500+02	.1000+00	0	DOLOM	CCL	77P001
1210140065	SS	BED	.2260+03	.5800+02	.1000+00	0	DOLOM	CCL	77P001
1210140065	SS	BED	.2210+03	.6600+02	.1000+00	0	DOLOM	CCL	77P001
1210140066	L2	ISL	.2380+03	.3600+02	.1000+00	0	MARBLE	CCL	77P001
1210140066	S1	MYF	.1490+03	.4200+02	.1000+00	0	MARBLE	CCL	77P001
1210140066	S1	MYF	.1300+03	.3000+02	.1000+00	0	MARBLE	CCL	77P001
1210140066	S1	MYF	.1130+03	.4000+02	.1000+00	0	MARBLE	CCL	77P001
1210140066	S1	MYF	.8900+02	.2800+02	.1000+00	0	MARBLE	CCL	77P001

LOCALE	FABELT	TYCODE	STR	DPL	SIZE	TAG	LITHCO	METHOD	REFER
1210140066	S1	MYF	.1780+03	.2600+02	.1000+00	0	MARBLE	CCL	77P001
1210140066	S1	MYF	.1700+03	.3300+02	.1000+00	0	MARBLE	CCL	77P001
1210140066	S2	FRC	.6300+02	.8400+02	.1000+00	0	MARBLE	CCL	77P001
1210140067	SS	BED	.2290+03	.6300+02	.1000+00	0	DOLOM	CCL	77P001
1210140067	SS	BED	.2400+03	.5200+02	.1000+00	0	DOLOM	CCL	77P001
1210140067	SS	BED	.2380+03	.4800+02	.1000+00	0	DOLOM	CCL	77P001
1210140067	SS	BED	.2350+03	.5800+02	.1000+00	0	DOLOM	CCL	77P001
1210140068	SS	BED	.2290+03	.6000+02	.1000+00	0	DOLOM	CCL	77P001
1210140068	SS	BED	.2470+03	.5100+02	.1000+00	0	DOLOM	CCL	77P001
1210140068	SS	BED	.2330+03	.5600+02	.1000+00	0	DOLOM	CCL	77P001
1210140068	SS	BED	.2310+03	.5200+02	.1000+00	0	DOLOM	CCL	77P001
1210140069	SS	BED	.2070+03	.5500+02	.1000+00	0	DOLOM	CCL	77P001
1210140070	SS	BED	.4800+02	.5800+02	.1000+00	0	DOLOM	CCL	77P001
1210140070	SS	BED	.2900+02	.7500+02	.1000+00	0	DOLOM	CCL	77P001
1210140070	SS	BED	.1200+02	.6700+02	.1000+00	0	DOLOM	CCL	77P001
1210140070	SS	BED	.1000+02	.6200+02	.1000+00	0	DOLOM	CCL	77P001
1210140071	SS	BED	.1570+03	.4600+02	.1000+00	0	DOLSH	CCL	77P001
1210140071	SS	BED	.1560+03	.6000+02	.1000+00	0	DOLSH	CCL	77P001
1210140071	SS	BED	.1550+03	.4700+02	.1000+00	0	DOLSH	CCL	77P001
1210140071	SS	BED	.1540+03	.5800+02	.1000+00	0	DOLSH	CCL	77P001
1210140072	SS	BED	.1490+03	.1900+02	.1000+00	0	QTZPSH	CCL	77P001
1210140073	S1	MYF	.1020+03	.3200+02	.1000+00	0	MARBLE	CCL	77P001
1210140073	S1	MYF	.1210+03	.3900+02	.1000+00	0	MARBLE	CCL	77P001
1210140073	S1	MYF	.1100+03	.2400+02	.1000+00	0	MARBLE	CCL	77P001
1210140073	S1	MYF	.1260+03	.2300+02	.1000+00	0	MARBLE	CCL	77P001
1210140074	SS	BED	.1970+03	.5900+02	.1000+00	0	DOLOM	CCL	77P001
1210140074	SS	BED	.2020+03	.5600+02	.1000+00	0	DOLOM	CCL	77P001
1210140074	SS	BED	.2000+03	.6600+02	.1000+00	0	DOLOM	CCL	77P001
1210140074	SS	BED	.2150+03	.6800+02	.1000+00	0	DOLOM	CCL	77P001
1210140075	SS	BED	.9000+02	.2900+02	.1000+00	0	DOLOM	CCL	77P001
1210140076	SS	BED	.2470+03	.3700+02	.1000+00	0	DOLOM	CCL	77P001
1210140076	SS	BED	.2440+03	.3400+02	.1000+00	0	DOLOM	CCL	77P001
1210140076	SS	BED	.2500+03	.3800+02	.1000+00	0	DOLOM	CCL	77P001
1210140076	SS	BED	.2490+03	.3400+02	.1000+00	0	DOLOM	CCL	77P001
1210140077	SS	BED	.2180+03	.2900+02	.1000+00	0	QTZPSH	CCL	77P001
1210140077	SS	BED	.2040+03	.1800+02	.1000+00	0	QTZPSH	CCL	77P001
1210140077	SS	BED	.2480+03	.2700+02	.1000+00	0	QTZPSH	CCL	77P001
1210140077	SS	BED	.2420+03	.3300+02	.1000+00	0	QTZPSH	CCL	77P001
1210140077	SS	BED	.2340+03	.3000+02	.1000+00	0	QTZPSH	CCL	77P001
1210140077	SS	BED	.2240+03	.3100+02	.1000+00	0	QTZPSH	CCL	77P001
1210140077	SS	BED	.2770+03	.6000+02	.1000+00	0	QTZPSH	CCL	77P001
1210140077	SS	BED	.2700+03	.8000+02	.1000+00	0	QTZPSH	CCL	77P001
1210140078	L1	FAX	.2810+03	.2000+02	.1000+00	0	QTZPSH	CCL	77P001
1210140078	SS	BED	.2500+03	.3300+02	.1000+00	0	QTZPSH	CCL	77P001
1210140078	SS	BED	.2690+03	.3400+02	.1000+00	0	QTZPSH	CCL	77P001
1210140078	SS	BED	.2570+03	.3200+02	.1000+00	0	QTZPSH	CCL	77P001
1210140078	SS	BED	.2520+03	.2400+02	.1000+00	0	QTZPSH	CCL	77P001
1210140079	SF	JNT	.3600+02	.5700+02	.1000+00	0	DOLOM	CCL	77P001
1210140079	SF	JNT	.8900+02	.5000+02	.1000+00	0	DOLOM	CCL	77P001
1210140079	SS	BED	.2520+03	.4500+02	.1000+00	0	DOLOM	CCL	77P001

LOCALE	FABELT	TYCODE	STR	DPL	SIZE	TAG	LITHCO	METHOD	REFER
1210140079	SS	BED	.2590+03	.4100+02	.1000+00	0	DOLOM	CCL	77P001
1210140079	SS	BED	.2580+03	.3800+02	.1000+00	0	DOLOM	CCL	77P001
1210140079	SS	BED	.2600+03	.4300+02	.1000+00	0	DOLOM	CCL	77P001
1210140080	SS	BED	.2410+03	.4600+02	.1000+00	0	DOLOM	CCL	77P001
1210140080	SS	BED	.2480+03	.5000+02	.1000+00	0	DOLOM	CCL	77P001
1210140080	SS	BED	.2440+03	.6000+02	.1000+00	0	DOLOM	CCL	77P001
1210140080	SS	BED	.2700+03	.4900+02	.1000+00	0	DOLOM	CCL	77P001
1210140081	SS	BED	.2340+03	.8300+02	.1000+00	2	DOLOM	CCL	77P001
1210140081	SS	BED	.2430+03	.5000+02	.1000+00	1	DOLOM	CCL	77P001
1210140081	SS	BED	.2420+03	.7200+02	.1000+00	2	DOLOM	CCL	77P001
1210140081	SS	BED	.2540+03	.7400+02	.1000+00	2	DOLOM	CCL	77P001
1210140081	SS	BED	.2530+03	.4400+02	.1000+00	1	DOLOM	CCL	77P001
1210140081	SS	BED	.2520+03	.5300+02	.1000+00	1	DOLOM	CCL	77P001
1210140081	SS	BED	.2450+03	.4300+02	.1000+00	1	DOLOM	CCL	77P001
1210140082	SS	BED	.2600+03	.6400+02	.1000+00	0	DOLOM	CCL	77P001
1210140082	SS	BED	.2590+03	.7200+02	.1000+00	0	DOLOM	CCL	77P001
1210140082	SS	BED	.2570+03	.6900+02	.1000+00	0	DOLOM	CCL	77P001
1210140082	SS	BED	.2560+03	.6700+02	.1000+00	0	DOLOM	CCL	77P001
1210140082	SS	BED	.2550+03	.7800+02	.1000+00	0	DOLOM	CCL	77P001
1210140082	SS	BED	.2520+03	.6300+02	.1000+00	0	DOLOM	CCL	77P001
1210140083	L1B	BDA	.2570+03	.1800+02	.1000+00	0	MARBLE	CCL	77P001
1210140083	L1X	MEL	.3390+03	.1900+02	.1000+00	0	MARBLE	CCL	77P001
1210140083	L1X	MEL	.3590+03	.2000+02	.1000+00	0	MARBLE	CCL	77P001
1210140083	L1X	MEL	.3500+03	.2200+02	.1000+00	0	MARBLE	CCL	77P001
1210140083	S1	MYF	.2300+03	.2900+02	.1000+00	0	MARBLE	CCL	77P001
1210140083	S1	MYF	.2260+03	.1900+02	.1000+00	0	MARBLE	CCL	77P001
1210140083	S1	MYF	.2350+03	.2600+02	.1000+00	0	MARBLE	CCL	77P001
1210140083	S1	MYF	.2330+03	.2400+02	.1000+00	0	MARBLE	CCL	77P001
1210140084	L1X	MEL	.3550+03	.1600+02	.1000+00	0	MARBLE	CCL	77P001
1210140084	L1X	MEL	.3470+03	.1500+02	.1000+00	0	MARBLE	CCL	77P001
1210140084	S1	MYF	.2600+03	.1500+02	.1000+00	0	MARBLE	CCL	77P001
1210140084	S1	MYF	.2220+03	.2000+02	.1000+00	0	MARBLE	CCL	77P001
1210140085	SS	BED	.3130+03	.6200+02	.1000+00	0	DOLOM	CCL	77P001
1210140086	S1	MYF	.2090+03	.3700+02	.1000+00	0	MARBLE	CCL	77P001
1210140087	L1X	MEL	.3080+03	.3700+02	.1000+00	2	MARBLE	CCL	77P001
1210140087	SS	BED	.2250+03	.5000+02	.1000+00	1	DOLOM	CCL	77P001
1210140088	L1B	ISL	.3360+03	.1200+02	.1000+00	0	MARBLE	CCL	77P001
1210140088	S1	MYF	.1880+03	.3400+02	.1000+00	0	MARBLE	CCL	77P001
1210140089	SS	BED	.2700+03	.2000+02	.1000+00	0	DOLOM	CCL	77P001
1210140090	SS	BED	.1170+03	.4500+02	.1000+00	0	QTZITE	CCL	77P001
1210140091	SS	BED	.2800+02	.4600+02	.1000+00	0	DOLOM	CCL	77P001
1210140091	SS	BED	.2700+02	.5700+02	.1000+00	0	DOLOM	CCL	77P001
1210140091	SS	BED	.6000+02	.5100+02	.1000+00	0	DOLOM	CCL	77P001
1210140091	SS	BED	.5300+02	.4800+02	.1000+00	0	DOLOM	CCL	77P001
1210140091	SS	BED	.3600+02	.3000+02	.1000+00	0	DOLOM	CCL	77P001
1210150001	SS	BED	.3070+03	.7700+02	.1000+00	0	DOLOM	CCL	77P001
1210150001	SS	BED	.3480+03	.7800+02	.1000+00	0	DOLOM	CCL	77P001
1210150002	SS	BED	.3180+03	.7600+02	.1000+00	0	DOLOM	CCL	77P001
1210150003	SS	BED	.2700+02	.4900+02	.1000+00	0	DOLOM	CCL	77P001
1210150004	S1	MYF	.1710+03	.7200+02	.1000+00	0	MARBLE	CCL	77P001

LOCALE	FABELT	TYCODE	STR	DPL	SIZE	TAG	LITHCO	METHOD	REFER
1210150004	S1	MYF	.1790+03	.3500+02	.1000+00	0	MARBLE	CCL	77P001
1210150005	L2	FAX	.1670+03	.4000+01	.1000+00	1	BLSMAR	CCL	77P001
1210150005	SS	BED	.2600+02	.4000+01	.1000+00	1	BLSMAR	CCL	77P001
1210150005	S1	MYF	.2600+02	.2100+02	.1000+00	2	BLSMAR	CCL	77P001
1210150005	S1	MYF	.3560+03	.8100+02	.1000+00	2	BLSMAR	CCL	77P001
1210150005	S1	MYF	.3070+03	.5600+02	.1000+00	2	BLSMAR	CCL	77P001
1210150005	S1	MYF	.2840+03	.7300+02	.1000+00	2	BLSMAR	CCL	77P001
1210150005	S1	MYF	.2230+03	.8800+02	.1000+00	1	BLSMAR	CCL	77P001
1210150005	S1	MYF	.6600+02	.2200+02	.1000+00	2	BLSMAR	CCL	77P001
1210150006	S1	MYF	.2390+03	.7000+02	.1000+00	0	MARBLE	CCL	77P001
1210150006	S1	MYF	.2480+03	.6200+02	.1000+00	0	MARBLE	CCL	77P001
1210150007	SS	BED	.2150+03	.2900+02	.1000+00	0	QTZITE	CCL	77P001
1210150008	SS	BED	.2480+03	.1900+02	.1000+00	0	BLSTN	CCL	77P001
1210150009	L1X	MEL	.3490+03	.1800+02	.1000+00	0	MARBLE	CCL	77P001
1210150009	S1	MYF	.2050+03	.2600+02	.1000+00	0	MARBLE	CCL	77P001
1210150010	L1	FAX	.3150+03	.2300+02	.1000+00	1	MARBLE	CCL	77P001
1210150010	L1	FAX	.3220+03	.2200+02	.1000+00	2	MARBLE	CCL	77P001
1210150010	S1	BCL	.1890+03	.2800+02	.1000+00	3	MARBLE	CCL	77P001
1210150010	S1	FAP	.2020+03	.3100+02	.1000+00	1	MARBLE	CCL	77P001
1210150010	S1	FAP	.1960+03	.3000+02	.1000+00	2	MARBLE	CCL	77P001
1210150011	SS	BED	.2000+03	.4900+02	.1000+00	0	DOLOM	CCL	77P001
1210150011	S1	BCL	.1810+03	.1800+02	.1000+00	0	DOLOM	CCL	77P001
1210150011	S1	MYF	.1050+03	.4300+02	.1000+00	0	MARBLE	CCL	77P001
1210150011	S1	MYF	.1020+03	.2900+02	.1000+00	0	MARBLE	CCL	77P001
1210150011	S1	MYF	.9800+02	.1400+02	.1000+00	0	MARBLE	CCL	77P001
1210150011	S1	MYF	.6400+02	.7600+02	.1000+00	0	MARBLE	CCL	77P001
1210150011	S1	MYF	.3560+03	.1800+02	.1000+00	0	MARBLE	CCL	77P001
1210150011	S1	MYF	.2590+03	.6200+02	.1000+00	0	MARBLE	CCL	77P001
1210150011	S1	MYF	.2570+03	.7500+02	.1000+00	0	MARBLE	CCL	77P001
1210150011	S1	MYF	.2540+03	.3500+02	.1000+00	0	MARBLE	CCL	77P001
1210150011	S1	MYF	.2440+03	.6900+02	.1000+00	0	MARBLE	CCL	77P001
1210150011	S1	MYF	.2380+03	.6900+02	.1000+00	0	MARBLE	CCL	77P001
1210150012	SS	BED	.1910+03	.4600+02	.1000+00	0	DOLOM	CCL	77P001
1210150012	SS	BED	.1860+03	.2300+02	.1000+00	0	DOLOM	CCL	77P001
1210150013	L1	FAX	.2510+03	.1700+02	.1000+00	0	QTZPSH	CCL	77P001
1210150013	L1	FAX	.2580+03	.1800+02	.1000+00	0	QTZPSH	CCL	77P001
1210150013	SS	BED	.2270+03	.3600+02	.1000+00	0	QTZPSH	CCL	77P001
1210150013	SS	BED	.2330+03	.5400+02	.1000+00	0	QTZPSH	CCL	77P001
1210150013	SS	BED	.2480+03	.3800+02	.1000+00	0	QTZPSH	CCL	77P001
1210150013	S1	FAP	.2120+03	.2600+02	.1000+00	0	QTZPSH	GCS	77P001
1210150014	L1	FAX	.2600+03	.2600+02	.1000+00	0	QTZPSH	CCL	77P001
1210150014	SS	BED	.6600+02	.4200+02	.1000+00	0	QTZPSH	CCL	77P001
1210150014	SS	BED	.2290+03	.8200+02	.1000+00	0	QTZPSH	CCL	77P001
1210150014	SS	BED	.1750+03	.3200+02	.1000+00	0	QTZPSH	CCL	77P001
1210150014	SS	BED	.1540+03	.2800+02	.1000+00	0	QTZPSH	CCL	77P001
1210150014	SS	BED	.1530+03	.3600+02	.1000+00	0	QTZPSH	CCL	77P001
1210150014	SS	BED	.1490+03	.3100+02	.1000+00	0	QTZPSH	CCL	77P001
1210150014	SS	BED	.1360+03	.2300+02	.1000+00	0	QTZPSH	CCL	77P001
1210150014	SS	BED	.8800+02	.6200+02	.1000+00	0	QTZPSH	CCL	77P001
1210150014	SS	BED	.8200+02	.7500+02	.1000+00	0	QTZPSH	CCL	77P001

LOCALE	FABELT	TYCODE	STR	DPL	SIZE	TAG	LITHCO	METHOD	REFER
1210150014	SS	BED	.2460+03	.6900+02	.1000+00	0	QTZPSH	CCL	77P001
1210150015	SS	BED	.2190+03	.1900+02	.1000+00	0	DOLOM	CCL	77P001
1210150015	SS	BED	.2340+03	.2800+02	.1000+00	0	DOLOM	CCL	77P001
1210150016	SS	BED	.2150+03	.8200+02	.1000+00	0	BLSTN	CCL	77P001
1210150016	S1	BCL	.2070+03	.8400+02	.1000+00	0	BLSTN	CCL	77P001
1210150016	S1	BCL	.2000+03	.6200+02	.1000+00	0	BLSTN	CCL	77P001
1210150017	L1B	ISL	.2250+03	.3500+02	.1000+00	0	PELITE	CCL	77P001
1210150017	SS	BED	.1270+03	.2600+02	.1000+00	0	QTZITE	CCL	77P001
1210150018	SS	BED	.2170+03	.7000+02	.1000+00	0	QTZITE	CCL	77P001
1210150020	SS	BED	.2110+03	.5100+02	.1000+00	0	CONGLQ	CCL	77P001
1210150021	L1X	MEL	.3170+03	.4200+02	.1000+00	0	BLSTN	CCL	77P001
1210150021	L1X	MEL	.3060+03	.3300+02	.1000+00	0	BLSTN	CCL	77P001
1210150021	S1	CLE	.2160+03	.4200+02	.1000+00	0	BLSTN	CCL	77P001
1210150021	S1	CLE	.2120+03	.3400+02	.1000+00	0	BLSTN	CCL	77P001
1210150021	S1	CLE	.2110+03	.4300+02	.1000+00	0	BLSTN	CCL	77P001
1210150022	S1	MYF	.1790+03	.4400+02	.1000+00	0	MARBLE	CCL	77P001
1210150022	S1	MYF	.1990+03	.3800+02	.1000+00	0	MARBLE	CCL	77P001
1210150023	L2	CRL	.2990+03	.4200+02	.1000+00	0	MARBLE	CCL	77P001
1210150023	S1	MYF	.2090+03	.5700+02	.1000+00	0	MARBLE	CCL	77P001
1210150023	S1	MYF	.2050+03	.5000+02	.1000+00	0	MARBLE	CCL	77P001
1210150023	S1	MYF	.2140+03	.5300+02	.1000+00	0	MARBLE	CCL	77P001
1210150024	L1	FAX	.1520+03	.1600+02	.1000+00	2	DOLOM	CCL	77P001
1210150024	SS	BED	.1400+02	.5400+02	.1000+00	1	DOLOM	CCL	77P001
1210150024	SS	BED	.1000+02	.5700+02	.1000+00	1	DOLOM	CCL	77P001
1210150024	SS	BED	.3550+03	.4300+02	.1000+00	1	DOLOM	CCL	77P001
1210150024	SS	BED	.3410+03	.4900+02	.1000+00	2	DOLOM	CCL	77P001
1210150024	SS	BED	.3340+03	.5700+02	.1000+00	1	DOLOM	CCL	77P001
1210150024	SS	BED	.3310+03	.4600+02	.1000+00	1	DOLOM	CCL	77P001
1210150024	SS	BED	.1700+02	.3000+02	.1000+00	2	DOLOM	CCL	77P001
1210150024	S1	MYF	.2290+03	.7600+02	.1000+00	3	MARBLE	CCL	77P001
1210150024	S1	MYF	.2300+03	.7900+02	.1000+00	3	MARBLE	CCL	77P001
1210150024	S1	MYF	.2300+03	.7600+02	.1000+00	3	MARBLE	CCL	77P001
1210150024	S1	MYF	.2320+03	.8100+02	.1000+00	3	MARBLE	CCL	77P001
1210150025	SS	BED	.2280+03	.5100+02	.1000+00	0	QTZDOL	CCL	77P001
1210150026	SS	BED	.1540+03	.5300+02	.1000+00	0	QTZDOL	CCL	77P001
1210150026	SS	BED	.2470+03	.9000+02	.1000+00	0	QTZDOL	CCL	77P001
1210150027	SS	BED	.2340+03	.4100+02	.1000+00	0	QTZPSH	CCL	77P001
1210150028	SS	BED	.9900+02	.5900+02	.1000+00	0	QTZPSH	CCL	77P001
1210150029	SS	BED	.2400+03	.5800+02	.1000+00	0	QTZPSH	CCL	77P001
1210150030	L1B	ISL	.2600+02	.9000+01	.1000+00	0	PSH	CCL	77P001
1210150030	SS	BED	.1500+02	.2800+02	.1000+00	0	PSH	CCL	77P001
1210150031	SS	BED	.2650+03	.6000+02	.1000+00	0	DOLOM	CCL	77P001
1210150032	SS	BED	.4700+02	.5200+02	.1000+00	0	DOLOM	CCL	77P001
1210150033	L1	FAX	.2120+03	.2200+02	.1000+00	0	MARBLE	CCL	77P001
1210150033	L1X	MEL	.2050+03	.2100+02	.1000+00	0	MARBLE	CCL	77P001
1210150033	L1X	MEL	.2050+03	.9000+01	.1000+00	0	MARBLE	CCL	77P001
1210150033	L1X	MEL	.2040+03	.1800+02	.1000+00	0	MARBLE	CCL	77P001
1210150033	S1	MYF	.4600+02	.3500+02	.1000+00	0	MARBLE	CCL	77P001
1210150033	S1	MYF	.9400+02	.1800+02	.1000+00	0	MARBLE	CCL	77P001
1210150033	S1	MYF	.7300+02	.2600+02	.1000+00	0	MARBLE	CCL	77P001

LOCALE	FABELT	TYCODE	STR	DPL	SIZE	TAG	LITHCO	METHOD	REFER
1210150033	S1	MYF	.6300+02	.2900+02	.1000+00	0	MARBLE	CCL	77P001
1210150034	SS	BED	.2180+03	.3700+02	.1000+00	0	BLSTN	CCL	77P001
1210150034	SS	BED	.2330+03	.3900+02	.1000+00	0	BLSTN	CCL	77P001
1210150034	SS	BED	.2260+03	.3000+02	.1000+00	0	BLSTN	CCL	77P001
1210150034	SS	BED	.2190+03	.3300+02	.1000+00	0	BLSTN	CCL	77P001
1210150035	SS	BED	.2480+03	.4100+02	.1000+00	0	BLSTN	CCL	77P001
1210150036	S1	BCL	.2710+03	.9000+02	.1000+00	0	BLSTN	CCL	77P001
1210150037	SS	BED	.2520+03	.5400+02	.1000+00	0	DOLOM	CCL	77P001
1210150038	SS	BED	.2470+03	.4900+02	.1000+00	0	DOLOM	CCL	77P001
1210150039	SS	BED	.1820+03	.5100+02	.1000+00	0	DOLOM	CCL	77P001
1210150040	SS	BED	.2580+03	.3700+02	.1000+00	3	QTZITE	CCL	77P001
1210150040	SS	BED	.2460+03	.4900+02	.1000+00	1	DOLBLS	CCL	77P001
1210150040	SS	BED	.2420+03	.4500+02	.1000+00	2	PELITE	CCL	77P001
1210150041	SS	BED	.2750+03	.3800+02	.1000+00	0	QTZITE	CCL	77P001
1210150042	SS	BED	.2400+03	.4900+02	.1000+00	2	BLSTN	CCL	77P001
1210150042	SS	BED	.2370+03	.4600+02	.1000+00	3	PELITE	CCL	77P001
1210150042	SS	BED	.2250+03	.5000+02	.1000+00	1	DOLOM	CCL	77P001
1210150043	SS	BED	.5000+02	.6400+02	.1000+00	2	BLSTN	CCL	77P001
1210150043	SS	BED	.2470+03	.4200+02	.1000+00	1	QTZITE	CCL	77P001
1210150044	L1	FAX	.2590+03	.1000+02	.1000+00	2	PELITE	CCL	77P001
1210150044	SS	BED	.2430+03	.2500+02	.1000+00	2	PELITE	CCL	77P001
1210150044	SS	BED	.2420+03	.1900+02	.1000+00	1	QTZITE	CCL	77P001
1210150045	SS	BED	.7000+02	.3800+02	.1000+00	0	BLSTN	CCL	77P001
1210150046	S1	MYF	.2590+03	.6400+02	.1000+00	0	MARBLE	CCL	77P001
1210150047	L1	FAX	.4100+02	.3500+02	.1000+00	0	MARBLE	CCL	77P001
1210150047	L1X	MEL	.1200+02	.4900+02	.1000+00	0	MARBLE	CCL	77P001
1210150047	L1X	MEL	.3440+03	.4900+02	.1000+00	0	MARBLE	CCL	77P001
1210150047	S1	MYF	.2420+03	.5000+02	.1000+00	0	MARBLE	CCL	77P001
1210150047	S1	MYF	.2520+03	.5000+02	.1000+00	0	MARBLE	CCL	77P001
1210150048	S1	MYF	.2520+03	.5700+02	.1000+00	0	MARBLE	CCL	77P001
1210150049	L1	FAX	.2400+02	.2100+02	.1000+00	0	MARBLE	CCL	77P001
1210150049	S1	MYF	.2420+03	.4200+02	.1000+00	0	MARBLE	CCL	77P001
1210150050	L1	FAX	.4500+02	.2000+02	.1000+00	0	MARBLE	CCL	77P001
1210150050	S1	MYF	.2360+03	.4300+02	.1000+00	0	MARBLE	CCL	77P001
1210150051	S1	MYF	.2110+03	.4700+02	.1000+00	0	MARBLE	CCL	77P001
1210150052	L1X	MEL	.2660+03	.2300+02	.1000+00	0	SLATE	GCS	77P001
1210150052	S1	SLC	.2530+03	.6200+02	.1000+00	0	SLATE	CCL	77P001
1210150053	L1	FAX	.2900+02	.2800+02	.1000+00	0	MARBLE	CCL	77P001
1210150053	S1	FAP	.2130+03	.5300+02	.1000+00	0	MARBLE	CCL	77P001
1210150054	L1X	MEL	.3460+03	.4000+02	.1000+00	0	MARBLE	CCL	77P001
1210150054	S1	MYF	.2430+03	.4000+02	.1000+00	0	MARBLE	CCL	77P001
1210150055	L1B	ISL	.2390+03	.4000+01	.1000+00	0	SLATE	GCS	77P001
1210150055	SS	BED	.2280+03	.2400+02	.1000+00	0	SLATE	GCS	77P001
1210150055	S1	SLC	.2370+03	.6900+02	.1000+00	0	SLATE	CCL	77P001
1210150056	SS	BED	.2530+03	.4100+02	.1000+00	0	DOLOM	CCL	77P001
1210150056	SS	BED	.2500+03	.4500+02	.1000+00	0	DOLOM	CCL	77P001
1210150056	SS	BED	.2540+03	.3200+02	.1000+00	0	DOLOM	CCL	77P001
1210150057	SS	BED	.2360+03	.4300+02	.1000+00	0	DOLOM	CCL	77P001
1210150058	SS	BED	.2400+03	.4200+02	.1000+00	0	DOLOM	CCL	77P001
1210150059	SS	BED	.2220+03	.5800+02	.1000+00	0	DOLOM	CCL	77P001

LOCALE	FABELT	TYCODE	STR	DPL	SIZE	TAG	LITHCO	METHOD	REFER
1210150060	SS	BED	.2130+03	.4300+02	.1000+00	0	CQTZTE	CCL	77P001
1210150061	SS	BED	.1890+03	.1500+02	.1000+00	0	DOLOM	CCL	77P001
1210150062	SS	BED	.1680+03	.3300+02	.1000+00	0	DOLOM	CCL	77P001
1210150063	LS	XBISL	.1950+03	.3100+02	.1000+00	0	CQTZTE	GCS	77P001
1210150063	L1	FAX	.2490+03	.6000+01	.1000+00	0	CQTZTE	CCL	77P001
1210150063	SS	BED	.4000+02	.5600+02	.1000+00	0	CQTZTE	CCL	77P001
1210150063	SS	BED	.5400+02	.4500+02	.1000+00	0	CQTZTE	CCL	77P001
1210150064	SS	BED	.2100+03	.3600+02	.1000+00	0	CQTZTE	CCL	77P001
1210150065	S1	MYF	.2640+03	.6200+02	.1000+00	0	MARBLE	CCL	77P001
1210150066	S1	MYF	.2470+03	.4700+02	.1000+00	0	MARBLE	CCL	77P001
1210150067	S1	MYF	.2400+03	.6500+02	.1000+00	0	MARBLE	CCL	77P001
1210150068	S1	MYF	.2630+03	.4300+02	.1000+00	0	MARBLE	CCL	77P001
1210150069	L1	FAX	.2530+03	.1500+02	.1000+00	0	MARBLE	CCL	77P001
1210150069	SF	JNT	.1590+03	.8900+02	.1000+00	0	MARBLE	CCL	77P001
1210150069	S1	MYF	.2030+03	.2300+02	.1000+00	0	MARBLE	CCL	77P001
1210150070	L1X	MEL	.1710+03	.1100+02	.1000+00	0	MARBLE	CCL	77P001
1210150070	S1	MYF	.1630+03	.1900+02	.1000+00	0	MARBLE	CCL	77P001
1210150070	S1	MYF	.1300+03	.2000+02	.1000+00	0	MARBLE	CCL	77P001
1210150070	S1	MYF	.1260+03	.2300+02	.1000+00	0	MARBLE	CCL	77P001
1210150070	S1	MYF	.1220+03	.1600+02	.1000+00	0	MARBLE	CCL	77P001
1210150071	SS	BED	.2580+03	.3800+02	.1000+00	0	DOLOM	CCL	77P001
1210150072	SS	BED	.2340+03	.6600+02	.1000+00	0	DOLOM	CCL	77P001
1210150073	SS	BED	.2270+03	.4000+02	.1000+00	0	DOLOM	CCL	77P001
1210150074	SS	BED	.2430+03	.7700+02	.1000+00	0	DOLOM	CCL	77P001
1210150075	S1	MYF	.2080+03	.3200+02	.1000+00	0	MARBLE	CCL	77P001
1210150076	L1	FAX	.1000+01	.1800+02	.1000+00	0	MARBLE	CCL	77P001
1210150076	L1B	BDA	.2670+03	.2800+02	.1000+00	0	MARBLE	CCL	77P001
1210150076	S1	MYF	.2150+03	.3200+02	.1000+00	0	MARBLE	CCL	77P001
1210150077	SS	BED	.2480+03	.2600+02	.1000+00	0	QTZPSH	CCL	77P001
1210150078	SS	BED	.1940+03	.3800+02	.1000+00	0	DOLOM	CCL	77P001
1210150078	SS	BED	.2230+03	.3700+02	.1000+00	0	DOLOM	CCL	77P001
1210150078	SS	BED	.2210+03	.3200+02	.1000+00	0	DOLOM	CCL	77P001
1210150078	SS	BED	.2230+03	.4200+02	.1000+00	0	DOLOM	CCL	77P001
1210150079	L1	FAX	.2180+03	.1900+02	.1000+00	0	DOLOM	CCL	77P001
1210150079	SS	BED	.5000+02	.2100+02	.1000+00	0	DOLOM	CCL	77P001
1210150079	SS	BED	.3800+02	.9000+02	.1000+00	0	DOLOM	CCL	77P001
1210150079	SS	BED	.2070+03	.3900+02	.1000+00	0	DOLOM	CCL	77P001
1210150079	SS	BED	.1970+03	.3100+02	.1000+00	0	DOLOM	CCL	77P001
1210150079	SS	BED	.1920+03	.3800+02	.1000+00	0	DOLOM	CCL	77P001
1210150079	SS	BED	.1580+03	.1900+02	.1000+00	0	DOLOM	CCL	77P001
1210150079	SS	BED	.1260+03	.1900+02	.1000+00	0	DOLOM	CCL	77P001
1210150080	SS	BED	.2220+03	.3600+02	.1000+00	0	DOLOM	CCL	77P001
1210150081	L1	FAX	.3180+03	.1900+02	.1000+00	0	QTZPSH	CCL	77P001
1210150081	SS	BED	.1820+03	.2900+02	.1000+00	0	QTZPSH	CCL	77P001
1210150081	S1	FAP	.2240+03	.2700+02	.1000+00	0	QTZPSH	CCL	77P001
1210150082	SS	BED	.2300+03	.3500+02	.1000+00	0	DOLOM	CCL	77P001
1210150083	SS	BED	.2000+03	.3400+02	.1000+00	0	DOLOM	CCL	77P001
1210150084	SF	FAULT	.2910+03	.9000+02	.1000+00	0	DOLOM	CCL	77P001
1210150085	SS	BED	.1590+03	.5600+02	.1000+00	0	QTZITE	CCL	77P001
1210150086	SS	BED	.2520+03	.1700+02	.1000+00	0	DOLOM	CCL	77P001

LOCALE	FABELT	TYCODE	STR	DPL	SIZE	TAG	LITHCO	METHOD	REFER
1210150087	S1	MYF	.2000+03	.8000+01	.1000+00	0	MARBLE	CCL	77P001
1210150088	L1	FAX	.2420+03	.5000+01	.1000+00	0	DOLOM	CCL	77P001
1210150088	SS	BED	.2440+03	.2400+02	.1000+00	0	DOLOM	CCL	77P001
1210150088	SS	BED	.8200+02	.3200+02	.1000+00	0	DOLOM	CCL	77P001
1210150089	SS	BED	.2600+03	.5100+02	.1000+00	0	CQTZTE	CCL	77P001
1210150090	SS	BED	.2510+03	.5300+02	.1000+00	0	DOLOM	CCL	77P001
1210150091	SS	BED	.2580+03	.4600+02	.1000+00	0	CQTZTE	CCL	77P001
1210150092	SS	BED	.2330+03	.4200+02	.1000+00	0	CQTZTE	CCL	77P001
1210150093	SS	BED	.2140+03	.3600+02	.1000+00	0	CQTZTE	CCL	77P001
1210150094	SS	BED	.2100+03	.1700+02	.1000+00	0	CQTZTE	CCL	77P001
1210150095	SS	BED	.2580+03	.6100+02	.1000+00	0	DOLOM	CCL	77P001
1210150096	SS	BED	.2450+03	.5200+02	.1000+00	0	DOLOM	CCL	77P001
1210150097	SS	BED	.2750+03	.5200+02	.1000+00	0	CQTZTE	CCL	77P001
1210150098	SS	BED	.2440+03	.7000+02	.1000+00	0	DOLOM	CCL	77P001
1210150099	SS	BED	.2250+03	.6000+02	.1000+00	0	DOLOM	CCL	77P001
1210150100	S1	MYF	.2580+03	.6200+02	.1000+00	0	BLSMAR	CCL	77P001
1210150101	SS	BED	.2230+03	.6000+02	.1000+00	0	DOLOM	CCL	77P001
1210150102	S1	MYF	.2450+03	.7700+02	.1000+00	0	MARBLE	CCL	77P001
1210150103	SS	BED	.2380+03	.5800+02	.1000+00	0	DOLOM	CCL	77P001
1210150104	SS	BED	.2180+03	.5600+02	.1000+00	0	DOLOM	CCL	77P001
1210150105	SS	BED	.1700+03	.4300+02	.1000+00	0	DOLOM	CCL	77P001
1210150105	SS	BED	.1540+03	.5200+02	.1000+00	0	DOLOM	CCL	77P001
1210150105	SS	BED	.2220+03	.5700+02	.1000+00	0	DOLOM	CCL	77P001
1210150105	SS	BED	.2160+03	.5800+02	.1000+00	0	DOLOM	CCL	77P001
1210150105	SS	BED	.1890+03	.3800+02	.1000+00	0	DOLOM	CCL	77P001
1210150106	LS	RPM	.1600+02	.3000+02	.1000+00	0	QTZITE	CCL	77P001
1210150106	SS	BED	.2220+03	.4300+02	.1000+00	0	QTZITE	CCL	77P001
1210150107	L1	FAX	.2630+03	.2000+02	.1000+00	1	MARPHY	CCL	77P001
1210150107	L2	FAX	.2550+03	.1100+02	.1000+00	2	MARPHY	GCS	77P001
1210150107	SF	JNT	.1630+03	.8500+02	.1000+00	2	MARPHY	CCL	77P001
1210150107	S1	BCL	.1410+03	.1200+02	.1000+00	2	MARPHY	CCL	77P001
1210150107	S1	BCL	.1220+03	.1400+02	.1000+00	2	MARPHY	CCL	77P001
1210150107	S1	BCL	.8400+02	.4900+02	.1000+00	2	MARPHY	CCL	77P001
1210150107	S1	FAP	.1750+03	.2000+02	.1000+00	1	MARPHY	CCL	77P001
1210150107	S2	FAP	.2470+03	.5500+02	.1000+00	2	MARPHY	GCS	77P001
1210150107	S2	TEV	.1100+02	.7000+02	.1000+00	1	MARPHY	GCS	77P001
1210150107	S2	TEV	.1400+02	.7100+02	.1000+00	1	MARPHY	GCS	77P001
1210150107	S2	TEV	.1300+02	.7100+02	.1000+00	1	MARPHY	GCS	77P001
1210150107	S2	TEV	.1700+02	.7200+02	.1000+00	1	MARPHY	GCS	77P001
1210150108	SF	JNT	.1470+03	.8400+02	.1000+00	1	MARBLE	CCL	77P001
1210150108	SF	JNT	.1540+03	.8600+02	.1000+00	1	MARBLE	CCL	77P001
1210150108	S1	BCL	.8600+02	.1000+02	.1000+00	1	MARBLE	CCL	77P001
1210150108	S1	MYF	.2880+03	.1900+02	.1000+00	2	MARBLE	CCL	77P001
1210150109	L1	FAX	.3330+03	.4000+01	.1000+00	0	MARBLE	CCL	77P001
1210150109	S1	MYF	.1080+03	.6000+01	.1000+00	0	MARBLE	CCL	77P001
1210150110	S1	MYF	.1700+02	.2400+02	.1000+00	0	MARBLE	CCL	77P001
1210150110	S1	MYF	.1520+03	.3600+02	.1000+00	0	MARBLE	CCL	77P001
1210150110	S1	MYF	.1450+03	.4100+02	.1000+00	0	MARBLE	CCL	77P001
1210150110	S1	MYF	.6900+02	.1100+02	.1000+00	0	MARBLE	CCL	77P001
1210150111	L1X	MEL	.3320+03	.2600+02	.1000+00	0	MARBLE	CCL	77P001

LOCALE	FABELT	TYCODE	STR	DPL	SIZE	TAG	LITHCO	METHOD	REFER
1210150111	L1X	MEL	.3400+03	.2500+02	.1000+00	0	MARBLE	CCL	77P001
1210150111	L1X	MEL	.3330+03	.2700+02	.1000+00	0	MARBLE	CCL	77P001
1210150111	L1X	MEL	.3320+03	.2700+02	.1000+00	0	MARBLE	CCL	77P001
1210150111	S1	MYF	.2290+03	.2700+02	.1000+00	0	MARBLE	CCL	77P001
1210150111	S1	MYF	.2360+03	.2700+02	.1000+00	0	MARBLE	CCL	77P001
1210150111	S1	MYF	.2310+03	.2800+02	.1000+00	0	MARBLE	CCL	77P001
1210150111	S1	MYF	.2300+03	.2800+02	.1000+00	0	MARBLE	CCL	77P001
1210150112	L1B	ISL	.1000+01	.2000+02	.1000+00	1	MARBLE	CCL	77P001
1210150112	L1X	MEL	.3220+03	.2500+02	.1000+00	1	MARBLE	CCL	77P001
1210150112	L1X	MEL	.3170+03	.2000+02	.1000+00	0	MARBLE	CCL	77P001
1210150112	L1X	MEL	.3170+03	.2400+02	.1000+00	0	MARBLE	CCL	77P001
1210150112	S1	MYF	.2230+03	.2500+02	.1000+00	0	MARBLE	CCL	77P001
1210150112	S1	MYF	.2310+03	.2600+02	.1000+00	1	MARBLE	CCL	77P001
1210150112	S1	MYF	.2300+03	.1800+02	.1000+00	0	MARBLE	CCL	77P001
1210150112	S1	MYF	.2300+03	.2100+02	.1000+00	0	MARBLE	CCL	77P001
1210150113	SS	BED	.7600+02	.3500+02	.1000+00	0	DOLOM	CCL	77P001
1210150113	SS	BED	.1440+03	.3100+02	.1000+00	0	DOLOM	CCL	77P001
1210150113	SS	BED	.1200+03	.2000+02	.1000+00	0	DOLOM	CCL	77P001
1210150113	SS	BED	.1030+03	.3500+02	.1000+00	0	DOLOM	CCL	77P001
1210150113	SS	BED	.1030+03	.3100+02	.1000+00	0	DOLOM	CCL	77P001
1210150113	SS	BED	.8600+02	.4400+02	.1000+00	0	DOLOM	CCL	77P001
1210150114	SS	BED	.5600+02	.7400+02	.1000+00	0	DOLOM	CCL	77P001
1210150114	SS	BED	.6200+02	.5900+02	.1000+00	0	DOLOM	CCL	77P001
1210150114	SS	BED	.5900+02	.5500+02	.1000+00	0	DOLOM	CCL	77P001
1210150114	SS	BED	.6700+02	.6000+02	.1000+00	0	DOLOM	CCL	77P001
1210150114	SS	BED	.6400+02	.4500+02	.1000+00	0	DOLOM	CCL	77P001
1210150115	L1	FAX	.2960+03	.3000+02	.1000+00	0	QTZPSH	CCL	77P001
1210150115	SF	FAULT	.2410+03	.3500+02	.1000+00	0	QTZPSH	CCL	77P001
1210150115	SS	BED	.2270+03	.4900+02	.1000+00	0	QTZPSH	CCL	77P001
1210150115	SS	BED	.2240+03	.3900+02	.1000+00	0	QTZPSH	CCL	77P001
1210150115	SS	BED	.1820+03	.1700+02	.1000+00	0	QTZPSH	CCL	77P001
1210150115	SS	BED	.1180+03	.7300+02	.1000+00	0	QTZPSH	CCL	77P001
1210150115	SS	BED	.2930+03	.9000+02	.1000+00	0	QTZPSH	CCL	77P001
1210150115	SS	BED	.2830+03	.4900+02	.1000+00	0	QTZPSH	CCL	77P001
1210150115	SS	BED	.2820+03	.4400+02	.1000+00	0	QTZPSH	CCL	77P001
1210150115	SS	BED	.2800+03	.5500+02	.1000+00	0	QTZPSH	CCL	77P001
1210150115	SS	BED	.2710+03	.4500+02	.1000+00	0	QTZPSH	CCL	77P001
1210150115	SS	BED	.2360+03	.4100+02	.1000+00	0	QTZPSH	CCL	77P001
1210150115	SS	BED	.2320+03	.3200+02	.1000+00	0	QTZPSH	CCL	77P001
1210150115	SS	BED	.2320+03	.3700+02	.1000+00	0	QTZPSH	CCL	77P001
1210150115	S1	FAP	.2460+03	.3200+02	.1000+00	0	QTZPSH	CCL	77P001
1210150116	L1	FAX	.3020+03	.3300+02	.1000+00	0	QTZPSH	CCL	77P001
1210150116	L1	FAX	.3060+03	.3100+02	.1000+00	0	QTZPSH	CCL	77P001
1210150116	L1	FAX	.3040+03	.3900+02	.1000+00	0	QTZPSH	CCL	77P001
1210150116	SS	BED				0	QTZPSH		77P001
1210150117	L1	FAX	.2270+03	.6000+01	.1000+00	1	MARPHY	CCL	77P001
1210150117	L1B	ISL	.2730+03	.2500+02	.1000+00	3	SHALE	CCL	77P001
1210150117	SS	BED	.2260+03	.2500+02	.1000+00	3	SHALE	CCL	77P001
1210150117	S1	BCL	.2120+03	.3700+02	.1000+00	1	MARPHY	CCL	77P001
1210150117	S1	BCL	.2070+03	.3200+02	.1000+00	2	MARPHY	CCL	77P001

LOCALE	FABELT	TYCODE	STR	DPL	SIZE	TAG	LITHCO	METHOD	REFER
1210150117	S1	BCL	.2070+03	.3500+02	.1000+00	2	MARPHY	CCL	77P001
1210150117	S1	BCL	.2050+03	.3600+02	.1000+00	1	MARPHY	CCL	77P001
1210150117	S1	BCL	.2040+03	.3300+02	.1000+00	2	MARPHY	CCL	77P001
1210150117	S1	BCL	.2000+03	.2800+02	.1000+00	1	MARPHY	CCL	77P001
1210150117	S1	BCL	.2000+03	.3400+02	.1000+00	2	MARPHY	CCL	77P001
1210150117	S1	SLC	.2450+03	.4300+02	.1000+00	3	SHALE	CCL	77P001
1210150117	S2	TEV	.7200+02	.5800+02	.1000+00	3	SHALE	CCL	77P001
1210150117	S2	TEV	.3390+03	.6400+02	.1000+00	1	MARPHY	GCS	77P001
1210150119	L1	FAX	.2230+03	.1500+02	.1000+00	1	SHALE	CCL	77P001
1210150119	L1B	ISL	.2560+03	.8000+01	.1000+00	0	SHALE	CCL	77P001
1210150119	SS	BED	.2010+03	.1600+02	.1000+00	1	SHALE	CCL	77P001
1210150119	SS	BED	.1260+03	.1500+02	.1000+00	2	SHALE	CCL	77P001
1210150119	SS	BED	.5900+02	.6700+02	.1000+00	1	SHALE	CCL	77P001
1210150119	S1	FAP	.2190+03	.3500+02	.1000+00	1	SHALE	CCL	77P001
1210150119	S1	FRC	.2390+03	.3600+02	.1000+00	2	SHALE	CCL	77P001
1210150119	S1	FRC	.2220+03	.2200+02	.1000+00	2	SHALE	CCL	77P001
1210150119	S1	FRC	.2190+03	.1900+02	.1000+00	2	SHALE	CCL	77P001
1210150119	S1	FRC	.2100+03	.2900+02	.1000+00	1	SHALE	CCL	77P001
1210150120	S1	MYF	.1630+03	.2000+02	.1000+00	0	MARBLE	CCL	77P001
1210150120	S1	MYF	.1050+03	.6500+02	.1000+00	0	MARBLE	CCL	77P001
1210150120	S1	MYF	.1020+03	.5800+02	.1000+00	0	MARBLE	CCL	77P001
1210150120	S1	MYF	.1010+03	.8600+02	.1000+00	0	MARBLE	CCL	77P001
1210150120	S1	MYF	.2260+03	.3300+02	.1000+00	0	MARBLE	CCL	77P001
1210150120	S1	MYF	.2000+03	.2600+02	.1000+00	0	MARBLE	CCL	77P001
1210150121	SS	BED	.2520+03	.4500+02	.1000+00	0	DOLOM	CCL	77P001
1210150122	L1	FAX	.8000+02	.2600+02	.1000+00	0	DOLOM	CCL	77P001
1210150122	SS	BED	.2770+03	.4900+02	.1000+00	0	DOLOM	CCL	77P001
1210150122	SS	BED	.5300+02	.5000+02	.1000+00	0	DOLOM	CCL	77P001
1210150122	S1	FAP	.8000+02	.9000+02	.1000+00	0	DOLOM	CCL	77P001
1210150123	SS	BED	.2630+03	.4200+02	.1000+00	0	DOLOM	CCL	77P001
1210150124	L1	FAX	.3100+03	.4000+02	.1000+00	2	MARBLE	CCL	77P001
1210150124	L1	FAX	.2660+03	.2000+02	.1000+00	3	MARBLE	CCL	77P001
1210150124	L1X	MEL	.1000+01	.5400+02	.1000+00	2	MARBLE	CCL	77P001
1210150124	S1	BCL	.2330+03	.2800+02	.1000+00	3	MARBLE	CCL	77P001
1210150124	S1	FAP	.2390+03	.4800+02	.1000+00	2	MARBLE	CCL	77P001
1210150124	S1	FAP	.2310+03	.3000+02	.1000+00	3	MARBLE	CCL	77P001
1210150124	S1	MYF	.2280+03	.3800+02	.1000+00	1	MARBLE	CCL	77P001
1210150124	S1	MYF	.2240+03	.3900+02	.1000+00	1	MARBLE	CCL	77P001
1210150124	S1	MYF	.2650+03	.5600+02	.1000+00	2	MARBLE	CCL	77P001
1210150124	S1	MYF	.2580+03	.5600+02	.1000+00	2	MARBLE	CCL	77P001
1210150124	S1	MYF	.2550+03	.4700+02	.1000+00	2	MARBLE	CCL	77P001
1210150124	S1	MYF	.2540+03	.5000+02	.1000+00	2	MARBLE	CCL	77P001
1210150124	S1	MYF	.2300+03	.4100+02	.1000+00	1	MARBLE	CCL	77P001
1210150124	S1	MYF	.2300+03	.4000+02	.1000+00	1	MARBLE	CCL	77P001
1210150125	S1	BCL	.2130+03	.3800+02	.1000+00	1	DOLMAR	CCL	77P001
1210150125	S1	BCL	.2080+03	.3800+02	.1000+00	1	DOLMAR	CCL	77P001
1210150125	S1	BCL	.2290+03	.5300+02	.1000+00	2	DOLMAR	CCL	77P001
1210150125	S1	BCL	.2150+03	.3900+02	.1000+00	1	DOLMAR	CCL	77P001
1210150126	S1	MYF	.2360+03	.5400+02	.1000+00	0	MARBLE	CCL	77P001
1210150126	S1	MYF	.2210+03	.4700+02	.1000+00	0	MARBLE	CCL	77P001

LOCALE	FABELT	TYCODE	STR	DPL	SIZE	TAG	LITHCO	METHOD	REFER
1210150126	S1	MYF	.2430+03	.3300+02	.1000+00	0	MARBLE	CCL	77P001
1210150126	S1	MYF	.2420+03	.4600+02	.1000+00	0	MARBLE	CCL	77P001
1210150127	SS	BED	.2720+03	.3300+02	.1000+00	0	DOLOM	CCL	77P001
1210150127	SS	BED	.1430+03	.3100+02	.1000+00	0	DOLOM	CCL	77P001
1210150128	SS	BED	.2660+03	.3400+02	.1000+00	0	DOLOM	CCL	77P001
1210150128	SS	BED	.2590+03	.3900+02	.1000+00	0	DOLOM	CCL	77P001
1210150128	SS	BED	.2570+03	.3100+02	.1000+00	0	DOLOM	CCL	77P001
1210150128	SS	BED	.2570+03	.3100+02	.1000+00	0	DOLOM	CCL	77P001
1210150129	S1	BCL	.1770+03	.2600+02	.1000+00	0	BLSMAR	CCL	77P001
1210150129	S1	BCL	.1770+03	.2500+02	.1000+00	0	BLSMAR	CCL	77P001
1210150129	S1	BCL	.1700+03	.4800+02	.1000+00	0	BLSMAR	CCL	77P001
1210150129	S1	BCL	.1660+03	.3600+02	.1000+00	0	BLSMAR	CCL	77P001
1210150129	S1	BCL	.1880+03	.3200+02	.1000+00	0	BLSMAR	CCL	77P001
1210150129	S1	BCL	.1880+03	.3500+02	.1000+00	0	BLSMAR	CCL	77P001
1210150130	L1B	ISL	.2960+03	.2800+02	.1000+00	0	BLSGSH	CCL	77P001
1210150130	S1	CLE	.2580+03	.7500+02	.1000+00	0	BLSGSH	CCL	77P001
1210150130	S1	CLE	.2900+03	.6100+02	.1000+00	0	BLSGSH	CCL	77P001
1210150130	S1	CLE	.2710+03	.6200+02	.1000+00	0	BLSGSH	CCL	77P001
1210150130	S1	CLE	.2690+03	.6400+02	.1000+00	0	BLSGSH	CCL	77P001
1210150131	L1	FAX	.4000+02	.1400+02	.1000+00	0	MARBLE	CCL	77P001
1210150131	L1X	MEL	.3190+03	.5000+02	.1000+00	0	MARBLE	CCL	77P001
1210150131	S1	MYF	.2240+03	.5300+02	.1000+00	0	MARBLE	CCL	77P001
1210150131	S1	MYF	.2270+03	.6500+02	.1000+00	0	MARBLE	CCL	77P001
1210150131	S1	MYF	.2250+03	.7200+02	.1000+00	0	MARBLE	CCL	77P001
1210150131	S1	MYF	.2290+03	.7200+02	.1000+00	0	MARBLE	CCL	77P001
1210150132	L1	FAX	.2830+03	.6800+02	.1000+00	0	MARBLE	CCL	77P001
1210150132	S1	MYF	.2560+03	.6700+02	.1000+00	0	MARBLE	CCL	77P001
1210150133	SS	BED	.2370+03	.3400+02	.1000+00	0	DOLOM	CCL	77P001
1210150133	SS	BED	.2470+03	.3900+02	.1000+00	0	DOLOM	CCL	77P001
1210150133	SS	BED	.2400+03	.4200+02	.1000+00	0	DOLOM	CCL	77P001
1210150133	SS	BED	.2390+03	.4300+02	.1000+00	0	DOLOM	CCL	77P001
1210150134	SS	BED	.2740+03	.4300+02	.1000+00	0	DOLOM	CCL	77P001
1210150134	SS	BED	.2940+03	.4000+02	.1000+00	0	DOLOM	CCL	77P001
1210150134	SS	BED	.2860+03	.4100+02	.1000+00	0	DOLOM	CCL	77P001
1210150134	SS	BED	.2790+03	.3400+02	.1000+00	0	DOLOM	CCL	77P001
1210150134	SS	BED	.2760+03	.2900+02	.1000+00	0	DOLOM	CCL	77P001
1210150135	S1	MYF	.1790+03	.6400+02	.1000+00	0	MARBLE	CCL	77P001
1210150135	S1	MYF	.1770+03	.5700+02	.1000+00	0	MARBLE	CCL	77P001
1210150135	S1	MYF	.1730+03	.5600+02	.1000+00	0	MARBLE	CCL	77P001
1210150135	S1	MYF	.1720+03	.7000+02	.1000+00	0	MARBLE	CCL	77P001
1210150135	S1	MYF	.1680+03	.7000+02	.1000+00	0	MARBLE	CCL	77P001
1210150137	L1X	MEL	.3550+03	.3300+02	.1000+00	1	PHYLL	CCL	77P001
1210150137	L1X	MEL	.3580+03	.2200+02	.1000+00	1	PHYLL	CCL	77P001
1210150137	S1	MYF	.2400+03	.3000+02	.1000+00	2	DOLMAR	CCL	77P001
1210150137	S1	MYF	.2450+03	.3900+02	.1000+00	2	DOLMAR	CCL	77P001
1210150137	S1	PHF	.2300+03	.1800+02	.1000+00	1	PHYLL	CCL	77P001
1210150137	S1	PHF	.2390+03	.2400+02	.1000+00	1	PHYLL	CCL	77P001
1210150137	S1	PHF	.2330+03	.2700+02	.1000+00	1	PHYLL	CCL	77P001
1210150137	S1	PHF	.2420+03	.3300+02	.1000+00	1	PHYLL	CCL	77P001
1210150138	SS	BED	.2000+01	.9300+02	.1000+00	0	DOLOM	CCL	77P001

LOCALE	FABELT	TYCODE	STR	DPL	SIZE	TAG	LITHCO	METHOD	REFER
1210150138	SS	BED	.1900+02	.7100+02	.1000+00	0	DOLOM	CCL	77P001
1210150138	SS	BED	.7000+01	.7800+02	.1000+00	0	DOLOM	CCL	77P001
1210150138	SS	BED	.1900+03	.5300+02	.1000+00	0	DOLOM	CCL	77P001
1210150138	SS	BED	.1870+03	.4800+02	.1000+00	0	DOLOM	CCL	77P001
1210150138	SS	BED	.1700+03	.4200+02	.1000+00	0	DOLOM	CCL	77P001
1210150138	SS	BED	.1680+03	.4400+02	.1000+00	0	DOLOM	CCL	77P001
1210150138	SS	BED	.1460+03	.4400+02	.1000+00	0	DOLOM	CCL	77P001
1210150138	SS	BED	.1430+03	.3300+02	.1000+00	0	DOLOM	CCL	77P001
1210150138	SS	BED	.1260+03	.3400+02	.1000+00	0	DOLOM	CCL	77P001
1210150138	SS	BED	.1150+03	.3100+02	.1000+00	0	DOLOM	CCL	77P001
1210150139	L1	FAX	.3230+03	.2500+02	.1000+00	2	MARBLE	CCL	77P001
1210150139	L1	FAX	.2360+03	.1000+02	.1000+00	1	MARBLE	CCL	77P001
1210150139	S1	FAP	.2220+03	.3000+02	.1000+00	2	MARBLE	CCL	77P001
1210150139	S1	FAP	.2160+03	.2600+02	.1000+00	1	MARBLE	CCL	77P001
1210150139	S1	MYF	.2010+03	.2200+02	.1000+00	3	MARBLE	CCL	77P001
1210150139	S1	MYF	.1990+03	.2700+02	.1000+00	3	MARBLE	CCL	77P001
1210150139	S1	MYF	.1980+03	.2300+02	.1000+00	3	MARBLE	CCL	77P001
1210150139	S1	MYF	.1920+03	.2100+02	.1000+00	3	MARBLE	CCL	77P001
1210150140	SS	BED	.2020+03	.3800+02	.1000+00	0	DOLOM	CCL	77P001
1210150140	SS	BED	.2010+03	.4600+02	.1000+00	0	DOLOM	CCL	77P001
1210150140	SS	BED	.2200+03	.4400+02	.1000+00	0	DOLOM	CCL	77P001
1210150140	SS	BED	.2120+03	.4300+02	.1000+00	0	DOLOM	CCL	77P001
1210150140	SS	BED	.2050+03	.4200+02	.1000+00	0	DOLOM	CCL	77P001
1210150140	SS	BED	.2040+03	.4600+02	.1000+00	0	DOLOM	CCL	77P001
1210160001	SS	BED	.3390+03	.4400+02	.1000+00	0	QTZITE	CCL	77P001
1210160002	SS	BED	.3360+03	.6400+02	.1000+00	0	DOLOM	CCL	77P001
1210160003	SS	BED				0	QTZPSH		77P001
1210160004	SS	BED	.3100+03	.6000+02	.1000+00	0	DOLOM	CCL	77P001
1210160006	S1	MYF	.2530+03	.5900+02	.1000+00	0	MARBLE	CCL	77P001
1210160006	S1	MYF	.2510+03	.5800+02	.1000+00	0	MARBLE	CCL	77P001
1210160006	S1	MYF	.2620+03	.6200+02	.1000+00	0	MARBLE	CCL	77P001
1210160007	S1	BCL	.1670+03	.6200+02	.1000+00	0	DOLOM	CCL	77P001
1210160007	S1	BCL	.2450+03	.7500+02	.1000+00	0	DOLOM	CCL	77P001
1210160007	S1	BCL	.2280+03	.6500+02	.1000+00	0	DOLOM	CCL	77P001
1210160007	S1	BCL	.3130+03	.8900+02	.1000+00	0	DOLOM	CCL	77P001
1210160007	S1	BCL	.2550+03	.7400+02	.1000+00	0	DOLOM	CCL	77P001
1210160007	S1	BCL	.2500+03	.7600+02	.1000+00	0	DOLOM	CCL	77P001
1210160008	S1	MYF	.2650+03	.4600+02	.1000+00	0	MARBLE	CCL	77P001
1210160008	S1	MYF	.2800+03	.4400+02	.1000+00	0	MARBLE	CCL	77P001
1210160009	SS	BED	.2070+03	.5200+02	.1000+00	0	DOLOM	CCL	77P001
1210160011	SS	BED	.2740+03	.4500+02	.1000+00	0	DOLOM	CCL	77P001
1210160012	SS	BED	.3010+03	.5600+02	.1000+00	0	QTZITE	CCL	77P001
1210160013	SS	BED	.2740+03	.6200+02	.1000+00	0	CQTZTE	CCL	77P001
1210160014	SS	BED	.2770+03	.6200+02	.1000+00	0	CQTZTE	CCL	77P001
1210160015	SS	BED	.2750+03	.2800+02	.1000+00	0	CQTZTE	CCL	77P001
1210160015	SS	BED	.1100+03	.4200+02	.1000+00	0	CQTZTE	CCL	77P001
1210160016	SS	BED	.2820+03	.3300+02	.1000+00	1	CQTZTE	CCL	77P001
1210160016	SS	BED	.2750+03	.2600+02	.1000+00	1	CQTZTE	CCL	77P001
1210160016	SS	BED	.2620+03	.2400+02	.1000+00	1	CQTZTE	CCL	77P001
1210160017	SS	BED	.1000+03	.4200+02	.1000+00	0	DOLOM	CCL	77P001

LOCALE	FABELT	TYCODE	STR	DPL	SIZE	TAG	LITHCO	METHOD	REFER
1210160018	SS	BED	.1150+03	.5200+02	.1000+00	0	DOLOM	CCL	77P001
1210160019	SS	BED	.2780+03	.7200+02	.1000+00	0	CQTZTE	CCL	77P001
1210160020	SS	BED	.1540+03	.3000+02	.1000+00	0	CQTZTE	CCL	77P001
1210160021	SS	BED	.1240+03	.4400+02	.1000+00	0	DOLOM	CCL	77P001
1210160022	SS	BED	.7800+02	.6900+02	.1000+00	0	DOLOM	CCL	77P001
1210160023	SS	BED	.2550+03	.5000+01	.1000+00	0	DOLOM	CCL	77P001
1210160024	L1X	MEL	.3230+03	.2100+02	.1000+00	3	PHYMAR	CCL	77P001
1210160024	L1X	MEL	.3140+03	.2200+02	.1000+00	2	PHYMAR	CCL	77P001
1210160024	L1X	MEL	.3330+03	.2400+02	.1000+00	1	PHYMAR	CCL	77P001
1210160024	S1	PHF	.2470+03	.2400+02	.1000+00	1	PHYMAR	CCL	77P001
1210160024	S1	PHF	.2820+03	.3900+02	.1000+00	3	PHYMAR	CCL	77P001
1210160024	S1	PHF	.2680+03	.3100+02	.1000+00	2	PHYMAR	CCL	77P001
1210160025	SS	BED	.1030+03	.2500+02	.1000+00	0	DOLOM	CCL	77P001
1210160026	SS	BED	.8000+02	.1900+02	.1000+00	0	DOLOM	CCL	77P001
1210160027	SS	BED	.2850+03	.2500+02	.1000+00	0	DOLOM	CCL	77P001
1210160028	SS	BED	.1200+02	.2000+02	.1000+00	2	DOLOM	CCL	77P001
1210160028	SS	BED	.3270+03	.3100+02	.1000+00	2	DOLOM	CCL	77P001
1210160028	SS	BED	.3030+03	.6500+02	.1000+00	2	DOLOM	CCL	77P001
1210160028	SS	BED	.2880+03	.6500+02	.1000+00	1	DOLOM	CCL	77P001
1210160028	SS	BED	.1010+03	.2400+02	.1000+00	2	DOLOM	CCL	77P001
1210160029	SS	BED	.2940+03	.4200+02	.1000+00	0	DOLOM	CCL	77P001
1210170001	L1	FAX	.2220+03	.1000+01	.1000+00	0	QTZITE	CCL	77P001
1210170002	L1B	ISL	.3100+02	.9000+01	.1000+00	0	PELITE	CCL	77P001
1210170002	SS	BED	.7000+01	.2700+02	.1000+00	0	PELITE	CCL	77P001
1210170002	S1	FAP	.2360+03	.2000+02	.1000+00	0	PELITE	GCS	77P001
1210170002	S1	FAP	.2360+03	.2000+02	.1000+00	0	PELITE	GCS	77P001
1210170005	SS	BED	.1320+03	.3300+02	.1000+00	0	QTZITE	CCL	77P001
1210170006	SS	BED	.1390+03	.4300+02	.1000+00	0	QTZITE	CCL	77P001
1210170007	L2	PEN	.3460+03	.2900+02	.1000+00	0	QTZITE	CCL	77P001
1210170008	SS	BED	.1320+03	.2400+02	.1000+00	0	DOLSH	CCL	77P001
1210170010	SS	BED	.2130+03	.2300+02	.1000+00	0	DOLOM	CCL	77P001
1210170011	SS	BED	.2720+03	.4400+02	.1000+00	0	BLSTN	CCL	77P001
1210170011	SS	BED	.2790+03	.6500+02	.1000+00	0	BLSTN	CCL	77P001
1210170012	L1	FAX	.3360+03	.3300+02	.1000+00	0	BLSTN	CCL	77P001
1210170012	L1	FAX	.3360+03	.3300+02	.1000+00	0	BLSTN	GCS	77P001
1210170012	SS	BED	.2080+03	.2800+02	.1000+00	0	BLSTN	CCL	77P001
1210170012	SS	BED	.3360+03	.9000+02	.1000+00	0	BLSTN	CCL	77P001
1210170012	SS	BED	.2650+03	.2900+02	.1000+00	0	BLSTN	CCL	77P001
1210170012	SS	BED	.2470+03	.3900+02	.1000+00	0	BLSTN	CCL	77P001
1210170012	SS	BED	.2430+03	.3400+02	.1000+00	0	BLSTN	CCL	77P001
1210170013	SS	BED	.2120+03	.3100+02	.1000+00	0	QTZITE	CCL	77P001
1210170014	L1	FAX	.3520+03	.3200+02	.1000+00	0	QTZITE	CCL	77P001
1210170014	SS	BED	.2300+03	.2500+02	.1000+00	0	QTZITE	CCL	77P001
1210170014	SS	BED	.2600+03	.2600+02	.1000+00	0	QTZITE	CCL	77P001
1210170014	SS	BED	.3230+03	.4700+02	.1000+00	0	QTZITE	CCL	77P001
1210170014	SS	BED	.2920+03	.3200+02	.1000+00	0	QTZITE	CCL	77P001
1210170014	SS	BED	.2740+03	.1800+02	.1000+00	0	QTZITE	CCL	77P001
1210170015	SS	BED	.2020+03	.5600+02	.1000+00	0	CONGL	CCL	77P001
1210170016	SS	BED	.2810+03	.3900+02	.1000+00	0	BLSTN	CCL	77P001
1210170017	SS	BED	.2300+03	.5000+02	.1000+00	0	BLSTN	CCL	77P001

LOCALE	FABELT	TYCODE	STR	DPL	SIZE	TAG	LITHCO	METHOD	REFER
1210170018	SS	BED	.1690+03	.4700+02	.1000+00	0	DOLBLS	CCL	77P001
1210170019	SS	BED	.2740+03	.3200+02	.1000+00	0	BLSTN	CCL	77P001
1210170020	SS	BED	.2020+03	.1400+02	.1000+00	0	SLTSTN	CCL	77P001
1210170020	SS	BED	.6400+02	.2100+02	.1000+00	0	SLTSTN	CCL	77P001
1210170020	SS	BED	.4500+02	.1200+02	.1000+00	0	SLTSTN	CCL	77P001
1210170021	SS	BED	.2720+03	.7200+02	.1000+00	0	DOLOM	CCL	77P001
1210170022	SS	BED	.2600+03	.3000+02	.1000+00	0	CQTZTE	CCL	77P001
1210170022	SS	BED	.2550+03	.3600+02	.1000+00	0	CQTZTE	CCL	77P001
1210170022	SS	BED	.2540+03	.2800+02	.1000+00	0	CQTZTE	CCL	77P001
1210170023	SS	BED	.2350+03	.6300+02	.1000+00	0	BLSTN	CCL	77P001
1210170024	SS	BED	.2350+03	.4200+02	.1000+00	1	BLSTN	CCL	77P001
1210170024	SS	BED	.2330+03	.5400+02	.1000+00	1	BLSTN	CCL	77P001
1210170024	SS	BED	.2320+03	.5400+02	.1000+00	1	BLSTN	CCL	77P001
1210170024	SS	BED	.2300+03	.5500+02	.1000+00	2	BLSTN	CCL	77P001
1210170025	L1B	ISL	.2080+03	.1600+02	.1000+00	0	DOLOM	CCL	77P001
1210170025	SS	BED	.1370+03	.2800+02	.1000+00	0	DOLOM	CCL	77P001
1210170025	SS	BED	.1910+03	.4200+02	.1000+00	0	DOLOM	CCL	77P001
1210170025	SS	BED	.1720+03	.6300+02	.1000+00	0	DOLOM	CCL	77P001
1210170025	S1	PSF	.2070+03	.7500+02	.1000+00	0	DOLOM	CCL	77P001
1210170026	SS	BED	.2020+03	.4000+02	.1000+00	0	BLSTN	CCL	77P001
1210170027	L1B	ISL	.2490+03	.3700+02	.1000+00	0	SHALE	GCS	77P001
1210170027	SS	BED	.2020+03	.4300+02	.1000+00	0	SHALE	CCL	77P001
1210170027	S1	CLE	.2220+03	.5900+02	.1000+00	0	SHALE	CCL	77P001
1210170028	SS	BED	.2750+03	.2300+02	.1000+00	1	QTZITE	CCL	77P001
1210170028	SS	BED	.2690+03	.4900+02	.1000+00	2	DOLOM	CCL	77P001
1210170029	SS	BED	.2630+03	.5000+02	.1000+00	0	SHALE	CCL	77P001
1210170030	SS	BED	.2630+03	.4200+02	.1000+00	0	QTZITE	CCL	77P001
1210170031	SS	BED	.2480+03	.4400+02	.1000+00	0	QTZITE	CCL	77P001
1210170032	LS	RPM	.3300+02	.2100+02	.1000+00	0	QTZITE	CCL	77P001
1210170032	SS	BED	.2290+03	.4900+02	.1000+00	0	QTZITE	CCL	77P001
1210170033	SS	BED	.2510+03	.5600+02	.1000+00	0	DOLOM	CCL	77P001
1210170034	S1	BCL	.2080+03	.4300+02	.1000+00	0	BLSTN	CCL	77P001
1210170035	SS	BED	.2450+03	.5400+02	.1000+00	0	QTZITE	CCL	77P001
1210170036	SS	BED	.1930+03	.5200+02	.1000+00	2	BLSTN	CCL	77P001
1210170036	SS	BED	.2590+03	.5900+02	.1000+00	1	DOLOM	CCL	77P001
1210170037	SS	BED	.2630+03	.4900+02	.1000+00	0	QTZITE	CCL	77P001
1210170038	SS	BED	.2600+03	.4400+02	.1000+00	0	QTZITE	CCL	77P001
1210170039	SS	BED	.2390+03	.4700+02	.1000+00	0	QTZITE	CCL	77P001
1210170040	SS	BED	.2360+03	.4200+02	.1000+00	0	CQTZTE	CCL	77P001
1210170041	SS	BED	.1780+03	.8000+01	.1000+00	0	CQTZTE	CCL	77P001
1210170042	SS	BED	.1020+03	.6300+02	.1000+00	0	DOLOM	CCL	77P001
1210170043	SS	BED	.9500+02	.5800+02	.1000+00	2	QTZITE	CCL	77P001
1210170043	SS	BED	.1070+03	.5600+02	.1000+00	1	QTZITE	CCL	77P001
1210170043	SS	XBED	.1160+03	.7300+02	.1000+00	2	QTZITE	CCL	77P001
1210170044	S1	BCL	.7100+02	.5800+02	.1000+00	0	SLTSTN	CCL	77P001
1210170045	SS	BED	.2820+03	.3800+02	.1000+00	0	QTZITE	CCL	77P001
1210170046	SS	BED	.4100+02	.8500+02	.1000+00	0	BLSTN	CCL	77P001
1210170047	SS	BED	.2220+03	.5000+02	.1000+00	0	BLSTN	CCL	77P001
1210170048	SS	BED	.2400+03	.7000+02	.1000+00	0	BLSTN	CCL	77P001
1210170049	SS	BED	.2270+03	.5000+02	.1000+00	0	BLSTN	CCL	77P001

LOCALE	FABELT	TYCODE	STR	DPL	SIZE	TAG	LITHCO	METHOD	REFER
1210170050	SS	BED	.2370+03	.3700+02	.1000+00	0	BLSTN	CCL	77P001
1210170051	SS	BED	.2750+03	.2600+02	.1000+00	0	CONGLQ	CCL	77P001
1210170052	SS	BED	.2510+03	.1500+02	.1000+00	0	CONGLQ	CCL	77P001
1210170053	SS	BED	.2410+03	.4300+02	.1000+00	0	CQTZTE	CCL	77P001
1210170054	SS	BED	.5800+02	.5400+02	.1000+00	0	QTZITE	CCL	77P001
1210170055	SS	BED	.6700+02	.2600+02	.1000+00	0	QTZITE	CCL	77P001
1210170056	SS	BED	.2570+03	.4700+02	.1000+00	0	QTZITE	CCL	77P001
1210170057	SF	JNT	.5200+02	.2200+02	.1000+00	0	QTZITE	CCL	77P001
1210170058	SS	BED	.2200+03	.3400+02	.1000+00	0	DOLOM	CCL	77P001
1210170059	SS	BED	.7100+02	.1800+02	.1000+00	0	QTZITE	CCL	77P001
1210170060	SS	BED	.2390+03	.6000+02	.1000+00	0	QTZITE	CCL	77P001
1210170061	S1	BCL	.3180+03	.6700+02	.1000+00	0	BLSTN	CCL	77P001
1210170062	SS	BED	.2220+03	.4500+02	.1000+00	0	QTZITE	CCL	77P001

NAUKLUFT LOCATION DATA FILE

LOCALE	IDENTIFICATION	X	Y	Z	TAG	SHEET	METHOD	REFER
1210110001		.2169250+06	.8617500+05	.1200000+04	25	2316CC	MANPLT	77P001
1210110002		.2171500+06	.8620000+05	.1220000+04	25	2316CC	MANPLT	77P001
1210110003		.2173000+06	.8620000+05	.1260000+04	25	2316CC	MANPLT	77P001
1210110004		.2174250+06	.8617500+05	.1310000+04	25	2316CC	MANPLT	77P001
1210110005		.2177500+06	.8602500+05	.1355000+04	25	2316CC	MANPLT	77P001
1210110006		.2186500+06	.8507500+05	.1300000+04	25	2316CC	MANPLT	77P001
1210110007		.2184500+06	.8517500+05	.1300000+04	25	2316CC	MANPLT	77P001
1210110008		.2181250+06	.8512500+05	.1250000+04	25	2316CC	MANPLT	77P001
1210110009		.2178500+06	.8505000+05	.1220000+04	25	2316CC	MANPLT	77P001
1210110010		.2176500+06	.8455000+05	.1200000+04	25	2316CC	MANPLT	77P001
1210110011		.2171000+06	.8485000+05	.1200000+04	25	2316CC	MANPLT	77P001
1210110012		.2170000+06	.8487500+05	.1230000+04	25	2316CC	MANPLT	77P001
1210110013		.2170250+06	.8467500+05	.1245000+04	25	2316CC	MANPLT	77P001
1210110014		.2169250+06	.8460000+05	.1280000+04	25	2316CC	MANPLT	77P001
1210110015		.2169500+06	.8450000+05	.1290000+04	25	2316CC	MANPLT	77P001
1210110016		.2169000+06	.8437500+05	.1300000+04	25	2316CC	MANPLT	77P001
1210110017		.2169750+06	.8430000+05	.1300000+04	25	2316CC	MANPLT	77P001
1210110018		.2171500+06	.8440000+05	.1295000+04	25	2316CC	MANPLT	77P001
1210110019		.2169250+06	.8387500+05	.1340000+04	25	2316CC	MANPLT	77P001
1210110020		.2168750+06	.8360000+05	.1370000+04	25	2316CC	MANPLT	77P001
1210110021		.2166250+06	.8372500+05	.1360000+04	25	2316CC	MANPLT	77P001
1210110022		.2165500+06	.8342500+05	.1370000+04	25	2316CC	MANPLT	77P001
1210110023		.2168500+06	.8327500+05	.1425000+04	25	2316CC	MANPLT	77P001
1210110024		.2169750+06	.8315000+05	.1435000+04	25	2316CC	MANPLT	77P001
1210110025		.2184250+06	.8677500+05	.1160000+04	25	2316CC	MANPLT	77P001
1210110026		.2186250+06	.8675000+05	.1160000+04	25	2316CC	MANPLT	77P001
1210110027		.2187750+06	.8650000+05	.1180000+04	25	2316CC	MANPLT	77P001
1210110028		.2189500+06	.8640000+05	.1175000+04	25	2316CC	MANPLT	77P001
1210110029		.2190000+06	.8622500+05	.1190000+04	25	2316CC	MANPLT	77P001
1210110030		.2191750+06	.8595000+05	.1200000+04	25	2316CC	MANPLT	77P001
1210110031		.2193250+06	.8595000+05	.1230000+04	25	2316CC	MANPLT	77P001
1210110032		.2196500+06	.8595000+05	.1265000+04	25	2316CC	MANPLT	77P001
1210110033		.2198750+06	.8595000+05	.1290000+04	25	2316CC	MANPLT	77P001
1210110034		.2200250+06	.8597500+05	.1330000+04	25	2316CC	MANPLT	77P001
1210110035		.2203750+06	.8585000+05	.1440000+04	25	2316CC	MANPLT	77P001
1210110036		.2160750+06	.7867500+05	.1280000+04	25	2316CC	MANPLT	77P001
1210110037		.2161500+06	.7865000+05	.1280000+04	25	2316CC	MANPLT	77P001
1210110038		.2161250+06	.7857500+05	.1280000+04	25	2316CC	MANPLT	77P001
1210110039		.2162500+06	.7840000+05	.1285000+04	25	2316CC	MANPLT	77P001
1210110040		.2163500+06	.7847500+05	.1290000+04	25	2316CC	MANPLT	77P001
1210110041		.2164250+06	.7820000+05	.1300000+04	25	2316CC	MANPLT	77P001
1210110042		.2172750+06	.7745000+05	.1330000+04	25	2316CC	MANPLT	77P001
1210110043		.2172000+06	.7755000+05	.1400000+04	25	2316CC	MANPLT	77P001
1210110044		.2171500+06	.7765000+05	.1410000+04	25	2316CC	MANPLT	77P001
1210110045		.2173000+06	.7767500+05	.1420000+04	25	2316CC	MANPLT	77P001
1210110046		.2175000+06	.7775000+05	.1430000+04	25	2316CC	MANPLT	77P001
1210110047		.2177500+06	.7785000+05	.1420000+04	25	2316CC	MANPLT	77P001
1210110048		.2180000+06	.7772500+05	.1380000+04	25	2316CC	MANPLT	77P001
1210110049		.2181500+06	.7775000+05	.1380000+04	25	2316CC	MANPLT	77P001
1210110050		.2182250+06	.7772500+05	.1385000+04	25	2316CC	MANPLT	77P001

LOCALE	IDENTIFICATION	X	Y	Z	TAG	SHEET	METHOD	REFER
1210110051		.2184500+06	.7790000+05	.1380000+04	25	2316CC	MANPLT	77P001
1210110052		.2183750+06	.7707500+05	.1385000+04	25	2316CC	MANPLT	77P001
1210110053		.2120500+06	.7690000+05	.1410000+04	25	2316CC	MANPLT	77P001
1210110054		.2128750+06	.7707500+05	.1380000+04	25	2316CC	MANPLT	77P001
1210110055		.2139000+06	.7657500+05	.1460000+04	25	2316CC	MANPLT	77P001
1210110056		.2140500+06	.7647500+05	.1520000+04	25	2316CC	MANPLT	77P001
1210110057		.2123000+06	.7615000+05	.1320000+04	25	2316CD	MANPLT	77P001
1210110058		.2109750+06	.7490000+05	.1360000+04	25	2316CD	MANPLT	77P001
1210110059		.2102000+06	.7417500+05	.1420000+04	25	2316CD	MANPLT	77P001
1210110060		.2102250+06	.7552500+05	.1370000+04	25	2316CD	MANPLT	77P001
1210110061		.2124250+06	.7505000+05	.1370000+04	25	2316CD	MANPLT	77P001
1210110062		.2123250+06	.7467500+05	.1370000+04	25	2316CD	MANPLT	77P001
1210110063		.2120250+06	.7417500+05	.1390000+04	25	2316CD	MANPLT	77P001
1210110064		.2122750+06	.7400000+05	.1410000+04	25	2316CD	MANPLT	77P001
1210110065		.2124500+06	.7435000+05	.1390000+04	25	2316CD	MANPLT	77P001
1210110066		.2128250+06	.7445000+05	.1490000+04	25	2316CD	MANPLT	77P001
1210110067		.2136250+06	.7360000+05	.1420000+04	25	2316CD	MANPLT	77P001
1210110068		.2186250+06	.7490000+05	.1420000+04	25	2316CD	MANPLT	77P001
1210110069		.2190500+06	.7530000+05	.1480000+04	25	2316CD	MANPLT	77P001
1210110070		.2189000+06	.7527500+05	.1440000+04	25	2316CD	MANPLT	77P001
1210110071		.2185500+06	.7520000+05	.1410000+04	25	2316CD	MANPLT	77P001
1210110072		.2181750+06	.7525000+05	.1475000+04	25	2316CD	MANPLT	77P001
1210120001		.1990250+06	.6892500+05	.1770000+04	25	2316CD	MANPLT	77P001
1210120002		.2045250+06	.6985000+05	.1470000+04	25	2316CD	MANPLT	77P001
1210120003		.2047000+06	.7110000+05	.1470000+04	25	2316CD	MANPLT	77P001
1210120004		.2050000+06	.7127500+05	.1550000+04	25	2316CD	MANPLT	77P001
1210120005		.2054000+06	.7057500+05	.1650000+04	25	2316CD	MANPLT	77P001
1210120006		.2055000+06	.6975000+05	.1680000+04	25	2316CD	MANPLT	77P001
1210120007		.2055500+06	.6962500+05	.1670000+04	25	2316CD	MANPLT	77P001
1210120008		.2047250+06	.6480000+05	.1820000+04	25	2316CD	MANPLT	77P001
1210120009		.2048500+06	.6520000+05	.1870000+04	25	2316CD	MANPLT	77P001
1210120010		.2050500+06	.6527500+05	.1850000+04	25	2316CD	MANPLT	77P001
1210120011		.2053500+06	.6557500+05	.1860000+04	25	2316CD	MANPLT	77P001
1210120012		.2054000+06	.6585000+05	.1855000+04	25	2316CD	MANPLT	77P001
1210120013		.2052500+06	.6600000+05	.1865000+04	25	2316CD	MANPLT	77P001
1210120014		.2047500+06	.6635000+05	.1910000+04	25	2316CD	MANPLT	77P001
1210120015		.2047500+06	.6605000+05	.1910000+04	25	2316CD	MANPLT	77P001
1210120016		.2051750+06	.6637500+05	.1870000+04	25	2316CD	MANPLT	77P001
1210120017		.2055500+06	.6615000+05	.1855000+04	25	2316CD	MANPLT	77P001
1210120018		.2059500+06	.6652500+05	.1870000+04	25	2316CD	MANPLT	77P001
1210120019		.2061000+06	.6695000+05	.1865000+04	25	2316CD	MANPLT	77P001
1210120020		.2062500+06	.6722500+05	.1855000+04	25	2316CD	MANPLT	77P001
1210120021		.2062250+06	.6765000+05	.1845000+04	25	2316CD	MANPLT	77P001
1210120022		.2081000+06	.6562500+05	.1720000+04	25	2316CD	MANPLT	77P001
1210120023		.2082000+06	.6632500+05	.1780000+04	25	2316CD	MANPLT	77P001
1210120024		.2079750+06	.6652500+05	.1755000+04	25	2316CD	MANPLT	77P001
1210120025		.2078000+06	.6645000+05	.1760000+04	25	2316CD	MANPLT	77P001
1210120026		.2074250+06	.6620000+05	.1760000+04	25	2316CD	MANPLT	77P001
1210120027		.2080250+06	.6700000+05	.1765000+04	25	2316CD	MANPLT	77P001
1210120028		.2082000+06	.6682500+05	.1720000+04	25	2316CD	MANPLT	77P001

LOCALE	IDENTIFICATION	X	Y	Z	TAG	SHEET	METHOD	REFER
1210120029		.2083250+06	.6680000+05	.1695000+04	25	2316CD	MANPLT	77P001
1210120030		.2085250+06	.6697500+05	.1710000+04	25	2316CD	MANPLT	77P001
1210120031		.2085250+06	.6665000+05	.1720000+04	25	2316CD	MANPLT	77P001
1210120032		.2086500+06	.6647500+05	.1720000+04	25	2316CD	MANPLT	77P001
1210120033		.2097500+06	.6760000+05	.1590000+04	25	2316CD	MANPLT	77P001
1210120034		.2098000+06	.6772500+05	.1590000+04	25	2316CD	MANPLT	77P001
1210120035		.2101000+06	.6795000+05	.1560000+04	25	2316CD	MANPLT	77P001
1210120036		.2105250+06	.6805000+05	.1560000+04	25	2316CD	MANPLT	77P001
1210120037		.2097000+06	.6835000+05	.1720000+04	25	2316CD	MANPLT	77P001
1210120038		.2095750+06	.6820000+05	.1750000+04	25	2316CD	MANPLT	77P001
1210120039		.2107250+06	.6785000+05	.1570000+04	25	2316CD	MANPLT	77P001
1210120040		.2105750+06	.6745000+05	.1600000+04	25	2316CD	MANPLT	77P001
1210120041		.2099500+06	.6660000+05	.1570000+04	25	2316CD	MANPLT	77P001
1210120042		.2101000+06	.6657500+05	.1580000+04	25	2316CD	MANPLT	77P001
1210120043		.2102000+06	.6650000+05	.1585000+04	25	2316CD	MANPLT	77P001
1210120044		.2104750+06	.6625000+05	.1590000+04	25	2316CD	MANPLT	77P001
1210120045		.2108000+06	.6647500+05	.1645000+04	25	2316CD	MANPLT	77P001
1210120046		.2109000+06	.6650000+05	.1670000+04	25	2316CD	MANPLT	77P001
1210120047		.2112000+06	.6615000+05	.1640000+04	25	2316CD	MANPLT	77P001
1210120048		.2121500+06	.6660000+05	.1640000+04	25	2316CD	MANPLT	77P001
1210120049		.2131000+06	.6747500+05	.1725000+04	25	2316CD	MANPLT	77P001
1210120050		.2129500+06	.6757500+05	.1720000+04	25	2316CD	MANPLT	77P001
1210120051		.2129500+06	.6840000+05	.1570000+04	25	2316CD	MANPLT	77P001
1210120052		.2127750+06	.6880000+05	.1540000+04	25	2316CD	MANPLT	77P001
1210120053		.2126750+06	.6902500+05	.1540000+04	25	2316CD	MANPLT	77P001
1210120054		.2129000+06	.6947500+05	.1515000+04	25	2316CD	MANPLT	77P001
1210120055		.2130000+06	.6965000+05	.1570000+04	25	2316CD	MANPLT	77P001
1210120056		.2130500+06	.6982500+05	.1580000+04	25	2316CD	MANPLT	77P001
1210120057		.2134000+06	.6952500+05	.1560000+04	25	2316CD	MANPLT	77P001
1210120058		.2133500+06	.6957500+05	.1560000+04	25	2316CD	MANPLT	77P001
1210120059		.2147500+06	.7075000+05	.1535000+04	25	2316CD	MANPLT	77P001
1210120060		.2152250+06	.7002500+05	.1500000+04	25	2316CD	MANPLT	77P001
1210120061		.2155000+06	.6957500+05	.1515000+04	25	2316CD	MANPLT	77P001
1210120062		.2152250+06	.6920000+05	.1570000+04	25	2316CD	MANPLT	77P001
1210120063		.2151000+06	.6925000+05	.1580000+04	25	2316CD	MANPLT	77P001
1210120064		.2120750+06	.7077500+05	.1470000+04	25	2316CD	MANPLT	77P001
1210120065		.2116250+06	.7085000+05	.1480000+04	25	2316CD	MANPLT	77P001
1210120066		.2110250+06	.7085000+05	.1520000+04	25	2316CD	MANPLT	77P001
1210120067		.2108000+06	.7067500+05	.1550000+04	25	2316CD	MANPLT	77P001
1210120068		.2102500+06	.7020000+05	.1590000+04	25	2316CD	MANPLT	77P001
1210120069		.2098250+06	.6975000+05	.1640000+04	25	2316CD	MANPLT	77P001
1210120070		.2102500+06	.6930000+05	.1630000+04	25	2316CD	MANPLT	77P001
1210120071		.2103000+06	.6920000+05	.1580000+04	25	2316CD	MANPLT	77P001
1210120072		.2102000+06	.6885000+05	.1570000+04	25	2316CD	MANPLT	77P001
1210120073		.2099750+06	.6865000+05	.1660000+04	25	2316CD	MANPLT	77P001
1210120074		.2098250+06	.6860000+05	.1710000+04	25	2316CD	MANPLT	77P001
1210120075		.2108750+06	.6940000+05	.1550000+04	25	2316CD	MANPLT	77P001
1210130001		.2367750+06	.7790000+05	.1510000+04	25	2416AA	MANPLT	77P001
1210130002		.2366000+06	.7835000+05	.1410000+04	25	2416AA	MANPLT	77P001
1210130003		.2363250+06	.7755000+05	.1380000+04	25	2416AA	MANPLT	77P001

LOCALE	IDENTIFICATION	X	Y	Z	TAG	SHEET	METHOD	REFER
1210130004		.2346750+06	.7212500+05	.1420000+04	25	2416AB	MANPLT	77P001
1210130005		.2344500+06	.7185000+05	.1460000+04	25	2416AB	MANPLT	77P001
1210130006		.2335000+06	.6950000+05	.1470000+04	25	2416AB	MANPLT	77P001
1210130007		.2335500+06	.6945000+05	.1460000+04	25	2416AB	MANPLT	77P001
1210130008		.2341000+06	.6937500+05	.1450000+04	25	2416AB	MANPLT	77P001
1210130009		.2293500+06	.6895000+05	.1600000+04	25	2416AB	MANPLT	77P001
1210130010		.2182000+06	.5830000+05	.1660000+04	25	2316CD	MANPLT	77P001
1210130011		.2182500+06	.5832500+05	.1670000+04	25	2316CD	MANPLT	77P001
1210130012		.2182000+06	.5860000+05	.1690000+04	25	2316CD	MANPLT	77P001
1210130013		.2171500+06	.5935000+05	.1675000+04	25	2316CD	MANPLT	77P001
1210130014		.2175000+06	.5937500+05	.1675000+04	25	2316CD	MANPLT	77P001
1210130015		.2177250+06	.5935000+05	.1690000+04	25	2316CD	MANPLT	77P001
1210130016		.2177750+06	.5947500+05	.1685000+04	25	2316CD	MANPLT	77P001
1210130017		.2181750+06	.5985000+05	.1720000+04	25	2316CD	MANPLT	77P001
1210130018		.2188500+06	.5997500+05	.1725000+04	25	2316CD	MANPLT	77P001
1210130019		.2216500+06	.5885000+05	.1670000+04	25	2416AB	MANPLT	77P001
1210130020		.2215000+06	.5917500+05	.1670000+04	25	2316CD	MANPLT	77P001
1210130021		.2206500+06	.5977500+05	.1740000+04	25	2316CD	MANPLT	77P001
1210130022		.2214500+06	.6000000+05	.1720000+04	25	2316CD	MANPLT	77P001
1210130023		.2220000+06	.6120000+05	.1740000+04	25	2416AB	MANPLT	77P001
1210130024		.2209500+06	.5965000+05	.1690000+04	25	2316CD	MANPLT	77P001
1210130025		.2186000+06	.5870000+05	.1675000+04	25	2316CD	MANPLT	77P001
1210130026		.2184000+06	.5877500+05	.1690000+04	25	2316CD	MANPLT	77P001
1210130027		.2327000+06	.7555000+05	.1340000+04	25	2416AB	MANPLT	77P001
1210130028		.2326250+06	.7562500+05	.1380000+04	25	2416AB	MANPLT	77P001
1210130029		.2322250+06	.7597500+05	.1485000+04	25	2416AB	MANPLT	77P001
1210130030		.2325500+06	.7525000+05	.1330000+04	25	2416AB	MANPLT	77P001
1210130031		.2323750+06	.7522500+05	.1360000+04	25	2416AB	MANPLT	77P001
1210130032		.2323000+06	.7530000+05	.1400000+04	25	2416AB	MANPLT	77P001
1210130033		.2320750+06	.7505000+05	.1420000+04	25	2416AB	MANPLT	77P001
1210130034		.2319000+06	.7512500+05	.1450000+04	25	2416AB	MANPLT	77P001
1210130035		.2320250+06	.7475000+05	.1410000+04	25	2416AB	MANPLT	77P001
1210130036		.2320750+06	.7462500+05	.1380000+04	25	2416AB	MANPLT	77P001
1210130037		.2320750+06	.7432500+05	.1340000+04	25	2416AB	MANPLT	77P001
1210130038		.2301500+06	.7155000+05	.1390000+04	25	2416AB	MANPLT	77P001
1210130039		.2299500+06	.7120000+05	.1480000+04	25	2416AB	MANPLT	77P001
1210130040		.2297250+06	.7097500+05	.1570000+04	25	2416AB	MANPLT	77P001
1210130041		.2296500+06	.7085000+05	.1620000+04	25	2416AB	MANPLT	77P001
1210130042		.2295750+06	.7055000+05	.1580000+04	25	2416AB	MANPLT	77P001
1210130043		.2295250+06	.7030000+05	.1620000+04	25	2416AB	MANPLT	77P001
1210130044		.2297250+06	.7247500+05	.1560000+04	25	2416AB	MANPLT	77P001
1210130045		.2294250+06	.7277500+05	.1620000+04	25	2416AB	MANPLT	77P001
1210130046		.2302500+06	.6970000+05	.1450000+04	25	2416AB	MANPLT	77P001
1210130047		.2301750+06	.6985000+05	.1550000+04	25	2416AB	MANPLT	77P001
1210130048		.2300750+06	.6950000+05	.1530000+04	25	2416AB	MANPLT	77P001
1210130049		.2299750+06	.6955000+05	.1570000+04	25	2416AB	MANPLT	77P001
1210130050		.2298750+06	.6962500+05	.1600000+04	25	2416AB	MANPLT	77P001
1210130051		.2297250+06	.6972500+05	.1680000+04	25	2416AB	MANPLT	77P001
1210130052		.2283000+06	.6860000+05	.1470000+04	25	2416AB	MANPLT	77P001
1210130053		.2280750+06	.6872500+05	.1510000+04	25	2416AB	MANPLT	77P001

LOCALE	IDENTIFICATION	X	Y	Z	TAG	SHEET	METHOD	REFER
1210130054		.2280000+06	.6875000+05	.1540000+04	25	2416AB	MANPLT	77P001
1210130055		.2279000+06	.6877500+05	.1570000+04	25	2416AB	MANPLT	77P001
1210130056		.2286500+06	.6840000+05	.1440000+04	25	2416AB	MANPLT	77P001
1210130057		.2285000+06	.6780000+05	.1720000+04	25	2416AB	MANPLT	77P001
1210130058		.2287250+06	.6785000+05	.1710000+04	25	2416AB	MANPLT	77P001
1210130059		.2288750+06	.6790000+05	.1720000+04	25	2416AB	MANPLT	77P001
1210130060		.2291750+06	.6800000+05	.1620000+04	25	2416AB	MANPLT	77P001
1210130061		.2322500+06	.6827500+05	.1390000+04	25	2416AB	MANPLT	77P001
1210130062		.2323500+06	.6825000+05	.1410000+04	25	2416AB	MANPLT	77P001
1210130063		.2327750+06	.6847500+05	.1520000+04	25	2416AB	MANPLT	77P001
1210130064		.2327500+06	.6865000+05	.1520000+04	25	2416AB	MANPLT	77P001
1210130065		.2326000+06	.6852500+05	.1450000+04	25	2416AB	MANPLT	77P001
1210130066		.2361000+06	.7837500+05	.1350000+04	25	2416AA	MANPLT	77P001
1210130067		.2365500+06	.7842500+05	.1400000+04	25	2416AA	MANPLT	77P001
1210130068		.2366750+06	.7780000+05	.1500000+04	25	2416AA	MANPLT	77P001
1210130069		.2304500+06	.8025000+05	.1240000+04	25	2416AA	MANPLT	77P001
1210130070		.2303000+06	.8037500+05	.1280000+04	25	2416AA	MANPLT	77P001
1210130071		.2302500+06	.8035000+05	.1310000+04	25	2416AA	MANPLT	77P001
1210130072		.2306750+06	.8032500+05	.1240000+04	25	2416AA	MANPLT	77P001
1210130073		.2297750+06	.8205000+05	.1240000+04	25	2416AA	MANPLT	77P001
1210130074		.2340750+06	.6925000+05	.1420000+04	25	2416AB	MANPLT	77P001
1210130075		.2341000+06	.6947500+05	.1470000+04	25	2416AB	MANPLT	77P001
1210130076		.2340000+06	.6950000+05	.1480000+04	25	2416AB	MANPLT	77P001
1210130077		.2339750+06	.6957500+05	.1520000+04	25	2416AB	MANPLT	77P001
1210130078		.2339000+06	.6960000+05	.1500000+04	25	2416AB	MANPLT	77P001
1210130079		.2292000+06	.6890000+05	.1580000+04	25	2416AB	MANPLT	77P001
1210140001		.2363250+06	.6485000+05	.1540000+04	25	2416AB	MANPLT	77P001
1210140002		.2363000+06	.6510000+05	.1490000+04	25	2416AB	MANPLT	77P001
1210140003		.2361000+06	.6460000+05	.1590000+04	25	2416AB	MANPLT	77P001
1210140004		.2332000+06	.6205000+05	.1680000+04	25	2416AB	MANPLT	77P001
1210140005		.2328000+06	.6220000+05	.1600000+04	25	2416AB	MANPLT	77P001
1210140006		.2341500+06	.6255000+05	.1570000+04	25	2416AB	MANPLT	77P001
1210140007		.2342500+06	.6290000+05	.1730000+04	25	2416AB	MANPLT	77P001
1210140008		.2344500+06	.6285000+05	.1740000+04	25	2416AB	MANPLT	77P001
1210140009		.2345500+06	.6335000+05	.1720000+04	25	2416AB	MANPLT	77P001
1210140010		.2337000+06	.6330000+05	.1690000+04	25	2416AB	MANPLT	77P001
1210140011		.2339500+06	.6370000+05	.1720000+04	25	2416AB	MANPLT	77P001
1210140012		.2330000+06	.6575000+05	.1500000+04	25	2416AB	MANPLT	77P001
1210140013		.2330000+06	.6530000+05	.1610000+04	25	2416AB	MANPLT	77P001
1210140014		.2332500+06	.6550000+05	.1610000+04	25	2416AB	MANPLT	77P001
1210140015		.2333000+06	.6550000+05	.1600000+04	25	2416AB	MANPLT	77P001
1210140016		.2334000+06	.6550000+05	.1600000+04	25	2416AB	MANPLT	77P001
1210140017		.2335500+06	.6550000+05	.1570000+04	25	2416AB	MANPLT	77P001
1210140018		.2337000+06	.6565000+05	.1480000+04	25	2416AB	MANPLT	77P001
1210140019		.2320750+06	.6215000+05	.1765000+04	25	2416AB	MANPLT	77P001
1210140020		.2318750+06	.6235000+05	.1750000+04	25	2416AB	MANPLT	77P001
1210140021		.2319000+06	.6225000+05	.1780000+04	25	2416AB	MANPLT	77P001
1210140022		.2317500+06	.6235000+05	.1740000+04	25	2416AB	MANPLT	77P001
1210140023		.2317000+06	.6215000+05	.1785000+04	25	2416AB	MANPLT	77P001
1210140024		.2318000+06	.6282500+05	.1760000+04	25	2416AB	MANPLT	77P001

LOCALE	IDENTIFICATION	X	Y	Z	TAG	SHEET	METHOD	REFER
1210140025		.2317000+06	.6297500+05	.1740000+04	25	2416AB	MANPLT	77P001
1210140026		.2320000+06	.6332500+05	.1760000+04	25	2416AB	MANPLT	77P001
1210140027		.2317750+06	.6335000+05	.1750000+04	25	2416AB	MANPLT	77P001
1210140028		.2303750+06	.6090000+05	.1670000+04	25	2416AB	MANPLT	77P001
1210140029		.2310250+06	.6320000+05	.1720000+04	25	2416AB	MANPLT	77P001
1210140030		.2310250+06	.6330000+05	.1740000+04	25	2416AB	MANPLT	77P001
1210140031		.2310250+06	.6345000+05	.1760000+04	25	2416AB	MANPLT	77P001
1210140032		.2310500+06	.6352500+05	.1770000+04	25	2416AB	MANPLT	77P001
1210140033		.2310750+06	.6380000+05	.1810000+04	25	2416AB	MANPLT	77P001
1210140034		.2310250+06	.6420000+05	.1830000+04	25	2416AB	MANPLT	77P001
1210140035		.2310000+06	.6437500+05	.1830000+04	25	2416AB	MANPLT	77P001
1210140036		.2309750+06	.6452500+05	.1830000+04	25	2416AB	MANPLT	77P001
1210140037		.2309000+06	.6460000+05	.1830000+04	25	2416AB	MANPLT	77P001
1210140038		.2305750+06	.6492500+05	.1760000+04	25	2416AB	MANPLT	77P001
1210140039		.2306250+06	.6487500+05	.1780000+04	25	2416AB	MANPLT	77P001
1210140040		.2307000+06	.6477500+05	.1820000+04	25	2416AB	MANPLT	77P001
1210140041		.2308000+06	.6467500+05	.1820000+04	25	2416AB	MANPLT	77P001
1210140042		.2307000+06	.6437500+05	.1820000+04	25	2416AB	MANPLT	77P001
1210140043		.2305750+06	.6407500+05	.1815000+04	25	2416AB	MANPLT	77P001
1210140044		.2306500+06	.6375000+05	.1770000+04	25	2416AB	MANPLT	77P001
1210140045		.2307500+06	.6367500+05	.1800000+04	25	2416AB	MANPLT	77P001
1210140046		.2309000+06	.6335000+05	.1770000+04	25	2416AB	MANPLT	77P001
1210140047		.2313750+06	.6320000+05	.1760000+04	25	2416AB	MANPLT	77P001
1210140048		.2313000+06	.6330000+05	.1780000+04	25	2416AB	MANPLT	77P001
1210140049		.2313500+06	.6360000+05	.1800000+04	25	2416AB	MANPLT	77P001
1210140050		.2313500+06	.6385000+05	.1800000+04	25	2416AB	MANPLT	77P001
1210140051		.2312000+06	.6390000+05	.1760000+04	25	2416AB	MANPLT	77P001
1210140052		.2313500+06	.6552500+05	.1825000+04	25	2416AB	MANPLT	77P001
1210140053		.2313750+06	.6585000+05	.1790000+04	25	2416AB	MANPLT	77P001
1210140054		.2312250+06	.6527500+05	.1835000+04	25	2416AB	MANPLT	77P001
1210140055		.2320500+06	.6415000+05	.1760000+04	25	2416AB	MANPLT	77P001
1210140056		.2327000+06	.6450000+05	.1755000+04	25	2416AB	MANPLT	77P001
1210140057		.2334500+06	.6445000+05	.1490000+04	25	2416AB	MANPLT	77P001
1210140058		.2334500+06	.6470000+05	.1470000+04	25	2416AB	MANPLT	77P001
1210140059		.2358750+06	.6482500+05	.1600000+04	25	2416AB	MANPLT	77P001
1210140060		.2357750+06	.6465000+05	.1720000+04	25	2416AB	MANPLT	77P001
1210140061		.2356500+06	.6442500+05	.1750000+04	25	2416AB	MANPLT	77P001
1210140062		.2356000+06	.6417500+05	.1760000+04	25	2416AB	MANPLT	77P001
1210140063		.2358750+06	.6520000+05	.1440000+04	25	2416AB	MANPLT	77P001
1210140064		.2357250+06	.6390000+05	.1780000+04	25	2416AB	MANPLT	77P001
1210140065		.2355250+06	.6362500+05	.1790000+04	25	2416AB	MANPLT	77P001
1210140066		.2354500+06	.6345000+05	.1740000+04	25	2416AB	MANPLT	77P001
1210140067		.2353250+06	.6325000+05	.1755000+04	25	2416AB	MANPLT	77P001
1210140068		.2349500+06	.6310000+05	.1760000+04	25	2416AB	MANPLT	77P001
1210140069		.2341750+06	.6335000+05	.1780000+04	25	2416AB	MANPLT	77P001
1210140070		.2340750+06	.6382500+05	.1760000+04	25	2416AB	MANPLT	77P001
1210140071		.2340000+06	.6397500+05	.1740000+04	25	2416AB	MANPLT	77P001
1210140072		.2339250+06	.6422500+05	.1700000+04	25	2416AB	MANPLT	77P001
1210140073		.2339250+06	.6440000+05	.1680000+04	25	2416AB	MANPLT	77P001
1210140074		.2339000+06	.6452500+05	.1680000+04	25	2416AB	MANPLT	77P001

LOCALE	IDENTIFICATION	X	Y	Z	TAG	SHEET	METHOD	REFER
1210140075		.2338500+06	.6470000+05	.1650000+04	25	2416AB	MANPLT	77P001
1210140076		.2322500+06	.6682500+05	.1500000+04	25	2416AB	MANPLT	77P001
1210140077		.2320750+06	.6667500+05	.1560000+04	25	2416AB	MANPLT	77P001
1210140078		.2322000+06	.6630000+05	.1680000+04	25	2416AB	MANPLT	77P001
1210140079		.2320500+06	.6617500+05	.1720000+04	25	2416AB	MANPLT	77P001
1210140080		.2320250+06	.6590000+05	.1740000+04	25	2416AB	MANPLT	77P001
1210140081		.2319250+06	.6570000+05	.1750000+04	25	2416AB	MANPLT	77P001
1210140082		.2319000+06	.6555000+05	.1770000+04	25	2416AB	MANPLT	77P001
1210140083		.2356500+06	.6535000+05	.1410000+04	25	2416AB	MANPLT	77P001
1210140084		.2356750+06	.6500000+05	.1540000+04	25	2416AB	MANPLT	77P001
1210140085		.2355750+06	.6520000+05	.1450000+04	25	2416AB	MANPLT	77P001
1210140086		.2355000+06	.6517500+05	.1450000+04	25	2416AB	MANPLT	77P001
1210140087		.2353750+06	.6532500+05	.1430000+04	25	2416AB	MANPLT	77P001
1210140088		.2351250+06	.6512500+05	.1430000+04	25	2416AB	MANPLT	77P001
1210140089		.2352000+06	.6472500+05	.1520000+04	25	2416AB	MANPLT	77P001
1210140090		.2348250+06	.6480000+05	.1460000+04	25	2416AB	MANPLT	77P001
1210140091		.2348000+06	.6460000+05	.1530000+04	25	2416AB	MANPLT	77P001
1210150001		.2371750+06	.6667500+05	.1480000+04	25	2416AB	MANPLT	77P001
1210150002		.2375500+06	.6660000+05	.1520000+04	25	2416AB	MANPLT	77P001
1210150003		.2367500+06	.6630000+05	.1430000+04	25	2416AB	MANPLT	77P001
1210150004		.2339500+06	.6887500+05	.1390000+04	25	2416AB	MANPLT	77P001
1210150005		.2339750+06	.6865000+05	.1440000+04	25	2416AB	MANPLT	77P001
1210150006		.2336000+06	.6770000+05	.1450000+04	25	2416AB	MANPLT	77P001
1210150007		.2358500+06	.6635000+05	.1470000+04	25	2416AB	MANPLT	77P001
1210150008		.2358000+06	.6640000+05	.1520000+04	25	2416AB	MANPLT	77P001
1210150009		.2359750+06	.6625000+05	.1410000+04	25	2416AB	MANPLT	77P001
1210150010		.2396250+06	.6735000+05	.1660000+04	25	2416AB	MANPLT	77P001
1210150011		.2372250+06	.6575000+05	.1460000+04	25	2416AB	MANPLT	77P001
1210150012		.2371250+06	.6582500+05	.1480000+04	25	2416AB	MANPLT	77P001
1210150013		.2370250+06	.6600000+05	.1550000+04	25	2416AB	MANPLT	77P001
1210150014		.2370250+06	.6595000+05	.1510000+04	25	2416AB	MANPLT	77P001
1210150015		.2353000+06	.6630000+05	.1410000+04	25	2416AB	MANPLT	77P001
1210150016		.2352500+06	.6645000+05	.1440000+04	25	2416AB	MANPLT	77P001
1210150017		.2353000+06	.6650000+05	.1480000+04	25	2416AB	MANPLT	77P001
1210150018		.2351500+06	.6675000+05	.1500000+04	25	2416AB	MANPLT	77P001
1210150019		.2397500+06	.6900000+05	.1760000+04	25	2416AB	MANPLT	77P001
1210150020		.2368000+06	.6720000+05	.1440000+04	25	2416AB	MANPLT	77P001
1210150021		.2367500+06	.6735000+05	.1480000+04	25	2416AB	MANPLT	77P001
1210150022		.2369500+06	.6715000+05	.1440000+04	25	2416AB	MANPLT	77P001
1210150023		.2381000+06	.6740000+05	.1660000+04	25	2416AB	MANPLT	77P001
1210150024		.2412500+06	.7025000+05	.1800000+04	25	2416AB	MANPLT	77P001
1210150025		.2423500+06	.6990000+05	.1830000+04	25	2416AB	MANPLT	77P001
1210150026		.2423000+06	.7025000+05	.1850000+04	25	2416AB	MANPLT	77P001
1210150027		.2429000+06	.7065000+05	.1840000+04	25	2416AB	MANPLT	77P001
1210150028		.2430500+06	.7090000+05	.1860000+04	25	2416AB	MANPLT	77P001
1210150029		.2427500+06	.7040000+05	.1850000+04	25	2416AB	MANPLT	77P001
1210150030		.2328500+06	.6795000+05	.1470000+04	25	2416AB	MANPLT	77P001
1210150031		.2329000+06	.6815000+05	.1490000+04	25	2416AB	MANPLT	77P001
1210150032		.2333250+06	.6802500+05	.1350000+04	25	2416AB	MANPLT	77P001
1210150033		.2334250+06	.6782500+05	.1370000+04	25	2416AB	MANPLT	77P001

LOCALE	IDENTIFICATION	X	Y	Z	TAG	SHEET	METHOD	REFER
1210150034		.2400000+06	.6920000+05	.1820000+04	25	2416AB	MANPLT	77P001
1210150035		.2401500+06	.6952500+05	.1810000+04	25	2416AB	MANPLT	77P001
1210150036		.2403500+06	.6982500+05	.1820000+04	25	2416AB	MANPLT	77P001
1210150037		.2403250+06	.6995000+05	.1800000+04	25	2416AB	MANPLT	77P001
1210150038		.2404750+06	.7010000+05	.1800000+04	25	2416AB	MANPLT	77P001
1210150039		.2407000+06	.7035000+05	.1810000+04	25	2416AB	MANPLT	77P001
1210150040		.2407750+06	.7017500+05	.1810000+04	25	2416AB	MANPLT	77P001
1210150041		.2409250+06	.7020000+05	.1805000+04	25	2416AB	MANPLT	77P001
1210150042		.2409750+06	.7042500+05	.1810000+04	25	2416AB	MANPLT	77P001
1210150043		.2410250+06	.7020000+05	.1820000+04	25	2416AB	MANPLT	77P001
1210150044		.2406500+06	.6980000+05	.1800000+04	25	2416AB	MANPLT	77P001
1210150045		.2398500+06	.6905000+05	.1805000+04	25	2416AB	MANPLT	77P001
1210150046		.2383000+06	.6880000+05	.1700000+04	25	2416AB	MANPLT	77P001
1210150047		.2382500+06	.6885000+05	.1710000+04	25	2416AB	MANPLT	77P001
1210150048		.2383250+06	.6897500+05	.1710000+04	25	2416AB	MANPLT	77P001
1210150049		.2384500+06	.6917500+05	.1690000+04	25	2416AB	MANPLT	77P001
1210150050		.2385500+06	.6932500+05	.1660000+04	25	2416AB	MANPLT	77P001
1210150051		.2387000+06	.6942500+05	.1640000+04	25	2416AB	MANPLT	77P001
1210150052		.2392500+06	.7035000+05	.1630000+04	25	2416AB	MANPLT	77P001
1210150053		.2391750+06	.7030000+05	.1650000+04	25	2416AB	MANPLT	77P001
1210150054		.2391000+06	.7037500+05	.1690000+04	25	2416AB	MANPLT	77P001
1210150055		.2389750+06	.7035000+05	.1740000+04	25	2416AB	MANPLT	77P001
1210150056		.2387500+06	.7002500+05	.1800000+04	25	2416AB	MANPLT	77P001
1210150057		.2386000+06	.6985000+05	.1800000+04	25	2416AB	MANPLT	77P001
1210150058		.2383250+06	.6945000+05	.1780000+04	25	2416AB	MANPLT	77P001
1210150059		.2380750+06	.6932500+05	.1810000+04	25	2416AB	MANPLT	77P001
1210150060		.2380000+06	.6890000+05	.1800000+04	25	2416AB	MANPLT	77P001
1210150061		.2385250+06	.7015000+05	.1780000+04	25	2416AB	MANPLT	77P001
1210150062		.2387000+06	.7035000+05	.1790000+04	25	2416AB	MANPLT	77P001
1210150063		.2386250+06	.7080000+05	.1840000+04	25	2416AB	MANPLT	77P001
1210150064		.2387250+06	.7072500+05	.1860000+04	25	2416AB	MANPLT	77P001
1210150065		.2389750+06	.7075000+05	.1850000+04	25	2416AB	MANPLT	77P001
1210150066		.2385000+06	.7090000+05	.1820000+04	25	2416AB	MANPLT	77P001
1210150067		.2379500+06	.7115000+05	.1820000+04	25	2416AB	MANPLT	77P001
1210150068		.2384750+06	.7107500+05	.1840000+04	25	2416AB	MANPLT	77P001
1210150069		.2358250+06	.6585000+05	.1420000+04	25	2416AB	MANPLT	77P001
1210150070		.2358750+06	.6577500+05	.1430000+04	25	2416AB	MANPLT	77P001
1210150071		.2359250+06	.6585000+05	.1480000+04	25	2416AB	MANPLT	77P001
1210150072		.2361000+06	.6580000+05	.1570000+04	25	2416AB	MANPLT	77P001
1210150073		.2361750+06	.6572500+05	.1550000+04	25	2416AB	MANPLT	77P001
1210150074		.2338250+06	.6865000+05	.1400000+04	25	2416AB	MANPLT	77P001
1210150075		.2367500+06	.6647500+05	.1450000+04	25	2416AB	MANPLT	77P001
1210150076		.2367000+06	.6650000+05	.1460000+04	25	2416AB	MANPLT	77P001
1210150077		.2370500+06	.6650000+05	.1440000+04	25	2416AB	MANPLT	77P001
1210150078		.2373000+06	.6645000+05	.1470000+04	25	2416AB	MANPLT	77P001
1210150079		.2374250+06	.6652500+05	.1480000+04	25	2416AB	MANPLT	77P001
1210150080		.2375750+06	.6652500+05	.1500000+04	25	2416AB	MANPLT	77P001
1210150081		.2376000+06	.6660000+05	.1510000+04	25	2416AB	MANPLT	77P001
1210150082		.2377500+06	.6660000+05	.1520000+04	25	2416AB	MANPLT	77P001
1210150083		.2377250+06	.6672500+05	.1520000+04	25	2416AB	MANPLT	77P001

LOCALE	IDENTIFICATION	X	Y	Z	TAG	SHEET	METHOD	REFER
1210150084		.2375000+06	.6650000+05	.1480000+04	25	2416AB	MANPLT	77P001
1210150085		.2394500+06	.6717500+05	.1700000+04	25	2416AB	MANPLT	77P001
1210150086		.2390000+06	.6680000+05	.1750000+04	25	2416AB	MANPLT	77P001
1210150087		.2386500+06	.6692500+05	.1750000+04	25	2416AB	MANPLT	77P001
1210150088		.2385250+06	.6670000+05	.1755000+04	25	2416AB	MANPLT	77P001
1210150089		.2376250+06	.7130000+05	.1880000+04	25	2416AB	MANPLT	77P001
1210150090		.2375500+06	.7115000+05	.1880000+04	25	2416AB	MANPLT	77P001
1210150091		.2376000+06	.7092500+05	.1860000+04	25	2416AB	MANPLT	77P001
1210150092		.2374750+06	.7067500+05	.1860000+04	25	2416AB	MANPLT	77P001
1210150093		.2373500+06	.7052500+05	.1875000+04	25	2416AB	MANPLT	77P001
1210150094		.2369250+06	.7000000+05	.1860000+04	25	2416AB	MANPLT	77P001
1210150095		.2376000+06	.7185000+05	.1900000+04	25	2416AB	MANPLT	77P001
1210150096		.2377750+06	.7205000+05	.1905000+04	25	2416AB	MANPLT	77P001
1210150097		.2380750+06	.7185000+05	.1855000+04	25	2416AB	MANPLT	77P001
1210150098		.2377500+06	.7042500+05	.1860000+04	25	2416AB	MANPLT	77P001
1210150099		.2374500+06	.7000000+05	.1845000+04	25	2416AB	MANPLT	77P001
1210150100		.2374000+06	.6967500+05	.1850000+04	25	2416AB	MANPLT	77P001
1210150101		.2375750+06	.6940000+05	.1830000+04	25	2416AB	MANPLT	77P001
1210150102		.2375000+06	.6942500+05	.1840000+04	25	2416AB	MANPLT	77P001
1210150103		.2373500+06	.6942500+05	.1850000+04	25	2416AB	MANPLT	77P001
1210150104		.2366250+06	.6927500+05	.1830000+04	25	2416AB	MANPLT	77P001
1210150105		.2367500+06	.6935000+05	.1830000+04	25	2416AB	MANPLT	77P001
1210150106		.2368750+06	.6935000+05	.1840000+04	25	2416AB	MANPLT	77P001
1210150107		.2358000+06	.6585000+05	.1420000+04	25	2416AB	MANPLT	77P001
1210150108		.2359500+06	.6595000+05	.1400000+04	25	2416AB	MANPLT	77P001
1210150109		.2360000+06	.6590000+05	.1430000+04	25	2416AB	MANPLT	77P001
1210150110		.2360000+06	.6585000+05	.1460000+04	25	2416AB	MANPLT	77P001
1210150111		.2369250+06	.6690000+05	.1450000+04	25	2416AB	MANPLT	77P001
1210150112		.2367500+06	.6680000+05	.1450000+04	25	2416AB	MANPLT	77P001
1210150113		.2368250+06	.6600000+05	.1500000+04	25	2416AB	MANPLT	77P001
1210150114		.2368750+06	.6620000+05	.1480000+04	25	2416AB	MANPLT	77P001
1210150115		.2371750+06	.6650000+05	.1460000+04	25	2416AB	MANPLT	77P001
1210150116		.2371000+06	.6655000+05	.1460000+04	25	2416AB	MANPLT	77P001
1210150117		.2392250+06	.6772500+05	.1680000+04	25	2416AB	MANPLT	77P001
1210150118		.2356750+06	.6612500+05	.1570000+04	25	2416AB	MANPLT	77P001
1210150119		.2359750+06	.6720000+05	.1580000+04	25	2416AB	MANPLT	77P001
1210150120		.2358750+06	.6737500+05	.1680000+04	25	2416AB	MANPLT	77P001
1210150121		.2354000+06	.6765000+05	.1760000+04	25	2416AB	MANPLT	77P001
1210150122		.2354500+06	.6755000+05	.1770000+04	25	2416AB	MANPLT	77P001
1210150123		.2356500+06	.6750000+05	.1790000+04	25	2416AB	MANPLT	77P001
1210150124		.2338500+06	.6740000+05	.1410000+04	25	2416AB	MANPLT	77P001
1210150125		.2341250+06	.6745000+05	.1460000+04	25	2416AB	MANPLT	77P001
1210150126		.2342000+06	.6775000+05	.1460000+04	25	2416AB	MANPLT	77P001
1210150127		.2348250+06	.6820000+05	.1605000+04	25	2416AB	MANPLT	77P001
1210150128		.2352750+06	.6832500+05	.1665000+04	25	2416AB	MANPLT	77P001
1210150129		.2350000+06	.6835000+05	.1640000+04	25	2416AB	MANPLT	77P001
1210150130		.2351250+06	.6837500+05	.1670000+04	25	2416AB	MANPLT	77P001
1210150131		.2357500+06	.6917500+05	.1710000+04	25	2416AB	MANPLT	77P001
1210150132		.2355500+06	.6847500+05	.1660000+04	25	2416AB	MANPLT	77P001
1210150133		.2357000+06	.6847500+05	.1690000+04	25	2416AB	MANPLT	77P001

LOCALE	IDENTIFICATION	X	Y	Z	TAG	SHEET	METHOD	REFER
1210150134		.2358250+06	.6860000+05	.1735000+04	25	2416AB	MANPLT	77P001
1210150135		.2353500+06	.6840000+05	.1650000+04	25	2416AB	MANPLT	77P001
1210150136		.2410500+06	.6845000+05	.1540000+04	25	2416AB	MANPLT	77P001
1210150137		.2409000+06	.6852500+05	.1610000+04	25	2416AB	MANPLT	77P001
1210150138		.2416000+06	.6857500+05	.1640000+04	25	2416AB	MANPLT	77P001
1210150139		.2420500+06	.6855000+05	.1760000+04	25	2416AB	MANPLT	77P001
1210150140		.2423000+06	.6880000+05	.1790000+04	25	2416AB	MANPLT	77P001
1210160001		.2438250+06	.9050000+05	.1620000+04	25	2416AA	MANPLT	77P001
1210160002		.2424250+06	.8700000+05	.1920000+04	25	2416AA	MANPLT	77P001
1210160003		.2417750+06	.8642500+05	.1930000+04	25	2416AA	MANPLT	77P001
1210160004		.2428750+06	.8767500+05	.1895000+04	25	2416AA	MANPLT	77P001
1210160005		.2425000+06	.9235000+05	.1450000+04	25	2416AA	MANPLT	77P001
1210160006		.2439500+06	.7307500+05	.1900000+04	25	2416AB	MANPLT	77P001
1210160007		.2440750+06	.7702500+05	.1905000+04	25	2416AA	MANPLT	77P001
1210160008		.2443750+06	.7697500+05	.1915000+04	25	2416AA	MANPLT	77P001
1210160009		.2445500+06	.7725000+05	.1905000+04	25	2416AA	MANPLT	77P001
1210160010		.2457250+06	.7790000+05	.1915000+04	25	2416AA	MANPLT	77P001
1210160011		.2463250+06	.7835000+05	.1910000+04	25	2416AA	MANPLT	77P001
1210160012		.2476250+06	.7845000+05	.1870000+04	25	2416AA	MANPLT	77P001
1210160013		.2476750+06	.7867500+05	.1845000+04	25	2416AA	MANPLT	77P001
1210160014		.2475250+06	.7865000+05	.1870000+04	25	2416AA	MANPLT	77P001
1210160015		.2471500+06	.7847500+05	.1890000+04	25	2416AA	MANPLT	77P001
1210160016		.2469750+06	.7840000+05	.1890000+04	25	2416AA	MANPLT	77P001
1210160017		.2496500+06	.7857500+05	.1630000+04	25	2416AC	MANPLT	77P001
1210160018		.2496250+06	.7792500+05	.1805000+04	25	2416AC	MANPLT	77P001
1210160019		.2495000+06	.7737500+05	.1860000+04	25	2416AC	MANPLT	77P001
1210160020		.2497000+06	.7710000+05	.1860000+04	25	2416AC	MANPLT	77P001
1210160021		.2497750+06	.7725000+05	.1800000+04	25	2416AC	MANPLT	77P001
1210160022		.2499000+06	.7720000+05	.1750000+04	25	2416AC	MANPLT	77P001
1210160023		.2490000+06	.7995000+05	.1680000+04	25	2416AA	MANPLT	77P001
1210160024		.2422750+06	.8195000+05	.1885000+04	25	2416AA	MANPLT	77P001
1210160025		.2465500+06	.8247500+05	.1915000+04	25	2416AA	MANPLT	77P001
1210160026		.2465000+06	.8280000+05	.1915000+04	25	2416AA	MANPLT	77P001
1210160027		.2466500+06	.8357500+05	.1930000+04	25	2416AA	MANPLT	77P001
1210160028		.2463500+06	.8327500+05	.1930000+04	25	2416AA	MANPLT	77P001
1210160029		.2449750+06	.8217500+05	.1905000+04	25	2416AA	MANPLT	77P001
1210170001		.2452000+06	.9102500+05	.1480000+04	25	2416AA	MANPLT	77P001
1210170002		.2456500+06	.9065000+05	.1470000+04	25	2416AA	MANPLT	77P001
1210170003		.2457500+06	.8832500+05	.1550000+04	25	2416AA	MANPLT	77P001
1210170004		.2455250+06	.8607500+05	.1700000+04	25	2416AA	MANPLT	77P001
1210170005		.2457500+06	.8607500+05	.1640000+04	25	2416AA	MANPLT	77P001
1210170006		.2458750+06	.8640000+05	.1635000+04	25	2416AA	MANPLT	77P001
1210170007		.2460500+06	.8707500+05	.1595000+04	25	2416AA	MANPLT	77P001
1210170008		.2440250+06	.9062500+05	.1595000+04	25	2416AA	MANPLT	77P001
1210170009		.2433000+06	.9350000+05	.1470000+04	25	2416AA	MANPLT	77P001
1210170010		.2580000+06	.8205000+05	.1770000+04	25	2416AC	MANPLT	77P001
1210170011		.2542000+06	.7770000+05	.1400000+04	25	2416AC	MANPLT	77P001
1210170012		.2542000+06	.7785000+05	.1440000+04	25	2416AC	MANPLT	77P001
1210170013		.2541500+06	.7800000+05	.1500000+04	25	2416AC	MANPLT	77P001
1210170014		.2541500+06	.7815000+05	.1570000+04	25	2416AC	MANPLT	77P001

LOCALE	IDENTIFICATION	X	Y	Z	TAG	SHEET	METHOD	REFER
1210170015		.2541500+06	.7850000+05	.1720000+04	25	2416AC	MANPLT	77P001
1210170016		.2550000+06	.7920000+05	.1870000+04	25	2416AC	MANPLT	77P001
1210170017		.2548500+06	.7885000+05	.1860000+04	25	2416AC	MANPLT	77P001
1210170018		.2546500+06	.7880000+05	.1830000+04	25	2416AC	MANPLT	77P001
1210170019		.2544500+06	.7870000+05	.1810000+04	25	2416AC	MANPLT	77P001
1210170020		.2510500+06	.7760000+05	.1470000+04	25	2416AC	MANPLT	77P001
1210170021		.2508750+06	.7755000+05	.1480000+04	25	2416AC	MANPLT	77P001
1210170022		.2506250+06	.7745000+05	.1550000+04	25	2416AC	MANPLT	77P001
1210170023		.2508000+06	.7775000+05	.1510000+04	25	2416AC	MANPLT	77P001
1210170024		.2509250+06	.7785000+05	.1560000+04	25	2416AC	MANPLT	77P001
1210170025		.2510000+06	.7782500+05	.1580000+04	25	2416AC	MANPLT	77P001
1210170026		.2510500+06	.7770000+05	.1540000+04	25	2416AC	MANPLT	77P001
1210170027		.2509500+06	.7770000+05	.1520000+04	25	2416AC	MANPLT	77P001
1210170028		.2511500+06	.7732500+05	.1485000+04	25	2416AC	MANPLT	77P001
1210170029		.2513500+06	.7732500+05	.1510000+04	25	2416AC	MANPLT	77P001
1210170030		.2515500+06	.7737500+05	.1600000+04	25	2416AC	MANPLT	77P001
1210170031		.2515000+06	.7752500+05	.1610000+04	25	2416AC	MANPLT	77P001
1210170032		.2518000+06	.7750000+05	.1590000+04	25	2416AC	MANPLT	77P001
1210170033		.2517500+06	.7722500+05	.1595000+04	25	2416AC	MANPLT	77P001
1210170034		.2520000+06	.7720000+05	.1580000+04	25	2416AC	MANPLT	77P001
1210170035		.2519250+06	.7742500+05	.1570000+04	25	2416AC	MANPLT	77P001
1210170036		.2521250+06	.7780000+05	.1585000+04	25	2416AC	MANPLT	77P001
1210170037		.2519750+06	.7780000+05	.1590000+04	25	2416AC	MANPLT	77P001
1210170038		.2526750+06	.7812500+05	.1590000+04	25	2416AC	MANPLT	77P001
1210170039		.2524750+06	.7742500+05	.1520000+04	25	2416AC	MANPLT	77P001
1210170040		.2503000+06	.7847500+05	.1580000+04	25	2416AC	MANPLT	77P001
1210170041		.2501000+06	.7855000+05	.1610000+04	25	2416AC	MANPLT	77P001
1210170042		.2496750+06	.7835000+05	.1720000+04	25	2416AC	MANPLT	77P001
1210170043		.2497250+06	.7800000+05	.1790000+04	25	2416AC	MANPLT	77P001
1210170044		.2501000+06	.7720000+05	.1700000+04	25	2416AC	MANPLT	77P001
1210170045		.2514750+06	.7780000+05	.1660000+04	25	2416AC	MANPLT	77P001
1210170046		.2516250+06	.7800000+05	.1680000+04	25	2416AC	MANPLT	77P001
1210170047		.2516500+06	.7832500+05	.1805000+04	25	2416AC	MANPLT	77P001
1210170048		.2518500+06	.7862500+05	.1840000+04	25	2416AC	MANPLT	77P001
1210170049		.2518000+06	.7915000+05	.1870000+04	25	2416AC	MANPLT	77P001
1210170050		.2524000+06	.7972500+05	.1850000+04	25	2416AC	MANPLT	77P001
1210170051		.2489000+06	.7970000+05	.1690000+04	25	2416AA	MANPLT	77P001
1210170052		.2489500+06	.7902500+05	.1820000+04	25	2416AA	MANPLT	77P001
1210170053		.2482500+06	.7992500+05	.1885000+04	25	2416AA	MANPLT	77P001
1210170054		.2488250+06	.8115000+05	.1900000+04	25	2416AA	MANPLT	77P001
1210170055		.2477500+06	.8140000+05	.1900000+04	25	2416AA	MANPLT	77P001
1210170056		.2477250+06	.8255000+05	.1920000+04	25	2416AA	MANPLT	77P001
1210170057		.2470250+06	.8265000+05	.1905000+04	25	2416AA	MANPLT	77P001
1210170058		.2606000+06	.9452500+05	.1705000+04	25	2416AC	MANPLT	77P001
1210170059		.2608250+06	.9557500+05	.1755000+04	25	2416AC	MANPLT	77P001
1210170060		.2600500+06	.9600000+05	.1710000+04	25	2416AC	MANPLT	77P001
1210170061		.2604000+06	.9627500+05	.1635000+04	25	2416AC	MANPLT	77P001
1210170062		.2592750+06	.9110000+05	.1735000+04	25	2416AC	MANPLT	77P001

CHAPTER A-II

DYNAMIC ANALYSIS OF SLOW FINITE DEFORMATION IN INHOMOGENEOUS VISCOUS SOLIDS : A CONTRIBUTION TO THE THEORY OF CONGLOMERATE DEFORMATION

A. THE CONTINUUM MECHANICS APPROACH TO STRUCTURAL GEOLOGY

1. Introduction

Continuum mechanics is the mechanics of extended bodies. In contrast to Newtonian mechanical tradition, where the central idea is that of the mass point, the central concept in Eulerian mechanical tradition is the material continuum, infinite in extent and indefinitely divisible. Continuum mechanics, in other words, adopts the *field*, rather than the *corpuscle*, as its basic model of nature. It thus shares a common basis with other branches of *classical field theory* (Truesdell & Toupin, 1960).

Continuum mechanics provides a unified theoretical basis for a number of previously distinct and more or less specialised disciplines, all concerned with the mechanical properties and behaviour of various natural and artificial materials. A more generalised science of material behaviour has resulted, in which different modes of response to various thermodynamic fields are treated with due regard for their possible interconnections. The continuum mechanics approach, as it has developed recently in applied Earth sciences such as soil and rock mechanics, thus gradually supersedes the idealized plastic or elastic models of behaviour on which they were originally founded. Recent developments in structural geology can be viewed in this general scientific context. For example, the restatement of the formal theory of finite homogeneous strain as the basis of structural geology (Ramsay, 1967) and the extension of this development to include the formal theory of finite inhomogeneous deformation (Ramsay & Graham, 1970; Hobbs, 1971), is of fundamental importance for the understanding of the purely kinematic aspects of rock deformation. Likewise, the analysis of the buckling behaviour of layered systems in visco-elastic or viscuous fluid

(iv) *Initial and boundary conditions*, which describe the geometric, kinematic and dynamic configurations and/or constraints relevant to the particular system being analysed.

The element (i) and (ii) are completely general, whereas (iii) and (iv) are specific to particular materials and particular problems, respectively.

2. Constitutive equations for crustal rock

a. Review of theory

Geological phenomena such as folding and "shearing" (large, finite, ductile deformation) of rock in widespread parts of the Earth's crust, testify to the ability of solid rock to behave plastically over long periods and to flow or "creep" at very slow rates. The first problem, in attempting a quantitative physical analysis of these phenomena, is the specification of constitutive relationships for rock under the various pressure and temperature conditions which prevail in the crust. In view of the chemical and physical variability of crustal materials and the variability of crustal physical conditions, this is a formidable task. In fact, there may be no unique constitutive equation describing rock behaviour under all conditions, but rather a set of fields in stress-temperature space (the "deformation map" concept : Stocker & Ashby, 1973), in which one kind of deformation mechanism dominates all others and hence confers its own characteristic equation of state on the rock under certain specific conditions.

The investigation of these problems falls mostly within the scope of experimental structural geology and involves the deformation of rocks and minerals in the laboratory under conditions of elevated pressure and temperature at very slow strain rates (Price, 1975; Heard, 1976). It also entails the microscopic comparison of deformation structures and fabrics in naturally and experimentally deformed rocks to check if the mechanisms have been the same in each case (White, 1973). Field structural analysis and the quantitative analysis of macroscopic tectonic phenomena cannot, however, be suspended pending the outcome of experimental and laboratory investigations. It is necessary,

therefore, to begin with relatively simple assumptions about constitutive relationships in rock and to modify or sophisticate these where comparison between theory and observational or experimental evidence requires it.

The most convenient starting assumption about the rheological constitution or flow behaviour of crustal rocks is that there is a linear relationship between viscous stress (i.e. the deviatoric or non-hydrostatic part of the stress tensor) and strain or deformation rate; that rock behaves, in the long-term, as an ideal isotropic Newtonian fluid. The constitutive equation for a general Newtonian fluid is thus

$$\tau_{ij} = K_{ijpq} D_{pq} \tag{1}$$

where τ_{ij} is the *viscuous stress tensor*, Dpq is the *rate of deformation tensor*, and the constants K_{ijpq} are *viscosity coefficients* (Mase, 1970). Using the above equation and the customary resolution of the *stress tensor* σ_{ij} into viscous stress and hydrostatic pressure components

$$\sigma_{ij} = -p\delta_{ij} + \tau_{ij} \tag{2}$$

where p is the *pressure* and δ_{ij} is the *Kronecker delta*, it can be shown that the constitutive equation for an *isotropic homogeneous Newtonian* fluid is

$$\sigma_{ij} = -p_{ij} + \lambda^{*}\delta_{ij} D_{kk} + 2\mu^{*} D_{ij} \tag{3}$$

(Jaeger, 1969; Mase, 1970), where λ^{*} and μ^{*} are *viscosity coefficients* analogous to *Lame's parameters* of elasticity theory. The *mean normal stress* in the fluid is given by

$$\frac{\sigma_{ii}}{3} = -p + \frac{3\lambda^{*} + 2\mu^{*}}{3} D_{ii} = -p + \kappa^{*} D_{ii} \tag{4}$$

where $\kappa^{*} = \lambda^{*} + \frac{2}{3}\mu^{*}$ is the *coefficient of bulk viscosity*. *Deviator components* of stress and rate of deformation are defined (Mase, 1970) as

$$s_{ij} = \sigma_{ij} - \delta_{ij}\frac{\sigma_{kk}}{3} \tag{5}$$

and

$$D'_{ij} = D_{ij} - \delta_{ij}\frac{p_{kk}}{3} \tag{6}$$

respectively. Using these equation (3) becomes

$$s_{ij} + \delta_{ij}\frac{\sigma_{kk}}{3} = -p\delta_{ij} + \delta_{ij}\left(\lambda^* + \frac{2\mu^*}{3}\right)D_{kk} + 2\mu^* D'_{ij} \qquad (7)$$

In view of equation (4), this is accordingly expressed by the pair of equations

$$s_{ij} = 2\mu^* D'_{ij} \qquad (8)$$

$$\sigma_{ii} = -3p + 3\kappa^* D_{ii} \qquad (9)$$

the first of which relates shear effects in the fluid and the second of which gives the volume relationship since D_{ii} is the *dilatation rate*. In the case of an *incompressible* Newtonian fluid, the additional constraint that $D_{ii} = 0$ exists. A constitutive equation of the form of equation (8) can be shown to apply to a polycrystalline aggregate such as rock if, from a microscopic point of view, the dominant mechanism of slow deformation is a form of intracrystalline *diffusion creep* or diffusion-accommodated *grain-boundary sliding* (Elliott, 1973; Stocker & Ashby, 1973). For this type of creep, the rate of deformation is given by

$$D_{ij} = A\,\frac{D_e^* G V^*}{kT\ d^2}\left\{\frac{s_{ij}}{G}\right\} \qquad (10)$$

Nabarro, 1948; Herring, 1950; Raj & Ashby, 1971) where in addition to those quantities already defined above

- D_e – effective diffusivity (diffusion coefficient)
- G – elastic shear modulus of medium
- k – Boltzmann's constant
- T – absolute temperature
- V^* – atomic or molecular volume of diffusing species
- d – grain diameter
- A – constant having a value of 21, being a function of source and sink geometry of diffusing lattice vacancies

The quantity (s_{ij}/G) in the above equation is the "normalized" deviator stress.

The two constraints implicit in the derivation of this equation are:

(i) grains must individually suffer the same shape change as the bulk polycrystalline aggregate;

(ii) grains may not change their neighbours.

When these constraints are relaxed (Ashby & Verrall, 1973), another form of diffusion-accommodated grain-boundary sliding becomes possible, which appears to be the phenomenon underlying "superplasticity" in metals (Stocker & Ashby, 1973, p.396). The creep rate equation for this second sort of diffusion flow is the same as equation (10) to a first approximation, but the constant $\mathring{A}$ is about 100 instead of 21, i.e. the flow goes somewhat faster (Ashby & Verrall, 1973; Stocker & Ashby, 1973).

If, however, intracrystalline mechanisms of plastic flow involving the glide or climb of *dislocations* are dominant, then the macroscopic flow behaviour of the polycrystalline material is *non-Newtonian* (also called *Stokesian*: Mase, 1970). Theoretical analysis based on different models of possible dislocation interactions and experimental evidence, suggest a constitutive equation having the form

$$D_{11} = A \frac{D_v^* G b}{kT} \left\{ \frac{\sigma_{11}}{G} \right\}^n \qquad (11)$$

(Mukherjee, Bird & Dorn, 1969; Stocker & Ashby, 1973) where, in addition to quantities already defined,

D_{11} - tensile or compressional strain rate
σ_{11} - applied axial or normal stress
D_v^* - volume or lattice diffusivity
b - Burger's vector
A - constant parameter
n - dimensionless power.

Dislocation creep mechanisms thus lead to a power-law relationship between strain rate and stress. The constant parameters A and n are probably temperature and pressure independent (Stocker & Ashby, 1973). For *subgrain creep*, a variety of dislocation creep, n has a value of 3 (Weertman, 1970).

b. Argument for linear flow law in low-grade, upper-crustal rock.

For the present purposes, it will be assumed that a constitutive relationship of the general form of equation (3) or equations (8) and (9) characterises the flow behaviour of rock in the upper parts of the Earth's crust, i.e. the upper 15 km or so. The main reasons for this assumption are:

(i) abundant microscopic evidence, in the form of microfractures and displacements, for "cataclastic flow" (Paterson, 1969) and grain-boundary sliding mechanisms in the ductile deformation of upper-crustal, sedimentary and low-grade metamorphic rocks;

(ii) much petrographic evidence, dating back to Sorby's (1863, 1879) first descriptions, for the role of pressure solution phenomena in upper-crustal rock deformation which, as Elliott (1973) has shown, involves a form of diffusion creep mechanism (called "fluid phase transport" by Stocker & Ashby, 1973);

(iii) seismological and rock-mechanical evidence for the occurrence of significant "dilatancy" associated with strains in rock masses adjacent to large earthquake faults (Scholz, Sykes, Aggarwal, 1973), which, in turn, implies the contemporary occurrence of widespread cataclastic flow and grain-boundary sliding in large volumes of rock in the upper-crust.

There seems, therefore, to be no immediate justification for challenging the phenomenological basis from which the Biot-Ramberg and Gay theories of rock deformation, for example, proceed. Despite there being also microscopic evidence for the operation of dislocation creep mechanisms in upper-crustal rocks, Newtonian flow mechanisms are to be preferred.

Rutter (1976) has shown, on deformation maps for calcite and quartz (*op. cit.*, Figs. 8 & 9) that, at temperatures below 400-600°C and differential stress levels below 100 MPa, pressure solution is far more competitive in producing high strain rates than Coble (grain-boundary diffusion) or dislocation creep mechanisms in these minerals. Strain-rate contours in the pressure solution field have a sinusoidal shape with a minimum at about 200°C in the case of cal-

cite and about 400°C in the case of quartz, related to changes in concentration of the diffusing molecular species in the intercrystalline fluid phase and the solubility of the solid phase with changes in pressure and temperature. "Most geologists would agree that textures characteristic of diffusive mass transfer by pressure solution are common in rocks deformed at temperatures up to about 400°C and that crystal plastic flow textures dominate at high temperatures" (*op. cit.*, p.213).

This is contrary to a view which has been expressed, that temperatures of at least 400-500°C and confining pressures of 300-400 MPa are required for rocks to deform by steady-state viscous (or pseudoviscous) flow at reasonable geological strain rates (e.g. Gay & Fripp, 1976) and the concept that rocks at deep crustal levels (> 20 km) may behave as Newtonian fluids while upper-crustal rocks do not. Penetrative cleavage and finite strain, almost entirely as a result of massive pressure solution, is observed to become a dominant feature in rocks which have reached metamorphic temperatures ⩾ 250°C (Elliott, 1973, 1976). With normal and orogenic geothermal gradients these temperatures are reached between depths of 5 and 10 km. Conditions favouring diffusive mass transfer deformation mechanisms are likely to persist at least to depths of 15-20 km.

The constitutive equation for "fluid phase transport" derived by Stocker & Ashby (1973) is :

$$D_{ij} = A \frac{C_o D_l}{kT} \frac{G V^* f\{s_{ij}\}}{d^2 \{G\}} \qquad (12)$$

where: A – constant (usually 21)

C_o – concentration of diffusing species in fluid (liquid)

D_l – diffusivity of dissolved species in fluid

V^* – volume of the diffusing species

f – volume fraction of fluid phase

G – elastic shear modulus of solid phase

d – grain diameter of solid phase

T – temperature (°K)

k – Boltzmann's constant

The derivation assumes that there is no interfacial barrier to dissolution of the solid phase in the liquid one. For pressure solution at low stresses (σ_{11} < 30 MPa), Rutter (1976) has derived an approximate flow law

$$D_{11} = \frac{A\ C_o\ D_b\ \ w\ V^*\ \sigma_{11}}{\rho d^3 \qquad kT} \tag{13}$$

where: A – constant (=32)

D_b – grain boundary diffusivity

w – effective width of grain boundary

ρ – density of solid phase

and other symbols have their usual meanings.

It is assumed, therefore, that sedimentary and metasedimentary rocks in the upper-crust behave as Newtonian fluids with effective viscosities, μ^*, given by an expression such as

$$\mu^* = \frac{kTd^2}{22C_oD_lV^*f} \tag{14}$$

after Stocker & Ashby (1973). For a limestone with average grain diameter, d, equal to 1 mm, deforming at 200°C (473°K) by pressure solution through an intergranular fluid phase comprising 5% by volume (f = 0,05), the viscosity coefficient, μ^*, is found to be about 1,5 x 10^{18} Pa.s if values of 10^{-6}, 10^{-9} $m^2\ s^{-1}$ and 10^{-29} m^3 are assumed for C_o, D_l and V^*, respectively. This falls within the accepted range of rock viscosities derived from observations of surface or near-surface rock creep phenomena (deformation of pillars in mines, sagging of marble slabs in cemetries, cf. Biot, 1961, p.1607).

c. Problems

Diffusivity D^* (i.e. D_e^*, D_v^*, D_b^* or D_l^*) is temperature-dependent according to the relationship

$$D^* = D_o^* \exp\ (-H^*/kT) \tag{15}$$

where D_o^* is a particular diffusion constant and H^* is an activation enthalpy. This means that rock viscosity decreases markedly with an increase in temperature

T. As equation (14) shows, μ^* is also strongly related to the mean grain size, d, in the rock polycrystal, so that a decrease in grain size involves a marked decrease in viscosity. It is obvious then that a progressive decrease of grain size and a progressive increase in temperature *during* deformation - the first arising from a possible combination of pressure solution and cataclastic phenomena and the second arising from the operation of energy-dissipative flow in a medium of very low thermal conductivity - constitutes a significant source of thermo-mechanical "feedback" in the deforming system (Gruntfest, 1963; Griggs & Baker, 1969; Froidevaux & Schubert, 1975). In other words, the *constitutive relationships in rock do not remain unaltered during the deformation process*, but vary via the abovementioned thermal and microstructural couplings, with the actual course and rate of deformation.

The qualitative flow behaviour of rock is thus significantly different from that of most fluids with which we are familiar. There is also an obvious progression in most deformed rocks from an initial, more or less isotropic state to a final highly anisotropic or "foliated" state. This involves the use of the more general form of constitutive equation (1), in which there are many more coefficients of viscosity corresponding to the components of the fourth-order tensor K_{ijpq}. These facts inhibit the qualitative application of familiar fluid analogies to rock deformation and also impose important restrictions on the capability of classical techniques in mathematical analysis for realistically handling problems of ductile deformation in rock. However, new techniques in computer science offer a means of circumventing these restrictions and the application of one of them is illustrated below.

B. THE FINITE-ELEMENT METHOD

1. Evolution and general principles

In engineering, the alliance of matrix algebra techniques with the facilities for rapid automatic data-processing by digital computers resulted in the development of a method commonly known as *structural stiffness analysis* (cf. Livesley, 1964). Man-made structures can be visualised as an assemblage of structural elements interconnected at a discrete number of *nodal points*. The essence of the method is that, for each element, nodal forces are related to nodal displacements by a *stiffness matrix* and from the set of load-displacement equations for individual members, the load-displacement characteristics of the assembled structure are constructed according to the requirements of displacement compatibility and joint equilibrium. There is a further classification of the method according to which of the latter conditions is satisfied first. The more common variant, in which the compatibility conditions are used first, gives rise to equations of joint equilibrium and is therefore called the *equilibrium* or *displacement approach*; in this, the displacements of the joints are the basic unknowns of the problem. The converse is known as the *compatibility* or *force approach* (Livesley, 1964, p.11-12).

In an elastic or fluid continuum, the true number of interconnection points is infinite. The *finite-element method* (cf. Zienkiewicz, 1969, 1976), which has evolved from the technique outlined above, obviates this problem by assuming the continuum to be divided up into cells or *elements* interconnected only at a finite number of points or *nodes* at which the forces, statically representative of the distributed stresses on the element boundaries, are imagined to act. In the most common formulation of the method for elastic problems, the displacement of the nodes are the basic unknowns of the problem (Zienkiewicz, 1969, p.12) and the displacements - and hence the strains - within each element are related to these by *displacement functions*, the simplest of which are linear polynomials expressing homogeneous strain within each cell. Because adjacent elements share common nodes, the choice of linear displacement functions for each cell ensures that no "holes", tears or infinite strains

develop along the boundaries between them; thus the problem of satisfying strain compatibility requirements is solved, although the strains within each element are discrete.

The next important condition, that of stress equilibrium, is tackled by making use of a well-known principle of minimum potential energy (Sokolnikoff, 1956, p.384-385; Zienkiewicz, 1969, p.18-19). This states simply that, in an elastic body, of all the displacement configurations satisfying the requirements of compatibility and the prescribed boundary conditions, the one which by satisfying equilibrium actually takes place, is the one which makes the potential energy of the body assume a stationary (minimum) value.

Obviously a body divided up into finite elements is thereby limited in its response to prescribed boundary displacements or stresses and so will not reach the true energy minimum of the continuum which it is supposed to approximate. In general, though, it will converge on this minimum with increasing fineness of subdivision, as more nodes - and hence more degrees of freedom - are added to it. For situations in which solutions by exact analytical methods are not possible, an assessment of the accuracy of the finite-element technique requires an empirical study of this convergence for two or more stages of element subdivision. Ideally the finest possible mesh of elements should be taken, but in practice a balance usually has to be struck between the requirements of accuracy and those of computational economy.

2. Outline of the present technique

The present study has made use of the modified technique of finite-element analysis developed by Dieterich & Onat (1969). The essence of their method may be summarised in the following points:

(i) a viscous body is approximated by a model composed of a finite number of triangular elements;

(ii) it is assumed that each element deforms homogeneously, so that the velocity distribution within each at any time is a linear function of rectilinear co-ordinates, X and Y;

(iii) the velocity field for the whole system of elements in

the approximating body is defined in terms of the velocity components of the nodes;

(iv) these nodal velocities are determined from linear algebraic equations derived from a minimum principle to which the body is subject at all times, namely, that the velocity field minimises the rate of energy dissipation;

(v) this velocity field is allowed to operate on the system of elements for a small time increment;

(vi) since individual cells deform homogeneously, after each time increment of deformation the new configuration is still composed of the same number of triangular cells;

(vii) the procedure above is repeated many times, so that a finite deformation is built up by large numbers of increments of strain.

It is therefore evident that the technique is a combination of the finite-element method with a finite-difference procedure.

In solving for nodal velocities, instead of nodal displacements as in the usual elastic formulations of finite-element analysis, this method is based on a direct analogy with the elastic behaviour of solids. The constitutive equation used is

$$\sigma_{ij} = 2\mu^{*} D_{ij} + \lambda^{*} \delta_{ij} D_{kk} \qquad (16)$$

where the symbols represent quantities already defined in the previous section of this chapter. It was originally stated (*op. cit.*, 2082) that equation (16) represents a compressible Newtonian fluid for finite values of λ^{*}. Comparison with equation (3) above, shows that this is clearly not the case. It has been pointed out (Thompson & Mack, 1970) that equation (16) actually represents a *collapsible linearly viscous* (Newtonian) *fluid*. Multiplication of (16) by the Kronecker delta, δ_{ij}, yields the result

$$D_{kk} = \sigma_{kk} \; / \; (2\mu^{*} + 3\lambda^{*}) \qquad (17)$$

indicating that the dilation rate is directly proportional to the mean normal stress. Such a material shrinks continuously toward zero volume under the steady application of compressive hydrostatic stress.

It is considered (Thompson & Mack, 1970) that this important qualitative

behavioural difference between a Newtonian fluid and a collapsible material makes a direct application to geophysical situations involving high hydrostatic pressures questionable. In geophysical situations, however, the values of the viscosity coefficients, μ^* and λ^*, are also high, so the effect of equation (17) is quantitatively small. Results of the present study, moreover, reveal that the property of collapsibility introduces effects into the numerical experiment which appear to realistically simulate those of pressure solution in rocks. The possibility that upper-crustal rocks may be formally described as collapsible Newtonian fluids where pressure solution mechanisms are dominant in deformation is considered after discussion of these results.

C. APPLICATION OF THE FINITE-ELEMENT METHOD

1. Brief review of tectonic applications

The first application of the finite-element method to the study of tectonic problems in geology was made by Dieterich & Onat (1969), who laid out the theory of the technique for slow finite deformation in plane strain of viscous materials and illustrated it with two simple examples of some geological relevance. The method was subsequently applied to the analysis of stresses in folding layers (Dieterich & Carter, 1969), to the simulation of cleavage development in folded rocks (Dieterich, 1969) and to the study of the finite strain development of single- and multi-layer fold structures with viscosity contrasts (Dieterich, 1970). Another introduction to the geological application of the method has been given, for elastic and viscous problems, by Stephansson & Berner (1971), who illustrated their paper with examples drawn from widely different tectonic scales, showing how the finite-element method could be applied in geotectonics to the study of isostatic adjustment, sea-floor spreading and the development of mid-ocean ridge structures. Similarly, Bott & Dean (1972) used an elastic finite-element model to study crustal stresses associated with young continental margins. Crustal deformation caused by an underthrusting oceanic plate has been analysed using the finite-element method by Shimazaki (1974). Further applications to fold problems are illustrated by Stephansson (1976) and a general review of the method and its varied applications in geophysical problems is given by Zienkiewicz (1976).

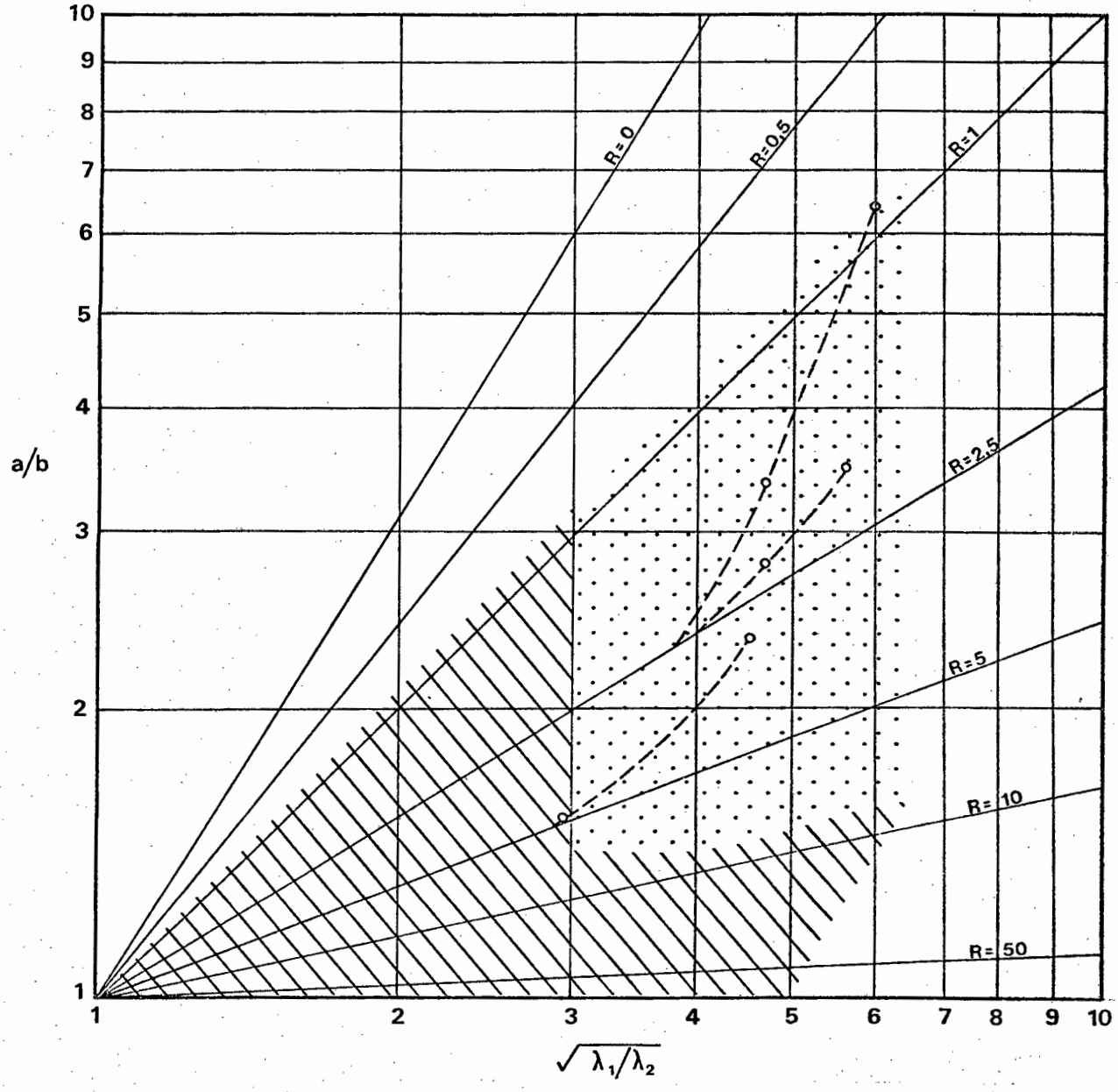

Figure AII-1. Graph of inclusion shape versus bulk strain for various values of viscosity contrast R (after Gay, 1968b) showing field (hachured) in which ethyl cellulose experiments confirmed theoretical predictions and also the field (stippled) in which experimental results differed from the theory.

2. Application to aspects of conglomerate deformation theory

a. Theoretical background

The present application of the finite-element method concerns two aspects of conglomerate deformation. These are:

(i) the change of shape of a viscous ellipsoidal inclusion embedded in a slowly deforming matrix of different viscosity;

(ii) the pattern of heterogeneous strain produced in the matrix around such an inclusion.

At the time that the present computer experiments were carried out, the only available treatment of these questions was that of Gay (1968a, b), who had derived the following relationship between the axial ratio of a cylindrical inclusion with an elliptical cross-section (a/b, where a represents the length of the major semi-axis and b, the minor semi-axis), the viscosity contrast ($R = \mu_i/\mu_m$, where μ_i is the viscosity coefficient of the inclusion and μ_m is the viscosity coefficient of the matrix) and a pure shear plane strain experienced by the inclusion-matrix system as a whole ($\sqrt{\lambda_1/\lambda_2}$, the square root of the ratio of principle quadratic extensions, corresponding to the axial ratio of the plane strain ellipse):

$$ln\ (a/b) = 5/(2R+3)\ ln\ (\sqrt{\lambda_1/\lambda_2}) \qquad (18)$$

In the theoretical model, the principal axes of pure shear strain coincide with the major and minor semi-axes of the elliptical section normal to the cylindrical axis.

A graph illustrating the results of this theory for an initially circular, cylindrical inclusion (Fig. 1*), shows the portions of the deformation field for which experimental verification, using ethyl cellulose-in-benzanol models, was attempted (Gay, 1968b). It is evident from this that divergence from prediction, generally toward greater particle deformation, was experienced at bulk strains ($\sqrt{\lambda_1/\lambda_2}$) greater than about 4 and that the theory could not be verified for bulk strains greater than 6.

Subsequent to the present computer experiments, the above theoretical equation was shown to be incorrectly derived (Bilby, Eshelby & Kundu, 1975;

---

* Note: Figure and table numbers in text are abbreviated so that e.g. Fig.1 refers to Fig. AII-1, Table 2 refers to Table AII-2, etc.

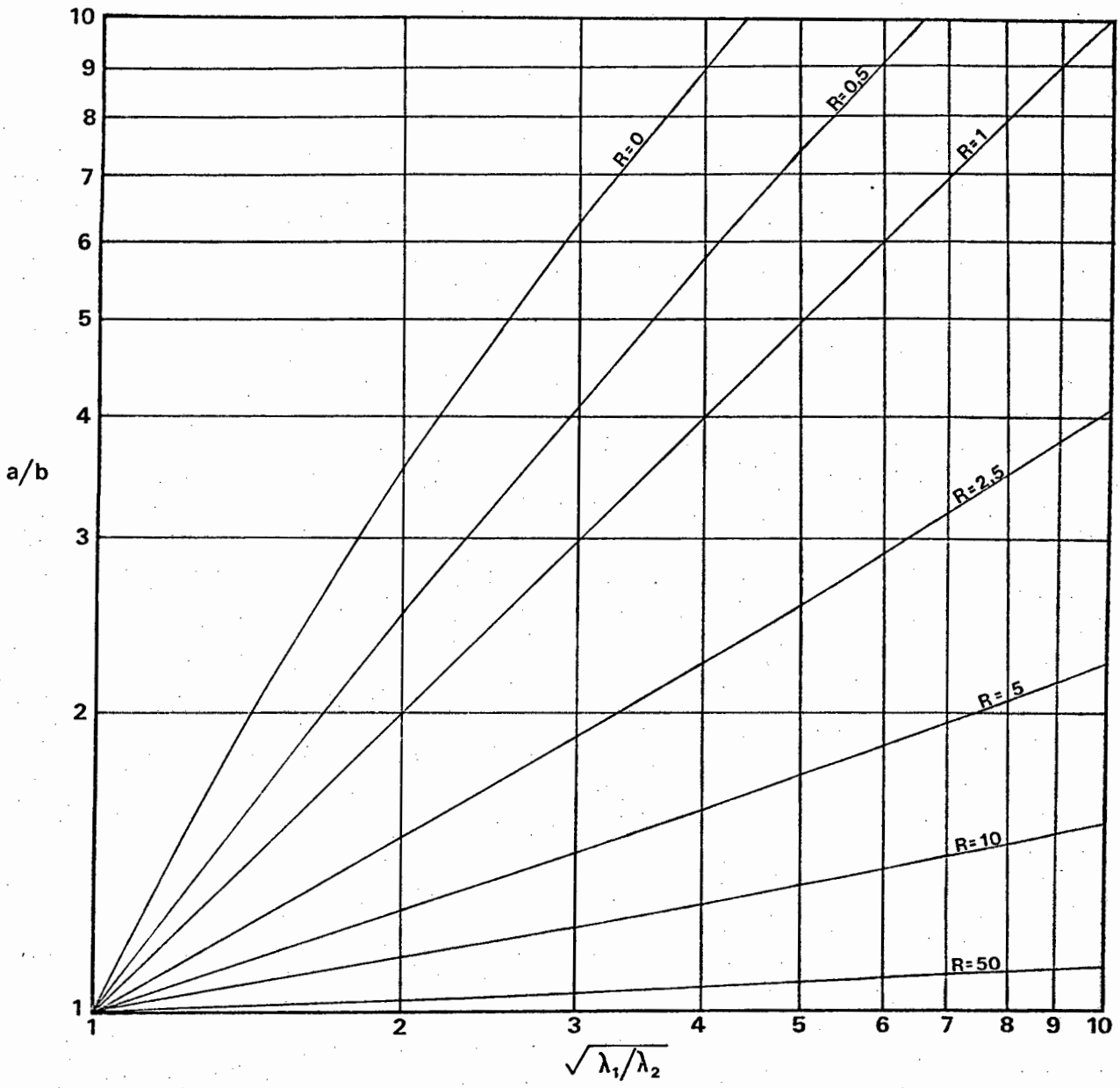

Figure AII-2. Graph of inclusion shape versus bulk strain for various values of viscosity contrast R (after Bilby *et al.*, 1975).

Bilby & Kolbuszewski, in discussion of Gay & Fripp, 1976). Deformation of an elliptical cylinder is instead described by the equation

$$ln(a/b)+(R-1)\left[\left\{(a/b)-1\right\}/\left\{(a/b)+1\right\}\right]=ln(\sqrt{\lambda_1/\lambda_2}) \qquad (19)$$

(Bilby *et al.*, 1975; Gay, 1976). The predictions of this theory for a range of low to moderate strains ($1<\sqrt{\lambda_1/\lambda_2}<10$) are illustrated in Fig. 2 . Comparing this with Fig. 1 , it can be seen that the difference between curves based on the two theories is rather slight for deviatoric strains less than about 10.

In the following section, the results of a set of finite-element experiments designed to test the original theory (Gay, 1968a) are described and thereafter comparisons of these results with the new correct theory are made.

b. The model configuration

The basic geometrical model adopted for the testing of that part of the theory dealing with the pure shear deformation of a single elliptical particle with its axes parallel to the strain axes (Gay, 1968a, p.215-218), was that of a circular cylinder, 2 cm in diameter, embedded in the centre of a rectangular "deformation box" measuring 24 cm along its Y-axis by 18 cm along its X-axis (see Fig. 3). The model is divided up into finite-elements of triangular shape in the manner indicated in Figs.3 and 4. Element size was so graded as to become finer towards the centre of the box, with the finest mesh occurring on either side of the particle-matrix interface, where the maximum gradients of strain were expected.

Because of geometrical symmetry, it is necessary to consider only one quarter of the model outlined above, which is a significant computational economy. A co-ordinate system centred on the particle was set up and the quadrant of positive X and positive Y was chosen for the finite-element study. Along the "internal" boundaries, however, cells from adjacent quadrants were included to ensure symmetry of deformation across the X = 0 and Y = 0 axes (see Fig. 3). In the computer routine, the co-ordinates of each node in the approximating body of finite-elements are generated automatically by the subroutine COORDS.

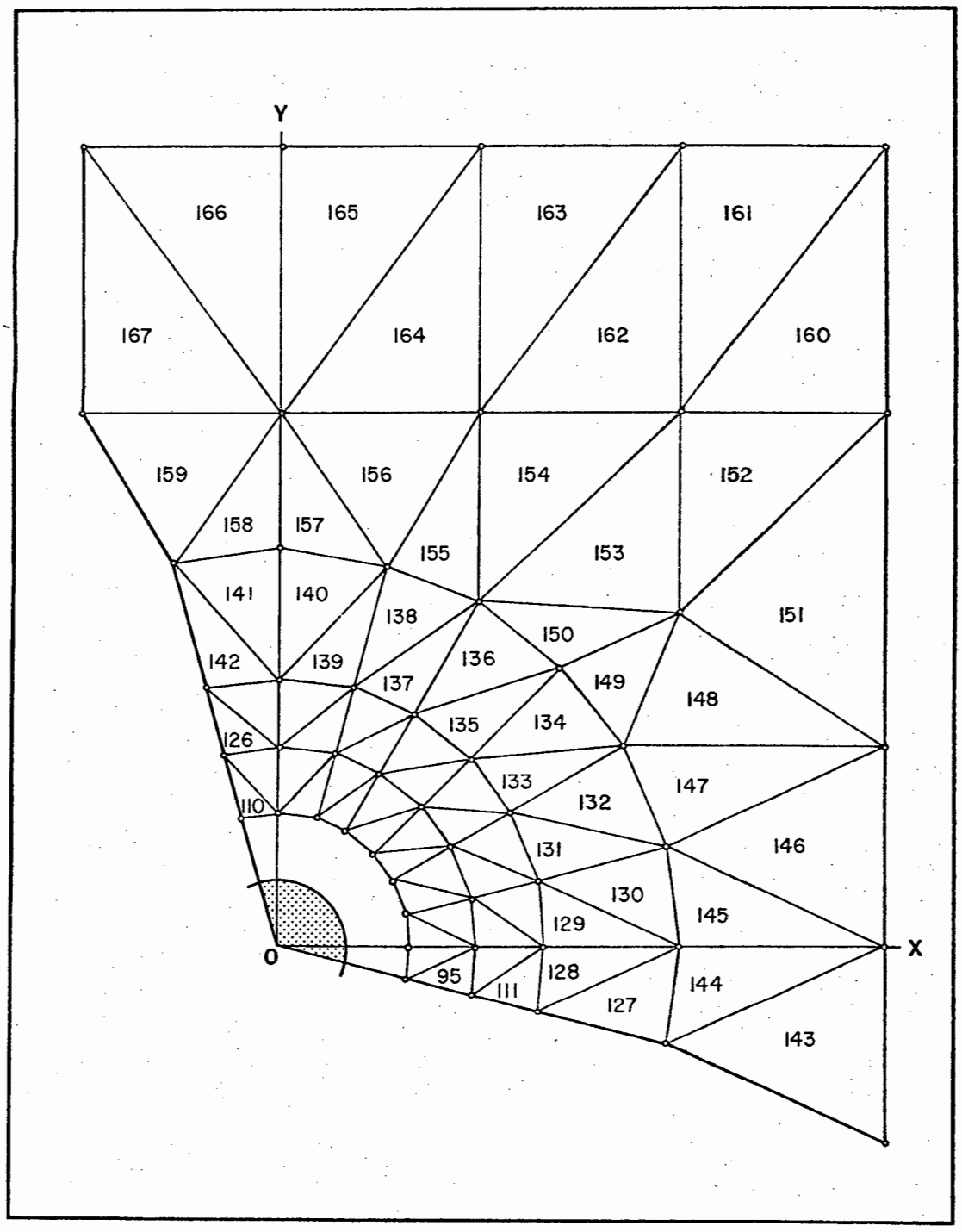

Figure AII-3. The present finite element model of a more viscous inclusion (stippled) surrounded by a less viscous matrix in a rectangular deformation box.

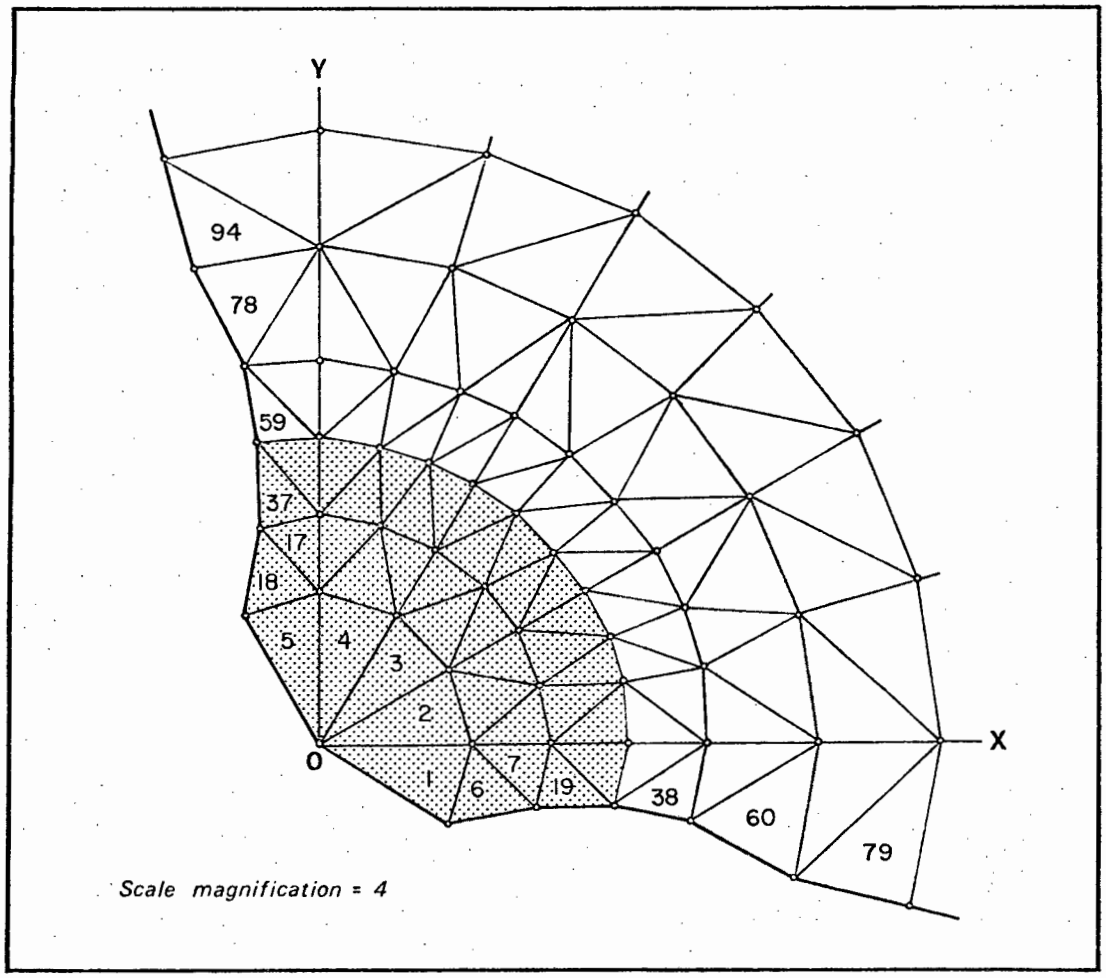

Figure AII-4. Detail of the interior part of the finite element model magnified four times to show the node and cell structure close to the inclusion-matrix interface.

c. Material properties

Following Dieterich & Onat (1969), the body described above was considered to be composed of viscous fluids obeying the constitutive law

$$\sigma_{ij} = 2\mu^* D_{ij} + \lambda^* \delta_{ij} D_{kk} \qquad (16)$$

where σ_{ij} and D_{ij} are the tensors of stress and strain rate respectively and μ^* and λ^* are positive constants, directly analogous to Lamé's parameters of elasticity theory (cf. Jaeger, 1969, p.56). This represents a *collapsible* Newtonian fluid (Thompson & Mack, 1970).

It should be noted here that the theory is concerned with ideally *incompressible* viscous fluids (Gay, 1968a, p.230). In the present study the ratio λ^*/μ^*, governing the degree of compressibility of the material (Dieterich & Onat, 1969, p.2082), was maintained at a value of 10 for all the results reported below. This gives a value of 0,4545 for ν, the Poisson's ratio equivalent in a fluid: a completely incompressible fluid has $\nu = 0{,}5$ exactly. It was found that, under the present method of finite-element analysis, it is not possible to use even greater values of λ^*/μ^* to approach ideal incompressibility even more closely, since in practice it appears that the technique begins to break down as λ^*/μ^* approaches and exceeds a value of about 100.

In the series of computer experiments CE4A-CE4F, the *matrix* (the set of elements external to the 37 cells of the *particle* clustered about the origin of the co-ordinate system) was assigned values of 10^{17} and 10^{18} Pa.s for μ^* and λ^* respectively. The value of 10^{17} Pa.s (10^{18}P) is deemed to be a reasonably realistic "geological" shear viscosity for a relatively incompetent rock (Biot, 1961, p.1067-1068). For values of crustal deviatoric stress less than or equal to about 200 MPa (which is considered to be above the likely maximum), the above viscosity yields strain rates of about $10^{-9}s^{-1}$ or less.

The *viscosity contrast*, R, in each experiment was obtained by assigning appropriate viscosity constants of equal or greater value to the 37 cells making up the particle. Thus μ^* for the particle varied between 10^{17} Pa.s for R = 1 in CE4A and 10^{20} Pa.s for R = 10^3 in CE4F. It may be noted that, in the present study, verification of the theory for values of R between 0 and 1

TABLE AII-1

INPUT PARAMETERS AND TECHNICAL DETAILS OF CE4 SERIES EXPERIMENTS

CE number	viscosity parameters: inclusion μ^* VMU(1) (Pa s)	inclusion λ^* VLA(1) (Pa s)	matrix μ^* VMU(2) (Pa s)	matrix λ^* VLA(2) (Pa s)	$\frac{\lambda^*}{\mu^*}$	viscosity contrast R	longitudinal strain rate STRATE (s^{-1})	time increment TIME (s)	D.I.	computer: CPU time (s)	computer: TYPE†
	($\times 10^{17}$)	($\times 10^{18}$)									
CE4A	1	1	10^{17}	10^{18}	10	1	10^{-10}	10^8	100	937,975	CDC 6400
CE4B	2,5	2,5	10^{17}	10^{18}	10	2,5	10^{-10}	10^8	100	409,808	CDC 6600
CE4C	5	5	10^{17}	10^{18}	10	5	10^{-10}	10^8	100	408,946	CDC 6600
CE4D	10	10	10^{17}	10^{18}	10	10	10^{-10}	10^8	100	948,671	CDC 6400
CE4E	50	50	10^{17}	10^{18}	10	50	10^{-10}	10^8	100	946,573	CDC 6400
CE4F	1000	1000	10^{17}	10^{18}	10	10^3	10^{-10}	10^8	100	412,547	CDC 6600
CE4G	25	25	10^{18}	10^{19}	10	2,5	10^{-10}	$0{,}25\times 10^8$	100	542,161	UNIVAC 1106
CE4H	25	25	10^{18}	10^{19}	10	2,5	10^{-10}	10^8	200	1081,525	UNIVAC 1106

† Computer installation at University of London Computer Centre : CDC 6600 and CDC 6400

Computer installation at University of Cape Town Computer Centre : UNIVAC 1106

D.I. Deformation increments

was not attempted.

d. Kinematic conditions

As can be seen in Fig. 3, the boundaries of the approximating body are of two types. There are two rectilinear "external" boundaries - i.e. boundaries to the deformation box as a whole - and two "internal" boundaries dividing the model from those parts of the deformation box which were excluded on the grounds of symmetry.

(i) External boundaries

The kinematic deformation conditions imposed on the external boundary nodes were those of pure shear (hyperbolic) flow, in which the velocity components u, v in the X and Y directions respectively, are given by

$$\begin{aligned} u &= \dot{\varepsilon}x \\ v &= \dot{\varepsilon}y \end{aligned} \qquad (20)$$

where $\dot{\varepsilon}$ is the rate of *natural* strain (Jaeger, 1969, p.68) and x and y are the actual co-ordinate values of a node. The X co-ordinate is therefore the compressional axis and the Y co-ordinate is the extensional axis.

In the CE4 series of computer experiments, a rate of longitudinal strain (D_{11}) of $10^{-10}s^{-1}$ was prescribed in the parameter code-named STRATE. This represents a very fast deformation rate in geological terms, since the *representative geological strain rate* is generally taken to be $3 \times 10^{-14}\ s^{-1}$. As the procedure of building up a finite strain is an incremental one, in which the prescribed strain rate is allowed to operate over successive small periods to time, Δt, an idea of the speed of this deformation can be got by considering the total time taken to deform the model to an overall or bulk strain with ellipse axial ratio of about 7,32. Except in CE4G, the small time-increment, Δt - code-named TIME, was prescribed as 10^8 seconds (about three years). This entails an incremental longitudinal strain, (e), of 1% per increment (STRATE x TIME). The abovementioned strain was built up in a total of 100 increments of 1% strain; that is, over a period of about 300 years.

The rate of natural strain is given by

$$\dot{\varepsilon} = \frac{ln(1 + e)}{\Delta t} \qquad (21)$$

In the computer programme, this quantity is used in subroutine PSHEAR to set up the boundary velocity components for the external nodes on the basis of *equation* (20).

Complete specification of the velocity components at the "external" boundaries of the model system has implications for the system of boundary forces that is required, in principle, to produce this special kind of kinematic constraint. Brief consideration of this question indicates that it requires the model to be reflected in these boundaries as an infinitely-repeating array. This in turn means that the system being modelled corresponds actually with *a conglomerate consisting of an infinite array of regularly-spaced inclusions in a matrix of infinite extent* and that the kinematic boundary conditions imposed on the system are those of pure shear at infinity. This aspect was not appreciated at the time the original set of computer experiments (CE4A to CE4F) was carried out and shows that the chief problem in any geological modelling is to obtain boundary conditions equivalent to those in the real system which it is intended to study (cf. Service & Douglas, 1973).

(ii) "Internal" boundaries

The only condition imposed upon the nodes along the "internal" boundaries of the system was that their velocity components should be a mirror-image of those of their counterparts in the positive quadrant across the X = 0 and Y = 0 axes. This was achieved by modification of the matrix of energy dissipation coefficients after its compilation for the whole system. An exception was the node point at the co-ordinate system origin, for which velocity components were specified to be zero in order to "pin" the model down in space, as it were. Thus conditions across the internal boundaries reflect the symmetry which allows a more economical analysis of little more than one quarter of the total model. In fact, the cells adjacent to

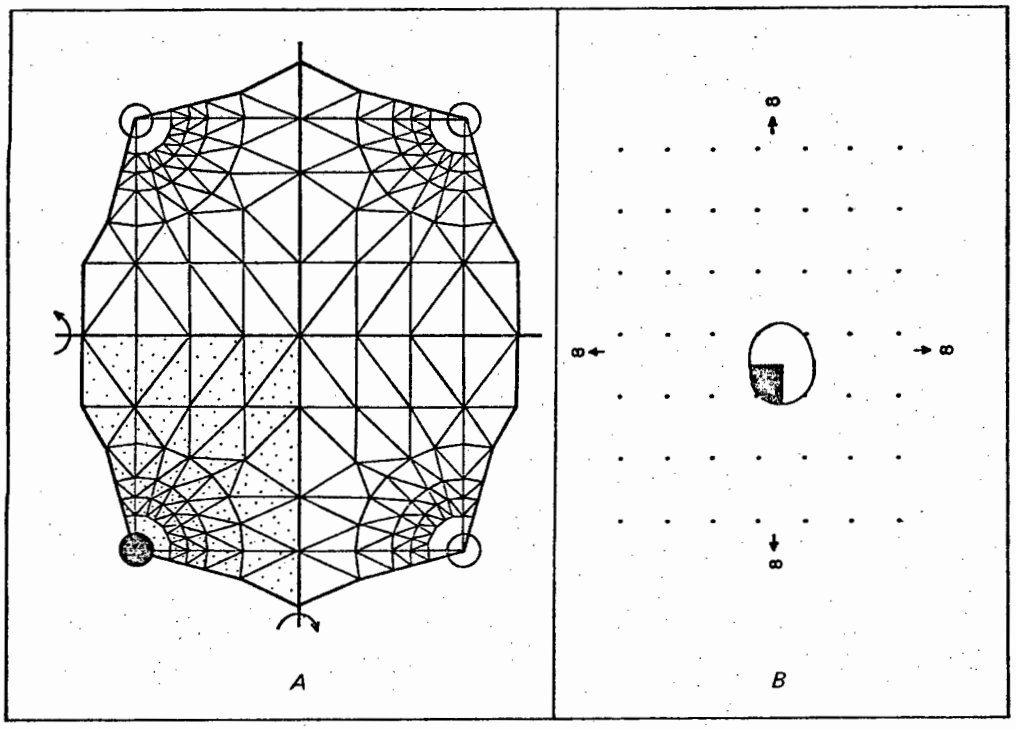

Figure AII-5. A. Reflection of the finite element model about its "external" boundaries causes the original single inclusion (black) to appear as a regular array of four inclusions. The external pure shear boundary conditions allow this interpretation of the model configuration.

B. The reflection condition imposed upon the "internal" boundaries of the finite element model results in a simulation of an infinite array of inclusions in which the four-inclusion array forms the "unit cell."

those of the positive quadrant were introduced into the model only at a rather late stage in the testing of the finite-element routine. It was previously found that, when the model consisted of positive quadrant elements only, certain problems arose. If the velocity components of the internal boundaries - then corresponding to the X = 0 and Y = 0 axes - were left completely unspecified (node at origin excepted), they deformed into curved shapes, thus destroying the symmetry of the full model. On the other hand if they were constrained to remain rectilinear by the prescription of zero velocity for the u and v components along the Y and X axes respectively, then anomalously inhomogeneous strain patterns arose in the adjacent nodes, as a result of induced tractional effects along these boundaries.

As mentioned above, however, it is a consequence of the boundary conditions imposed on this configuration that the "deformation box", which it was originally intended to simulate, is transformed into an idealised conglomerate of infinite extent (Fig. 5).

3. Results of computer experiment series CE4

In the present study a series of "computer experiments", involving the deformation of the finite element model described above, was carried out with inclusion-matrix viscosity contrasts ranging between 1 and 1000. This series has been called CE4, referring to the particular geometrical configuration adopted after trial investigations and individual experiments have been given the additional designation A - H. The results of the CE4 series can be separated into two parts: the first part concerns the comparison of inclusion axial ratios obtained by the numerical method with those predicted by Gay's exact theory (Gay, 1968a); the second part concerns the patterns of strain developed in the matrix surrounding a more viscous and therefore less deformed, inclusion.

a. Inclusion axial ratios

As a preliminary to the main series of finite element studies, an experiment (CE2 TEST) was conducted in which a similar approximating body was deformed

TABLE AII-2

SYNOPTIC TABLE OF PARTICLE AXIAL RATIO RESULTS

Deformation increment number	Computer Experiment Number						
	CE2 TEST	CE4A ($R = 1$)	CE4B ($R = 2,5$)	CE4C ($R = 5$)	CE4D ($R = 10$)	CE4E ($R = 50$)	CE4F ($R = 10^3$)
5	1,1046	1,1045	1,0651	1,0410	1,0246	1,0084	1,0040
10	1,2202	1,2199	1,1319	1,0803	1,0462	1,0130	1,0042
15	1,3479	1,3473	1,2029	1,1210	1,0681	1,0177	1,0045
20	1,4889	1,4880	1,2784	1,1633	1,0905	1,0225	1,0047
25	1,6447	1,6434	1,3591	1,2074	1,1136	1,0273	1,0049
30	1,8167	1,8149	1,4453	1,2535	1,1374	1,0321	1,0052
35	2,0068	2,0043	1,5377	1,3020	1,1620	1,0371	1,0054
40	2,2168	2,2135	1,6370	1,3530	1,1875	1,0422	1,0057
45	2,4487	2,4444	1,7441	1,4069	1,2142	1,0474	1,0060
50	2,7049	2,6994	1,8598	1,4641	1,2422	1,0529	1,0062
55	2,9879	2,9809	1,9851	1,5252	1,2717	1,0586	1,0065
60	3,3005	3,2918	2,1211	1,5904	1,3029	1,0646	1,0068
65	3,6458	3,6350	2,2692	1,6605	1,3361	1,0709	1,0071
70	4,0273	4,0139	2,4307	1,7359	1,3716	1,0777	1,0075
75	4,4486	4,4322	2,6070	1,8173	1,4096	1,0850	1,0078
80	4,9141	4,8940	2,7998	1,9053	1,4505	1,0927	1,0082
85	5,4282	5,4038	3,0108	2,0007	1,4944	1,1010	1,0086
90	5,9962	5,9665	3,2420	2,1042	1,5418	1,1100	1,0091
95	6,6235	6,5875	3,4955	2,2165	1,5929	1,1198	1,0096
100	7,3165	7,2731	3,7734	2,3385	1,6480	1,1303	1,0101

homogeneously by prescribing pure shear velocity components for the whole nodal array instead of just at the boundaries. A finite strain was thus built up incrementally with the same values of STRATE and TIME as obtained during the CE4A-CE4F experiments. The CE2 TEST, therefore, provided the numerical standard against which the results of the latter could be evaluated.

Inclusion axial ratios were computed from the co-ordinate values of the appropriate nodes - the two situated along the inclusion's major and minor axes on the inclusion-matrix interface - at each of the 100 deformation increments. In this way a record of the changing shape of the inclusion was kept. At the end of CE2 TEST, the originally circular shape had been deformed into an ellipse with an axial ratio (a/b) of 7,3165. In the first column of Table 2, values of a/b for this run are given for every fifth increment of deformation.

The subsequent columns of Table 2 show the axial ratio results obtained from experiments CE4A to CE4F. The results from CE4A, where there is no viscosity contrast, accord well with those of CE2 TEST, though the inclusion has suffered slightly less deformation and there is a small degree of inhomogeneity of strain throughout the system, as seen from a complete list of strain parameters for each element. These features may be due to technical aspects of the numerical method employed in the solution of the velocity component equations at the end of each deformation increment: the method is *Gauss-Siedel iteration*, hence solutions are approximate and might be expected to show a slight decrease in accuracy away from the boundaries for which velocities are fully prescribed. As the viscosity contrast between inclusion and matrix is increased, however, the deformation of the former drops off quite spectacularly.

The results from Table 2, with the exception of the major part of the CE4F column, have been plotted (Fig. 6) against the predictions of the original theory (solid lines) on a double logarithmic graph of the particle axial ratio (a/b) *versus* the axial ratio of the bulk strain ellipse ($\sqrt{\lambda_1/\lambda_2}$). CE2 TEST was taken as the base against which CE4 axial ratio values were plotted.

The numerical results show apparent good accordance with the theoretical predictions of the original theory (Gay, 1968a) for values of $\sqrt{\lambda_1/\lambda_2}$ up to about 4,0. After that, there is a deviation in the direction of greater strain

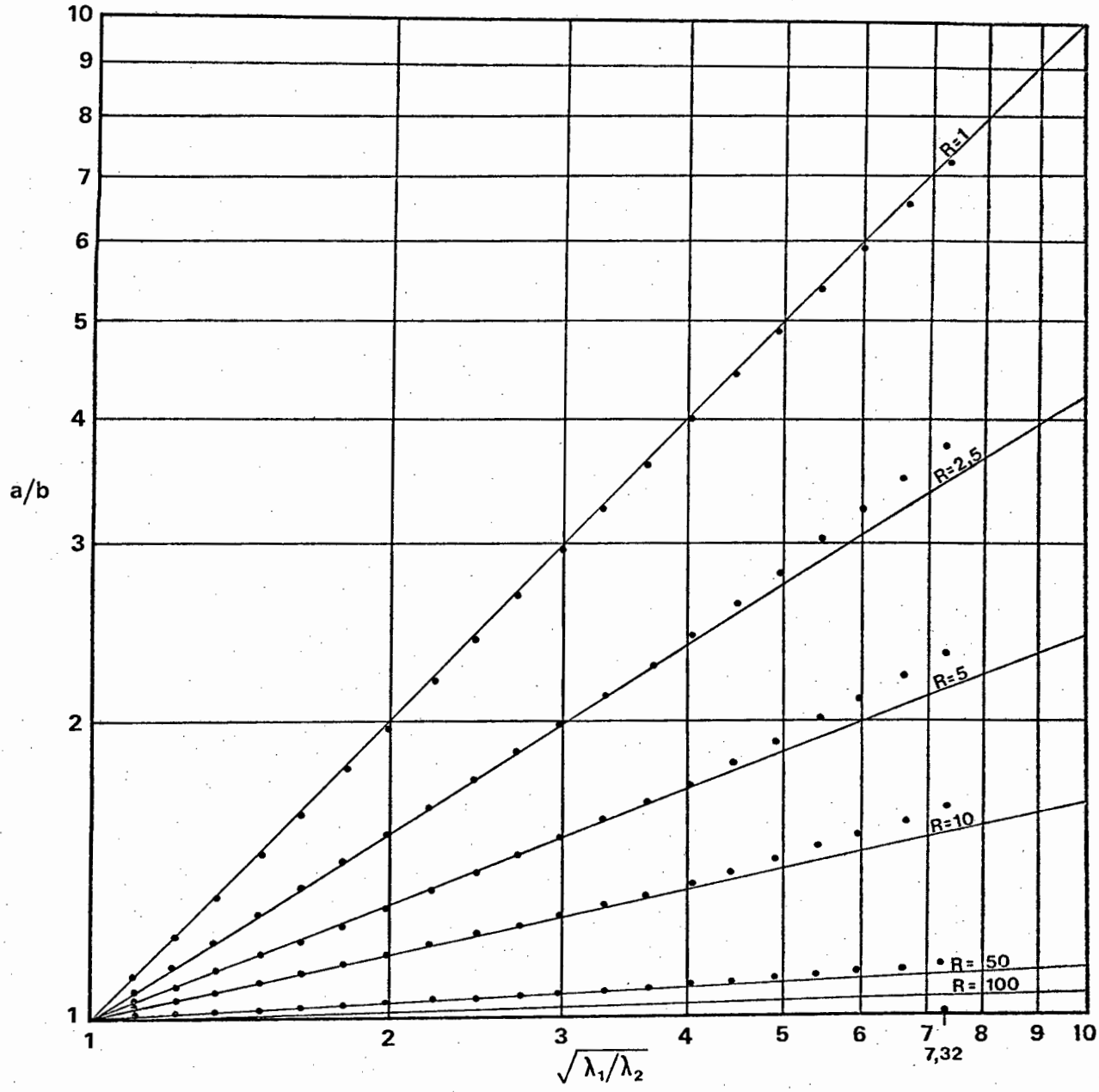

Figure AII-6. Comparison of the present finite element experimental results (dots) with Gay's (1968a) theoretical results (solid lines).

than anticipated, for systems with a viscosity contrast between inclusion and matrix. There may be a number of factors contributing to this deviation from prediction. These are:

(i) that the model of finite-elements is not exactly the continuous body with which the exact theory deals;

(ii) that the material of the model is slightly compressible and collapsible, whereas the mathematical theory deals with strictly incompressible materials;

(iii) that, under the incremental procedure adopted, the applied boundary conditions are not exactly those of ideal pure shear, there being a slight negative dilatation (i.e. area decrease) involved;

(iv) that errors of numerical approximation in the equation-solving subroutine SOLVE may be propagated from increment to increment and grow in the process; and

(v) that the boundary conditions of the experiments do not correspond to the boundary conditions of the exact theory.

Computer experiment CE4G was undertaken to test the possible influence of the finite-difference procedure for producing incremental deformation of the configuration. If differs from CE4B in the shorter time-increment, so that each deformation increment achieves only a 0,25% straining and also in a factor 10 increase in all viscosity coefficients. The results of CE4B and CE4G are compared in Table 3. It is evident that the CE4G results would fall below the CE4B curve in a plot of (a/b) *versus* $(\sqrt{\lambda_1/\lambda_2})$ and therefore correspond better with theory (Bilby *et al.*, 1975). The significant difference, however, is only in the third decimal place.

The notable feature of the computer experiments is that they deviate from the linear predictions of the original theory (Gay, 1968a) and trace curves similar in form to those of the later theory (Bilby *et al.*, 1975). Correspondence between experiments CE4B (R = 2,5) and CE4E (R = 50) and the exact theory is represented in Table 4, from which it can be seen that there is nevertheless a significant difference between experiment and theory. In both experiments, significantly higher inclusion axial ratios were achieved at bulk strains lower than theoretically predicted. For example, in CE4B, the final inclusion axial

TABLE AII-3

COMPARISON OF RESULTS OF EXPERIMENTS CE4B AND CE4G

CE4B			CE4G		
Deformation increment	Inclusion axial ratio a/b	Bulk strain $\sqrt{\lambda_1/\lambda_2}$	Deformation increment	Inclusion axial ratio a/b	Bulk strain $\sqrt{\lambda_1/\lambda_2}$
1	1,0139	1,0199	4	1,0129	1,0199
2	1,0268	1,0402	8	1,0253	1,0402
3	1,0395	1,0608	12	1,0370	1,0609
4	1,0522	1,0819	16	1,0507	1,0821
5	1,0651	1,1033	20	1,0637	1,1036
6	1,0782	1,1252	24	1,0767	1,1256
7	1,0914	1,1475	28	1,0900	1,1480
8	1,1048	1,1702	32	1,1034	1,1708
9	1,1182	1,1935	36	1,1169	1,1941
10	1,1319	1,2171	40	1,1306	1,2179
11	1,1458	1,2416	44	1,1445	1,2421
12	1,1598	1,2659	48	1,1586	1,2669
13	1,1740	1,2910	52	1,1729	1,2921
14	1,1883	1,3166	56	1,1873	1,3178
15	1,2029	1,3427	60	1,2019	1,3441
16	1,2176	1,3693	64	1,2167	1,3708
17	1,2325	1,3965	68	1,2317	1,3981
18	1,2476	1,4242	72	1,2468	1,4259
19	1,2629	1,4524	76	1,2622	1,4543
20	1,2784	1,4812	80	0,2778	1,4833
21	1,2941	1,5105	84	1,2936	1,5128
22	1,3101	1,5405	88	1,3095	1,5429
23	1,3262	1,5710	92	1,3257	1,5736
24	1,3425	1,6022	96	1,3422	1,6050
25	1,3591	1,6340	100	1,3588	1,6369

TABLE AII-4

COMPARISON OF EXPERIMENTAL RESULTS WITH EXACT THEORETICAL PREDICTION

Deformation increment	$\sqrt{\lambda_1/\lambda_2}$ Bulk strain in experiments	CE4B (R - 2,5) (a/b) exp.	CE4B (R - 2,5) $\sqrt{\lambda_1/\lambda_2}$ theory	CE4E (R - 50) (a/b) exp.	CE4E (R - 50) $\sqrt{\lambda_1/\lambda_2}$ theory
5	1,1046	1,0651	1,1167	1,0084	1,2378
10	1,2202	1,1319	1,2420	1,0130	1,3910
15	1,3479	1,2029	1,3811	1,0177	1,5642
20	1,4889	1,2784	1,5356	1,0225	1,7636
25	1,6447	1,3591	1,7077	1,0273	1,9873
30	1,8167	1,4453	1,8993	1,0321	2,2381
35	2,0068	1,5377	2,1130	1,0371	2,5315
40	2,2168	1,6370	2,3519	1,0422	2,8687
45	2,4487	1,7441	2,6195	1,0474	3,2567
50	2,7049	1,8598	2,9196	1,0529	3,7218
55	2,9879	1,9851	3,2566	1,0586	4,2707
60	3,3005	2,1211	3,6355	1,0646	4,9322
65	3,6458	2,2692	4,0624	1,0709	5,7321
70	4,0273	2,4307	4,5436	1,0777	6,7348
75	4,4486	2,6070	5,0860	1,0850	7,9979
80	4,9141	2,7998	5,6975	1,0927	9,5754
85	5,4282	3,0108	6,3867	1,1010	11,6088
90	5,9962	3,2420	7,1633	1,1100	14,2800
95	6,6235	3,4955	8,0377	1,1198	17,8566
100	7,3165	3,7734	9,0204	1,1303	22,6367

TABLE AII-5

COMPARISON OF COMPUTER EXPERIMENT AND THEORY FOR CE4H

Deformation increment	CE4H Inclusion axial ratio (a/b)	CE4H Bulk strain $\sqrt{\lambda_1/\lambda_2}$	Theory (R = 2,5)
10	1,1319	1,2171	1,2420
20	1,2784	1,4812	1,5356
30	1,4453	1,8026	1,8992
40	1,6370	2,1936	2,3519
50	1,8598	2,6696	2,9195
60	2,1211	3,2491	3,6356
70	2,4307	3,9547	4,5435
80	2,7998	4,8141	5,6975
90	3,2420	5,8610	7,1634
100	3,7734	7,1366	9,0205
110	4,4130	8,6910	11,3626
120	5,1833	10,5853	14,3002
130	6,1119	12,8939	17,9647
140	7,2321	15,7079	22,5133
150	8,5849	19,1382	28,1348
160	10,2199	23,3201	35,0563
170	12,1974	28,4187	43,5497
180	14,5895	34,6351	53,9395
190	17,4825	42,2146	66,6122
200	20,9799	51,4559	82,0292

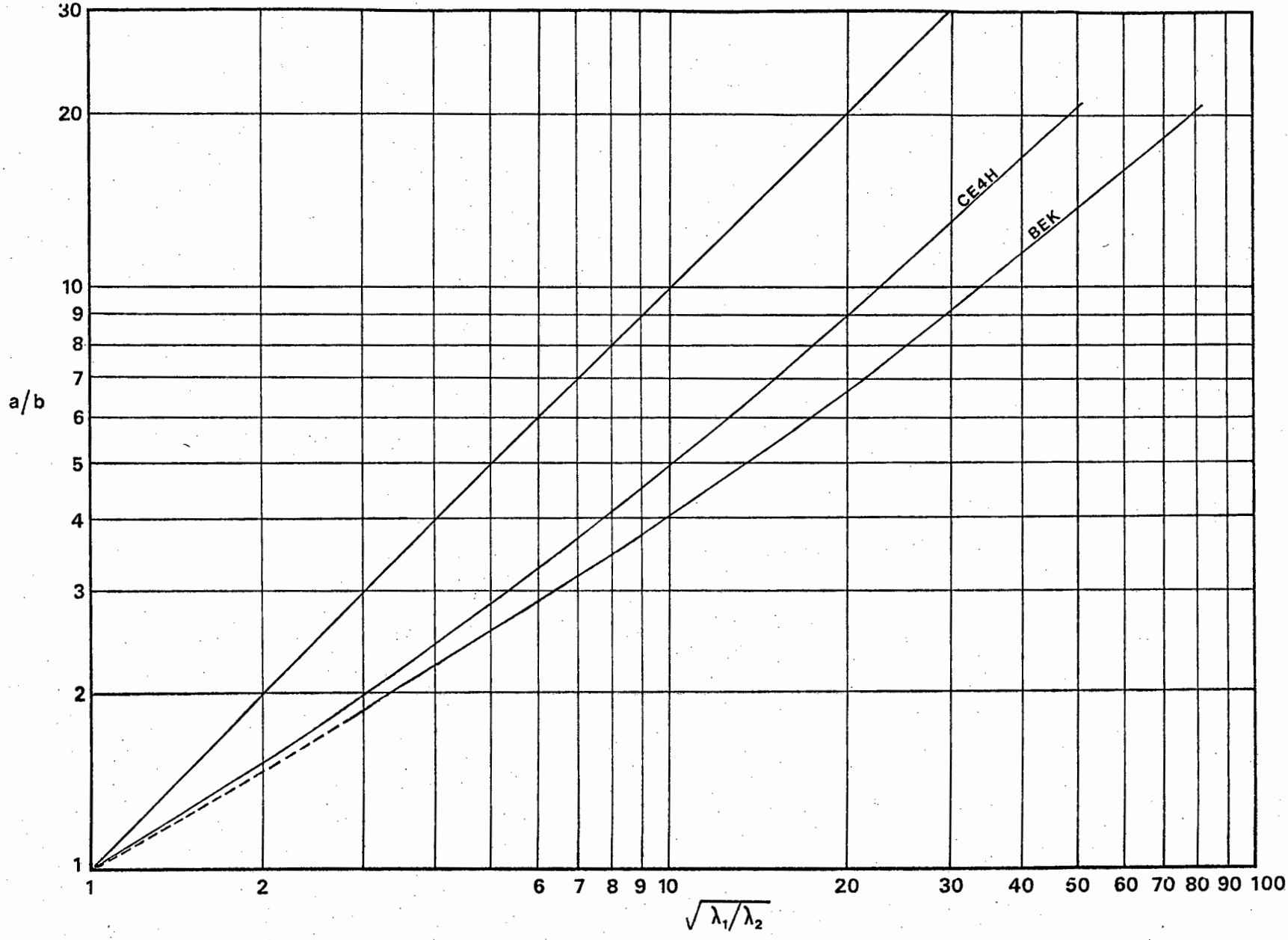

Figure AII-7. Comparison of finite element experimental results for a viscosity contrast of 2,5 with the theoretical predictions of Bilby *et al.*, (1975), represented as the curves CE4H and BEK respectively.

ratio of 3,77 is reached at an experimental bulk strain of 7,32, when according to theory it should be reached only when the bulk strain is 9.02.

This departure of experiment from theory is ascribed mainly to the different boundary conditions implicit in either analysis and not to any technical aspect of the finite-element method.

Comparison between theory and experiment is carried further in CE4H which is identical with CE4B, except that the greater viscosity coefficients of CE4G were maintained and that the deformation was carried on for 200 increments to a final bulk deviatoric strain of 51,46. At this stage the original 24 x 18 cm "deformation box" had been deformed into a 173,8 x 2,4 cm strip, containing a lensoid inclusion with an axial ratio of 21. Theoretically, however, this axial ratio should not have been reached for a viscosity contrast (R) of 2,5 until the bulk strain had reached 82 (Bilby *et al.*, 1975). Experimental results are given in Table 5, with theoretical data for comparison. These have been used in plotting Fig. 7 , which illustrates an interesting point. The experimental curve of CE4H is displaced way from the theoretical curve for R = 2,5 in the direction of lower viscosity contrast.

The graph, in fact, suggests an apparent viscosity contrast of about 2,0 for the CE4H system. The most likely explanation for this phenomenon, is that the effective viscosity of the matrix has been increased because the computer simulated system actually corresponds to a conglomerate, of which the regularly arrayed inclusions comprise about 3%. Closer analysis, discussed below, indicates that the apparent viscosity contrast varies systematically during deformation and is therefore not only related to the concentration of inclusions but also to their geometry and spacing along principal axes of strain.

b. Strain patterns in the matrix

A feature of the present finite-element routine is the provision for a detailed list of strain components to be obtained from each cell at the end of the deformation process. This is done in subroutine FSA2D by making use of the nodal co-ordinates of the *deformed* model and the stored nodal co-ordinates of the model in its original, undeformed state to derive the *deformation gradient matrix*

for each homogeneously strained element. From this matrix - erroneously called the *displacement gradient matrix* by Ramsay & Graham (1970, p.790) - it is possible to derive the fundamental features of the strain in each cell. These are:

(i) the maximum and minimum *principal quadratic elongations*, λ_1 and λ_2;

(ii) the angle, θ', between these axes and the X co-ordinate direction;

(iii) the rotational component, ω, reflecting the difference in orientation between the principal axes of strain in the undeformed and in the deformed state; and

(iv) the dilatation component, Δ, reflecting area change during deformation (since plane strain is assumed - no strain normal to XY plane - this implies volume change).

Where the plane-strain deformation gradient matrix (DGM) is given by

$$\begin{bmatrix} a & b \\ c & d \end{bmatrix}$$

the abovementioned strain components are obtained as follows

$$\lambda_1 = \tfrac{1}{2}(a^2+b^2+c^2+d^2 + \sqrt{(a^2+b^2+c^2+d^2)^2 - 4(ad-bc)^2}) \quad (22)$$

$$\lambda_2 = \tfrac{1}{2}(a^2+b^2+c^2+d^2 - \sqrt{(a^2+b^2+c^2+d^2)^2 - 4(ad-bc)^2}) \quad (23)$$

$$\tan 2\theta' = \frac{2(ac-bd)}{a^2+b^2-c^2-d^2} \quad (24)$$

$$\tan \omega = \frac{c-b}{a+d} \quad (25)$$

$$\Delta = (ad - bc) - 1 \quad (26)$$

after Ramsay (1967) and Ramsay & Graham (1970, p.790).

(i) CE2 TEST

CE2 TEST shows homogeneous strain throughout the model with λ_1 = 7,2444 and λ_2 = 0,1353. An ideal pure shear, the λ_1 value should correspond exactly to the axial-ratio of the strain ellipse, the *deviatoric strain ratio* given by $\sqrt{\lambda_1/\lambda_2}$, but here it obviously differs from the latter (which is about 7,317). The particle axial-ratio, too, is 7,3165. The reason for the discrepancy is shown by the component of dilatational strain (Δ or DEL) which indicates that there has been a reduction in area of about 1% over the whole of the model. The strain is therefore not ideal

pure shear and the explanation for this is to be sought in the method of incremental addition of small strains. If this were done in 200 steps of ½% incremental strain, rather than 100 steps of 1% strain, the effect would be greatly reduced. But the computing time would then be doubled.

In CE2 TEST the list of component θ' shows that the long axis of the strain ellipse is everywhere oriented parallel to the Y co-ordinate axis ($\theta' = 90^{o}$) and the list of ω shows that the deformation is effectively irrotational.

(ii) CE4A

Comparing the strain component list of CE4A with that of CE2 TEST, it can be seen that there is a systematic decrease in the λ_1 value and a corresponding increase in λ_2, as the vicinity of the inclusion is neared. This is believed to be due to less close approximation to an accurate solution away from the fully prescribed boundary nodal points. Further attention to subroutine SOLVE, such as the insertion of more iterative steps, would perhaps improve this, but again at the expense of increased computing time.

In addition, some slight departures from uniform ellipse orientations and completely irrotational strain were noted, but quantitatively these effects are negligible (of the order of $0{,}1^{o}$ or less). They may, however, be related to the more or less random variations in principal quadratic elongation values which are superimposed over the systematic variation noted above. Negative dilatational strain is again uniformly distributed and of the order of 1%.

In general, the CE4A results show a reasonably good pattern of approximately homogeneous, irrotational, pure shear strain : and they give some idea of the degree of confidence that may be attached to results from experiments CE4B to CE4H in which viscosity contrasts between inclusion and matrix have been introduced. In other words, they show the magnitude of strain variation resulting from experimental or numerical deficiencies to be not very great; indeed rather slight.

(iii) CE4B to CE4F

The strain component lists for CE4B to CE4F show that, in all cases, the inclusion displays a pattern of strain that is approximately homogeneous and irrotational. In other words, an initially *circular* inclusion always deforms to an elliptical shape, whatever the viscosity contrast. This carries with it the corollary that an initially *elliptical* inclusion orientated with its axes parallel to the principal axes of the imposed pure shear field remains elliptical, thus confirming an implicit assumption of the theory. It is therefore necessary only to consider patterns of strain variation in the surrounding matrix. Even for CE4B, which has the least viscosity contrast (R = 2,5),this variation is considerable.

General features that may be noted from the strain component list for the systems with viscosity contrasts are:

(i) distribution of strains both *higher* and *lower* than bulk strain($\sqrt{\lambda_1/\lambda_2}$ = 7,32) in the area between the inclusion - which shows much reduced strain - and the more external parts of the system - which show strains close to the bulk value;

(ii) variation in orientation of the principal axes of the strain ellipse in individual elements, becoming more notable as viscosity contrast is increased and occurring mainly in the area of the inclusion-matrix interface close to the long axis of the particle;

(iii) the occurrence of quite strongly rotational strains in the vicinity of the inclusion-matrix interface; and

(iv) the occurrence of strong dilatational strains in the vicinity of the inclusion-matrix interface.

The following discussion will centre primarily on points (i) and (iv) above.

In an attempt to illustrate strain patterns graphically and to indicate differences (and similarities) between patterns developed in systems with low R and those with high R, special attention has been concentrated on the results from CE4B (R = 2,5) and CE4E (R = 50).

In Fig. 8 and 9, sketches of the deformed CE4B and CE4E models around the inclusion have been made, indicating the shape of the inclusion-matrix interface and representing the deviatoric strain ratio variation in the surrounding

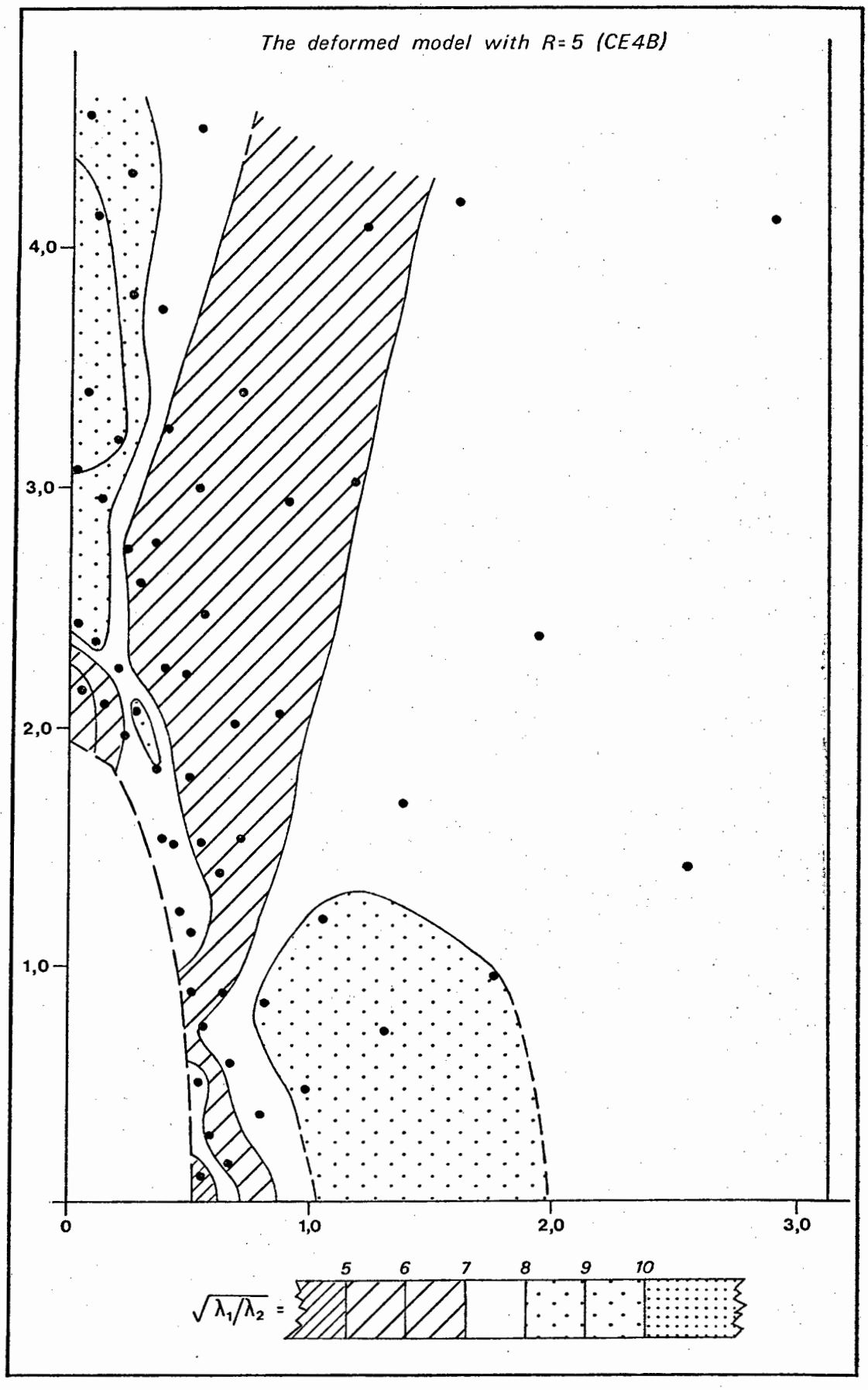

Figure AII-8. The pattern of deviatoric strain about a deformed inclusion where the viscosity contrast is 5 and the bulk strain attained is 7,32.

matrix. To derive them, deviatoric strain ratio values were plotted at the centroid positions (small dots) of each element and contours - coinciding with integral values of the ratio - were drawn manually to provide a general picture of their variation. It should be understood that, because the model is an *approximating body* of finite-elements - each of which has suffered a discrete, homogeneous strain, the patterns derived in this way are merely rather crude approaches to those which are to be expected from continuous materials. Obviously they could be improved by decreasing element size and increasing element number.

In CE4B (Fig. 8), the deviatoric strain ratio for the particle as a whole is close to 3,80. In the matrix, however, deviatoric ratios for individual cells vary between 4,61 and 9,75. As the contoured sketch shows, the highest deviatoric strains are located along the extended axis of the particle, rather than along the compressed direction as might intuitively have been expected. The *lowest* values of deviatoric strain are found along the compressed axis immediately adjacent to the deformed interface, in precisely the position in which one might have expected very high strains. In fact, the total strains in this position are really very high. What has happened here is that the deviatoric strain has been quite overshadowed by a strong component of *dilatational* strain (about 16%, negative) as inspection of the Δ column of the list for cells 39 and 40 shows.

Indeed, it appears that the area of low strain in an equivalent position on the extended (Y) axis may be explained in the same way, except that in this case the dilatational strain is strongly positive, signifying a marked area or volume increase (e.g. 31% and 39% in cells 54 and 56 respectively). It would therefore seem that the entire zone immediately external to the inclusion-matrix interface may be defined as one of potential *contact dilatational strain*, analogous to Ramberg's (1961) concept of deviatoric contact strain in the zone immediately adjacent to a buckling competent layer.

It is also interesting to note that, in the area not affected by marked dilatational strain, the true deviatoric strain "low" or "shadow" is located *off* the principal axes of the particle and not as might generally be believed,

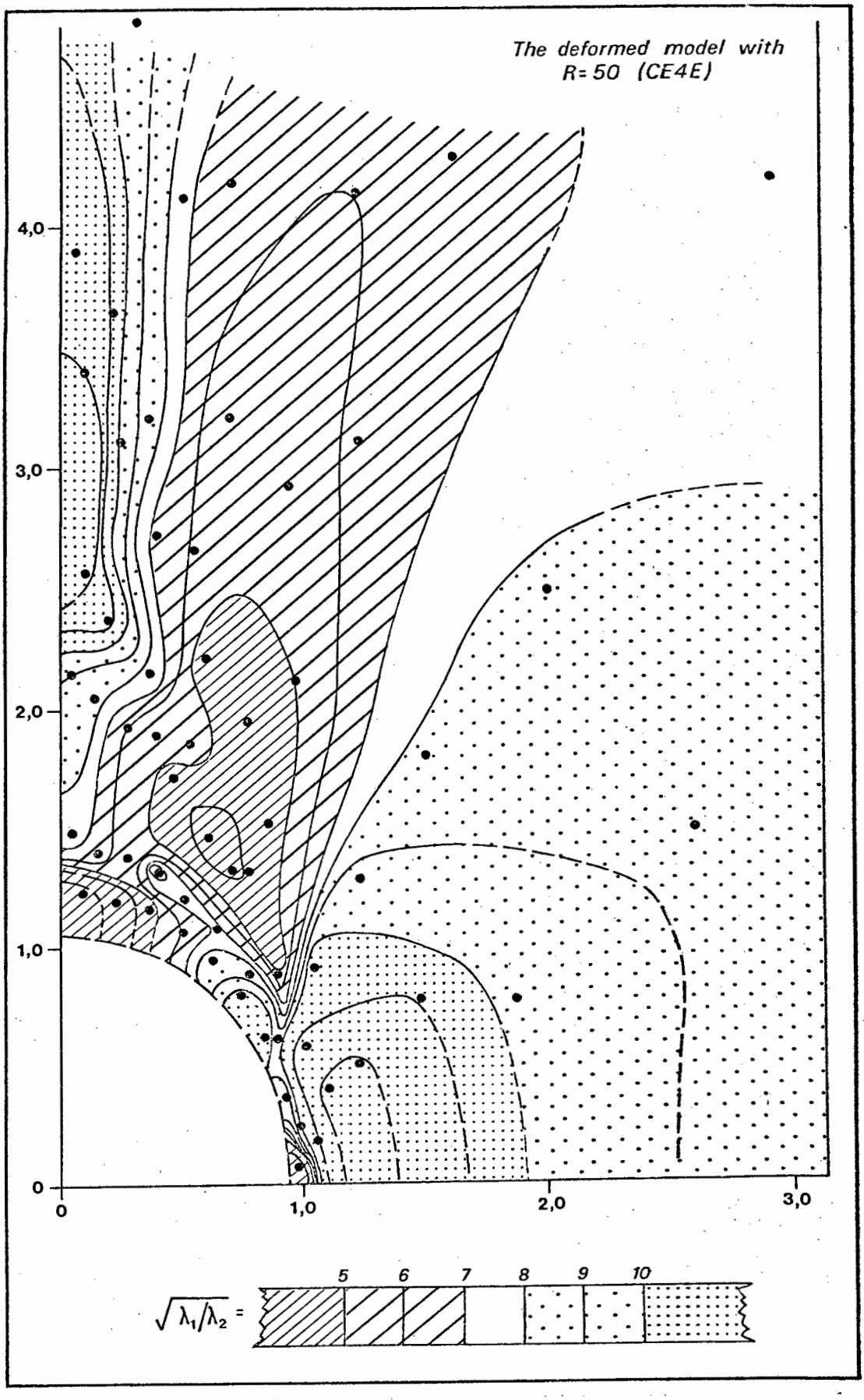

Figure AII-9. The pattern of deviatoric strain about a (hardly) deformed inclusion where the viscosity contrast is 50 and the bulk strain attained is 7,32.

along the extended axis of the body. The latter axis actually passes through the deviatoric strain *maximum* of the CE4B system.

In CE4E (Fig. 9) the greater viscosity contrast (R = 50) has rendered the matrix strain variation even more severe. The range of deviatoric ratios is between 2,66 and 12,77. The general pattern found in CE4B has also been brought out more clearly. The zone of contact dilatational strain is very pronounced and shows a pattern of deviatoric strain "lows" situated along the principal axes of the particle. At these points, negative and positive dilatational strains are very severe, reaching 57% and 117% respectively. On the other hand, those parts of the matrix which have suffered no significant degree of dilatation show a pattern of strain "highs" further out along the same axes. The true deviatoric strain shadow, as in Fig. 8 , is not situated along the extended axis of the particle, but in an intermediate position between the projected particle principal axes.

4. Discussion of the results

The original objective of the present study was the testing of the basic part of a theory dealing with the deformation of inhomogeneous viscous materials (Gay, 1968a), which was shown by Gay (1968b, 1969) to have some application to problems of strain determination in deformed conglomerates and other geologically granular systems (grits, oolitic limestones, etc.).

In fact, the present study does not precisely represent a test of either the above theory, or its later amendment (Bilby *et al.*, 1975) because the prescribed boundary conditions are different. The computer experiments actually appear to simulate the deformation of an infinite "conglomerate" of more viscous inclusions in a less viscous matrix, rather than a single inclusion embedded in an infinite matrix. The computer experiments are accordingly more realistic, in a sense, than the theory.

From this work, which appears to confirm the later theory (although in the field of geologically more relevant, low deviatoric strains, the two theories and the experimental results, are only marginally different in their quantitative predictions), two important features have emerged. Firstly, in connection

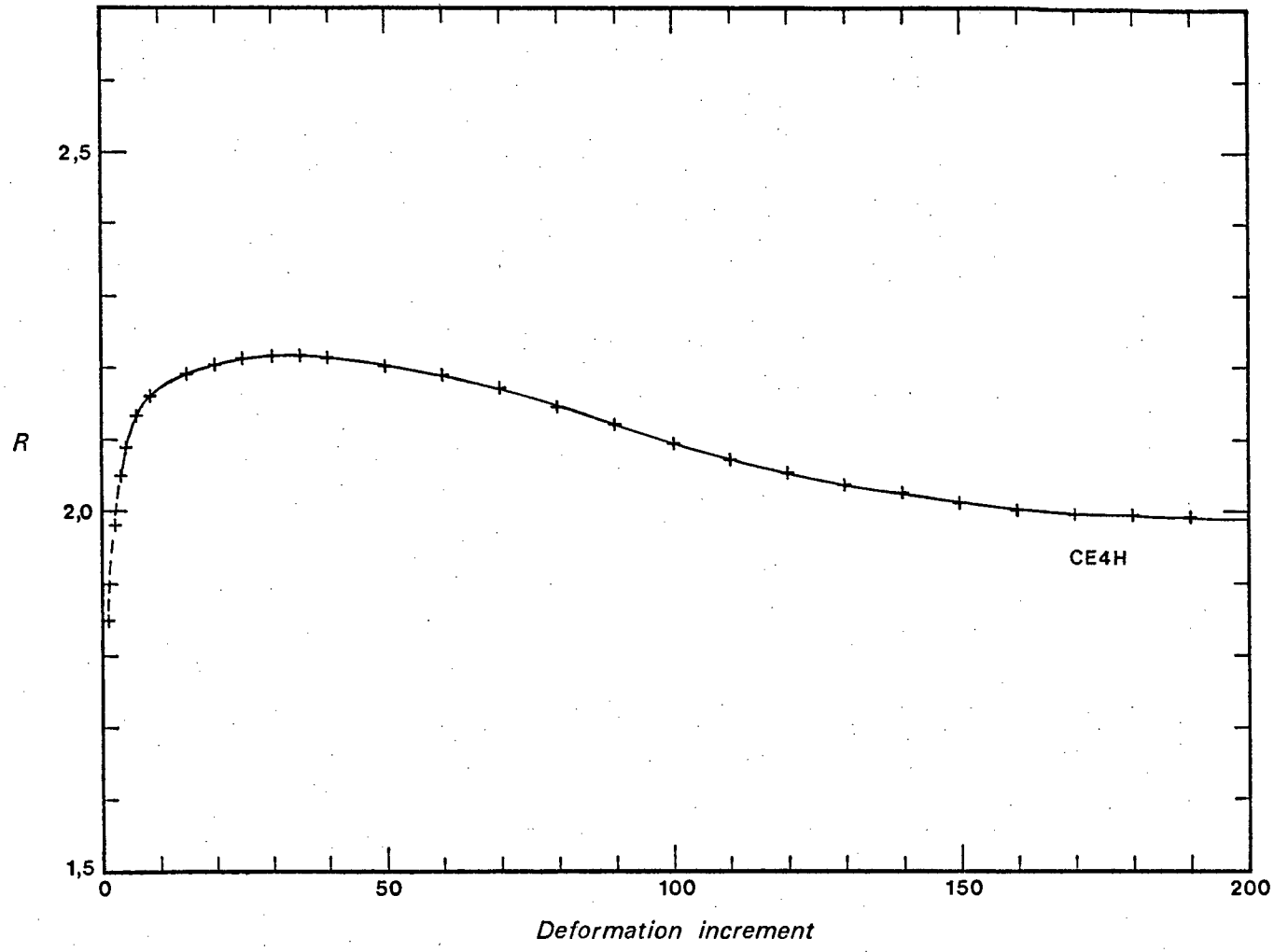

Figure AII-10. Apparent viscosity contrast R plotted against increasing bulk strain (represented by deformation increment number) for finite element experiment CE4H in which the assigned viscosity contrast was 2,5.

with the increase of inclusion axial ratio with progressive pure shear deformation, it has been noted that the apparent viscosity ratio is lower than that prescribed and that it may vary systematically with the deformation . Secondly, the phenomenon of "contact dilatational strain" in the matrix close to the inclusion has been recorded.

a. Inclusion-matrix apparent viscosity ratio

In order to test whether the experimentally derived curve in Fig. 7 could be fitted to an exact theoretical curve corresponding to a specific viscosity ratio (R) lower than that prescribed by the CE4H experimental input parameters, equation (19) was re-arranged to form

$$R = \left[\left\{ln(\sqrt{\lambda_1/\lambda_2}) - ln(a/b)\right\} \quad \frac{(a/b) + 1}{(a/b) - 1}\right] + 1 \qquad (27)$$

and the data of Table 5 (together with low increment-number data not included in the Table) was used to describe a curve of apparent viscosity ratio versus deformation increment number (Fig. 10). This shows that the lower apparent viscosity ratio is not constant throughout the experiment, but increases, rapidly at first, through to bulk deviatoric strain ratios around 2,0, and then decreases in apparently asymptotic form.

To guard slightly against the possibility that this might be an artifact of the experimental technique, the low deformation-increment data for experiment CE4G, having the same prescribed viscosity contrast, were processed in the same way and compared with CE4H results in Fig. 11. The same initially rapid increase in apparent viscosity contrast is evident in both sets of data.

The simple lowering of viscosity contrast is best explained by an increase in the effective viscosity of the infinite matrix surrounding the inclusion caused by the infinite array of similarly sized inclusions which it contains. Even though the inclusions comprise just under 3% of the whole system, their effect in lowering the viscosity contrast appears to be marked. In this respect, Gay (1968a, p.228) also noted that ethyl cellulose-benzanol experiments showed a more rapid rate of viscosity contrast decrease than that predicted theoretically by an equation which he derived (*op.cit.*, p.233-234).

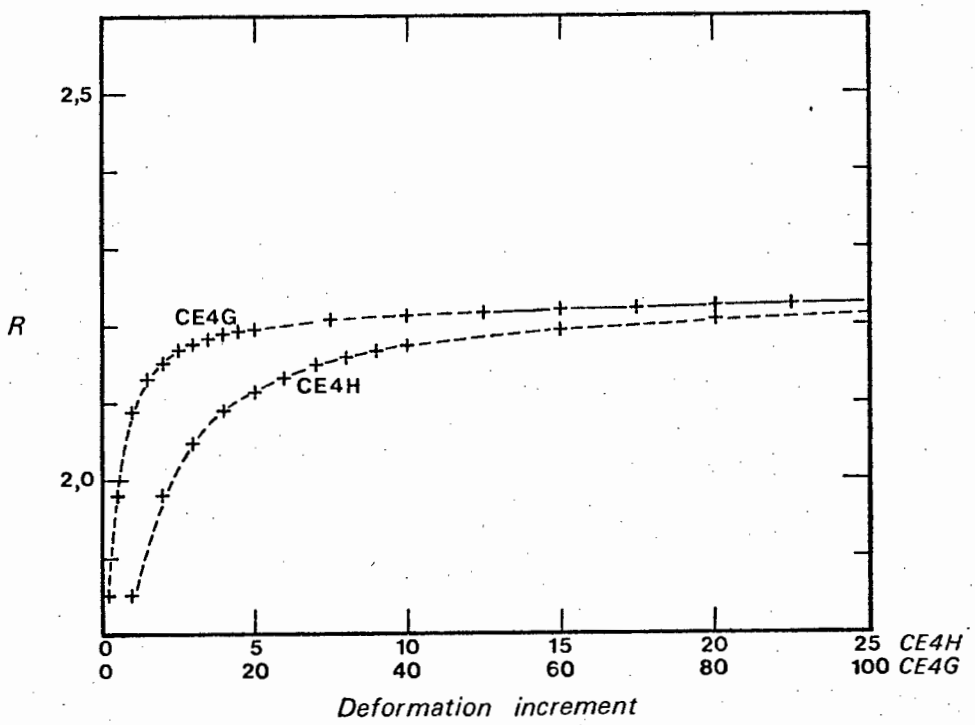

Figure AII-11. Apparent viscosity contrast R plotted against increasing bulk strain (represented by deformation increment numbers corresponding to nearly equal strains) for finite element experiments CE4G and CE4H in which the assigned viscosity contrasts were 2,5.

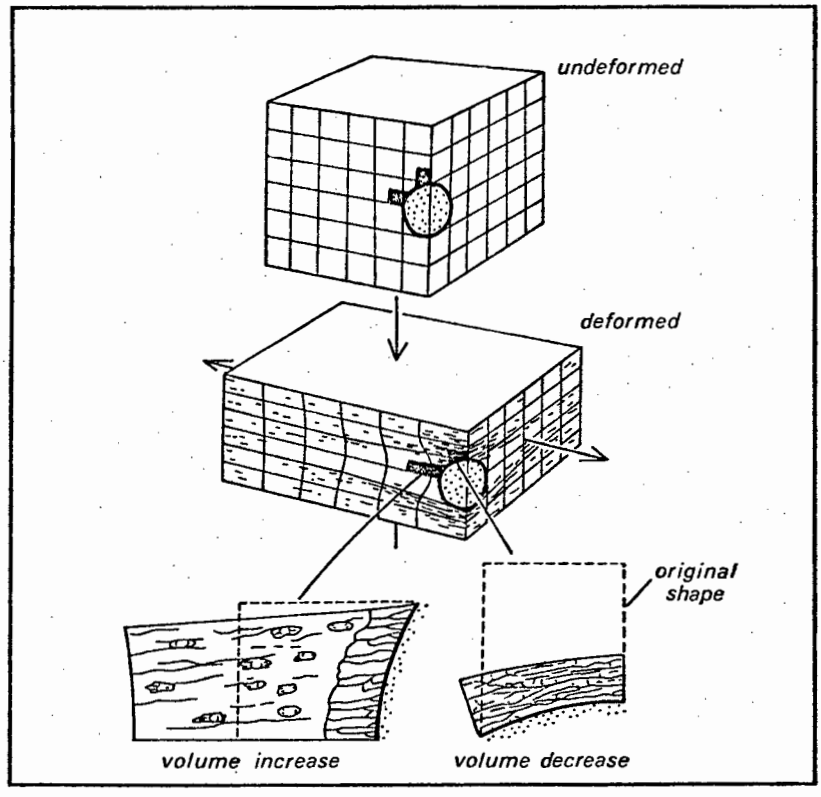

Figure AII-12. Model of pressure solution about a rigid inclusion (after Durney, 1976).

The regular variation in apparent viscosity contrast with progressive deformation noted above is less simply explained, but may be related to geometric factors. The latter may include:

(i) the different spacing of the inclusions along the two principal axes; and

(ii) the change in the rate of increase of the inclusion axial ratio with increasing deformation, as predicted by theory (Bilby *et al.*, 1975).

The gradually diminishing viscosity contrast at high strains can be perhaps accounted for by relating its decreasing distance between inclusion centres along the X-axis and the initial increase in the viscosity contrast may perhaps be related to the more rapidly increasing distance between originally more widely-spaced inclusion centres along the Y-axis at low strains. It is also possible that the ratio of centre-to-centre and interface-to-interface distances along the system axes is relevant to this behaviour. Obviously, more work with different configurations is required to confirm the phenomenon and explain its causes.

Alternatively it is possible that the effects of dilatational strain in the immediate region of the inclusion-matrix interface and their relationship to the changing shape of the inclusion, interferes with the inclusion-matrix viscosity contrast in some unspecified way. It is, in any case, possible that the effect might be suppressed at greater inclusion concentrations and hence might not be geologically important.

b. Contact dilatational strain

This phenomenom is of great geological relevance in connection with pressure solution effects around hard inclusions in low-grade metamorphic rocks. The latter usually show "pressure shadows", which are small areas where mineralogical compositions have been changed during the process of formation of the structure. The theory of pressure shadow formation has been treated using elastic inclusion theory (Savin, 1961) by Strömgård (1973) and has been interpreted as being promoted by gradients of mean normal stress which are set up around a hard object (*op. cit.*, Fig. 20).

The present model effectively simulates the *closed heterogeneously stressed system* described qualitatively by Durney (1976, p.235-236) and illustrated in Fig. 12. In all CE4 experiments, the phenomenon of negative dilatational strain in the matrix close to the inclusion surface along the compressional axis and positive dilatational strains close to the inclusion surface along the extensional axis, was noted. This is clearly related to the mean normal stress variation about the inclusion. The essential point, however, is that the pronounced dilatations actually occur in the model because of the assumption of material collapsibility. If the model were constituted by *incompressible* Newtonian viscous fluids, no dilatations would occur, by definition. If slight compressibility alone were assumed, as indicated by a λ^*/μ^* ratio of about 10, the dilatational effects around the more viscous inclusion would themselves be probably slight.

The relationship between rate of dilatation (D_{kk}) mean normal stress ($o_{kk}/3$) is given in equation (17) above. In the CE4 experiments it is dictated principally by the value of the viscosity parameter λ^*, since the shear viscosity parameter μ^* has been selected to correspond approximately with reasonable geological shear viscosity values inferred from experiment or field observation. If the value of λ^* were lowered significantly, the dilatational effects would be far more pronounced. Dieterich & Carter (1969), for example, report local dilatations as high as 29% using the ratio $\lambda^*/\mu = 4$.

A question remains about the use of a collapsible viscous fluid in computer modelling of pressure solution phenomena in nature. It is certainly a convenient assumption from the point of view of the ease of programming the method for the computer (cf. Thompson & Mack, 1970 for problems otherwise experienced), but there is doubt about its quantitative geophysical applicability. Does the phenomenon of pressure solution necessarily imply that rock, permeated by a fluid phase in low-grade metamorphic environments, is properly regarded as a collapsible material? And, if so, can the present-finite element model be used to quantify relationships between viscosity contrasts, deformation rates and diffusive mass transfer by solution in systems like the one described above?

REFERENCES - CHAPTER A-II

Ashby, M.F. & Verrall, R.A., 1973 - Diffusion accomodated flow and superplasticity. *Acta Metall.*, *21*, 149-163.

Bilby, B.A., Eshelby, J.D. & Kundu, A.K., 1975 - The change of shape of a viscous ellipsoidal region embedded in a slowly deforming matrix having a different viscosity. *Tectonophysics*, *28*, 265-274.

Biot, M.A., 1961 - Theory of folding of stratified visco-elastic media and its implications in tectonics and orogenesis. *Geol. Soc. Amer. Bull.*, *72*, *(11)*, 1595-1620.

Bott, M.H.P. & Dean, D.S., 1972 - Stress systems at young continental margins. *Nature Physical Science*, *235*, 23-25.

Cable, M., 1968 - The physical chemistry of glassmaking. *Proc. Int. Congr. on Glass, London. Society of Glass Technology*, 163-178.

Dieterich, J.H., 1969 - Origin of cleavage in folded rocks. *Am. J. Sci.*, *267*, *(2)*, 155-165.

_____, 1970 - Computer experiments on mechanics of finite-amplitude folds. *Can. Jl Earth Sci. 7*, 467-476.

_____, & Carter, N.L., 1969 - Stress history of folding. *Am. J. Sci.*, *267*, *(2)*, 129-154.

_____, & Onat, E.T., 1969 - Slow finite deformation of viscous solids. *J. Geophys. Res. 74*, 2081-2088.

Douglas, A., 1970 - Finite elements for geological modelling. *Nature*, *226*, 630-631.

Durney, D.W., 1976 - Pressure-solution and crystallization deformation. *Phil. Trans. R. Soc. Lond. A.283*, 229-240.

Elliott, D., 1973 - Diffusion flow laws in metamorphic rocks. *Geol. Soc. Amer. Bull.*, *84*, 2645-2664.

Froidevaux, C. & Schubert, G. (1975) - Plate motion and structure of the continental asthenosphere: A realistic model of the upper mantle. *J. Geophys. Res.*, *80*, 2553-2564.

Gay, N.C., 1968a - Pure shear and simple shear deformation of inhomogeneous viscous fluids. I : Theory. *Tectonophysics*, *5*, *(3)*, 211-234.

_____, 1968b - Pure shear and simple shear deformation of inhomogeneous viscous fluids. 2 : The determination of the total finite strain in a rock from objects such as deformed pebbles. *Tectonophysics*, *5*, *(4)*, 295-302.

_____, 1969 - Analysis of strain in the Barberton mountain land, Eastern Transvaal, using deformed pebbles. *J. Geol.*, *77*, *(4)*, 377-396.

_____, 1976 - The change of shape of a viscous ellipsoidal region embedded in a slowly deforming matrix having a different viscosity - a discussion. *Tectonophysics*, *35*, 403-407.

Gay, N.C. & Fripp, R.E.P., 1976 - The control of ductility on the deformation of pebbles and conglomerates. *Phil. Trans. R. Soc. Lond.* A.283, 109-128.

Griggs, D.T. & Baker, D.W., 1969 - The origin of deep-focus earthquakes. In: Mark, H. & Fernbach, S. (eds.), *Properties of matter under unusual conditions.* John Wiley, New York, 23-42.

Gruntfest, I.J., 1963 - Thermal feedback in liquid flow : Plane shear at constant stress. *Trans. Soc. Rheol.*, 7, 195-208.

Heard, H.C., 1976 - Comparison of the flow properties of rocks at crustal conditions. *Phil. Trans. R. Soc. Lond.* A.283, 173-186.

Herring, C., 1950 - Diffusional viscosity of a polycrystalline solid *J. Appl. Phys.*, 21.

Hobbs, B.E., 1971 - The analysis of strain in folded layers. *Tectonophysics*, 11, 329-375.

Jaeger, J.C., 1969 - *Elasticity, Fracture and Flow.* (3rd ed.) Methuen, 268 p.

Livesley, R.K., 1964 - *Matrix Methods of Structural Analysis.* Pergamon, 265 p.

Mase, G.E., 1970 - *Theory and Problems of Continuum Mechanics.* McGraw-Hill, New York. 221 p.

Mukherjee, A.K., Bird, J.E. & Dorn, J.E., 1969 - Experimental correlations for high temperature creep. *ASM Trans. Quart.*, 62.

Nabarro, F.R.N., 1948 - Steady state diffusional creep. *Phol. Mag.* 16,

Paterson, M.S., 1969 - The ductility of rocks. In: Argon, A.S. (ed.), *Physics of Strength and Plasticity,* M.I.T. Press, Cambridge, Mass. 377-392.

_____, 1976 - Some current aspects of experimental rock deformation. *Phil. Trans. R. Soc. Lond.* A.283, 163-172.

Price, N.J., 1975 - Rates of deformation - *J. Geol. Soc. Lond.*, 131, 553-575 .

Raj, R. & Ashby, M.F., 1971 - On grain boundary sliding and diffusional creep. *Metall. Trans.*, 2, 1113-1127.

Ramberg, H., 1961 - Contact strain and folding instability of a multi-layered body under compression. *Geol. Rdsch.*, 51, (2), 405-439.

_____, 1963 - Fluid dynamics of viscous buckling applicable to folding of layered rocks. *Bull. Am. Assoc. Petrol. Geologists*, 47, 484-505.

Ramsay, J.G., 1967 - *Folding and Fracturing of Rocks.* McGraw-Hill, New York, 568 p.

_____, J.G. & Graham, R.H., 1970 - Strain variation in shear belts. *Can. J. Earth Sci.* 7, (3), 786-813.

Rutter, E.H., 1976 - The kinetics of rock deformation by pressure solution. *Phil. Trans. R. Soc. Lond., A.283,* 203-219.

Savin, G.N., 1961 - *Stress Concentration around Holes.* Pergamon Press, Oxford, 430 p.

Scholz, C.H., Sykes, L.R. & Aggarwal, Y.P., 1973 - Earthquake prediction: a physical basis. *Science, 181,* 803-810.

Service, K.G. & Douglas, A., 1973 - Boundaries and fractures in finite element models of geological structures. *Geophys. J. Roy. astr. Soc., 32,* 1-14.

Shimazaki, K., 1974 - Pre-seismic crustal deformation caused by an underthrusting oceanic plate, in eastern Hokkaido, Japan. *Phys. Earth Planet. Interiors, 8,* 148-157.

Sokolnikoff, I.S., 1956 - *Mathematical Theory of Elasticity.* McGraw-Hill, N.Y.

Sorby, H.C., 1863 - On the original nature and subsequent alteration of mica-schist. *Q. Jl Geol. Soc. Lond., 19,* 401-406.

_____, H.C., 1879 - The structure and origin of limestones. *Q. Jl geol. Soc. Lond., 35,* 56-95.

Stephansson, O., 1976 - Finite element analysis of folds. *Phil. Trans. R. Soc. Lond., A.283,* 153-161.

_____, O. & Berner, H., 1971 - The finite element method in tectonic processes. *Phys. Earth Planet. Interiors, 4,* 301-321.

Stocker, R.L. & Ashby, M.F., 1973 - On the rheology of the upper mantle. *Rev. Geophys. Space Phys., 11,* 391-426.

Strömgård, K.E., 1973 - Stress distribution during formation of boudinage and pressure shadows. *Tectonophysics, 16,* 215-248.

Thompson, E.G. & Mack, L.R., 1970 - Remarks on paper by J.H. Dietrich and E.T. Onat, "Slow finite deformations of viscous solids." *J. Geophys. Res., 75,* 1625-1627.

Truesdell, C. & Toupin, R., 1960 - The Classical field theories. In: Flugge, S., (ed.), *Encyclopaedia of Physics : Volume III/1. Principles of Classical Mechanics and Field Theory.* Springer-Verlag, Berlin, 226-793.

Weertman, J., 1970 - The creep strength of the earth's mantle. *Rev. Geophys. Space Phys., 8,* 145-168.

White, S., 1973 - The dislocation structures responsible for the optical effects in some naturally-deformed quartzes. *J. Mater. Sci., 8,* 490-499.

Zienkiewicz, O.C., 1969 - *The Finite Element Method in structural and continuum mechanics.* McGraw-Hill, London, 274 p.

_____, O.C., 1976 - The finite element method and the solution of some geophysical problems. *Phil. Trans. R. Soc. Lond., A.283,* 139-151.

Aufschluß	27	131–132	2 Abb.	Heidelberg April 1976

Kristallwachstum an einer geologischen Deckenbahn

Von Hans-Georg MÜNCH, Heidelberg

In Südwestafrika, 200 km südlich der Hauptstadt Windhoek, tritt eine Gesteinsfolge ohne Beziehung zu ihrem Ablagerungsraum als tektonische Schubmasse auf: das exotische Naukluft-Deckensystem. Es wird aufgebaut aus jungpräkambrischen Sedimenten, wie Karbonatgesteinen, Quarziten und Tonschiefern und liegt tektonisch diskordant auf ebenfalls jungpräkambrischen Gesteinen – wiederum Karbonate, Tonschiefer und Quarzite – der Nama-Gruppe.

Die auffälligste Erscheinung des mindestens 30 km weit transportierten, 1600 km^2 großen Naukluft-Deckensystems ist seine Hauptbewegungsbahn, die – annähernd horizontal verlaufend – die tektonischen Strukturen des von weither Bewegten (Allochthon) von denen des Bodenständigen (Autochthon) scharf abschneidet.

Die Hauptbewegungsbahn des Deckensystems wird durch eine schichtförmige, zweiseitig-symmetrische Serie zertrümmerter (kataklastischer) und durch Bewegung veränderter (dynamometamorpher) karbonatischer Gesteine markiert. Diese bis 30 m mächtig werdende Gesteinsserie bildet in ihrer Gesamtheit das Deckenschmiermittel, das eine Reibungsbrekzie besonderer Art ist, die durch und während der Deckenbewegung entlang der Bewegungsbahn entstand.

Die Zentralzone des Deckenschmiermittels, die auch die Symmetrieebene der Zertrümmerungszone darstellt, wird von einem nach dem Stillstand der Decke (postkinematisch) umkristallisierten, sandkörnigen Gesteinszerreibsel (Protomylonit) gebildet, der intrusive Eigenschaften aufweist, d.h., daß er wie eine Schmelze vor allem nach oben auf Klüften und Spalten eingedrungen ist und so in Gängen und Adern auftritt. Der Protomylonit besteht aus einer grobkristallinen karbonatischen Matrix, in der regellos verteilt idiomorphe, grobe Kristalle (Blasten) von Quarz, Feldspäten, Dolomit, Calcit, Turmalin, Muskovit, Chlorit, Haematit und Pyrit auftreten.

Das nach dem Abklingen der Deckenbewegung eingetretene Kristall-Neuwachstum ist nicht nur auf die Zentralzone beschränkt, sondern umfaßt – wenn auch in abgeschwächter Form – das gesamte Deckenschmiermittel sowie die autochthonen und allochthonen Sedimentgesteine in der näheren Umgebung der Bewegungsfläche.

In den der Bewegungsfläche benachbarten karbonatischen Sedimenten finden sich bis 10 cm große, wasserklare, milchweiße, graue und schwarze Dolomitkristalle (Blasten), die ganz oder doch fast idiomorph ausgebildet sind. An der in Abb. 1 und 2 gezeigten Dolomitprobe ist deutlich zu erkennen, wie ein Dolomitkristall ungestört durch die primäre Sedi-

Anschrift des Verfassers: Dipl.-Geol. Hans-Georg MÜNCH, Geologisches Institut der Universität Heidelberg, Im Neuenheimer Feld 234, 6900 Heidelberg.

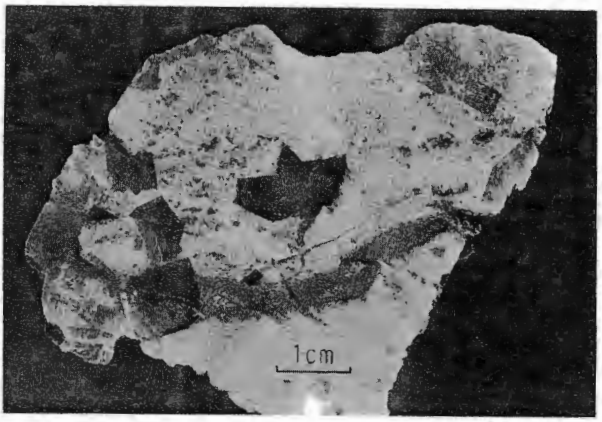

Abb. 1. Dolomitkristalle von Farm Remhoogte 227. Sandlagiger weißer Dolomit mit milchweißen bis klaren, idiomorphen und subidiomorphen Dolomitblasten bis 3 cm Größe (Probe HGM 405a im Geol. Inst. Heidelberg).

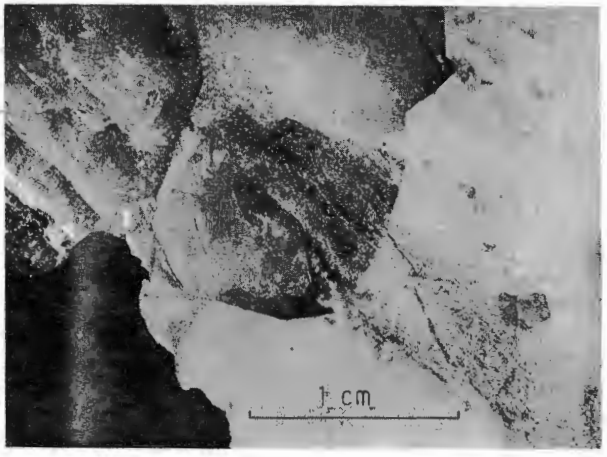

Abb. 2. Ausschnitt aus Abb. 1, linke untere Ecke ca. 45° nach rechts gedreht. Ein Dolomitkristall hat die ursprüngliche sedimentäre Struktur des Wirtsgesteins durchwachsen und diese ungestört in sich aufgenommen.

Fotos: K. SCHACHERL, Geol. Inst. d. Univ. Heidelberg.

mentstruktur – im Bild: lagige Einschaltung von Quarzkörnern – des Wirtsgesteins hindurchwächst und diese, ohne sie zu verschieben, in sich aufnimmt.

Der Verfasser hält die hier vorgestellte Probe für ein eindrucksvolles Beispiel dafür, wie stark einerseits die Kristallblastese sein kann und wie andererseits ein wachsender Kristall die Fähigkeit besitzt, Fremdmaterial zu umschließen und in sich aufzunehmen. Das Fremdmaterial wird ohne Lageveränderung in den Kristall aufgenommen, der damit poikiloblastisch wird, d.h. er hat eine ungestörte Kristallgestalt, in die jedoch körniges Fremdmaterial eingebaut ist.

Deckenschmiermittel an der Basis bewegter Gesteinsmassen sind äußerst selten beschrieben worden; in den Alpen rechnet man bisher nur den Lochseitenkalk dazu.

Für Informationen über die geologische Situation werden folgende Arbeiten genannt:

KORN, H. & MARTIN, H: Gravity Tectonics in the Naukluft Mountains of South West Africa. – Bull. Geol. Soc. Am. **70**, 1047–1078, 1959.

MÜNCH, H.G.: Die Geologie des Naukluft-Deckensystems, Südwestafrika (Vorläufiger Bericht). – N. Jb. Geol. Paläont. Mh. **11**, 657–663, Stuttgart 1975.

GEOLOGICAL MAP OF THE NAUKLUFT AREA

SCALE 1:100 000

2 1 0 1 2 3 4 5 6 7 8 9 10 km

23°45'

24°00'

24°15'

24°30'

16°15'

16°30'

GEOGRAPHICAL KEY

- Sonop River — Intermittent stream with name
- 1918 — Spot height (in metres)
- 12 △ 1948 — Trigonometrical beacon (with height and number)
- Farm boundary
- ZAIS 6 — Farm name and number
- Dwelling
- Main road
- Prospecting trench

(Note: The farms Naukluft 9, Ubusis 3, Felseneck 124, Die Valle 226, Arbeit Adelt 5 and Lemoenputs 162 now comprise the Naukluft Mountain Zebra Park.)

GEOLOGICAL KEY

- Limit of rock outcrop
- Lithological contact
- Major overthrust
- Minor thrust fault
- Normal or wrench fault
- Shear belt
- Photogeological fracture trace
- 40 — Strike and dip of bedding
- Strike of vertical bedding
- 70 — Strike and dip of cleavage
- 30 — Trend and plunge of lineation

LEGEND

	Sand, alluvium, calcrete, scree		Tertiary–Recent
	Terrace deposits		
Ef	Arkosic sandstone		Etjo Formation (?)
Dw	Tillite		Dwyka Formation
Oz	Dolomite, bitum. limestone	Onis Mbr	Zebra River Formation
Oi	Grey dolomite	Onis Mbr	Zebra River Formation
L	Shale, conglomerate, limestone	Lemoenputs Mbr	Zebra River Formation
T	Dolomite, calc. quartzite	Tsams Mbr	Zebra River Formation
U	Sandstone, shale, local conglomerate	Ubusis Mbr	Zebra River Formation
Ne	Nepheline syenite	Neuras Mbr	Zebra River Formation
A	Conglomerate, arkose, purple quartzite	Aubschlucht Formation	Naukluft Nappe Complex
Ts	Volcaniclastic, dolomite, purple slate	Tsabisis Formation	Naukluft Nappe Complex
Bk	Limestone–dolomite breccia, limestone	Blässkranz Formation	Naukluft Nappe Complex
Kbr	Limestone, ls-dol. breccia, shale	Klipbokrivier Formation	Naukluft Nappe Complex
R	Phyllite, slate marble, breccia	Remhoogte Formation	Naukluft Nappe Complex
B	Dolomite, calc quartzite, purple shale	Büllsport Formation	Naukluft Nappe Complex
N'	Dolomite, dolomitic sandstone	Noab Formation	Naukluft Nappe Complex
Ro	Limestone, shale, dolomite	Rietoog nappe	
Sr	Sandstone, shale	Schwarzrand Formation	Nama Group
Ku	Bitum. limestone, shale, quartzite	Kuibis Formation	Nama Group
Bb	Pebbly mudstone (? tillite)	Blaubeker Formation	?
Ka	Quartzites, arkose, conglomerate	Kamtsas Formation	?
Kla	Quartzites, calc shales, conglomerate	Klein Aub Formation	Nuwedam Group
D	Red quartzite purple mudstones, felsic volcanics	Doornpoort Formation	Nuwedam Group
g	Pebbly quartzite, slate, mafic volcanics	Grauwater Formation	Nuwedam Group
Na	Felsic volcanics, clastics	Nauzerus Formation	
+ +	Granite	Gamsberg granite	
	Granodiorite	Piksteel granodiorite	
~E~	Schists, magnetite-quartzite, calc-silicates	Elim Formation	

Mapped and compiled by C.J. Hartnady, 1972–1978.
Basement geology in north modified from S.A. de Waal, 1966.
Drawn by Miss P. Eloff, 1978. Colour separation by
Miss R. Allanson and Mrs R. Kovàts, 1980, Precambrian Research
Unit, Department of Geology, University of Cape Town.©